



Philip Ringrose  
Mark Bentley

# Reservoir Model Design

A Practitioner's Guide

*Second Edition*

 Springer

---

# Reservoir Model Design

---

Philip Ringrose • Mark Bentley

# Reservoir Model Design

A Practitioner's Guide

Second Edition



Philip Ringrose  
Equinor ASA  
Norwegian University of Science  
and Technology  
Trondheim, Norway

Mark Bentley  
TRACS International Limited  
Heriot-Watt University  
Aberdeen and Edinburgh  
Scotland, UK

ISBN 978-3-030-70162-8      ISBN 978-3-030-70163-5 (eBook)  
<https://doi.org/10.1007/978-3-030-70163-5>

© Springer Nature Switzerland AG 2015, 2021

This work is subject to copyright. All rights are reserved by the Publisher, whether the whole or part of the material is concerned, specifically the rights of translation, reprinting, reuse of illustrations, recitation, broadcasting, reproduction on microfilms or in any other physical way, and transmission or information storage and retrieval, electronic adaptation, computer software, or by similar or dissimilar methodology now known or hereafter developed.

The use of general descriptive names, registered names, trademarks, service marks, etc. in this publication does not imply, even in the absence of a specific statement, that such names are exempt from the relevant protective laws and regulations and therefore free for general use.

The publisher, the authors, and the editors are safe to assume that the advice and information in this book are believed to be true and accurate at the date of publication. Neither the publisher nor the authors or the editors give a warranty, expressed or implied, with respect to the material contained herein or for any errors or omissions that may have been made. The publisher remains neutral with regard to jurisdictional claims in published maps and institutional affiliations.

Cover figure: Multiscale geological bodies and associated erosion, Lower Antelope Canyon, Arizona, USA. Photograph by Jonas Bruneau. © EAGE reproduced with permission of the European Association of Geoscientists and Engineers.

This Springer imprint is published by the registered company Springer Nature Switzerland AG  
The registered company address is: Gewerbestrasse 11, 6330 Cham, Switzerland

---

## Preface

This book is about the design and construction of subsurface reservoir models.

In the early days of the oil industry, oil and gas production was essentially an engineering activity, dominated by disciplines related to chemical and mechanical engineering. Three-dimensional (3D) geological reservoir modelling was non-existent, and petroleum geologists were mostly concerned with the interpretation of wire-line well logs and with the correlation of geological units between wells. Two important technological developments – computing and seismic imaging – stimulated the growth of reservoir modelling, with computational methods being applied to mapping, volumetrics and reservoir simulation. Geological or ‘static’ reservoir modelling was given further impetus from the development of geostatistical techniques, allowing the reservoir modeller to estimate inter-well reservoir properties and hence make statistical predictions. 3D reservoir modelling has now become the norm.

Reservoir models in themselves do not generate prospects or development scenarios, increase productivity or reduce risk and uncertainty. They are simply tools which reflect our ability to achieve these goals. Advances in reservoir modelling cannot therefore be compared to technology breakthroughs such as 4D seismic imaging, horizontal drilling or EOR methods. Reservoir modeling tools are, however, invaluable tools for integrating knowledge and for making strategic decisions.

As the world moves into the energy transition and oil and gas production is likely to decline, energy and transportation will be increasingly powered by renewable or low-emissions technologies. In this new era, CO<sub>2</sub> disposal and subsurface energy storage will become increasingly important and will make new demands of subsurface modelling. The fluids used and stored in the subsurface may change but the value of porous rock reservoirs will remain. We will never cease to need to know how these fluids move in the subsurface, and modelling of subsurface reservoirs will remain a tool for building this understanding and making useful forecasts.

\* \* \*

The explosion of reservoir modelling software packages and associated geostatistical methods has created high expectations but also led to periodic disappointments. This has given birth to an oft quoted mantra “*all models are wrong.*”

This book emerged from a series of industry and academic courses given by the authors and aimed at guiding the reservoir modeller through the pitfalls and benefits of reservoir modelling, in the search for a reservoir model design that is useful for forecasting. Reservoir modelling and simulation software packages often come with guidance about which buttons to press and menus to use for each operation, but less advice on the objectives and limitations of the model algorithms. The result is that whereas much time is devoted to model building, the outcomes of the models often fall short of their objectives.

Our central contention in this book is that problems with reservoir modelling tend not to stem from hardware limitations or lack of software skills but from the approach taken to the modelling – the *model design*. It is essential to think through the design and to build fit-for-purpose models that meet the requirements of the intended use. All models are *not* wrong, but in many cases models are used to answer questions which they were simply not designed to answer.

We cannot hope to cover all the possible model designs and approaches, and we have avoided as much as possible reference to specific software modelling packages. Our aim is to share our experience and present a generic approach to reservoir model design. Our design approach is geologically based – partly because of our inherent bias as geoscientists – but mainly because subsurface reservoirs are composed of rocks. The pore space which houses the ‘black gold’ of the oil age, the ‘golden age’ of gas or the fluids disposed and stored in the new ‘age of sustainability’, has been constructed by geological processes – the deposition of sandstone grains and clay layers, processes of carbonate cementation and dissolution, and the mechanics of fracturing and folding. Good reservoir model design is therefore founded on good geological interpretation.

There is always a balance between probability (the outcomes of stochastic processes) and determinism (outcomes controlled by limiting conditions). We develop the argument that deterministic controls rooted in an understanding of geological processes are the key to good model design. The use of probabilistic methods in reservoir modelling without these geological controls is a poor basis for decision making, whereas an intelligent balance between determinism and probability offers a promising path.

We also discuss the decision-making process involved in reservoir modelling. Human beings are notoriously bad at making good judgements – a theme widely discussed in the social sciences and behavioural psychology. The same applies to reservoir modelling – how do you know you have a fit-for-purpose reservoir model? There are many possible responses, but most commonly there is a tendency to trust the outcome of a reservoir modelling process without appreciating the inherent uncertainties.

We hope this book will prove to be a useful guide to practitioners and students of subsurface reservoir modelling in the fields of petroleum geoscience, environmental geoscience, CO<sub>2</sub> and energy storage and reservoir engineering – an introduction to the complex, fascinating, rapidly-evolving and multi-disciplinary field of subsurface reservoir modelling.

Trondheim, Norway

Philip Ringrose

Edinburgh, UK  
Tenby, UK

Mark Bentley

---

# Prologue: Model Design

---

## Successful Reservoir Modelling

This book offers practical advice and ready-to-use tips on the design and construction of reservoir models. This subject is variously referred to as ‘geological reservoir modelling,’ ‘static reservoir modelling,’ ‘3D reservoir modelling’ or ‘geomodelling,’ and our starting point is very much the geology. However, the end point is fundamentally the engineering representation of the subsurface and in this sense these notes will deal with the important interface with the world of dynamic, simulation modelling, with which static modelling is intrinsically integrated.

Our central argument is that whether models succeed in their goals is generally determined in the higher level issue of *model design* – building models which are fit for the purpose at hand.

Based on our own experiences and those of colleagues and groups we have worked with on courses and in reviews, we distinguish five root causes which commonly determine modelling success or failure:

1. Establishing the model purpose  
*Why are we logged on in the first place and what do we mean by ‘fit-for-purpose’?*
2. Building a 3D architecture with appropriate modelling elements  
*The fluid-dependent choice on the level of detail required in a model*
3. Understanding determinism and probability  
*Our expectations of geostatistical algorithms*
4. Model scaling  
*Reconciling the jump between the scale of data and cellular resolution of our models, and how to represent pore-scale fluid flow reasonably at a reservoir scale*
5. Uncertainty-handling  
*Moving from single to multi-models and where the design becomes subject to bias*

Strategies for addressing these underlying issues will be dealt with in the following chapters under the thematic headings of model purpose, the rock model, the property model, upscaling flow properties and uncertainty-handling.

In the later chapters we focus on specific reservoir types, as there are generic issues which predictably arise when dealing with certain reservoirs. We look specifically at how our experiences from modelling hydrocarbon reservoirs can be applied to modelling reservoirs (and their overburdens) for disposal and storage of CO<sub>2</sub> or hydrogen. We share our experience, gained from personal involvement in over a hundred modelling studies, significantly augmented by the experiences of others shared in reviews and reservoir modelling classes over the past 30 years.

Before we engage in technical issues, however, a reflection on the central theme of design.



Reservoir modellers in front of rocks, discussing design (Photograph by Philip Ringrose)

---

## Design in General

Design is an essential part of everyday life, compelling examples of which are to be found in architecture. We are aware of famous, elegant and successful designs, such as *the Gherkin* – a striking feature of the London skyline designed for the Swiss Re company by Norman Foster and Partners – but we are more likely to live and work in less glamorous but hopefully fit-for-purpose buildings. The Gherkin, or more correctly the 30 St. Mary Axe building, uses half the energy typically required by an office block, optimises the use of daylight and natural ventilation (Price 2009) and embodies both innovative and successful design, although with significant complexity.



There are many more examples, however, of office block and accommodation units that are unattractive and plagued by design faults and inefficiencies – the *carbuncles* that should never have been built.

This architectural analogy gives us a useful setting for considering the more exclusive art of constructing models of the subsurface.



Norman Foster building, 30 St. Mary Axe (Photograph from Foster and Blaser (1993) – reproduced with kind permission from Springer Science + Business Media B.V.)

What constitutes good design? In our context we suggest the essence of a *good* design is simply that it fulfils a specific purpose and is therefore *fit* for that purpose.

The Petter Daas museum in the small rural community of Alstahaug in northern Norway offers another architectural statement on design. This fairly small museum, celebrating a local poet and designed by the architectural firm Snøhetta, fits snugly and consistently into the local landscape. It is elegant and practical giving both light, shelter and warmth in a fairly extreme environment. Although lacking the complexity and scale of the Gherkin, it is equally fit-for-purpose. Significantly, in the context of this book, it rises out from and

fits into the Norwegian bedrock. It is an engineering design clearly founded in the geology – the essence of good reservoir model design.

When we build models of fluid resources in the subsurface we should never ignore the fact that those resources are contained within rock formations. Geological systems possess their own natural forms of design as depositional, diagenetic and tectonic processes generate intricate reservoir architectures. We rely on a firm reservoir architectural foundation, based on an understanding of geological processes, which can then be quantified in terms of rock properties and converted into a form useful to predict fluid flow behaviour.



The Petter Dass Museum, Alstahaug, Norway (The Petter Dass-museum, © Petter Dass-museum, reproduced with permission)

Good reservoir model design therefore involves the digital representation of the natural geological architecture and its translation into useful models of subsurface fluid resources. Sometimes the representations are complex – sometimes they can be very simple indeed.

---

## References

- Foster N, Blaser W (1993) Norman foster sketch book. Birkhauser, Basel  
Price B (2009) Great modern architecture: the world's most spectacular buildings. Canary Press, New York

---

## Acknowledgements

Before engaging with this subject, we must acknowledge the essential contributions of others. Firstly, and anonymously, we thank our many professional colleagues in the fields of petroleum geoscience, reservoir engineering, geostatistics and software engineering. Without their expertise and the products of their innovation (commercial reservoir modelling packages), we as users would not have the opportunity to attempt good reservoir model design in the first place. All the examples and illustrations used in this book are the result of collaborative work with others – by its very nature reservoir modelling is done within multi-disciplinary teams. We have endeavoured to credit our sources with reference to published studies where possible. Elsewhere, where unpublished case studies are used, these are the authors' own work, unless explicitly acknowledged.

More specifically we would like to thank our employers past and present – Shell, TRACS and AGR (M.B.), Statoil, Equinor and NTNU (P.R.) and Heriot-Watt University (M.B. & P.R.) for the provision of data, computational resources and, not least, an invaluable learning experience. The latest versions of this book have been honed and developed as part of the TRACS and RPS/Nautilus training programmes ([www.tracs.com](http://www.tracs.com) and [www.training.rpsgroup.com](http://www.training.rpsgroup.com), respectively). Participants of these courses have repeatedly given us valuable feedback, suggesting improvements which have become embedded in the chapters of this book. Patrick Corbett, Kjetil Nordahl, Gillian Pickup, Stan Stanbrook, Paula Wigley and Caroline Hern are thanked for constructive reviews of the book chapters. Thanks are due also to Fiona Swapp and Susan McLafferty at TRACS for producing many excellent graphics for the book and the associated courses.

Each reservoir modelling study discussed has benefited from the use of commercial software packages. We do not wish to promote or advocate any one package or the other – rather to encourage the growth of this technology in an open competitive market. We do however acknowledge the use of licensed software from several sources. The main software packages we have used in the examples discussed in this book include the Petrel E&P Software Platform (Schlumberger), the Integrated Irap RMS Solution Platform (Roxar), the Paradigm SKUA-GOCAD framework for subsurface modelling, the SBED and ReservoirStudio products from Geomodeling Technology Corp., and the

ECLIPSE suite of reservoir simulation software tools (Schlumberger). This is not an exhaustive list, just an acknowledgement of the tools we have used most often in developing approaches to reservoir modelling.

And finally, we would like to acknowledge our families and partners, who have kindly let us out to engage in rather too many reservoir modelling studies, courses and field trips on every continent (apart from Antarctica). We hope this book is a small compensation for their patience and support.

---

# Contents

|          |  |    |
|----------|--|----|
| <b>1</b> | <b>Model Purpose</b> . . . . .                                 | 1  |
| 1.1      | Modelling for Comfort? . . . . .                               | 1  |
| 1.2      | Models for Visualisation Alone . . . . .                       | 2  |
| 1.3      | Models for Volumes . . . . .                                   | 3  |
| 1.4      | Models as a Front End to Simulation . . . . .                  | 4  |
| 1.5      | Models for Well Planning . . . . .                             | 4  |
| 1.6      | Models for Seismic Modelling . . . . .                         | 5  |
| 1.7      | Models for IOR/EOR . . . . .                                   | 7  |
| 1.8      | Models for Storage . . . . .                                   | 7  |
| 1.9      | The Fit-for-Purpose Model . . . . .                            | 8  |
|          | References . . . . .   | 10 |
| <b>2</b> | <b>The Rock Model</b> . . . . .                                | 11 |
| 2.1      | The Rock Model . . . . .                                       | 12 |
| 2.2      | Model Concept . . . . .  | 13 |
| 2.3      | The Model Framework . . . . .                                  | 13 |
| 2.3.1    | Structural Data . . . . .                                      | 15 |
| 2.3.2    | Stratigraphic Data . . . . .                                   | 17 |
| 2.4      | Model Elements . . . . .                                       | 19 |
| 2.4.1    | Reservoir Models Not Geological Models . . . . .               | 20 |
| 2.4.2    | Building Blocks . . . . .                                      | 20 |
| 2.4.3    | Model Element Types . . . . .                                  | 20 |
| 2.4.4    | How Much Heterogeneity to Include?<br>‘Flora’s Rule’ . . . . . | 23 |
| 2.5      | Determinism and Probability . . . . .                          | 28 |
| 2.5.1    | Balance Between Determinism and Probability . . . . .          | 29 |
| 2.5.2    | Different Generic Approaches . . . . .                         | 31 |
| 2.5.3    | Forms of Deterministic Control . . . . .                       | 32 |
| 2.6      | Essential Geostatistics . . . . .                              | 34 |
| 2.6.1    | Key Geostatistical Concepts . . . . .                          | 34 |
| 2.6.2    | Intuitive Geostatistics . . . . .                              | 39 |
| 2.7      | Algorithm Choice and Control . . . . .                         | 43 |
| 2.7.1    | Object Modelling . . . . .                                     | 44 |
| 2.7.2    | Pixel-Based Modelling . . . . .                                | 47 |
| 2.7.3    | Texture-Based Modelling . . . . .                              | 50 |
| 2.7.4    | Algorithms Compared . . . . .                                  | 51 |

|          |   |           |
|----------|---|-----------|
| 2.7.5    | Process-Based Modelling . . . . .                                   | 53        |
| 2.7.6    | The Importance of Deterministic Trends . . . . .                    | 54        |
| 2.7.7    | Alternative Rock Modelling Methods – A<br>Comparison . . . . .      | 58        |
| 2.8      | Summary . . . . .   | 61        |
| 2.8.1    | Rock Model QC . . . . .   | 61        |
| 2.8.2    | Synopsis – Rock Modelling Guidelines . . . . .                      | 61        |
|          | References . . . . .  | 62        |
| <b>3</b> | <b>The Property Model . . . . .</b>                                 | <b>65</b> |
| 3.1      | Which Properties? . . . . .   | 65        |
| 3.2      | Understanding Permeability . . . . .                                | 70        |
| 3.2.1    | Darcy’s Law . . . . .   | 70        |
| 3.2.2    | Upscaled Permeability . . . . .                                     | 70        |
| 3.2.3    | Permeability Variation in the Subsurface . . . . .                  | 72        |
| 3.2.4    | Permeability Averages . . . . .                                     | 72        |
| 3.2.5    | Numerical Estimation of Block Permeability . . . . .                | 75        |
| 3.2.6    | Permeability in Fractures . . . . .                                 | 77        |
| 3.3      | Handling Statistical Data . . . . .                                 | 78        |
| 3.3.1    | Introduction . . . . .  | 78        |
| 3.3.2    | Variance and Uncertainty . . . . .                                  | 80        |
| 3.3.3    | The Normal Distribution and Its Transforms . . . . .                | 82        |
| 3.3.4    | Handling $\phi$ -k Distributions and Cross Plots . . . . .          | 86        |
| 3.3.5    | Hydraulic Flow Units . . . . .                                      | 88        |
| 3.4      | Modelling Property Distributions . . . . .                          | 89        |
| 3.4.1    | Kriging . . . . .   | 89        |
| 3.4.2    | The Variogram . . . . .   | 90        |
| 3.4.3    | Gaussian Simulation . . . . .                                       | 91        |
| 3.4.4    | Bayesian Statistics . . . . .                                       | 92        |
| 3.4.5    | Property Modelling: Object-Based Workflow . . . . .                 | 93        |
| 3.4.6    | Property Modelling: Seismic-Based Workflow . . . . .                | 95        |
| 3.5      | Use of Cut-Offs and N/G Ratios . . . . .                            | 97        |
| 3.5.1    | Introduction . . . . .  | 97        |
| 3.5.2    | The Net-to-Gross Method . . . . .                                   | 99        |
| 3.5.3    | Total Property Modelling . . . . .                                  | 101       |
| 3.6      | Vertical Permeability and Barriers . . . . .                        | 105       |
| 3.6.1    | Introduction to $k_v/k_h$ . . . . .                                 | 105       |
| 3.6.2    | Modelling Thin Barriers . . . . .                                   | 106       |
| 3.6.3    | Modelling of Permeability Anisotropy . . . . .                      | 108       |
| 3.7      | Saturation Modelling . . . . .                                      | 110       |
| 3.7.1    | Capillary Pressure . . . . .  | 110       |
| 3.7.2    | Saturation-Height Functions . . . . .                               | 111       |
| 3.7.3    | Tilted Oil-Water Contacts . . . . .                                 | 112       |
| 3.8      | Modelling Fracture Properties . . . . .                             | 115       |
| 3.8.1    | Terminology and Type . . . . .                                      | 116       |
| 3.8.2    | Fault Zone Properties . . . . .                                     | 119       |
| 3.8.3    | Modelling Open Fracture Properties . . . . .                        | 124       |
| 3.8.4    | Capturing the Effects of Stress on<br>Fracture Properties . . . . . | 126       |

|          |   |            |
|----------|---|------------|
| 3.8.5    | Summary – Fracture Properties . . . . .   | 127        |
| 3.9      | Summary . . . . .   | 127        |
|          | References . . . . .  | 128        |
| <b>4</b> | <b>Upscaling Flow Properties . . . . .</b>  | <b>131</b> |
| 4.1      | Multi-scale Flow Modelling . . . . .  | 132        |
| 4.2      | Multi-phase Flow . . . . .  | 135        |
| 4.2.1    | Two-Phase Flow Equations . . . . .  | 135        |
| 4.2.2    | Two-Phase Steady-State Upscaling Methods . . . . .                                | 138        |
| 4.2.3    | Heterogeneity and Fluid Forces . . . . .  | 142        |
| 4.3      | Multi-scale Reservoir Modelling Concepts . . . . .                                | 144        |
| 4.3.1    | Geology and Scale . . . . .   | 144        |
| 4.3.2    | How Many Scales to Model and Upscale? . . . . .                                   | 146        |
| 4.3.3    | Which Scales to Focus On? (The REV) . . . . .                                     | 148        |
| 4.3.4    | Handling Variance as a Function of Scale . . . . .                                | 151        |
| 4.3.5    | Construction of Geomodel and Simulator<br>Grids . . . . .                         | 155        |
| 4.3.6    | Which Heterogeneities Matter? . . . . .   | 157        |
| 4.4      | The Way Forward . . . . .   | 159        |
| 4.4.1    | Potential and Pitfalls . . . . .  | 159        |
| 4.4.2    | Pore-to-Field Workflow . . . . .  | 160        |
| 4.4.3    | Essentials of Multi-scale Reservoir Modelling . . . . .                           | 160        |
|          | References . . . . .  | 161        |
| <b>5</b> | <b>Model-Based Uncertainty Handling . . . . .</b>                                 | <b>165</b> |
| 5.1      | The Issue . . . . .   | 166        |
| 5.1.1    | Modelling for Comfort . . . . .   | 166        |
| 5.1.2    | Modelling for Discomfort – Quantifying<br>Uncertainty and Exposing Risk . . . . . | 166        |
| 5.2      | Differing Methodologies . . . . .   | 169        |
| 5.2.1    | Best Guess, or ‘Rationalist’ Approaches . . . . .                                 | 169        |
| 5.2.2    | Multiple Stochastic Approaches . . . . .  | 170        |
| 5.2.3    | Multiple Deterministic Approaches . . . . .                                       | 170        |
| 5.3      | Bias . . . . .  | 172        |
| 5.3.1    | The Limits of Rationalism . . . . .   | 172        |
| 5.3.2    | The Limits of Geostatistics . . . . .   | 173        |
| 5.3.3    | Cognitive Limits – Heuristics . . . . .   | 175        |
| 5.4      | Towards an Unbiased Methodology . . . . .   | 177        |
| 5.4.1    | The Uncertainty List . . . . .  | 178        |
| 5.4.2    | Scenario Trees . . . . .  | 178        |
| 5.5      | Post-processing the Ensemble . . . . .  | 181        |
| 5.5.1    | Scenarios . . . . .   | 182        |
| 5.5.2    | Exhaustive Deterministic Ensembles . . . . .                                      | 182        |
| 5.5.3    | Variance Mapping . . . . .  | 183        |
| 5.5.4    | Sampling Probabilistic Ensembles . . . . .  | 185        |
| 5.5.5    | Experimental Design and Sensitivity Analysis . . . . .                            | 185        |
| 5.5.6    | Clustering . . . . .  | 187        |
| 5.5.7    | Updating Reservoir Uncertainty with New<br>Information . . . . .                  | 189        |

|          |   |            |
|----------|---|------------|
| 5.5.8    | Distinguishing and Illustrating Risk<br>vs. Uncertainty . . . . .               | 190        |
| 5.6      | Summary . . . . .   | 191        |
|          | References . . . . .  | 192        |
| <b>6</b> | <b>Reservoir Model Types . . . . .</b>  | <b>195</b> |
| 6.1      | Aeolian Reservoirs . . . . .  | 196        |
| 6.1.1    | Elements . . . . .  | 196        |
| 6.1.2    | Effective Properties . . . . .  | 196        |
| 6.1.3    | Stacking . . . . .  | 199        |
| 6.1.4    | Aeolian System Anisotropy . . . . .   | 199        |
| 6.1.5    | Laminae-Scale Effects . . . . .   | 200        |
| 6.2      | Fluvial Reservoirs . . . . .  | 201        |
| 6.2.1    | Fluvial Systems . . . . .   | 201        |
| 6.2.2    | Geometry . . . . .  | 202        |
| 6.2.3    | Connectivity and Percolation Theory . . . . .                                   | 202        |
| 6.2.4    | Hierarchy . . . . .   | 205        |
| 6.3      | Tidal Deltaic Sandstone Reservoirs . . . . .                                    | 206        |
| 6.3.1    | Tidal Characteristics . . . . .   | 206        |
| 6.3.2    | Handling Heterolithics . . . . .  | 207        |
| 6.4      | Shallow Marine Sandstone Reservoirs . . . . .                                   | 207        |
| 6.4.1    | Tanks of Sand? . . . . .  | 207        |
| 6.4.2    | Stacking and Laminations . . . . .  | 209        |
| 6.4.3    | Large-Scale Impact of Small-Scale<br>Heterogeneities . . . . .                  | 209        |
| 6.5      | Deep Marine Sandstone Reservoirs . . . . .                                      | 211        |
| 6.5.1    | Relative Confinement . . . . .  | 213        |
| 6.5.2    | Seismic Limits . . . . .  | 213        |
| 6.5.3    | Thin Beds . . . . .   | 214        |
| 6.5.4    | Small-Scale Heterogeneity in High<br>Net-to-Gross ‘Tanks’ . . . . .             | 215        |
| 6.5.5    | Summary . . . . .   | 216        |
| 6.6      | Carbonate Reservoirs . . . . .  | 217        |
| 6.6.1    | Depositional Architecture . . . . .   | 218        |
| 6.6.2    | Pore Fabric . . . . .   | 221        |
| 6.6.3    | Diagenesis . . . . .  | 223        |
| 6.6.4    | Fractures and Karst . . . . .   | 225        |
| 6.6.5    | Hierarchies of Scale – The Carbonate REV . . . . .                              | 225        |
| 6.6.6    | Conclusion: Forward-Modelling or Inversion? . . . . .                           | 228        |
| 6.7      | Fractured Reservoirs . . . . .  | 228        |
| 6.7.1    | Fracture Concepts . . . . .   | 229        |
| 6.7.2    | Low Density, Compartmentalised Fracture<br>Systems (Fault-Dominated) . . . . .  | 229        |
| 6.7.3    | Low Density Fracture Systems, Open to Flow<br>(Fault-Dominated) . . . . .       | 234        |
| 6.7.4    | High Density Fractured Reservoirs – Open<br>to Flow (Joint-Dominated) . . . . . | 239        |



|          |  |            |
|----------|--|------------|
| 6.7.5    | Forward-Modelling or Inversion in Fractured Reservoirs? . . . . .      | 244        |
| 6.8      | Fit-for-Purpose Recapitulation . . . . .                               | 246        |
|          | References . . . . .   | 247        |
| <b>7</b> | <b>Models for Storage</b> . . . . .                                    | <b>251</b> |
| 7.1      | Displacements of Different Fluids . . . . .                            | 252        |
| 7.2      | Geological Storage of CO <sub>2</sub> . . . . .                        | 252        |
| 7.3      | CO <sub>2</sub> Storage Modelling Objectives . . . . .                 | 254        |
| 7.4      | Understanding the CO <sub>2</sub> Storage Process . . . . .            | 257        |
| 7.5      | The Influence of Geological Heterogeneity . . . . .                    | 264        |
| 7.6      | Handling Pressure and Rock Deformation . . . . .                       | 267        |
| 7.7      | Model Design Futures for the Energy Transition . . . . .               | 273        |
|          | References . . . . .   | 274        |
| <b>8</b> | <b>Modelling Workflows</b> . . . . .                                   | <b>277</b> |
| 8.1      | The Detailed, Full-Field Model Default . . . . .                       | 278        |
| 8.2      | Resource and Decision Models . . . . .                                 | 278        |
| 8.3      | Iterative Workflows – The Forth Bridge . . . . .                       | 280        |
| 8.4      | Handling Dynamic Data . . . . .  | 283        |
| 8.4.1    | History-Matching . . . . .   | 283        |
| 8.4.2    | History-Comparing . . . . .  | 284        |
| 8.5      | ‘Truth Models’ . . . . .   | 285        |
|          | References . . . . .   | 288        |
| <b>9</b> | <b>Epilogue – Modelling for the Energy Transition</b> . . . . .        | <b>291</b> |
| 9.1      | Synopsis – The Story So Far . . . . .                                  | 292        |
| 9.2      | Use of Analogues and Data . . . . .                                    | 294        |
| 9.3      | Restoring Lost Heterogeneity . . . . .                                 | 296        |
| 9.4      | New Workflows . . . . .  | 296        |
| 9.4.1    | Surface-Based Models . . . . .   | 297        |
| 9.4.2    | Disposable Grids . . . . .   | 298        |
| 9.5      | Stepping Beyond the Solution – ‘Modelling for Understanding’ . . . . . | 300        |
|          | References . . . . .   | 302        |
|          | <b>Nomenclature</b> . . . . .  | <b>305</b> |
|          | <b>Solutions</b> . . . . .   | <b>307</b> |
|          | <b>Appendix A: A Template for Model Design</b> . . . . .               | <b>311</b> |
|          | <b>Index</b> . . . . .   | <b>315</b> |

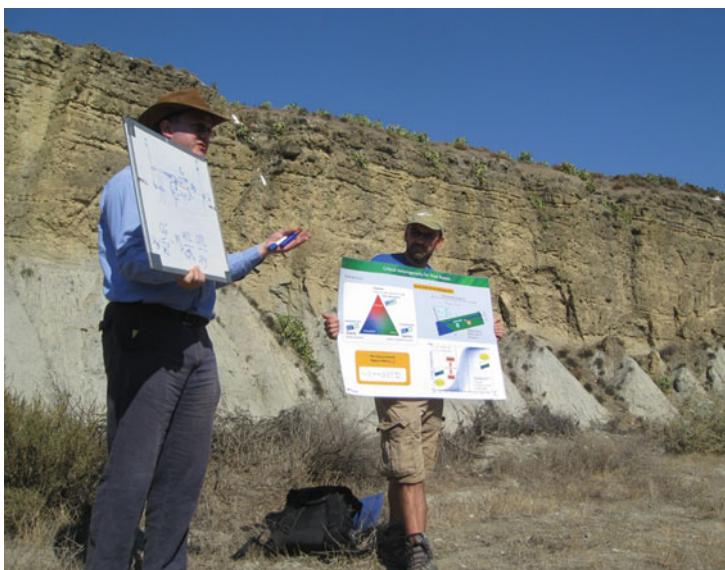
## Abstract

Should we aspire to build detailed full-field reservoir models with a view to using those models to answer business questions?

In this chapter it is suggested the answer to the above question is ‘not necessarily’. Instead

we argue the case for building for fit-for-purpose models, which may or may not be detailed and may or may not be full-field.

This choice triggers the question: ‘what is our purpose?’ The answer to this question determines the model design.



*A reservoir engineer and a geoscientist establish model purpose against an outcrop analogue*

## Keywords

Design · Reservoir modelling · Simulation · Energy transition · Fit-for-purpose · Volumetrics · Well planning · Forecasting · Development planning

## 1.1 Modelling for Comfort?

There are two broad schools of thought on the purpose of models:

1. To provide a 3D, digital representation of a hydrocarbon reservoir, which can be built and maintained as new data becomes available, and used to support on-going lifecycle needs such as volumetric updates, well planning and, via reservoir simulation, production forecasting.
2. That there is little value in maintaining a single ‘field model’. Instead, we should build and maintain a field database, from which several fit-for-purpose models can be built quickly to support specific decisions.

The first approach seems attractive, especially if a large amount of effort is invested in the first build prior to a major investment decision. However, the ‘all-singing, all-dancing’ full-field approach tends to result in large, detailed models, generally working at the limit of the available software/hardware and which are cumbersome to update and difficult to pass hand-to-hand as people move between jobs. Significant effort can be invested simply in the on-going maintenance of these models, to the point that the need for the model ceases to be questioned and the purpose of the model is no longer apparent. In the worst case, the maintenance of the model becomes a job in itself and the investment in modelling technology may just be satisfying an urge for technical rigour in the lead up to a business decision – simply ‘modelling for comfort’ (Bentley 2015).

We argue that the route to happiness lies with the second approach: building fit-for-purpose models which are equally capable of creating comfort or discomfort around a business decision. Choosing this approach immediately raises the

question “*what purpose?*”, as the model design will vary according to that purpose. To illustrate this, the following sections look at contrasting purposes of reservoir modelling, and the distinctive design of the models associated with these differing contexts.

## 1.2 Models for Visualisation Alone

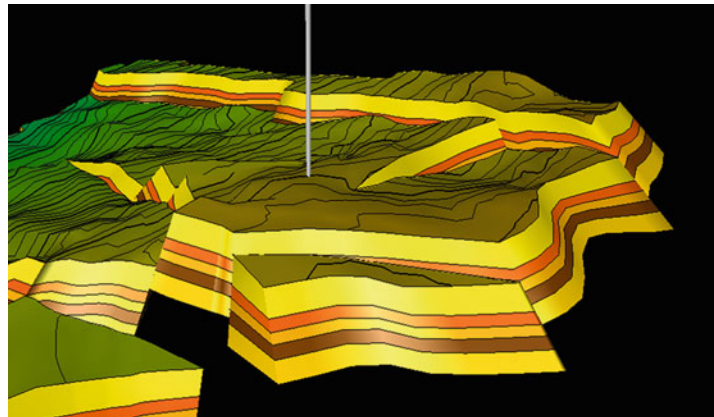
Simply being able to visualise the reservoir in 3D was identified early in the development of modelling tools as a potential benefit of reservoir modelling. Simply having a 3D box in which to view the available data is beneficial in itself.

This is the most intangible benefit of modelling, as there is no output other than a richer mental impression of the subsurface, which is difficult to measure. However, most people benefit from 3D visualisation (Fig. 1.1), consciously or unconsciously, particularly where cross-disciplinary issues are involved.

Some common examples are:

- To show the *geophysicist* the 3D structural model based on their seismic interpretations. Do they like it? Does it make geological sense? Have seismic artefacts been inadvertently included?
- To show the *petrophysicist* (well-log specialist) the 3D property model based on the well-log data supplied in 1D. Has the 3D property modelling been appropriate or have features been introduced which are inconsistent with the 1D knowledge along the wells,

**Fig. 1.1** The value of visualisation: appreciating structural and stratigraphic architecture, during well planning



e.g. correlations and geological or petrophysical trends?

- To show the *reservoir engineer* the geo-model grid, which will be the basis for subsequent flow modelling. Is it usable? Does it conflict with prior perceptions of reservoir unit continuity?
- To show the *well engineer* what you are trying to target in 3D with the complex well path you have just planned. Does it look feasible?
- To show the *asset team* how a conceptual reservoir model sketched on a piece of paper actually transforms into a 3D volume.
- To show the *manager* or investment fund holder what the subsurface resource actually looks like. That oil and gas do not come from a ‘hole in the ground’ but from a heterogeneous pore-system requiring significant technical skills to access, and a different set of skills when we come to consider storing or permanently disposing of fluids in the subsurface.

Getting a strong shared understanding of the subsurface concept tends to generate useful discussions on commercial risks and uncertainties, and looking at models or data in 3D often facilitates this process. The value of visualisation alone is the improved understanding it gives.

If this is a prime purpose then the model need not be complex – it depends on the audience. In

many cases, the model is effectively a 3D visual data base and many of the steps described in the subsequent chapters in this book are not required to achieve the desired understanding.

### 1.3 Models for Volumes

Knowing how much oil and gas is in place or how much fluid can be stored or disposed of is usually one of the first goals of reservoir modelling. This may be done using a simple map-based approach, but the industry has now migrated to 3D software packages, which is appropriate given that volumetrics are intrinsically a 3D property. The tradition of calculating volumes from 2D maps was a necessary simplification, no longer required.

3D mapping to support volumetrics should be quick, and is ideal for quickly screening uncertainties for their impact on volumetrics, as in the case shown in Fig. 1.2, where the volumetric sensitivity to fluid contact uncertainties is being tested, as part of a quick asset evaluation.

Models designed for this purpose can be relatively coarse, containing only the outline fault pattern required to define discrete blocks and the gross layering in which the volumes will be reported. The reservoir properties involved (e.g. porosity and net-to-gross) are statistically *additive* (see Chap. 3 for further discussion)

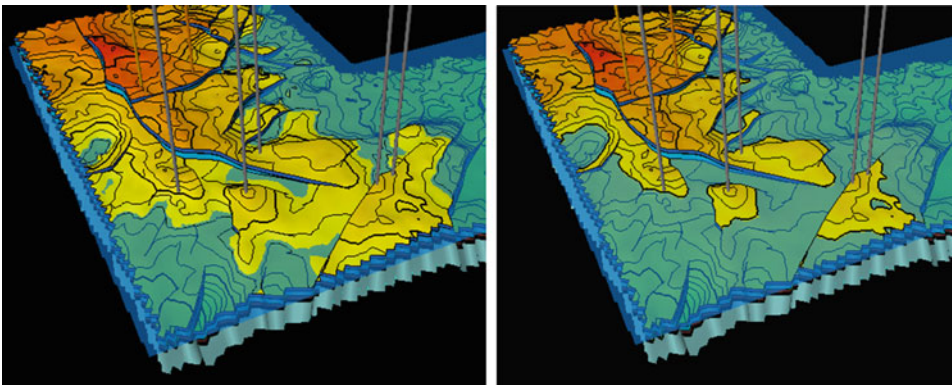


**Fig. 1.2** Two models for different fluid contact scenarios built specifically for volumetrics

which means cell sizes can be large. There is no requirement to create permeability models and, if this is for quick screening only, it may be sufficient to run 3D volumes for gross rock volume only, combining the remaining reservoir properties on spreadsheets.

Models designed for volumetrics should be coarse and fast.

### 1.4 Models as a Front End to Simulation

The majority of reservoir models, however, are built for input to flow simulators. To be successful, such models have to capture the essential permeability heterogeneity which will impact on reservoir performance. If the static models fail to capture this, the subsequent simulation forecasts may be useless.

The requirement for capturing connected permeability usually means finer scale modelling is required because permeability is a *multiplicative* rather than an additive property. Unlike models for volumetrics, the scope for simple averaging of detailed heterogeneity is limited. Issues of grid geometry and cell shape are also more pressing for flow models (Fig. 1.3); strategies for dealing with this are discussed in Chap. 4.

At this point it is sufficient to simply appreciate that taking a static geological model through to simulation automatically requires additional design, with a focus on permeability architecture.

### 1.5 Models for Well Planning

If the purpose of the modelling exercise is to assist well planning and geosteering, the model may require no more than a top structure map, nearby well ties and seismic attribute maps. Wells may also be planned using simulation models, allowing for alternative well designs to be tested against likely productivity.

It is generally preferable to design well paths in reservoir models which capture all factors likely to impact a fairly costly investment decision. Most geoscience software packages have good well design functionality allowing for accurate well-path definition in a high resolution static model. Figure 1.4 shows an example model for a proposed horizontal well, the trajectory of which has been optimised to access oil volumes (HCIIP) by careful geo-steering with reference to expected stratigraphic and structural surfaces.

Some thought is required around the determinism-probability issue referred to in the prologue and explored further in Chap. 2 because, although there are many possible statistical simulations of a reservoir, there will only be one final well path. It is therefore only reasonable to target the wells at the more deterministic features in the model – features that are placed in 3D by the modeller and determined by the underlying reservoir concept. These typically include fault blocks, key stratigraphic rock units, and high porosity features which are well determined, such as channel belts or seismic amplitude ‘sweet spots.’ It is wrong to target wells at highly

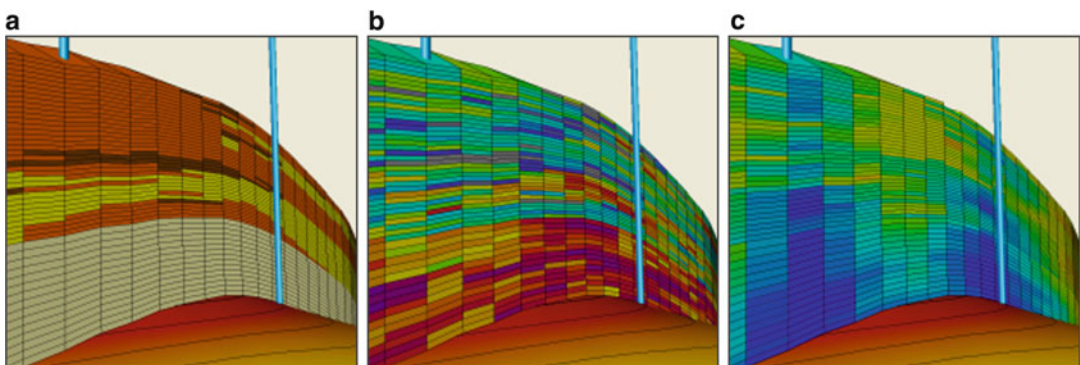


**Fig. 1.3** Rock model (a) and property model (b) designed for reservoir simulation for development planning (c)

**Fig. 1.4** Example planned well trajectory with an expected fault, base reservoir surface and well path targets

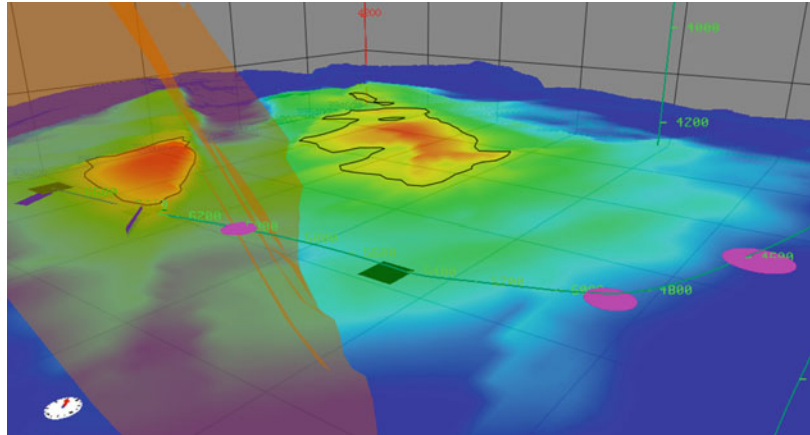
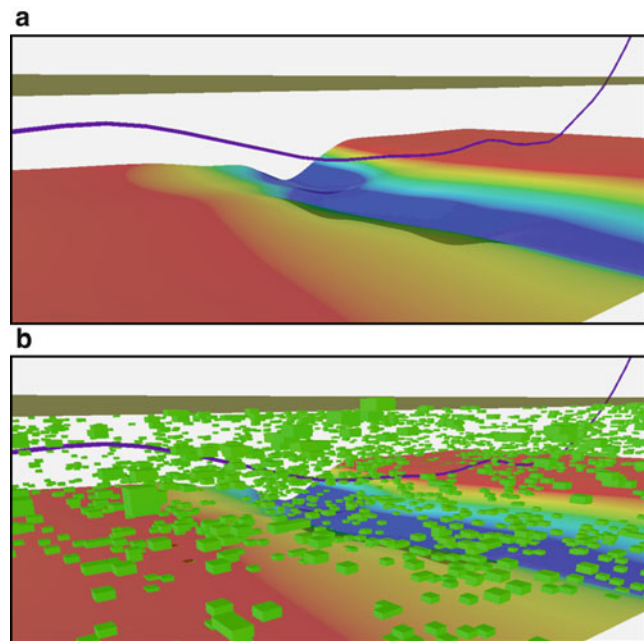


**Fig. 1.5** Modelling for horizontal well planning based on deterministic data (a) vs. a model with significant stochastic elements (b)



stochastic model features, such as a simulated random channel, stochastic porosity highs or small-scale probabilistic bodies (Fig. 1.5).

The dictum is that wells should only target highly probable features; this means well prognoses (and geosteering plans) can only be confidently conducted on models designed to be largely deterministic. If we try and drill a probabilistic rock body, we will probably be disappointed.

Having designed the well path it can be useful to monitor the actual well path (real-time updates) by incrementally reading in the well deviation file to follow the progress of the ‘actual’ well vs. the

‘planned’ well, including uncertainty ranges. Using visualisation, it is easier to understand surprises as they occur, particularly during geosteering (e.g. Fig. 1.4).

## 1.6 Models for Seismic Modelling

Over the last few decades, geophysical imaging has led to great improvements in reservoir characterisation – better seismic imaging allows us to ‘see’ progressively more of the subsurface. However, an image based on sonic wave reflections requires translation into rock and

fluid properties. Geological reservoir models are therefore important as *a priori* input to Quantitative Interpretation (QI) seismic studies.

This may be as simple as providing the layering framework for routine seismic inversion, or as complex as using Bayesian probabilistic rock and fluid prediction to merge seismic and

well data. The nature of the required input model varies according to the QI process being followed – this needs to be discussed with the geophysicist.

In the example shown here (Fig. 1.6), a reservoir model (top) has been passed through to the simulation stage to predict the acoustic

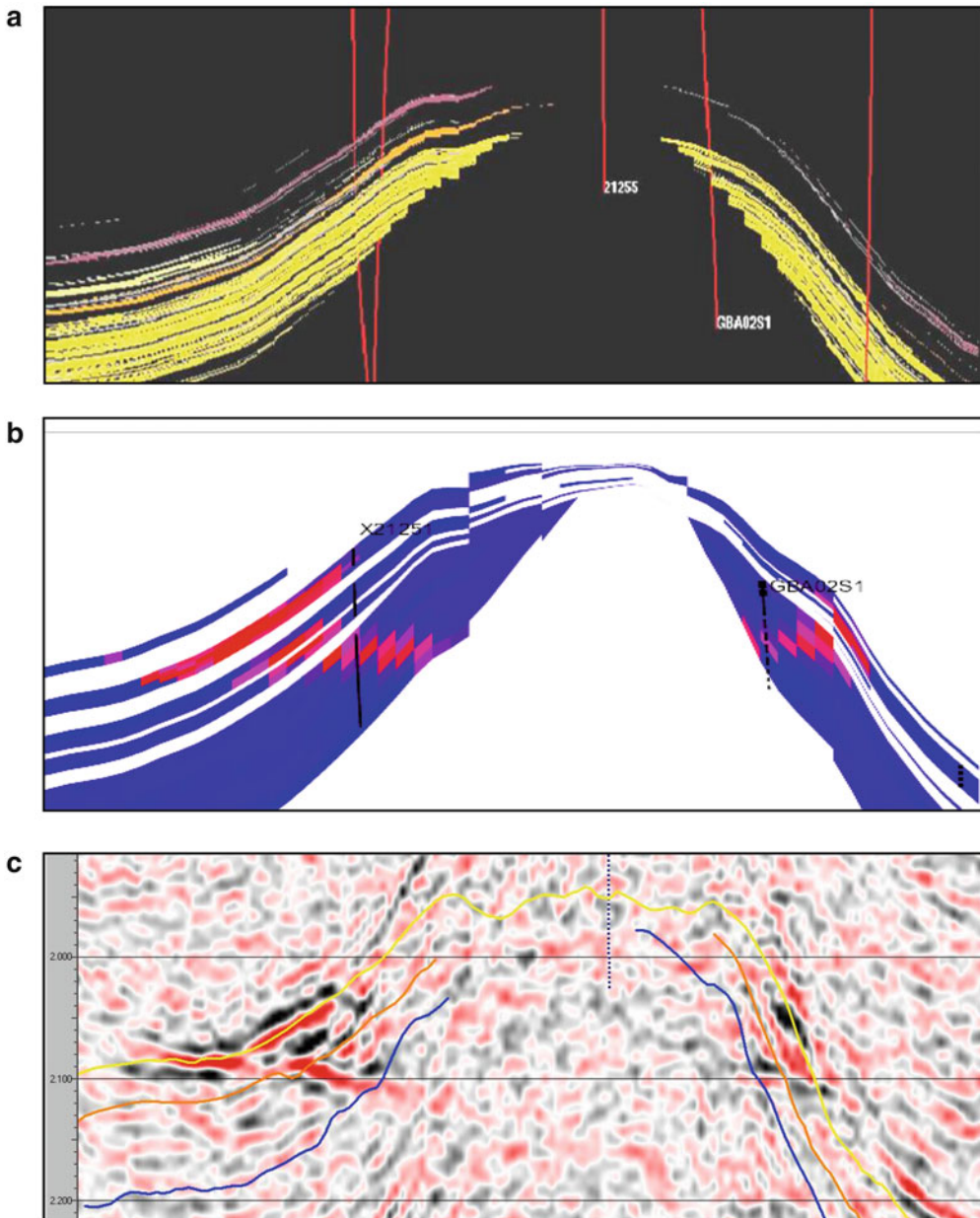


**Fig. 1.6** Reservoir modelling in support of seismic interpretation: (a) rock model; (b) forecast of acoustic impedance change between seismic surveys; (c) 4D seismic difference cube to which the reservoir simulation was

matched (Bentley and Hartung 2001). (Redrawn from Bentley and Hartung 2001, ©EAGE reproduced with kind permission of EAGE Publications B.V., The Netherlands)

impedance change to be expected on a 4D seismic survey (middle). The actual time-lapse (4D) image from seismic (bottom) is then compared to the synthetic acoustic impedance change, and the simulation is history-matched to achieve a fit.

If input to geophysical analysis is the key issue, the focus of the model design shifts to the properties relevant to geophysical modelling, notably models of velocity and density changes. There is, in this case, no need to pursue the intricacies of high resolution permeability architecture, and simpler (coarser) model designs may therefore be appropriate.

---

## 1.7 Models for IOR/EOR

Efforts to extract maximum possible volumes from oil and gas reservoirs usually fall under the banner of Improved Oil Recovery (IOR) or Enhanced Oil recovery (EOR). IOR tends to include all options including novel well design solutions, use of time-lapse seismic and secondary or tertiary flooding methods (water-based or gas-based injection strategies), while EOR generally implies tertiary flooding methods, i.e. something more advanced than primary depletion or secondary waterflood. CO<sub>2</sub> flooding and Water Alternating Gas (WAG) injection schemes are typical EOR methods. We will use IOR to encompass all the options.

We started by arguing that there is little value in ‘fit-for-all purposes’ detailed full-field models. However, IOR schemes generally require very detailed models to give very accurate answers, such as “exactly how much more oil will I recover if I start a gas injection scheme?” This requires detail, but not necessarily at a full-field scale. Many IOR solutions are best solved using detailed sector or near-well models, with relatively simple and coarse full-field grids to handle the reservoir management.

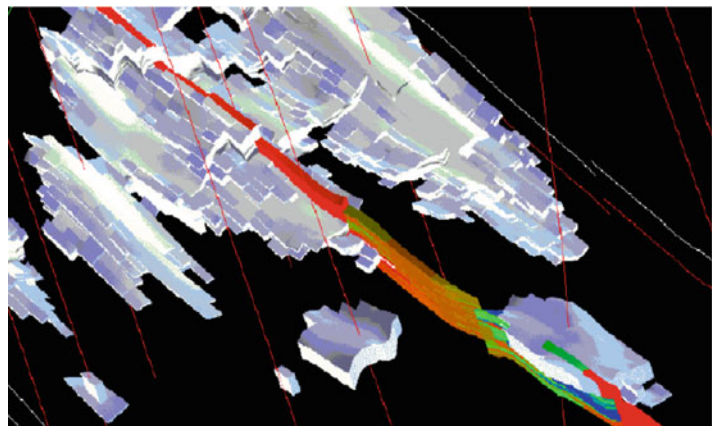
Figure 1.7 shows an example IOR model (Brandsæter et al. 2001). Gas injection was simulated in a high-resolution sector model with fine-layering (metre-thick cells) and various fault scenarios for a gas condensate field with difficult fluid phase behaviour. The insights from this IOR sector model were then used to constrain the coarse-grid full-field reservoir management model.

---

## 1.8 Models for Storage

The growing interest in CO<sub>2</sub> storage as a means of controlling greenhouse gas emissions brings a new challenge for reservoir modelling. Here there is a need for both initial scoping models (for capacity assessment) and for more detailed models to understand injection strategies and to assess long-term storage integrity. Some of the issues are similar – find the good permeability

**Fig. 1.7** Gas injection patterns (white) in a thin-bedded tidal reservoir (coloured section) modelled using a multi-scale method and incorporating the effects of faults in the reservoir simulation model

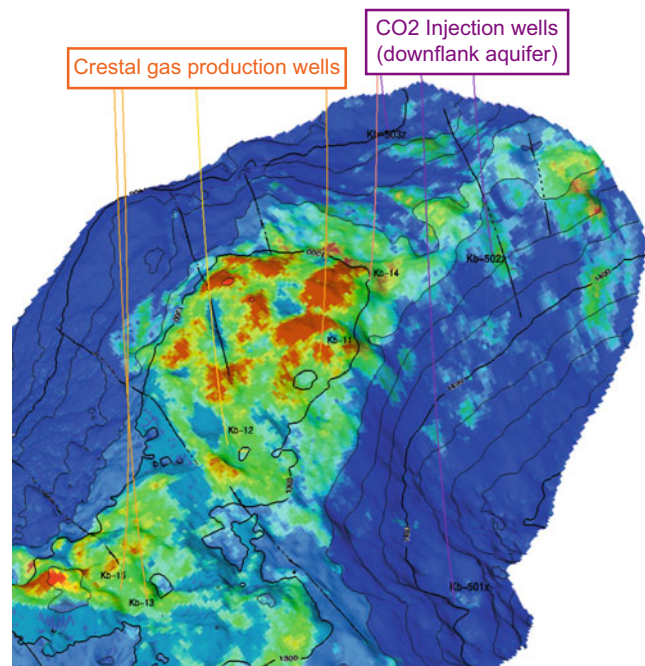




zones, identify important flow barriers and pressure compartments – but other issues are rather different, such as understanding formation response to elevated pressures and geochemical reactions due to CO<sub>2</sub> dissolved in brine. CO<sub>2</sub> is also normally compressed into the liquid or dense phase to be stored at depths of c.1–3 km, so that understanding fluid behaviour is also an important factor. CO<sub>2</sub> storage generally requires the assessment of quite large aquifer/reservoir volumes and the caprock system – presenting significant challenges for grid resolution and the level of detail required.

An example geological model for CO<sub>2</sub> storage is shown in Fig. 1.8 from the In Salah CO<sub>2</sub> injection project in Algeria (Ringrose et al. 2011). Here CO<sub>2</sub>, removed from several CO<sub>2</sub>-rich gas fields, has been stored in the down-flank aquifer of a producing gas field. Injection wells were placed on the basis of a seismic porosity inversion, and analysis of seismic and well data was used to monitor the injection performance and verify the integrity of the storage site. Geological models at a range of scales were required, from near-wellbore models of flow behaviour to large-scale models of the geomechanical response.

**Fig. 1.8** Models for CO<sub>2</sub> storage: Faulted top structure map with seismic-based porosity model and positions of injection wells



## 1.9 The Fit-for-Purpose Model

Given the variety of models described above, we argue that it is best to abandon the notion of a single, all-knowing, all-purpose, full-field model, and replace this with the idea of flexible, faster models based on thoughtful model design, tailored to answer specific questions at hand. Such models have a short shelf life and are built with specific ends in mind, i.e. there is a clear model purpose. The design of these models is informed by that purpose, as the contrast between the models illustrated in this chapter has shown.

With a fit-for-purpose mind set, the long-term handover items between geoscientists are not a set of 3D property models, but the underlying building blocks from which those models were created, notably the reservoir database (which should remain updated and ‘clean’) and the reservoir concept, which should be clear and explicit, to the point that it can be sketched.

It is also often practical to hand-over some aspects of the model build, such as a fault model if the software in use allows this to be updated easily, or workflows and macros, if these can be

understood and edited readily. The pre-existing model outputs (property models, rock models, volume summaries, etc.) are best archived.

The rest of this book develops this theme in more detail – how to achieve a design which addresses the model purpose whilst representing the essential features of the geological architecture (Fig. 1.9).

When setting about a reservoir modelling project, an overall workflow is required and

this should be decided up-front before significant modelling effort is expended. There is no ‘correct’ workflow, because the actual steps to be taken are an output of the fit-for-purpose design. However, it may be useful to refer to a general workflow (Fig. 1.10) which represents the main steps outlined in this book (see also Cannon 2018 for a description of the standard workflow).

**Fig. 1.9** Geological architecture. (Image of geomodel built in SBED Studio™ merged with photograph of Petter Dass Museum (Refer Chap. 1))

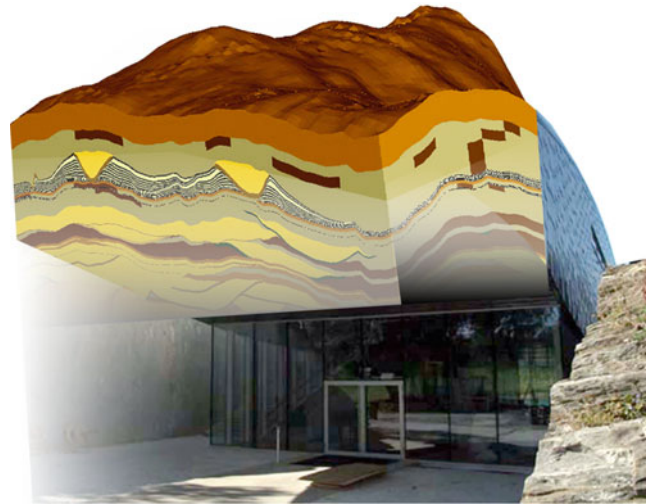
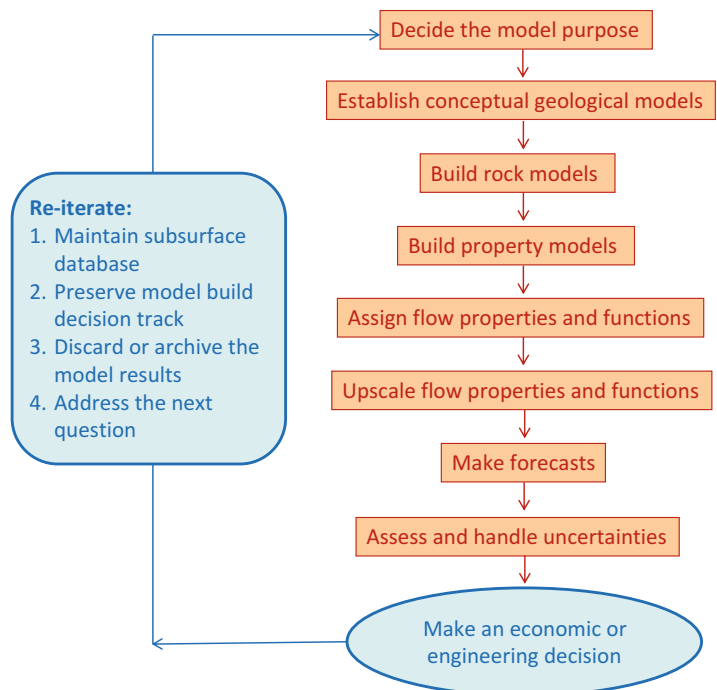


**Fig. 1.10** Generic reservoir modelling workflow



## References

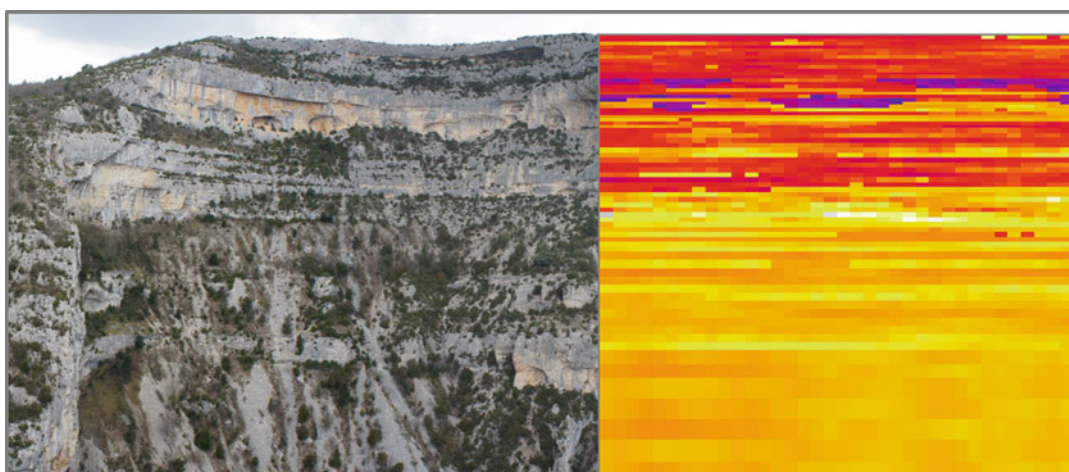
- Bentley MR (2015) Modelling for Comfort. *Pet Geosci* 22:3–10
- Bentley MR, Hartung M (2001) A 4D surprise at Gannet B. Presented at 63rd EAGE conference & exhibition, Amsterdam (extended abstract)
- Brandsæter I, Ringrose PS, Townsend CT, Omdal S (2001) Integrated modeling of geological heterogeneity and fluid displacement: Smørbukk gas-condensate field, Offshore Mid-Norway. Paper SPE 66391 presented at the SPE reservoir simulation symposium held in Houston, Texas, 11–14 February 2001
- Cannon S (2018) Reservoir modelling – a practical guide. John Wiley & Sons, pp. 312
- Ringrose P, Roberts DM, Raikes S, Gibson-Poole C, Iding M, Østmo S, Taylor M, Bond C, Wightman R, Morris J (2011) Characterisation of the Krechba CO<sub>2</sub> storage site: critical elements controlling injection performance. *Energy Procedia* 4:4672–4679

## Abstract

If you can sketch it, you can model it

Many static model practitioners embark on exercises of ‘geological modelling’, attempting to create a digital version of the geology as seen at outcrop. In practice this is futile. Even relatively high resolution models such as that for the Urgonian Shuiba analogue shown in below are clearly unlike the outcrop and close inspection of the outcrop would reveal a huge amount of missing detail.

Fortunately all the detail is rarely, if ever, required and we are saved the daunting task of capturing it all. We are in the business of building *model representations*: cellular proxies which capture the essence of the underlying complexity, extracting only the detail which is necessary to address commercial questions such as forecasts of resource volumes or fluid flow rates over time. We are building *reservoir models* rather than *geological models* and our focus is therefore on achieving a reasonable representation.



Outcrop view and model representation of the Urgonian Limestone at the Gorges de la Nesque, Provence (hot colours = high permeability)

## Keywords

Reservoir elements · Reservoir architecture · Correlation · Hierarchy · Concept sketching · Geostatistics · Algorithms · Variograms · Multi-point statistics · Seismic conditioning · Fluid flow · Darcy

## 2.1 The Rock Model

Most of the outputs from reservoir modelling are quantitative and derive from property models, so the main purpose of a rock model is to get the properties in the right place – to guide the spatial property distribution in 3D. In an applied geoscience and reservoir engineering world, rock modelling is rarely an end in itself. For certain model designs, the rock model component is minimal, for others it is essential.

In a generic reservoir modelling workflow, the construction of a rock or ‘facies’ model usually precedes the property modelling (Fig. 1.10). Effort is focussed on capturing contrasting rock types identified from sedimentology and representing these in 3D. This is often seen as the most ‘geological’ part of the model build along with the fault modelling, and it is generally assumed that a ‘good’ final model is one which is

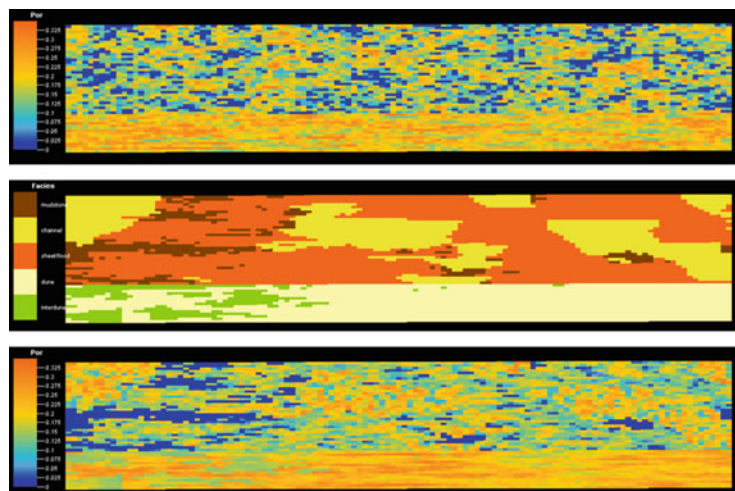
founded on a thoughtfully-constructed rock model. However, given that the rock model is rarely a model deliverable in itself, some reservoirs *do not require* rock models.

Figure 2.1 shows a porosity model which has been built with and without a rock model. If the upper porosity model is deemed a reasonable representation of the reservoir, then a rock model is not required. If, however, the porosity distribution is believed to be significantly influenced by the rock contrasts shown in the middle image, then the lower porosity model is the one to go for. Rock modelling is therefore a means to an end rather than an end in itself, an optional step which is useful if it helps to build an improved property model.

The details of rock model input are software-specific and are not covered here. Typically, the model requires specification of variables such as sand body sizes, facies proportions and reference to directional data such as dip-logs. These are part of a standard model build and need consideration, but are not viewed here as critical to the higher level issue of model design. Moreover, many of these variables cannot be specified precisely enough to determine the modelling outcome: rock body databases are only there as a guide, albeit a very useful one. Most critical to the design are the issues identified below,

**Fig. 2.1** To model rocks, or not to model rocks?

*Upper image:* porosity model built directly from porosity logs; *middle image:* a rock model capturing reservoir heterogeneity; *lower image:* the porosity model rebuilt, conditioned to the rock model



mishandling of which is a common source of a poor model build:

- *Reservoir concept* – is the architecture understood in a way which readily translates into a reservoir model?
- *Model elements* – from the range of observed structural components and sedimentological facies types, has the correct selection of elements been made on which to base the model?
- *Model build* – is the conceptual model carried through *intuitively* into the statistical component of the build?
- *Determinism and probability* – is the balance of determinism and probability in the model understood, and is the conceptual model firmly represented in the deterministic model components?

These four questions are used in this chapter to structure the discussion on the rock model, followed by a summary of more specific rock model build choices.

---

## 2.2 Model Concept

The best hope of building robust and sensible models is to use conceptual models to guide the model design. We favour this in place of purely data-driven modelling because of the issue of under-sampling (see later). The geologist should have a mental picture of the reservoir and use modelling tools to convert this into a quantitative geocellular representation. Using system defaults, or treating the package as a black box that somehow adds value or knowledge to the model, will always result in models that make little or no geological sense, and which usually have poor predictive capacity.

The form of the reservoir concept is not complex. It may be an image from a good outcrop analogue or, better, a conceptual sketch. The sketch may be an aerial view of depositional elements or a 3D block view of the same, incorporating the preserved form of the reservoir (Fig. 2.2). Satellite images are extremely

appealing visually, as are interpreted areal sketches, but suffer from being present-day snap-shots in 2D rather than images of the preserved reservoir. 3D blocks are much better, but many find them hard to construct.

A good starting point is often a simple 2D conceptual sketch in section, which can be built with guidance from log and core data. Figure 2.3 is an example built after a day in the core store interpreting heterogeneities in a fluvial reservoir. Elements have been chosen which reflect depositional facies and diagenetic alteration and the sketch illustrates how these elements connect architecturally. The elements are petrophysically distinct and the image was built up in the core store based on a geological-petrophysical conversation.

The ability to draw a conceptual sketch section is highly informative and brings clarity to the mental image of the reservoir held by the modeller. If this conceptual sketch is not clear, the process of model building is unlikely to make it any clearer. If there is no clear up-front conceptual model then the model output is effectively a random draw, hence:

If you can sketch it, you can model it

An early question to address is “what are the fundamental building blocks for the reservoir concept?” These have been referred to here as the ‘model elements’ and discussed further below. For the moment, the key thing to appreciate is that:

model elements  $\neq$  facies types

With the idea established of a reservoir concept as an architectural sketch constructed from model elements, we will look at the issues surrounding the build of the model framework then return to consider how to select elements to place within that framework in Sect. 2.4.

---

## 2.3 The Model Framework

The structural framework for all reservoir models is defined by a combination of structural inputs (faults and surfaces from seismic to impart gross

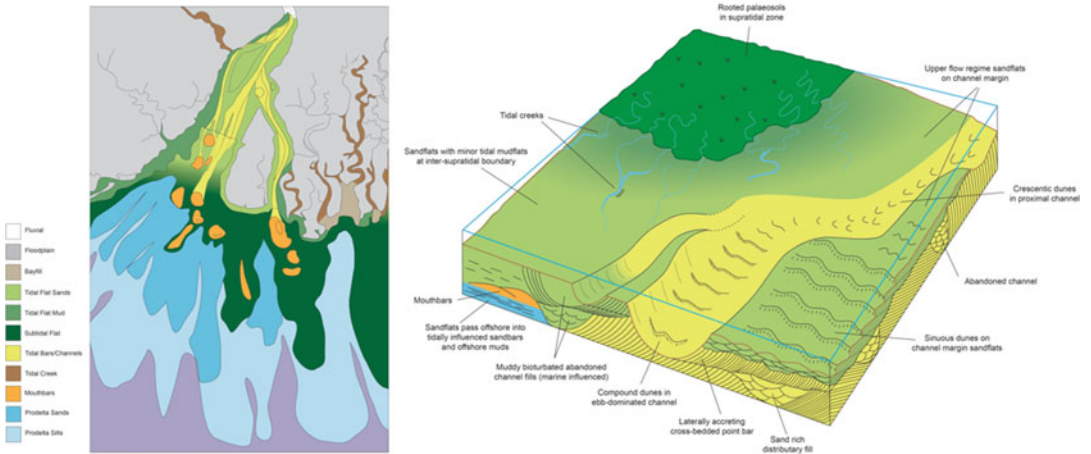


**Fig. 2.2** Capturing the reservoir concept for a tidal reservoir outcrop in the Lajas Formation in Patagonia (top image) in terms of an analogue depositional environment

from the Hugli delta in Bangladesh, or a generic block diagram sketch. (Block diagram adapted from McIlroy et al. 2005)

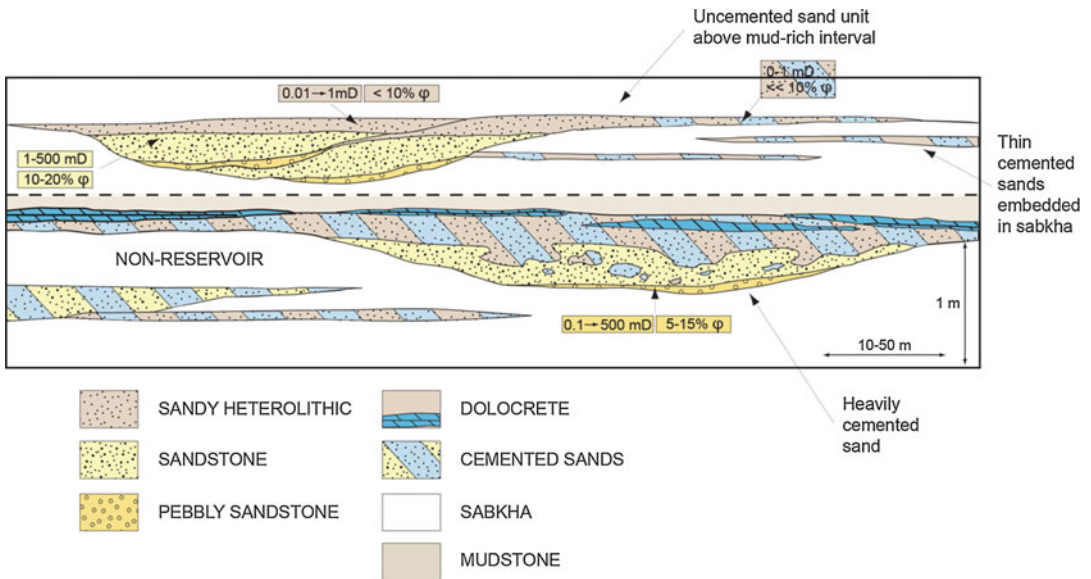


**Fig. 2.3** Capturing the reservoir concept in a simple sketch showing the architectural arrangement of distinct reservoir elements observed in core from a Triassic fluvial reservoir

geometry) and stratigraphic inputs (to define internal layering).

The main point we wish to consider here is *what are the structural and stratigraphic issues that a modeller should be aware of when thinking through a model design?* These are discussed below.

### 2.3.1 Structural Data

Building a fault model tends to be one of the more time-consuming and manual steps in a modelling workflow, and is therefore commonly done with each new generation of seismic interpretation. In the absence of new seismic, a fault model may be passed on between users and adopted simply to avoid the inefficiency of repeating the manual fault-building.

Such an inherited fault framework therefore requires quality control. The principal question

is whether the fault model reflects the seismic interpretation only or whether it has been adjusted with reference to a conceptual structural interpretation. We recommend the latter, as a direct expression of a seismic interpretation will tend to be a conservative representation of the fault architecture – it is limited to the resolution of the data.

Facets of an incomplete structural interpretation (Fig. 2.4) are:

- Fault networks tend to be incomplete, e.g. faults may be missing in areas of poor seismic quality.
- Faults may not be joined (under-linked networks) due to lack of sufficient seismic resolution in areas of fault intersections.
- Horizon interpretations may stop short of faults due to poorer seismic resolution around the fault zone.
- Horizon interpretations may be extended down fault planes or unconformities, i.e. the fault or

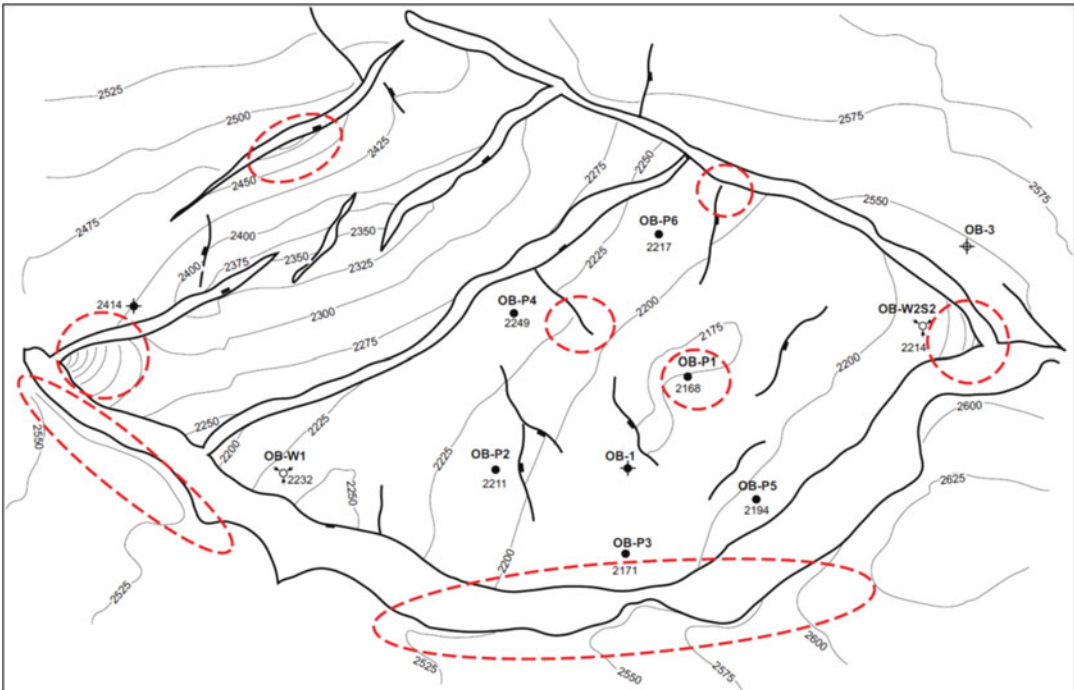


**Fig. 2.4** Incomplete structural interpretations, inappropriate for modelling. Highlighted areas pick out well-surface misties, disconnections in the fault network and unlikely

surface geometries around faults, presumably interpreted or gridded without reference to the fault planes



unconformity is not identified independently from each horizon, or not identified at all.

- Faults may be interpreted on seismic noise (artefacts).

Although models made from such ‘raw’ seismic interpretations are honest reflections of that data, the structural representations are incomplete and a structural interpretation should be overlain on the seismic outputs as part of the model design. To achieve this, the workflow similar to that shown in Fig. 2.5 is recommended.

Rather than start with a gridded framework constructed directly from seismic interpretation, the structural build should start with the raw, depth-converted seismic picks and the fault sticks. This is preferable to starting with horizon grids, as these will have been gridded without access to the final 3D fault network. Working with pre-gridded surfaces means the starting

inputs are smoothed, not only within-surface but more importantly around faults, the latter tending to have systematically reduced fault displacements.

A more rigorous structural model workflow is to:

1. Determine the structural concept – are faults expected to die out laterally or to link? Are *en echelon* faults separated by relay ramps? Are there small, possibly sub-seismic connecting faults? Make a sketch of the desired fault architecture to clarify.
2. Input the fault sticks and grid them as fault planes (Fig. 2.5a).
3. Link faults into a network consistent with the concept (1, above, also Fig. 2.5b).
4. Import depth-converted horizon picks and remove spurious points, e.g. those erroneously picked along fault planes rather

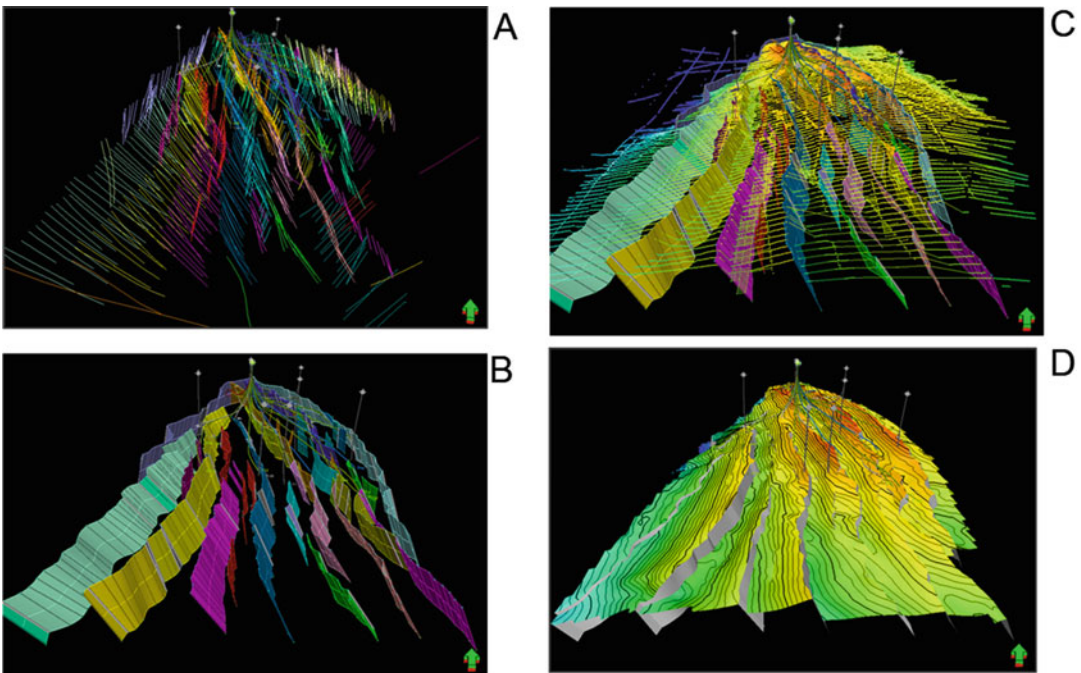


**Fig. 2.5** A structural build based on fault sticks from seismic (a), converted into a linked fault system (b), integrated with depth-converted horizon picks (c) to yield a conceptually acceptable structural framework which honours all inputs (d). The workflow can equally well be followed using time data, then converted to depth

using a 3D velocity model. The key feature of this workflow is the avoidance of intermediate surface gridding steps which are made independently of the final interpreted fault network. Example from the Douglas Field, East Irish Sea. (Bentley and Elliott 2008)

than stratigraphic surfaces (Fig. 2.5c) to avoid the structural errors shown in Fig. 2.4.

5. Edit the fault network to ensure optimal positioning relative to the raw picks; this may be an iterative process with the geophysicist, particularly if potentially spurious picks are identified.
6. Grid surfaces against the edited fault network (Fig. 2.5d).
7. Iterate steps 2–6 to capture alternative potential fault networks to capture structural uncertainties.

### 2.3.2 Stratigraphic Data

There are two main considerations in the selection of stratigraphic inputs to the geological framework model: *correlation* and *hierarchy*.

#### 2.3.2.1 Correlation

In the subsurface, correlation usually begins with markers picked from well data – *well picks*. Important information also comes from correlation surfaces picked from seismic data. Numerous correlation picks may have been defined in the interpretation of well data and these picks may have their origins in lithological, biostratigraphical or chronostratigraphical correlations – all of these being influenced directly or indirectly by sequence stratigraphy (see for example Van Wagoner et al. 1990; Van Wagoner and Bertram 1995). If multiple stratigraphic correlations are available these may produce surfaces which spatially cross, such as timelines crossing lithostratigraphic correlations. Not all these surfaces are needed in reservoir modelling. A choice is therefore required and as with the structural framework the selection of surfaces should be made with reference to the conceptual sketch, which is in turn driven by the model purpose.

For models built for exploration purposes or for in-place resource calculations only, correlation lines which track the distribution of reservoir properties are ideal, as the geostatistical simulation of properties will follow the 3D grid stratigraphy, which is in turn influenced by the zone

correlation. For static models which are to go forward to dynamic modelling, the best correlation lines for modelling are those which most closely reflect paths of fluid-flow during production or injection.

The choice of correlation surfaces hugely influences the resulting model architecture, as illustrated in Fig. 2.6. The example is for a shoreface system, broadly cleaning upwards. A ‘geological’ solution would identify time-lines and correlate genetic parasequences (Fig. 2.6a). In this case, for the water injection scenario illustrated, the flow in the highly permeable upper part of the sequence will simply follow the high permeability pathway which may or may not cross timelines. In the lower part of the sequence, however, the low  $k_v/k_h$  ratio associated with lower and middle shorefaces will direct flow lines from the horizontal, will result in poorer macroscopic sweep and will predict unswept intervals in the left-hand well. A lithostratigraphic interpretation (Fig. 2.6b) will predict an uneven floodfront, but with a different production profile and a prediction that all zones will ultimately be swept. The correct model representation is the one which captures how the fluid will ‘see’ the reservoir, and this depends on the permeability architecture, and an idea for how sensitive the reservoir fluids are to heterogeneity (guidance on this is given in Sect. 2.4.4).

An excellent example of the same issue for from a lacustrine reservoir system is given by Ainsworth et al. (1999).

#### 2.3.2.2 Use of Hierarchy

Different correlation schemes have different influences on the issue of hierarchy, as the stratigraphy of most reservoir systems is inherently hierarchical (Campbell 1967) and for reservoir modelling this impacts on the representation of length scales, an issue which is central to rock and property geostatistics. For a sequence stratigraphic correlation scheme, a low-stand systems tract may have a length-scale of tens of kilometres and contain stacked parasequences with a length-scale of kilometres (e.g. Fig. 2.6a). These parasequences in turn act as the container for individual reservoir elements with dimensions of

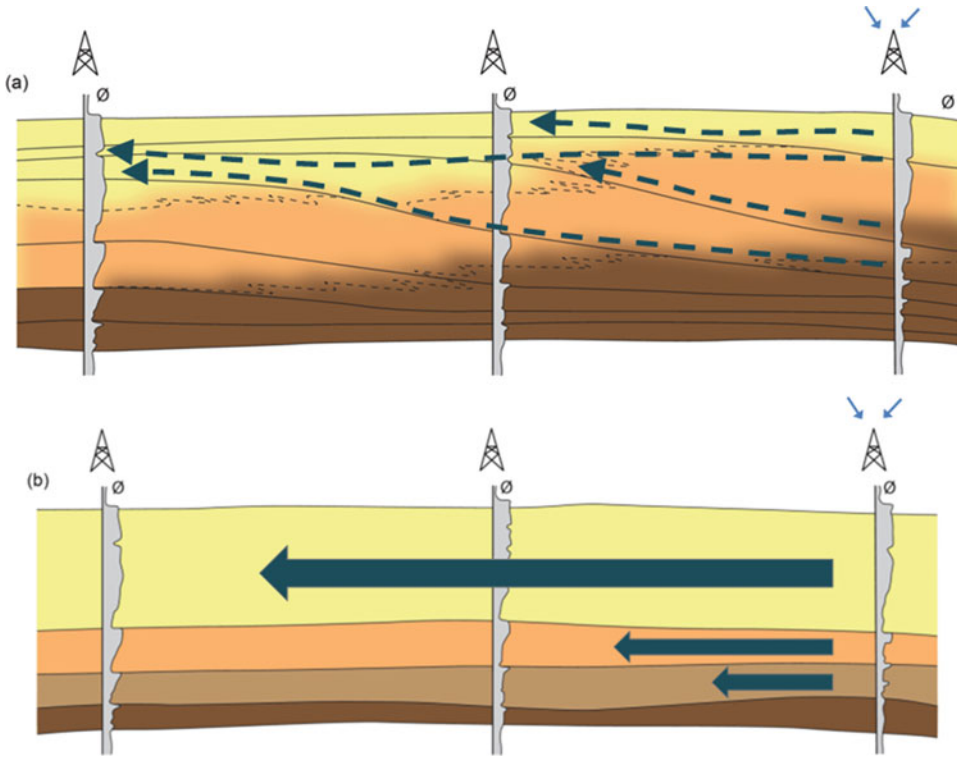


**Fig. 2.6** Alternative (a) chronostratigraphic and (b) lithostratigraphic correlations of the same sand observations in three wells; the choice of correlation

lines directly influences flow lines in a dynamic model simulation. Note: the chronostratigraphic correlation invokes an additional hierarchical level in the stratigraphy

tens to hundreds of metres. Lower levels of the hierarchy are *always* associated with shorter length scales.

The reservoir model should aim to capture the levels in the stratigraphic hierarchy which influence the spatial distribution of significant heterogeneities (determining ‘significance’ will be discussed in Sect. 2.4.4). Bounding surfaces within the hierarchy (e.g. flooding surfaces in a marginal marine interval) may or may not act as flow barriers – so they may represent important model elements in themselves or they may merely control the distribution of model elements within that hierarchy. This applies to structural model elements as well as the more familiar sedimentological elements, as features such as fracture density can be controlled by mechanical stratigraphy – implicitly related to the stratigraphic hierarchy.

Particular care is required if a sequence stratigraphic approach has been used to correlate. The method yields a framework of timelines, often based on picking the most shaley parts of non-reservoir intervals so a rock model for an interval between two flooding surfaces should contain a shaley portion at both the top and the base of the interval. The probabilistic aspects of the subsequent geostatistical modelling, however, can easily degrade the correlatable nature of the flooding surfaces, with inter-well shales becoming scattered incorrectly throughout the zone. This particular case can be resolved by applying deterministic trends; this will be pursued further in Sect. 2.7.4.

In general, hierarchical order is intrinsic to reservoirs and some degree of hierarchy is usually captured in standard software workflows, but not necessarily all. The modeller is required to work

out if the default hierarchy is sufficient to capture the required concept. If not, the workflow should be modified, most commonly by applying logical operations. An example of this is illustrated in Fig. 2.7, from a reservoir model in which the first two hierarchical levels were captured by the default software workflow: tying layering to seismic horizons (first level) then infilled by conformant sub-seismic stratigraphy (second level, Fig. 2.7a). An additional hierarchical level was required because an important permeability heterogeneity existed between lithofacies types *within* a particular model element (the main channels). The chosen solution was to build the channel model using channel objects and creating a separate, in this case probabilistic, model which contained the information about the distribution

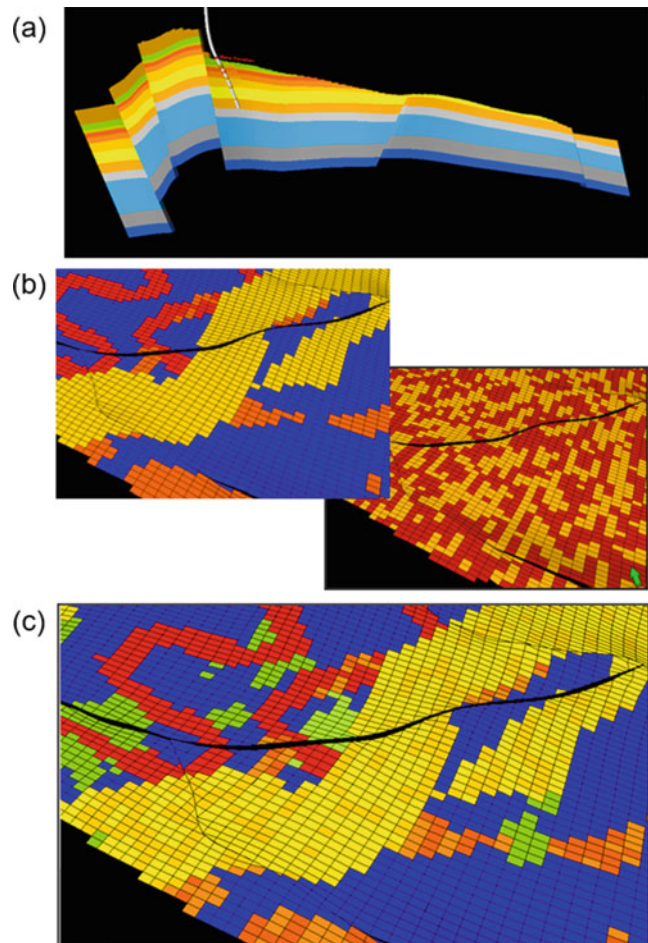
of the two lithofacies elements. The two rock models were then combined using a logical property model operation, which imposed the texture of the fine-scale lithofacies heterogeneity, but only within the relevant channels. Effectively this created a third hierarchical level within the model.

One way or another hierarchy can be represented, but only rarely by using default model workflows.

## 2.4 Model Elements

Having established a structural/stratigraphic model framework, we can now return to the model concept and consider how to fill the

**Fig. 2.7** The addition of hierarchy by logical combination: (a) stratigraphical framework; (b) single-hierarchy channel model (*left*, blue = mudstone, yellow = main channel) built in parallel with a probabilistic model of lithofacies types (*right*, yellow = better quality reservoir sands); (c) logical combination of lithofacies detail in the main channel only – an additional level of hierarchy



framework to create an optimal architectural representation.

### 2.4.1 Reservoir Models Not Geological Models

The rich and detailed geological story that can be extracted from days or weeks of analysis of the rock record from the core store need not be incorporated directly into the reservoir model, and this is a good thing. There is a natural tendency to ‘include all the detail’ just in case something minor turns out to be important. Models therefore have a tendency to be over-complex from the outset, particularly for novice modellers. The amount of detail required in the model can, to a large extent, be anticipated.

There is also a tendency for modellers to seize the opportunity to build ‘real 3D geological pictures’ of the subsurface and to therefore make these as complex as the geology is believed to be. This is a hopeless objective as the subsurface is considerably more complex in detail than we are capable of modelling explicitly and, thankfully, much of that detail is irrelevant to economic or engineering decisions. We are building *reservoir models* – reasonable representations of the detailed geology – not geological models.

### 2.4.2 Building Blocks

Hence the view of the components of a reservoir model as *model elements* – the fundamental building blocks of the 3D architecture. The use of this term distinguishes model elements from geological terms such as ‘facies’, ‘lithofacies’, ‘facies associations’ and ‘genetic units’ and from production-related terms such as ‘hydraulic units’ or ‘flow units’.

The geological terms are required to help interpret the richness of the geological story, but are not necessarily the things we need to put into reservoir models – they usually carry more detail than we need (see Sect. 2.4.4). Moreover, key elements of the reservoir model may be small-scale structural or diagenetic features, often

(perhaps incorrectly) excluded from descriptions of ‘facies’.

The flow-based terms tend to be well-centric views which, when converted into a 3D reservoir model, generally lead to a layer-based representation. For truly ‘layer-cake’ reservoirs (*sensu* Webber and van Guens 1990) this may be a sufficient representation. Our aim is to define building blocks for any 3D reservoir architecture, including parts of a field remote from well and production data – a broader mission.

Modelling elements are defined here as:

three-dimensional rock bodies which are petrophysically and/or geometrically distinct from each other in the specific context of the reservoir fluid system

Elements are therefore similar to petrophysical ‘rock types’, but include a geometric distinction, i.e. two rocks which are petrophysically similar would be distinguished if they were contained within two differently-shaped rock bodies such as sheets and channels. This is because bodies with different geometries stack together differently to produce different architectures. Also, petrophysical rock types can often be combined to make one modelling element, depending on the demands of the fluid system. The fluid-fill factor is important as it highlights the fact that different levels of heterogeneity are important for different types of fluid, e.g. gas reservoirs behave more homogeneously than oil reservoirs for a given reservoir type (see Sect. 2.4.4 below for handy guidance on this).

### 2.4.3 Model Element Types

If we can work beyond the traditional use of depositional facies to define rock bodies for modelling, a broad spectrum of elements can be considered for use, i.e. making the sketch of the reservoir as it is intended to be modelled. Six candidate model element types are considered below.

#### 2.4.3.1 Lithofacies Types

This is sedimentologically-driven and is the traditional way of defining the components of a rock

model. Typical lithofacies elements may be coarse sandstones, mudstones or grainstones, and will generally be defined from core and or log data (e.g. Fig. 2.8).

**2.4.3.2 Genetic Elements**

In reservoir modelling, genetic elements are a component of a sedimentary sequence which are

related by a depositional process. These include the rock bodies which typical modelling packages are most readily designed to incorporate, such as channels, sheet sands or heterolithics. These usually comprise several lithofacies, for example, a fluvial channel might include conglomeratic, cross-bedded sandstone and mudstone lithofacies. Figure 2.9 shows an example for a

**Fig. 2.8** Example lithofacies elements; *left*: coarse, pebbly sandstone; *right*: massively-bedded coarse-grained sandstone

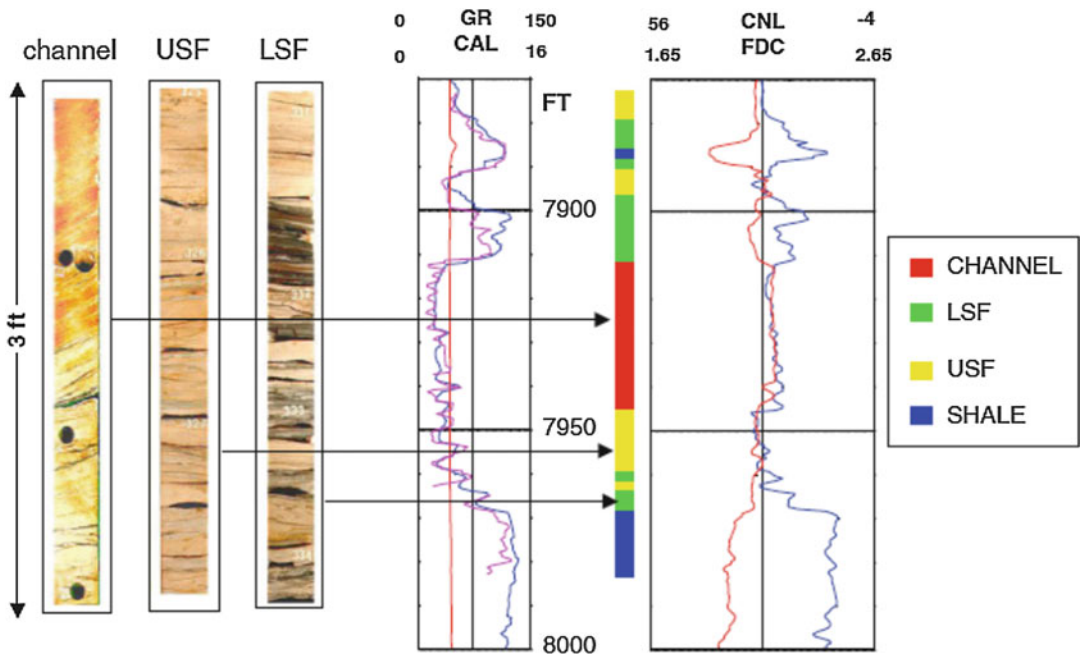
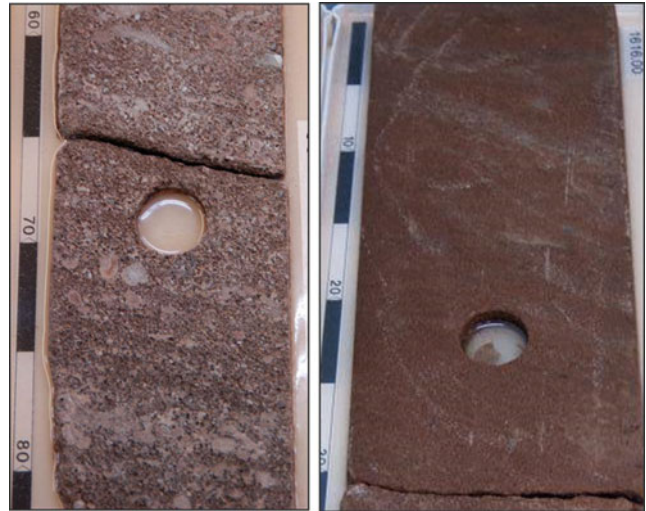


**Fig. 2.9** Genetic Units: lithofacies types grouped into channel, upper shoreface (USF) and lower shoreface (LSF) genetic depositional elements. (Image courtesy of Simon Smith)

shoreface in which genetic elements are identified from core and log data.

### 2.4.3.3 Stratigraphic Elements

For models based on a sequence stratigraphic framework, the fine-scale components of the scheme may be the predominant model elements. These may be parasequence sets organised within a larger-scale sequence-based framework, e.g. Fig. 2.10.

### 2.4.3.4 Diagenetic Elements

Diagenetic elements commonly overprint lithofacies types, may cross major stratigraphic boundaries and are often the predominant feature of carbonate reservoir models. Typical diagenetic elements could be zones of meteoric flushing, dolomitisation or de-dolomitisation (Fig. 2.11).

### 2.4.3.5 Structural Elements

Assuming a definition of model elements as three-dimensional features, structural model elements should be considered when the properties of a reservoir volume are dominated

by structural rather than sedimentological or stratigraphic aspects. Fault damage zones are important volumetric structural elements (e.g. Fig. 2.12) as are mechanical layers (strata-bound fracture sets) with properties driven by small-scale jointing or cementation. These are discussed further in Sect. 6.7.

### 2.4.3.6 Exotic Elements

The list of potential model elements matches the diversity of reservoir types. Reservoirs in volcanic rocks are a good example (Fig. 2.13), in which the key model elements may be zones of differential cooling and hence differential fracture density.

\* \* \*

The important point about using the term ‘model element’ is to stimulate broad thinking about the model concept, a thought process which runs across the reservoir geological sub-disciplines (stratigraphy, sedimentology, structural geology, even volcanology). For avoidance of doubt, the main difference between the

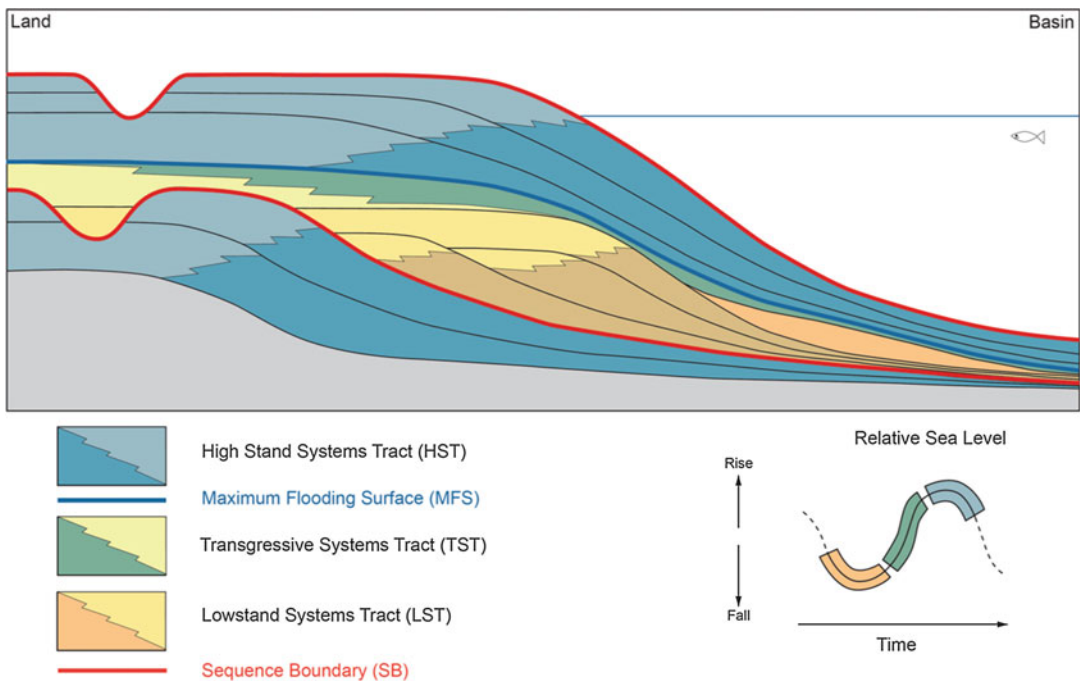


**Fig. 2.10** Sequence stratigraphic elements

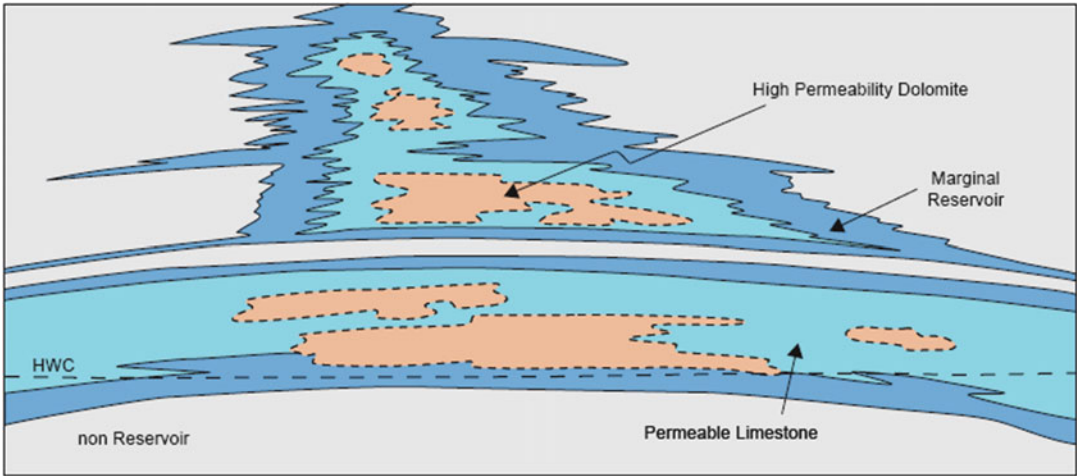
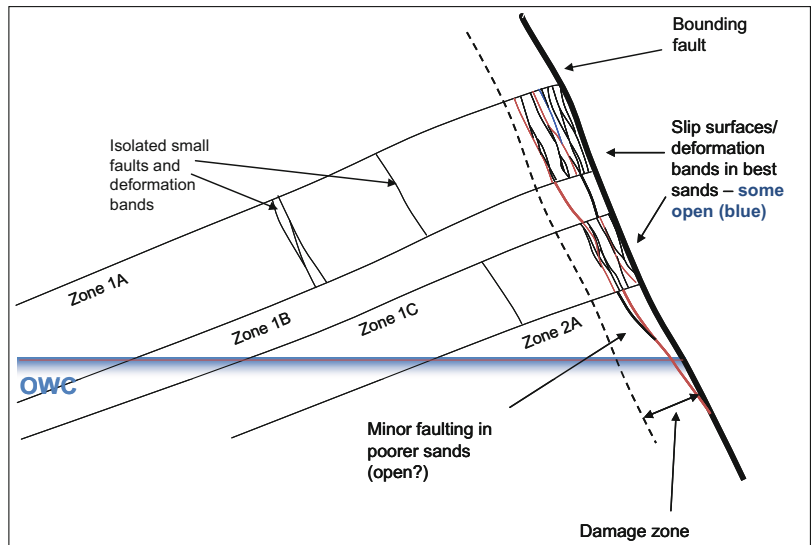


**Fig. 2.11** Diagenetic elements in a carbonate build-up; where reservoir property contrasts are driven by differential development of dolomitisation

**Fig. 2.12** Structural elements: volumes dominated by minor fracturing in a fault damage zone next to a major block-bounding fault. (Bentley and Elliot 2008)



model framework and the model elements is that 2D features are used to define the model framework (faults, unconformities, sequence boundaries, simple bounding surfaces) whereas it is 3D model elements which fill the volumes within that framework.

Having defined the framework and identified the candidate elements, the next question is how much detail to carry explicitly into the modelling process. Everything that can be identified need not be modelled.

### 2.4.4 How Much Heterogeneity to Include? ‘Flora’s Rule’

The answer to this fundamental question depends on the interaction of geology and flow physics. The key criteria for distinguishing which model elements are required for the model build are:

1. The identification of potential elements from a large number of ‘candidates’;



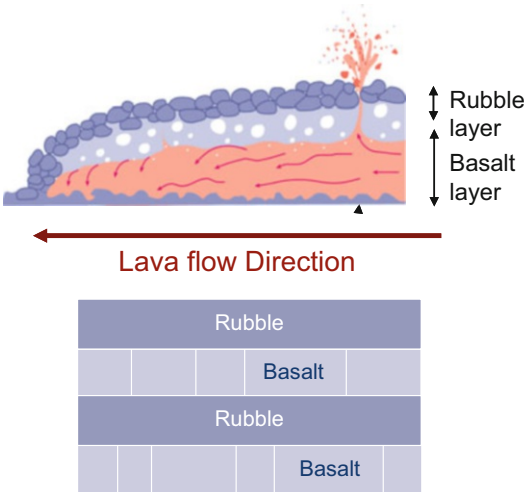


**Fig. 2.13** Exotic elements: reservoir breakdown for a bimodal-permeability gas-bearing volcanic reservoir in which model elements are driven by cooling behaviour in a set of stacked lava flows. (Image courtesy of Jenny Garnham)

2. The permeability contrasts between the candidate elements;
3. The fluid type;
4. The production and/or injection mechanism.

The four items above then need to be considered in terms of the length scales of the underlying heterogeneities and the scale associated with the original model purpose.

The first steps are illustrated in Fig. 2.14 in which six candidate elements have been identified from core and log data (step 1), placed in an analogue context (step 2) and their rock property contrasts compared (step 3). The six candidate elements seem to cluster into three, but is it right to lump these together? How great does a contrast have to be to be 'significant'? Here we can invoke some useful guidance.

A simple way of combining the factors above is to consider what level of permeability contrast would generate significant flow heterogeneities for a given fluid type and production mechanism. The handy rule of thumb is as follows (Fig. 2.15):

- Gas reservoirs are generally sensitive to 3 or more orders of magnitude permeability variation;

- Oil reservoirs under depletion are sensitive to 2 or more orders of magnitude permeability variation;
- Heavy oil reservoirs or lighter crudes under secondary or tertiary recovery tend to be sensitive to 1 order of magnitude permeability contrasts

This simple rule of thumb, which has become known to us as 'Flora's Rule' (after an influential and much-respected reservoir engineering colleague of one of the authors), has its foundation in the viscosity term in the Darcy flow equation:

$$u = \frac{-k}{\mu} \nabla(P) \quad (2.1)$$

where:

- $u$  = fluid velocity
- $k$  = permeability
- $\mu$  = fluid viscosity
- $\nabla P$  = pressure gradient

Because the constant of proportionality between flow velocity and the pressure gradient is  $k/\mu$ , low viscosity results in a weaker dependence of flow on the pressure gradient whereas higher viscosities give increasingly higher dependence of flow on the pressure gradient. Combine this with a consideration of the mobility ratio in a two-phase flow system, and the increased sensitivity of secondary and tertiary recovery to permeability heterogeneity becomes clear.

Using these criteria, some candidate elements which contrast geologically in core may appear rather similar to a fluid passing through them. The same heterogeneities that are shown to have an important effect in a  $\text{CO}_2$  disposal scheme (see Chap. 7) may have absolutely no effect in a hydrocarbon gas reservoir under depletion. The importance of some 'borderline' heterogeneities may be unclear – and these could be included on a 'just in case' basis. Alternatively, a quick static/dynamic sensitivity run may be enough to demonstrate that a specific candidate element can be dropped or included with confidence.

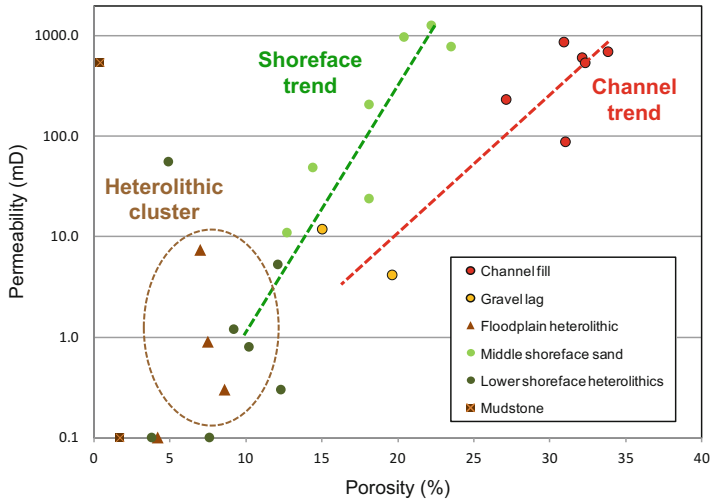
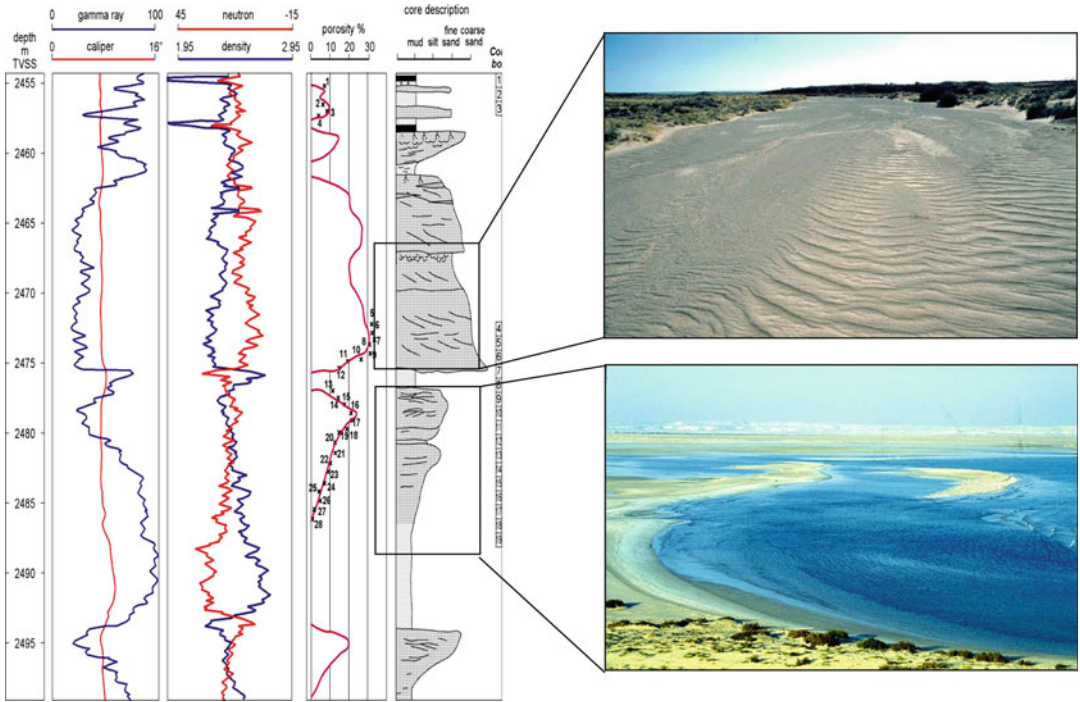


**Fig. 2.14** Six candidate model elements and one non-reservoir element identified from core and log data and clustered into three on a k/phi cross plot – how do we decide if it is acceptable to lump these together?

**Fig. 2.15** Critical order of magnitude permeability contrasts for a range of fluid and production mechanisms – ‘Flora’s Rule’

|                                       |                        |                          |  |
|---------------------------------------|------------------------|--------------------------|--|
| <b>Critical permeability contrast</b> | <b>3 orders</b>        | <b>2 orders</b>          | <b>1 order</b>                         |
| <b>Fluid fill</b>                     | dry gas                | wet gas                  | light oil<br>heavy oil                 |
| <b>Production mechanism</b>           | depletion (no aquifer) | depletion (with aquifer) | water injection<br>gas/steam injection |

The outcome of this line of argument is that some reservoirs may not require complex 3D reservoir models at all (Fig. 2.16). Gas-charged reservoirs require high degrees of permeability heterogeneity in order to justify a complex modelling exercise – they often deplete as simple tanks. Fault compartments and active aquifers may stimulate heterogeneous flow production in gas fields, but even in this case the model required to capture key fault blocks can be quite coarse. By contrast, heavy oil fields under water or steam injection or CO<sub>2</sub> storage schemes are highly susceptible to minor heterogeneities, and benefit from detailed modelling. The difficulty here lies in assessing the architecture of these heterogeneities, which can often be on a very fine, poorly-sampled scale.

The decision as to which candidate elements to include in a model is therefore not primarily a

geological one. Geological and petrophysical analyses are required to define the degree of permeability variation and to determine the spatial architecture, but it is the fluid type and the production or injection process which determine the level of geological detail needed in the reservoir model and hence the selection of ‘model elements’.

Beyond the considerations above, there remains the question of whether a significant heterogeneity should be modelled *explicitly* or captured *implicitly* in a well-selected average. This comes down to length scales, specifically the difference between the length scale of the significant uncertainty and the length scale of the question being addressed in the modelling exercise (Fig. 2.17).

Heterogeneity length scales are an established concept and will be discussed fully in Chap. 4 in

**Fig. 2.16** What type of reservoir model? A choice based on heterogeneity and fluid type

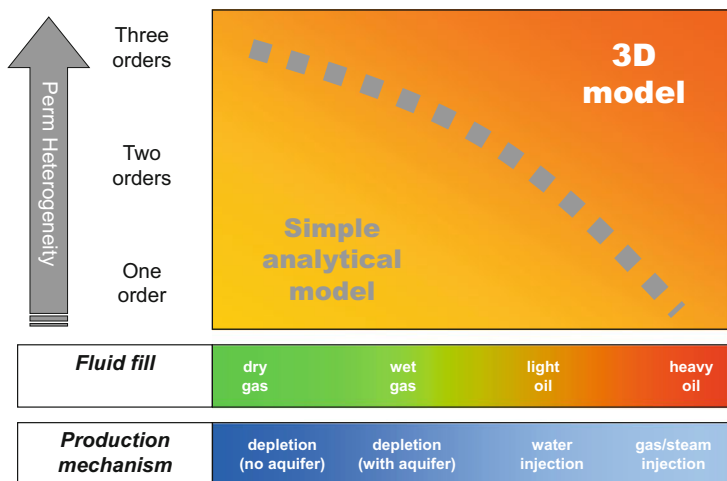
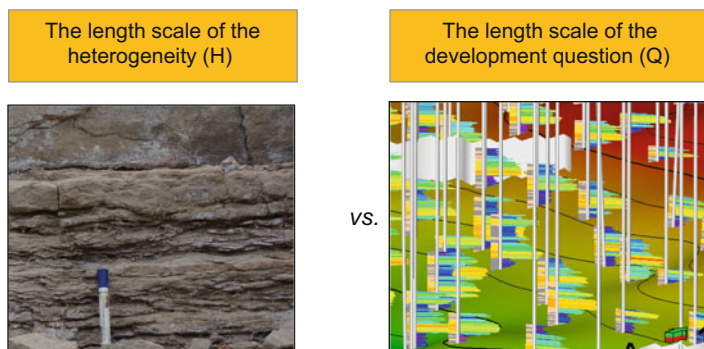


**Fig. 2.17** A comparison of length scales to assess the option of implicit vs. explicit element representation



the context of models scales and the REV (the Representative Elementary Volume). Here it suffices to say that the length scale is an assessment of the distance over which the heterogeneity varies: systems with high point-to-point variations over short distances are said to have short length scales, variations over long distances are said to have long length scales. The concept of questions having scales may be less commonly considered, but holds true for most subsurface decisions; every model has a purpose, the purpose relates to a question which is being asked and that question generally has a scale. For infill drilling, the scale of the question is the proposed well spacing, typically a few hundred metres and typically shorter onshore than offshore. For gas depletion the scale of the question is the size of the reservoir compartment being blown down, which may be the full field. For CO<sub>2</sub> storage schemes it is the size of the storage complex. For well-test interpretations the scale is much smaller – typically the radius of investigation of the well test.

The reason the comparison is important is that the subsurface has a dispersive effect on fluid flow, which is also rate-dependent. This is illustrated in Fig. 2.18 which shows a simple cross-sectional flow experiment involving water injecting into an oil reservoir. The homogeneous flow model (a) shows simple piston-like displacement, distorted only by the effect of gravity. The heterogeneous flow model (b) clearly shows the sensitivity to the underlying permeability heterogeneity but the shape of the flood front is not significantly impacted as the length of the heterogeneity is small compared to the length scale of the question, which is the well spacing (in this experiment this is the width of the model). The model is literally ‘so heterogeneous, it is homogeneous’. Only as the length scale of the heterogeneity (H) approaches the length scale of the development question (Q) does the floodfront start to deviate from the simple homogeneous case (the lower two sets of figures).

In all cases in Fig. 2.18b–d the heterogeneity is significant in terms of impacting flow. The

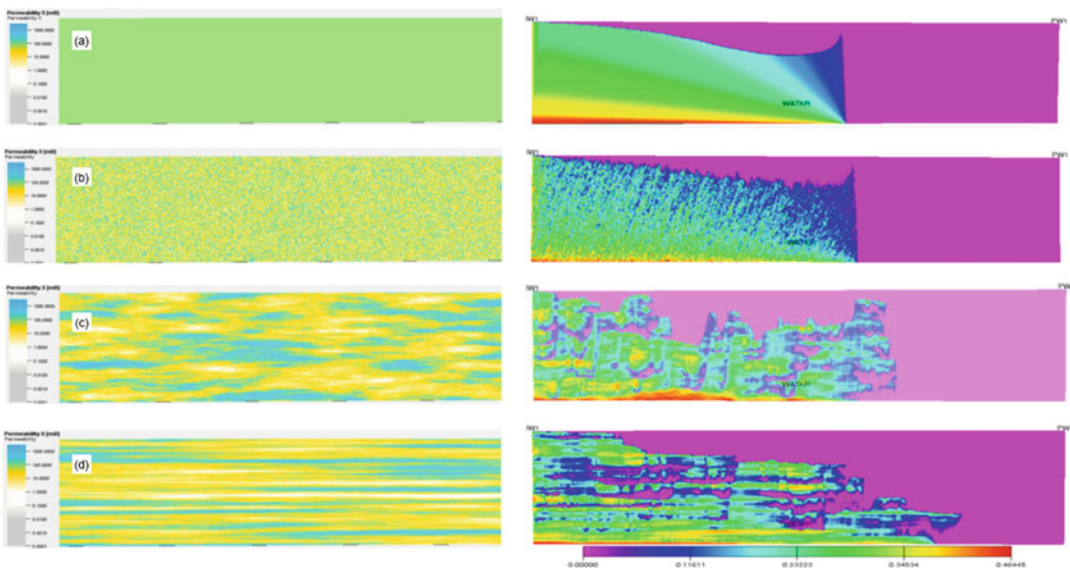


**Fig. 2.18** The impact of contrasting heterogeneity length scales vs. a fixed length scale of the development question (the well spacing): left-hand models are static permeability, right-hand models are paired water injection simulations, injecting from the left; ornament is water saturation. (a) homogeneous permeability model; (b)

heterogeneous model with very short length scales ( $H \ll Q$ ); (c) & (d) models in which the heterogeneity length scales approach that of the scale of the development question (where  $H \sim Q$ ). Images produced courtesy of Rayyan Hussein and Ed Stephens

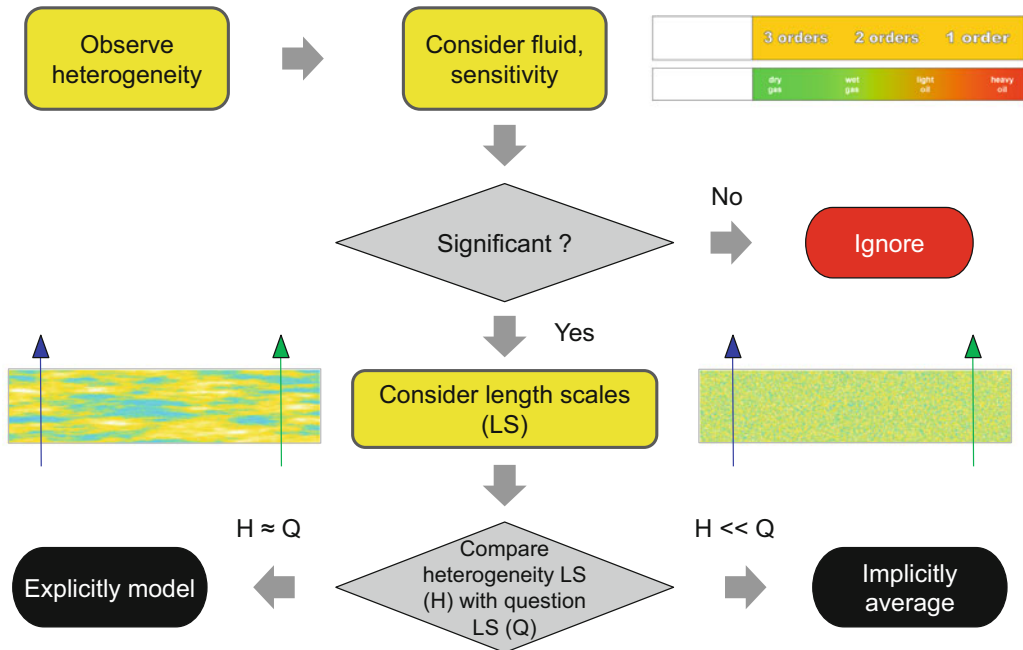


**Fig. 2.19** How much detail needs to be incorporated in a static modelling exercise? Assuming the ultimate purpose is flow modelling, it depends on the magnitude and the

length scale of the contrasts, the reservoir fluid and production mechanism and the scale of the question the model is addressing

difference is that in Fig. 2.18b it can be captured using a simple average, whereas in Fig. 2.18c–d it needs to be explicitly modelled. The averaging options are discussed in Chap. 4, but for now the question of how many elements need to be incorporated in a model can be summarised in the flow chart in Fig. 2.19. It relates to the magnitude of the heterogeneity compared to the fluid fill and the production mechanism (‘Flora’s Rule’) and a consideration of the length scales of the heterogeneity and the development question at hand.

If the fluid doesn’t sense the heterogeneity, the heterogeneity need not be modelled.

## 2.5 Determinism and Probability

The use of geostatistics in reservoir modelling became widely fashionable in the early 1990s (e.g. Haldorsen and Damsleth 1990; Journel and Albert 1990) and was generally received as a welcome answer to some tricky questions such as how to handle uncertainty and how to represent

geological heterogeneities in 3D reservoir models.

However, the promise of geostatistics (and ‘knowledge-based systems’) to solve reservoir forecasting problems sometimes led to disappointment. Probabilistic attempts to predict desirable outcomes, such as the presence of a sand body, yield naïve results if applied simply (Fig. 2.20).

This potential for disappointment is unfortunate as the available geostatistical library of tools is excellent for applying quantitative statistical algorithms rigorously and routinely, and is essential for filling the inter-well volume in a 3D reservoir model. The disappointments come from incorrect application, nicely summarised by Pырcz and Deutch (2014):

Geostatistical methods aim to reproduce (the) input statistics; geostatistical models have no predictive power with respect to these statistics

At the heart of this is an appreciation of the interplay of determinism and probability in the reservoir model build.

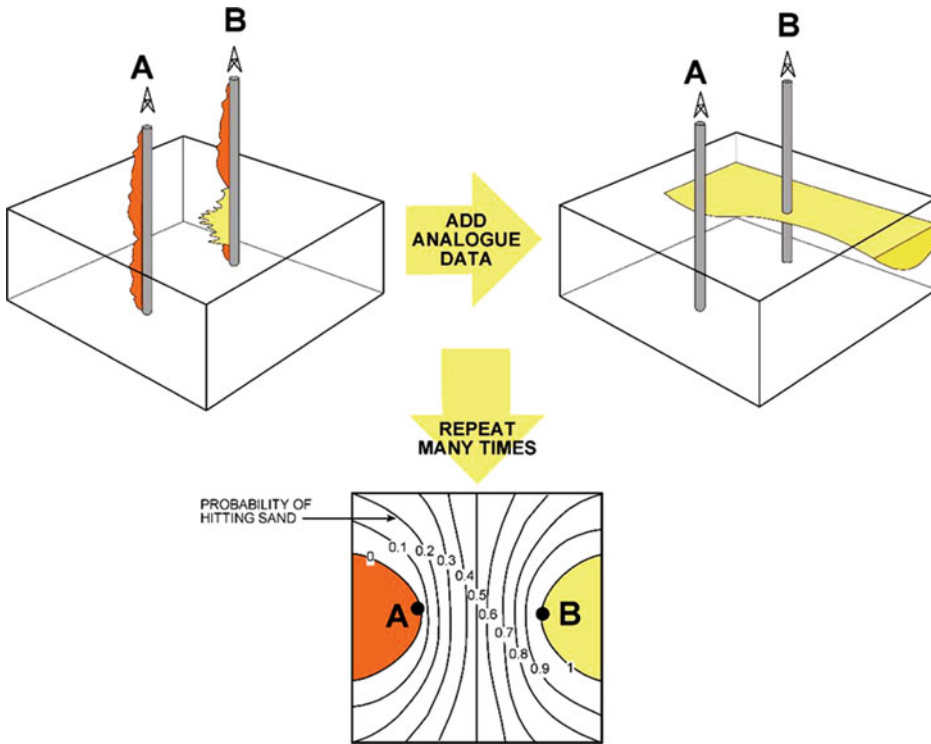


**Fig. 2.20** A naïve example of an expectation from geostatistical forecasting – the final mapped result simply illustrates where the wells are

### 2.5.1 Balance Between Determinism and Probability

The underlying design issue we stress is the balance between determinism and probability in a model, and whether the modeller is aware of, and in control of, this balance.

To define the terminology as used here:

- *Determinism* is taken to mean an aspect of a model which is fixed by the user and imposed on the model, such as placing a fault in the model or precisely fixing the location of a particular rock body;
- *Probability* refers to aspects of the model which are guided by a random (stochastic) outcome from running a probabilistic algorithm.

To complete the terminology, a *stochastic process* (from the Greek *stochas* for ‘aiming’ or

‘guessing’) is one whose behaviour is completely non-deterministic. A *probabilistic* method is one in which likelihood or probability theory is employed. Monte Carlo methods, referred to especially in relation to uncertainty handling, are a class of algorithms that rely on repeated random sampling to compute a probabilistic result. Although not strictly the same, the terms *probabilistic* and *stochastic* are often treated synonymously and in this book we will restrict the discussion to the contrast between deterministic and probabilistic approaches applied in reservoir modelling.

Put simply: probability involves dice, but in determinism there are no dice. The subtlety is that the balance of deterministic and probabilistic influences on a reservoir model is not as black and white as it may at first seem. Consider the simple range of cases shown in Fig. 2.21, showing three generic types of rock body:

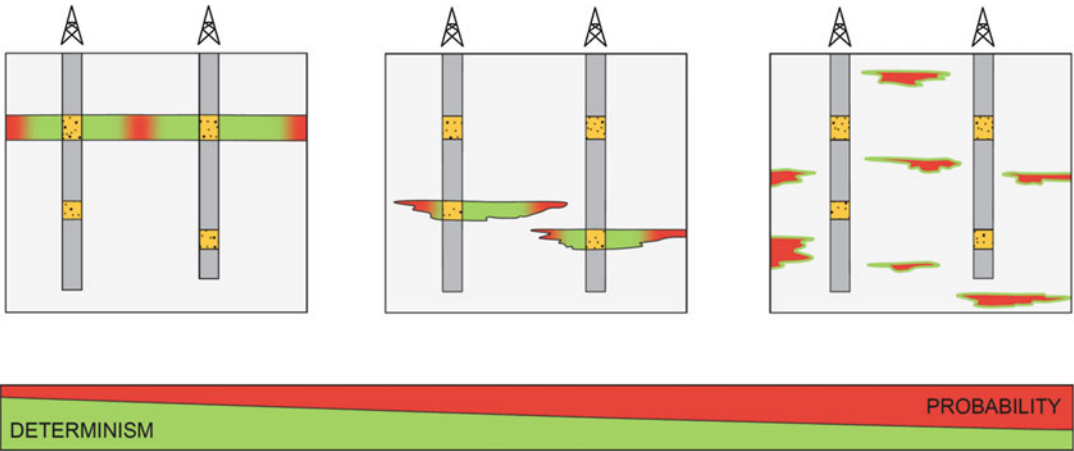


**Fig. 2.21** Different rock body types as an illustration of the deterministic/probabilistic spectrum

1. *Correlatable bodies* (Fig. 2.21, left). These are largely determined by correlation choices between wells, e.g. sand observations are made in two wells and interpreted as occurrences of the same extensive sand unit and are correlated. This is a deterministic choice, not an outcome of a probabilistic algorithm. The resulting body is not a 100% determined ‘fact’, however, as the interpretation of continuity between the wells is just that – an interpretation. At a distance from the wells, the sand body has a probabilistic component in its interpretation, if not its algorithmic emplacement.
2. *Non-correlated bodies* (Fig. 2.21, centre). These are bodies encountered in one well only. At the well, their presence is determined. At increasing distances from the well, the location of the sand body is progressively less well determined, and is eventually controlled almost solely by the roll of the dice. These bodies are each partly deterministic and partly probabilistic.
3. *Probabilistic bodies* (Fig. 2.21, right). These are the bodies not encountered by wells, the position of which will be chosen by a probabilistic algorithm. Even these, however, are not 100% probabilistic as their appearance in the model is not a completely random surprise.

Deterministic constraints will have been placed on the algorithm to make sure bodies are not unrealistically large or small, and are appropriately numerous.

So, if everything is a mixture of determinism and probability, what’s the problem? The issue is that although any reservoir model is rightfully a blend of deterministic and probabilistic processes, the richness of the blend is a choice of the user so this is an issue of model design. Some models are highly deterministic, some are highly probabilistic and which end of the spectrum a model sits at influences the uses to which it can be put. A single, highly probabilistic model is not suitable for planning one well (probabilistic rock bodies will probably not be encountered as prognosed). A highly deterministic model may be inappropriate, however, for simulations of reservoirs with small rock bodies and little well data. Furthermore, different modellers might approach the same reservoir with more deterministic or more probabilistic mindsets.

The balance of probability and determinism in a model is therefore a subtle issue, and needs to be understood and controlled as part of the model design. We suggest here that greater happiness is generally to be found in models built with strong deterministic control, as the deterministic inputs are the direct carrier of the reservoir concept.

### 2.5.2 Different Generic Approaches

To emphasise the importance of user choice in the approach to determinism and probability, two approaches to model design are summarised graphically. The first is a data-driven approach to modelling (Fig. 2.22). In this case, the model process starts with an analysis of the data, from which statistical guidelines can be drawn. These guidelines are input to a rich statistical model of the reservoir which in turn informs a geostatistical algorithm. The outcome of the algorithm is a model, from which a forecast emerges.

This is the approach which most closely resembles the default path in reservoir modelling, resulting from the linear workflow of a standard reservoir modelling software package, as outlined in Fig. 1.10.

The limit of a simple data-driven approach such as this is that there is a reliance on the rich geostatistical algorithm to generate the desired model outcome. This in turn relies on the statistical content of the underlying data set, *yet for most of our reservoirs, the underlying data set is statistically insufficient*. This is a critical issue and distinguishes reservoir modelling from other types of geostatistical modelling in earth sciences such as mining and soil science. In the latter cases, there is often a much richer underlying

data set, which can yield clear statistical guidance for a model build. In reservoir modelling we are typically dealing with more sparse data, an exception being direct conditioning of the reservoir model by high quality 3D seismic data (e.g. Doyen 2007).

An alternative is to take a more concept-driven, top-down approach (Fig. 2.23). In this case, the modelling still starts with an analysis of the data, but the analysis is used to generate alternative conceptual models for the reservoir. The reservoir concept should honour the data at its geographic location but, as the dataset is generally statistically insufficient, the full 3D model should not be limited to it. The model build is strongly concept-driven, has a strong deterministic component, and less reliance is placed on geostatistical algorithms to produce the desired product. The final outcome is not a single forecast, but a set of forecasts based on the uncertainties associated with the underlying reservoir concepts.

The difference between the data- and concept-driven approaches described above is the expectation they place on the geostatistical algorithm in the context of data insufficiency. The result is a greater emphasis on deterministic model aspects, which therefore need some more consideration.

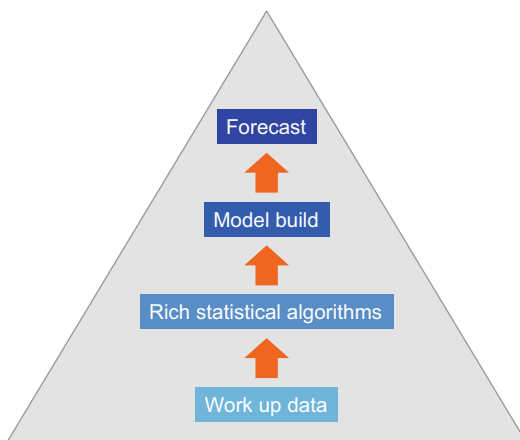


**Fig. 2.22** The data-driven approach to reservoir modelling

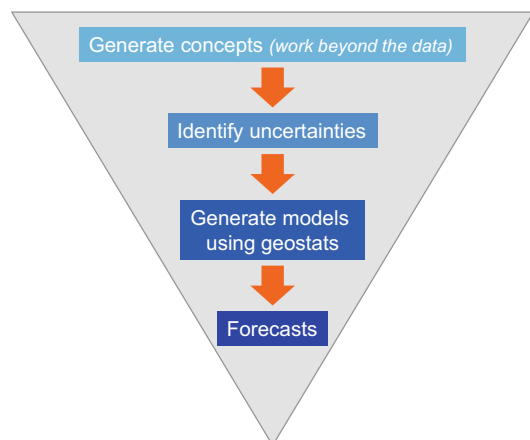


**Fig. 2.23** The concept-driven approach to reservoir modelling



### 2.5.3 Forms of Deterministic Control

The deterministic controls on a model can be seen as a toolbox of options with which to realise an architectural concept in a reservoir model. These will be discussed further in the last section of this chapter, and are introduced below.

#### 2.5.3.1 Faulting

With the exception of some (relatively) specialist structural modelling packages, large scale structural features are strongly deterministic in a reservoir model. Thought is required as to whether the structural framework is to be geophysically or geologically led, that is, are only features resolvable on seismic to be included, or will features be included which are kinematically likely to occur in terms of rock deformation. This in itself is a model design choice, introduced in the discussion on model frameworks (Sect. 2.3) and the choice will be imposed deterministically.

#### 2.5.3.2 Correlation and Layering

The correlation framework (Sect. 2.3) is deterministic, as is any imposed hierarchy. The probabilistic algorithms work entirely within this framework – layer boundaries are not moved in common software packages. Ultimately the flowlines in any simulation will be influenced by the fine layering scheme and this is all set deterministically.

#### 2.5.3.3 Choice of Algorithm

There are no hard rules as to which geostatistical algorithm gives the ‘correct’ result yet the choice of pixel-based or object-based modelling approaches will have a profound effect on the model outcome (Sect. 2.7). The best solution is the algorithm or combination of algorithms which most closely reflect the desired reservoir concept, and this is a deterministic choice.

#### 2.5.3.4 Boundary Conditions for Probabilistic Algorithms

All algorithms work within limits, which will be given by arbitrary default values unless imposed. These limits include correlation lengths, object

dimensions and statistical success criteria (Sect. 2.6). In the context of the concept-driven logic described above, these limits need to be deterministically chosen rather than a simple consequence of the spread of a statistically insufficient well data set.

#### 2.5.3.5 Seismic Conditioning

The great hope for detailed deterministic control is exceptionally good seismic data. This hope is often forlorn, as even good quality seismic data is not generally resolved at the level of detail required for a reservoir model. All is not lost, however, and it is useful to distinguish between *hard* and *soft* conditioning.

*Hard conditioning* is applicable in cases where extremely high quality seismic, sufficiently resolved at the scale of interest, can be used to directly define the architecture in a reservoir model. An example of this is seismic geobodies in cases where the geobodies are believed to directly represent important model elements. Some good examples of this have emerged from deepwater clastic environments, but in many of these cases detailed investigation (or more drilling) ends up showing that reservoir pay extends sub-seismically, or that the geobody is itself a composite, heterogeneous feature.

*Soft conditioning* is the more generally useful approach for rock modelling, where information from seismic is used to give a general guide to the probabilistic algorithms (Fig. 2.24). In this case, the link between the input from seismic and the probabilistic algorithm may be as simple as a correlation coefficient. It is the level of the coefficient which is now the deterministic control; and the decision to use seismic as either a hard or soft conditioning tool is also a deterministic one.

One way of viewing the role of seismic in reservoir modelling is to adapt the frequency/amplitude plot familiar from geophysics (Fig. 2.25). These plots are used to show the frequency content of a seismic data set and can be used to indicate how improved seismic acquisition and processing can extend the frequency content towards the ends of the spectrum. Fine-scale reservoir detail sits below the resolution of the seismic data. The low end of the frequency

spectrum – the large scale layering – is also beyond the range of the seismic sample unless broadband technologies are in use (e.g. Soubaras and Dowle 2010). Even in the case of broadband seismic, there is a requirement to construct a low

frequency ‘earth model’ to support seismic inversion work.

The plot is a convenient backdrop for arranging the components of a reservoir model, and the frequency/amplitude axes can be alternatively labelled as ‘scale of heterogeneity’ and ‘content’. The reservoir itself exists on all scales and is represented by the full ‘rectangle of truth’, which is only partially covered by seismic data. The missing areas are completed by the framework model at the low frequency end, by core and log-scale detail at the high frequency end and by interpretation in between these data scales.

The only full-frequency data set is a well exposed outcropping reservoir analogue, as it is only in the field that the reservoir can be accessed on all scales. Well facilitated excursions to outcrop analogues are thereby conveniently justified (an often neglected activity, the value of which is summarised in Howell et al. 2014).

Is all the detail necessary? Here we can refer back to Flora’s Rule and the model purpose, which will inform us how much of the full spectrum is required to be modelled in any particular case. In terms of seismic conditioning, it is only in the case where the portion required for modelling *exactly* matches the blue area in Fig. 2.25 that we

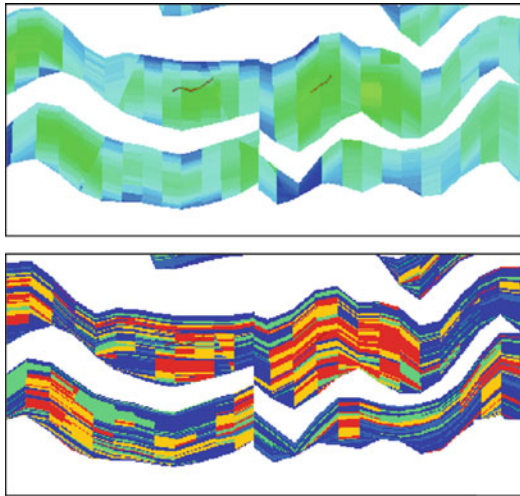
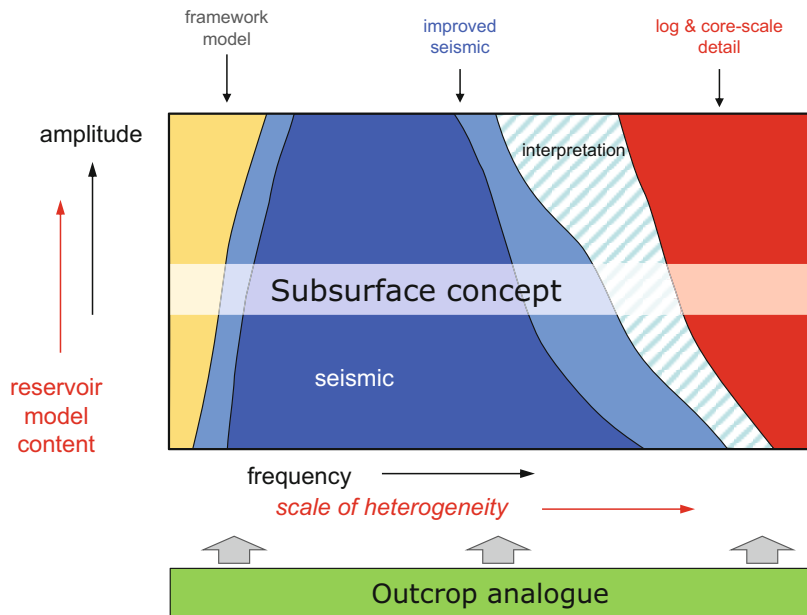


**Fig. 2.24** Deterministic model control in the form of seismic ‘soft’ conditioning of a rock model. *Upper image:* AI volume rendered into cells. *Lower image:* Best reservoir properties (red, yellow) preferentially guided by high AI values (Image courtesy of Simon Smith)

**Fig. 2.25** Seismic conditioning in the context of the ‘rectangle of truth’ – the full frequency spectrum only observed at the outcropping reservoir analogues



can confidently apply hard conditioning using geobodies in the reservoir model, and this happy coincidence is rarely the case.

\* \* \*

With the above considered, there can be some logic as to the way in which deterministic control is applied to a model, and establishing this is part of the model design process. The probabilistic aspects of the model should be clear, to the point where the modeller can state whether the design is strongly deterministic or strongly probabilistic and identify where the deterministic and probabilistic components sit.

Both components are implicitly required in any model and it is argued here that the road to happiness lies with strong deterministic control. The outcome from the probabilistic components of the model should be largely predictable, and should be a clear reflection of the input data combined with the deterministic constraints imposed on the algorithms.

Disappointment occurs if the modeller expects the probabilistic aspects of the software to take on the role of model determination, and fill in the knowledge and interpretational gaps in their own mind.

So how to approach geostatistics? The first step is to ensure we have a firm understanding of the underlying concepts behind the algorithms – just the essentials.

## 2.6 Essential Geostatistics

Good introductions to the use of statistics in reservoir modelling can be found in Yarus and Chambers (1994), Holden et al. (1998), Dubrule and Damsleth (2001), Caers (2011) and Pyrcz and Deutsch (2014) and these will not be superseded here. In the spirit of a practitioners guide, our interest lies in the application of the techniques – seeing the wood for the trees and finding the key levers and points of qualitative assumption – the points in the workflow where the ‘intuitive leaps’ happen. Very often the reservoir modeller is

confounded by complex geostatistical terminology which is difficult to translate into the modelling process. Take for example this quotation from the excellent but fairly theoretical treatment of geostatistics by Isaacs and Srivastava (1989):

in an ideal theoretical world the sill is either the stationary infinite variance of the random function or the dispersion variance of data volumes within the volume of the study area.

The problem for many of us is that we don’t work in an *ideal theoretical world* and are unfamiliar with the concepts and terminology that are used in statistical theory. This section therefore aims to extract just those statistical concepts which are essential for an *intuitive* understanding of what happens in the statistical engines of reservoir modelling packages.

### 2.6.1 Key Geostatistical Concepts

A central concept in geostatistics which must be understood is that of *variance*. Variance,  $\sigma^2$ , is a measure of the average difference between individual values and the mean of the dataset they come from. It is a measure of the *spread* of the dataset:

$$\sigma^2 = \Sigma(x_i - \mu)^2 / N \quad (2.2)$$

where:

$x_i$  = a value for the variable in question,

$N$  = the number of values in the data set, and

$\mu$  = the mean of that data set

Variance-related concepts underlie much of reservoir modelling. Two such occurrences are summarised below: the use of correlation coefficients and the variogram.

The correlation coefficient measures the strength of the dependency between two parameters by comparing how far pairs of values ( $x, y$ ) deviate from a straight line function, and is given by the function:

$$\rho = \frac{1/N \sum_{n=1}^{n=N} (x_i - \mu_x)(y_i - \mu_y)}{\sigma_x \sigma_y} \quad (2.3)$$

where:

$N$  = number of points in the data set

$x_i, y_i$  = values of point in the two data sets

$\mu_x, \mu_y$  = mean values of the two data sets, and

$\sigma_x, \sigma_y$  = standard deviations of the two data sets  
(the square of the variance)

If the outcome of the above function is positive then higher values of  $x$  tend to occur with higher values of  $y$ , and the data sets are said to be ‘positively correlated’. If the outcome is  $\rho = 1$  then the relationship between  $x$  and  $y$  is a simple straight line. A negative outcome means high values of one data set correlate with low values of the other: ‘negative correlation’. A zero result indicates no correlation.

Note that correlation coefficients assume the data sets are both linear. For example, two data sets which have a log-linear relationship might have a very strong correlation but still display a poor correlation coefficient. Of course, a coefficient can still be calculated if the log-normal data set, e.g. permeability, is first converted to a linear form by taking the logarithm of the data.

Correlation between datasets (e.g. porosity versus permeability) is typically entered into reservoir modelling packages as a value between 0 and 1, in which values of 0.7 or higher generally indicate a strong relationship. The value is commonly described as the ‘dependency’.

Correlation coefficients reflect the variation of values within a dataset, but say nothing about how those values vary spatially. For reservoir modelling we need to express the spatial variation of parameters, and the central concept controlling this is the *variogram*.

The variogram captures the relationship between the different values between pairs of data points, *and the distance separating those two points*. Numerically, this is expressed as the averaged squared differences between the pairs of data in the data set, given by the empirical

variogram function, which is most simply expressed as:

$$2\gamma = (1/N) \sum (z_i - z_j)^2 \quad (2.4)$$

where:

$z_i$  and  $z_j$  are pairs of points in the dataset

For convenience we generally use the semivariogram function:

$$\gamma = (1/2N) \sum (z_i - z_j)^2 \quad (2.5)$$

The semivariogram function can be calculated for all pairs of points in a data set, whether or not they are regularly spaced, and can therefore be used to describe the relationship between data points from, for example, irregularly scattered wells.

The results of variogram calculations can be represented graphically as a scatterplot (Fig. 2.26a) to establish the relationship between the separation distance (known as the ‘lag’) and the average  $\gamma$  value for pairs of points which are that distance apart. The data is grouped into distance bins to do the averaging; hence only one value appears for any given lag in Fig. 2.26b.

A more formal definition of semi-variance, incorporating the separation distance term, is given by:

$$\gamma(h) = \frac{1}{2} E \{ [Z(x+h) - Z(x)]^2 \} \quad (2.6)$$

where:

$E$  = the expectation (or mean)

$Z(x)$  = the value at a point in space

$Z(x+h)$  = the value at a separation distance,  $h$  (the lag)

Generally,  $\gamma$  increases as a function of separation distance. Where there is some relationship between the values in a spatial dataset,  $\gamma$  shows smaller values for points which are closer together in space, and therefore more likely to

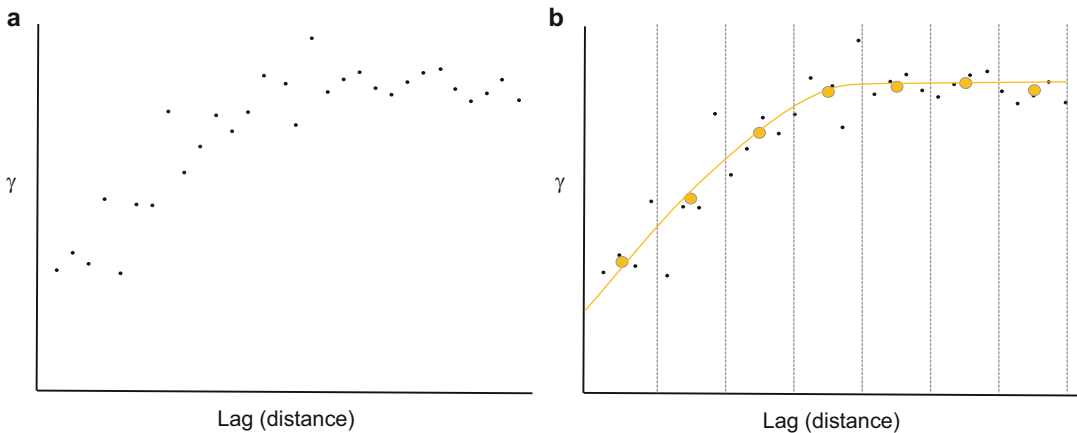


**Fig. 2.26** The variogram: a systematic change in variance between data points with increasing distance between those points; left: the raw  $\gamma$  values plotted versus the lag; right: the data binned, averaged and a line-fit applied

have similar values. As the separation distance increases the difference between the paired samples tends to increase. The variogram thus provides a quantified measure of spatial heterogeneity – ‘spatial correlation’.

The trend line through the points on a semivariogram plot yields the *semivariogram model* (Fig. 2.27) and it is this model which may be used as input to geostatistical packages during parameter modelling.

A semivariogram model has three defining features:

- *the sill*, which is a constant  $\gamma$  value that may be approached for widely-spaced pairs and approximates the variance;
- *the range*, which is the separation distance at which the sill is reached, and
- *the nugget*, which is the extrapolated  $\gamma$  value at zero separation.

Now recall the definition of the sill, from Isaaks and Srivastava (1989), quoted at the start of this section. In simple terms, the sill is the point at which the semivariogram function is equal to the variance, and the key measure for reservoir modelling is the range – the distance at which pairs of data points no longer bear any relationship to each other. A large range means that data points remain correlated over a large area,

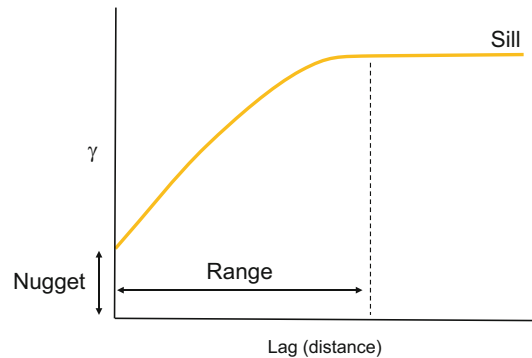


**Fig. 2.27** A semivariogram model for the data in Fig. 2.26 with annotated components

i.e. they are more homogeneously spread; a small range means the parameters are highly variable over short distances i.e. they are heterogeneous on a smaller scale. The presence of a nugget means that although the dataset displays correlation, quite sudden variations between neighbouring points can occur, such as when gold miners come across a nugget, hence the name. The nugget is also related to the sample scale – an indication that there is variation at a scale smaller than the scale of the measurement.

The impact on reservoir models of adjusting the range in a variogram function is illustrated simply in Fig. 2.28. The geostatistical simulation technique itself will be discussed in Sect. 2.7 but

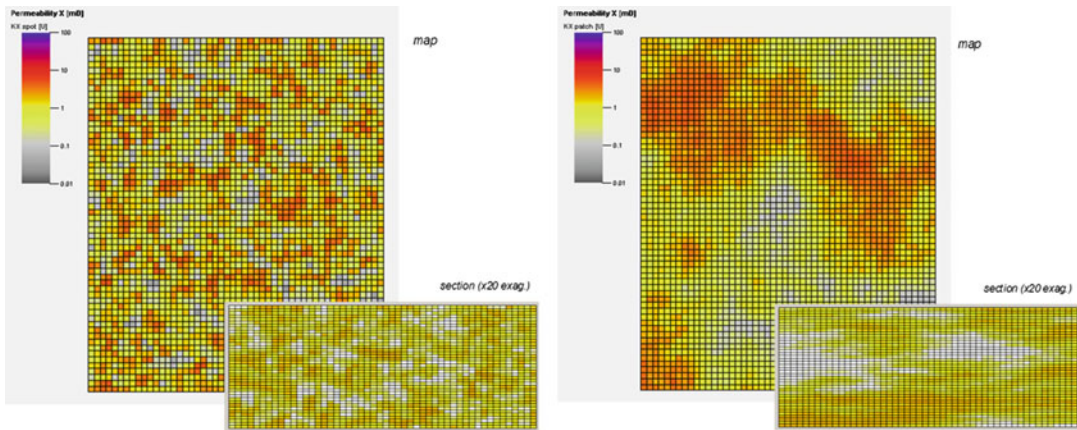


**Fig. 2.28** Contrasting reservoir models built from a common data set, but modelled with different ranges: short range to the left (short length scale heterogeneity); long range to the right (long length scale heterogeneity)

for the moment the connection to make is the link between the variogram range and heterogeneity length scales. Short ranges correspond to short length scale heterogeneities, long ranges to long length scale heterogeneities.

There are several standard functions which can be given to semivariogram models, and which appear as options on reservoir modelling software packages. Six types are illustrated in Fig. 2.29. Three are options present in most modelling packages (spherical, exponential and gaussian); the spherical model is probably the most widely used, and is appropriate for most purposes.

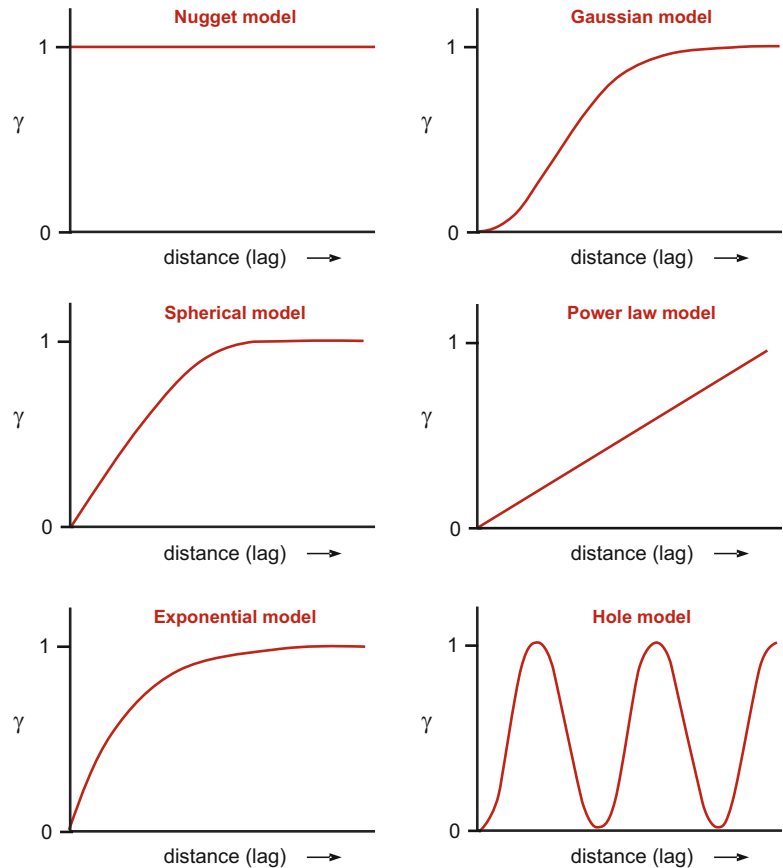
The power law semivariogram describes data sets which continue to get more dissimilar with distance. A simple example would be depth points on a tilted surface or a vertical variogram through a data set with a porosity/depth trend. The power law semivariogram has no sill.

It should also be appreciated that, in general, sedimentary rock systems often display a ‘hole effect’ when data is analysed vertically (Fig. 2.29, lower right). This is a feature of any rock system that shows cyclicity (Jensen et al. 1995), where the  $\gamma$  value decreases as the repeating bedform is encountered. In practice this is generally not required for the vertical definition of layers in a reservoir model, as the layers are usually created deterministically from log data, or introduced using vertical trends (Sect. 2.7).

A final important feature of variograms is that they can vary with direction. The spatial variation represented by the variogram model can be orientated on any geographic axis, N-S, E-W, etc. This has an important application to modelling in sedimentary rocks, where a trend can be estimated based on the depositional environment. For example, reservoir properties may be more strongly correlated along a channel direction, or along the strike of a shoreface. This directional control on spatial correlation leads to anisotropic variograms. Anisotropy is imposed on the reservoir model by indicating the direction of preferred continuity and the strength of the contrast between the maximum and minimum continuity directions, usually represented as an oriented ellipse.

Anisotropic correlation can also occur in the vertical plane, controlled by features such as sedimentary bedding. In most reservoir systems vertical length scales are shorter than horizontal length scales because sedimentary systems tend to be layered. It is generally much easier to calculate vertical variograms directly from subsurface data, because continuous data come from logs in sub-vertical wells. Vertical length scales in layered systems are short, and vertical variograms therefore tend to have short ranges, *often less than that set by default in software packages.*

**Fig. 2.29** Standard semivariogram models, with  $\gamma$  normalised to 1. (Redrawn from Deutsch 2002, © Oxford University Press, by permission of Oxford University Press, USA ([www.oup.com](http://www.oup.com)))



Horizontal variograms are likely to have much longer ranges, and may not reach the sill at the scale of the reservoir model. This is illustrated conceptually in Fig. 2.30, based on work by Deutsch (2002).

As vertical semivariograms can be easier to estimate, one approach for geostatistical analysis is to *measure* the vertical correlation (from well data) and then estimate the likely horizontal semivariogram using a vertical/horizontal anisotropy ratio based on a general knowledge of sedimentary systems. Considerable care should be taken if this is attempted, particularly to ensure that the vertical semivariograms are sampled within distinct (deterministic) zones. Deutsch has estimated ranges of typical anisotropy ratios by sedimentary environment (Table 2.1) and these offer a general guideline.

The figures in Table 2.1 summarise important and useful contrasts but also reflect the residual uncertainty in predicting the range of a horizontal semivariogram model, which is the key parameter required in any model build using variograms. Attempts can be made to derive horizontal semivariograms directly from any data set, but the dataset is only a sample, most likely an imperfect one. This is a particular issue for well data, especially sparse offshore well data, which is generally statistically insufficient for the model purpose. For many datasets, the horizontal variogram is difficult to estimate, and the modeller is therefore often required to choose a variogram model 'believed' to be representative of the system being modelled. *This is the intuitive leap* and it is an intuitive application of geostatistics that we advocate.

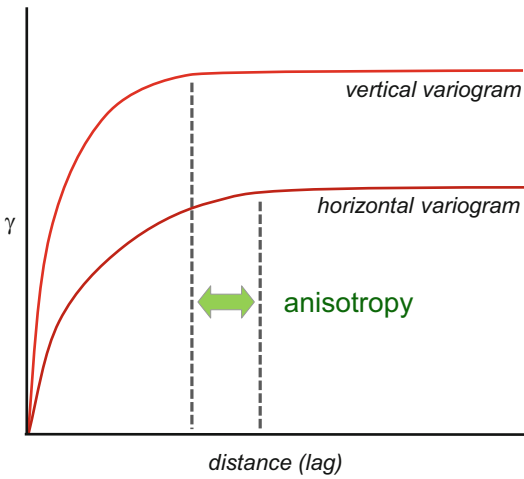


**Fig. 2.30** Horizontal-vertical anisotropy ratio in semivariograms. (Redrawn from Deutsch 2002, © Oxford University Press, by permission of Oxford University Press, USA ([www.oup.com](http://www.oup.com)))

**Table 2.1** Typical ranges in variogram anisotropy ratios

| Element             | Anisotropy ratio |
|---------------------|------------------|
| Point bars          | 10:1–20:1        |
| Braided fluvial     | 20:1–100:1       |
| Aeolian             | 30:1–120:1       |
| Estuarine           | 50:1–150:1       |
| Deepwater           | 80:1–200:1       |
| Deltaic             | 100:1–200:1      |
| Platform carbonates | 200:1–1000:1     |

From Deutsch (2002)

### 2.6.2 Intuitive Geostatistics

In the discussion of key geostatistical principles above we have tried to make the link between geostatistics and the underlying reservoir concepts which should drive modelling. Although this link is difficult to define precisely, an intuitive link can always be made between the variogram and the reservoir architectural concept.

In the discussion below we develop that link using a satellite image adopted as a conceptual analogue for a potential reservoir system. The image is of a wide fluvial channel complex opening out into a tidally-influenced delta. Assuming the analogue is appropriate, we extract the guidance required for the model design by estimating

the variogram range and anisotropy from this image. We assume the image intensity is an indicator for sand, and extract this quantitatively from the image by pixelating the image, converting to a greyscale and treating the greyscale as a proxy for ‘reservoir’. This process is illustrated in Figs. 2.31, 2.32, 2.33, 2.34, 2.35 and 2.36.

This example shows how the semivariogram emerges from quite variable line-to-line transects over the analogue image to give a picture of *average* variance. The overall result suggests pixel ranges of 22 pixels in an E-W direction (Fig. 2.35) and 32 in a N-S direction (Fig. 2.36), reflecting the N-S orientation of the sand system and a 32:22 (1.45:1) horizontal anisotropy ratio.

This example is not intended to suggest that quantitative measures should be derived from satellite images and applied simply to reservoir modelling: there are issues of depositional vs. preserved architecture to consider, and for a sand system such as that illustrated above the system would most likely be broken down into elements which would not necessarily be spatially modelled using variograms alone (see next section).

The example is designed to guide our thinking towards an intuitive connection between the



**Fig. 2.31** Image of a present-day sand system – an analogue for lower coastal plain fluvial systems and tidally-influenced deltas. The Brahmaputra Delta (NASA shuttle image)



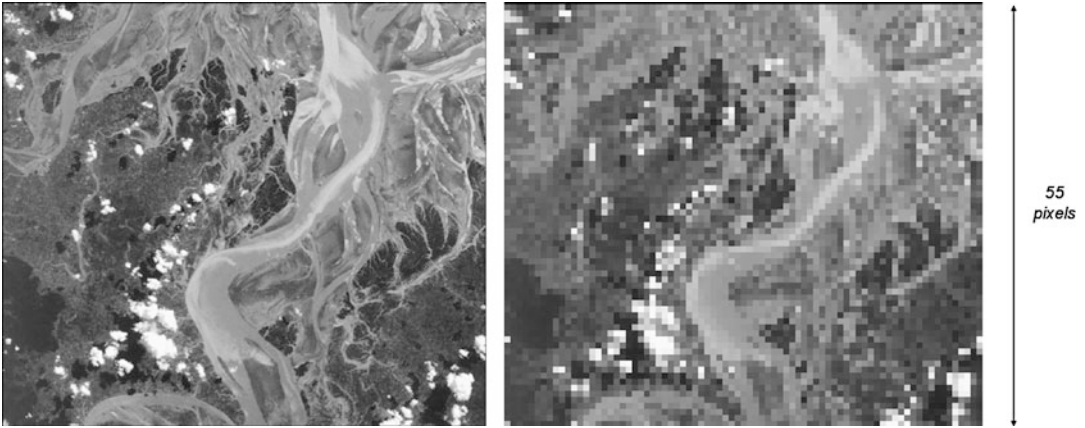


**Fig. 2.32** Figure 2.31 converted to greyscale (*left*), and pixelated (*right*)

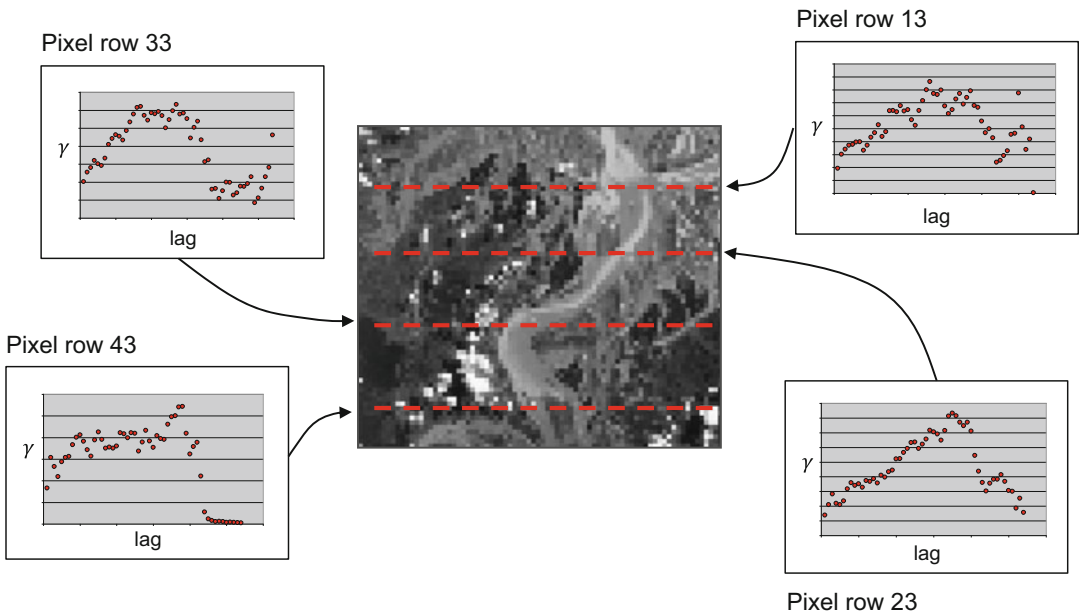


**Fig. 2.33** Semivariograms for pixel pairs on selected E-W transects

variogram (geostatistical variance) and reservoir heterogeneity (our concept of the variation). In particular, the example highlights the role of *averaging* in the construction of variograms. Individual transects over the image vary widely, and there are many parts of the sand system which are not well represented by the final averaged variogram. The variogram is in a sense quite crude and the application of variograms to either rock or property modelling assumes it is

reasonable to convert actual spatial variation to a representative average and then apply this average over a wide area. Using sparse well data as a starting point this is a big assumption, and its validity depends on the architectural concept we have for the reservoir. The concept is not a statistical measure; hence the need to make an intuitive connection between the reservoir concept and the geostatistical tools we use to generate reservoir heterogeneity.

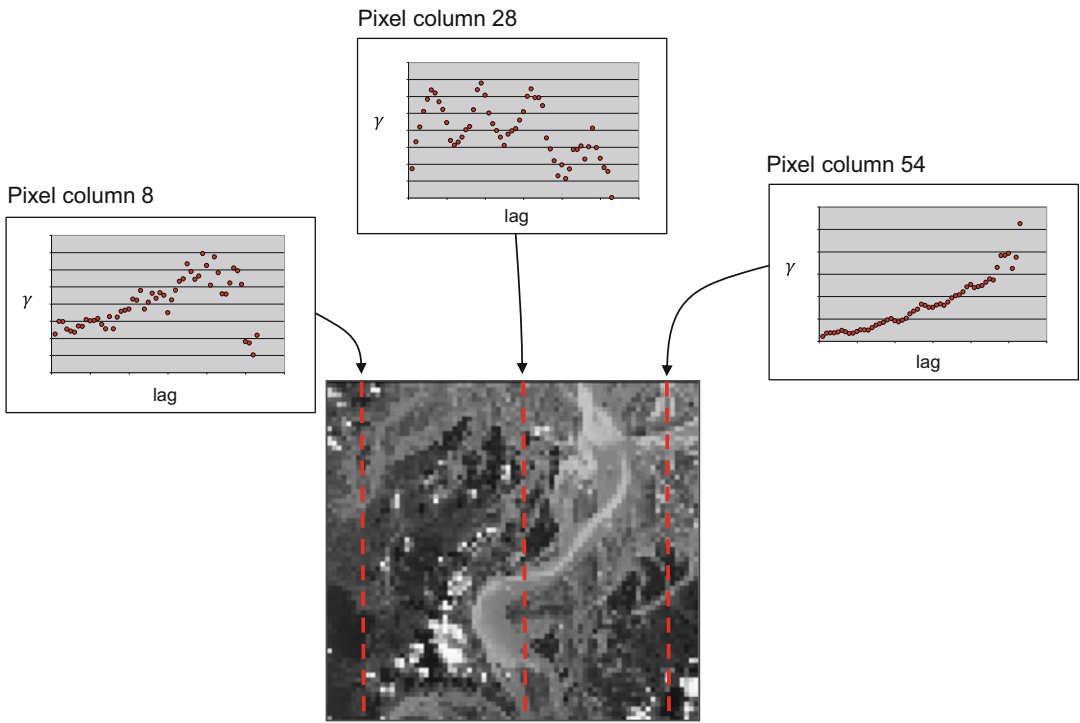


**Fig. 2.34** Semivariograms for pixel pairs on selected N-S transects

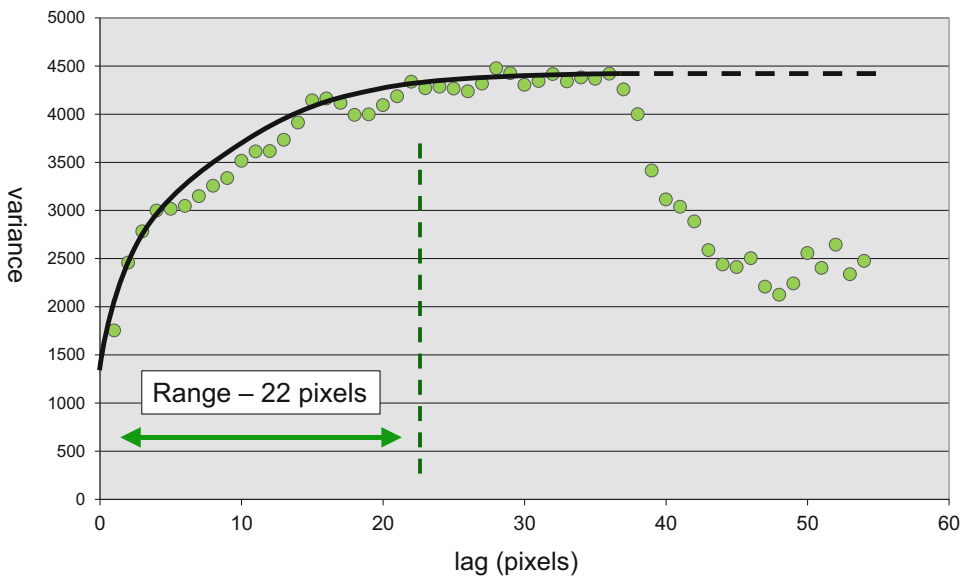


**Fig. 2.35** Semivariogram based on all E-W transects

The intuitive leap in geostatistical reservoir modelling is therefore to repeat this exercise for an analogue of the reservoir being modelled and use the resulting variogram to guide

the geostatistical model, *assuming* the application of an average variogram model is valid. The basic steps are as follows:

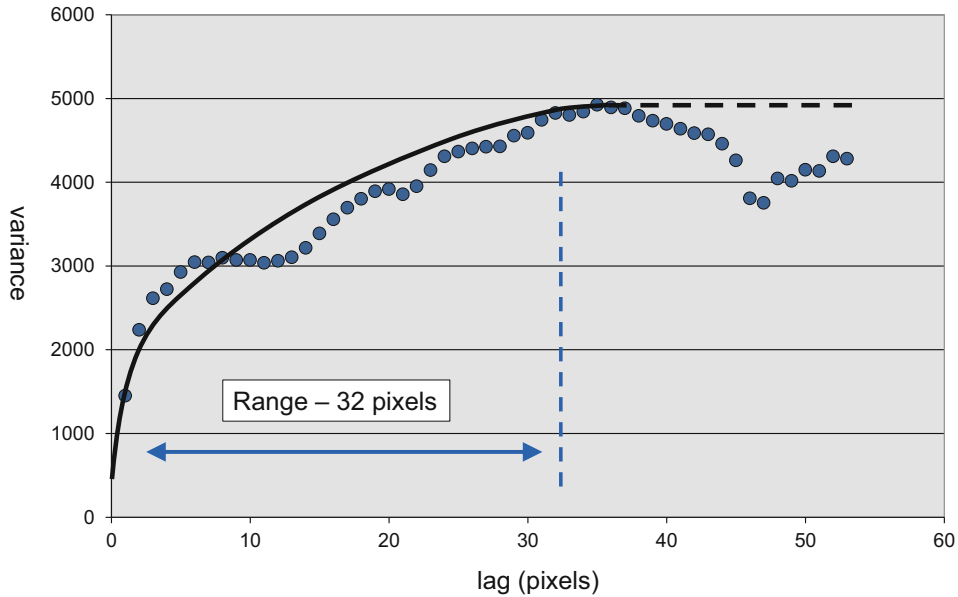


**Fig. 2.36** Semivariogram based on all N-S transects

1. Select (or imagine) an outcrop analogue.
  2. Choose the rock model elements which appropriately characterise the reservoir.
  3. Sketch their spatial distribution (the architectural concept sketch) guided by a suitable analogue dataset.
  4. Estimate appropriate variogram ranges for individual elements (with different variogram ranges for the horizontal and vertical directions).
  5. Estimate the anisotropy in the horizontal plane.
  6. Input these estimates directly to a variogram-based algorithm if pixel-based techniques are selected (see next section).
  7. Carry through the same logic for modelling reservoir properties, if variogram-based algorithms are chosen.
- Highly heterogeneous systems, e.g. glacial clastic systems, should have short ranges and are relatively isotropic in (x, y).
  - Shoreface systems generally have long ranges, at least for their reservoir properties, and the maximum ranges will tend to be along the strike of the system.
  - In high net fluvial systems, local coarse-grained components (if justifiably extracted as model elements) may have very short ranges, often only a nugget effect.
  - In carbonate systems, it needs to be clear whether the heterogeneity is driven by diagenetic or depositional elements, or a blend of both; single-step variography described above may not be sufficient to capture this (see Chap. 6 for suggested solutions).

The approach above offers an intuitive route to the selection of the key input parameters for a geostatistical rock model. The approach is concept-based and deterministically steers the probabilistic algorithm which will populate the 3D grid.

There are some generalities to bear in mind:

- There should be greater variance across the grain of a sedimentary system than along it (represented by the shorter E-W range for the example above).

Often these generalities may not be apparent from a statistical analysis of the well data, but they make intuitive sense. The outcome of an 'intuitive' variogram model should of course be sense-checked for consistency against the well data – any significant discrepancy should prompt a re-evaluation of either the concept or the approach to the handling of the data, e.g. the choice of model elements. However, this intuitive approach to geostatistical reservoir modelling is recommended in preference to simple conditioning of the variogram model to the well data –

which is nearly always statistically unrepresentative.

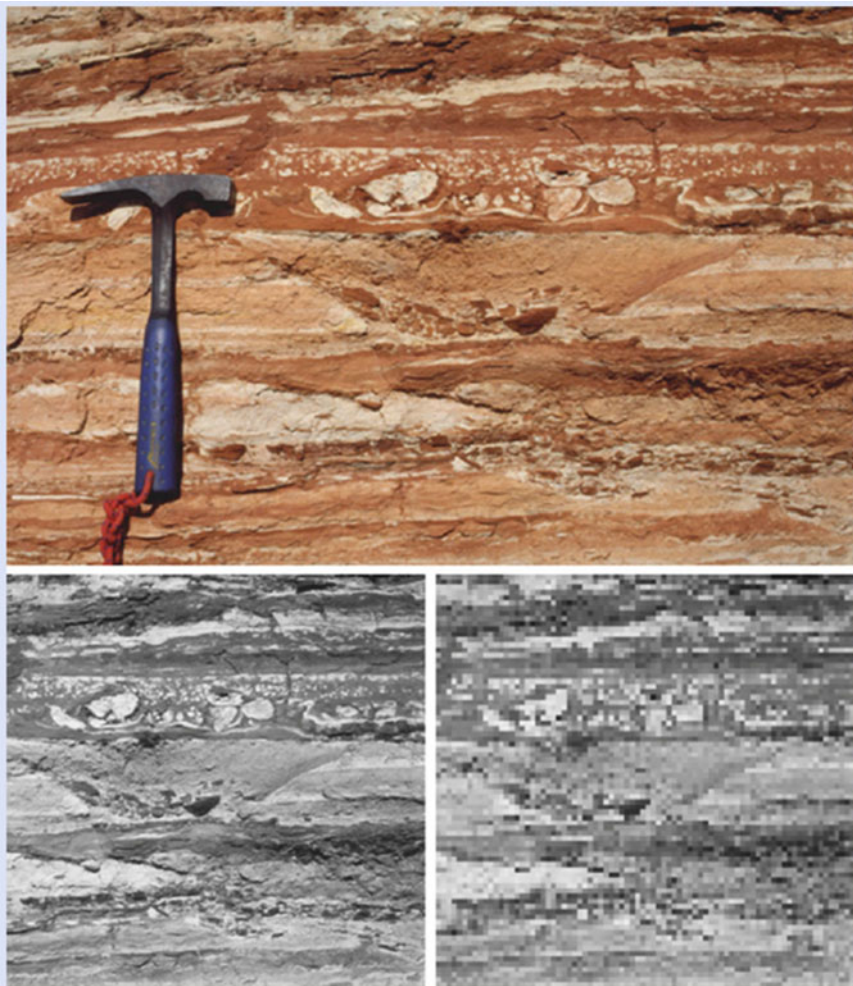
### Exercise 2.1 Estimate Variograms from an Outcrop Image

The image below shows an example photo of bedding structures from an outcrop section of a fluvial sedimentary sequence. Redox reactions (related to paleo-groundwater flows) give a strong visible contrast between high porosity (white) and low porosity (red) pore types. Small scours with lag deposits and soft-sediment deformation features are also present.

Sketch estimated semivariogram functions for the horizontal and vertical directions assuming that colour (grey-scale) indicates rock quality. The hammer head is 10 cm across. Use the grey-scale image and pixelated grey-scale images to guide you.

## 2.7 Algorithm Choice and Control

The preceding sections presented the basis for the design of the rock modelling process:



Grey scale image is  $22.5 \times 22.5$  cm; pixelated grey-scale image is 55 by 55 pixels

1. Form geological concepts and decide whether rock modelling is required;
2. Select the model elements;
3. Set the balance between determinism and probability;
4. Intuitively set parameters to guide the geostatistical modelling process, consistent with the architectural concepts.

The next step is to select an algorithm and decide what controls are required to move beyond the default settings that all software packages offer. Algorithms can be broadly grouped into four:

- *Object modelling*, placing bodies with discrete shapes into 3D space for which another model element, or group of elements, has been defined as the background.
- *Pixel-based methods*, using indicator variograms to create the model architecture by assigning the model element type on a cell-by-cell basis. The indicator variogram is simply a variogram that has been adapted for discrete rather than continuous variables. There are several variants of pixel modelling including Sequential Indicator Simulation (SIS), indicator kriging and various facies trend or facies belt methods which attempt to capture gradational lateral facies changes.

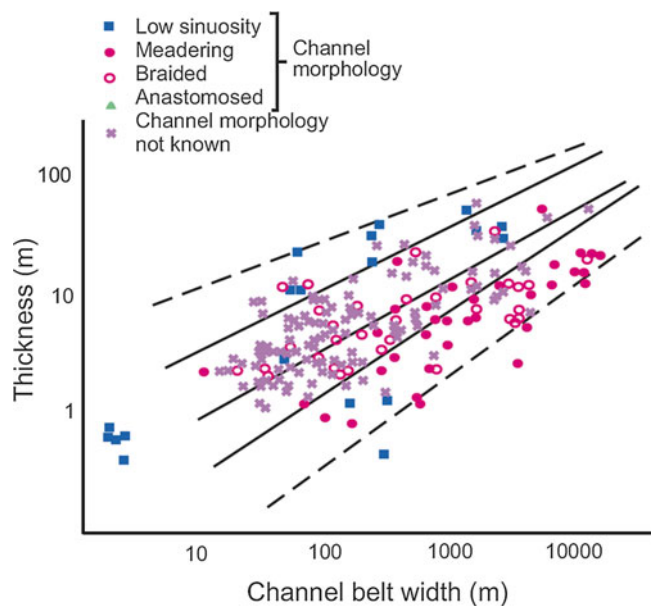
- *Texture-based methods*, using training images to recreate the desired architecture. Although this has been experimented with since the early days of reservoir modelling this has only recently ‘come of age’ through the development of practical multi-point statistical (MPS) algorithms (Strebelle 2002).
- *Process-based methods*, in which an architecture is built up stratigraphically, often using 2D grids to define the upper and lower surfaces of a rock body or layer.

The pros and cons of these algorithms, including some common pitfalls, are explored below.

### 2.7.1 Object Modelling

Object modelling uses various adaptations of the ‘marked point process’ (Holden et al. 1998). A position in the 3D volume, the marked point, is selected at random and a point defined within a modelled 3D body (ellipse, half moon, channel etc.) is attached to that point in space. The main inputs for object modelling are an upscaled element log, a shape template and a set of geometrical parameter distributions such as width, orientation and body thickness, derived from outcrop data (e.g. Fig. 2.37).

**Fig. 2.37** An early example of outcrop-derived data used to define geometries in object models. (Redrawn from Fielding and Crane 1987, © SEPM Society for Sedimentary Geology [1987], reproduced with permission)



The algorithm works by implanting objects with dimensions selected from the prescribed input distributions and then rejecting objects which do not satisfy the well constraints (in statistics, the ‘prior model’). For example, a channel object which is placed in 3D but intersects a well without a channel observed at that location is rejected. This process continues iteratively until a target proportion of each element is achieved, constrained by the expected total volume fraction of the object, e.g. 30% channels. Objects that do not intersect the wells are also simulated if needed to achieve the specified element proportions. However, spatial trends of element abundance or changing body thickness are not automatically honoured because most algorithms assume *stationarity* (no interwell trends). Erosional, or intersection, rules are applied so that an object with highest preservation potential can replace previously simulated objects (Fig. 2.38).

There are issues of concern with object modelling which require user control and awareness of the algorithm limitations. Firstly, it is important to appreciate that the algorithm can generate bodies that cross multiple wells if intervals of the requisite element appear at the right depth intervals in the wells. That is, the algorithm can generate probabilistic correlations without user guidance – something that may or may not be desirable. Some algorithms allow the

user to control multiple well intersections of the same object but this is not commonplace.

Secondly, the distribution of objects at the wells does not influence the distribution of inter-well objects because of the assumption of stationarity in the algorithm. Channel morphologies are particularly hard to control because trend maps only influence the location of the ‘marked point’ for the channel object and not the rest of the body, which generally extends throughout the model.

A key issue with object modelling, therefore, is that things can easily go awry in the inter-well area. Figure 2.39 shows an example of ‘funnelling’, in which the algorithm has found it difficult to position channel bodies without intersecting wells with no channel observations; the channels have therefore been preferentially funnelled into the inter-well area. Again, some intuitive geological sense is required to control and if necessary reject model outcomes. The issue illustrated in Fig. 2.39 can easily be exposed by making a net sand map of the interval and looking for bulls-eyes around the wells.

Thirdly, the element proportions of the final model do *not* necessarily give guidance as to the quality of the model. Many users compare the element (‘facies’) proportions of the model with those seen in the wells as a quantitative check on the result, but matching the well intersections is the main statistical objective of the algorithm so

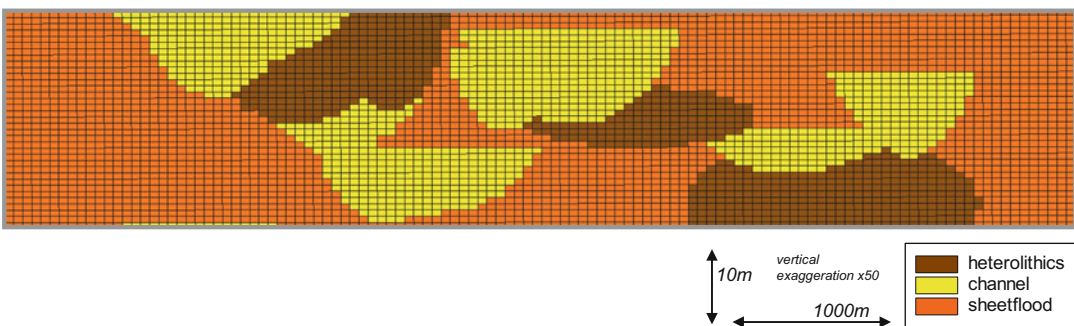
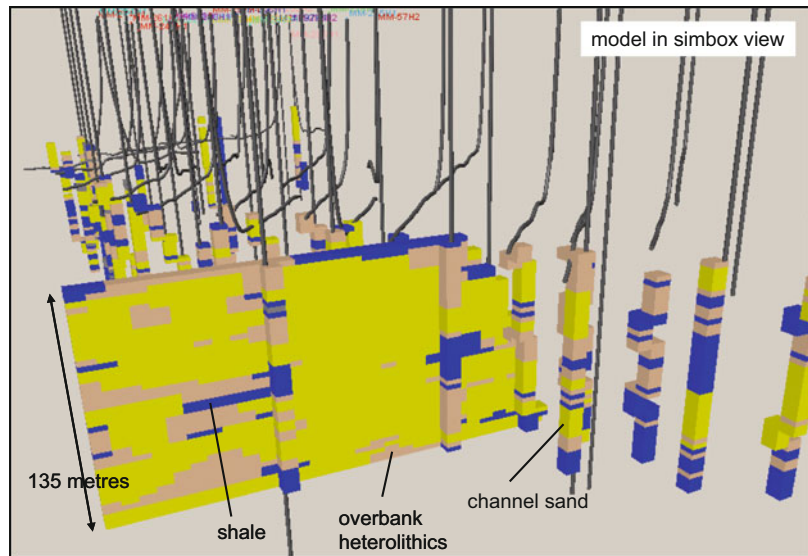


**Fig. 2.38** Cross section through the ‘Moray Field’ model, an outcrop-based model through Triassic fluvial clastics in NE Scotland. Figures 2.38, 2.40, 2.41 and 2.42 follow the

same section line through models which are conditioned to the same well data, with the same choice of elements, differing only in the selection of rock modelling algorithm

**Fig. 2.39** ‘Funnelling’ – over-concentration of objects (channels, yellow) in between wells which have lower concentrations of those objects; a result of inconsistencies between well data, guidance of the model statistics and the model concept (Image courtesy of Simon Smith)



there is a circular logic to this type of QC. The key thing to check is the degree of ‘well match’ *and* the spatial distributions *and* the total element proportions (together). Repeated mismatches or anomalous patterns point to inconsistencies between wells, geometries and element proportions.

Moreover, it is highly unlikely that the element proportions seen in the wells truly represent the distribution in the subsurface as the wells dramatically under-sample the reservoir. It is always useful to check the model element distributions against the well proportions, and the differences should be explained, but differences should be *expected*. The ‘right’ element proportion is the one which matches the underlying concept.

The following list of observations and tips provides a useful checklist for compiling body geometries in object modelling:

1. Do not rely on the default geometries.
2. Recall that thickness distributions have to be customised for the reservoir. Depending on the software package in use, the upscaled facies parameter can be based on the *measured* thickness from deviated wells – not necessarily the stratigraphic thicknesses.
3. Spend some time customising the datasets and collating your own data from analogues. There are a number of excellent data sources available to support this; they do not provide instant answers but do give good guidance on realistic *preserved* body geometries.
4. The obvious object shape to select for a given element is not always the best one to use. Channels are a good example of this, as the architecture of a channel belt is sometimes better constructed using ellipse- or crescent-shaped objects rather than channel objects *per se*, which are often more representative of the shape of the rivers that formed the channel belts, rather than the preserved belt geometries of nested barforms. Also, these body shapes are less extensive than the channel shapes, rarely go all the way through a model area and so reflect the trend map inputs more closely and are less prone to the ‘bull’s eye’ effect.
5. There may be large differences between the geometry of a modern feature and that preserved in the rock record. The example above of channels is a case in point; carbonate reservoirs offer a more extreme example as any original depositional architecture may have been completely overprinted by subsequent diagenetic effects. Differential compaction effects (sands vs. muds and coals) may also change the vertical geometry of the original sediment body.
6. It is important to distinguish *uncertainty* from *variability*. Uncertainty about the most

appropriate analogue may result in a wide spread of geometrical options. It is incorrect, however, to combine different analogue datasets and so create spuriously large amounts of variation. It is better to make two scenarios using different data sets and then quantify the differences between them.

7. Get as much information as possible from the well and seismic data sets. Do well correlations constrain the geometries that can be used? Is there useful information in the seismic?
8. We will never know what geometries are correct. The best we can do is to use our conceptual models of the reservoir to select a series of different analogues that span a plausible range of geological uncertainty and quantify the impact. This is pursued further in Chap. 5.

### 2.7.2 Pixel-Based Modelling

Pixel-based modelling is a fundamentally different approach, based on assigning properties using geostatistical algorithms on a cell-by-cell basis, rather than by implanting objects in 3D. It can be achieved using a number of algorithms, the commonest of which are summarised below.

*Kriging* is the most basic form of interpolation used in geostatistics, developed by the French mathematician Georges Matheron and his student Daniel Krige (Matheron 1963). The technique is applicable to property modelling (next section) but rock models can also be made using an adaptation of the algorithm called *Indicator Kriging*.

The kriging algorithm attempts to minimise the estimation error at each point in the model grid. This means the most likely element at each location is estimated using the well data and the variogram model – there is no random sampling. Models made with indicator kriging typically show smooth trends away from the wells, and the wells themselves are often highly visible as ‘bulls-eyes’, especially in very sparse data sets. These models will have different element proportions to the wells because the algorithm does not attempt to match those proportions to the frequency distribution at the wells. Indicator kriging can be useful for capturing lateral trends *if* these are well represented in the well data set, and if a high degree of correlation between wells is desired.

In general, it is a poor method for representing reservoir heterogeneity because the lateral heterogeneity in the resulting model is too heavily influenced by the well spacing. For fields with dense, regularly-spaced wells and relatively long correlation lengths in the parameter being modelled, it may still be useful.

Figure 2.40 shows an example of indicator Kriging applied to the Moray data set – it is first and foremost an interpolation tool.

*Sequential Gaussian Simulation* (SGS) is most commonly used for modelling continuous petrophysical properties (Sect. 3.4), but one variant, *Sequential Indicator Simulation* (SIS), is quite commonly used for rock modelling (Journel and Alabert 1990). SIS builds on the underlying geostatistical method of kriging, but then introduces heterogeneity using a sequential stochastic method to draw Gaussian realisations

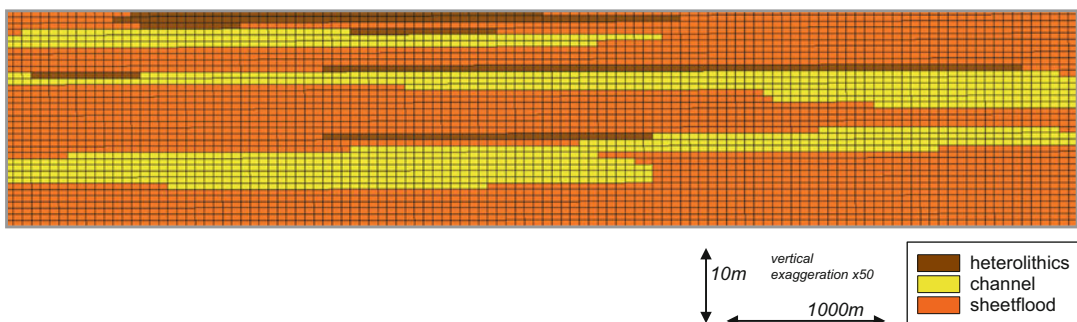


**Fig. 2.40** Rock modelling using indicator kriging



using an indicator transform. The indicator is used to transform a continuous distribution to a discrete distribution (e.g. element 1 vs. element 2).

When applied to rock modelling, SIS will generally assume the reservoir shows no lateral or vertical trends of element distribution – the principle of stationarity again – although trends can be superimposed on the simulation (see the important comment on trends at the end of this section).

Models built with SIS should, by definition, honour the input element proportions from wells, and each geostatistical realisation will differ when different random seeds are used. Only when large ranges or trends are introduced will an SIS model realisation differ statistically from the input well data.

The main limitation with such pixel-based methods is that it is difficult to build architectures with well-defined margins and discrete shapes because the geostatistical algorithms tend to create smoothly-varying fields (e.g. Fig. 2.41). Pixel-based methods tend to generate models with limited linear trends, controlled instead by the principal axes of the variogram. Where the rock units have discrete, well-defined geometries or they have a range of orientations (e.g. radial patterns), object-based methods are preferable to SIS.

SIS is useful where the reservoir elements do not have discrete geometries either because they have irregular shapes or variable sizes. SIS also gives good models in reservoirs with many closely-spaced wells and many well-to-well correlations. The method is more robust than object modelling for handling complex well-

conditioning cases and the funnelling effect is avoided. The method also avoids the bulls-eyes around wells which are common in indicator kriging.

The algorithm can be used to create correlations by adjusting the variogram range to be greater than the well spacing. In the example in Fig. 2.42, correlated shales (shown in blue) have been modelled using SIS. These correlations contain a probabilistic component, will vary from realisation to realisation and will not necessarily create 100% presence of the modelled element between wells. Depending on the underlying concept, this may be desirable.

When using the SIS method as commonly applied in commercial packages, we need to be aware of the following:

1. Reservoir data is generally statistically insufficient and rarely enough to derive meaningful experimental variograms. This means that the variogram used in the SIS modelling must be derived by intuitive reasoning (see previous section).
2. The range of the variogram is not the same as the element body size. The range is related to the *maximum* body size, and actual simulated bodies can have sizes anywhere along the slope of the variogram function. The range should therefore *always* be set larger than your expected average body size, as a rule of thumb – twice the size.
3. The choice of the type of kriging used to start the process off can have a big effect. For *simple kriging* a universal mean is used and

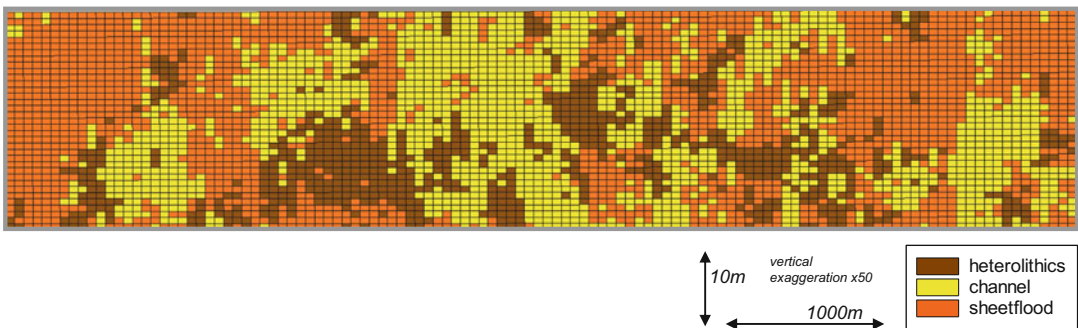
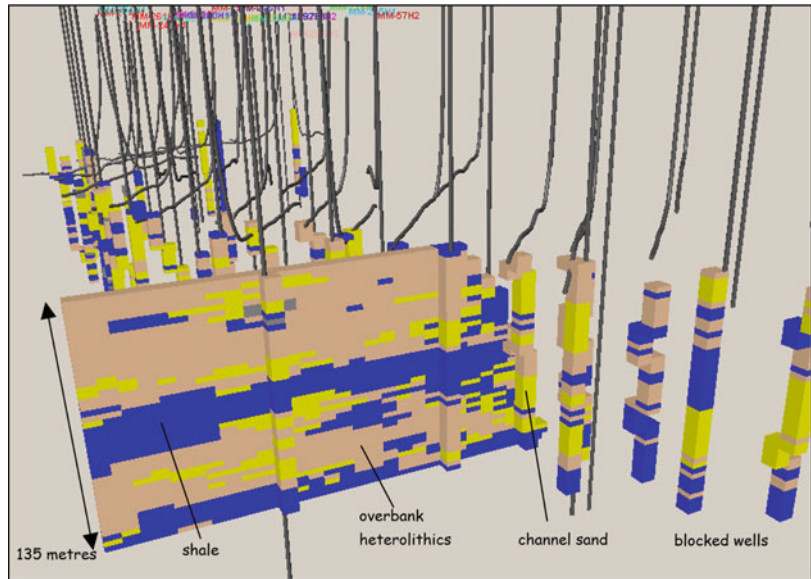


**Fig. 2.41** Rock modelling using SIS

**Fig. 2.42** Creating correlatable shale bodies (shown in *blue*) in a fluvial system using SIS (Image courtesy of Simon Smith)



the algorithm assumes stationarity. For *ordinary kriging* the mean is estimated locally throughout the model, and consequently allows lateral trends to be captured. Ordinary kriging works well with large numbers of wells and well-defined trends, but can produce unusual results with small data sets.

4. Some packages allow the user to specify local azimuths for the variogram. This information can come from the underlying architectural concept and can be a useful way of avoiding the regular linear striping which is typical for indicator models, especially those conditioned to only a small number of wells.
5. Variograms make *average* statements about spatial correlation in a given direction. This places a limit on the textures that can be modelled; variogram modelling is often described as a two-point process. The impact of this simplification is illustrated in Fig. 2.43, in which the image from Sect. 2.6.2 is revisited. In that case, the exhaustive, true dataset was available and a variogram analysis of that data yielded length scales (variogram ranges) and a horizontal anisotropy ratio of 1.45:1. Yet if those same ranges and ratio are fed back into an SIS run the channelised image does not reappear (Fig. 2.43, left-hand image).

Instinctively, the anisotropy should be more pronounced, perhaps 10:1, but feeding this ratio through an SIS run will also not reproduce the original (Fig. 2.43, right-hand image). In short: the SIS algorithm is robust but has limitations; an alternative is required *if* the desire is to reproduce an model similar to the centre image in Fig. 2.43.

The *facies trend simulation* algorithm is a modified version of SIS which attempts to honour a logical lateral arrangement of elements, for example, an upper shoreface passing laterally into a lower shoreface and then into mudstone.

Figure 2.44 shows an example applied to the Moray data set. The facies trend approach, because it uses SIS, gives a more heterogeneous pattern than indicator kriging and does not suffer from the problem of well bulls-eyes. The latter is because the well data is honoured at the well position, but not necessarily in the area local to the well.

The user can specify stacking patterns, directions, angles and the degree of inter-fingering. The approach can be useful, but it is often very hard to get the desired inter-fingering throughout the model. The best applications tend to be shoreface environments where the logical

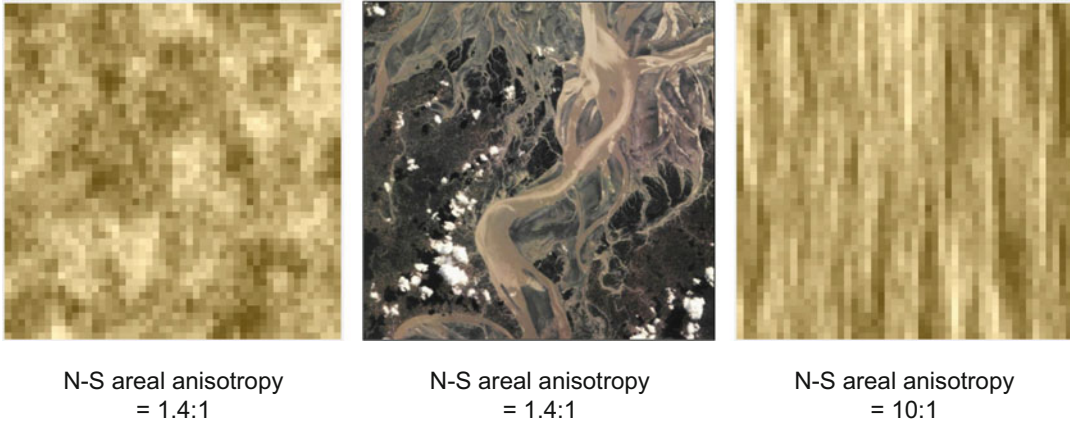


**Fig. 2.43** Attempts to recreate a complex image using SIS. Centre: the original image; left: an SIS realisation based on the measured spatial correlation and *average*

anisotropy in the centre image; right: an alternative run with increased anisotropy. The complexity of the image is beyond the reach of a standard variogram workflow

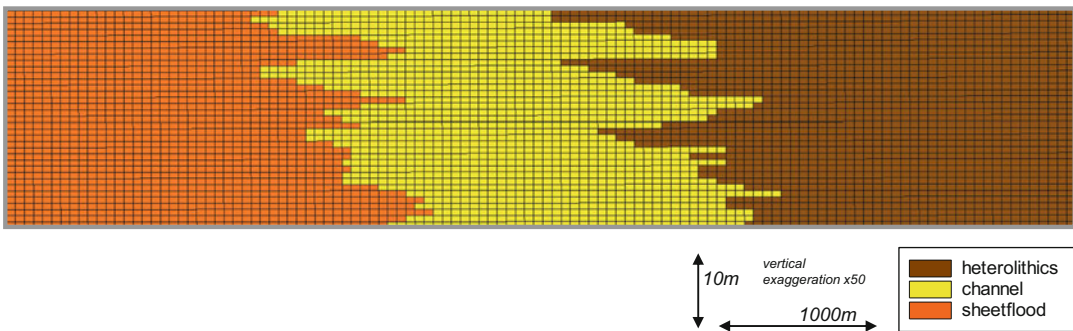


**Fig. 2.44** Rock modelling using facies trend simulation

sequence of elements, upper to lower shoreface, transition on a large scale. Similar modelling effects can also be achieved by the manual application of trends (see below).

### 2.7.3 Texture-Based Modelling

An alternative approach to the averaging of variography is the emergence of algorithms which aim to honour texture directly. Although there are parallels with very early techniques such as simulated annealing (Yarus and Chambers 1994, Chapter 1 by Srivistava) the approach has become more widely available through the multi-

point statistics (MPS) technique (Strebelle 2002; Caers 2003).

The approach starts with a pre-existing training image, a cellular model or a scanned image, which is analysed for textural content. Using a geometric template, the frequency of instances of a model element occurring next to similar and different elements are recorded, as is their relative position (to the west, the east, diagonally etc.). As the cellular model framework is sequentially filled, the record of textural content in the training image is referred to in order to determine the likelihood of a particular cell having a particular model content, given the content of the surrounding cells (Fig. 2.45).

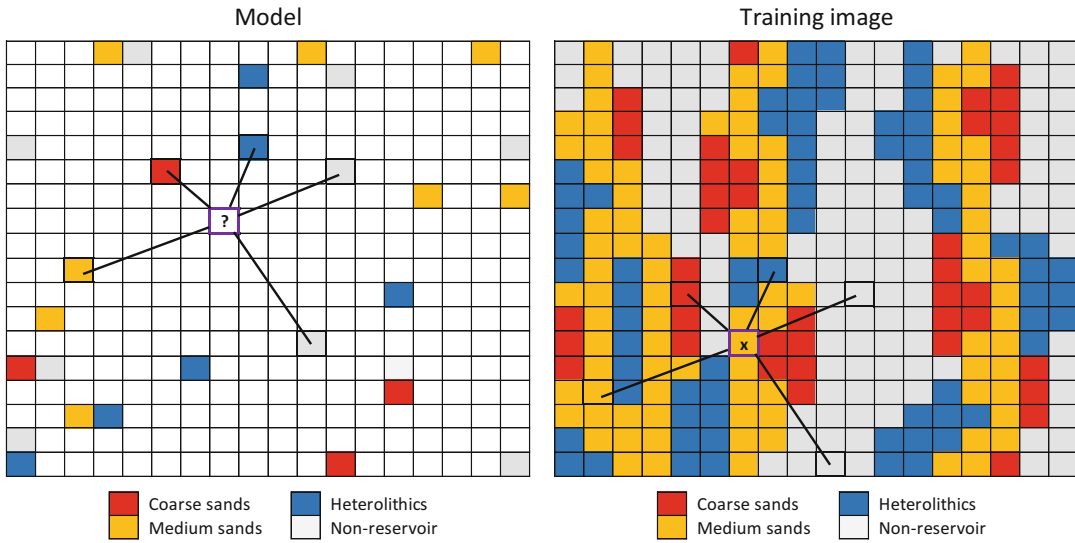


**Fig. 2.45** The Multi-Point Statistics (MPS) approach to rock modelling

Although the approach is pixel-based, the key step forward is the emphasis on potentially complex texture rather than relatively simple ‘two-point’ statistics of variography. The prime limitation of variogram-based approaches – the need to derive simple rules for *average* spatial correlation – is therefore surmounted by modelling instead an *average texture*.

An example is shown in Fig. 2.46 – a cross-sectional model based on a sketch of a single bed in a dryland river system. The sketch was hand-drawn, drafted neatly, scanned and input to an MPS algorithm resulting in the digital model illustrated.

MPS is arguably the most desirable algorithm for building 3D reservoir architectures because architecture itself is a heterogeneous textural feature and MPS is designed to model these textures directly. In spite of this there are two reasons why MPS is not necessarily the algorithm of choice:

1. A training image is required, and this is a 3D architectural interpretation in itself. MPS models are therefore not as ‘instantaneous’ as the simpler pixel-based techniques such as SIS, and require more pre-work. The Moray Field example shown in Fig. 2.47 was built using a training data set which was itself extracted from a model combining object-

- and SIS-based architectural elements. The MPS algorithm does not ‘work alone.’
2. The additional effort of generating and checking a training image may not be required in order to generate the desired architecture; 2-point geostatistics or object modelling may be sufficient.

Despite the above, the technique can provide very realistic-looking architectures which overcome both the simplistic textures of older pixel-based techniques and the simplistic shapes and sometimes unrealistic architectures produced by object modelling.

### 2.7.4 Algorithms Compared

A comparison of the techniques above is shown in Fig. 2.48. These are the same images shown in Figs. 2.38, 2.40, 2.41, 2.44 and 2.47 but now placed together and shown with less vertical exaggeration. All models are based on the same underlying data set and all are architectural arrangements of the same three elements of an ephemeral braided fluvial system from the ‘Moray Field’ training set.

There is no technical error in the construction of the models in Fig. 2.48 and each would pass a

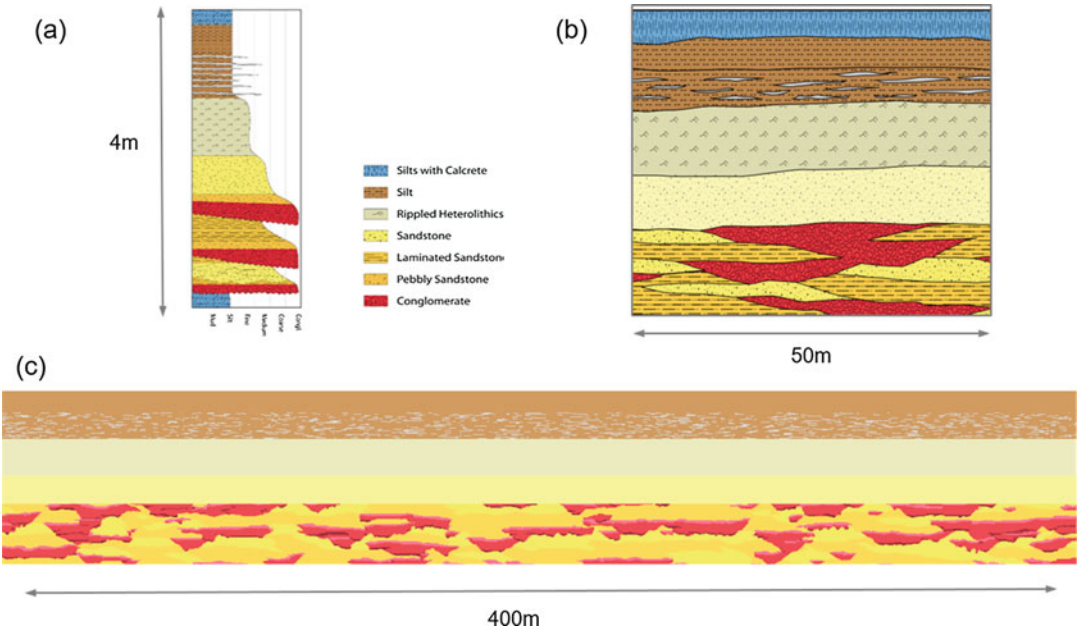


**Fig. 2.46** MPS model based on a sketch of a bed in a dryland fluvial system: (a) graphic log through a type section of the bed; (b) conceptual sketch of the arrangement of elements within the bed over 50 m used as a training image; (c) MPS realization of the bed over 400 m based on the training image (model courtesy of Tom Buckle and Rhona Hutton)

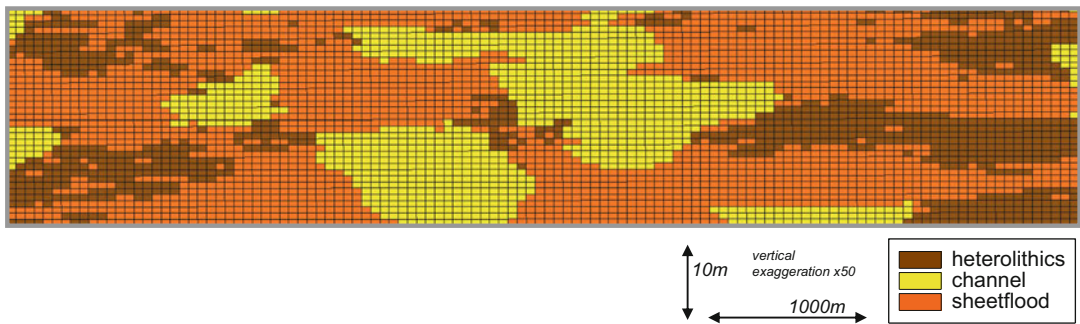


**Fig. 2.47** Rock modelling using MPS

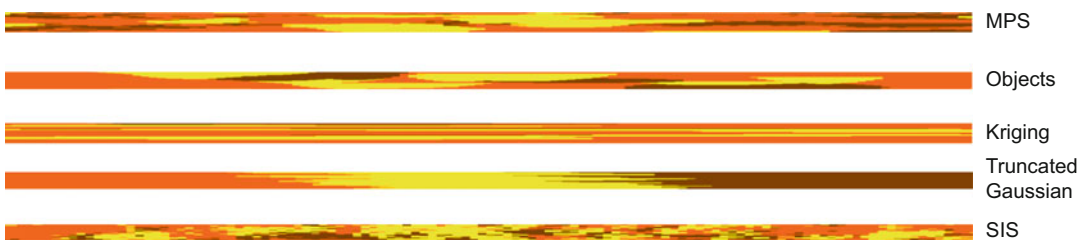


**Fig. 2.48** True-scale comparison of five techniques applied to the Moray Field outcrop-based model

statistical QC, yet the images are clearly very different and subsequent flow modelling would yield very different results.

Which is correct? We argue, it is the one which best matches the underlying conceptual interpretation drawn before the modelling began – the sketch.

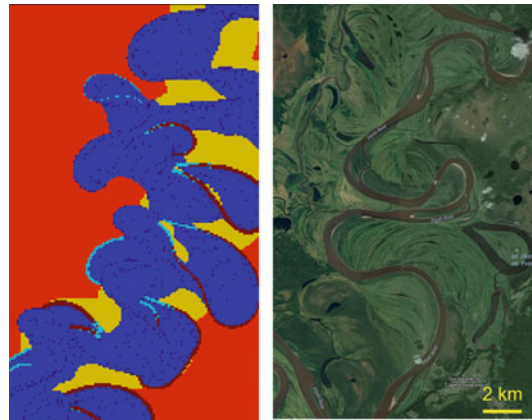
### 2.7.5 Process-Based Modelling

The section above compared modelling algorithms widely available in software packages used in the E&P industry. There are another approaches, however, and these can be considered for use in addition to the standard workflow if the approaches above fail to produce the desired architectures.

Figure 2.49 shows the model outcome from a process-based model for a meandering fluvial system. The image is a map view of a 3D model built stratigraphically with the modelling algorithm depositing layers guided by process sedimentological parameters. These parameters can be varied to produce different architectures, as shown in Fig. 2.50 which compares variations in aggradation rate with preserved net sand volumes. The process can be tuned not only to understand key ‘tipping’ points for architectural connectivity but also to provide a range of architectures for forward-modelling.

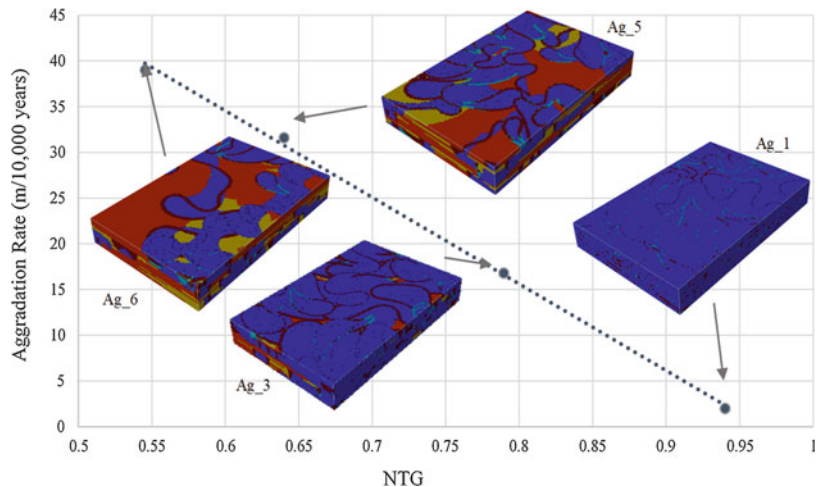
Models such as that in Figs. 2.49 and 2.50 can be used to provide a template for modelling in standard software packages. This can be done by using the models as training images for MPS or, as in the case in Figs. 2.51 and 2.52 mapping the process model grid onto a standard 3D modelling grid for onward property modelling (Da Pra et al. 2017).

Process models can become extremely elaborate as more realistic parameters are introduced to the algorithm. The example in Fig. 2.53 is a 3D process model mimicking the evolution of the Nile Delta which was generated by solving



**Fig. 2.49** Map view of a process-based fluvial model (left), mimicking a meandering fluvial system (right). Image courtesy of Tom Buckle

**Fig. 2.50** Four process-based model versions of Fig. 2.49, exploring the relationship between aggradation rate and net-to-gross (NTG). Image courtesy of Tom Buckle



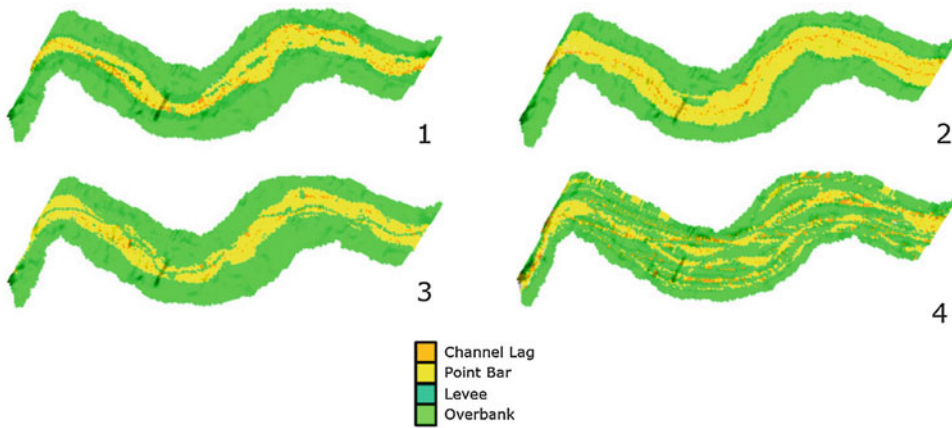


**Fig. 2.51** Process-based models for a fluvial system; four contrasting map views of the models (Da Pra et al. 2017). Image reproduced courtesy of the EAGE

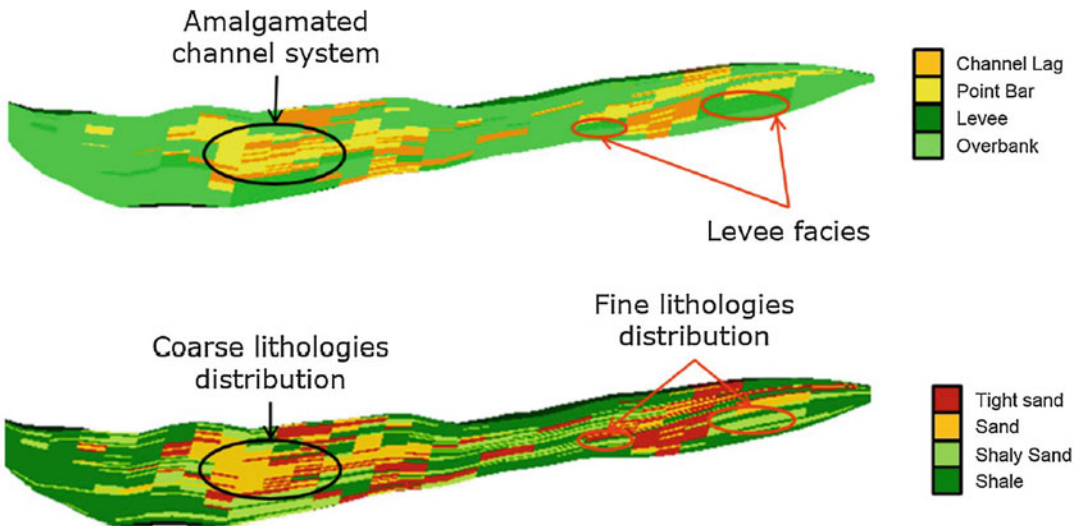


**Fig. 2.52** Cross-sections through the fluvial model after translating the process-based model onto a standard modelling grid (upper image) and infilling with the desired

reservoir elements (lower image), (Da Pra et al. 2017). Image reproduced courtesy of the EAGE

interactions between bathymetry, hydrodynamics and sediment transport. These are complex models which do not go forward simply into a fluid flow simulation. The models are primarily aiming to create realistic architectures, including distribution of sediment bodies and grain size variations within them, which can then be used as training images for rock modelling (Aarnes et al. 2019).

## 2.7.6 The Importance of Deterministic Trends

All of the algorithms above involve a probabilistic component. In Sect. 2.5 the balance between determinism and probability was discussed and it was proposed that strong deterministic control is generally required to realise the desired architectural concept.

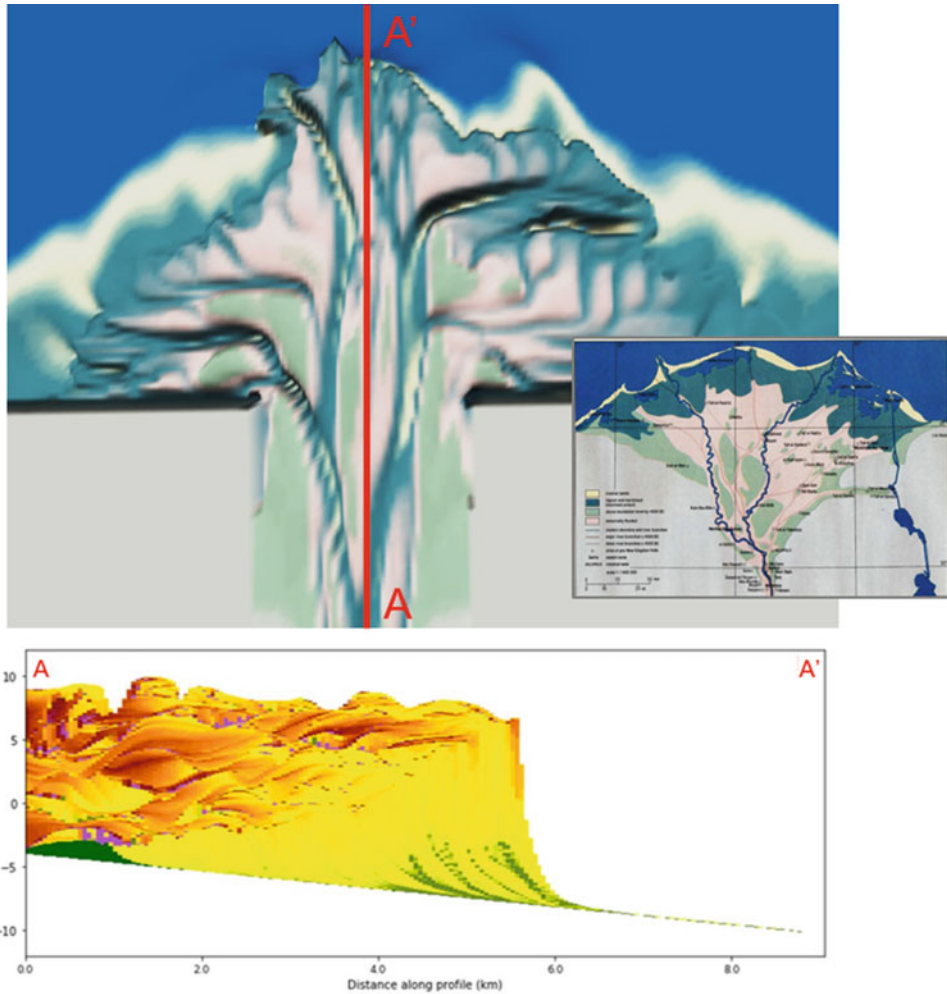


**Fig. 2.53** Plan view of a process-based model of the Nile Delta. Generated by solving interaction between bathymetry, hydrodynamics and sediment transport. Image reproduced courtesy of TUDelft

Having discussed the pros and cons of the algorithms, the final consideration is therefore how to overlay deterministic control. In statistical terms, this is about overcoming the *stationarity* that probabilistic algorithms assume as a default. Stationarity is a prerequisite for the algorithms and assumes that elements are randomly but homogeneously distributed in the inter-well space. This is at odds with geological systems, in which elements are heterogeneously distributed and show significant non-stationarity: they are commonly clustered and show patterns in their distribution. Non-stationarity is the

geological norm, indeed, *Walther's Law* – the principle that vertical sequences can be used to predict lateral sequences – is a statement of non-stationarity.

Deterministic trends are therefore *required*, whether to build a model using object- or pixel-based techniques, or to build a training image for a texture-based technique.

### 2.7.6.1 Vertical Trends

Sedimentary systems typically show vertical organisation of elements which can be observed in core and on logs and examined quantitatively



in the data-handling areas of modelling packages. Any such vertical trends are typically switched *off* by default – the assumption of stationarity.

As a first assumption, observed trends in the form of vertical probability curves should be switched *on*, unless there are compelling reasons not to use them. More significantly, these trends can be manually adjusted to help realise an architectural concept perhaps only partly captured in the raw well data.

Figure 2.54 shows an edited vertical element distribution which represents a concept of a depositional system becoming sand-prone upwards. This is a simple pattern, common in sedimentary sequences, but will not be integrated in the modelling process by default.

Thought is required when adjusting these profiles because the model is being consciously steered away from the statistics of the well data. Unless the well data is a perfect statistical sample of the reservoir (rarely the case and never provable) this is not a problem, but the modeller should be aware that hydrocarbon volumes are

effectively being adjusted up and down away from well control. The adjustments therefore require justification which comes, as ever, from the underlying conceptual model.

### 2.7.6.2 Horizontal Trends

Horizontal trends are most simply introduced as 2D maps which can be applied to a given interval. Figure 2.55 shows the application of a sand trend map to a low net-to-gross system following the steps below:

1. Sand elements are identified in wells based on core and log interpretation.
2. A net-to-gross (sand) value is extracted at each well and gridded in 2D to produce a map illustrating any sand trend apparent from well data alone.
3. The 2D map is hand-edited to represent the desired concept, with most attention being paid to the most poorly sampled areas (in the example shown, the trend grid is also

**Fig. 2.54** Vertical probability trends; each colour represents a different reservoir element and the probability represents the likelihood of that element occurring at that point in the cell stratigraphy (blue = mudstone; yellow = sandstone)

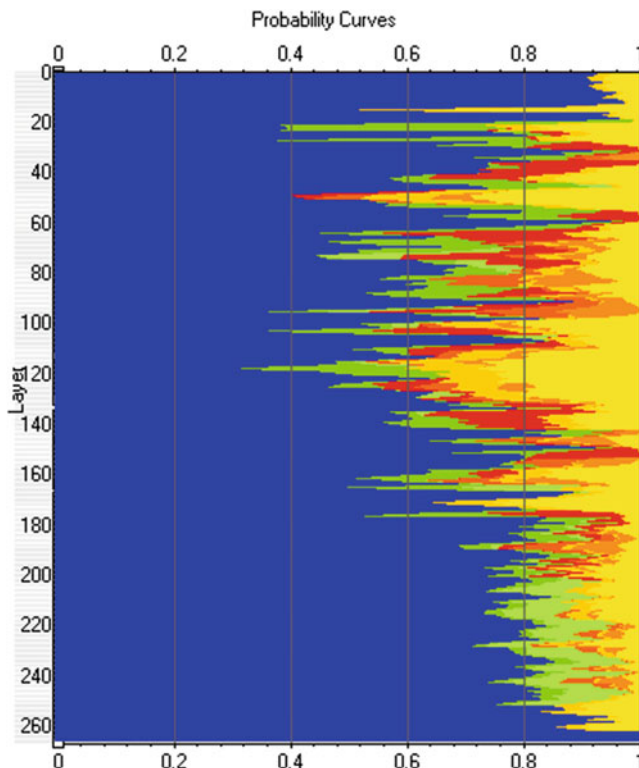
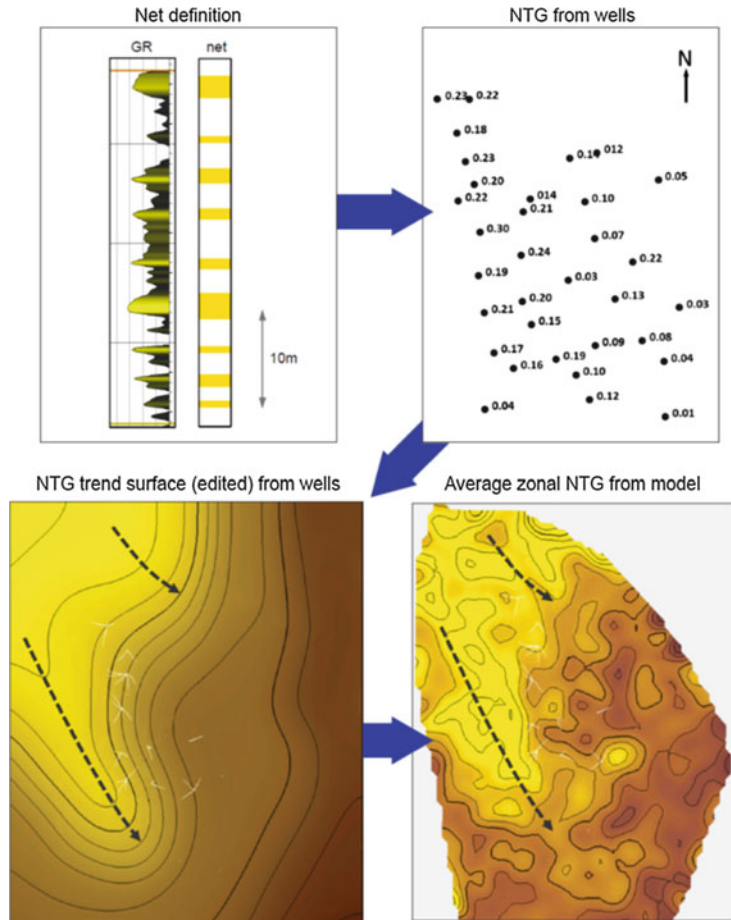


**Fig. 2.55** Deterministic application of a horizontal trend



smoothed – the level of detail in the trend map should match the scale of the sand distribution concept).

4. The trend map is input to, in this case, an SIS algorithm for rock modelling.
5. As a check, the interval average net-to-gross is backed-out of the model as a map and compared with the concept. The map shows more heterogeneity because the variogram ranges have been set low and the model has been tied to the actual well observations; the desired deterministic trends, however, clearly control the overall pattern.

The influence of the trend on the model is profound in this case as the concept is for the sand system to finger eastwards into a poorly drilled, mud-dominated environment. The fluid volumes in the trended case are *half* that calculated

for a model with the trends removed, with all other model variables unchanged. Stationarity is overcome and the concept dominates the modelling.

The source of the trend can be an extension of the underlying data, as in the example above, or a less data-independent concept based on a regional model, or a trend surface derived from seismic attributes – the ‘soft conditioning’ described in Sect. 2.5.

### 2.7.6.3 3D Probability Volumes

The 3D architecture can be directly conditioned using a 3D volume – a natural extension of the process above. The conditioning volume can be built in a modelling exercise as a combination of the horizontal/vertical trends described above, or derived from a 3D data source, typically a seismic volume.

Seismic conditioning directly in 3D creates some issues:

1. The volume needs QC. It is generally easier to check simpler data elements, so if the desired trends are separately captured in 2D trend surfaces and vertical proportion curves then combination into a 3D trend volume is not necessary.
2. If conditioning to a 3D seismic volume, the resolution of the model framework needs to be consistent with the intervals the seismic attribute is derived from. For example, if the parameter being conditioned is the sand content within a 25 m thick interval, it must be assumed that the seismic data from which the seismic attribute is derived is also coming from that 25 m interval. This is unlikely to be the case from a simple amplitude extraction and a better approach is to condition from inverted seismic data. The questions to ask are therefore what the seismic inversion process was inverting for (was it indeed the sand content) and was the earth model used for the inversion the same one as the reservoir model is being built on?
3. If the criteria for using 3D seismic data (2, above) are met, can a probabilistic seismic inversion be called upon? This is the ideal input to condition to.
4. If the criteria in point 2, above, are not met, the seismic can still be used for soft conditioning, but will be more artefact-free and easier to QC if applied as a 2D trend. The noisier the data, the softer the conditioning will need to be, i.e. the lower the correlation coefficient.

### 2.7.7 Alternative Rock Modelling Methods – A Comparison

An example is given below, to which alternative algorithms have been applied. The case is taken from a fluvio-deltaic reservoir – the Franken Field – based on a type log with a well-defined conceptual geological model (Fig. 2.56). The main reservoir is the Shelley, which divides into a clearly fluvial Lower Shelley characterised by sheetfloods, and an Upper Shelley, the

sedimentology for which is less clear and can be viewed as either a lower coastal plain or a river-dominated delta.

Rock model realisations have been built from element distributions in 19 wells. Cross-sections taken at the same location through the models are illustrated in Figs. 2.57, 2.58 and 2.59 for a 2-, 4- and 7-interval correlation, respectively. The examples within each layering scheme explore object vs. pixel (SIS) modelling and the default model criteria (stationarity maintained) vs. the use of deterministic trends (stationarity overwritten).

The models contrast greatly and the following observations can be made:

1. The more heavily subdivided models are naturally more ‘stripy’. This is partly due to the ‘binning’ of element well picks into zones, which starts to break down stationarity by picking up any systematic vertical organisation of the elements, irrespective of the algorithm chosen and without separate application of vertical trends.
2. The stripy architecture is further enhanced in the 7-zone model because the layering is based on a flooding surface model, the unit boundaries for which are preferentially picked on shales. The unit boundaries are therefore shale-rich by design and prone to generating correlatable shales if the shale dimension is big enough (for object modelling) or the shale variogram range long enough (for SIS).
3. Across all frameworks, the object-based models are consistently more ‘lumpy’ and the SIS-based models consistently more ‘spotty’, a consequence of the different underlying principles of the algorithms.
4. The untrended object model for the two zone realisation is the one most dominated by stationarity, and looks the least realistic geologically.
5. The addition of deterministic trends, both vertical and lateral, creates more ordered, less random-looking models, as the assumption of stationarity is overridden by the conceptual model.

Any of above models presented in Figs. 2.57, 2.58 and 2.59 could be offered as a ‘best guess’, and could be supported at least superficially with

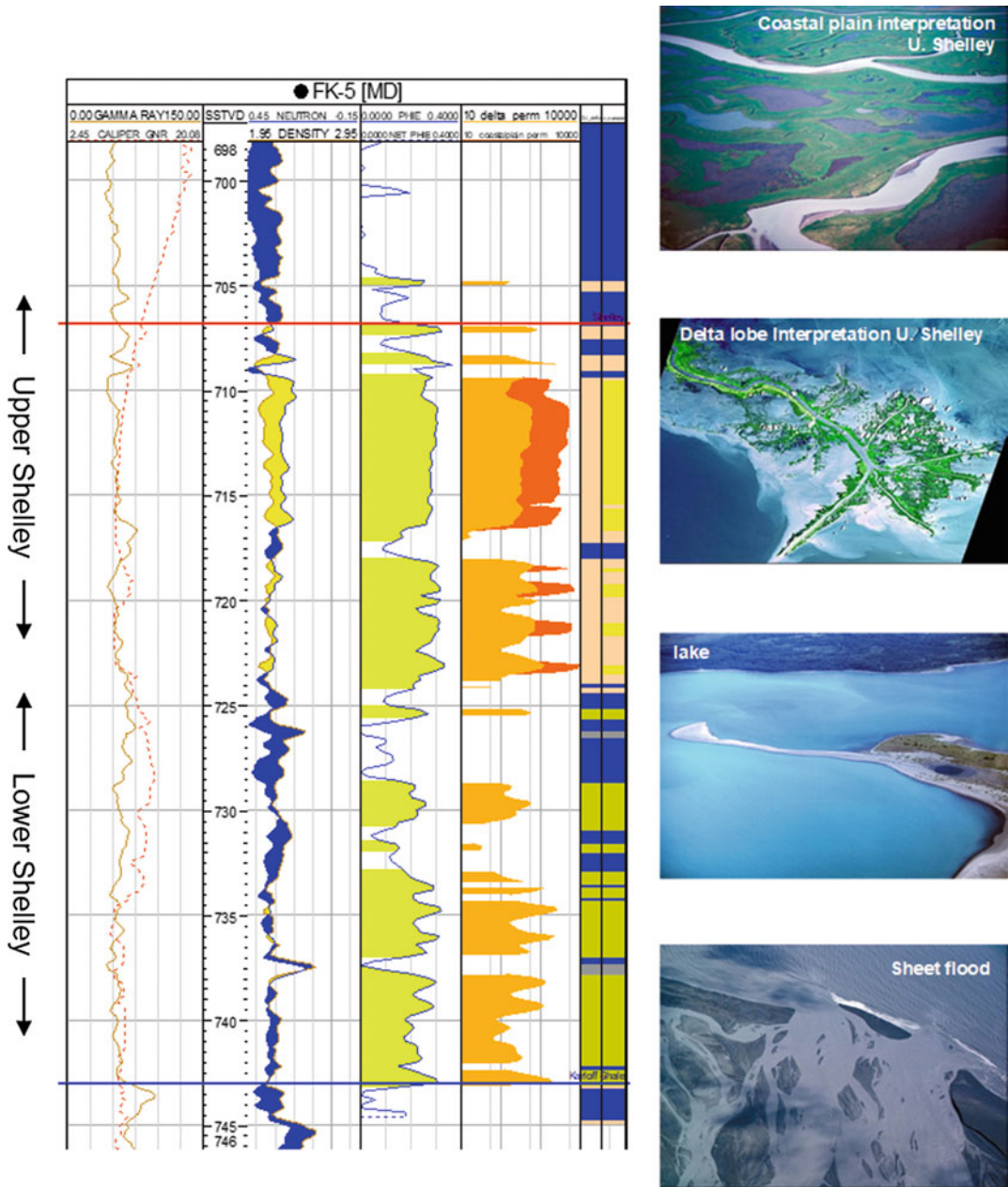


**Fig. 2.56** The Franken Field reservoir – type log and proposed depositional environment analogues. The model elements are shown on the *right-hand coloured* logs, one of which is associated with a delta interpretation

for the Upper Shelley, the other for an alternative coastal plain model for the Upper Shelley. Sands are marked in *yellow*, muds in *blue*, intermediate lithologies in intermediate colours. (Image courtesy of Simon Smith)

an appropriate story line. Presenting multiple models using different layering schemes and alternative algorithms also appears thorough and in a peer-review it would be hard to know which

of these models is a ‘good’ or ‘bad’ representation of the reservoir. However, a number of the models were made quickly using system defaults and have little substance; stationarity (within

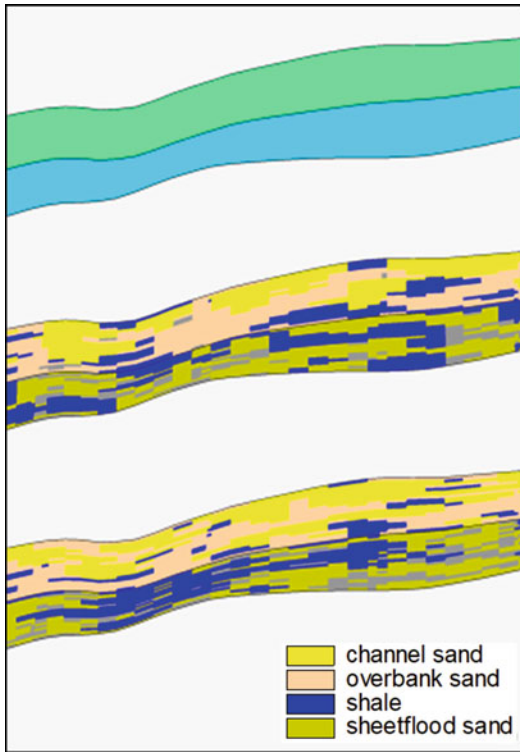


**Fig. 2.57** The Franken Field. *Top image:* the two zone subdivision; *middle image:* object model (no trends applied, stationarity maintained); *bottom image:* trended object model

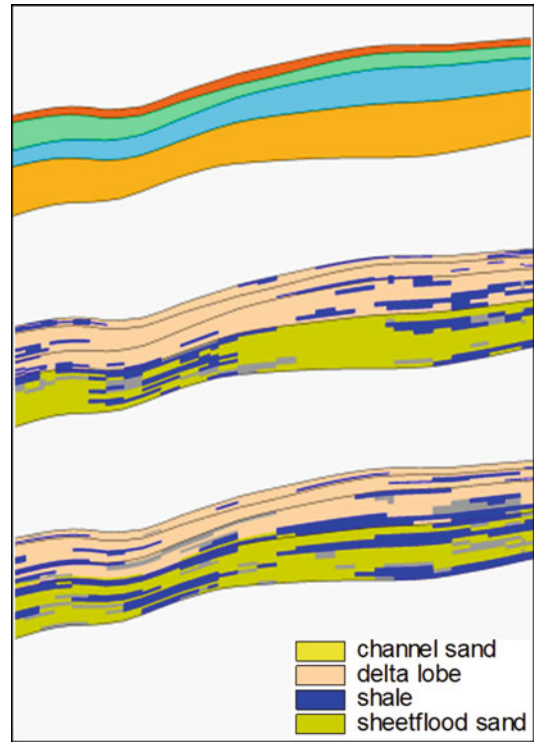


**Fig. 2.58** The Franken Field: *Top image:* the four zone subdivision; *middle image:* pixel (SIS) model (no trends applied, stationarity maintained); *bottom image:* trended pixel (SIS) model

zones) is dominant and although the models are statistically valid, they lack an underlying concept and have poor deterministic control. Only the lower models in each figure take account of the trends associated with the underlying reservoir concept, and it is these which are the superior representations – at least matching the quality of the conceptual interpretation.

The main point to take away from this example is that all the models match the well data and no mechanical modelling errors have been made in their construction, yet the models differ drastically owing to the algorithm choice, the style of correlation and the use of trends. The comparison reinforces the importance of the underlying reservoir concept as the tool for assessing which of the resulting rock models are acceptable representations of the reservoir.

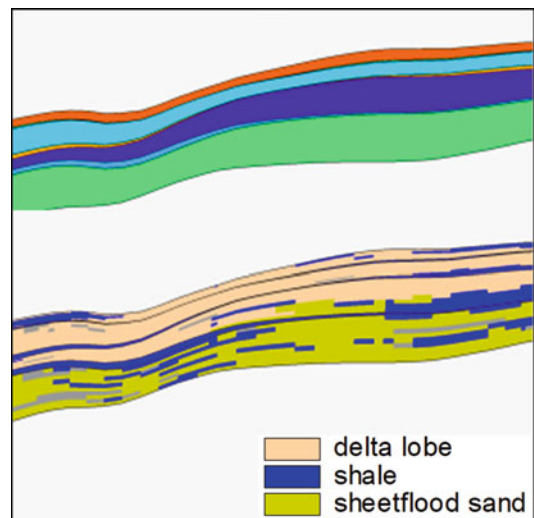


**Fig. 2.59** The Franken Field: *Top image:* the seven zone subdivision; *bottom image:* trended SIS model

## 2.8 Summary

In this section we have offered an overview of approaches to rock modelling and reviewed a range of geostatistically-based methods, whilst holding the balance between probability and determinism and the primacy of the underlying concept as the core issues. Reservoir modelling is not simply a process of applying numerical tools to the available dataset – there is always an element of subjective design involved – *an intuitive leap*.

Overall the rock model must make geological sense and to summarise this we offer a brief resume of practical things which can be done to check the quality of the rock model – the QC process.

### 2.8.1 Rock Model QC

- Make architectural sketches along depositional strike and dip showing the key features of the conceptual models. During the model build, switch the model display to stratigraphic (*simbox*) view to remove the structural deformation. How do the models compare with the sketches?
  - Watch out for the individual well matches reported by the software package – well by well. These are more useful and diagnostic than the overall ‘facies’ proportions. Anomalous wells point to weaknesses in the model execution.
  - Make element proportion maps for each element in each zone and check these against well data and the overall concept. This is an important check on the inter-well probabilistic process.
  - Assuming trends have been applied, check the statistics of the modelled element distribution against that for the well data alone; they are highly unlikely to be the same because of the undersampling of the wells, but the differences should be explicable in terms of any applied trends and the spatial location of the wells.
- Make net sand isochore maps for each zone without wells posted; imposed trends should be visible and the well locations should not (no bulls-eyes around wells).
  - Make full use of the visualisation tools, especially the ability to scroll through the model vertically, layer by layer, to look for anomalous geometries, e.g. spikes and pinch-outs.

### 2.8.2 Synopsis – Rock Modelling Guidelines

The first decision to be made is whether or not a rock model is truly required. If rock modelling can add useful control upon the desired distribution of reservoir properties, then it is needed. If the desired property distributions can be achieved directly by property modelling, then rock modelling is not necessary at all.

If it is decided that a rock model is required, it then needs some thought and design. The use of system default values is unlikely to be successful.

This chapter has attempted to stress the following things:

1. The *model concept* needs to be formed before the modelling begins, otherwise the modeller is ‘flying blind’. A simple way of checking your (or someone else’s) grasp of the conceptual reservoir model is to make a sketch section of the reservoir, or request a sketch, showing the desired architecture. *If you can sketch it, you can model it.*
2. The model concept needs to be expressed in terms of the chosen *model elements*, the selection of which is based on not only a consideration of the heterogeneity, but with a view to the fluid type and production mechanism. Some fluid types are more sensitive to heterogeneity than others; if the fluid molecules do not sense the heterogeneity, there is no need to model it – reference ‘Flora’s Rule’ as a handy rule of thumb.
3. Rock models are mixtures of *deterministic* and *probabilistic* inputs. Well data tends to be statistically insufficient, so attempts to extract

statistical models from the well data are often not successful. The road to happiness therefore generally lies with strong deterministic control, as determinism is the most direct method of carrying the underlying reservoir concept into the model.

4. To achieve the desired reservoir architecture, the *variogram model* has a leading influence if pixel-based methods are employed; we suggest the *variogram range* and its spatial anisotropy is the most important geostatistical input to reconcile with the conceptual sketch.
5. To get a reasonable representation of the model concept it is generally necessary to impose *trends* (both vertical and lateral) on the modelling algorithm, irrespective of the chosen algorithm, unless a process-based modelling tool is used to forward-model the likely trends.
6. Guide the geostatistical algorithms during a rock model build by an intuitive understanding of the relationship between the underlying reservoir concept and the geostatistical rules which guide the chosen algorithm.
7. It is unlikely that the element proportions in the model will match those seen in the wells – do not expect this to be the case; the data and the model are statistically different – this is discussed further in the next chapter.

## References

- Aarnes I, van der Vegy H, Hauge R, Fjellvoll B, Nordahl K (2019) Using sedimentary process-based models as training images for multipoint facies simulations. *Bull Can Petrol Geol* 67:217–230
- Ainsworth RB, Sanlung M, Duivenvoorden STC (1999) Correlation techniques, perforation strategies and recovery factors. An integrated 3-D reservoir modeling study, Sirikit Field, Thailand. *Am Assoc Petrol Geol Bull* 83(10):1535–1551
- Bentley MR, Elliott AA (2008) Modelling flow along fault damage zones in a sandstone reservoir: an unconventional modelling technique using conventional modelling tools in the Douglas Field Irish Sea UK. SPE paper 113958 presented at SPE Europec/EAGE conference and exhibition. Society of Petroleum Engineers (SPE). <https://doi.org/10.2118/113958-MS>
- Caers J (2003) History matching under training-image-based geological model constraints. *SPE J* 8 (3):218–226
- Caers J (2011) *Modeling uncertainty in the earth sciences*. Wiley, Hoboken
- Campbell CV (1967) Lamina, laminaset, bed, bedset. *Sedimentology* 8:7–26
- Da Pra A, Anastasi P, Corradi C, Sprega G (2017) 3D process based model integration in reservoir modeling – a real case application. Presented at the 79th EAGE Conference and Exhibition 2017, Paris, extended abstract
- Deutsch CV (2002) *Geostatistical reservoir modeling*. Oxford University Press, Oxford, p 376
- Doyen PM (2007) *Seismic reservoir characterisation*. EAGE Publications, Houten
- Dubrule O, Damsleth E (2001) Achievements and challenges in petroleum geostatistics. *Pet Geosci* 7:1–7
- Fielding CR, Crane RC (1987) An application of statistical modelling to the prediction of hydrocarbon recovery factors in fluvial reservoir sequences, vol 39. Society of Economic Paleontologists and Mineralogists (SEPM) special publication
- Haldorsen HH, Damsleth E (1990) Stochastic modelling. *J Petrol Technol* 42:404–412
- Holden L, Hauge R, Skare Ø, Skorstad A (1998) Modeling of fluvial reservoirs with object models. *Math Geol* 30 (5):473–496
- Howell J, Martinius A, Good T (2014) The application of outcrop analogues in geological modelling: a review, present status and future outlook. *Geol Soc London Spec Publ* 387:1–25
- Isaaks EH, Srivastava RM (1989) *Introduction to applied geostatistics*. Oxford University Press, Oxford
- Jensen JL, Corbett PWM, Pickup GE, Ringrose PS (1995) Permeability semivariograms, geological structure and flow performance. *Math Geol* 28(4):419–435
- Journel AG, Alabert FG (1990) New method for reservoir mapping. *J Petrol Technol* 42:212–218
- Matheron G (1963) *Principles of geostatistics*. *Econ Geol* 58:1246–1266
- McIlroy D, Flint S, Howell J, Timms N (2005) Sedimentology and the tide-dominated Jurassic Lajas Formation, Neuquen Basin, Argentina. *Geol Soc London Spec Publ* 252:83–107
- Pyrz MJ, Deutsch CV (2014) *Geostatistical Reservoir Modelling*, 2nd edn. Oxford University Press, Oxford
- Soubaras R, Dowle R (2010) Variable-depth streamer – a broadband marine solution. *First Break* 28:89–96
- Strebelle S (2002) Conditional simulation of complex geological structures using multiple-point statistics. *Math Geol* 34(1):1–21
- Van Wagoner JC, Bertram GT (eds) (1995) *Sequence stratigraphy of Foreland basin deposits*. American Association of Petroleum Geologists (AAPG), AAPG Memoir 64:137–224
- Van Wagoner JC, Mitchum RM, Campion KM, Rahmanian VD (1990) Siliciclastic sequence stratigraphy in well logs, cores, and outcrops. AAPG methods

- in exploration series, vol 7. American Association of Petroleum Geologists (AAPG)
- Webber KJ, Van Geuns LC (1990) Framework for constructing clastic reservoir simulation models. *J Pet Technol* 42:1–248
- Yarus JM, Chambers RL (1994) Stochastic modeling and geostatistics principals, methods, and case studies. AAPG computer applications in geology, vol 3. American Association of Petroleum Geologists (AAPG), p 379

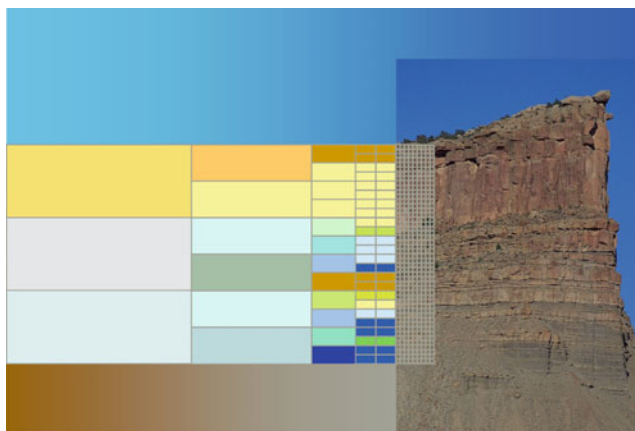


## Abstract

Now let's say you have a beautiful fit-for-purpose rock model of your reservoir – let's open the box and find out what's inside? All too often the properties used within the geo-model are woefully inadequate. What we need are appropriately-scaled property estimates based on statistical analysis of the available data – not just random guesses!

The aim of this chapter is to ensure the properties of your model are also fit-for-purpose and not, like Pandora's box, full of “all the evils of mankind.”

*Eros warned her not to open the box once Persephone's beauty was inside[...] but as she opened the box Psyche fell unconscious upon the ground. (from The Golden Ass by Apuleius)*



*Pixelated rocks*

## Keywords

Permeability · Effective permeability · Porosity · Averaging · Property distributions · Geostatistics · Gaussian simulation · Seismic conditioning · Net-to-gross · Anisotropy · Saturation

## 3.1 Which Properties?

First let us recall the purpose of building a reservoir model in the first place. We propose that the overall aim in reservoir model design is:

To capture knowledge of the subsurface in a quantitative form in order to evaluate and engineer the reservoir

This definition combines knowledge capture, the process of collecting all relevant information, with the engineering objective – the practical outcome of the model (Fig. 3.1). Deciding how to do this is the job of the geo-engineer – a geoscientist with sufficient knowledge of the Earth and the ability to quantify that knowledge in a way that is useful for the engineering decision at hand. A mathematician, physicist or engineer with sufficient knowledge of Earth science can make an equally good geo-engineer (Fig. 3.2).

A static model of a reservoir is the basis for most reservoir or CO<sub>2</sub> storage unit evaluation and engineering decisions. This resolves in to a number of purposes (reviewed in Chap. 1), roughly in order of complexity and detail:

- Making estimates of fluid volumes in place;
- Scoping reservoir development plans;
- Defining well targets;
- Designing detailed well plans, and
- Optimising fluid recovery (usually for IOR/EOR schemes).

The type of decision involved affects the property modelling approach used. Simple averaging

**Fig. 3.1** Knowledge capture and the engineering decision

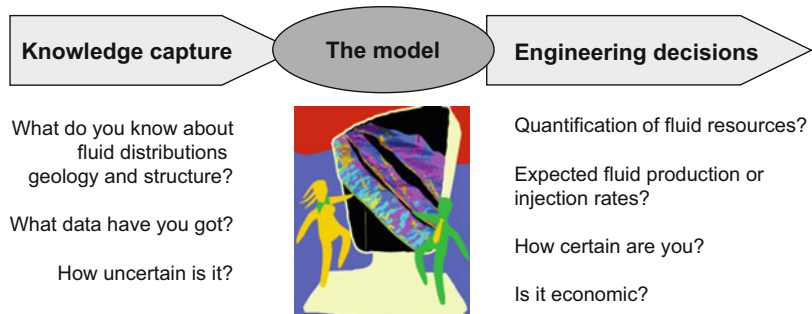


**Fig. 3.2** The geo-engineer. (Photo, Equinor image archive, © Equinor ASA, reproduced with permission)



or mapping of properties are more likely to be appropriate for initial volume estimates whereas advanced modelling with explicit upscaling is mostly employed when designing well plans (Fig. 3.3) or as part of improved reservoir displacement plans or enhanced oil recovery (EOR) strategies.

The next question is: “which petrophysical properties do we want to model?” The focus in this chapter will be on modelling porosity ( $\phi$ ) and permeability ( $k$ ), the latter an essential parameter in the flow equation (Darcy’s law). The methods discussed here for handling  $\phi$  and  $k$  can also be applied to other properties, such as formation bulk density ( $\rho_b$ ) or sonic p-wave velocity ( $v_p$ ), volume fraction of shale ( $V_{\text{shale}}$ ) or fracture density ( $F_d$ ), to name but a few. Table 3.1 lists the most commonly modelled rock properties, but the choice should not be limited to these, and indeed a key element of the design should be careful consideration of which properties should or can be usefully represented. Integration of dynamic data with seismic and well data will generally require modelling of several petrophysical properties and their cross-correlations.

Permeability is generally the most challenging property to define because it is highly variable in nature and is a tensor property dependent on flow boundary conditions. Permeability is also, in general, a non-additive property, that is:

$$k^{\Delta V} \neq \sum_1^n k_i^{\delta v} \quad (3.1)$$

In contrast, porosity is essentially an additive property:

$$\phi^{\Delta V} = \sum_1^n \phi_i^{\delta v} \quad (3.2)$$

where:

$\Delta V$  is a large scale volume

$\delta v[n]$  is the exhaustive set of small scale volumes filling the large-scale volume

Put in practical terms, if you have defined all the cell porosity values in your reservoir model then the total reservoir porosity is precisely equal to the sum of the cell porosities divided by the number cells (i.e. the arithmetic average),

**Fig. 3.3** Defining the well target

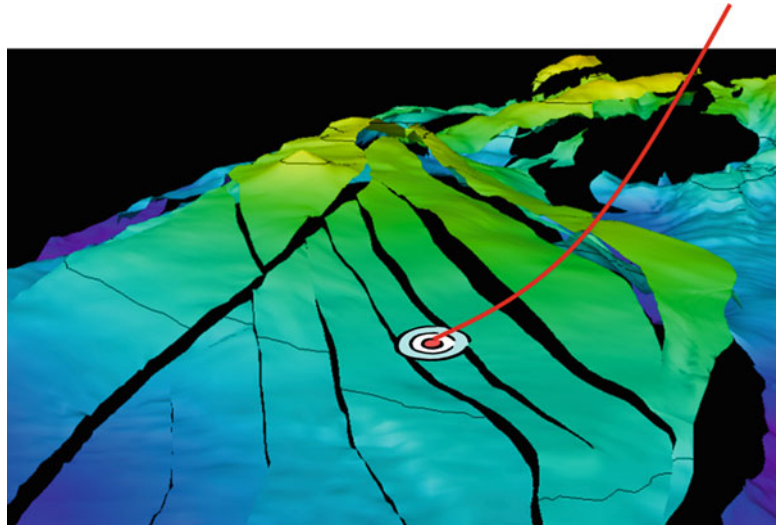


**Table 3.1** List of properties typically included in geological reservoir models

|                   | Symbol                            | Property   | Units<br>[typical range]                   |  |
|-------------------|-----------------------------------|--|--|--|
| All reservoirs    | $\phi$                            | Porosity   | Fraction<br>[0, 0.4]                       |  |
|                   | $\phi_m, \phi_f$                  | Matrix porosity, fracture porosity                   | Fraction<br>[0, 0.4]                       |  |
|                   | $K_h, k_v$                        | Horizontal permeability, vertical permeability       | Millidarcy, mD<br>[0.001, 10,000]          |  |
|                   | $k_v/k_h$                         | Ratio of vertical to horizontal permeability         | Millidarcy, mD<br>[ $10^{-5}$ , 1]         |  |
|                   | $V_{shale}, V_{sand}, V_{cement}$ | Volume fraction<br>(shale, sandstone, cement)        | Fraction<br>[0, 1]                         |  |
|                   | $N/G_{sand}, N/G_{res}$           | Net to gross ratio (sandstone, reservoir)            | Fraction<br>[0, 1]                         |  |
|                   | $S_w, S_o, S_g, S_c$              | Fluid saturation (water, oil, gas, CO <sub>2</sub> ) | Fraction<br>[0, 1]                         |  |
|                   | $SAT_{num}$                       | Relative permeability saturation function index      | Integer<br>[1, N]                          |  |
|                   | Fractured reservoirs              | $\phi_m, \phi_f$                                     | Matrix porosity, fracture porosity         | Fraction<br>[0, 0.4]                     |
|                   |                                   | $k_f, k_m$   | Fracture permeability, matrix permeability | Millidarcy, mD<br>[ $10^{-3}$ , $10^5$ ] |
| $F_d$             |                                   | Fracture density                                     | Number per metre,<br>$m^{-1}$<br>[0.1, 10] |  |
| $F_a$             |                                   | Fracture aperture                                    | m<br>[ $10^{-6}$ , $10^{-3}$ ]             |  |
| $C_{mean}$        |                                   | Mean surface curvature                               | 2nd derivative<br>[ $-x > 0 < +x$ ]        |  |
| Seismic inversion |                                   | *symbol below should be here                         | Bulk density                               | g/cc ( $kg/m^3$ )                        |
|                   |                                   | $\rho_b$   |  | [1–2]                                    |
|                   | $V_p$                             | Seismic velocity (p-wave)                            | m/s<br>[1400–5000]                         |  |
|                   | $V_p/V_s$                         | Ratio of compression-wave to shear-wave velocity     | m/s<br>[700–3000]                          |  |
|                   | $Al_p, Al_s$                      | Acoustic (seismic) impedance<br>(p-wave, s-wave)     | m/s.g/cc ( $pa.s/m^3$ )<br>[6000, 14,000]  |  |
|                   | $\phi_{AVO}$                      | Porosity from AVO inversion                          | Fraction<br>[0, 0.4]                       |  |

whereas for permeability this is not the case. We will discuss appropriate use of various permeability averages in the following chapter.

**Exercise 3.1**

Which methods to use?

Think through the following decision matrix for an oilfield development to decide which approaches are appropriate for which decisions?

| Method (for a given reservoir interval)   | Choice | Purpose   |
|---|--------|---|
| Conceptual geological sketch of proposed reservoir analogue   |        | Initial fluids-in-place volume estimate   |
| Simple average of porosity, $\phi$ , permeability, $k$ , and fluid saturation, $S_w$                          |        | Preliminary reserves estimates  |
| 2D map of $\phi$ , $k$ and $S_w$ (e.g. interpolation or kriging between wells)                                |        | Reserve estimates for designing top-side facilities (number of wells, platform type)  |
| 3D model of $\phi$ , $k$ and $S_w$ in the reservoir unit (from well data)                                     |        | Definition of appraisal or development well drilling plan   |
| 3D model of $\phi$ , $k$ and $S_w$ for each of several model elements (from well data)                        |        | Submitting detailed well design for final approval  |
| 3D model of $\phi$ , $k$ and $S_w$ conditioned to seismic inversion cube (seismic facies)                     |        | Designing optimized long-term CO <sub>2</sub> storage strategy for investment decision                                      |
| 3D model of $\phi$ , $k$ , $S_w$ and facies conditioned to dynamic data (production pressures and flow rates) |        | Designing improved oil recovery (IOR) strategy and additional well targets  |
| 3D model of $\phi$ , $k$ , $S_w$ and facies integrating multi-scale static and dynamic data                   |        | Implementing enhanced oil recovery (EOR) strategy using an injection blend (e.g. water alternating gas or CO <sub>2</sub> ) |

\*\*

Another important question to address is: “which reservoir or rock unit do we want to average?” There are many related concepts used

to define flowing rock intervals: flow units, hydraulic units, geological units or simply ‘the reservoir’. The most succinct term for defining the rock units in reservoir studies is the Hydraulic Flow Unit (HFU), which is defined as representative rock volume with consistent petrophysical properties distinctly different from other rock units. Hence the direct relationship between flow units and the ‘model elements’ introduced in the preceding chapter.

**Exercise 3.2**

Additive properties

*Additivity* involves a mathematical function in which a property can be expressed as a weighted sum of some independent variable(s). The concept is important to a wide range of statistical methods used in many science disciplines. Additivity has many deeper facets and definitions that are discussed in mathematics and statistical literature.

It is useful to consider a wider selection of petrophysical properties and think through whether they are essentially additive or non-additive (i.e. multiplicative) properties.

What would you conclude about these terms?

- Net-to-gross ratio
- Fluid saturation
- Permeability
- Porosity
- Bulk density
- Formation resistivity
- Seismic velocity,  $V_p$  or  $V_s$
- Acoustic Impedance, AI

\*\*

Abbaszadeh et al. (1996) define the HFU in terms of the Kozeny-Carmen equation to extract Flow Zone Indicators which can be used quantitatively to define specific HFUs from well data. We will return the definition of representative volumes and flow units in Chap. 4 when we look at upscaling, but first we need to understand permeability.

### 3.2 Understanding Permeability

#### 3.2.1 Darcy's Law

The basic permeability equation is founded on the observations and field experience of Henri Darcy (1803–1858), made while engineering a pressurized water distribution system in the town of Dijon, France. His equation relates flow rate to the head of water draining through a pile of sand (Fig. 3.4):

$$Q = KA(\Delta H/L) \tag{3.3}$$

where:

- Q = volume flux of water
- K = constant of hydraulic conductivity or coefficient of permeability
- A = cross sectional area
- ΔH = height of water column
- L = length of sand column

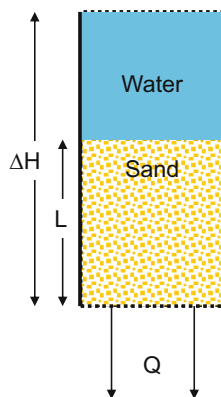
From this we can derive the familiar Darcy's Law – a fundamental equation for flow in porous media, based on dimensional analysis and the Navier-Stokes equations for flow in cylindrical pores:

$$u = \frac{-k}{\mu} \nabla(P + \rho gz) \tag{3.4}$$

where:

- u = intrinsic fluid velocity
- k = intrinsic permeability

**Fig. 3.4** Darcy's experiment



- μ = fluid viscosity
- ∇P = applied pressure gradient
- ρgz = pressure gradient due to gravity
- ∇P (grad P) is the pressure gradient, which can be solved in a cartesian coordinate system as:

$$\nabla P = \frac{dP}{dx} + \frac{dP}{dy} + \frac{dP}{dz} \tag{3.5}$$

The pressure gradient due to gravity is then ρg∇z. For a homogeneous, uniform medium k has a single value, which represents the medium's ability to permit flow (independent of the fluid type). For the general case of a heterogeneous rock medium, k is a tensor property.

#### Exercise 3.3

Dimensions of permeability.

What are the dimensions of permeability? Do a dimensional analysis for Darcy's Law.

For the volumetric flux equation: Q = KA(ΔH/L).

The dimensions are: [L<sup>3</sup>T<sup>-1</sup>] = [LT<sup>-1</sup>] [L<sup>2</sup>].

Therefore the SI unit for K is: ms<sup>-1</sup>.

Do the same for Darcy's Law: u = - (k/μ). ∇(P + ρgz).

The dimensions are: [ ] = ([ ]/[ ]). [ ].

Therefore the SI unit for k is ...?

\*\*

#### 3.2.2 Upscaled Permeability

In general terms, *upscaled permeability* refers to the permeability of a larger volume given some fine scale observations or measurements. The concept is widely used, and abused, and requires some care in its use and application. It is also rather fundamental – if it was a simple thing to estimate the correctly upscaled permeability for a reservoir unit, there would be much less value in reservoir modelling (apart from simple volume estimates).

The upscaled (or block) permeability, k<sub>b</sub>, is defined as the permeability of a homogeneous block, which under the same pressure boundary

conditions will give the same average flows as the heterogeneous region the block is representing (Fig. 3.5). The upscaled block permeability could be estimated, given a set of values in a permeability field or model, or it could be measured at the larger scale (e.g. in a well test or core analysis), in which case the fine-scale permeabilities need not be known.

The *effective permeability* is defined strictly in terms of effective medium theory and is an intrinsic large-scale property which is independent of the boundary conditions. The main theoretical conditions for estimation of the effective permeability,  $k_{\text{eff}}$ , are:

- That the flow is linear and steady state.
- That the medium is statistically homogeneous at the large scale.

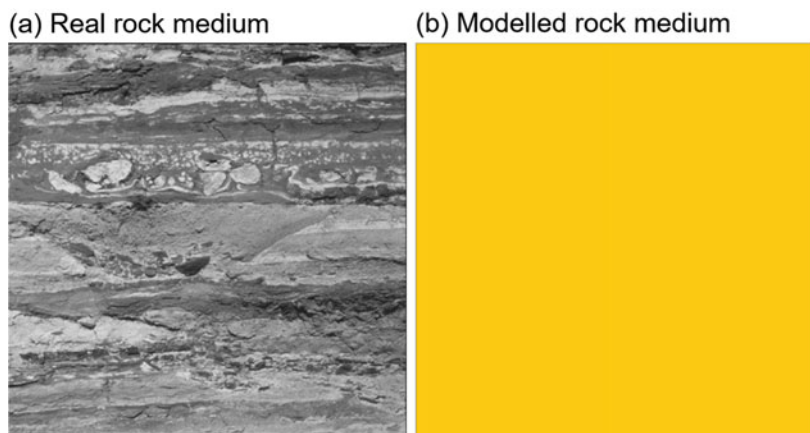
When the upscaled domain is large enough, such that these conditions are nearly satisfied, then  $k_b$  approaches  $k_{\text{eff}}$ . The term *equivalent permeability* is also used (Renard and de Marsily 1997) and refers to a general large-scale permeability which can be applied to a wide range of boundary conditions, to some extent encompassing both  $k_b$  and  $k_{\text{eff}}$ . These terms are often confused or misused, and in this treatment we will refer to the permeability upscaled from a model as the *block permeability*,  $k_b$ , and use *effective permeability* as the ideal upscaled permeability we would generally wish to estimate if we could satisfy the necessary conditions. In

reservoir modelling we are usually estimating  $k_b$  in practice, because we rarely fully satisfy the demands of effective medium theory. However,  $k_{\text{eff}}$  is an important concept with many constraints that we try to satisfy when estimating the upscaled (block) permeability.

Note that in petrophysical analysis, the term ‘effective porosity’ refers to the porosity of moveable fluids excluding micro-porosity and chemically bound water, while total porosity encompasses all pore types. Although effective porosity and effective permeability both represent properties relevant to, and controlling, macroscopic flow, they are defined on different bases. Effective permeability is essentially a larger scale property requiring statistical homogeneity in the medium, whereas effective porosity is essentially a pore-scale physical attribute. Of course, if both properties are estimated at, or rescaled to, the same appropriate volume, they may correspond and can then be correctly used together in flow modelling. They should not, however, be automatically associated. For example, in an upscaled heterogeneous volume there could be effective porosity elements (e.g. vuggy pores) which do not contribute to the flow and therefore do not influence the effective permeability.

In general,  $k_b$  is a tensor property (Fig. 3.6) where, for example,  $k_{xy}$  represents flow in the  $x$  direction due to a pressure gradient in the  $y$  direction. In practice  $k_b$  is commonly assumed to be a diagonal tensor where off-diagonal terms are neglected. A further simplification in many

**Fig. 3.5** Effective permeability and upscaled block permeability (a) Real rock medium has some (unknown) effective permeability. (b) Modelled rock medium has an estimated block permeability with the same average flow as the real thing



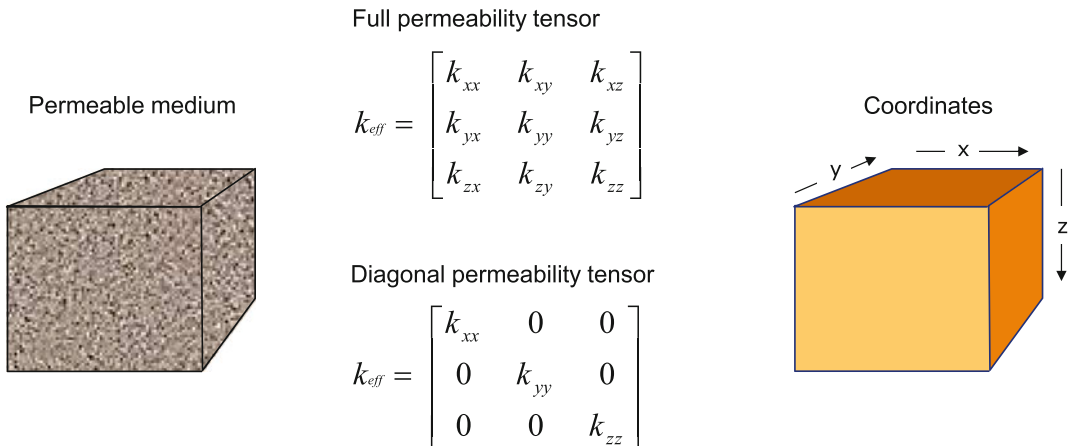


**Fig. 3.6** The permeability tensor

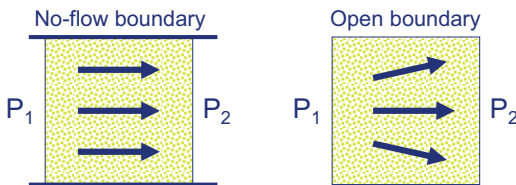


**Fig. 3.7** Simple illustration of flow boundary conditions:  $P_1$  and  $P_2$  are fluid pressures applied at the *left* and *right* hand sides and *arrows* illustrate flow vectors

reservoir modelling studies is the assumption that  $k_h = k_{xx} = k_{yy}$  and that  $k_v = k_{zz}$ .

The calculation or estimation of  $k_b$  is dependent on the boundary conditions (Fig. 3.7). Note that the assumption of a no-flow or sealed side boundary condition, forces the result to be a diagonal tensor. This is useful, but may not of course represent reality. Renard and de Marsily (1997) give an excellent review of effective permeability, and Pickup et al. (1994, 1995) give examples of the permeability tensor estimated for a range of realistic sedimentary media.

### 3.2.3 Permeability Variation in the Subsurface

There is an extensive literature on the measurement of permeability (e.g. Goggin et al. 1988; Hurst and Rosvoll 1991; Ringrose et al. 1999) and its application for reservoir modelling (e.g. Begg et al. 1989; Weber and van Geuns

1990; Corbett et al. 1992). All too often, rather idealised permeability distributions have been assumed in reservoir models, such as a constant value or the average of a few core plug measurements.

In reality, permeability in a rock medium is a highly variable property. In sedimentary basins as a whole we expect variations of at least 10 orders of magnitude (Fig. 3.8), with a general decrease from surface to depth due to compaction and diagenesis. Good sandstone units may have permeabilities typically in the 10–1000 mD range, but the silt and clay rich units pull the permeability down to around  $10^{-3}$  mD or lower. Deeply buried mudstones forming cap-rocks and seals have permeabilities in the microdarcy to nanodarcy range. Even within a single reservoir unit, permeability may vary by at least 5 orders of magnitude. In the example shown in Fig. 3.9 the wide range in observed permeabilities is due both to lithofacies (heterolithic elements tend to be lower than sandy elements) and due to cementation (each element is highly variable mainly due to the effects of variable degrees of quartz cementation).

### 3.2.4 Permeability Averages

Due to its highly variable nature, some form of averaging of permeability is generally needed. The question is which average? There are well-



**Fig. 3.8** Typical ranges of permeability for near-surface aquifers and North Sea oil reservoirs:  
 1 = Holocene aquifers.  
 (From Bierkins 1996),  
 2 = Example North Sea datasets (anonymous)

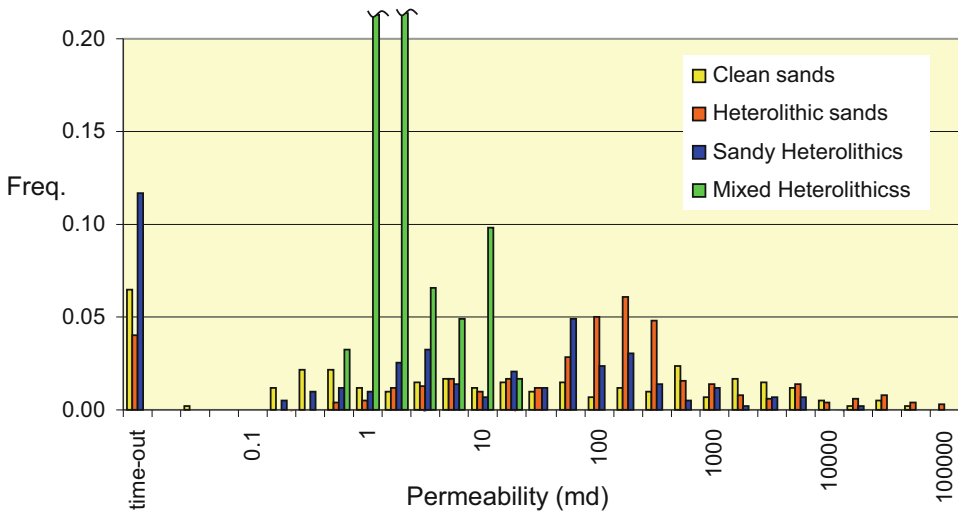
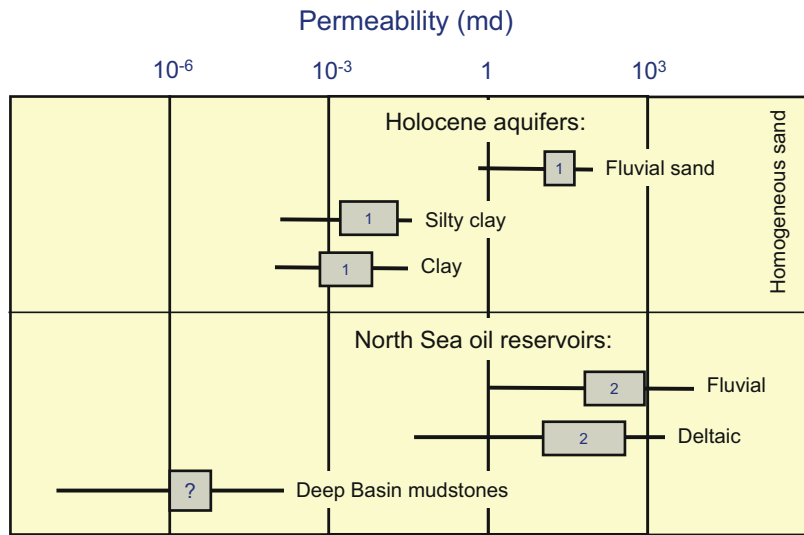


**Fig. 3.9** Probe permeameter measurements from a highly variable, deeply-buried, tidal-deltaic reservoir interval (3 m of core) from offshore Norway

known limits for the estimation of  $k_{eff}$  in ideal systems. For flow along continuous parallel layers the arithmetic average gives the correct effective permeability, while for flow perpendicular to continuous parallel layers the harmonic average is the correct solution (Fig. 3.10).

If the layers are in any way discontinuous or variable or the flow is not perfectly parallel or perpendicular to the layers then the true effective permeability will lie in between these averages.

This gives us the outer bounds to effective permeability:


$$k_{harmonic} \leq k_{eff} \leq k_{arithmetic}$$

More precise limits to  $k_{eff}$  have also been proposed, such as the arithmetic mean of harmonic means of each row of cells parallel to flow (lower bound) and *vice versa* for the upper bound (Cardwell and Parsons 1945). However, for most practical purposes the arithmetic and

**Fig. 3.10** Calculation of effective permeability using averages for ideal layered systems: (a) The arithmetic average for flow along continuous parallel layers; (b) The harmonic average for flow perpendicular to continuous parallel layers ( $k_i$  and  $t_i$  are the permeability and thickness of layer  $i$ )

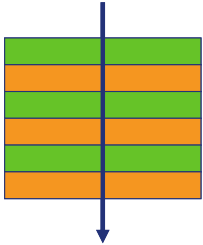
(a)

$$k_{arithmetic} = \frac{\sum_1^n k_i t_i}{\sum_1^n t_i}$$



(b)

$$k_{harmonic} = \left[ \frac{\sum_1^n t_i / k_i}{\sum_1^n t_i} \right]^{-1}$$



harmonic means are quite adequate limiting values, especially given that we seldom have an exhaustive set of values to average (the sampling problem, discussed in Sect. 3.3).

The geometric average is often proposed as a useful or more correct average to use for more variable rock systems. Indeed for flow in a correlated random 2D permeability field with a log-normal distribution and a low variance the effective permeability is equal to the geometric mean:

$$k_{geometric} = \exp \left[ \sum_1^n \ln k_i / n \right] \quad (3.6)$$

This can be adapted for 3D as long as the variance of the distribution is also taken account of. Gutjahr et al. (1978) showed that for a log-normally distributed permeability field in 3D:

$$k_{eff} = k_{geometric} (1 + \sigma^2 / 6) \quad (3.7)$$

where:

$\sigma^2$  is the variance of  $\ln(k)$

Thus in 3D, the theoretical effective permeability is slightly higher than the geometric

average, or indeed significantly higher if the variance is large.

An important condition for  $k_{eff} \approx k_{geometric}$  is that correlation length,  $\lambda$ , of the permeability variation must be significantly smaller than the size of the averaging volume,  $L$ . That is:

$$\lambda_x \lambda_y \lambda_z \ll L_x L_y L_z$$

This relates to the condition of statistical homogeneity. In practice, we have found that  $\lambda$  needs to be at least 5 times smaller than  $L$  for  $k_b \rightarrow k_{geometric}$  for a log-lognormal permeability field. This implies that the assumption (sometimes made) that  $k_{geometric}$  is the ‘right’ average for a heterogeneous reservoir interval is not generally true. Neither does the existence of a log-normal permeability distribution imply that the geometric average is the right average. This is evident in the case of a perfectly layered system with permeability values drawn from a log normal distribution – in such a case  $k_{eff} = k_{arithmetic}$ .

Averages between the outer-bound limits to  $k_{eff}$  can be generalised in terms of the power average (Kendall and Stuart 1977; Journel et al. 1986):

$$k_{power} = \left[ \sum k_i^p / n \right]^{1/p} \quad (3.8)$$

where:

$p = -1$  corresponds to the harmonic mean,  $p \sim 0$  to the geometric mean and  $p = 1$  to the arithmetic mean ( $p = 0$  is invalid and the geometric mean is calculated using Eq. 3.6)

For a specific case with some arbitrary heterogeneity structure, a value for  $p$  can be found, e.g. by finding a  $p$  value which gives best fit to results of numerical simulations. This can be a very useful form of the permeability average. For example, after some detailed work on estimating the permeability of a particular reservoir unit or facies (based on a key well or near-well model) one can derive plausible values for  $p$  for general application in the full field reservoir model (e.g. Ringrose et al. 2005). In general,  $p$  for  $k_h$  will be positive and  $p$  for  $k_v$  will be negative.

Note that for the general case, when applying averages to numerical models with varying cell sizes, we use volume weighted averages. Thus, the most general form of the permeability estimate using averages is:

$$k_{estimate} = \left[ \int k^p dV / \int dV \right]^{1/p} \quad \langle -1 < p < 1 \rangle \quad (3.9)$$

where:

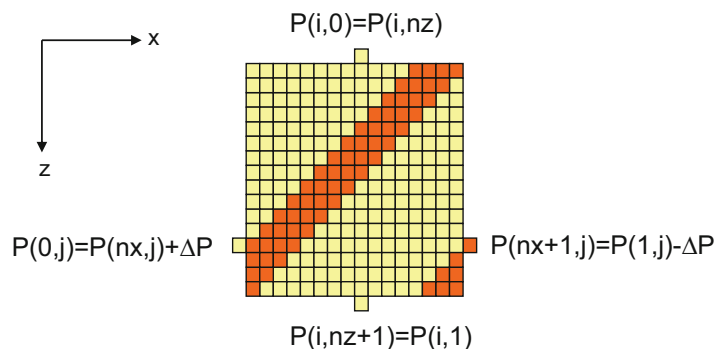
$p$  is estimated or postulated

### 3.2.5 Numerical Estimation of Block Permeability

For the general case, where an average permeability cannot be assumed, *a priori*, numerical methods must be used to calculate the block permeability ( $k_b$ ). This subject has occupied many minds in the fields of reservoir engineering and there is a large literature on this subject. The numerical methods used are based on the assumptions of conservation of mass and energy, and generally assume steady-state conditions. The founding father of the subject in the petroleum field is arguably Muskat (1937), while Matheron (1967) founded much of the theory related to estimation of flow properties. De Marsilly (1986) gives an excellent foundation from a groundwater perspective and Renard and de Marsily (1997) give a more recent review on the calculation of equivalent permeability. Some key papers on the calculation of permeability for heterogeneous rock media include White and Horne (1987), Durlofsky (1991) and Pickup et al. (1994).

To illustrate the numerical approach we take an example proposed by Pickup and Sorbie (1996) shown in Fig. 3.11. Assuming a fine-scale grid of permeability values,  $k_i$ , we want to calculate the upscaled block permeability tensor,  $k_b$ . An assumption on the boundary conditions must be made, and we will assume a period boundary condition (Durlofsky 1991) – where fluids exiting from one edge are assumed to enter from the opposite edge – and apply this to a periodic permeability field (where the model

**Fig. 3.11** Periodic pressure boundary conditions applied to a periodic permeability field, involving an inclined layer. Example boundary cell pressure conditions are shown



geometry repeats in all directions). This arrangement of geometry and boundary conditions gives us an exact solution.

First a pressure gradient  $\Delta P$  is applied to the boundaries in the x direction. For the boundaries parallel to the applied pressure gradient, the periodic condition means that P in cell (i, 0) is set as equal to P in cell (i, nz), where n is the number of cells. A steady-state flow simulation is carried out on the fine-scale grid, and as all the permeabilities are known, it is possible to find the cell pressures and flow values (using matrix computational methods).

We then solve Darcy's Law for each fine-scale block:

$$\vec{u} = -(1/\mu) \underline{k} \cdot \nabla P \quad (3.10)$$

where:

$\vec{u}$  is the local flow vector

$\mu$  is the fluid viscosity

$\underline{k}$  is the permeability tensor

$\Delta P$  is the pressure gradient

Usually, at the fine scale we assume the local permeability is not a tensor so that only one value of k is required per cell.

We then wish to know the upscaled block permeability for the whole system. This is a

relatively simple step once all small scale Darcy equations are solved, and involves the following steps:

1. Solve the fine-scale equations to give pressures,  $P_{ij}$  for each block.
2. Calculate inter-block flows in the x-direction, using Darcy's Law.
3. Calculate total flow, Q, by summing individual flows between any two planes.
4. Calculate  $k_b$  using Darcy's Law applied to the upscaled block.
5. Repeat for the y and z directions.

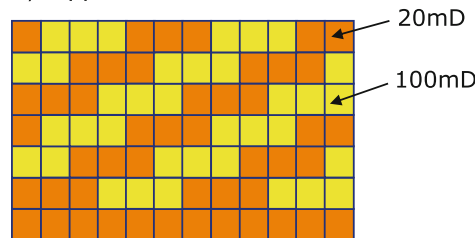
For the upscaled block this results in a set of terms governing flow in each direction, such that:

$$\begin{aligned} u_x &= -\frac{1}{\mu} \left( k_{xx} \frac{\partial P}{\partial x} + k_{xy} \frac{\partial P}{\partial y} + k_{xz} \frac{\partial P}{\partial z} \right) \\ u_y &= -\frac{1}{\mu} \left( k_{yx} \frac{\partial P}{\partial x} + k_{yy} \frac{\partial P}{\partial y} + k_{yz} \frac{\partial P}{\partial z} \right) \\ u_z &= -\frac{1}{\mu} \left( k_{zx} \frac{\partial P}{\partial x} + k_{zy} \frac{\partial P}{\partial y} + k_{zz} \frac{\partial P}{\partial z} \right) \end{aligned} \quad (3.11)$$

For example, the term  $k_{zx}$  is the permeability in the z direction corresponding to the pressure gradient in the x direction. These off-diagonal terms are intuitive when one looks at the permeability field. Take the vertical (x, z) geological model section shown in Fig. 3.12. If the inclined

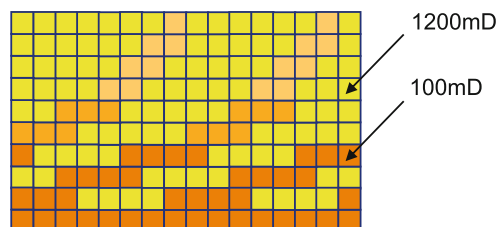
**Fig. 3.12** Example tensor permeability matrices calculated for simple 2D models of common sedimentary structures

a) Ripple laminaset



$$\underline{k} = \begin{bmatrix} 48 & -7.1 \\ -7.1 & 34 \end{bmatrix}$$

b) Trough crossbed set



$$\underline{k} = \begin{bmatrix} 759 & -63 \\ -63 & 336 \end{bmatrix}$$

orange layers have lower permeability, then flow applied in the +x direction (to the right) will tend to generate a flux in the -z direction (i.e. upwards). This results in a vertical flow and requires a  $k_{zx}$  permeability term in the Darcy equation (for a 2D tensor).

Example solutions of permeability tensors for simple geological models are given by Pickup et al. (1994) and illustrated in Fig. 3.12. Ripple laminasets and trough cross-beds are two common architectures found in deltaic and fluvial depositional settings – ripple laminasets tend to be 2–4 cm in height while trough cross-bed sets are typically 10–50 cm in height. These simple models are two dimensional and capture typical geometry and permeability variation (measured on outcrop samples) in a section parallel to the depositional current. In both cases, the tensor permeability matrices have relatively large off-diagonal terms, 15 and 8% of the  $k_{xx}$  value, respectively. The negative off-diagonal terms reflect the chosen coordinate system with respect to flow direction (flow left to right with z increasing downwards). Vertical permeability is also significantly lower than the horizontal permeability due to the effects of the continuous low permeability bottomset.

Geological elements like these will tend to fill the volume within a particular reservoir unit, imparting their flow anisotropy and cross-flow tendencies on the overall reservoir unit. Of course, real rock systems will have natural variability in both architecture and petrophysical

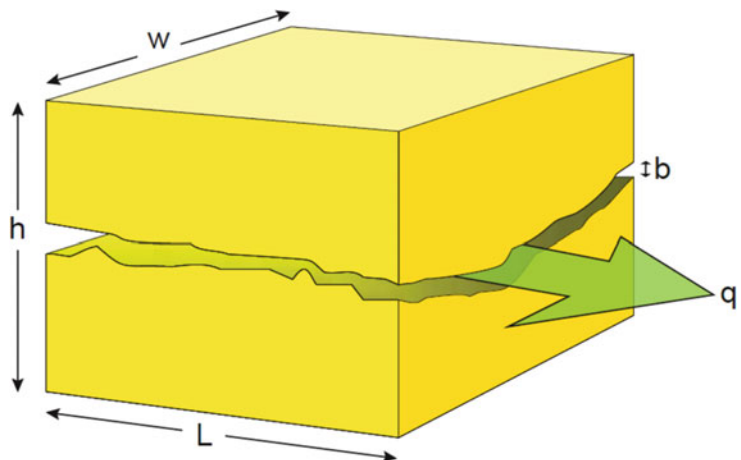
properties, and our aim is therefore to represent the expected flow behaviour. The effects of geological architecture on flow are frequently neglected – for example, it may be assumed that a Gaussian random field represents the inter-well porosity and permeability architecture. More advanced, geologically-based, flow modelling will, however, allow us to assess the potential effects of geological architecture on flow, and attempt to capture these effects as a set of upscaled block permeability values. Structural architecture in the form of fractures or small faults may also generate pervasive tendencies for strongly tensorial permeability within a rock unit. By aligning grid cells to geological features (faults, dominant fracture orientations, or major bed-set boundaries) the cross-flow terms can be kept to a minimum. However, typically one aligns the grid to the largest-scale geological architecture (e.g. major fault blocks) and so other smaller-scale features inevitably generate some cross-flow.

### 3.2.6 Permeability in Fractures

Understanding permeability in fractured reservoirs requires some different flow physics – Darcy’s law does not apply.

Flow within a fracture (Fig. 3.13) is described by Poiseuille’s Law, which for a parallel-plate geometry gives (Mourzenko et al. 1995):

**Fig. 3.13** Flow in a fracture



$$q = \frac{w b^3 \Delta P}{12\mu L} \quad (3.12)$$

where:

$q$  is the volumetric flow rate

$w$  is the fracture width

$b$  is the fracture aperture

$\mu$  is the fluid viscosity

$\Delta P/L$  is the pressure gradient

Note that the flow rate is proportional to  $b^3$ , and thus highly dependent on fracture aperture. In practice, the flow strongly depends on the stress state and the fracture roughness (Witherspoon et al. 1980), but the underlying concept still holds. To put some values into this simple equation – a 1 mm wide fracture in an impermeable rock matrix would have an effective permeability of around 100 darcys.

Unfortunately, fracture aperture is not easily measured, and generally has to be inferred from pressure data. This makes fracture systems much harder to model than conventional non-fractured reservoirs.

In practice, there are two general approaches for modelling fracture permeability:

- Implicitly, where we model the overall rock permeability (matrix and fractures) and assume we have captured the ‘effect of fractures’ as an effective permeability.
- Explicitly, where we represent the fractures in a model.

For the explicit case, there are then several options for how this may be done:

1. *Discrete Fracture Network (DFN) models*, where individual fractures with explicit geometry are modelled in a complex network.
2. *Dual permeability models*, where the fracture and matrix permeability are explicitly represented (but fracture geometry is implicitly represented by a shape factor).
3. *Dual porosity models*, where the fracture and matrix porosity are explicitly represented, but the permeability is assumed to occur only in

the fractures (and the fracture geometry is implicitly represented by a shape factor).

Fractured reservoir modelling is discussed in detail by Nelson (2001) and covered in most reservoir engineering textbooks. In Sect. 3.8, below, we discuss the handling of fault and fracture properties in further detail, and in Chap. 6 we describe approaches for handling fractured reservoir models. The important thing to keep in mind in the context of understanding permeability, is that fractures behave quite differently (and follow different laws) from the general Darcy-flow concept for flow in permeable (granular) rock media.

Before considering faults and fractures in more detail, we need to appreciate the statistical aspects of estimating and modeling rock properties.

## 3.3 Handling Statistical Data

### 3.3.1 Introduction

Many misunderstandings about upscaled permeability, or any other reservoir property, are caused by incorrect understanding or use of probability distributions. The treatment of probability distributions is an extensive subject covered in a number of textbooks. Any of the following are suitable for geoscientists and engineers wanting to gain deeper appreciation of statistics and the Earth sciences: Size 1987; Isaaks and Srivastava 1989; Olea 1991; Jensen et al. 2000, and Davis 2003. Here we will identify some of the most important issues related to property modelling, namely:

- Understanding sample versus population statistics;
- Using log-normal and other transforms;
- Use and implications of applying cut-off values.

Our overall aim in reservoir modelling is to estimate and compare distributions for:

- The well data (observations);
- The reservoir model (a hypothesis or postulate);
- The population (the unknown ‘true’ reservoir properties).

We must always remember not to confuse observations (data) with the model (a hypothesis) and both of these with the ‘ground truth’ (an unknown). This leads us to one of the most important axioms of reservoir modelling:

$$Data \neq Model \neq Truth$$

Of course, we want our models to be consistent with the available data (from wells, seismic, and dynamic data) and we hope they will give us a good approximation of the truth, but too often the reservoir design engineer tries to force an artificial match which leads inevitably to great disappointment. A common mistake is to try to manipulate the data statistics to obtain an apparent match between the model and data. You may have heard versions of the following statements:

- A “We matched the well test permeability ( $k_h$ ) to the log-derived permeability data by applying a cut-off and using a geometric average.”, or
- B “The previous models were all wrong, but this one must be right because it matches all the data we have.”

Statement A sounds good but begs the questions: “what cut-off was applied?” and “is the geometric

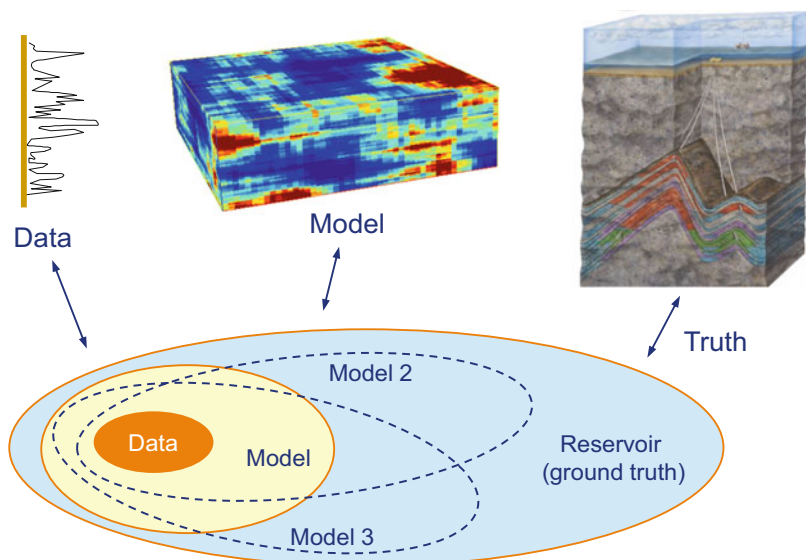
average indeed the appropriate average to use?” Statement B is clearly arrogant but in fact captures the psychology of every reservoir model builder – we try to do our best with the available data but are reluctant to admit to the errors that must be present. Versions of these statements that would be more consistent with the inequality above might be:

- A “We were able to match the well test permeability ( $k_h$ ) to within 10 % of the log-derived permeability data by applying the agreed cut-off and using a geometric average, and a power average with  $p = 0.3$  gave us an even better match to within 1 %.”
- B “The previous models had several serious errors and weaknesses, but this latest set of three (or more) models incorporates the latest data and captures the likely range of subsurface behaviour.”

Figure 3.14 illustrates what the statistical objective of modelling should be. The available data is some limited subset of the true subsurface, and the model should extend from the data in order to make estimates of the true subsurface. In terms of set theory:

$$Data \in Model \in Truth$$

**Fig. 3.14** Illustration of the axiom:  $Data \neq Model \neq Truth$



Our models should be consistent with that data (in that they encompass it) but should aim to capture a wider range, approaching reality, using both geological concepts and statistical methods. In fact, as we shall see later (in this section and in Sect. 3.4) bias in the data sample and upscaling transforms further complicate this picture whereby the data itself can be misleading.

Table 3.2 illustrates this principle using the simple case of estimating the sand volume fraction,  $V_s$  (or  $N/G_{\text{sand}}$ ), at different stages in a field development. We might quickly infer that the 30 well case gives us the most correct estimate and that the earlier 2 and 5 well cases are in error due to limited sample size. In fact, by applying the N-zero statistic (explained below) we can conclude that the 5-well estimate is accurate to within 20% of the true mean, and that by the 30-well stage we still lie within the range estimated at the 5-well stage. In other words, it is better to proceed with a realistic estimate of the range in  $V_s$  from the available data than to assume that the data you have gives the ‘correct’ value. In this case,  $V_s = 36\% \pm 7\%$  constitutes a good model at the 5-well stage in this field development.

### 3.3.2 Variance and Uncertainty

There are a number of useful measures that can guide the reservoir model practitioner in gaining a realistic impression of the uncertainty involved in using the available data. To put it simply, *variance* refers to the spread of the data you have (in front of you), while *uncertainty* refers to some unknown variability beyond the

information at hand. From probability theory we can establish that ‘most’ values lie close to the mean. What we want to know is “how close?” – or how sure we are about the mean value. The fundamental difficulty here is that the true (population) mean is unknown and we have to employ the theory of confidence intervals to give us an estimate. Confidence limit theory is treated well in most books on statistics; Size (1987) has a good introduction.

*Chebyshev’s inequality* gives us the theoretical basis (and mathematical proof) for quantifying how many values lie within certain limits. For example, for a Gaussian distribution 75% of the values are within the range of two standard deviations from the mean. Stated simply, Chebyshev’s theory gives:

$$P(|x - \mu| \geq \kappa\sigma) \leq \frac{1}{\kappa^2} \quad (3.13)$$

where:

$\kappa$  is the number of standard deviations

The *standard error* provides a simple measure of uncertainty. If we have a sample from a population (assuming a normal distribution and statistically independent values), then the standard error of the mean value,  $\bar{x}$ , is the standard deviation of the sample divided by the square root of the sample size:

$$SE_{\bar{x}} = \frac{\sigma_s}{\sqrt{n}} \quad (3.14)$$

where:

$\sigma_s$  is the standard deviation of the sample and  $n$  is the sample size.

**Table 3.2** Statistics for a simple example of estimation of the sand volume fraction,  $V_s$ , in a reservoir unit at different stages of well data support

|          | With 2 wells | With 5 wells | With 30 wells |
|----------|--------------|--------------|---------------|
| Mean     | 38.5         | 36.2         | 37.4          |
| $\sigma$ | 4.9          | 6.6          | 7.7           |
| SE       | 3.5          | 3.0          | 1.4           |
| $C_v$    | –            | 0.18         | 0.21          |
| $N_0$    | –            | 3            | 4             |
| N        | 2            | 5            | 30            |



The standard error can also be used to calculate confidence intervals. For example, the 95% confidence interval is given by  $(\bar{x} \pm SE_{\bar{x}} * 1.96)$ .

The *Coefficient of Variation*,  $C_v$ , is a normalized measure of the dispersion of a probability distribution, or put simply a normalised standard deviation:

$$C_v = \frac{\sqrt{Var(p)}}{E(p)} \tag{3.15}$$

where:

$Var(p)$  and  $E(p)$  are the variance and expectation of the variable,  $p$ .

The  $C_v$  can be estimated from a sample by:

$$C_v \approx \frac{\sigma(p)}{\bar{p}} \tag{3.16}$$

where:

$\sigma(p)$  and  $\bar{p}$  are the standard deviation and mean of the sample

Corbett and Jensen (1992) proposed a simple classification of  $C_v$  values using a large selection of permeability data from petroleum reservoirs and outcrop analogues (Fig. 3.15).

$C_v < 0.5$  implies an effectively homogeneous dataset:

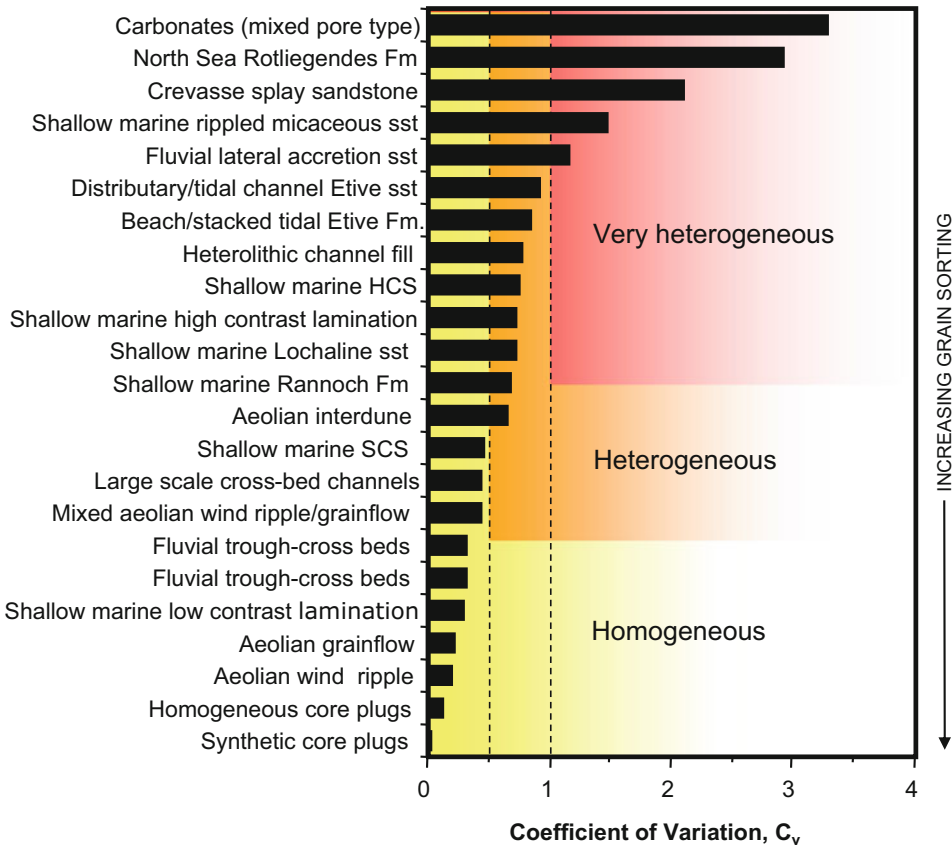


**Fig. 3.15** Reservoir heterogeneity for a large range of reservoir and outcrop permeability datasets ranked by the Coefficient of Variation,  $C_v$ , (redrawn from Corbett and

Jensen 1992; ©EAGE reproduced with kind permission of EAGE Publications B.V., The Netherlands)

- $0.5 < C_v < 1$  is termed ‘heterogeneous’
- $C_v > 1$  is termed ‘very heterogeneous’

The N-zero ( $N_o$ ) statistic (Hurst and Rosvoll 1991) captures these underlying statistical theories into a practical guideline for deciding how confident one can be given a limited dataset. The  $N_o$  statistic indicates the sample number required to estimate the true mean to within a 20% tolerance (at a 95% confidence level) as a function of the Coefficient of Variation,  $C_v$ :

$$N_o = (10 C_v)^2 \quad (3.17)$$

If the actual sample number is significantly less than  $N_o$  then a clear inference can be made that the sample is insufficient and that the sample statistics must be treated with extreme caution. For practical purposes we can use  $N_o$  as rule of thumb to indicate data sufficiency (e.g. Table 3.2). This simple approach assumes a Gaussian distribution and statistical representivity of the sample, so the approach is only intended as a first approximation. More precise estimation of the error associated with the mean of a given sample dataset can be made using confidence interval theory (e.g. Isaaks and Srivastava 1989; Jensen et al. 2000).

This analysis gives a useful framework for judging how variable your reservoir data really is. Note that more than half the datasets included in Fig. 3.14 are heterogeneous or very heterogeneous. Carbonate reservoirs and highly laminated or inter-bedded formations show the highest  $C_v$  values. This plot should in no way be considered as definitive for reservoirs for any particular depositional environment. We shall see later (Chap. 4), that the scale of measurement is a key factor within essentially multi-scale geological reservoir systems. Also keep in mind that your dataset may be too limited to make a good assessment of the true variability – the  $C_v$  from a sample dataset is an estimate. Jensen et al. (2000) give a

fuller discussion of the application of the  $C_v$  measure to petrophysical reservoir data.

### 3.3.3 The Normal Distribution and Its Transforms

Probability theory is founded in the properties of the Normal (or Gaussian) Distribution. A variable  $X$  is a *normal random variable* when the *probability density function* is given by:

$$g(x) = \frac{1}{\sigma\sqrt{2\pi}} e^{-\frac{(x-\mu)^2}{2\sigma^2}} \quad (3.18)$$

where:

$\mu$  is the mean and  $\sigma^2$  is the variance.

This bell-shaped function is completely determined by the mean and the variance. Carl Friedrich Gauss became associated with the function following his analysis of astronomical data (atmospheric scatter from point light sources), but the function was originally proposed by Abraham de Moivre in 1733 and developed by one of the founders of mathematics, Pierre-Simon de Laplace in his book *Analytical Theory of Probabilities* in 1812. Since that time, a wide range of natural phenomena in the biological and physical sciences have been found to be closely approximated by this distribution – not least measurements in rock media. The function is also fundamental to a wide range of statistical methods and the basis for most geostatistical modelling tools. It is also important to say that many natural phenomena do not conform to the Gaussian distribution – they may, for example, be better approximated by another function such as the Poisson distribution and in geology distributions have a strong tendency to be more complex and multimodal.

Permeability data is often found to be approximated by a log-normal distribution. A

variable  $X$  is *log-normally distributed* if its natural logarithmic transform  $Y$  is normally distributed with mean  $\mu_Y$  and standard deviation  $\sigma_Y$ . The probability density function for  $X$  is given by:

$$f(x) = \frac{1}{\sqrt{2\pi}\sigma_Y x} e^{-\frac{[\ln(x)-\mu_Y]^2}{2\sigma_Y^2}} \quad \text{if } x > 0 \quad (3.19)$$

The variable statistics,  $\mu_X$  and  $\sigma_X^2$  are related to the log transform parameters  $\mu_Y$  and  $\sigma_Y^2$  as follows:

$$\mu_X = e^{\mu_Y + 0.5\sigma_Y^2} \quad (3.20a)$$

$$\sigma_X^2 = \mu_X^2 (e^{\sigma_Y^2} - 1) \quad (3.20b)$$

This can lead to some confusion, and it is important that the reservoir modelling practitioner keeps close track of which distributions relate to which statistics. For  $\sigma = 0$  the mean obeys the simple law of the log transform,  $\mu_x = e^{\mu_Y}$ , but generally ( $\sigma > 0$ ),  $\mu_x > e^{\mu_Y}$ .

Log-normal distributions are appealing and useful because (a) they capture a broad spread of observations in one statistic, and (b) they are easily manipulated using log transforms. However, they also present some difficulties in reservoir modelling:

- They tend to generate excessive distribution tails.
- It is tempting to apply them to multimodal data.
- They can cause confusion, e.g. “*what is the average?*”

Note that the correct ‘average’ for a log-normal distribution of permeability is the geometric average – equivalent to a simple average of  $\ln(k)$  – but this does not necessarily mean that this is the ‘correct’ average for flow calculations. In fact, for a layered model with layer values drawn from a log-normal distribution the layer-parallel effective permeability is given by the arithmetic average (see previous section).

There are several useful transforms other than the log-normal transform. The Box–Cox

transform (Box and Cox 1964), also known as a power transform, is one of the most versatile and is essentially a generalisation of the log normal transform. It is given by:

$$x^{(\lambda)} = \begin{cases} \frac{(x^\lambda - 1)}{\lambda} & \text{if } \lambda \neq 0 \\ \ln(x) & \text{if } \lambda = 0 \end{cases} \quad (3.21)$$

where:

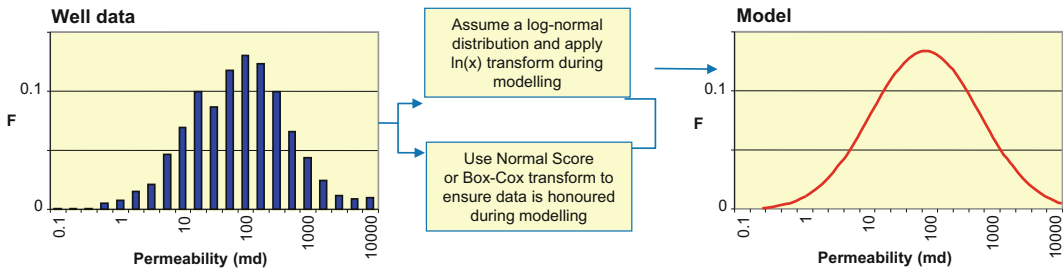
the power  $\lambda$  determines the transformed distribution  $x^{(\lambda)}$

the square-root transform is given by  $\lambda = 1/2$  and for  $\lambda = 0$  the transform is the log-normal transform

Another transform widely used in reservoir property modelling is the *normal score transform (NST)* in which an arbitrary distribution is transformed into a normal distribution, using a form of ranking (Deutsch and Journel 1992; Journel and Deutsch 1997). This is done using a cumulative distribution function (CDF) where each point on the CDF is mapped into a standard normal distribution using a transform (the score). There are several ways of doing this but the most common (and simple) is the linear method in which a linear factor is applied to each step (bin) of the cumulative distribution (for a fuller explanation see Soares 2001). This allows any arbitrary distribution to be represented and modelled in a geostatistical process (e.g. Sequential Gaussian Simulation). Following simulation, the results must be back transformed to the original distribution.

These transforms are illustrated graphically in Fig. 3.16. We should add an important note of caution when selecting appropriate transforms in any reservoir modelling exercise. It may be tempting to allow default transforms in a given modelling package (notably the NST) to automatically handle a series of non-Gaussian input data, e.g. Figure 3.16b. This can be very misleading and essentially assumes that your data CDFs are very close to the true population statistics. This is

a. Good, approximately log-normal dataset



b. Poor, non-Gaussian dataset

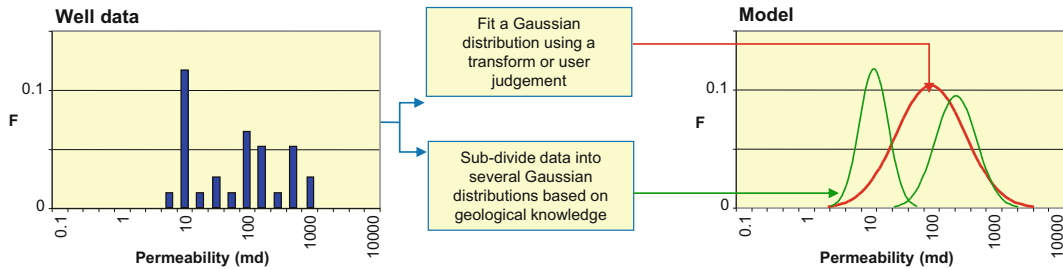
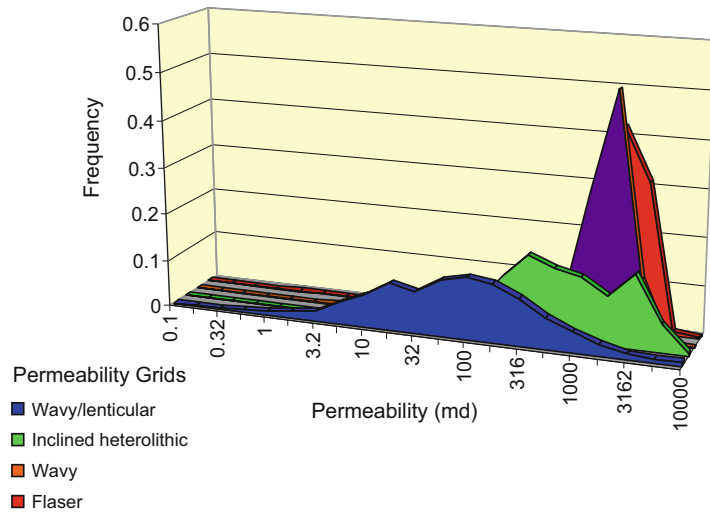


**Fig. 3.16** Illustration of data-to-model transforms for (a) a well-sampled dataset, and (b) a poorly-sampled datasets

**Fig. 3.17** Probe permeability datasets using a 2 mm-spaced measurements on a 10 cm grid of reservoir core slabs from facies in a tidal deltaic reservoir unit



in conflict with the  $Data \neq Truth$  axiom. It is preferable to control and select the transforms being used, and only employ the Normal Score Transform when clearly justified. The selection of the model elements (Chap. 2) is the first step to deconstructing a complex distribution, after which the normal score transform may indeed be applicable: one for each model element.

Two examples of something close to ‘true’ reservoir permeability distributions are shown in Fig. 3.17. Here, exhaustive probe permeability datasets have been assembled using a 2 mm-spaced measurements on a 10 cm grid of reservoir core slabs from facies in a tidal deltaic reservoir unit. In one case, the permeability distribution is close to log-normal, while the others they are

clearly not – more root normal or multi-modal. So it cannot be generally true that permeability is lognormally distributed – it often is, but not necessarily so.

With more conventional data sets, e.g. log datasets, we also have the problem of under-sampling to contend with. Figure 3.18 shows three contrasting log-based porosity datasets. The first (a) could be successfully represented by a normal distribution while the second (b) is clearly neither normal nor log-normal. The third (c) is a typical under-sampled dataset where the user needs to infer a ‘restored’ porosity distribution.

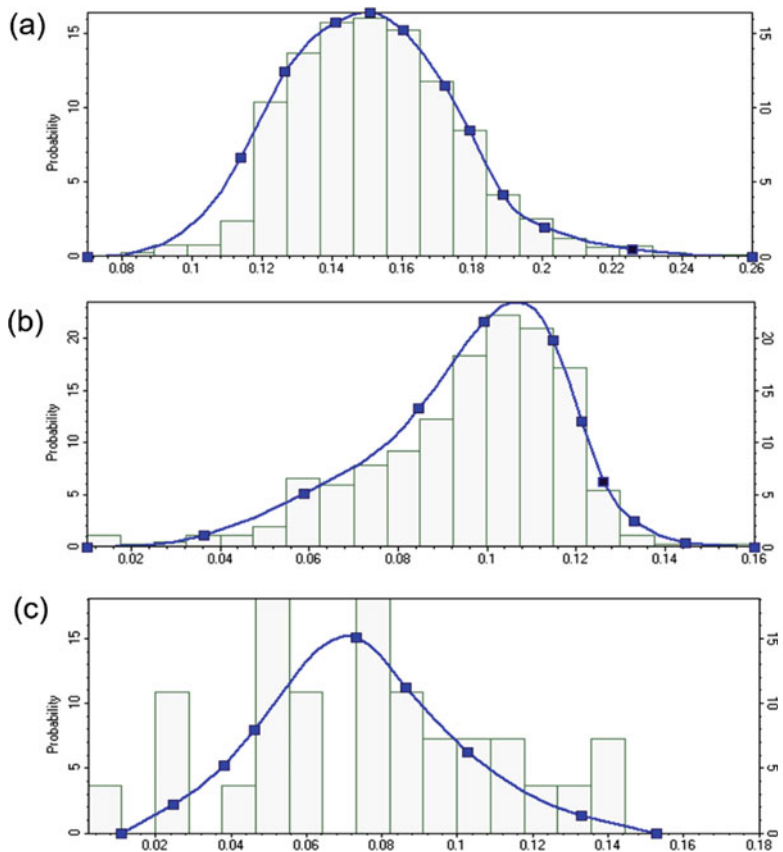
Whatever the nature of the underlying distributions in a reservoir dataset, we should bear in mind an important principle embodied

by the *Central Limit Theorem* which can be summarized as follows:

The distribution of sample means from a large number of independent random variables usually approximates a normal distribution regardless of the nature of the underlying population distribution functions.

For example, let us assume we have  $N$  wells with permeability data for a given reservoir unit. For each well, we have observed distributions of  $k$  which appear to be approximately log-normally distributed (a common observation). However, the distribution of the average well-interval permeability between wells (the mapped parameter) is found to be normally distributed. This is quite consistent, and indeed for a large number of wells

**Fig. 3.18** Example sandstone reservoir porosity distributions (*histograms*) and possible model distributions fitted to the data: (a) approximately normal, (b) neither normal nor log-normal, (c) under-sampled



this is expected from central limit theory. Similar arguments can apply when upscaling – fine-scale permeability distributions may be quite complex (log-normal or multi-modal) whereas coarse-scale distributions tend towards a normal distribution. An important constraint for the Central Limit Theorem is that the samples should be statistically independent and reasonably large.

### 3.3.4 Handling $\phi$ -k Distributions and Cross Plots

Plots of porosity ( $\phi$ ) versus permeability ( $k$ ) are fundamental to the process of reservoir modelling (loosely referred to as ‘poro-perm cross-plots’). Porosity represents the available fluid volume and permeability represents the ability of the fluid to flow. In petroleum engineering, porosity is the essential factor determining fluids in place whereas permeability is the essential factor controlling production and reserves (in groundwater hydrology and in gas storage the term ‘storativity’, a function of the effective porosity and the hydraulic conductivity, are often used).

Poro-perm cross-plots are used to perform many functions:

- To compare measured porosity and permeability from core data.
- To estimate permeability from log-based porosity functions in uncored wells.
- To model the distribution of porosity and permeability in the inter-well volume; reservoir property modelling.

Good reservoir model design involves careful use of  $\phi$ -k functions whereas poor handling of this fundamental transform can lead to gross errors. It is generally advisable to regress permeability (the dependent variable) on porosity (as the independent variable).

In general, we often observe permeability data to be log-normally distributed whereas porosity data is more likely to be normally distributed. This has led to a common practice of plotting porosity versus the log of permeability and finding a best-fit function by linear regression.

Although useful, this assumption has pitfalls:

- Theoretical models and well-sampled datasets show that true permeability versus porosity functions depart significantly from a log-linear function. For example, Bryant and Blunt (1992) calculated absolute permeability – using a pore network model – for randomly packed spheres with different degrees of cementation to predict a function (Fig. 3.19) that closely matches numerous measurements of the Fontainebleau sandstone (Bourbie and Zinszner 1985).
- Calculations based on an exponential trend line fitted to log-transformed permeability data can lead to serious bias due to a statistical pitfall (Delfiner 2007).
- Multiple rock types (model elements) can be grouped inadvertently into a common cross plot which gives a misleading and unrepresentative function.
- Sampling errors, including application of cut-offs, lead to false conclusions about the correlation between porosity and permeability.

Delfiner (2007) reviews some of the important pitfalls in the  $k$ - $\phi$  transform process, and in particular recommends using a permeability estimator based on percentiles – Swanson’s mean. Swanson’s mean permeability,  $k_{SM}$ , for a given class of porosity (e.g. 15–20%) is given by:

$$k_{SM} = 0.3 X_{10} + 0.4 X_{50} + 0.3 X_{90} \quad (3.22)$$

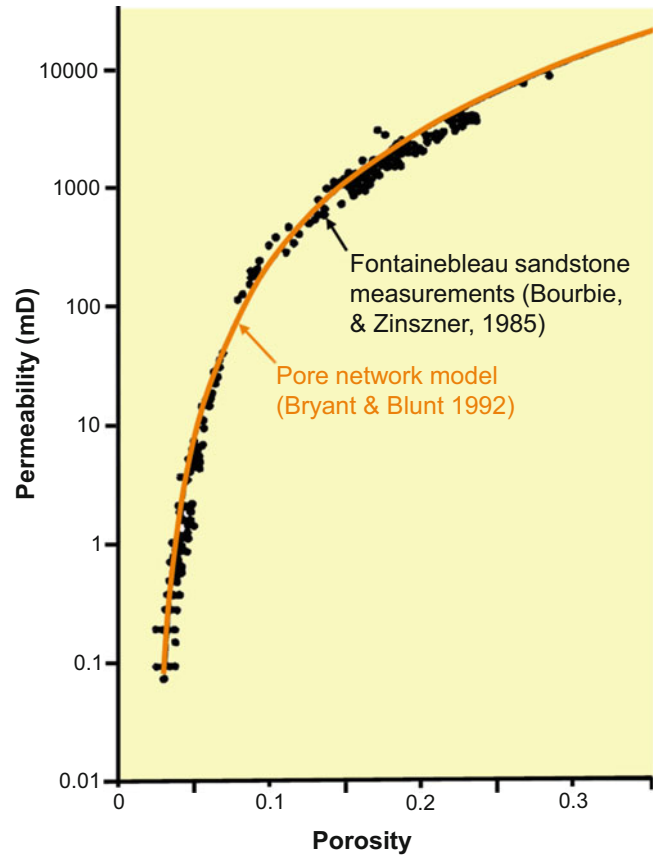
where:

$X_{10}$  is the tenth percentile of the permeability values in the porosity class.

The resulting mean is robust to the log-linear transform and insensitive to the underlying distribution (log-normal or not). The result is a significantly higher  $k_{mean}$  than obtained by a simple trend-line fit through the data.

Figure 3.20 illustrates the use of the  $k$ - $\phi$  transform within the Data  $\neq$  Model  $\neq$  Truth paradigm. True pore systems have a non-linear relation between porosity and permeability, depending on the specific mechanical and chemical history

**Fig. 3.19** Pore-network model of a porosity-permeability function closely matched to data from the Fontainebleau sandstone



of that rock (compaction and diagenesis). We use the Fontainebleau sandstone trend to represent the ‘true’ (but essentially unknown)  $k$ - $\phi$  relationship (Fig. 3.20a). Core data may, or may not, give us a good estimate of the true relationship between porosity and permeability, and the inferred function is strongly dependent on the selection of elements (Sect. 2.4) and sample size. For example, in Fig. 3.20b, the correlation coefficient ( $R^2$ ) for a single element is significantly lower than for the total reservoir unit (due to reduced sample size). Furthermore, for the whole dataset, Swanson’s mean gives a higher permeability trend than with a simple exponential fit to the data. The modelled  $k$ - $\phi$  transform (Fig. 3.20c) should be designed to both faithfully represent the data and capture rock trends or populations that may not be fully represented by the measured data. Upscaling leads to further transformations of the  $k$ - $\phi$  model. In general, we

should expect a reduction in variance (therefore improved correlation) in the  $k$ - $\phi$  transform as the length-scale is increased (see discussion on variance in Chap. 4).

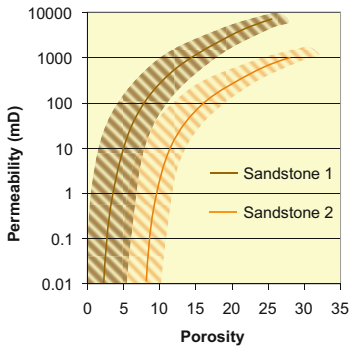
We have introduced two end member approaches to modelling:

1. Concept-driven;
2. Data-driven.

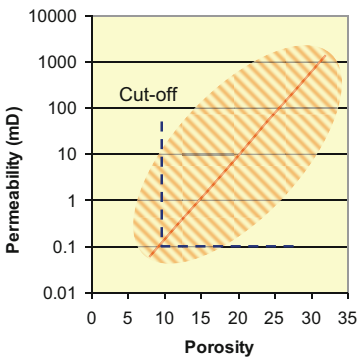
The concept-driven approach groups the data into a number of distinct model elements, each with their own  $k$ - $\phi$  transform. Simple log transforms and best-fit functions are used to capture trends but  $k$ - $\phi$  cross-correlation is poor and belief in the data support is weak. The process is ‘model-driven’ and the explicitly modelled rock elements capture the complex relationship between porosity and permeability.

The data-driven approach assumes a representative dataset and a minimal number of model

(a) True k-φ relationship (unknown)



(c) Modelled k-φ relationship



(b) Analysis of k-φ data

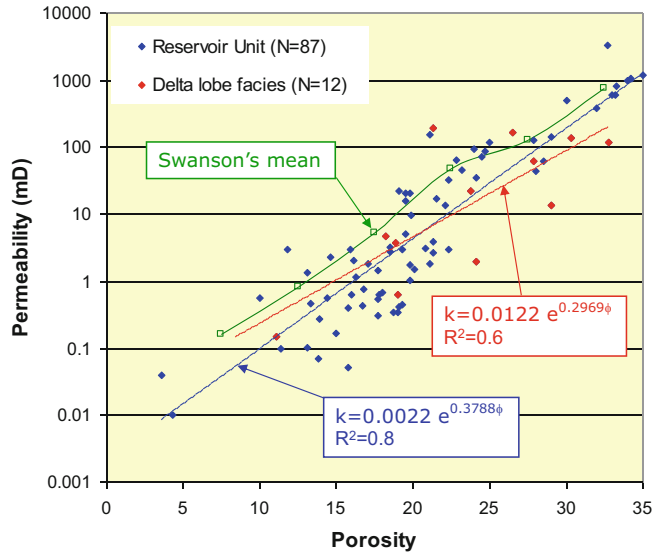


**Fig. 3.20** Use of the k-φ transform: (a) True pore systems exhibit a non-linear relationship with dispersion, (b) Data analysis is sensitive to the choice of elements and

statistical analysis method; (c) The model function should be constrained by data and fit-for-purpose

elements are distinguished (perhaps only one). Care is taken to correctly model the observed k-φ transform, using for example a piecewise or percentile-based formula (e.g. Swanson’s mean). The reservoir model is ‘data-driven’ and the carefully-modelled k-φ transform aims to capture the complex relationship between porosity and permeability.

used to capture the shape factor and tortuosity terms.

Modifying the Kozeny-Carmen equation gives:

$$0.0314 \sqrt{\frac{k}{\phi_e}} = \frac{\phi_e}{1 - \phi_e} F_{zi} \quad (3.23)$$

where:

k is in mD.  
 $\phi_e$  is the effective porosity.

$F_{zi}$  is a function of the tortuosity,  $\tau$ , the shape factor,  $F_s$ , and the surface area per unit grain volume,  $S_{gv}$ :

$$F_{zi} = \frac{1}{\tau \sqrt{F_s} S_{gv}} \quad (3.24)$$

### 3.3.5 Hydraulic Flow Units

The Hydraulic Flow Unit (HFU) concept offers a useful way of classifying properties on the k-φ cross-plot, and can be linked to the definition of model elements in a modelling study. Abbaszadeh et al. (1996) defined HFU’s in terms of a modified Kozeny-Carmen equation in which a Flow Zone Indicator,  $F_{zi}$ , was



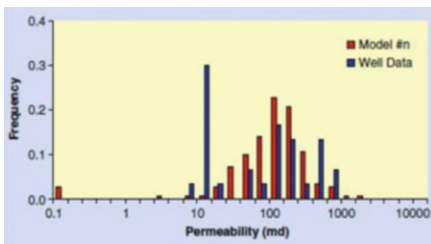
The  $F_{zi}$  term thus gives a formal relationship between  $k$  and  $\phi$  which is related to pore-scale flow physics (laminar flow in a packed bed of spherical particles).

**Exercise 3.4**

Comparing model distributions to data.

The plot and table below show a comparison of well data with the output of a model realisation designed to represent the data in a geological model. The well data are from a cored well interval identified as a deltaic sandstone facies. The model has used Gaussian statistical modelling to represent the spatial distribution of permeability. The two distributions appear to match quite well – they cover a similar range and have a similar arithmetic mean. However, analysis of the data statistics reveals some strange behaviour – the geometric and harmonic means are quite different.

What is going on here? And is this in fact a good model for the given data?



| Statistics                  | Well data | Model #n |
|-----------------------------|-----------|----------|
| Number of data values/cells | 30        | 150      |
| Arithmetic mean             | 119.9     | 115.7    |
| Geometric mean              | 45.9      | 90.8     |
| Harmonic mean               | 17.19     | 0.87     |

\*\*

**3.4 Modelling Property Distributions**

Assuming we have a geological model with certain defined components (i.e. zones, model elements), how should we go about distributing properties within those volumes? There are a number of widely used methods. We will first summarise these methods and then discuss the choice of method and input parameters.

The basic input for modelling spatial petrophysical distribution in a given volume requires the following:

- Mean and deviation for each parameter (porosity, permeability, etc.).
- Cross-correlation between properties, e.g. how well porosity correlates with permeability.
- Spatial correlation of the properties, i.e. how rapidly the property varies with position in the reservoir.
- Vertical or lateral trends, how the mean values vary with position.
- Conditioning points (known data values at the wells).

The question is “how should we use these input data sensibly?” Commercial reservoir modelling packages offer a wide range of options, usually based on two or three underlying geostatistical methods (e.g. Hohn 1999; Pyrcz and Deutsch 2014). Our purpose is to understand what these methods do and how to use them wisely in building a reservoir model.

**3.4.1 Kriging**

*Kriging* is a fundamental spatial estimation technique related to statistical regression. The approach was first developed by Matheron (1967) and named after his student Daniel Krige who first applied the method for estimating average gold grades at the Witwatersrand gold-bearing reef complex in South Africa. To gain a basic appreciation of Kriging, take the simple case of an area we want to map given a few data points, such as wells which intersect the reservoir layer (Fig. 3.21).

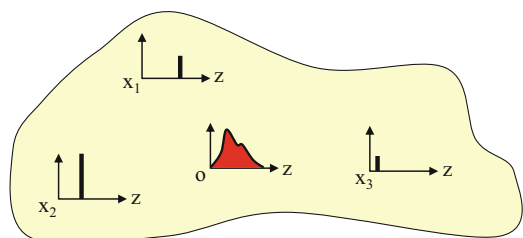


**Fig. 3.21** Illustration of the Kriging method

We want to estimate a property,  $Z^*$  at an unmeasured location,  $o$ , based on known values of  $Z_i$  at locations  $x_i$ . Kriging uses an interpolation function:

$$Z^* = \sum_{i=1}^n \omega_i Z_i \quad (3.25)$$

where:

$\omega_i$  are the weights.  
the *objective function* minimises variance.

That is to say, a set of weights are found to obtain a minimum expected variance given the available known data points.

The algorithm finds values for  $\omega$  such that the objective function is honoured. The correlation function ensures gradual changes, and Kriging will tend to give a smooth function which is close to the local mean. Mathematically there are several ways of Kriging, depending on the assumptions made. *Simple Kriging* is mathematically the simplest, but assumes that the mean and distribution are known and that they are statistically stationary, i.e. a global mean. *Ordinary Kriging* is more commonly used because it assumes slightly weaker constraints, namely that the mean is unknown but constant, i.e. a local mean, and that the variogram function is known. Fuller discussion of the Kriging method can be found in many textbooks; Jensen et al. (2000) and Leuangthong et al. (2011) give very accessible accounts for non-specialists.

### 3.4.2 The Variogram

The variogram function describes the expected spatial variation of a property. In Chap. 2 we discussed the ability of the variogram to represent element length scales and hence architecture. Here we employ the same function as a modelling tool to estimate spatial property variations within that architecture.

We recall that the semi-variance is half the expected value of the squared differences in values separated by  $h$ :

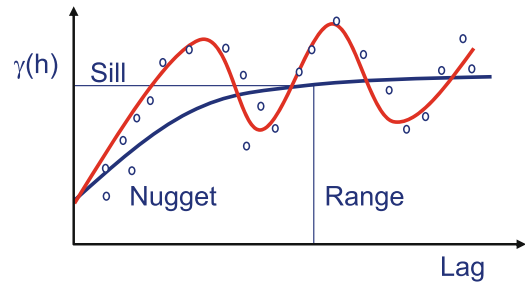


**Fig. 3.22** Sketch of the semi-variogram (*blue* = theoretical function; *red* = function through observed data points)

$$\gamma(h) = \frac{1}{2} E \{ [Z(x+h) - Z(x)]^2 \} \quad (3.26)$$

The semi-variogram (Fig. 3.22) has several important features. The ‘lag’ ( $h$ ) is the separation between two points. Two adjacent points will tend to be similar and have a  $\gamma(h)$  close to zero. A positive value at zero lag is known as the ‘nugget’. As the lag increases the chance of two points having a similar value decreases, and at some distance a sill is reached where the average difference between two points is large, and in fact close to the variance of the population. The range (equivalent to the correlation length) describes the ‘separation distance’ at which this occurs. A theoretical semi-variogram has a smooth function rising up towards the variance while measured/observed semi-variogram often has oscillations and complex variations due to, for example, cyclicity in rock architecture.

The most common functions for the semi-variogram are spherical, Gaussian and exponential – each giving a different rate of rise towards the sill value (Fig. 2.23). Note that for a specific situation (second order stationarity) the semi-variogram is the inverse of the covariance (de Marsilly 1986, p. 292). Jensen et al. (1995) and Jensen et al. (2000) give a more extensive discussion on the application of the semi-variogram to permeability data in reservoirs. One important observation here is that most reservoir property modelling workflows assume the spherical model. This is partly due to experience with rock property datasets (which typically show a steady increase towards the range) but also

because it is modelled with a simple polynomial expression with the form:

$$\gamma(h) = \left(1.5 \frac{h}{a} - 0.5 \frac{h^3}{a^3}\right) \text{ if } h \leq a \quad (3.27)$$

where:

$a$  is the range

See Deutsch (2002) or Isaaks and Srivastava (1989) for a fuller explanation of semi-variogram models. Application of the semi-variogram for rock modelling is discussed in Chap. 2.

### 3.4.3 Gaussian Simulation

Gaussian Simulation covers a number of related approaches for estimating reservoir properties away from known points (well observations). The Sequential Gaussian Simulation (SGS) method can be summarized by the following steps (Jensen et al. 2000):

1. Transform the sampled data to be Gaussian.
2. Assign unconditioned cells (inter-well) = conditioned cells (wells).
3. Define a random path to visit each cell.
4. For each cell locate a specified number of conditioning data (the neighbourhood).
5. Perform Kriging in the neighbourhood to determine the local mean and variance, using the variogram as a constraint.
6. Draw a random number to sample the Gaussian distribution (from step 5).
7. Add the new simulated value to the ‘known’ data and repeat step 4.

Repeating steps 4–7 gives one realisation of a Gaussian random distribution conditioned to known points. Repeating step 3 gives a new realisation. The average of a large number of realisations will approach the kriged result. In this way we can use Gaussian simulation to give a spatial statistical model of reservoir properties that includes lateral and vertical heterogeneity. A good geostatistical model should give a realistic

picture of petrophysical structure and variability and can be used for flow simulation and for studies to define drilling targets. However, one realisation is only one possible outcome, and many realisations normally need to be simulated to assess variability and probability of occurrence. To put this in practical terms, a single realisation might be useful to define static heterogeneity for a flow simulation model, but a single realisation would be little value in planning a new well location, hence the importance of establishing clear model purpose (see Sect. 1.5). For well planning or reserves estimation, the average expectation from many realisations, or a Kriged model, would be a more statistically stable estimate.

*Truncated Gaussian Simulation* (TGS) is a simple modification of SGS where a particular threshold value of the simulated Gaussian random field is used to identify a model element or petrophysical property group, such as porosity  $> X$  (Fig. 3.22). *Sequential Indicator Simulation* (SIS) uses a similar approach but treats the conditioning data and the probability function as a discrete (binary) variable from the outset (Journel and Alabert 1990). The indicator transform is defined by:

$$i(\vec{u}; z) = \begin{cases} 1, & \text{if } z(\vec{u}) \leq z \\ 0, & \text{if not} \end{cases} \quad (3.28)$$

where:

$z$  is the cut-off value for a field of values  $\vec{u}$ .

The field  $\vec{u}$  could be derived from, for example, porosity data, the gamma-ray log or seismic impedance. The important decision is the choice of the indicator value. Both these methods are useful for modelling rock elements (Sect. 2.7) as well as for modelling property distributions within elements.

Figure 3.23 illustrates the different methods of Gaussian simulation. The methods can be used in a number of ways, for example to define several nested groups of model elements and the properties within them. Gaussian simulation is an essential part of the tool kit for property

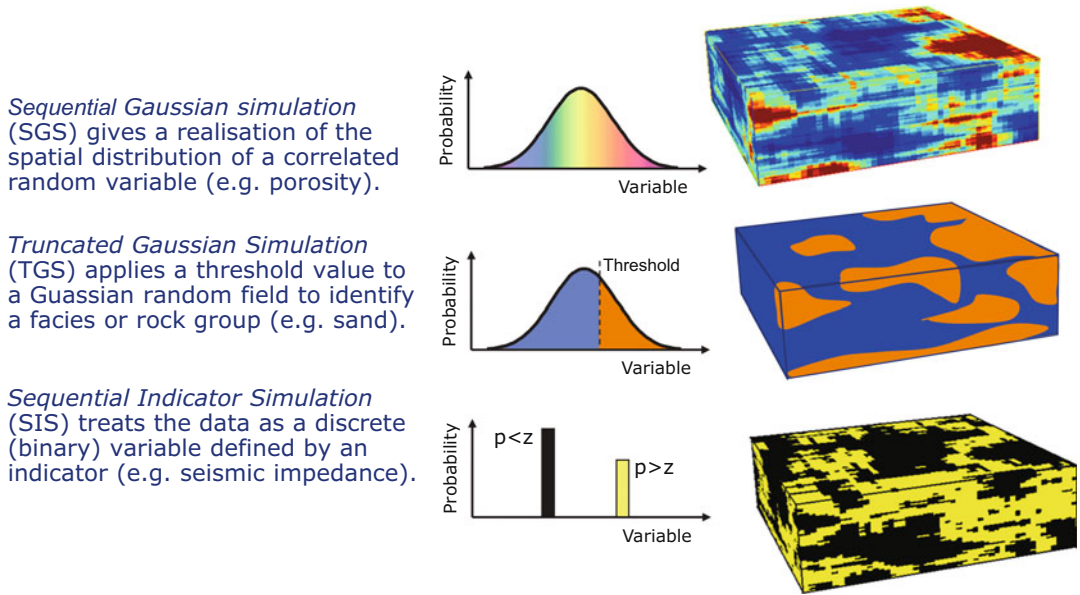


**Fig. 3.23** Illustration of the different methods for property modelling using Gaussian simulation

modelling and also a key tool for data integration, especially for combining well data with seismic inversion data. Doyen (2007) gives an in-depth account of seismic-based rock property modelling including a detailed description of the application of the SGS and SIS methods to seismic datasets.

### 3.4.4 Bayesian Statistics

We have now reviewed the main statistical tools employed in property modelling; however, one important concept is missing. We argued in Chap. 2 that reservoir modelling must find a balance between determinism and probability, and that more determinism is generally desirable. Using Gaussian simulation methods without firm control from the known data is generally unhelpful and dissatisfying. We ideally want geostatistical property models rooted in geological concepts and conditioned to observations (well, seismic and dynamic data), and this is where Bayes comes in. Thomas Bayes (1701–1761) developed a theorem for updating beliefs about the natural world and then later his ideas were developed and formalised by Laplace (in *Théorie analytique des probabilités*, 1812).

Subsequently, over the last 50 years, Bayesian theory has revolutionised many fields of statistical analysis, not least reservoir modelling.

Bayesian inference derives one uncertain parameter (the posterior probability) from another (the prior probability) via a likelihood function. Bayes' rule states that:

$$P(A|B) = \frac{P(B|A)P(A)}{P(B)} \quad (3.29)$$

where:

$P(A|B)$  is the *posterior* – the probability of A assuming B is observed

$P(A)$  is the *prior* – the probability of A before B was observed

$P(B|A)$  is the *likelihood* (of what was actually observed)

$P(B)$  is the underlying evidence (also termed the marginal likelihood)

This comparison of prior and posterior probabilities may at first appear confusing, but is easily explained using a simple example (Exercise 3.5), and fuller discussion can be found elsewhere (e.g. Howson and Urbach 1991). The

essence of Bayesian estimation is that a probabilistic variable (the posterior) can be estimated given some constraints (the prior). This allows probabilistic models to be constrained by data and observations, even when those data are incomplete or uncertain. This is exactly what probabilistic reservoir models need: a dependence on, or conditioning to, observations. Bayesian methods are used to condition reservoir models to seismic, well data and dynamic data, and are especially valuable for integrating seismic and well data.

### Exercise 3.5

Bayes and the cookie jar.

A simple example to illustrate Bayes theory is the ‘cookie jar’ example. There are two cookie jars. One jar has 10 chocolate chip cookies and 30 plain cookies, while the second jar has 20 of each. Fred picks a jar at random, and then picks a cookie at random – he gets a plain one. We all know intuitively he could have picked from either jar, but most likely picked from jar 1. Use Bayes theory Eq. (3.29) to find probability that Fred picked the cookie from Jar 1.

The answer is 0.6 – but why?

\*\*

Given that we have a set of recipes for different property modelling methods, how do we combine them to make a good property model? Remember that the mark of a good model is that it is geologically-based and fit for purpose. To illustrate the different approaches to property model design we describe two approaches based on case studies:

- An object-based model of channelised elements based on detailed outcrop data.
- A seismic-based rock model, exploiting good 3D seismic data.

### 3.4.5 Property Modelling: Object-Based Workflow

Rock modelling using object-based methods was explained in Chap. 2. The geological objects

(i.e. model elements such as channels, bar forms, or sheet deposits) need petrophysical properties to be defined. This could be done in a very simplistic manner – such as the assumption that all channel objects have a constant porosity and permeability – or can be done by ‘filling’ the objects with continuous properties using a Gaussian simulation method. Each model element is assigned the statistical parameters required to define a continuous property field (using Sequential Gaussian Simulation) which applies only to that element. This process can become quite complicated, but allows enormous flexibility and the ability to condition geological reservoir models to different datasets for multiple reservoir zones.

This process is illustrated for an object-based model used for stochastic simulation of permeability for an outcrop model (Brandsæter et al. 2005). A section from the Lajas Formation in Argentina (McIlroy et al. 2005) was modelled due to its value as an analogue to several reservoirs in the Hatnbanken oil and gas province offshore mid Norway. The model is 700 m by 400 m in area and covers about 80 m of stratigraphy – it is thus a very-high resolution model, highly constrained by detailed outcrop data. The model illustrates how an object model based on outcrop data can be combined with Gaussian simulation of petrophysical properties using well data from the Heidrun oilfield offshore Norway. Note that in this case we assign reservoir properties to the outcrop model, whereas normally we would make a reservoir model assuming geological object dimensions derived from outcrop studies.

Table 3.3 summarises some of the dimensions assumed for the geological objects in this model. Object lengths are in the range of 500 m to 1000 m, with widths slightly smaller, whereas object thicknesses are in the in 0.5–2 m range. These values have some uncertainty but are relatively well known as they are based on detailed study of the outcrop. However, the correlation lengths,  $\lambda_x$ ,  $\lambda_y$ ,  $\lambda_z$ , that are required to control property distributions within objects are much less well constrained. In this study, a plausible range of correlation lengths (Table 3.3) was assumed and used as input to a sensitivity

**Table 3.3** Example object dimensions and correlation lengths from the Lajas outcrop model study

| Facies  | Object length (m)  | Object width (m) | Object thickness (m)                         |
|---|--|------------------|--|
| Meandering channels                               | 1000   | 300              | 2  |
| Trough cross-bedded cannels                       | 1000   | 100              | 1.5  |
| Mixed tidal flats                                 | 500  | 400              | 0.5  |
| Correlation lengths for properties within objects | Horizontal correlation length $\lambda_x, \lambda_y$ (m) |                  | Vertical correlation length, $\lambda_z$ (m) |
| All facies  | 50–500   |                  | 0.5–5.0                                      |

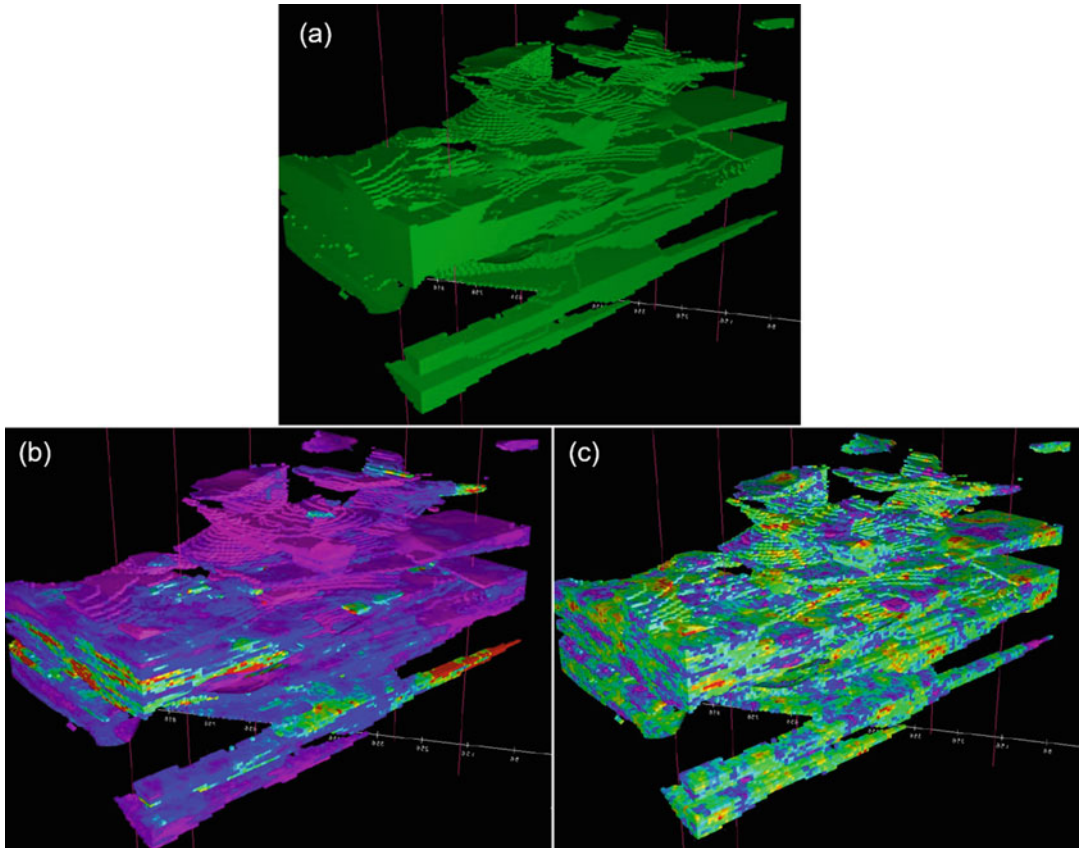


**Fig. 3.24** Property model examples from the Lajas tidal delta outcrop model (Brandsæter et al. 2005): (a) Modelled tidal channel objects; (b) Permeability realisation assuming a short correlation length of 50 m horizontally and 0.5 m vertically; (c) Permeability

realisation assuming a long correlation length 500 m horizontally and 5 m vertically. *Yellow and red* indicate high permeability values while *blue and purple* indicate low permeability values

analysis. The range was chosen to test the effects of highly-varying or gradually-varying properties within objects (Fig. 3.24). Sensitivity analysis showed that oil production behaviour is very sensitive to this value, alongside the effects of anisotropy and rock model (Brandsæter et al. 2005).

In general, we expect there to be some property variation within rock objects, therefore  $\lambda_x, \lambda_y, \lambda_z < \text{object dimension}$ . The question is how much variation? The choice of correlation lengths for property modelling is therefore very uncertain and also rather important for flow modelling. In

practice, sensitivity to this parameter needs to be evaluated as part of the model design. The value range should be constrained to any available geological data and to evidence from dynamic data, such as the presence or absence of pressure communication between wells in the same model element or reservoir unit.

A useful guideline is to test the following hypotheses:

- Properties are relatively constant within geological objects:  $\lambda \approx$  object dimension.
- Properties are quite variable within geological objects:  $\lambda \approx 1/3$  object dimension.
- Properties are highly variable within geological objects:  $\lambda \approx 1/10$  object dimension.

Note that the grid size needs to significantly smaller than the correlation length being modelled, e.g.  $\lambda \approx 1/10$  object dimension would require a very fine grid.

### 3.4.6 Property Modelling: Seismic-Based Workflow

Seismic imaging has made enormous leaps and bounds in the last decades – from simple detection of rock layers that might contain oil or gas to 3D imaging of reservoir units that almost certainly do contain oil and gas (using direct hydrocarbon indicators) to high-resolution broadband imaging of CO<sub>2</sub> storage prospects. In this book we have assumed that seismic imaging is always available in some form to define the reservoir container, e.g. the top reservoir surface and bounding faults. Here we are concerned with the potential for using seismic data to obtain information about the reservoir properties – such as porosity or the spatial distribution of high porosity sandstones.

There are numerous recipes available for obtaining reservoir properties from seismic data, e.g. Doyen 2007. These are all based on the underlying theory of seismology in which reflected or refracted seismic waves are controlled by changes in the density ( $\rho$ ) and velocity ( $V_P$ ,  $V_S$ ) of rock formations. More specifically,

seismic imaging is controlled by the acoustic impedance,  $AI = \rho V_P$  (for a compressional wave). Zoeppritz, in 1919, determined the set of equations which control the partitioning of seismic wave energy at a planar interface, and then subsequently many others (notably Shuey 1985) developed approaches for determining rock properties from seismic waves. Because there is a relationship between the reflection coefficient,  $R$ , and the angle of incidence,  $\theta$ , analysis of seismic amplitude variations with offset (AVO) or angle (AVA) allows rock properties of specific rock layers to be estimated.

The simplest form of the AVO equations, known as the Shuey approximation is:

$$R(\theta) = R(0) + G \sin^2\theta \quad (3.30)$$

where:

$R(0)$  and  $R(\theta)$  are the reflection coefficients for normal incidence and offset angle  $\theta$ .

$G$  is a function of  $V_P$  and  $V_S$ , given by:

$$G = \frac{1}{2} \frac{\Delta V_P}{V_P} - 2 \frac{V_S^2}{V_P^2} \left( \frac{\Delta \rho}{\rho} + 2 \frac{\Delta V_S}{V_S} \right) \quad (3.31)$$

Subsequently, using empirical correlations, it is then possible to estimate porosity from  $V_P$ ,  $V_S$  and  $\rho$ . Assuming that information on rock properties can be gained from seismic data, the next challenge is to find a way of integrating seismic information with well data and the underlying geological concepts. The real challenge here is that well data and seismic data rarely tell the same story – they need to be reconciled. Both seismic data and well data have associated uncertainties. They also sample different volumes with the reservoir – well data needs to be upscaled and seismic data needs to be downscaled (depending on the grid resolution and seismic resolution of the case in hand). This is where the Bayesian method comes into play.

Buland et al. (2003) developed a particularly elegant and effective method for estimating rock properties from AVO data, employing Bayesian inference and the Fourier transform. This approach allows the reservoir modeller to

reconcile different scales of data (seismic versus well data, using the Fourier transform) within a robust Bayesian statistical framework: finding the best seismic inversion given the well data – a P (AIB) problem. Nair et al. (2012) have illustrated this workflow for reservoir characterisation, combining elastic properties (from seismic) with facies probability parameters (from wells) to condition probabilistic property models.

Having first extracted elastic properties ( $V_P$ ,  $V_S$  and  $\rho$ ) from the seismic AVA data (Fig. 3.25), the challenge is then to relate elastic properties to flow properties.

Because flow properties are essentially estimated from well data (cores and logs), we need to merge (or correlate) the seismic elastic properties with elastic and flow properties at the wells. This is a complicated process. We need a velocity model to convert seismic data from time to depth and we need a way of handling the scale transition, as well data has high frequency content not present in the seismic data. Using Bayesian reasoning, Buland et al. (2003) and Nair et al. (2012) use the following steps:

1. Assign the elastic properties from well data as a prior probability model,  $p(m)$ .
2. Treat the seismic AVA data ( $d$ ) as a likelihood model,  $p(d|m)$ .

3. The Bayesian inversion is then posterior probability model,  $p(m|d)$ .

To handle the band-limitations of the seismic data a low frequency background model is needed. This is estimated from vertical and lateral trends in the well log data using Kriging to generate a smoothed background model. This background model itself should capture the underlying geological concepts (sand fairways, porosity trends) but is also critical to the seismic inversion. Figure 3.26 shows an example comparison of raw versus inverted  $V_P$  logs, an important step in quality control of the process.

The solutions to seismic AVA inversion are non-unique and entail large amounts of data: wavelets and reflection coefficients for each offset angle throughout the volume of interest. By transferring the data into the Fourier domain (the frequency spectrum), Buland et al. (2003) used a fast Fourier transform to handle the seismic covariance matrices and to separate the signal and noise terms. Figure 3.27 compares AI from seismic inversion (the prediction) with two stochastic realisations of simulated AI, incorporating both seismic data and well data. Notice the finer resolution of simulated cases because of inclusion of higher frequency well data with the seismic data in this Bayesian workflow.

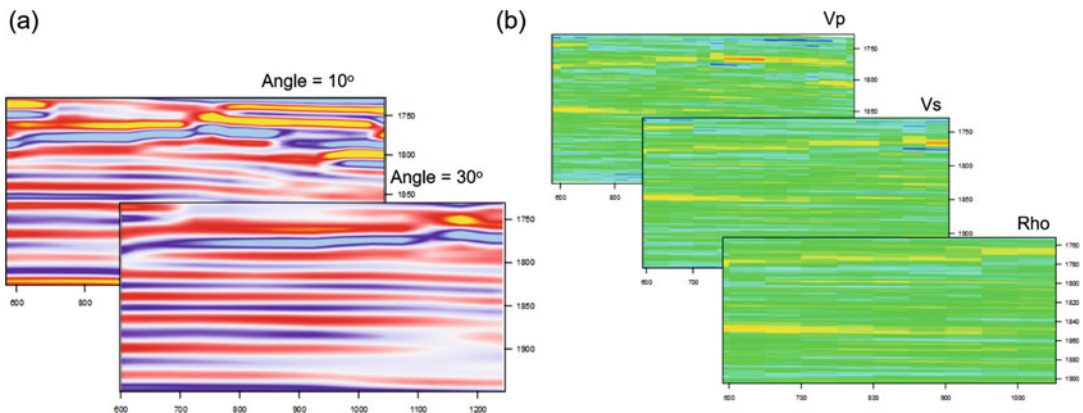


**Fig. 3.25** (a) Angle stacks and (b) corresponding inverted elastic parameters from seismic inversion case study. (Redrawn from Nair et al. 2012, ©EAGE

reproduced with kind permission of EAGE Publications B.V., The Netherlands)



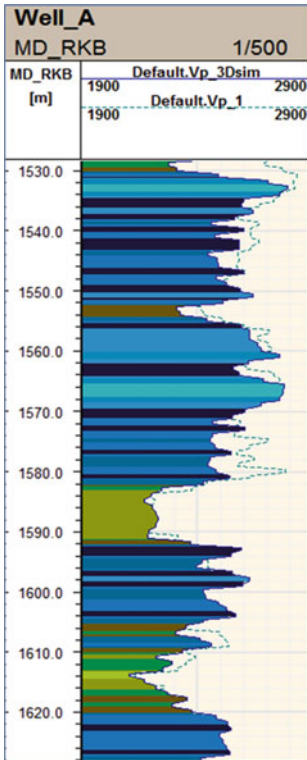


**Fig. 3.26** Comparison of raw  $V_p$  logs (*dashed lines*) with  $V_p$  logs extracted along the well from the inverted 3D seismic data (*continuous lines*). (Redrawn from Nair et al. 2012, ©EAGE reproduced with kind permission of EAGE Publications B.V., The Netherlands)

The potential for deriving rock properties from seismic data is enormous. The  $V_p/V_s$  versus impedance plot, e.g. Figure 3.28, is widely used as a rock physics template, giving the potential for estimation of facies and flow properties from seismic data. Exactly how successfully this can be done depends on the case at hand and the data quality. We should add a cautionary reminder to seismic inversion enthusiasts – the transform from elastic properties to flow properties is not a simple one, and there are many pitfalls. However, in the hands of an experienced reservoir modeller the Bayesian statistical framework offers a rather elegant way of making that leap from 3D seismic data to predictive flow property models.

## 3.5 Use of Cut-Offs and N/G Ratios

### 3.5.1 Introduction

The concept of the net-to-gross ratio (N/G) is widespread in the oil business and consequently reservoir modelling. Unfortunately, the concept is applied in widely differing ways and poor use can lead to serious errors. In this section, we consider appropriate ways to handle N/G in the context of a typical reservoir modelling work flow and discuss an alternative approach termed ‘Total Property Modelling’.

In the simplest case, a clastic reservoir can be divided into sand and shale components:

$$N/G = \text{Sand volume fraction} / \text{Gross rock volume (GRV)}$$

In most cases, rocks have variable sand content and the sands themselves have variable reservoir quality such that:

$$N/G_{\text{reservoir}} \neq \text{Sand volume fraction} / \text{GRV}.$$

The term ‘net sand’ is commonly defined with respect to the gamma and porosity logs, as in the logical expression [IF Gamma < X AND Poro > Y THEN NET]. In such a case, ‘net sand’ has a rather weak and arbitrary association with the geological rock type ‘sandstone.’ Worthington and Cosentino (2005) discuss this problem at length and show how widely the assumptions vary in the definition of net sand or net reservoir. To avoid any further confusion with terminology we adopt their definitions (Table 3.4). Many problems arise from misunderstanding of these basic concepts especially when different disciplines – petrophysics, geoscience and reservoir engineering – assume different definitions.

Another common piece of folklore, often propagated within different parts of the petroleum industry is that oil and gas reservoirs have specific values for permeability cut-off that should be applied: for example the assumption that the cut-off value for an oil reservoir should be 1 mD

**Fig. 3.27** Comparison of AI predicted from seismic inversion with two stochastic simulations integrating both the seismic and the fine-scale well data. (Redrawn from Nair et al. 2012, ©EAGE reproduced with kind permission of EAGE Publications B.V., The Netherlands)

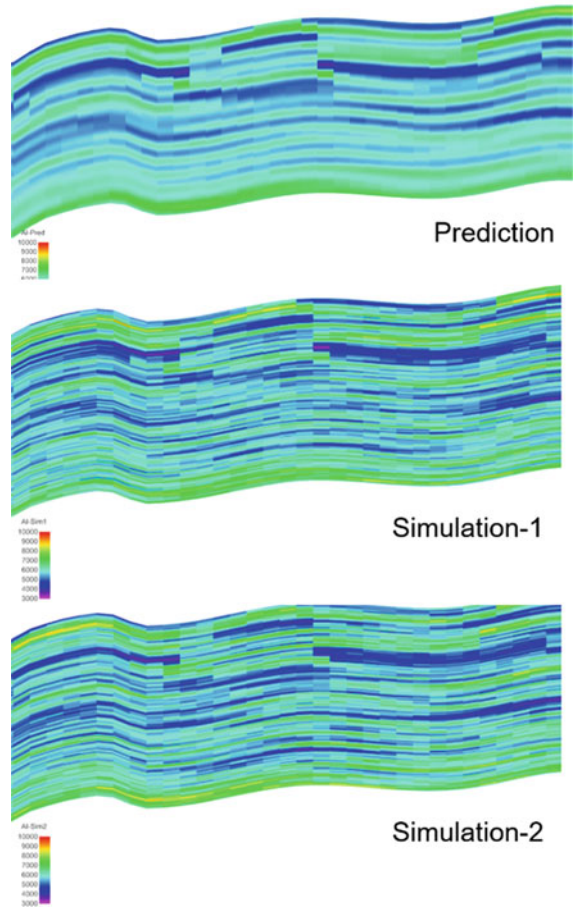


**Fig. 3.28** Plot of  $V_p/V_s$  versus P-wave Impedance illustrating the separation of facies categories from logs. (Redrawn from Nair et al. 2012, ©EAGE reproduced with kind permission of EAGE Publications B.V., The Netherlands)

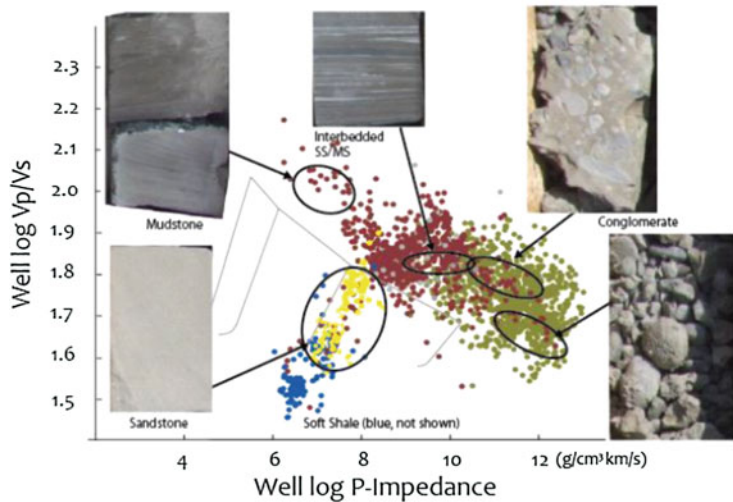


**Table 3.4** Definition of terms used to describe the Net-to-Gross ratio

| Term          | Definition   | Comment   |
|---------------|--|---|
| Net sand      | A lithologically-clean sedimentary rock  | Can only be proved in core but inferred from log data |
| Net reservoir | Net sand intervals with useful reservoir properties  | Usually defined by a log-derived porosity cut-off     |
| Net pay       | Net reservoir intervals containing hydrocarbons  | Usually defined by a log-derived saturation cut-off   |
| Net-to-gross  | A ratio defined explicitly with reference to one of the above, e.g. $N/G_{\text{reservoir}}$ | $N/G_{\text{sand}} \neq N/G_{\text{reservoir}}$       |

but 0.1 mD for gas reservoirs. This concept is based on Darcy's law and is best understood in terms of a dynamic cut-off (Cosentino 2001), in which it is the ratio of permeability,  $k$ , to viscosity,  $\mu$ , that defines the flow potential (the mobility ratio). For example, the following cut-offs are equivalent:

$$\left(\frac{0.01 \text{ md}}{0.05 \text{ cp}}\right)^{\text{gas}} \equiv \left(\frac{1 \text{ md}}{5 \text{ cp}}\right)^{\text{oil}} \quad (3.32)$$

Worthington and Cosentino (2005) argue that the most consistent way to handle cut-offs is to cross-plot porosity versus the  $k/\mu$  ratio to decide on an appropriate and consistent set of cut-off criteria (Fig. 3.29). The cut-off criterion  $(k/\mu)_c$  is arbitrary but based on a reservoir engineering decision concerning the flow rate that is economic for the chosen production well concept and the design life of the oil field. It may be the case that later on in the field life the appropriate  $(k/\mu)_c$  criterion is revised (to lower values) on account of advances in oil recovery technology and introduction of enhanced oil recovery methods.

Because of these difficulties with terminology and the underlying arbitrary nature of the cut-off assumptions, the key guideline for good reservoir model design is to:

Use net-to-gross and cut-off criteria in a consistent way between geological reservoir descriptions, petrophysical interpretations and reservoir flow simulations.

In the following discussion, we consider two end-members of a range of possible approaches – the net-to-gross method and a more general Total Property Modelling approach.

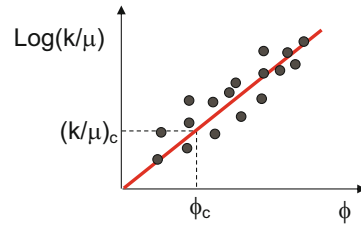


**Fig. 3.29** Cross plot of porosity,  $\phi$ , versus the  $k/\mu$  ratio to define a consistent set of cut-off criteria,  $\phi_c$  and  $k_c$ . (Redrawn from Ringrose 2008, ©2008, Society of Petroleum Engineers Inc., reproduced with permission of SPE. Further reproduction prohibited without permission)

### 3.5.2 The Net-to-Gross Method

From a geological perspective, the ideal case of a reservoir containing clean (high porosity) sandstone set in a background of homogeneous mudstones or shale does not occur in reality. However, for certain cases the pure sand/shale assumption is an acceptable approximation and gives us a useful working model. When using this N/G ratio approach it is important that we define net sand on a geological basis making clear and explicit simplifications. For example, the following statements capture some of the assumptions typically made:

- We assume a fluvial channel is 100% sand (although the channel can contain significant thin shale layers).
- If the net-sand volume fraction in the model grid is within 2% of the continuous-log net-sand volume fraction, then this is considered as an acceptable error and ignored.
- The estuarine bar facies is given a constant sand volume fraction of 60% in the model,

but in reality it varies between about 40 and 70%.

- Tightly-cemented sandstones are included with the mudstone volume fraction and are collectively and loosely referred to as ‘shale’.

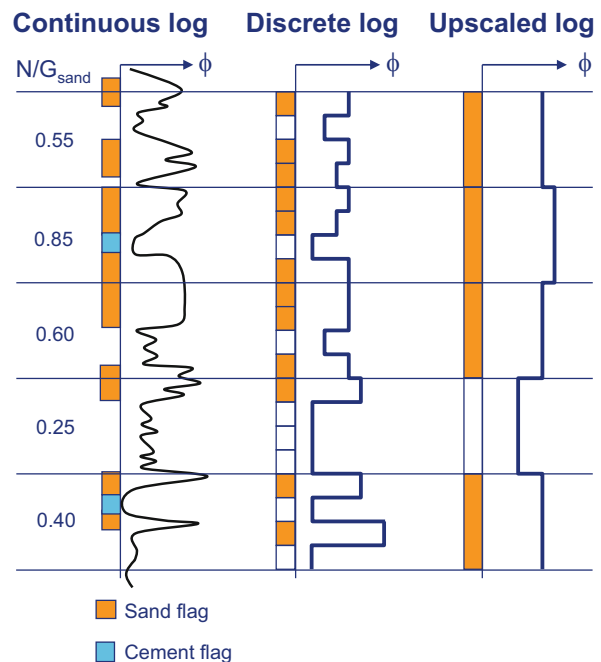
Having made the geological assumptions clear and explicit, it is important to then proceed to an open discussion (between geologists, petrophysicists, reservoir engineers and the economic decision makers) in order to agree the definition of net reservoir cut-off criteria. For example, a typical decision might be:

- We assume that net reservoir is defined in the well-log data by: IF (Gamma <40API AND (Poro >0.05 OR Perm >0.1 mD) THEN (Interval =  $N/G_{\text{reservoir}}$ ).
- After averaging, reservoir modelling and upscaling, the simulation model  $N/G_{\text{reservoir}}$  may differ from average well-data  $N/G_{\text{reservoir}}$  by a few percent and will be adjusted to ensure a match.

Hidden within the discussion above is the problem of upscaling. That is, the  $N/G$  estimate is likely to change as a function of scale between well data and full-field reservoir simulation model. This is illustrated in Fig. 3.30 for a simplified workflow. There are several important biasing factors which tend to occur in this process:

- Blocked sand intervals are likely to contain non-sand, and the converse for non-sand intervals (blocking refers to the process of creating a discrete parameter from a higher frequency dataset).
- Upscaling will bias the volume fractions in favour of the majority volume fraction. This is illustrated in Fig. 3.30 where, for example, in the top layer the  $N/G_{\text{sand}}$  increases from 0.55 to 0.75 to 1.0 in the transition from continuous log to discrete log to upscaled log.
- Cemented sand is not the same as shale, and will typically be included as part of the shale fraction, unless care is taken to avoid this.

**Fig. 3.30** Upscaling of net-sand logs



- As we require net sand properties we must filter the data accordingly. That is, only the fine-scale net-sand values for  $k$  and  $\phi$  should be included in the upscaled net-sand values.
- We have to assume something about the non-net sand volume – typically we assume it has zero porosity and some arbitrarily low (or zero) value for vertical permeability.

This tendency to introduce bias when upscaling from a fine-scale well-log to the reservoir model can lead to significant errors. Similar blocking errors are introduced for the case of rock modelling (Fig. 3.31), such that modelled volume fractions of a sand element can differ from the well data (due to blocking) in addition to the bias related to modelling net sand properties. The errors can be contained and limited by careful tracking of the correct N/G value in the modelling process.

The common assumption in reservoir flow simulation is that the N/G ratio is used to factor down the cell porosity and the horizontal permeability,  $k_h$ , in order to derive the correct inter-cell transmissibility. However, no explicit N/G factor is generally applied to the vertical permeability,  $k_v$ , as it is assumed that this is independently assigned using a  $k_v/k_h$  ratio. This is illustrated in Fig. 3.32. A potential error is to double calculate

the N/G effect, where, for example the geologist calculates a total block permeability of 600 mD and the reservoir engineer then multiplies this again by 0.6 to give  $k_x = 360$  mD.

When using the N/G approach the main products from the geological model to the reservoir simulation model are as follows:

- A model for the spatial distribution of N/G.
- Net sand properties, e.g.  $\phi$ ,  $k_h$ ,  $S_w$ .
- Multi-phase flow functions for net-sand, e.g.  $k_{ro}(S_w)$ .
- $k_v/k_h$  ratios to be applied to each cell.
- Information on stratigraphic barriers and faults.

The N/G ratio approach is widely used and can be consistently and successfully applied through the re-scaling process – from well data to geological model to reservoir-simulation model. However, significant errors can be introduced and care should be taken to ensure that the model correctly represents the underlying assumptions made.

### 3.5.3 Total Property Modelling

Total Property Modelling (TPM, Ringrose 2008) refers to an approach where all rock properties are

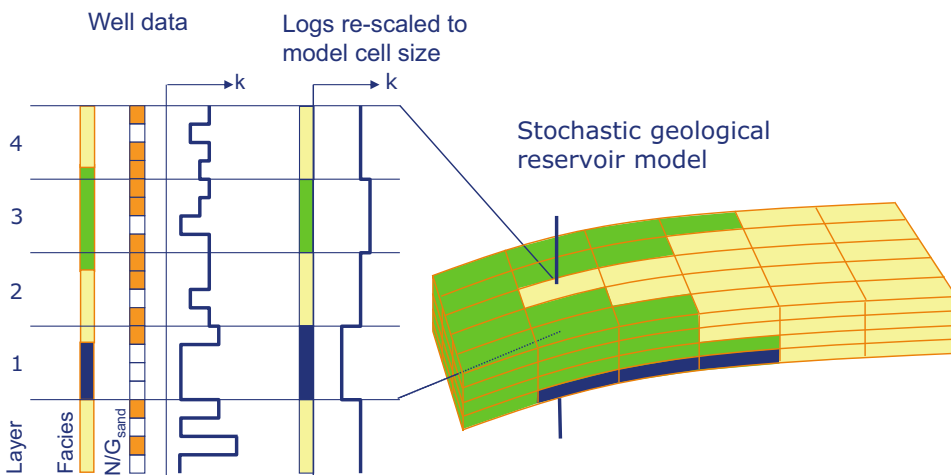


**Fig. 3.31** Handling net-sand within a rock model. Block and upscaling can affect both the element volume fraction and the net-sand volume fraction. (Redrawn from

Ringrose 2008, ©2008, Society of Petroleum Engineers Inc., reproduced with permission of SPE. Further reproduction prohibited without permission)

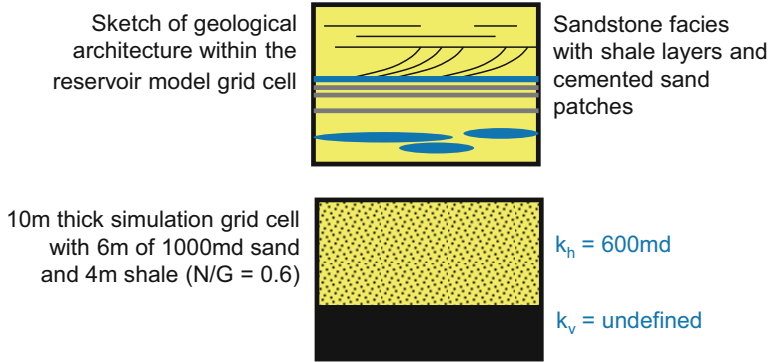


**Fig. 3.32** Simple example of a reservoir grid block where the N/G assumption is correctly used to estimate a horizontal block permeability of 600 mD in the case where the net sand has an upscaled permeability of 1000 mD.

(Redrawn from Ringrose 2008, ©2008, Society of Petroleum Engineers Inc., reproduced with permission of SPE. Further reproduction prohibited without permission)

explicitly modelled and where the cut-offs are only applied after modelling (if at all). In this way cut-offs, or net to gross criteria, are not embedded in the modelling workflow. This is a more comprehensive approach and is used in many academic studies where economic cut-off factors, e.g. oil reserves, are not a major concern. This approach is especially appropriate where:

1. Reservoir properties are highly variable or marginal;
2. Cementation is as important as the sand/shale issue;
3. Carbonates comprise the main reservoirs.

The TPM method is illustrated in Fig. 3.33. Note that net-reservoir is still defined in this case but only after modelling and upscaling. As shaly or cemented elements are modelled explicitly alongside better quality sandstones (or carbonates) it is easy to test the effect of assuming different cut-offs – such as “How will an 8 % versus a 10 % porosity cut-off affect the reserves forecast?”

An important prerequisite for this approach is that the petrophysical data must have been handled appropriately. Net sand concepts are often embedded in petrophysical logging procedures – partly by dint of habit but also because shaly and cemented rock properties are more difficult to measure. Therefore, a major challenge for the total property modelling approach is that property estimation in

poor reservoir quality units is difficult or imprecise. However, if it is understood that very low porosity and permeability rock elements will be eventually discounted, it is appropriate to assign a *reasonable guess* to the low-quality reservoir units. This is illustrated by the dataset from a very heterogeneous reservoir unit shown in Fig. 3.34.

Numerical upscaling is generally required when applying the TPM approach (with the N/G approach simple averaging is often assumed). Valid application of numerical upscaling methods requires that a number of criteria are met, related to flow boundary conditions and the statistical validity of the upscaled volume (discussed in Chap. 4). The TPM approach may often challenge these criteria and can be difficult to apply. However, by using statistical analysis of the rock populations present in the reservoir and careful choice of optimum model length-scales (grid resolution), these problems can be reduced and made tractable.

With the TPM approach, the main products from the geological model to the reservoir simulation model are:

- Upscaled porosity and fluid saturation.
- Effective permeabilities for all directions ( $k_x$ ,  $k_y$ ,  $k_z$ ).
- Multi-phase flow functions for the total grid block.
- Information on stratigraphic barriers/faults.

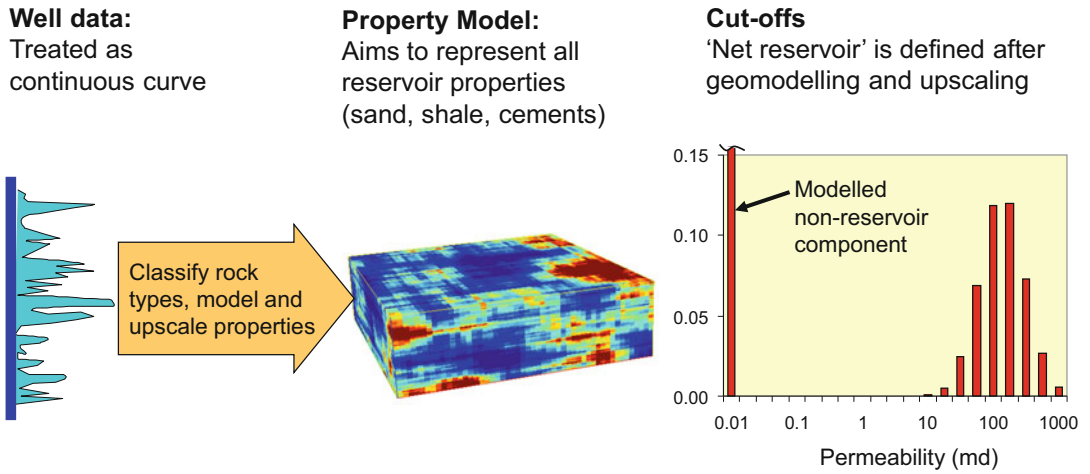


**Fig. 3.33** Illustration of the total property modelling approach. (Redrawn from Ringrose 2008, ©2008, Society of Petroleum Engineers Inc., reproduced with permission of SPE. Further reproduction prohibited without permission)

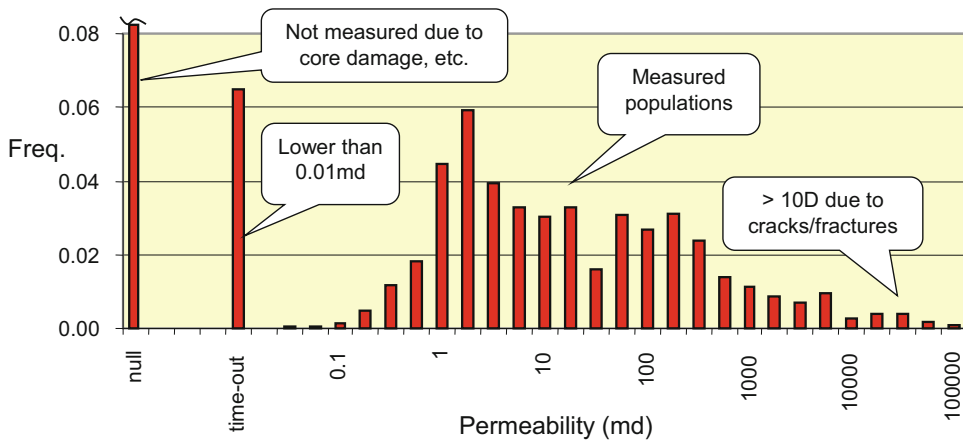


**Fig. 3.34** Probe permeability dataset (5 mm-spaced sampling for a 3 m reservoir interval) where permeabilities between 0.01 mD and 10 Darcy have been measured, and where the ‘lower-than measurable’ population has been

identified. (Redrawn from Ringrose 2008, ©2008, Society of Petroleum Engineers Inc., reproduced with permission of SPE. Further reproduction prohibited without permission)

After upscaling, all blocks with upscaled properties less than the chosen cut-off criteria may be declared ‘non-reservoir’. An important feature of this approach is that, for example, thin sands will be correctly upscaled where they would have been discounted in the N/G approach (Fig. 3.35).

It is best to illustrate and contrast these approaches by applying them to an example dataset. The example is from a 3 m interval core interval from a deeply buried tidal deltaic

reservoir from the Smørbukk Field, offshore Norway (Ringrose 2008). This thin-bedded reservoir interval was characterised using high-resolution probe permeability data, sampled at 5 mm intervals, and calibrated to standard core plugs. The thin-bed data set is assumed to give the ‘ground truth’, with lower-than-measurable permeability values set to 0.0001 mD.

Figure 3.36 shows the results of the analyses. For the N/G approach (Fig. 3.36a) the fine-scale

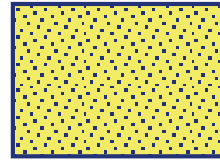
**Fig. 3.35** Example of a reservoir grid block modelled using the total property modelling approach.  $N/G$  is assumed = 1. Upscaled horizontal block permeability is correctly estimated as 100.1 mD (while the 'net sand' method would have assigned the block to be non-reservoir)

Sketch of geological architecture within the reservoir model grid cell



Mudstone-dominated rock unit with thin-bedded sandstone layers

Simulation Cell:  
10m thick cell  
9m of 0.01md shale  
1m of thin 1D sands



$k_x = 100.01\text{md}$

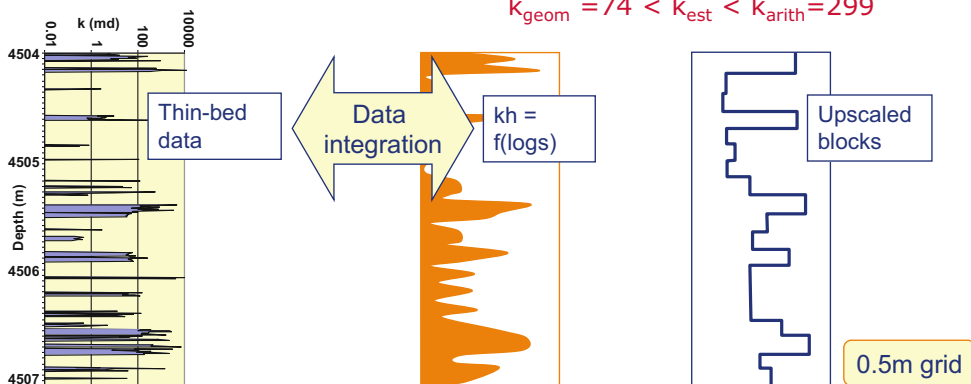
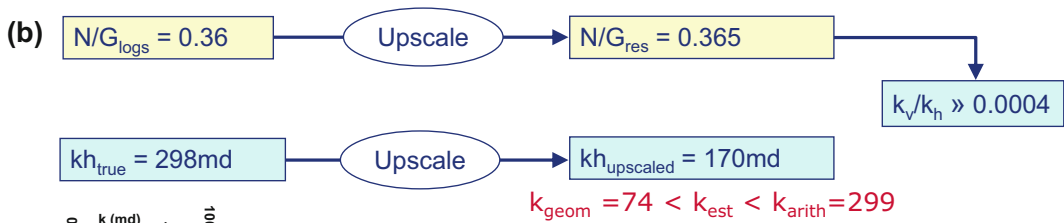
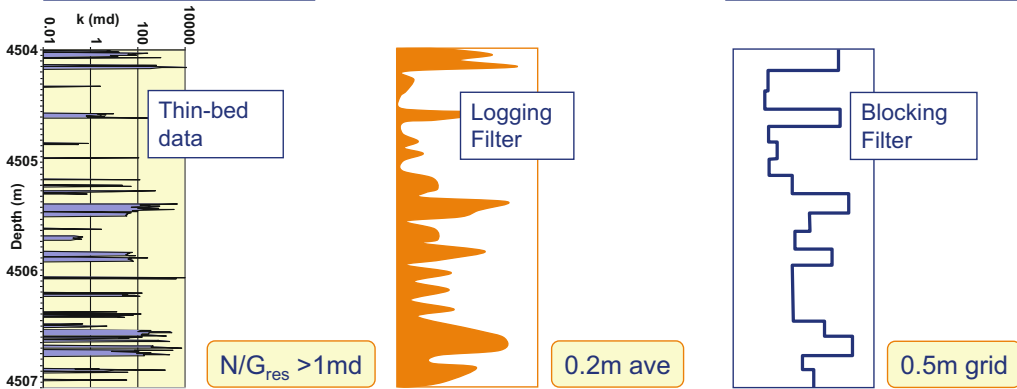
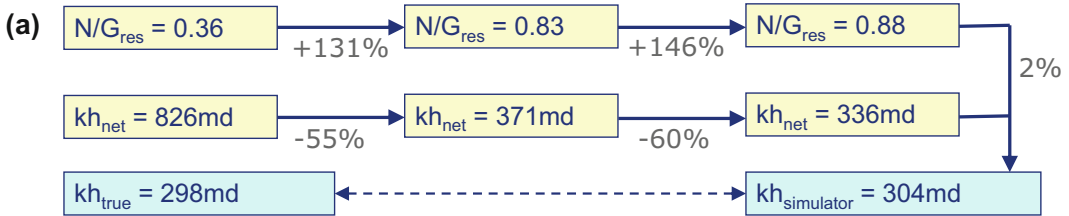


**Fig. 3.36** Application of (a) the  $N/G$  approach and (b) the total property modelling approach to an example thin-bed permeability dataset



data are transformed using a 0.2 m running average (to represent a logging process) and then are blocked to create a 0.5 m discrete log (to represent the gridding process). A  $N/G_{\text{res}}$  cutoff criterion of 1 mD is assumed, leading to estimates of  $k_h(\text{net})$  and  $N/G_{\text{res}}$  at each upscaling step. At the logging stage the (apparent)  $kh_{\text{net}} = 371$  mD and the  $N/G_{\text{res}}$  is 0.83 and when the blocking filter is applied the  $k_h(\text{net}) = 336$  mD and the  $N/G_{\text{res}}$  is 0.88. These transforms result in significant over-estimation of  $N/G$  and underestimation of net horizontal permeability,  $k_h(\text{net})$ . The upscaled  $k_h(\text{simulator})$  is then estimated by  $k_h(\text{net}) \times N/G_{\text{res}}$  for each 0.5 m cell value (representing a typical reservoir-simulation procedure).

The resulting upscaled  $k_h(\text{simulator})$  for the whole interval is 304 mD, which is only slightly higher than the true value (298 mD). However, this apparently satisfactory result hides several errors embedded in the process. The  $N/G_{\text{res}}$  has been significantly over-estimated while the  $k_h(\text{net})$  has been underestimated (errors are shown in Fig. 3.36a). The two errors tend to cancel one another out, but unfortunately two wrongs don't make a right.  $k_v$  is also neglected inherently in this procedure and must be estimated independently.

For the TPM approach (Fig. 3.36b), the fine-scale data are transformed directly to the 0.5 m discrete log by blocking the thin-bed data set (using values for net and non-net reservoir). The discrete-log  $N/G_{\text{res}}$  estimate is quite accurate, as smoothing has not been applied. Upscaled cell values ( $k_h$  and  $k_v$ ) are then estimated using functions proposed by Ringrose et al. (2003) for permeability in heterolithic bedding systems (described in Sect. 3.6 below). These functions represent the numerical (single-phase) upscaling step in the TPM workflow. The TPM approach preserves both an accurate estimate for  $N/G_{\text{res}}$  and  $k_h$  throughout the procedure, and also gives a sound basis for estimation of upscaled  $k_h$  and  $k_v$ . The upscaled  $k_h$  (170 mD for the whole interval) is significantly lower than the arithmetic average  $k_h$  because of the effects of sandstone connectivity and the presence of shales and mudstone layers. A degree of validation that we have derived a 'reasonable estimate' for  $k_h$  is found in

the observation that  $k_h$  lies in the range  $k_{\text{geometric}}$  to  $k_{\text{arithmetic}}$  (Fig. 3.35b).

The main challenges of the TPM approach are:

1. The approach requires some form of explicit upscaling, and upscaling always has some associated errors.
2. Where only log data are available, i.e. in the absence of fine-scale core data, some form of indirect estimate of the fine-scale sand/mud ratios and rock properties is needed, and this inevitably introduces additional random error in the estimation of  $N/G_{\text{res}}$ .

However, for challenging, heterogeneous or low-permeability reservoirs, these (generally minor) errors are preferable to the errors associated with the inappropriate simplifications of the  $N/G$  approach.

In summary, the widely used  $N/G$  approach is simpler to apply and can be justified for relatively good-quality reservoirs or situations where quick estimates are warranted. The method tends to embed errors in the process of re-scaling from well data to reservoir model, and care should be taken to minimise and record these errors. The TPM approach is generally more demanding but aims to minimize the inherent upscaling errors by making estimates of the effective flow properties of the rock units concerned.  $N/G$  ratios can be calculated at any stage in the TPM modelling workflow.

---

## 3.6 Vertical Permeability and Barriers

### 3.6.1 Introduction to $k_v/k_h$

The ratio of vertical to horizontal permeability,  $k_v/k_h$ , is an important, but often neglected, reservoir modelling property. Too often, especially when using the net-sand modelling method, a value for the  $k_v/k_h$  ratio is assumed at the last minute (0.1 is a common default) with little basis in reality. Figure 3.37 captures a typical 'history' for this parameter; neglected or assumed = 1 in the early stages then rapidly dropping after unexpected barriers are

**Fig. 3.37** Typical 'history' of the  $k_v/k_h$  ratio

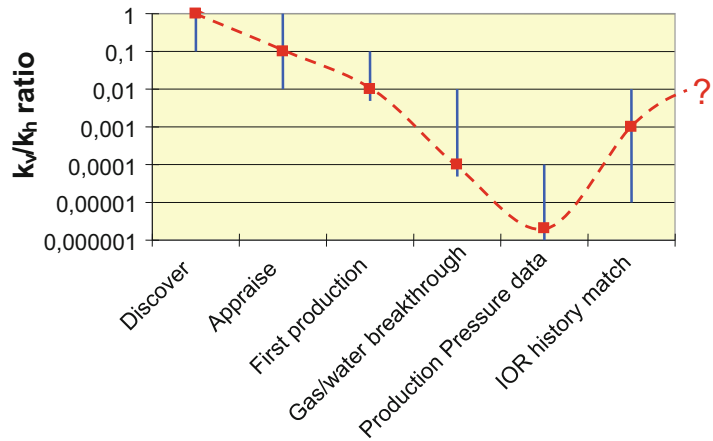
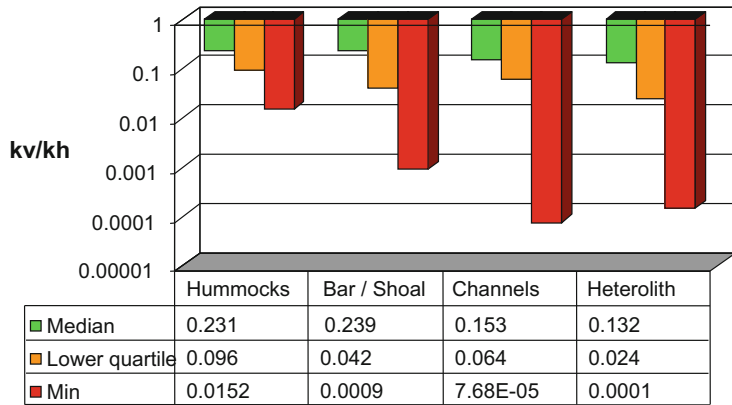


**Fig. 3.38** Statistics of measured  $k_v/k_h$  ratios from core plug pairs from an example reservoir interval



encountered and finally rising again to a more plausible value late in the field life.

The problem of vertical permeability is also further confounded because it is very difficult to measure. Routine core plug analysis usually gives some estimate of core-plug scale  $k_v/k_h$  but these data can be misleading due to severe under sampling or biased sampling (discussed by Corbett and Jensen 1992) and the measurement is in any case not generally made at the scale of interest for reservoir modelling (the cell scale).

Figure 3.38 illustrates some typical core plug anisotropy data. For this example we know from production data that the mean value is far too high (due to under sampling) and in fact the minimum observed plug  $k_v/k_h$  ratio gives a more realistic indication of the true values at the reservoir scale.

A frequent problem with modelling or estimating permeability anisotropy is confusion

between (or mixing the effects of) thin barriers and rock fabric anisotropy. The following two sections consider these two aspects separately.

### 3.6.2 Modelling Thin Barriers

Large extensive barriers are best handled explicitly in the geological reservoir model:

- Fault transmissibilities can be mapped onto to cell boundaries.
- Extensive shales and cemented layers can be modelled as objects and then transformed to transmissibility multipliers onto to cell boundaries.

Some packages allow simulation of sub-seismic faults as effective permeability

reduction factors within grid cells (see for example Manzocchi et al. 2002, or Lescoffit and Townsend 2005). Some modelling packages offer the option to assign a sealing barrier between specified layers. For the more general situation, the geo-modeller needs to stochastically simulate barriers and ensure they are applied in the simulation model. Pervasive, discontinuous thin shales and cements may also be modelled as cell-value reduction factors (an effective  $k_v/k_h$  multiplier).

Figure 3.39 shows an example of barrier modelling for calcite cements in an example reservoir. The fine-scale barriers are first modelled as geological objects and then assigned as vertical transmissibility values using single-phase upscaling.

Before plunging into stochastic barrier modelling, it is important to consider using well established empirical relationships that may save a lot of time. Several previous studies have considered the effects of random shales on a sandstone reservoir. Begg et al. (1989) proposed a

general estimator for the effective vertical permeability,  $k_{ve}$ , for a sandstone medium containing thin, discontinuous, impermeable mudstones, based on effective medium theory and geometry of ideal streamlines. They proposed:

$$k_{VE} = \frac{k_x(1 - V_m)}{(a_z + fd)^2} \quad (3.33)$$

where:

$V_m$  is the volume fraction of mudstone

$a_z$  is given by  $(k_{sv}/k_{sh})^{1/2}$

$k_{sh}$  and  $k_{sv}$  are the horizontal and vertical permeability of the sandstone

$f$  is the barrier frequency

$d$  is a mudstone dimension

( $d = L_m/2$  for a 2D system with mean mudstone length,  $L_m$ )

This method is valid for low mudstone volume fractions and assumes thin, uncorrelated, impermeable, discontinuous mudstone layers.

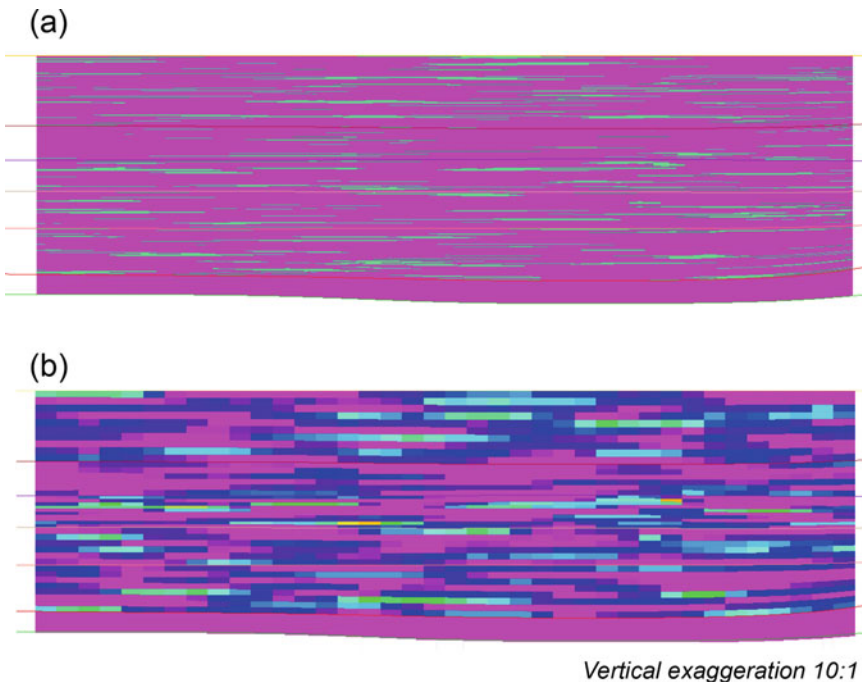


**Fig. 3.39** Example modelling of randomly distributed calcite cement barriers in an example reservoir (Reservoir is c. 80 m thick) (a) Fine-scale model of calcite barriers. (b) Upscaled  $k_v$  as vertical transmissibility multipliers

Desberats (1987) estimated effective permeability for a complete range of mudstone volume fractions in 2D and 3D, using statistical models with spatial covariance and a range of anisotropies. For strongly stratified media, the effective horizontal permeability,  $k_{he}$ , was found to approach the arithmetic mean, while  $k_{ve}$  was found to be closer to the geometric mean. Deutsch (1989) proposed using both power-average and percolation models to approximate  $k_{he}$  and  $k_{ve}$  for a binary permeability sandstone–mudstone model on a regular 3D grid, and showed how both the averaging power and the percolation exponents vary with the anisotropy ratio.

Whatever the chosen method, it is important to separate out the effects of thin barriers (or faults) from the more general rock permeability anisotropy (discussed below).

### 3.6.3 Modelling of Permeability Anisotropy

Using advances in small-scale geological modelling, it is now possible to accurately estimate  $k_v/k_h$  ratios for sandstone units. Ringrose et al. (2003, 2005) and Nordahl et al. (2005) developed this approach for some common bedding types found in tidal deltaic sandstone reservoirs: flaser, wavy and lenticular bedding. Their method gives a basis for general estimation

for facies-specific  $k_v/k_h$  ratios. Example results are shown in Figs. 3.40 and 3.41.

The method takes the following steps:

1. Perform a large number of bedding simulations to understand the relationship between  $k_{sand}$ ,  $k_{mud}$  and  $V_{mud}$  (simulations are unconditioned to well data and can be done rapidly).
2. Input values for the small-scale models are the typical values derived from measured core permeabilities.
3. Fit a curve to the simulations to estimate the  $k_v$  or  $k_v/k_h$  ratio as a function of other modelled parameters: e.g.  $k_h$ ,  $V_{mud}$ , or  $\phi$ .

The following function was found to capture the characteristic vertical permeability of this system (Ringrose et al. 2003):

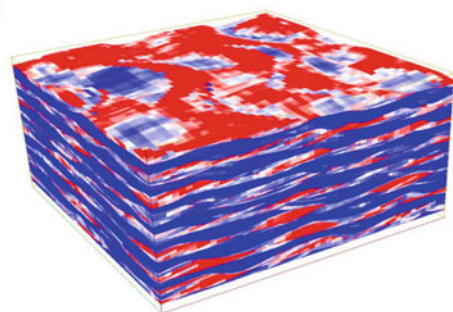
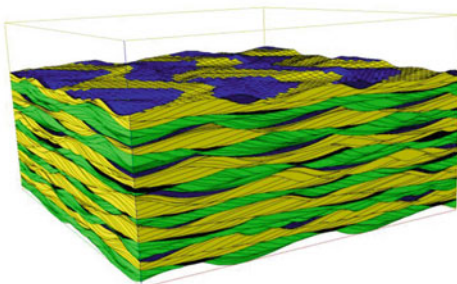
$$k_v = k_{sand} \left( \frac{k_{mud}}{k_{sand}} \right)^{\frac{V_m}{V_{mc}}} \quad (3.34)$$

where:

$V_{mc}$  is the critical mudstone volume fraction (or percolation threshold).

This formula is essentially a re-scaled geometric average constrained by the percolation threshold. This is consistent with the previous findings by Desberats (1987) and Deutsch (1989) who observed that the geometric average was close to

Tidal bedding model and permeability cube



Model size: 0.5m x 0.5m x 0.1m

**Fig. 3.40** Example model of heterolithic flaser bedding (left) with corresponding permeability model (right). Note the bi-directional sand lamina sets (green and yellow laminae) and the partially preserved mud drapes (dark

tones). Higher permeabilities indicated by hot colours. (Modified from Ringrose et al. 2005 *Petrol Geoscience*, Volume 11, © Geological Society of London [2005])

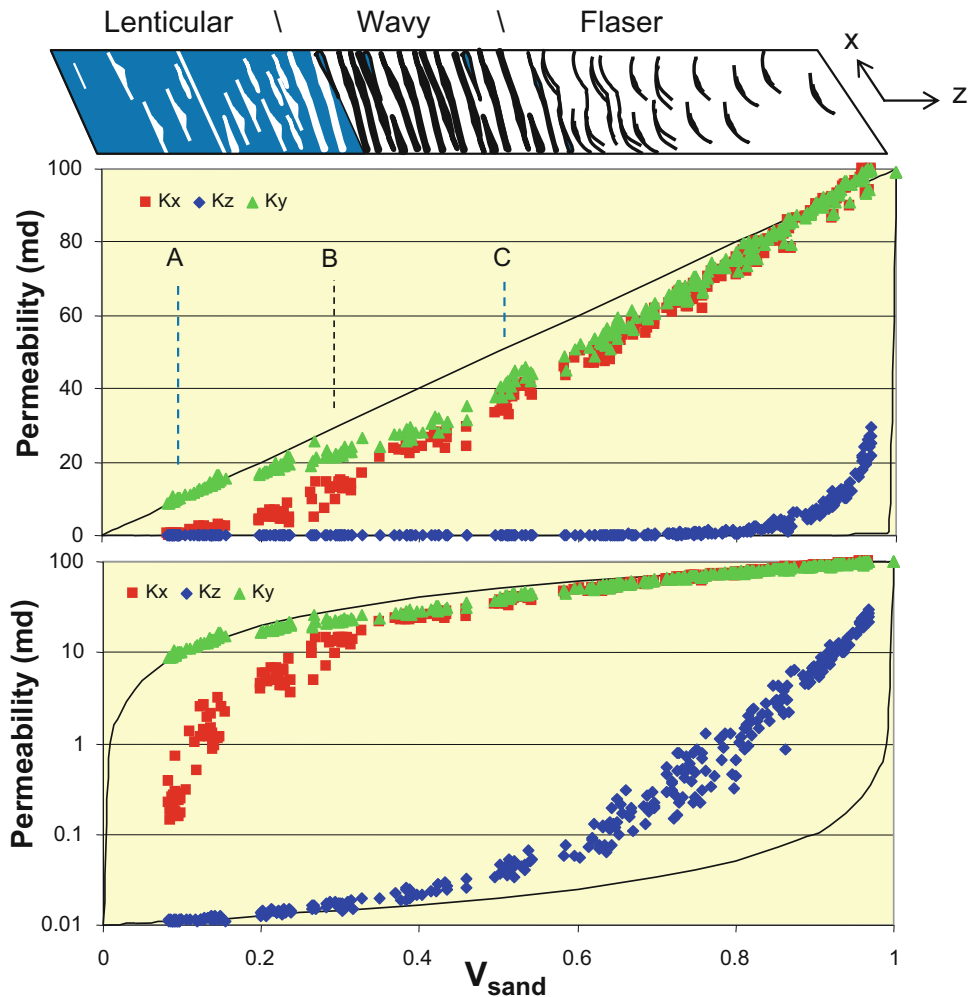


**Fig. 3.41** Results of sub-metre-scale simulation of heterolithic bedding in tidal deltaic reservoirs. Effective permeability simulation results are for the constant petrophysical properties case (i.e. sandstone and mudstone have constant permeability). Observed effective permeability is compared to bedding styles and the critical points

*A, B and C.* *A* is the percolation threshold for  $k_x$ , and *C* is the percolation threshold for  $k_z$ , while *B* is the theoretical percolation threshold for a simple 3D system. Thin lines are the arithmetic and harmonic averages. (Modified from Ringrose et al. 2005, *Petrol Geoscience*, Volume 11, © Geological Society of London [2005])

the simulated  $k_v$  for random shale systems, and also noted percolation behaviour in such systems. This equation captures the percolation behaviour (the percolation threshold is estimated for the geometry of a specific depositional system or facies), while still employing a general average function that can be easily applied in reservoir simulation.

The method has been applied to a full-field study by Elfenbein et al. (2005) and compared

to well-test estimates of anisotropy (Table 3.5). The comparison showed a very good match in the Garn 4 Unit but a poorer match in the Garn 1–3 Units. This can be explained by the fact that the lower Garn 1–3 Units have abundant calcite cements (which were modelled in the larger-scale full-field geomodel), illustrating the importance of understanding both the thin large-scale barriers and the inherent sandstone anisotropy (related to the facies and bedding architecture).

**Table 3.5** Comparison of simulated kv/kh ratios with well test estimates from the case study by Elfenbein et al. (2005)

| Reservoir unit | Modelled $k_v/k_h$ : Geometric average of simulation model | Modelled $k_v/k_h$ : Geometric average of well test volume | Well test $k_v/k_h$ : Analytical estimate  | Comments                     |
|----------------|--|--|--|------------------------------|
|                |  |  | Tyrihans south, well test in well 6407/1-2 |                              |
| Garn 4         | 0.031  | 0.043  | <0.05                                      | Test of garn 4 interval      |
| Garn 3         | 0.11   |  |  | Producing interval uncertain |
| Garn 2         | 0.22   |  |  | Complex two-phase flow       |
| Garn 1         | 0.11   |  |  |                              |
|                |  |  | Tyrihans north, well test in well 6407/1-3 |                              |
| Garn 4         | 0.025  |  |  |                              |
| Garn 3         | 0.123  | 0.19   | 0.055                                      | Test of garn 1 to 3 interval |
| Garn 2         | 0.24   |  |  | Analytical gas cap           |
| Garn 1         | 0.12   |  |  | Partial penetration model    |

## 3.7 Saturation Modelling

### 3.7.1 Capillary Pressure

An important interface between the static and dynamic models is the definition of initial water saturation. There are numerous approaches to this problem, and in many challenging situations analysis and modelling of fluid saturations requires specialist knowledge in the petrophysics and reservoir engineering disciplines. Here we introduce the important underlying concepts that will enable the initial saturation model to be linked to the geological model and its uncertainties.

The initial saturation model is usually based on the assumption of capillary equilibrium with saturations defined by the capillary pressure curve. We recall the basic definition for capillary pressure:

$$P_c = P_{\text{non-wetting phase}} - P_{\text{wetting-phase}} [P_c = f(S)] \quad (3.35)$$

The most basic form for this equation is given by:

$$P_c = AS_{wn}^{-b} \sqrt{\phi/k} \quad (3.36)$$

That is, capillary pressure is a function of the wetting phase saturation and the rock properties, summarized by  $\phi$  and  $k$ . The exponent  $b$  is related to the pore size distribution of the rock. Note the use of the normalised water saturation:

$$S_{wn} = (S_w - S_{wi}) / (S_{wor} - S_{wi}) \quad (3.37)$$

We can expand the  $P_c$  equation to include the fluid properties:

$$P_c(S_w) = \sigma \cos \theta J(S_w) \sqrt{\phi/k} \quad (3.38)$$

where:

$\sigma$  = interfacial tension  
 $\theta$  = interfacial contact angle  
 $J(S_w)$  = Leverett J-junction

Rearranging this we obtain the J-function:

$$J(S_w) = \frac{P_c(S_w)}{\sigma \cos \theta} \left( \frac{k}{\phi} \right)^{1/2} \quad (3.39)$$

Figure 3.42 shows two example J-functions for contrasting rock types.

To put this more simply, we could measure and model any number of capillary pressure curves,  $P_c = f(S)$ . However, the J-function method allows a number of similar functions to be normalized with respect to the rock and fluid properties and plotted with a single common curve.

### 3.7.2 Saturation-Height Functions

There are a number of ways of plotting the  $P_c = f(S)$  function to indicate how saturation varies with height in the reservoir. The following equation is a general form of the  $P_c$  equation, including all the key rock and fluid terms:

$$S_{wn}^{-b} = \frac{(\rho_w - \rho_o)gh}{\sigma \cos \theta} \left( \frac{k}{\phi} \right)^{1/2} \quad (3.40)$$

Here,  $P_c$  is defined by the fluid buoyancy term,  $\Delta(\rho)gh$ , where  $h$  is the height above the free water

level. This equation gives a useful basis for forward modelling water saturation, given some known rock and fluid properties.

For practical purposes we often want to estimate the  $S_w$  function from well log data. There are again several approaches to this (Worthington 2001 gives a review), but the simplest is the power law function which has the same form as the J-function:

$$S_w = C.h^d \quad (3.41)$$

A significant issue in reservoir modelling is how the apparent (and true) saturation-height function is affected by averaging of well data and/or upscaling of the fine-scale geological model data.

To illustrate these effects in the reservoir model, we take a simple case. We must first define the *free water level* (FWL) – the fluid-water interface in the absence of rock pores, i.e. resulting only from fluid forces (buoyancy and hydrodynamic pressure gradients). The effect of rock pores is to introduce another factor (capillary forces) to the oil-water distribution, so that the oil-water contact is different from the free water level.

A simple model for this behaviour is given by the following saturation-height function:

$$S_w = S_{wi} + (1 - S_{wi}) \left[ 0.1h\sqrt{k/\phi} \right]^{-2/3} \quad (3.42)$$

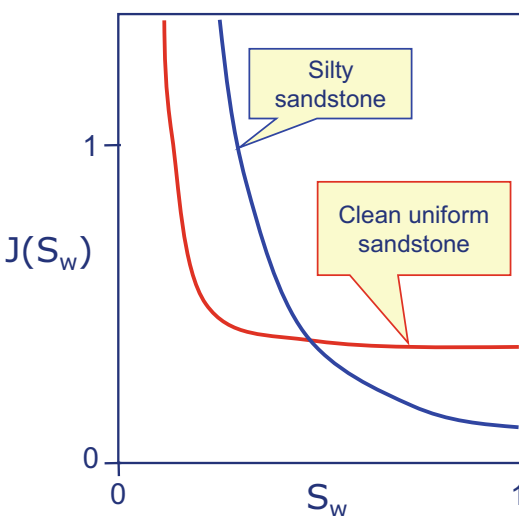
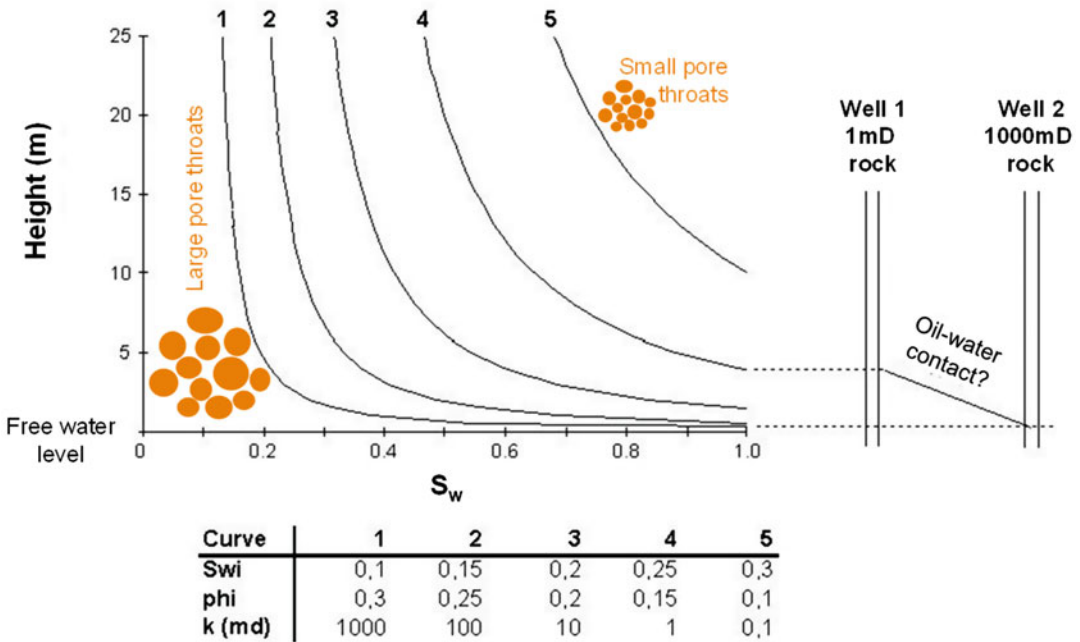


Fig. 3.42 Example capillary pressure J-functions

Figure 3.42 shows example curves, based on this function, and illustrates how at least 10 m variation in oil-water contact can occur due to changes in pore throat size. In general, for a high porosity/permeability rock  $OWC \approx FWL$ . However, for low permeability or heterogeneous reservoirs the fluid contact will vary considerably as a function of rock properties, and  $OWC \neq FWL$ .

Further difficulties in the interpretation of these functions come with upscaling or averaging saturations from heterogeneous systems. For example, suppose you had a thinly-bedded reservoir comprising alternating rock types 2 and 4 (Fig. 3.43), then the average saturation-height



**Fig. 3.43** Example saturation-height functions for the listed input parameters, illustrating how an apparent change in oil-water contact may be caused by rock property variations between wells

**Table 3.6** Selected examples of tilted oil-water contacts

| Field, Location            | Tilt of OWC (m/km) | References                    |
|----------------------------|--------------------|-------------------------------|
| South Glenrock, Wy. USA    | <95                | Dahlberg (1995)               |
| Norman Wells, NWT, Canada  | 75                 | Dahlberg (1995)               |
| Tin-Fouye, Algeria         | 10                 | Dahlberg (1995)               |
| Weyburn, Sask., Canada     | 10                 | Dahlberg (1995)               |
| Kraka, North Sea (Denmark) | 10                 | Thomassen and Jacobsen (1994) |
| Billings Nose, N.Da., USA  | 5                  | Berg et al. (1994)            |
| Knutson, N.Da., USA        | 3                  | Berg et al. (1994)            |

function (detected by a logging tool) would be close to curve 3. That is, the average  $S_w$  corresponds to the average  $k/\phi$ . However, if the thin beds were composed of an unknown random mix of rocks types 1, 2, 3, 4 and 5 then it would clearly be very difficult to infer the correct relationship between  $S_w$ ,  $k$  and  $\phi$ .

### 3.7.3 Tilted Oil-Water Contacts

Depending on which part of the world the petroleum geologist is working, tilted oil-water contacts are either part of accepted knowledge

or disputed folk law. In parts of the Middle East, North Africa and North America, there are numerous well-documented examples of tilted contacts. These occur in continental basins with appreciable levels of topographically driven groundwater flow, or hydrodynamic gradients. Dahlberg (1995) provides a fairly comprehensive study of the evidence for, and interpretation of, tilted oil water contacts. Berg et al. (1994) give good documentation of some examples from Dakota, USA. In the offshore continental shelf petroleum provinces, such as offshore NW Europe, the cases are fewer, but still evident. Table 3.6 lists a range of examples.



Here, we are concerned with the implications that tilted hydrocarbon-water contacts might have for dynamic modelling of fluid accumulations. For simplicity, we mainly consider oil-water contacts, but the theory applies to any fluid: gas, condensate or oil. The main principle governing this phenomenon is potentiometric head. If an aquifer contains flowing water driven by some pressure gradient (Fig. 3.44), then this pressure gradient causes a slope in the petroleum-water interface of any accumulation within that aquifer, defined by Hubbert (1953) as:

$$\Delta z/\Delta x \approx (\rho_w/\rho_w - \rho_o).(\Delta H_w/\Delta x) \quad (3.43)$$

where:

$\rho_w - \rho_o$  = density of water and petroleum

$\Delta z/\Delta x$  = slope of the hydrocarbon-water interface

$\Delta H_w/\Delta x$  = potentiometric surface in aquifer

The greater the difference in fluid density, i.e. the lighter the petroleum, the smaller the tilt of the fluid contact. It is important to differentiate the free-water level (FWL) from the oil-water contact (OWC). Where the capillary pressures are significant due to small pores, the difference between FWL and OWC can be significant (Fig. 3.44). In Eq. (3.44), the  $\Delta z/\Delta x$  term relates to the FWL (and only approximately to the OWC). A more comprehensive treatment of this topic is given by Muggeridge and Mahmode (2012), who include the terms for the effective permeability in the aquifer,  $k_{aq}$ , and reservoir,

$k_{res}$ , to derive a relationship between the hydrocarbon-water interface and the hydrodynamic pressure gradient in terms of steady-state flow:

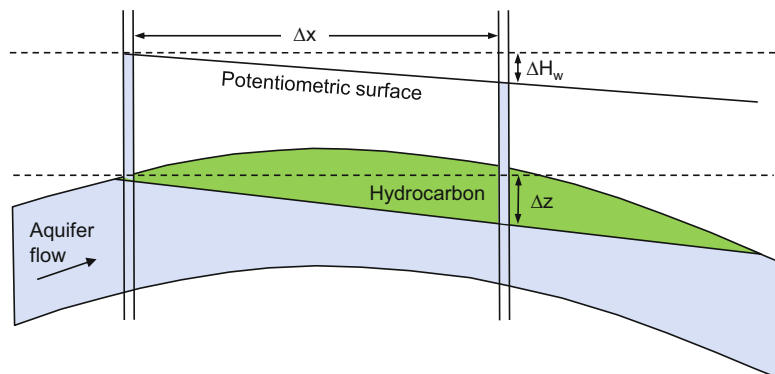
$$(\Delta z/\Delta x) = (k_{res}/k_{aq}\Delta\rho g).(\Delta H_w/\Delta x) \quad (3.44)$$

As can be seen from Table 3.6, the actual value of the tilted oil-water contact can be quite small (most documented examples are around 10 m/km), so that uncertainties in detection become important. There are many situations which can give an apparent tilt in an oil-water contact, including:

- Undetected faults (usually the first explanation to be proposed) or stratigraphic boundaries.
- Variations in reservoir properties – systematic changes in pore throat size across a field can lead to a variation in the oil-water contact of 5 m or more.
- Misinterpretation of paleo-oil-water contacts (marked by residual oil stains or tar mats) as present-day contacts.
- Errors in deviation data for well trajectories.

Thus, proof of the presence of a tilted oil-water contact requires either multiple well data explained by a common inclined surface (Fig. 3.45) or multiple data types explained coherently in terms of a common hydrodynamic model (as in the Kraka field example discussed below). Possible hydrodynamic aquifer influence on a static (passive) petroleum accumulation must also be considered alongside the concepts of a dynamic petroleum accumulation, e.g. on-going

**Fig. 3.44** Terms defining a tilted oil-water contact. (Redrawn from Dahlberg 1995 (Fig. 12.5), Springer-Verlag, New York, with kind permission from Springer Science and Business Media B.V)



migration or leakage, or pressure transients in the aquifer.

### 3.7.3.1 Kraka Field Example

This small chalk reservoir in the Danish sector of the North Sea provides an interesting account of the phenomenon of tilted oil-water contacts and their interpretation. The subtle nature of the tilt and the use of multiple data sources to confirm an initially doubtful interpretation are very informative. A study of the field by Jørgensen and

Andersen (1991) included some initial observations on a tilted oil-water contact, and a tentative argument that it was due to tectonic tilting during the Tertiary. A subsequent study by Thomasen and Jacobsen (1994), gave a detailed description and a more thorough basis for the interpretation of a  $0.6^\circ$  dip in both free water level and oil-water contact (Fig. 3.46).

Their main observations were:

- Repeat Formation Tester (RFT) data from three wells indicated a free-water level (interpreted from the change in slope of water and oil zones) falling by about 70 m over a 2 km distance (Fig. 3.46).
- Due to the heterogeneous and fractured nature of the chalk reservoir zone, logs from seven wells show highly variable saturations (Fig. 3.48). These were interpreted by best-fit capillary pressure saturation functions. Difficulties in fitting a function assuming a horizontal free-water level were resolved by fitting functions to individual wells and then identifying the implied tilt in free water level. The slope of the free-water level inferred from this was found to be close to the RFT pressure data model.
- An intra-reservoir seismic reflection interpreted as the matrix oil-water contact was mapped around the field and extrapolated to its intersection with top reservoir, and was again found to be in good agreement with the saturation model.

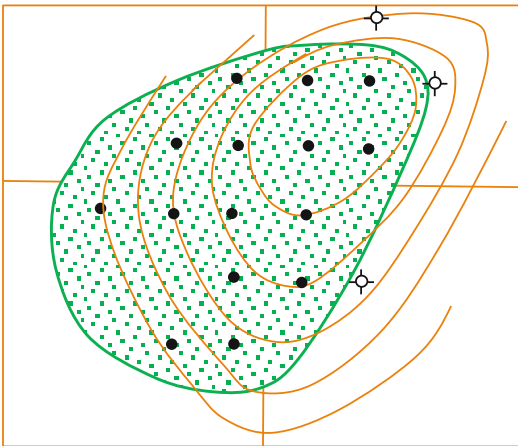


**Fig. 3.45** Map of the Cairo Pool oilfield, Arkansas showing a hydrodynamic offset of an oil accumulation (After Dahlberg 1995). Contours are 20 foot intervals; *black dots* = wells with oil in the reservoir interval, *open circles* = wells with water in the reservoir interval. (Redrawn from Dahlberg 1995 (Fig. 12.5), Springer-Verlag, New York, with kind permission from Springer Science and Business Media B.V)

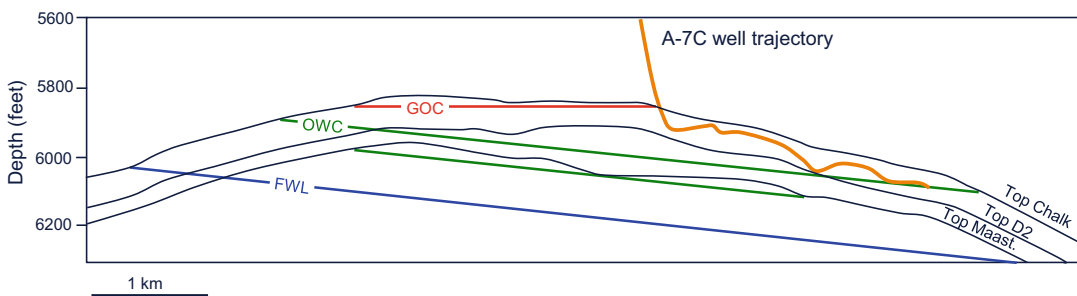
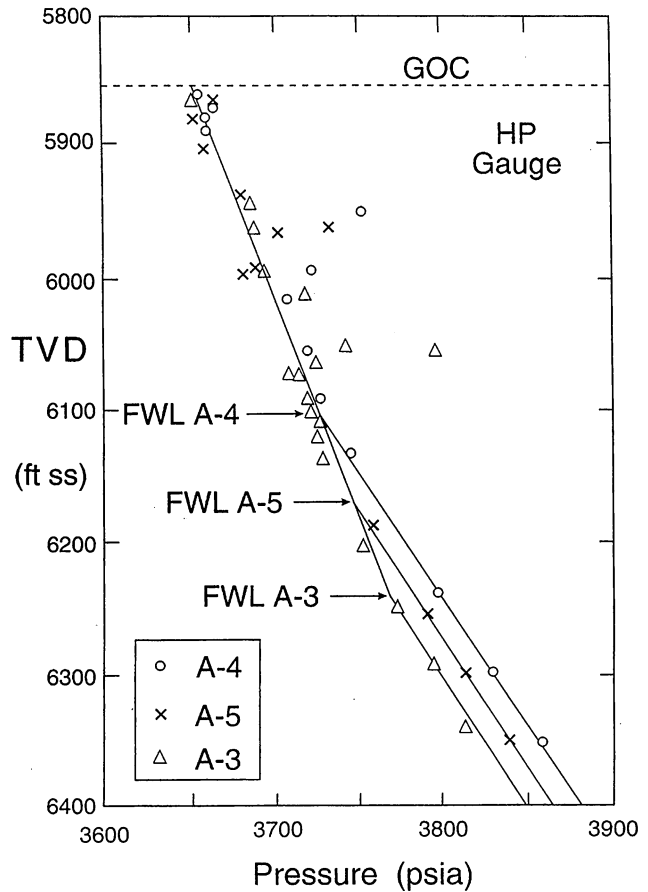


**Fig. 3.46** Cross-section through the Kraka field (From Thomasen and Jacobsen 1994) showing interpreted fluid contacts and horizontal well to exploit down-dip reserves. (Redrawn from Thomasen and Jacobsen 1994, ©1994,

Society of Petroleum Engineers Inc., reproduced with permission of SPE. Further reproduction prohibited without permission)

**Fig. 3.47** RFT data for three wells for the Kraka field. (Redrawn from Thomasen and Jacobsen 1994, ©1994, Society of Petroleum Engineers Inc., reproduced with permission of SPE. Further reproduction prohibited without permission)



- The orientation of the inferred hydrodynamic gradient (towards the SE) was found to be in agreement with regional gradients from inter-field pressure variations.

This integrated interpretation had a significant economic benefit in terms of the appropriate placement of horizontal wells in the thicker part of the accumulation, and in the estimation of inter-well permeability in this fairly marginal field development.

### 3.8 Modelling Fracture Properties

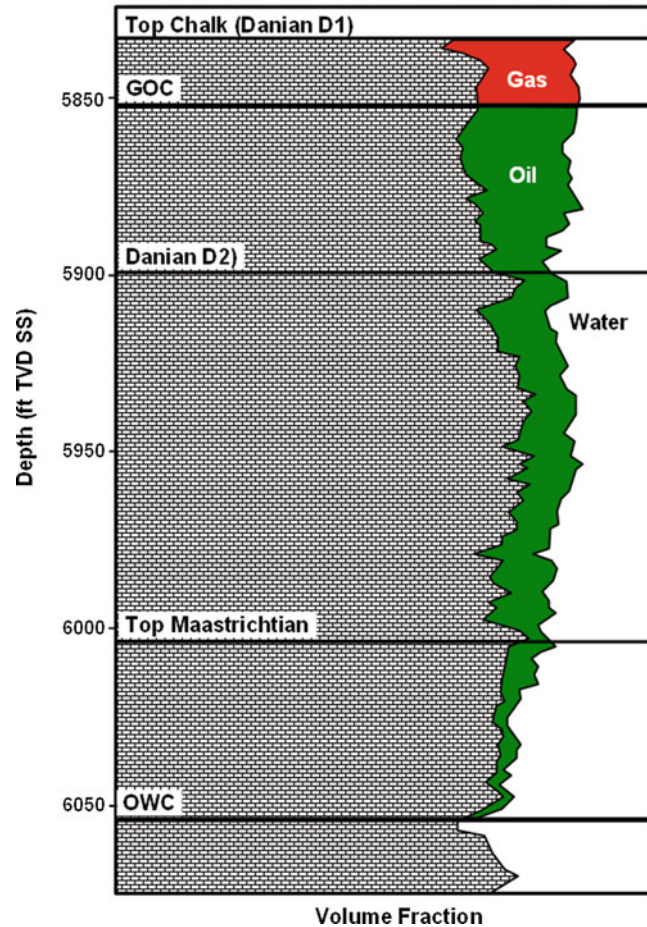
The discussion so far in this section has concerned the quantification of matrix properties, yet most reservoirs contain fractures, with widely varying properties. At one extreme they may be

closed, creating compartments, at the other extreme they can be open, in which case they will have a profound impact on flow performance.

However, in reservoir modelling and simulation, property modelling tends to focus on matrix properties, with the impact of fracture systems restricted to the mapping of 2D fault planes which may or may not be transmissible to flow normal to those planes. Fracture rock properties, if considered at all, are treated as an overlay. Very heavily fractured reservoirs – the ‘Type 1’ systems of Nelson (2001) – tend to be treated as a different type of reservoir, usually modelled using non-standard specialist software with matrix properties simplified or ignored.

We argue that all reservoirs are fractured to some extent and matrix and fracture properties are best regarded together. We see fractures as just

**Fig. 3.48** Type log for the Kraka field illustrating the variable oil saturations and the thick transition zone. (Redrawn from Thomasen and Jacobsen 1994, ©1994, Society of Petroleum Engineers Inc., reproduced with permission of SPE. Further reproduction prohibited without permission)



another model element, as even in reservoir systems with a low density fracture network these fractures are three-dimensional features which have a thickness:

“fractures are volumetric”

They should therefore be treated as discrete elements (as defined in Chap. 2) and considered petrophysically alongside the more familiar matrix elements.

In this section, the properties of fracture systems, both open and partially sealing, will be reviewed. In Chap. 6.7, options for modelling different types of fractured reservoirs in fields where the fracture component is significant, will be explored.

### 3.8.1 Terminology and Type

Fractures can be broadly viewed in terms of two end-member types: *joints* and *faults*.

Joints are extensional fractures, formed when rocks enter tensile space (the left-hand side of the Mohr diagram, Fig. 3.49) under a deviatoric stress in excess of the tensile rock strength. They tend to form regularly-spaced fractures (Figs. 3.49 and 3.50 left) often in more than one set, with sets mutually abutting. Lateral displacement on joints is minimal, although not necessarily zero as once a tensile fracture has formed there may be millions of years of isostatic activity to follow, during which some movement on any open fracture is inevitable.

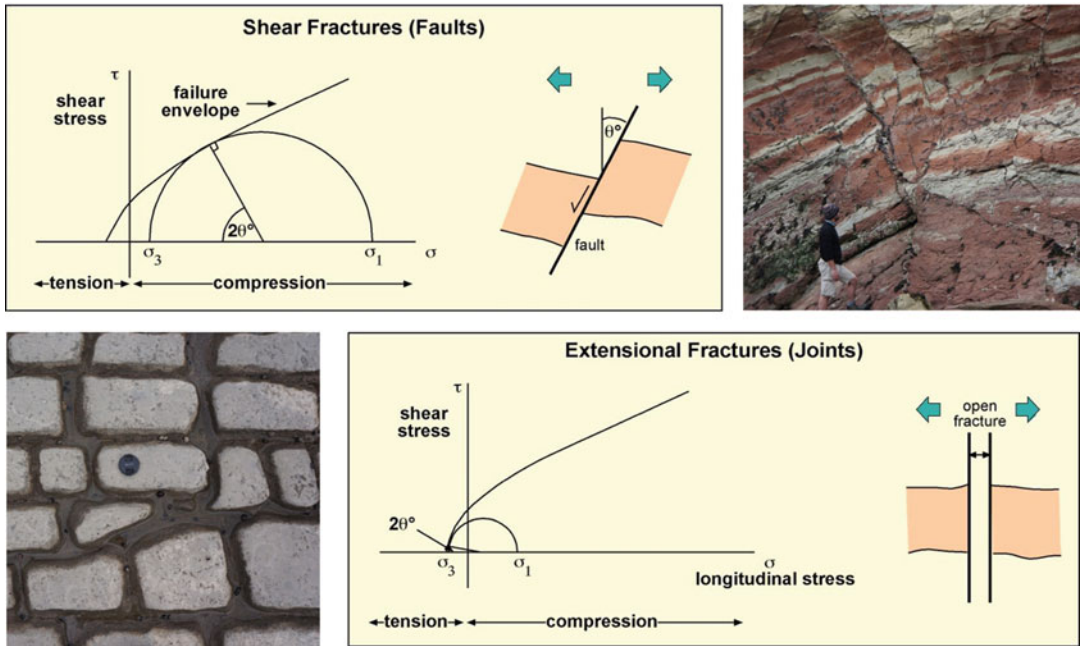


**Fig. 3.49** Contrasting modes of fracturing: tensile (jointing) vs. shear (faulting)



**Fig. 3.50** Contrasting fracture styles: tensile fracturing (jointing, left); shear fracturing (faulting, right), Somerset, UK

By contrast, a fault is a zone (a volume in 3D), either side of which relative displacement of the host rock has occurred during failure as a result of *shear* when the compressive deviatoric stress exceeds the rock strength (the right-hand side of the Mohr diagram, Fig. 3.49 upper, Fig. 3.50, right). Note that rocks are always in net compression at shear failure, irrespective of whether the

regional tectonic picture is described as ‘extensional’, ‘compressional’ or ‘strike-slip’. The latter terms simply describe the orientation of the principal stresses at failure.

Faults form as part of a fault network and a key characteristic of fault networks is their scale invariance – the same fault patterns can be observed on a range of scales. They are fractal.

Faults in reservoirs are not single 2D planes, but form zones in which many fractures coalesce. The result is a highly deformed fault core surrounded by a wider, less deformed damage zone containing a mixture of joints and small faults (Fig. 3.51).

The properties of joint sets are influenced strongly by the mechanical properties of the host rock – brittle rocks form joints more readily – so joints are often bed-limited. Mechanical

stratigraphy is therefore important in understanding joint patterns. Unlike fault networks the statistics of joint sets (in terms of frequency vs. size) are typically log-normal. The classic ‘naturally-fractured reservoir’ is typically a joint-network reservoir, in which production is dominated by flow from a pervasive, high-density fracture network such as those seen at outcrop in Fig. 3.50 (left) and Fig. 3.52.

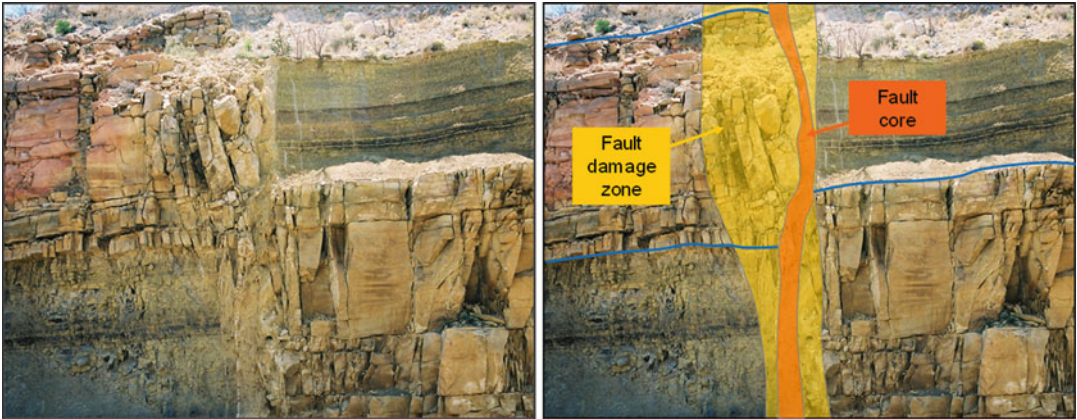


**Fig. 3.51** Fault-related fracturing: a fault damage zone, Brushy Canyon, USA

**Fig. 3.52** Bed-limited joint networks in Urgonian limestone, Cassis, France; note the contrast between the regular joint sets in the upper, mechanically homogeneous limestone, and the vertically less continuous joint sets in the lower interbedded limestones and marls



### 3.8.2 Fault Zone Properties

On the basis that faults are 3D volumes it follows that faults must have volumetric properties just like the matrix or host rock. Fault rock has porosity and permeability, and the latter can be expected to be highly anisotropic, particularly in a fault core.

In a reservoir with high phyllosilicate (clay mineral) content, faults will tend to seal either by juxtaposition of reservoir and non-reservoir layers or by the introduction of clay-rich material into the fault zone as a ‘fault gouge’ (Fig. 3.53) (Yielding et al. 1997; Fisher and Knipe 1998). Braathen et al. (2009) have developed these concepts further by defining a set of ‘fault facies’ enabling more quantitative fault description for 3D reservoir modelling.

Empirical data from fault systems has led to a set of quantitative methods for predicting the sealing properties of faults. The most widely used method is the shale gouge ratio, SGR, proposed by Yielding et al. (1997) who showed that the cumulative shale bed thickness in a faulted siliciclastic reservoir sequence could be used to predict fault seal based on observed across-fault pressure differences. They defined the SGR for a specific reservoir interval as:

$$SGR = \frac{\Sigma(\text{Shale bed thickness})}{\text{Fault throw}} \times 100 \% \quad (3.45)$$

Other factors used in fault seal analysis include the clay smear potential and the shale smear factor (Fig. 3.54), but the SGR method is most widely applied.

Modifications to the SGR method include corrections for the clay mineral content of shaly beds (Sperrevik et al. 2002) and field data from the Brent Group (Jolley et al. 2007). These authors have developed functional relationships between SGR and fault rock permeability, and these can be compared with permeability data gathered from faults either by direct measurement of core material or by modelling of production performance in and around fault zones (see Fig. 3.55, adapted from the compilation of Solum and Huisman 2017).

The effects of fault seal variation across fault zones intersecting a multi-layer reservoir interval can be mapped using fault juxtaposition diagrams, to which a measure of seal potential can be added (Bentley and Barry 1991; Knipe 1997). Combining this with a functional relationship between SGR and permeability, a workflow



**Fig. 3.53** Fault gouge (brown, left) in a phyllosilicate-rich clastic interval, Somerset, UK

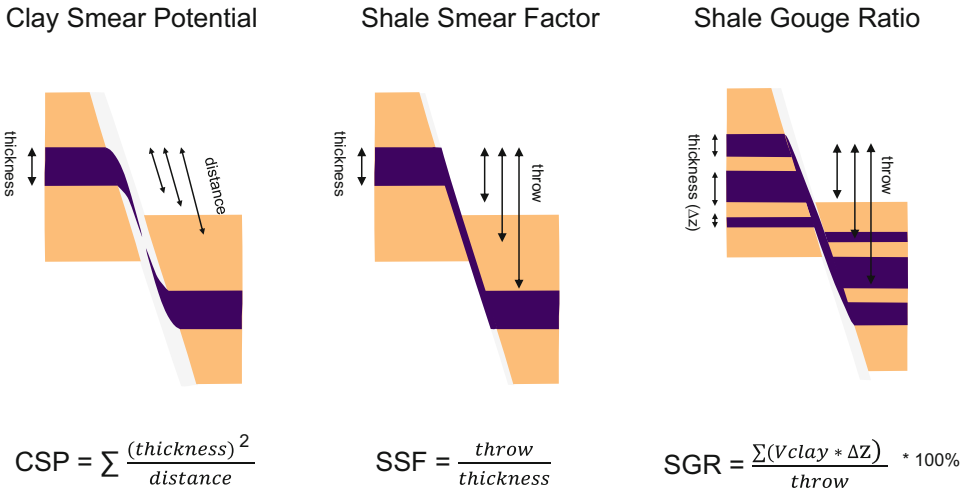


**Fig. 3.54** Common algorithms calculating the sealing potential of fault zones. (Modified from Yielding et al. 2010); SGR (right) remains the most widely used

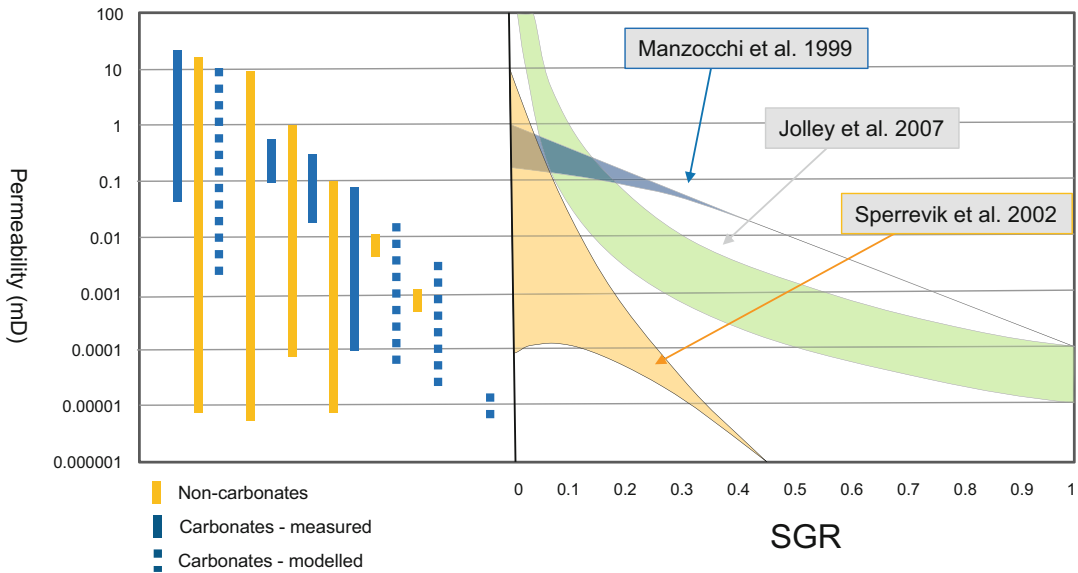


**Fig. 3.55** Relationships between Shale Gouge Ratio (SGR) and permeability shown against estimates of fault rock permeability from core plug measurements or models (based on a compilation by Solum and Huisman 2017)

can be completed which delivers a quantitative estimate of cell-to-cell transmissibility across fault zones in reservoir and simulation models (Manzocchi et al. 1999).

This workflow offers a method for forward-modelling the lateral seal potential of fault zones (it is assumed that no flow occurs along the fault zone) and allows for the recognition that although some faults do seal, others are only baffles to flow and the seal potential is a variable. This

recognition is a significant improvement to the modelling of faults as either simply ‘open’ or ‘closed’ features and the SGR workflow provides the utility to systematically quantify this, incorporating variable fault displacements and spatially variable lithology (via the use of a  $V_{clay}$  matrix property). It should be appreciated, however, that faults are highly complex geological features containing multiple elements acting both as flow conduits and barriers (e.g. Caine



et al. 1996; Manzocchi et al. 1998, 2010) and the SGR workflow is delivering a practical 2D (across-fault) solution to a more complex 3D problem.

The SGR examples relate to fault rocks which are phyllosilicate-rich but the data in Fig. 3.55 are a reminder that fault rocks without clays (carbonates, sandstones) can also have reduced permeabilities through the process of cataclasis (mechanical grain size reduction). In these cases there are predictable property changes as a fault zone is entered:

1. Reduction in porosity;
2. Reduction in permeability magnitude;
3. Increased permeability anisotropy;
4. A rotation of the permeability tensor.

This is illustrated in Fig. 3.56 for an analogue outcrop example in a very high net sand system. The consequence of this is that, unless the fault zone permeability is sufficiently reduced that the fault zone is fully sealing, the fault will remain open to flow but the preferential flow directions within the zone will be quite different from the surrounding host rock, as the rock fabric is so strongly altered by deformation. This may lead to the paradox that fault zones, when considered as 3D elements, may be both open and closed:

closed to flow perpendicular to the fault zone but open along the plane of the faulting.

A measured example of permeability reduction into a fault zone in a clean sandstone reservoir is described by Farrell and Healy (2017). They record the change in rock fabric into the fault zone and a decrease in permeability from 1D to less than 1 mD with a fault core largely cemented (Fig. 3.57). Any flow in the damage zone is preferentially along, rather than across, the fault zone.

An example of this from a producing field is described by Bentley and Elliott (2008) from a high net sand reservoir from the Irish Sea, and a modelling solution to represent it is described in Chap. 6.

\* \* \*

Considering faults as 3D volumes, and fault rocks as elements with properties, we can enrich our view of fault zones by recognizing they have multiphase flow properties related to capillary and surface tension effects. These effects can be subtle but quite substantial and in some cases cause a fault to retain an oil column of several 10's of metres while still being permeable to water.

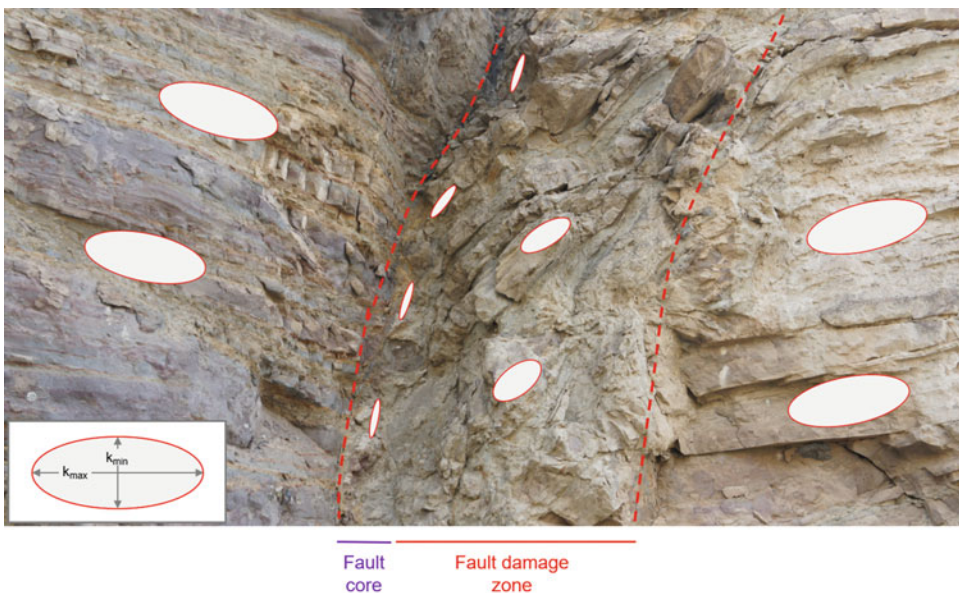


**Fig. 3.56** Fault rock properties in a sand-rich reservoir; permeability magnitude decreases into the fault zone, anisotropy increases and the permeability tensor rotates; flow across the zone becomes less likely and any flow in

the damage zone is more likely to occur along or up the zone. High NTG marine sandstone example from Tabernas, Spain

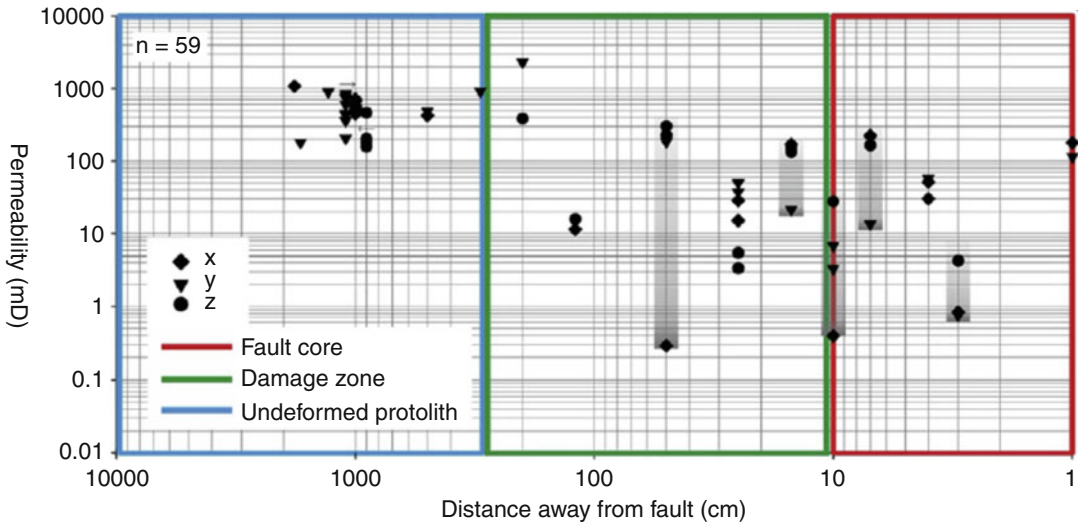


**Fig. 3.57** Permeability reduction in a quartz arenite as a fault with a ca.50 m displacement is approached; data from the Clashach Fault, Scotland (Farrell and Healy 2017)

For the simplest case of a water-wet low-permeability fault rock, we can define the capillary threshold pressure,  $P_{CT}$ , required to allow the non-wetting phase to flow (Manzocchi and Childs 2013), e.g. for a static oil-water system:

$$P_{CT} = (\rho_w - \rho_o)g h_o \quad (3.46)$$

where:

$h_o$  = oil column height.

If the fluid pressure of the oil column exceeds the  $P_{CT}$  of the fault then oil will flow across the fault, if not then the fault will be permeable only to water. Figure 3.58 shows an example of a set of leaky faults creating stepped fluid contacts as neighbouring faults have their capillary entry pressure exceeded at different heights.

In the case of non-static conditions, where natural hydrodynamic gradients exist or lateral pressures are applied (by injection or production) additional terms for lateral pressure gradients in the water or oil phase need to be taken into account (see Manzocchi and Childs 2013).

In addition to entry pressure effects causing an apparently ‘sealing’ fault to allow flow of the wetting phase (water), the simple presence of a fault rock which is tight relative to the surrounding host may have a baffling effect on

flow even if the fault is not sealing. This is a relative permeability effect and is illustrated in Fig. 3.59. The poorer quality (tighter) fault rock element will have a thicker transition zone than the host, and therefore even with oil either side of a permeable fault the relative permeability of the fault to oil will be lower than in the host rock, especially in the lower part of the oil column, creating a baffle.

Wherever faults are important in reservoir modelling studies, considerable efforts are needed to measure fault rock properties (e.g. Sperrevik et al. 2002). Figure 3.60 shows a compiled set of measured values for  $P_{CT}$  as a function of permeability. Despite some spread in the data, general empirical transforms between permeability and capillary threshold pressure can be established. The trends for faulted and un-faulted rock samples are broadly similar, although low-permeability clay-rich fault rocks tend to have significantly higher  $P_{CT}$ .

To summarise these challenges, in order to represent the effects of faults in reservoir simulation models, there are several options:

1. Represent the fault as a transmissibility multiplier on the simulation cell boundary which coincides with the fault plane (no multi-phase effects included).
2. Represent the fault as a two-phase flow transmissibility multiplier on the simulation cell boundary which coincides with the fault plane.

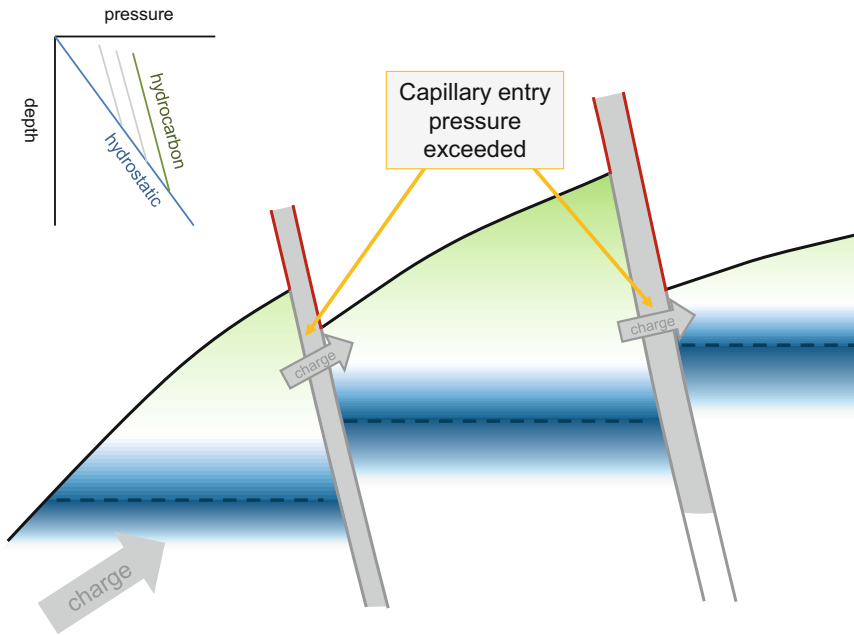


**Fig. 3.58** Stepped contacts across a series of fault blocks resulting from the exceedance of capillary entry pressure in successive fault rocks during hydrocarbon migration

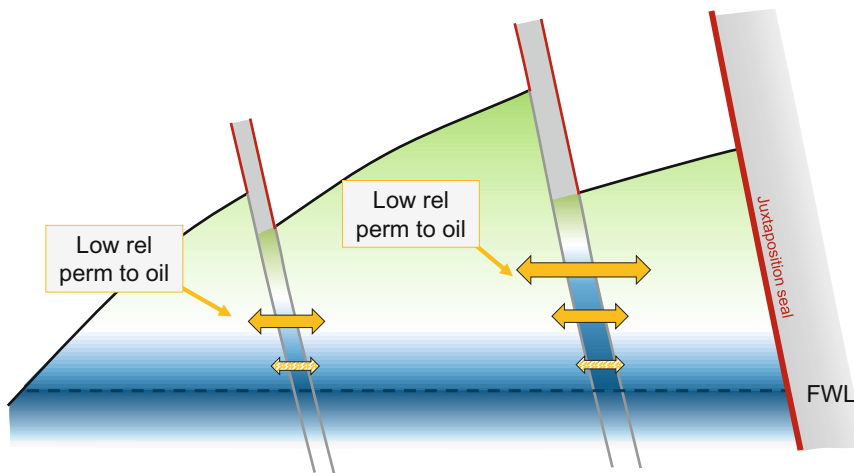


**Fig. 3.59** Relative permeability effects across low but non-zero permeability fault rocks; the effect is to create baffles to oil flow in the lower part of an oil column, even if the fault is not sealing

3. Represent the fault explicitly as a volume, placing grid cells within the fault zone and adjacent to the fault zone or damage zone (with multi-phase effects included).

The third option allows detailed analysis of the effects of faults on flow, but is rarely used because it may be computationally demanding.

The use of simple transmissibility multipliers allows for more efficient reservoir simulations, but neglects potentially important multi-phase flow effects. Manzocchi et al. (2002) proposed a versatile approach for inclusion of two-phase transmissibility multipliers to represent faults in reservoir simulation studies, allowing more structural geological detail to be included in reservoir

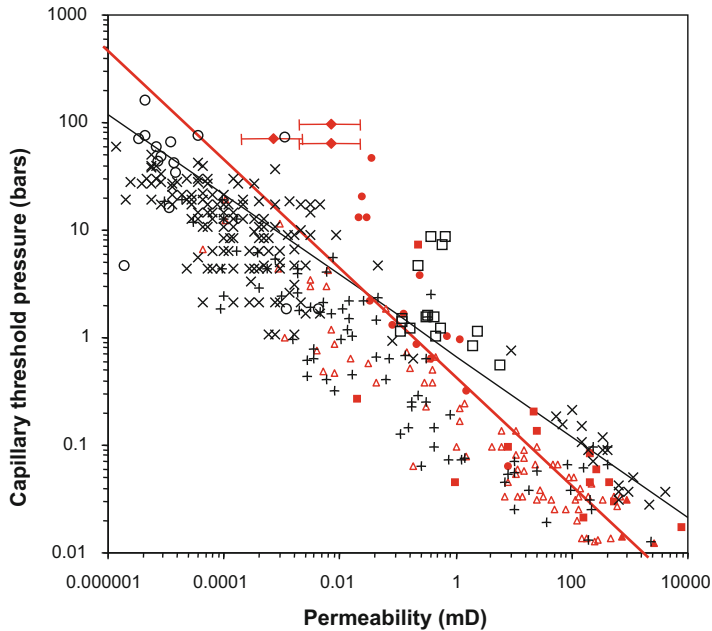


**Fig. 3.60** Capillary threshold pressure versus permeability from a compiled dataset of fault-rock samples (*solid symbols*) and unfaulted rock samples (*crosses and open symbols*) from Manzocchi et al. (2002) and T. Manzocchi (pers. comm.). The two lines are published model relationships for unfaulted rocks (*black line*, Ringrose

et al. 1993) and faulted rocks (*red line*, Harper and Lundin 1997). For sources of datasets see Manzocchi et al. (2002). Data have been normalized for a moderately water-wet oil-water system (redrawn from Manzocchi et al. 2002, Petroleum Geoscience, v. 8 © Geological Society of London [2002])

models (e.g. Brandsæter et al. 2001; Manzocchi et al. 2008a, b).

### 3.8.3 Modelling Open Fracture Properties

Modelling the flow properties of open fracture systems, whether open fractures in a fault damage zone or, more commonly, dense joint networks (Fig. 3.61), generally focuses on estimations of fracture density and fracture aperture.

Modelling workflows for these are discussed in Chap. 6. Here it is only necessary to emphasise the dramatic difference an open fracture makes to the effective permeability of a reservoir system. The underlying reason is the fundamental flow equation, as ‘Darcy flow’ familiar in matrix-only reservoirs is replaced by Poiseuille’s Law (introduced in Sect. 3.2.6) and flow is now a function of fracture geometry, notably the fracture aperture. The latter is important because fracture aperture is difficult to measure, hard to

estimate and is raised to the power three in the fundamental flow equation (Eq. 3.12). Practitioners new to fractured reservoir modelling typically overestimate aperture with first pass guesses such as ‘1 mm’, which lead to very large flow rates (a better starting guess would be one or two orders of magnitude lower). The prime consequence of not knowing this sensitive parameter is that forward modelling is very unreliable, and it is generally necessary to invert estimates from production data, re-emphasising the problem of sampling (data  $\neq$  truth  $\neq$  model). This is discussed further in Chap. 6.

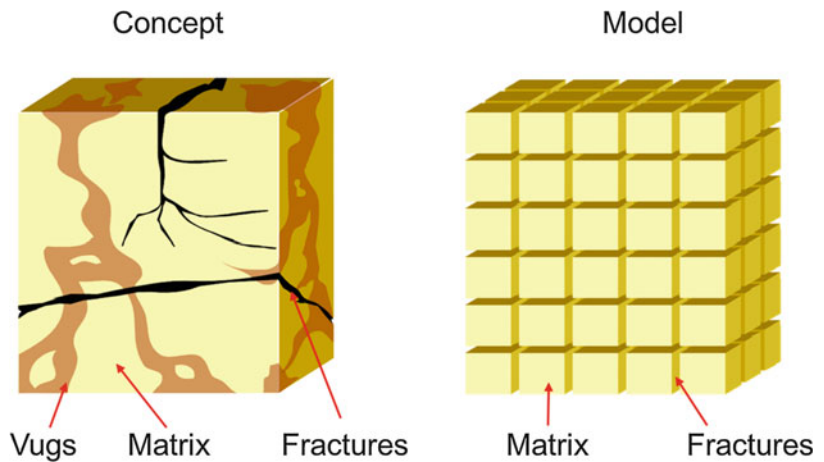
In terms of generating a starting estimate of effective reservoir properties for fractures at the simulation grid-cell scale, there are key steps:

1. Formulate a clear concept for the geometry of the network.
2. Ascertain the typical network geometry from image logs and any oriented core data.
3. Conclude from petrophysical data and well tests whether matrix *and* fractures are contributing to flow, or only the fractures.



**Fig. 3.61** Dense open fracture system in Urgonian Limestone, Cassis, France

**Fig. 3.62** Classical representation of a dense fracture system in a model



4. Generalise the complexity of the fracture pattern: in Fig. 3.62, a concept of irregular fracturing in a number of orientations is represented by a 'sugar cube' geometry; classical fractured reservoir engineering (Aguilera 1980) offers three templates depending on the number of fracture sets present: sheets, sticks and cubes.
5. Once selected, the geometrical relationship between matrix blocks and the fracture network can be quantified in terms of a general 'shape factor' parameter, sigma ( $\sigma$ ), capturing

the surface area over which matrix and fracture connect.

6. Understand the wettability of the matrix rock, as this determines the efficacy of the imbibition process required to encourage oil in a matrix block to move into the fracture network and hence to a producing well.

The workflows involved in extrapolating these cellular properties and the options for modelling across a field are discussed in Chap. 6.

### 3.8.4 Capturing the Effects of Stress on Fracture Properties

A prescient challenge for estimating fracture properties is capturing the effects of stress. The present-day stress system will act on the inherited sets of fractures to determine their fluid flow properties. Fractures which are favourably aligned to the present-day stress field will tend to be more open and conductive than fractures which are in compression. In reservoir modelling, conditioning static fracture models to dynamic data (well tests and production data) often acts as a proxy to stress-modelling, as the dynamic data indicates which fractures are actually flowing. This is not necessarily predictive, however, and it may be preferable to try and forward-model or ‘forecast’ which fractures are most likely to be conductive under long-term production.

Predicting the effects of the stress field on fracture flow properties is a significant challenge, so that a more realistic modelling objective is to allow fracture flow properties to be ‘stress sensitive’ – that is, to try to capture the relationship between fracture conductivity and orientation. Bond et al. (2013) successfully

demonstrated this approach by modelling fracture anisotropy as a parameter controlled by the stress field, for a CO<sub>2</sub> storage modelling study (Fig. 3.63). They used dilation tendency  $T_d$ , as the controlling factor:

$$T_d = (\sigma_1 - \sigma_n)(\sigma_3 - \sigma_n) \quad (3.47)$$

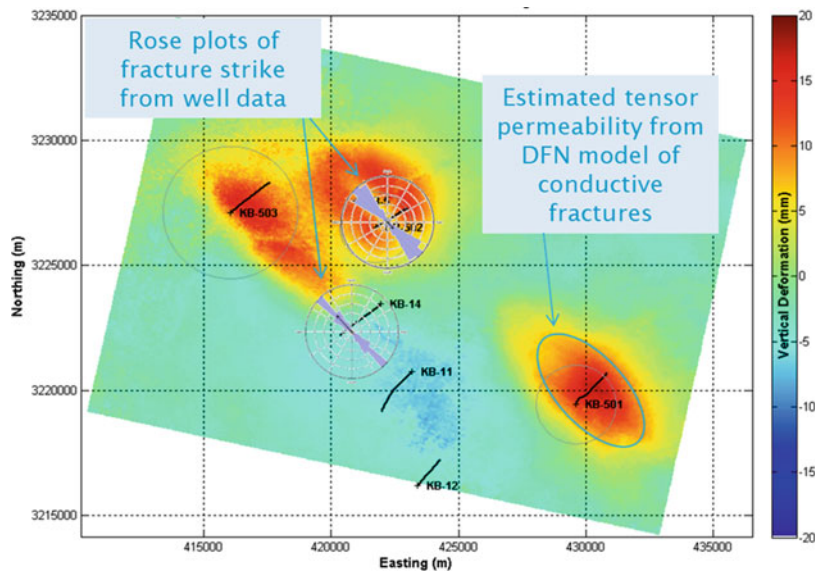
where:

$\sigma_n$  is the normal stress on the fracture plane.

This allows the stress field to operate as a control on the fracture flow properties, generating a tensor permeability matrix for the fracture permeability (see Sect. 3.2), which was found to give an excellent match to surface uplift data (Vasco et al. 2010) because ground deformation was controlled by the fracture permeability field (Fig. 3.63).

The fracture network properties still need to be calibrated to static and dynamic data such as image logs, seismic data and well tests, but in this way the effects of stress are also included. The stress field in itself may be hard to determine accurately, and alternative stress field scenarios may need to be evaluated, ideally within a framework of multiple deterministic scenarios, as was done in the study by Bond et al. (2013).

**Fig. 3.63** Comparison of modelled fracture permeability tensor (from Bond et al. 2013) with fractures orientations observed in wells at the In Salah CO<sub>2</sub> injection site. Data are overlain on a map of surface uplift based on InSAR data (Vasco et al. 2010) which reveals an anisotropic pressure field around each of the 3 CO<sub>2</sub> injector wells. The predicted anisotropic fracture flow vectors closely match the observed vertical deformation patterns (red areas with 10–20 mm uplift). Images modified from Bond et al. (2013) courtesy of Equinor ASA



### 3.8.5 Summary – Fracture Properties

Fractures are commonly modelled as simple 2D fault planes unless reservoir performance is completely dominated by fracture flow, and thereby unavoidable. The contribution of fracture properties to overall flow in a reservoir is therefore commonly underestimated.

A key step is to recognise fracture presence and build a concept for its impact on field performance, positive or negative, then attempt to quantify the fracture properties. This requires the conceptualisation of fractures as 3D reservoir elements, not simply 2D planes (Fig. 3.64). The complexity can appear daunting but this can also be a blessing: fracture systems are characterised by short length scale heterogeneity which can often be averaged. The averaging process is discussed in Chap. 4, and general approaches to modelling fractured reservoirs are outlined in Chap. 6.

## 3.9 Summary

We have covered a range of issues related to the petrophysical property modelling of reservoirs. The theoretical principles that underlie the modelling ‘buttons’ and workflows in reservoir modelling packages have been discussed along with many of the practical issues that govern the choice of parameters.

To summarise this chapter, we offer a checklist of key questions to ask before proceeding with your property modelling task:

1. Have you agreed with your colleagues across disciplines (geoscience, petrophysics and reservoir engineering):
  - the key geological issues you need to address – rock heterogeneity, sedimentary barriers, faults, etc., and
  - a consistent method for handling net-to-gross (N/G) and cut-off values?
2. Is your petrophysical data representative of the rock unit (sampling problems, tails of distributions), and if not how will you address that uncertainty?
3. Have you used appropriate averaging and/or upscaling methods?
4. Is the model output consistent with data input? Compare the statistics of input and output distributions. The variance may be as important as the mean.
5. Have you run sensitivities to check important assumptions?
6. Have you considered the effects of possible un-detected flow barriers in the system, especially given that the effects of fractures are often underestimated?

A final word about the future of property modelling – if we are looking for fit-for-purpose models for interpreting petrophysical well data, then we are probably talking about high-resolution near-wellbore models (Fig. 3.65).



**Fig. 3.64** Fracture zones: sometimes sealing, often open, always volumetric

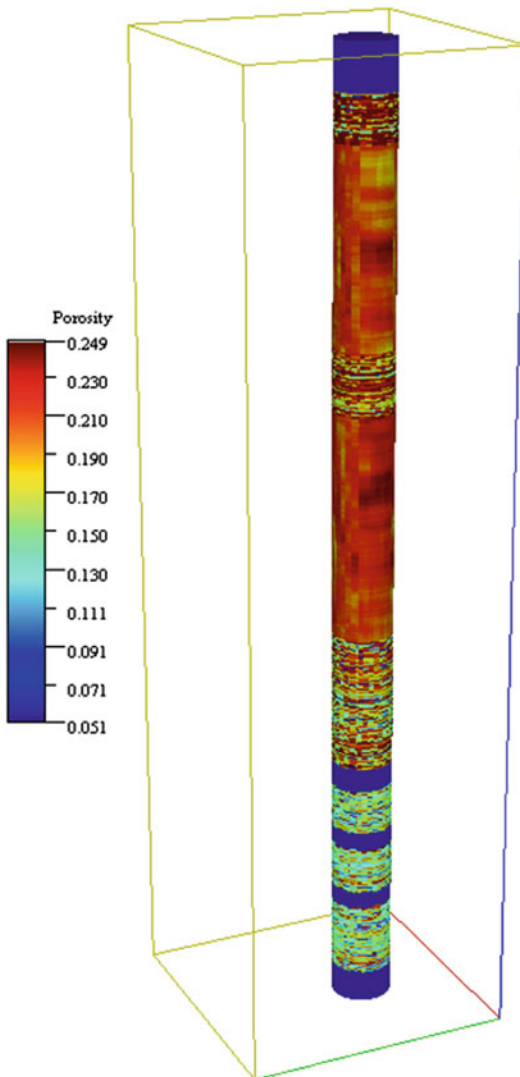


**Fig. 3.65** Near-wellbore porosity model ( $1 \text{ m}^2 \times 10 \text{ m}$ )

These models could be very detailed or could be just a simple equation. Either way they need to be focussed on the scale of the rock property variation – the subject of the next chapter.

## References

- Abbaszadeh M, Fujii H, Fujimoto F (1996) Permeability prediction by hydraulic flow units – theory and applications. *SPE Form Eval* 11(4):263–271
- Aguilera R (1980) Naturally fractured reservoirs. Penwell Corp, Tulsa. 521pp
- Begg SH, Carter RR, Dranfield P (1989) Assigning effective values to simulator gridblock parameters for heterogeneous reservoirs. *SPE Reserv Eng* 4:455–463
- Bentley MR, Barry JJ (1991) Representation of fault sealing in a reservoir simulation: cormorant block IV UK North Sea. SPE paper 22667 presented at the SPE annual technical conference and exhibition, Dallas, Texas, 6–9 October
- Bentley M, Elliott A (2008) Modelling flow along fault damage zones in a sandstone reservoir; an unconventional modelling technique using conventional modelling tools in the Douglas Field, Irish Sea, UK. SPE paper 113958 presented at Europec/EAGE conference and exhibition, Rome, Italy, 9–12 June 2008
- Berg RR, DeMis WD, Mitsdarffer AR (1994) Hydrodynamic effects on Mission Canyon (Mississippian) oil accumulations, Billings Nose area. *North Dakota AAPG Bull* 78(4):501–518
- Bierkins MFP (1996) Modeling hydraulic conductivity of a complex confining layer at various spatial scales. *Water Resour Res* 32(8):2369–2382
- Bond CE, Wightman R, Ringrose PS (2013) The influence of fracture anisotropy on CO<sub>2</sub> flow. *Geophys Res Lett* 40(7):1284–1289
- Bourbie T, Zinszner B (1985) Hydraulic and acoustic properties as a function of porosity in Fontainebleau sandstone. *J Geophys Res* 90(B13):11524–11532
- Box GEP, Cox DR (1964) An analysis of transformations. *J R Stat Soc Series B* 26:211–243, discussion 244–252
- Braathen A, Tveranger J, Fossen H, Skar T, Cardozo N, Semshaug SE, Bastesen E, Sverdrup E (2009) Fault facies and its application to sandstone reservoirs. *AAPG Bull* 93(7):891–917
- Brandsæter I, Ringrose PS, Townsend CT, Omdal S (2001) Integrated modeling of geological heterogeneity and fluid displacement: Smørbukk gas-condensate field, Offshore Mid-Norway. SPE reservoir simulation symposium. Society of Petroleum Engineers
- Brandsæter I, McIlroy D, Lia O, Ringrose PS (2005) Reservoir modelling of the Lajas outcrop (Argentina) to constrain tidal reservoirs of the Haltenbanken (Norway). *Pet Geosci* 11:37–46
- Bryant S, Blunt MJ (1992) Prediction of relative permeability in simple porous media. *Phys Rev A* 46:2004–2011
- Buland A, Kolbjørnsen O, Omre H (2003) Rapid spatially coupled AVO inversion in the fourier domain. *Geophysics* 68(1):824–836
- Caine JS, Evans JP, Forster CB (1996) Fault zone architecture and permeability structure. *Geology* 24(11):1025–1028
- Cardwell WT, Parsons RL (1945) Average permeabilities of heterogeneous oil sands. *Trans Am Inst Min Met Pet Eng* 160:34–42
- Corbett PWM, Jensen JL (1992) Estimating the mean permeability: how many measurements do you need? *First Break* 10:89–94
- Corbett PWM, Ringrose PS, Jensen JL, Sorbie KS (1992) Laminated clastic reservoirs: the interplay of capillary pressure and sedimentary architecture. SPE paper 24699, presented at the SPE annual technical conference, Washington, DC
- Cosentino L (2001) Integrated reservoir studies. Editions Technip, Paris, 310 pp



- Dahlberg EC (1995) Applied hydrodynamics in petroleum exploration, 2nd edn. Springer, New York
- Davis JC (2003) Statistics and data analysis in geology, 3rd edn. Wiley, New York, 638 pp
- de Marsilly G (1986) Quantitative hydrogeology. Academic, San Diego
- Delfiner P (2007) Three statistical pitfalls of phi-k transforms. *SPE Reserv Eval Eng* 10:609–617
- Desberats AJ (1987) Numerical estimation of effective permeability in sand-shale formations. *Water Resour Res* 23(2):273–286
- Deutsch C (1989) Calculating effective absolute permeability in sandstone/shale sequences. *SPE Form Eval* 4:343–348
- Deutsch CV (2002) Geostatistical reservoir modeling. Oxford University Press, Oxford, 376 pp
- Deutsch CV, Journel AG (1992) Geostatistical software library and user's guide, vol 1996. Oxford University Press, New York
- Doyen PM (2007) Seismic reservoir characterisation. EAGE Publications, Houten
- Durlowsky LJ (1991) Numerical calculations of equivalent grid block permeability tensors for heterogeneous porous media. *Water Resour Res* 27(5):699–708
- Elfenbein C, Husby Ø, Ringrose PS (2005) Geologically-based estimation of kv/kh ratios: an example from the garn formation, Tyrihans field, mid-Norway. In: Dore AG, Vining B (eds) Petroleum geology: North-West Europe and global perspectives. Proceedings of the 6th petroleum geology conference. The Geological Society, London
- Farrell NJC, Healy D (2017) Anisotropic pore fabrics in faulted porous sandstones. *J Struct Geol* 104:125–141
- Fisher QJ, Knipe R (1998) Fault sealing processes in siliciclastic sediments. *Geol Soc Lond Spec Publ* 147(1):117–134
- Goggin DJ, Chandler MA, Kocurek G, Lake LW (1988) Patterns of permeability variation in eolian deposits: page sandstone (Jurassic), N.E. Arizona. *SPE Form Eval* 3(2):297–306
- Gutjahr AL, Gelhar LW, Bakr AA, MacMillan JR (1978) Stochastic analysis of spatial variability in subsurface flows 2. Evaluation and application. *Water Resour Res* 14(5):953–959
- Harper TR, Lundin ER (1997) Fault seal analysis: reducing our dependence on empiricism. In: Møller-Pedersen P, Koestler AG (eds) Hydrocarbon seals: importance for exploration and production, Norwegian petroleum society special publications, 7. Elsevier, Amsterdam, pp 149–164
- Hohn ME (1999) Geostatistics and petroleum geology, 2nd edn. Kluwer, Dordrecht
- Howson C, Urbach P (1991) Bayesian reasoning in science. *Nature* 350:371–374
- Hubbert MK (1953) Entrapment of petroleum under hydrodynamic conditions. *AAPG Bull* 37(8):1954–2026
- Hurst A, Rosvoll KJ (1991) Permeability variations in sandstones and their relationship to sedimentary structures. In: Lake LW, Carroll HB Jr, Wesson TC (eds) Reservoir characterisation II. Academic, San Diego, pp 166–196
- Isaaks EH, Srivastava RM (1989) Introduction to applied geostatistics. Oxford University Press, Oxford
- Jensen JL, Corbett PWM, Pickup GE, Ringrose PS (1995) Permeability semivariograms, geological structure and flow performance. *Math Geol* 28(4):419–435
- Jensen JL, Lake LW, Corbett PWM, Goggin DJ (2000) Statistics for petroleum engineers and geoscientists, 2nd edn. Elsevier, Amsterdam
- Jolley SJ, Dijk H, Lamens JH, Fisher QT, Manzocchi T, Eikmans H, Huang Y (2007) Faulting and fault sealing in production simulation models: Brent Province, northern North Sea. *Pet Geosci* 13:321–340
- Jørgensen LN, Andersen PM (1991) Integrated study of the Kraka Field. SPE paper 23082, presented at the offshore Europe conference, Aberdeen, 3–6 Sept 1991
- Journel AG, Alabert FG (1990) New method for reservoir mapping. *J Petrol Technol* 42(02):212–218
- Journel AG, Deutsch CV (1997) Rank order geostatistics: a proposal for a unique coding and common processing of diverse data. *Geostat Wollongong* 96:174–187
- Journel AG, Deutsch CV, Desbarats AJ (1986) Power averaging for block effective permeability. SPE paper 15128, presented at SPE California regional meeting, Oakland, California, 2–4 April
- Kendall M, Stuart A (1977) The advanced theory of statistics, vol. 1: distribution theory, 4th edn. Macmillan, New York
- Knipe RJ (1997) Juxtaposition and seal diagrams to help analyze fault seals in hydrocarbon reservoirs. *AAPG Bull* 81(2):187–195
- Lescoffit G, Townsend C (2005) Quantifying the impact of fault modeling parameters on production forecasting for clastic reservoirs. In: Evaluating fault and cap rock seals, AAPG special volume Hedberg series, no. 2. American Association of Petroleum Geologists, Tulsa, pp 137–149
- Leuangthong O, Khan KD, Deutsch CV (2011) Solved problems in geostatistics. Wiley, New York
- Manzocchi T, Childs C (2013) Quantification of hydrodynamic effects on capillary seal capacity. *Pet Geosci* 19(2):105–121
- Manzocchi T, Ringrose PS, Underhill JR (1998) Flow through fault systems in high-porosity sandstones. *Geol Soc Lond Spec Publ* 127(1):65–82
- Manzocchi T, Walsh JJ, Nell P, Yielding G (1999) Fault transmissibility multipliers for flow simulation models. *Pet Geosci* 5(1):53–63
- Manzocchi T, Heath AE, Walsh JJ, Childs C (2002) The representation of two phase fault-rock properties in flow simulation models. *Pet Geosci* 8(2):119–132
- Manzocchi T, Carter JN, Skorstad A et al (2008a) Sensitivity of the impact of geological uncertainty on production from faulted and unfaulted shallow-marine oil reservoirs: objectives and methods. *Pet Geosci* 14:3–15
- Manzocchi T, Heath AE, Palanathakumar B, Childs C, Walsh JJ (2008b) Faults in conventional flow simulation models: a consideration of representational

- assumptions and geological uncertainties. *Pet Geosci* 14(1):91–110
- Manzocchi T, Childs C, Walsh JJ (2010) Faults and fault properties in hydrocarbon flow models. *Geofluids* 10 (1–2):94–113
- Matheron G (1967) *Éléments pour une théorie des milieux poreux*. Masson and Cie, Paris
- McIlroy D, Flint S, Howell JA, Timms N (2005) Sedimentology of the tide-dominated Jurassic Lajas Formation, Neuquen Basin, Argentina. *Geol Soc Lond Spec Publ* 252:83–107
- Mourzenko VV, Thovert JF, Adler PM (1995) Permeability of a single fracture; validity of the Reynolds equation. *J de Phys II* 5(3):465–482
- Muggeridge A, Mahmode H (2012) Hydrodynamic aquifer or reservoir compartmentalization? *AAPG Bull* 96 (2):315–336
- Muskat M (1937) *The flow of homogeneous fluids through porous media*. McGraw-Hill, New York. (Reprinted by the SPE and Springer 1982)
- Nair KN, Kolbjørnsen O, Skorstad A (2012) Seismic inversion and its applications in reservoir characterization. *First Break* 30:83–86
- Nelson RA (2001) *Geologic analysis of naturally fractured reservoirs*, 2nd edn. Butterworth-Heinemann, Boston
- Nordahl K, Ringrose PS, Wen R (2005) Petrophysical characterisation of a heterolithic tidal reservoir interval using a process-based modelling tool. *Pet Geosci* 11:17–28
- Olea RA (ed) (1991) *Geostatistical glossary and multilingual dictionary*, IAMG studies in mathematical geology no. 3. Oxford University Press, Oxford
- Pickup GE, Sorbie KS (1996) The scale-up of two-phase flow in porous media using phase permeability tensors. *SPE J* 1:369–381
- Pickup GE, Ringrose PS, Jensen JL, Sorbie KS (1994) Permeability tensors for sedimentary structures. *Math Geol* 26:227–250
- Pickup GE, Ringrose PS, Corbett PWM, Jensen JL, Sorbie KS (1995) Geology, geometry and effective flow. *Pet Geosci* 1:37–42
- Pyrz MJ, Deutsch CV (2014) *Geostatistical Reservoir Modelling*, 2nd edn. Oxford University Press, Oxford
- Renard P, de Marsily G (1997) Calculating equivalent permeability: a review. *Adv Water Resour* 20:253–278
- Ringrose PS (2008) Total-property modeling: dispelling the net-to-gross myth. *SPE Reserv Eval Eng* 11:866–873
- Ringrose PS, Sorbie KS, Corbett PWM, Jense JL (1993) Immiscible flow behaviour in laminated and cross-bedded sandstones. *J Pet Sci Eng* 9(2):103–124
- Ringrose PS, Pickup GE, Jensen JL, Forrester M (1999) The Ardross reservoir gridblock analogue: sedimentology, statistical representivity and flow upscaling. In: Schatzinger R, Jordan J (eds) *Reservoir characterization – recent advances*, AAPG memoir no. 71, pp 265–276
- Ringrose PS, Skjetne E, Elfeinbein C (2003) Permeability estimation functions based on forward modeling of sedimentary heterogeneity. SPE 84275, presented at the SPE annual conference, Denver, CO, USA, 5–8 Oct 2003
- Ringrose PS, Nordahl K, Wen R (2005) Vertical permeability estimation in heterolithic tidal deltaic sandstones. *Pet Geosci* 11:29–36
- Shuey RT (1985) A simplification of the Zoeppritz equations. *Geophysics* 50(4):609–614
- Size WB (ed) (1987) *Use and abuse of statistical methods in the earth sciences*, IAMG studies in mathematical geology, no. 1. Oxford University Press, Oxford
- Soares A (2001) Direct sequential simulation and cosimulation. *Math Geol* 33(8):911–926
- Solum JG, Huisman BAH (2017) Toward the creation of models to predict static and dynamic fault-seal potential in carbonates. *Pet Geosci* 23:70–91
- Sperrevik S, Gillespie PA, Fisher QJ, Halvorsen T, Knipe RJ (2002) Empirical estimation of fault rock properties. In: Koestler AG, Hunsdale R (eds) *Hydrocarbon seal quantification*, Norwegian petroleum society special publications, 11. Elsevier, Amsterdam, pp 109–125
- Thomassen JB, Jacobsen NL (1994) Dipping fluid contacts in the Kraka Field, Danish North Sea. SPE paper 28435, presented at the 69th SPE annual technical conference and exhibition, New Orleans, LA, USA, 25–28 September 1994
- Vasco DW, Rucci A, Ferretti A, Novali F, Bissell RC, Ringrose PS, Mathieson AS, Wright IW (2010) Satellite-based measurements of surface deformation reveal fluid flow associated with the geological storage of carbon dioxide. *Geophys Res Lett* 37(3):1–5
- Weber KJ, van Geuns LC (1990) Framework for constructing clastic reservoir simulation models. *J Pet Technol* 42:1248–1297
- White CD, Horne RN (1987) Computing absolute transmissibility in the presence of fine-scale heterogeneity. SPE paper 16011, presented at the 9th SPE symposium of reservoir simulation, San Antonio, TX, 1–4 Feb 1987
- Witherspoon PA, Wang JSY, Iwai K, Gale JE (1980) Validity of cubic law for fluid flow in a deformable rock fracture. *Water Resour Res* 16(6):1016–1024
- Worthington PF (2001) Scale effects on the application of saturation-height functions to reservoir petrofacies units. *SPE Reserv Eval Eng* 4(5):430–436
- Worthington PF, Cosentino L (2005) The role of cut-offs in integrated reservoir studies (SPE paper 84387). *SPE Reserv Eval Eng* 8(4):276–290
- Yielding G, Freeman B, Needham DT (1997) Quantitative fault seal prediction. *AAPG Bull* 81(6):897–917
- Yielding GPBS, Bretan P, Freeman B (2010) Fault seal calibration: a brief review. *Geol Soc Lond Spec Publ* 347(1):243–255

## Abstract

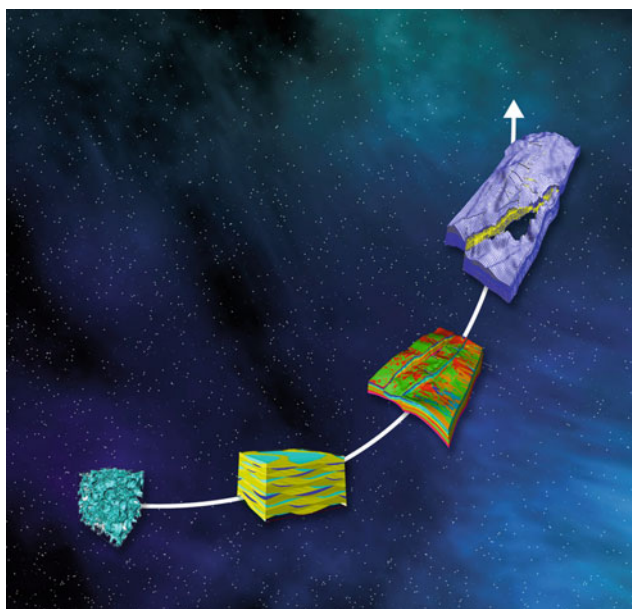
To ‘upscale flow properties’ means to estimate large-scale flow behaviour from smaller-scale measurements. Typically, we start with a few measurements of rock samples (length scale ~3 cm) and some records of flow rates and pressures in well tests (~100’s m). Our challenge is to estimate how the whole reservoir will flow (~1 km).

Flow properties of rocks vary enormously over a wide range of length scales, and

estimating upscaled flow properties can be quite a challenge. Unfortunately, many reservoir modellers choose to overlook this problem and blindly hope that a few measurements will correctly represent the whole reservoir.

The aim of this chapter is to help make intelligent estimates of large-scale flow properties and to avoid stupid pitfalls. In the words of Albert Einstein:

Two things are infinite: the universe and human stupidity; and I’m not sure about the universe.



*Upscaling – from pore to field, and beyond ...*

### Keywords

Multi-scale upscaling · Multi-phase flow · Steady-state methods · Heterogeneity · Fluid forces · Representative elementary volume (REV) · Gridding, pore-to-field

## 4.1 Multi-scale Flow Modelling

This chapter concerns the implementation of multi-scale flow modelling of permeable reservoir containing valuable fluid resources, e.g. hydrocarbons, water, CO<sub>2</sub> or hydrogen. Multi-scale flow modelling is defined here as:

any method which attempts to explicitly represent the flow properties at more than one scale within a reservoir.

We may, for example, have:

- an estimate of flow properties around a single well in a specific flow unit (or reservoir interval) and
- a rationale for using this estimate to calculate the flow properties in the whole reservoir.

This rationale could simply be a multiplication factor transforming the single-well flow property to the reservoir scale, or it might involve a 3D array (or grid) of values drawn from a statistical

population (which includes the single-well flow property).

In multi-scale modelling, the essence is that geological concepts are used to make the transition from smaller-scale measurements to larger-scale estimates (models) of reservoir properties or behaviour (Fig. 4.1). Reservoir modelling in itself is an art form requiring some intimate knowledge of the geological system – typically involving Picasso-type geologists (Fig. 4.2) with an interest in detail. For upscaling we require representative geological models in which the geological elements (e.g. layers of sandstone, siltstone, mudstone and limestone) are represented as properties relevant for fluid modelling – porosity, permeability, capillary pressure functions, etc.

This process inevitably involves some simplification of the intricate variability of rock architecture, as we aim to group the rock elements into flow units with similar properties. In the art analogy this process is more like the work of Mark Rothko, where broad bands of colour capture the essence of the object or concept being described (Fig. 4.2).

The process of transferring information between scales is referred to as *upscaling* or, more generally, *re-scaling*. Upscaling involves some form of numerical or analytical method for estimating effective or equivalent flow properties at a larger scale given some set of finer scale rock

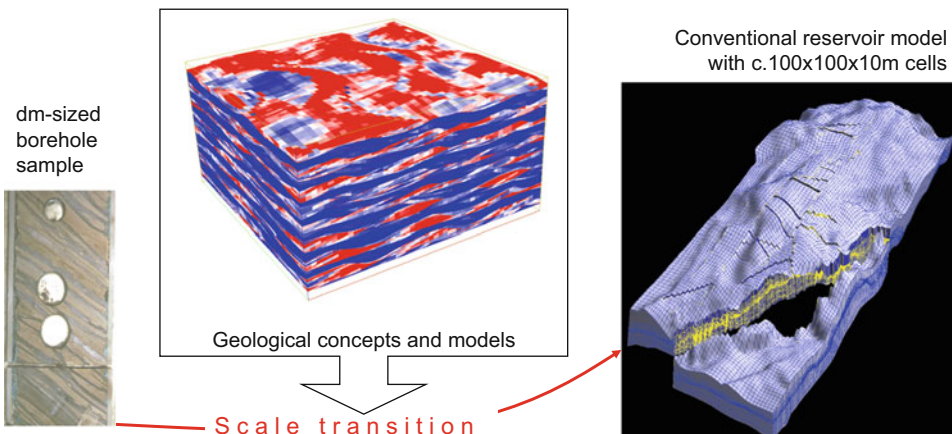
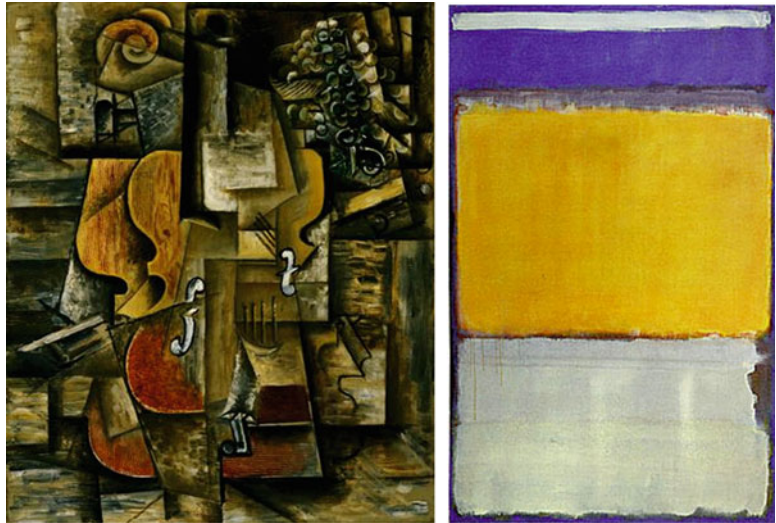


**Fig. 4.1** Scale transition in reservoir modelling and the role of geological concepts

**Fig. 4.2** The art of geological modelling: ‘Picasso-type geologists’ aim to represent fine detail in their art work while ‘Rothko-type geologists’ aim to capture only the representative flow units as essential colours. (Pablo Picasso, *Violins and Grapes*, oil on canvas (1912) and Mark Rothko, *No. 10*, 1950. Oil on canvas, 229.2 × 146.4 cm, reproduced with permission DIGITAL IMAGE © The Museum of Modern Art/Scala, Florence)



properties. Upscaling methods for single and multiphase flow are reviewed in detail by Renard and de Marsily (1997), Barker and Thibeau (1997), Ekran and Aasen (2000) and Pickup et al. (2005). We will review the methods involved and establish the principles which guide the flow upscaling process. The term *downscaling* has also been used (Doyen 2007) to mean the process by which smaller-scale properties are estimated from a larger-scale property. This is most commonly done in the context of seismic data where, for example, a porosity value estimated from seismic impedance is used to constrain the porosity values of thin layers below the resolution of the seismic wavelet. In more general terms, if we know all the fine-scale properties then the upscaled property can be estimated uniquely. Conversely, if we know only the large-scale property value then there are many alternative fine-scale property models that could be consistent with the upscaled property.

We will develop the argument that upscaling is essential in reservoir modelling – whether implicit or explicit. There is no such thing as the *correct* value for the permeability of a given hydraulic flow unit. The relevant permeability value depends on length-scale, the boundary conditions and flow process. Efforts to define the diagnostic characteristics for hydraulic flow

units (HFU) (e.g. Abbaszadeh et al. 1996) provide valuable approaches to petrophysical data analysis, but HFUs should always be related to a representative elementary volume (REV). As we will show it is not always simple to define the REV, and when flow processes are brought into play different REV's may apply to different flow processes. Hydraulic flow units are themselves multi-scale.

The framework we will use for upscaling involves a series of steps where smaller-scale models are nested within larger scale models. These steps essentially involve models or concepts at the pore-scale, geological concepts and models at the field-scale and reservoir simulations (Fig. 4.3).

The factors involved in these scale transitions are enormous; certainly a factor of around  $10^9$  as we go from the rock pore to the full-field reservoir model (Table 4.1), and important scale markers involved in reservoir modelling are best illustrated on a logarithmic scale (Fig. 4.4). Despite these large scale transitions, most flow processes average out the local variations – so that what we are looking for is the correct average flow behaviour at the larger scales. How we do this is the rationale for this chapter.

Flow simulation of detailed reservoir models is a fairly demanding exercise, involving many

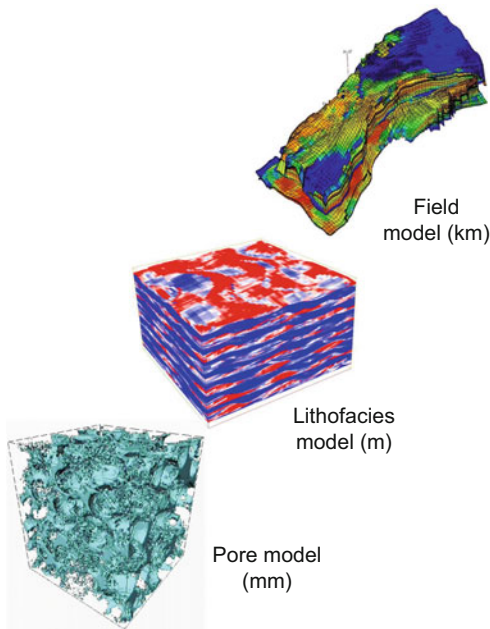


**Fig. 4.3** Reservoir models at different scales. (Equinor image archives, © Equinor ASA, reproduced with permission)

mathematical tools for creating and handling flow grids and calculating the flows and pressures between the grid cells. The mathematics of flow simulation is beyond the scope of this book, and will be treated only in an introductory sense. Mallet (2008) gives a useful review of the processes involved in the creation of numerical rock models and their use in flow simulation. King and Mansfield (1999) also give a fairly comprehensive discussion of flow simulation of geological reservoir models, in terms of managing and handling the grid and associated flow terms (transmissibility factors). In this chapter, we will take as our starting point the existence of a numerical rock model, created by some set of recipes in a geological modelling toolkit, and will focus on the methods involved for performing multi-scale upscaling. Before we do that we need to introduce, or recapitulate, some of the basic theory for multiphase fluid flow.

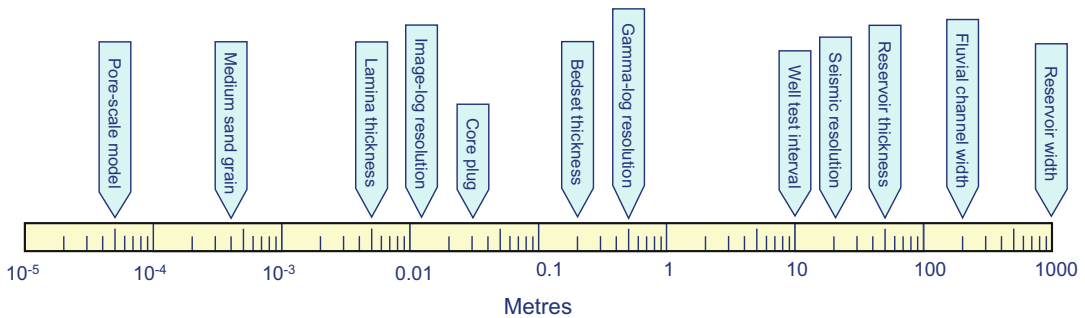


**Fig. 4.4** Important length scales involved in reservoir modelling

**Table 4.1** Typical dimensions for important volumes used in multi-scale reservoir modelling

|                  | X (m)              | Y(m)                | Z(m)                | Volume (m <sup>3</sup> ) | Cubic root (m) | Fraction of reservoir volume |
|------------------|--------------------|---------------------|---------------------|--------------------------|----------------|------------------------------|
| Pore-scale model | $5 \times 10^{-5}$ | $50 \times 10^{-5}$ | $50 \times 10^{-5}$ | $1.25 \times 10^{-13}$   | 0.00005        | 0.00000005                   |
| Core plug sample | 0.025              | 0.025               | 0.025               | 0.000031                 | 0.031          | 0.00003                      |
| Well test volume | 400                | 300                 | 10                  | 1,200,000                | 106            | 0.1                          |
| Reservoir model  | 8000               | 4000                | 40                  | 1,280,000,000            | 1086           | 1                            |

## 4.2 Multi-phase Flow

### 4.2.1 Two-Phase Flow Equations

In Chap. 3 we introduced the concept of permeability and the theoretical basis for estimating effective permeability using averages and numerical recipes. This introduced us to upscaling for single-phase flow properties. Here we extend this by looking at two-phase flow and the upscaling of multi-phase flow properties.

For a fuller treatment of multi-phase flow theory applied to oil and gas reservoir systems refer to reservoir engineering textbooks (e.g. Chierici 1994; Dake 2001; Towler 2002). A more geologically-based introduction to multi-phase flow in structured sedimentary media is given by Ringrose et al. (1993) and Ringrose and Corbett (1994).

The first essential concept in multiphase flow is the principal of mass balance. Any fluid which flows into a grid cell (mass accumulation) over a particular interval of time must be equal to the mass of fluids which have flowed out. This principle may be rather trivial for single phase flow, but becomes more critical for multiphase flow, where different fluids may have different densities, viscosities, and permeabilities. What goes in must be balanced by what comes out, and for a complex set of flow equations the zero-sum constraint for each grid cell is essential.

Fluid flow in porous media is represented by Darcy's Law (Sect. 4.3.2) which relates the fluid velocity,  $u$ , to the pressure gradient and two terms representing the rock and the fluid:

$$u = -\underline{k}/\mu \cdot \nabla(P + \rho gz) \quad (4.1)$$

The pressure term comprises an imposed pressure gradient,  $\nabla(P)$ , and a pressure gradient due to gravity,  $\nabla(\rho gz)$ . In Cartesian coordinates the gradient of pressure,  $\nabla P$ , is resolved as:

$$\nabla P = \frac{dP}{dx} + \frac{dP}{dy} + \frac{dP}{dz} \quad (4.2)$$

The rock (or the permeable medium) is represented by the permeability tensor,  $\underline{k}$ , and fluid by the viscosity,  $\mu$ .

When two or more fluid phases are flowing, it becomes necessary to introduce terms for the density, viscosity and permeability of each phase and for the interfacial forces (both fluid-fluid and fluid-solid). For two-phase immiscible flow (e.g. oil and water), the two-phase Darcy equation and the capillary pressure equation are used:

$$u_o = -\underline{k}k_{ro}/\mu_o \cdot \nabla(P_o + \rho_o gz) \quad (4.3)$$

$$u_w = -\underline{k}k_{rw}/\mu_w \cdot \nabla(P_w + \rho_w gz) \quad (4.4)$$

$$P_c = P_o - P_w \quad (4.5)$$

where:

$o$  and  $w$  refer to the oil and water phases

$k_{rw}$  and  $k_{ro}$  are the relative permeabilities of each phase

$\mu$  and  $\rho$  are fluid viscosity and density

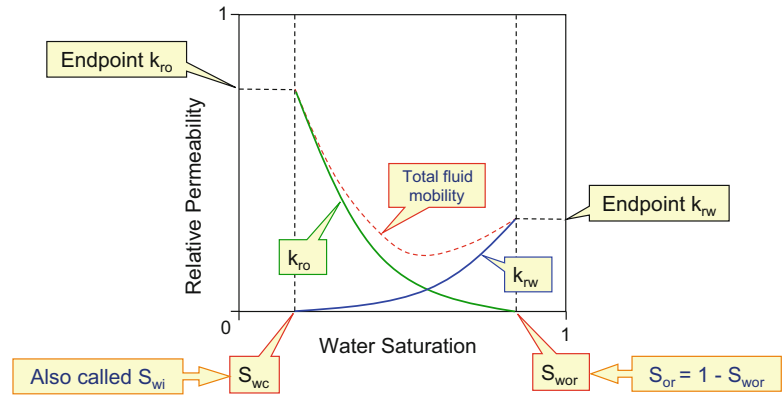
$P_c$  is the capillary pressure

$\nabla P_o$  is the gradient of pressure for the oil phase

The same form of equations can be applied to any pair of fluids, such as CO<sub>2</sub>-water, or air-water or methane-water. We can also generalize the fluid pairs into the non-wetting phase and the wetting phase. We will also limit our discussion here to the case of immiscible fluid pairs, e.g. oil-water or CO<sub>2</sub>-water, where there is a capillary interface between the two fluids. Some fluid pairs, such as CO<sub>2</sub> and oil can be miscible at certain ranges of pressure and temperature (Gozalpour et al. 2005), in which case different mixing, relative permeability and scaling laws apply (see Sorbie et al. 1994).

This set of equations for two-phase immiscible flow is non-linear as the  $k_{rw}$ ,  $k_{ro}$  and  $P_c$  terms are all functions of phase saturation,  $S_w$ , which is itself controlled by the flow rates. Thus, in order to solve these equations for a given set of initial and boundary conditions, numerical codes (reservoir simulators) are used, in which saturation-dependent functions for  $k_{rw}$ ,  $k_{ro}$  and  $P_c$  are given as input, and an iterative numerical recipe is used to estimate saturation and pressure. Figure 4.5 shows a typical set of oil-water relative permeability curves with the endpoint terminology.

**Fig. 4.5** Example oil-water relative permeability functions



Note that the total fluid mobility is  $<1$  (mobility is the permeability/viscosity ratio for the flowing phase). That is, the permeability of a rock containing more than one phase is significantly lower than a rock with only one phase. Clearly the fluid viscosity is a key factor but the fluid-fluid interactions also play a role. The functions are drawn between ‘endpoints,’ which as well as being a mathematical convenience are also based on physical phenomena – they represent the point at which the flow rate of one phase becomes insignificant. However, the endpoint values themselves are not physically fixed. For example, there exists a measurable irreducible water saturation, but its precise value depends on many things (e.g. oil phase pressure or temperature). Many of the problems and errors in upscaling arise from poor treatment or understanding of these endpoints.

The most common functions used for relative permeability are the Corey exponent functions:

$$k_{ro} = A(1 - S_{wn})^x \quad (4.6)$$

$$k_{rw} = B(S_{wn})^y \quad (4.7)$$

where:

$S_{wn}$  is the normalized saturation:

$$S_{wn} = (S_w - S_{wc}) / (S_{wor} - S_{wc}) \quad (4.8)$$

Typical values for a water-wet light oil might be:

$$\begin{aligned} k_{ro} &= 0.85(1 - S_{wn})^3 \text{ and } k_{rw} \\ &= 0.3(S_{wn})^3 \end{aligned} \quad (4.9)$$

A similar set of functions can be used to describe a gas-oil system (Fig. 4.6), where the functions are bounded by the critical gas saturation,  $S_{gc}$ , and the maximum gas saturation,  $S_{gmax}$ . However, gas-oil relative permeability curves tend to have less curvature (lower Corey exponents) and sometimes straight-line functions are assumed, implying perfect mixing or a fully-miscible gas-oil system. Relative permeability functions for  $\text{CO}_2$ -brine systems are discussed in Chap. 7, and use the same conceptual framework.

These functions describe the flows and pressures for multi-phase flow. The third equation required to completely define a two-phase flow system is the capillary pressure equation. For the general case (any fluid pair):

$$P_c = P_{\text{non-wetting phase}} - P_{\text{wetting-phase}} \quad [P_c = f(S)] \quad (4.10)$$

Capillary pressure,  $P_c$ , is a function of phase saturation, and must be defined by a set of functions. The capillary pressure curve is a summary of fluid-fluid interactions, and for any element of rock gives the average phase pressures for all the fluid-fluid contacts within the porous medium at a given saturation. For an individual pore,  $P_c$  can be related to measurable geometries (curvatures) and forces (interfacial tension), and defined theoretically – but for a real porous



**Fig. 4.6** Example gas-oil relative permeability functions

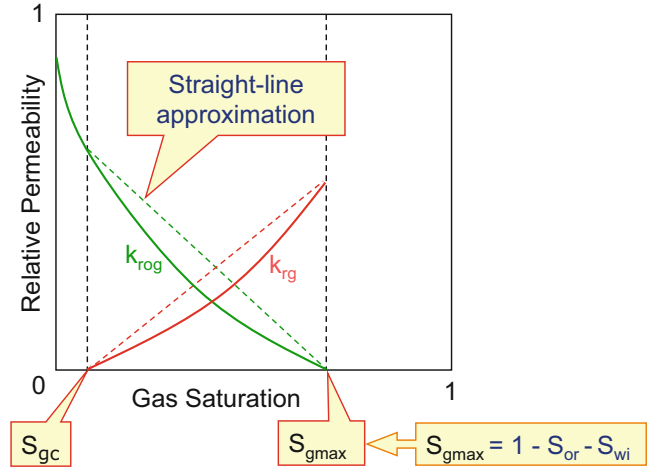
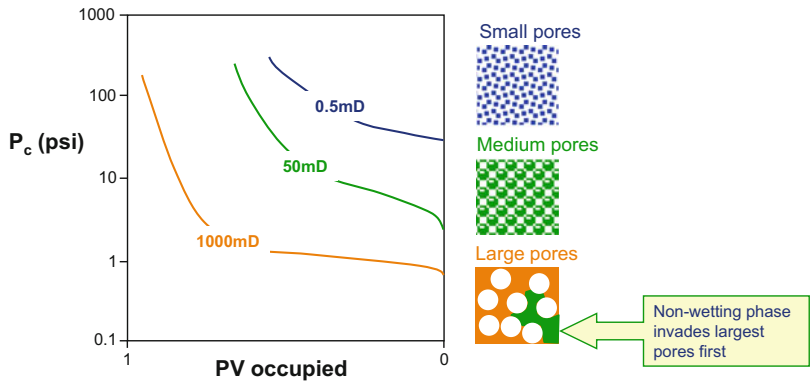


**Fig. 4.7** Example capillary pressure functions: capillary drainage curves based on mercury intrusion experiments measuring the non-wetting phase pressure required to invade a certain pore volume (PV)



medium it is an average property. Figure 4.7 shows some example measured  $P_c$  curves, based on mercury intrusion experiments (Neasham 1977).

The slope of the  $P_c$  curve is related to the pore size distribution. More uniform pore-size distributions have a fairly flat function (as for the 1000 mD curve in Fig. 4.7), whereas highly variable pore size distributions have a gradually rising function (as with the 50 mD curve in Fig. 4.7). The capillary entry pressure is a function of the largest accessible pore. Different  $P_c$  curves are followed for drainage (oil invasion) and imbibition (waterflood) processes. Similarly, the relative permeability curves and endpoints will be slightly different for the drainage and imbibition cycles. However, when upscaling we are typically interested in only one of these cycles

(either drainage or imbibition) such that one set of curves is often sufficient.

We summarise our introduction by noting that the complexities of multi-phase flow boil down to a set of rules governing how two or more phases interact in the porous medium. Figure 4.8 shows an example micro-model (an artificial etched-glass pore space network) in which fluid phase distributions can be visualised. Even for this comparatively simple pore space, the number and nature of the fluid-fluid and fluid-solid interfaces is bewildering. What determines whether gas, oil or water will invade the next available pore as the pressure in one phase changes?

One response – the modelling approach – is that good answers to this problem are found in mathematical modelling of pore networks (e.g. McDougall and Sorbie 1995; Blunt 1997;

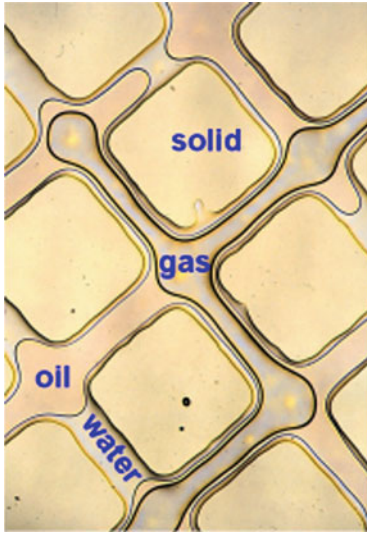


**Fig. 4.8** Example micro-model, where fluid distributions are visualised within an artificial laboratory pore-space. (Equinor archive image of micromodel experiment conducted at Heriot Watt University)

Øren and Bakke 2003; Behbahani and Blunt 2005). Another response – the laboratory approach – is that you need to measure the multi-phase flow behaviour in real rock samples at true reservoir conditions (pressures and temperatures). In practice, you need both measurements and modelling to obtain a good appreciation of the ‘rules’ governing multiphase flow. Our concern here is to understand how to handle and upscale these functions within the reservoir model.

#### 4.2.2 Two-Phase Steady-State Upscaling Methods

Multiphase flow upscaling involves the process of calculating the large-scale multiphase flows given a known distribution of the small-scale petrophysical properties and flow functions. There are many methods for doing this, but it is useful to differentiate two:

1. Dynamic methods
2. Steady-state methods

Fuller discussions of these methods are found in, for example, Barker and Thibeau (1997), Ekran and Aasen (2000) and Pickup et al. (2005).

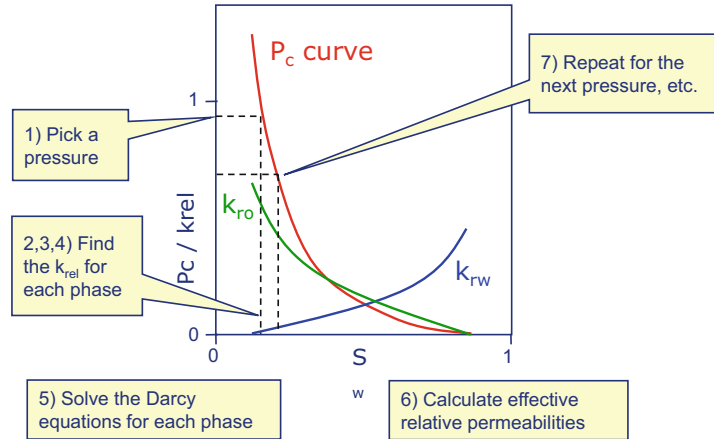
Reservoir simulators generally perform *dynamic* multi-phase flow simulations – that is, the pressures and saturations are allowed to vary with position and time in the simulation grid. The Kyte and Berry (1975) upscaling method is the most well-known dynamic two-phase upscaling method, but there have been many alternatives proposed, such as Stone’s (1991) method and Todd and Longstaff (1972) for miscible gas. The strength of the dynamic methods is that they attempt to capture the ‘true’ flow behaviour for a given set of boundary conditions. Their principle weaknesses are that they can be difficult and time-consuming to calculate and can be plagued by numerical errors.

In contrast, the steady-state methods are easier to calculate and understand and represent ideal multi-phase flow behaviour. There are three steady-state end-member assumptions:

- *Viscous limit* (VL): The assumption that the flow is steady-state at a given, constant fractional flow. Capillary pressure is assumed to be zero.
- *Capillary equilibrium* (CE): The assumption that the saturations are completely controlled by capillary pressure. Applied pressure gradients are assumed to be zero or negligible.
- *Gravity-Capillary equilibrium* (GCE): Similar to CE, except that in addition the saturations are also controlled by the effect of gravity on the fluid density difference.

Note that GCE is similar to the vertical equilibrium (VE) assumption also applied in reservoir simulation (Coats et al. 1971), except that VE assumes negligible capillary pressure and that gravity forces are much stronger than the lateral viscous forces. The VE upscaling approach has been successfully applied and adapted to CO<sub>2</sub> storage simulation by several groups (e.g. Nordbotten and Celia, 2011; Nilsen et al. 2011). However, in our discussion of geologically-based flow upscaling we will focus

**Fig. 4.9** Illustration of the capillary equilibrium steady-state upscaling method



on the VE and CE end-member cases as these capture the range of behaviours we might expect in multiphase flow modelling.

The viscous limit assumption is similar to a steady-state core flood experiment which is sometimes used in core analysis of multi-phase flow (referred to as special core analysis, or SCAL). Here, a known and constant fraction of the wetting and non-wetting phases is injected into the sample (let us say 20% oil and 80% water) and the permeability for each phase is calculated from the pressure drop and flow rate for that phase. The procedure is then repeated for a different fractional flow, and so on. It is assumed that capillary pressure and gravity have no effect. The method can be assumed to apply for a Darcy-flow-dominated two-phase flow system. The method is also considered to be a valid approximation at larger length scales, where capillary forces can generally be neglected, e.g. for model grid cell sizes greater than about 1 m vertically.

For the capillary equilibrium steady state assumption it is the Darcy flow effects that are neglected and all fluxes are deemed to be controlled by the capillary pressure curve. For a given pressure, the saturation is known from the  $P_c$  curve and the local phase permeability is then determined from the relative permeability curves. The calculation is then repeated for each chosen decrement of pressure until the saturation range is covered (Fig. 4.9). The method is considered to be valid at smaller length scales, where capillary forces are likely to dominate (e.g. at length scales



**Fig. 4.10** SEM image of laminae in an aeolian sandstone. (Image courtesy of British Gas)

less than about 0.2 m). There is also a rate-dependence for viscous and capillary forces – higher flow rates favour viscous forces while lower flow rates favour capillary forces. Note that layering in sedimentary rock media is often at the mm to cm scale (Fig. 4.10), and therefore capillary forces are likely to be important at this length scale.

The gravity-capillary equilibrium (GCE) method uses the same principle as the CE method except that a vertical pressure gradient is also applied, resulting in a vertical trend in the saturation at any chosen pressure reference (see Yortsos

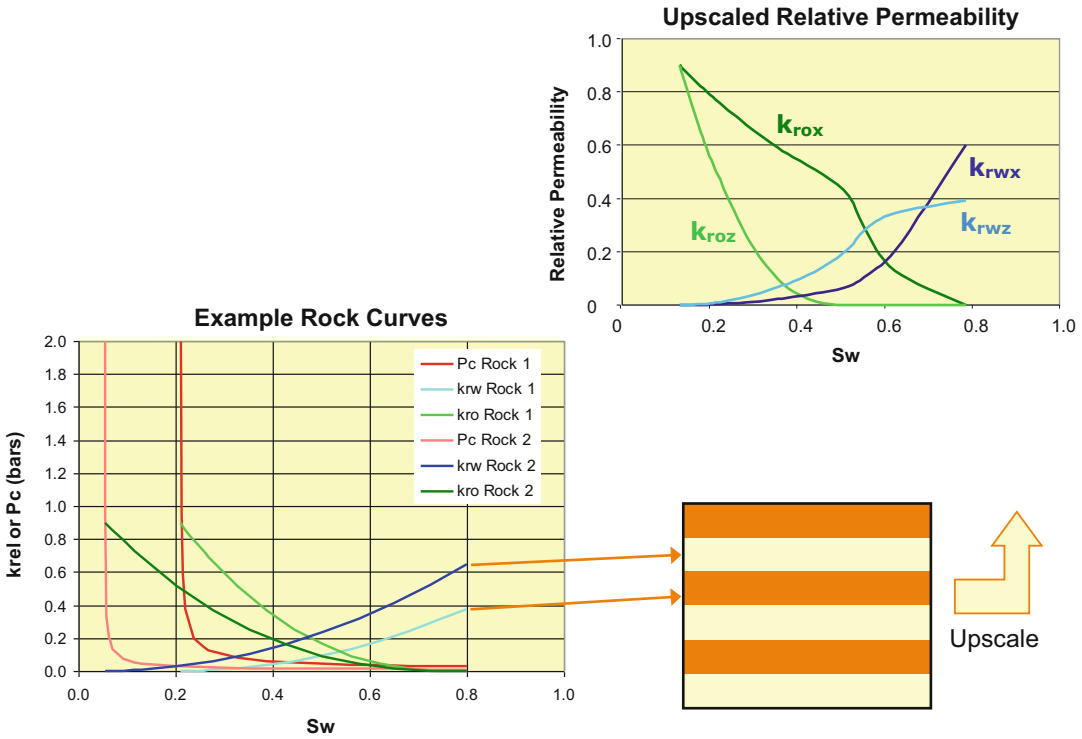


**Fig. 4.11** Capillary equilibrium steady-state upscaling method applied to a simple layered model

(1995) for a full discussion of vertical equilibrium theory and methods). The GCE solution should tend towards the CE solution as the length scale becomes increasingly small. The GCE assumption is also the basis for the initial saturation distribution in an oil or gas field (see Sect. 3.7.2) or the final saturation distribution in a CO<sub>2</sub> storage unit.

All three steady-state upscaling methods involve a series of independent single-phase flow calculations and therefore can employ a standard single-phase pressure solver algorithm. The methods can therefore be rapidly executed on standard computers.

The capillary equilibrium method can be easily calculated for a simple case, as illustrated in Fig. 4.11 by an example set of input functions for a regular layered model. Upscaled relative permeability curves for this simple case can be calculated analytically using a spreadsheet or calculator. The method uses the following steps (refer to Fig. 4.9):

1. Chose a value for pressure,  $P_{c1}$ .
2. Find the corresponding saturation value,  $S_{w1}$ .
3. Determine the relative permeability for oil and water for each rock type,  $k_{ro1}$ ,  $k_{rw1}$ ,  $k_{ro2}$ ,  $k_{rw2}$ .
4. Find the phase permeabilities, e.g.  $k_{o1} = k_1 * k_{ro1}$ .
5. Calculate the upscaled permeability for each direction and for each phase using the arithmetic and harmonic averages.
6. Invert back to upscaled relative permeability, e.g.  $k_{ro1} = k_{o1} / k_{upscaled}$  (once again the arithmetic and harmonic averages are used to obtain the upscaled absolute permeability).
7. Repeat for next value pressure,  $P_{c2}$ .

Note that the upscaled curves are highly anisotropic, and in fact sometimes lie outside the range of the input curves. This is because of the effects of capillary forces – specifically *capillary trapping* when flowing across layers. Capillary forces result in preferential imbibition of water (the wetting phase) into the lower permeability layers, making flow of oil (the non-wetting phase)

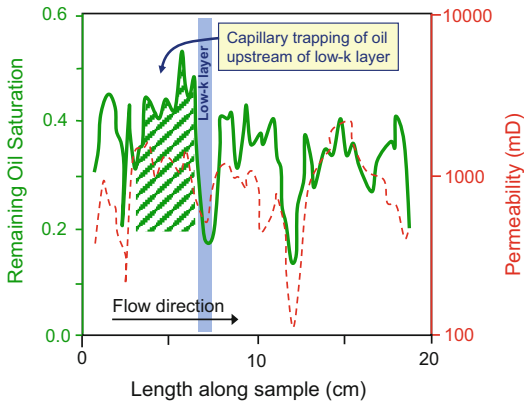


**Fig. 4.12** Summary of a waterflood experiment across a laminated water-wet rock sample (redrawn from Huang et al. 1995, ©1995, Society of Petroleum Engineers Inc., reproduced with permission of SPE. Further reproduction prohibited without permission)

into these low permeability layers even more difficult.

These somewhat non-intuitive effects of capillary pressure in laminated rocks can be demonstrated experimentally (Fig. 4.12). In the case of two-phase flow across layers in a water-wet laminated rock – a cross-bedded aeolian sandstone (Fig. 4.10) – oil becomes trapped in the high permeability layers upstream of low permeability layers due to water imbibition into the lower permeability layers (Huang et al. 1995).

The chosen flow rate for this experiment was at typical reservoir waterflood rate (around 0.1 m/day). This trapped oil can be mobilised either by reducing the capillary pressure (e.g. by modifying the interfacial tension by use of surfactant

chemicals) or by increasing the flow rate, and thereby the viscous forces. Alternatively, a modified flow strategy favouring flow along the rock layers (parallel to bedding) would result in less capillary trapping and a more efficient waterflood. In the more general case, where the rock has variable wettability the effects of capillary/viscous interactions become more complex (e.g. McDougall and Sorbie 1995; Huang et al. 1996; Behbahani and Blunt 2005).

**Exercise 4.1**

Relative permeability upscaling for a simple layered model.

The simple repetitive layered model shown in Fig. 4.11 can be used to illustrate single and multi-phase permeability upscaling using the ‘back of the envelope’ maths. We assume the two layers are regular and of equal thickness. Rock type 1 has a permeability of 100 md and rock type 2 has a permeability of 1000 md.

- (a) Calculate the upscaled horizontal and vertical single-phase permeability using averaging.
- (b) Calculate selected values for the upscaled two-phase relative permeability curves, assuming steady-state capillary equilibrium conditions. Use the flow functions shown in Fig. 4.11, as tabulated below, with water saturation,  $S_w$ ; relative permeability to water,  $k_{rw}$ ; relative permeability to oil,  $k_{row}$ ; capillary pressure,  $P_c$  (bars). Choose  $P_c$  values of 0.05 and 0.3 (shown in bold).

| Table for rock type 1 (100 mD) |               |              |            | Table for rock type 2 (1000 mD) |                 |              |             |
|--------------------------------|---------------|--------------|------------|---------------------------------|-----------------|--------------|-------------|
| $S_w$                          | $k_{rw}$      | $k_{row}$    | $P_c$      | $S_w$                           | $k_{rw}$        | $k_{row}$    | $P_c$       |
| 0.2092                         | 0.0           | 0.9          | 10.0       | 0.05432                         | 0.0             | 0.9          | 10.0        |
| 0.209791                       | 0.0000004     | 0.897752     | 2.744926   | 0.055066                        | 0.0             | 0.897752     | 0.976926    |
| 0.212154                       | 0.000009      | 0.888792     | 0.938248   | 0.058048                        | 0.000016        | 0.888792     | 0.333925    |
| 0.215108                       | 0.000038      | 0.877668     | 0.590923   | <b>0.059</b>                    | <b>0.000023</b> | <b>0.887</b> | <b>0.3</b>  |
| 0.221016                       | 0.000151      | 0.855673     | 0.372172   | 0.061777                        | 0.000065        | 0.877668     | 0.210311    |
| <b>0.226</b>                   | <b>0.0003</b> | <b>0.839</b> | <b>0.3</b> | 0.069234                        | 0.000259        | 0.855673     | 0.132457    |
| 0.238740                       | 0.000943      | 0.791683     | 0.201984   | 0.091604                        | 0.001618        | 0.791683     | 0.071887    |
| 0.256464                       | 0.002413      | 0.730655     | 0.147628   | 0.113974                        | 0.004141        | 0.730655     | 0.052541    |
| 0.26828                        | 0.003771      | 0.691590     | 0.127213   | <b>0.119</b>                    | <b>0.005</b>    | <b>0.718</b> | <b>0.05</b> |
| 0.32736                        | 0.015084      | 0.515190     | 0.080120   | 0.128888                        | 0.006471        | 0.691590     | 0.045275    |
| 0.38644                        | 0.033939      | 0.368967     | 0.061135   | 0.203456                        | 0.025884        | 0.515190     | 0.028515    |
| 0.44552                        | 0.060336      | 0.250969     | 0.050461   | 0.278024                        | 0.058239        | 0.368967     | 0.021758    |

(continued)

| Table for rock type 1 (100 mD) |              |              |             | Table for rock type 2 (1000 mD) |          |          |          |
|--------------------------------|--------------|--------------|-------------|---------------------------------|----------|----------|----------|
| Sw                             | krw          | krow         | Pc          | Sw                              | krw      | krow     | Pc       |
| <b>0.449</b>                   | <b>0.062</b> | <b>0.245</b> | <b>0.05</b> | 0.352592                        | 0.103536 | 0.250969 | 0.017959 |
| 0.5046                         | 0.094275     | 0.159099     | 0.043483    | 0.42716                         | 0.161775 | 0.159099 | 0.015476 |
| 0.56368                        | 0.135756     | 0.091074     | 0.038504    | 0.501728                        | 0.232956 | 0.091074 | 0.013704 |
| 0.62276                        | 0.184779     | 0.044366     | 0.034742    | 0.576296                        | 0.317079 | 0.044366 | 0.012365 |
| 0.68184                        | 0.241344     | 0.016099     | 0.031781    | 0.650864                        | 0.414144 | 0.016100 | 0.011311 |
| 0.74092                        | 0.305451     | 0.002846     | 0.029380    | 0.725432                        | 0.524151 | 0.002846 | 0.010456 |
| 0.8                            | 0.3771       | 0.000000     | 0.027386    | 0.8                             | 0.6471   | 0.000000 | 0.009747 |

\*\*\*

### 4.2.3 Heterogeneity and Fluid Forces

It is important to relate these multi-phase fluid flow processes to the heterogeneity being modelled. This is a fairly complex issue and fundamental to what reservoir model design is all about. As a way in to this topic we use the *balance of forces* concept to give us a framework for understanding which scales most affect a particular flow process. For example, we know that capillary forces are likely to be important for rocks with strong permeability variations at the small scale (less than 20 cm scale is a good rule of thumb).

Figure 4.13 shows a simple sketch of the end-members of the fluid force system. We have three end members: gravity-, viscous- and capillary-dominated. Reality will lie somewhere within the triangle, but appreciation of the end-member systems is useful to understand the expected flow-heterogeneity interactions. Note, that for the same rock system the flow behaviour will be completely different for a gravity-dominated, viscous-dominated or capillary-dominated flow regime. The least intuitive is the capillary-dominated case where water (for a water-wet system) imbibes preferentially into the lower permeability layers.

To treat this issue more formally, we use scaling group theory (Rapoport 1955; Li and Lake 1995; Li et al. 1996; Zhou et al. 1997) to understand the balance of forces. The viscous/capillary ratio and the gravity/capillary ratio are two of a number of dimensionless scaling group ratios that can be determined to represent the balance of

fluid forces. For example, for an oil-water system we can define the following force ratios:

$$\frac{\text{Viscous}}{\text{Capillary}} = \frac{u_x \Delta x \mu_o}{k_x (dP_c/dS)} \quad (4.11)$$

$$\frac{\text{Gravity}}{\text{Capillary}} = \frac{\Delta \rho g \Delta z}{(dP_c/dS)} \quad (4.12)$$

where:

$\Delta x$ ,  $\Delta z$  are system dimensions

$u_x$  is fluid velocity

$\mu_o$  is the oil viscosity

$k_x$  is the permeability in the x direction

$(dP_c/dS)$  is the slope of the capillary pressure function

$\Delta \rho$  is the fluid density difference and  $g$  is the constant due to gravity

The viscous/capillary ratio is essentially a ratio of Darcy's law with a capillary pressure gradient term, while the gravity/capillary ratio is the buoyancy term against the capillary pressure gradient.  $\Delta x$  and  $\Delta z$  represent the physical length scales – essentially the size of the model in the x and z directions. There are several different forms of derivation of these ratios depending on the physical assumptions and the mathematical approach, but the form given above should allow the practitioner to gain an appreciation of the factors involved. It is important that a consistent set of units are used to ensure the ratios remain dimensionless.

For example, a calculation to determine when capillary/heterogeneity interactions are important can be made by studying the ratio of capillary to viscous forces. Figure 4.14 shows a reference well pair assuming 1 km well spacing and a 150 psi pressure drawdown at the producing

**Fig. 4.13** The fluid forces triangle with sketches to illustrate how a multiphase flow system would behave with (blue) water displacing oil a layered rock (yellow = high permeability layers)

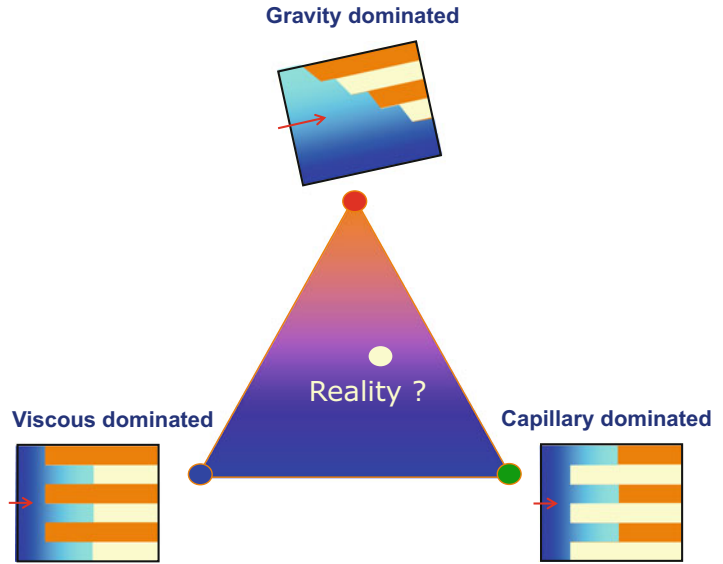
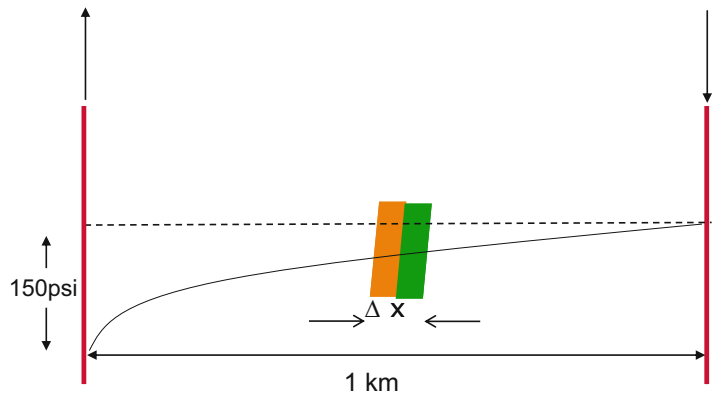


**Fig. 4.14** Sketch of pressure drawdown between an injection and production well pair for water-flooding an oil reservoir



well. We are interested in the balance of forces and a rock unit within the reservoir, represented by alternating permeability layers with a spacing of  $\Delta x$ . Figure 4.15 shows the result of the analysis of the viscous/capillary ratio for different layer contrasts and heterogeneity length-scales (Ringrose et al. 1996).

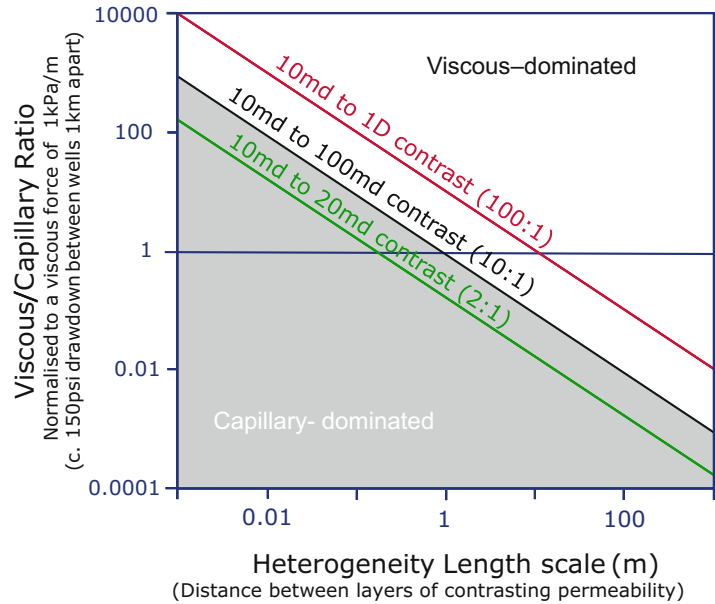
If the layering in a reservoir occurs at the  $>10$  m scale then viscous forces tend to dominate (or the Viscous/Capillary ratio must be very low for capillary forces to be significant at this scale). However, if the layers are in the mm-to-cm range then capillary forces are much more likely to be

important (or the Viscous/Capillary ratio must be very high to override capillary effects). Note, however, that the pressure gradients will vary as a function of spatial position and time and so in fact the Viscous/Capillary ratio will vary – viscous forces will be high close to the wells and lower in the inter-well region.

An important and related concept is the capillary number, most commonly defined as:

$$C_a = \frac{\mu q}{\gamma} \quad (4.13)$$

**Fig. 4.15** Example calculation of the viscous/capillary ratio for a layered system as a function of length scale, for selected permeability contrasts. (Redrawn from Ringrose et al. 1996, ©1996, Society of Petroleum Engineers Inc., reproduced with permission of SPE. Further reproduction prohibited without permission)



where:

$\mu$  is the viscosity

$q$  is the flow rate

$\gamma$  is the interfacial tension

This is a simpler ratio of the viscous force to the surface tension at the fluid-fluid interface. Capillary numbers around  $10^{-4}$  or lower are generally deemed to be capillary-dominated.

### 4.3 Multi-scale Reservoir Modelling Concepts

#### 4.3.1 Geology and Scale

The importance of multiple scales of heterogeneity for petroleum reservoir engineering has been recognised for some time. Haldorsen and Lake (1984) and Haldorsen (1986) proposed four conceptual scales associated with averaging properties in porous rock media:

- Microscopic (pore-scale);
- Macroscopic (representative elementary volume above the pore scale);
- Megascopic (the scale of geological heterogeneity and or reservoir grid blocks);
- Gigascopic (the regional or total reservoir scale).

Weber (1986) showed how common sedimentary structures including lamination, clay drapes and cross-bedding affect reservoir flow properties and Weber and van Geuns (1990) proposed a framework for constructing geologically-based reservoir models for different depositional environments. Corbett et al. (1992) and Ringrose et al. (1993) argued that multi-scale modelling of water-oil flows in sandstones should be based on a hierarchy of sedimentary architectures, with smaller scale heterogeneities being especially important for capillary-dominated flow processes (see Sect. 2.3.2.2 for an introduction to hierarchy). Campbell (1967) established a basic hierarchy of sedimentary features related to fairly universal processes of deposition, namely lamina, laminasets, beds and bedsets. Miall (1985) showed how the range of sedimentary bedforms can be defined by a series of bounding surfaces from a first order surface bounding the laminaset to fourth (and higher) order surfaces bounding, for example, composite point-bars in fluvial systems.

Figure 4.16 illustrates the geological hierarchy for a heterolithic sandstone reservoir. Lamina-scale, lithofacies-scale and sequence-stratigraphic scale elements can be identified. In addition to the importance of correctly describing the sedimentary length scales, structural (Fig. 4.16d) and diagenetic processes act to modify the primary depositional fabric.



**Fig. 4.16** Field outcrop sketches illustrating multi-scale reservoir architecture; (a) sandstone and siltstone lamina-sets from a weakly-bioturbated heterolithic sandstone; (b) sandy and muddy bed-sets in a tidal deltaic lithofacies; (c) prograding sedimentary sequences from a channelized tidal delta; (d) fault deformation fabric around a normal fault through an inter-bedded sandstone and silty clay sequence. (Redrawn from Ringrose et al. 2008, The Geological Society, London, Special Publications 309 © Geological Society of London [2008])

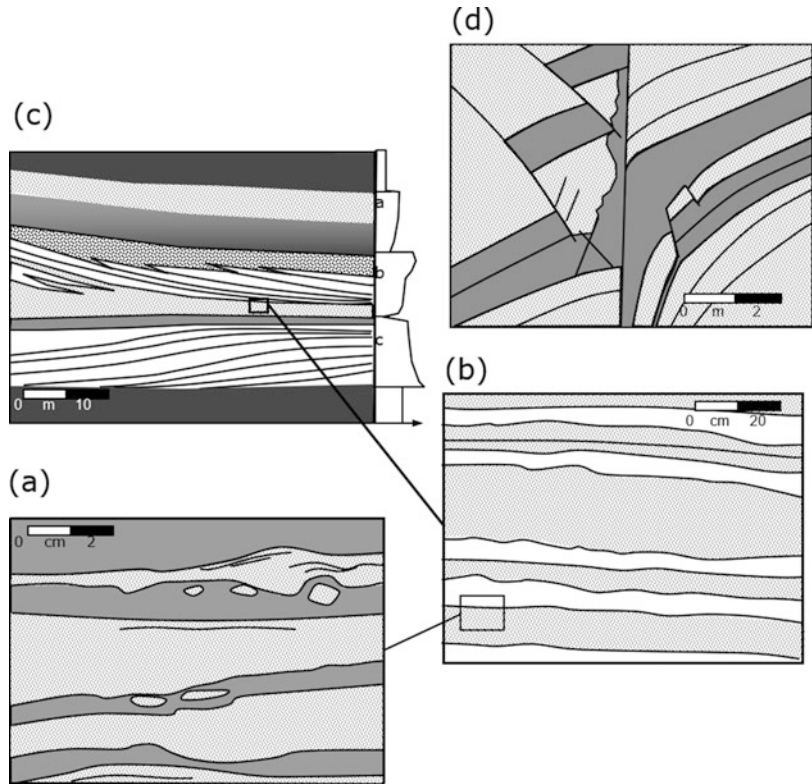
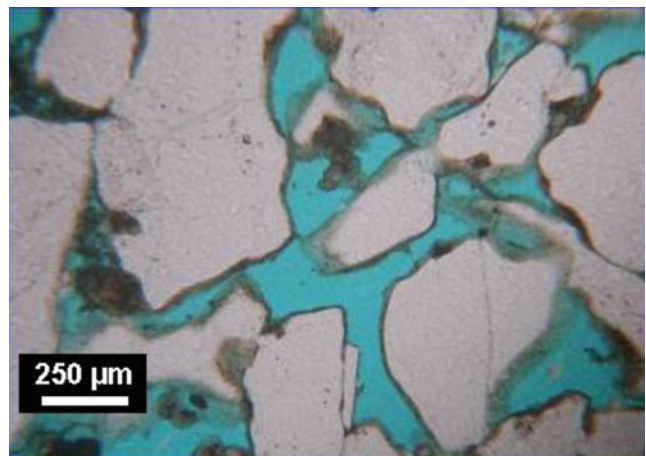


**Fig. 4.17** The pore scale – example thin section of pores in a sandstone reservoir. (Equinor image archive, © Equinor ASA, reproduced with permission)



At the most elemental level we are interested in the pore scale (Fig. 4.17) – the rock pores that contain fluids and determine the multi-phase flow behaviour. Numerical modelling at the pore scale has been widely used to better understand permeability, relative permeability and capillary pressure behaviour for representative pore

systems (e.g. Bryant and Blunt 1992; Bryant et al. 1993; McDougall and Sorbie 1995; Bakke and Øren 1997; Øren and Bakke 2003). Most laboratory analysis of rock samples is devoted to measuring pore-scale properties – resistivity, acoustic velocity, porosity, permeability, and relative permeability. Pore-scale modelling allows

these measured flow properties to be related to fundamental rock properties such as grain size, grain sorting and mineralogy. However, the application of pore-scale measurements and models in larger-scale reservoir models requires a framework for assigning pore-scale properties to the reservoir model elements described in Chap. 2. We do this by assigning flow properties to lamina-scale, lithofacies-scale or stratigraphic-scale models. This can be done quite loosely, with weak assumptions, or systematically within a multi-scale upscaling hierarchy.

Statistical methods for representing the spatial architecture of geological systems were covered in Chap. 2. What concerns us here is how we integrate geological models within a multi-scale hierarchy. This may require a re-evaluation of the scales of models needed to address different scale transitions.

Pixel-based modelling approaches (e.g. SGS, SIS) can be applied at pretty much any scale, whereas object-based modelling approaches will tend to have very clear associations with pre-defined length scales. In both cases the model grid resolution needs to be fine enough to

explicitly capture the heterogeneity being represented in the model. Process-based modelling methods (e.g. Rubin 1987; Wen et al. 1998; Ringrose et al. 2003) are particularly appropriate for capturing the effects of small-scale geological architecture within a multi-scale modelling framework.

In the following sections we look at some key questions the reservoir modelling practitioner will need to address in building multi-scale reservoir models:

1. How many scales to model and upscale?
2. Which scales to focus on?
3. How to best construct model grids?
4. Which heterogeneities matter most?

### 4.3.2 How Many Scales to Model and Upscale?

Despite the inherent complexities of sedimentary systems, dominant scales and scale transitions can be identified (Fig. 4.18). These dominant scales are based both on the nature of rock heterogeneity

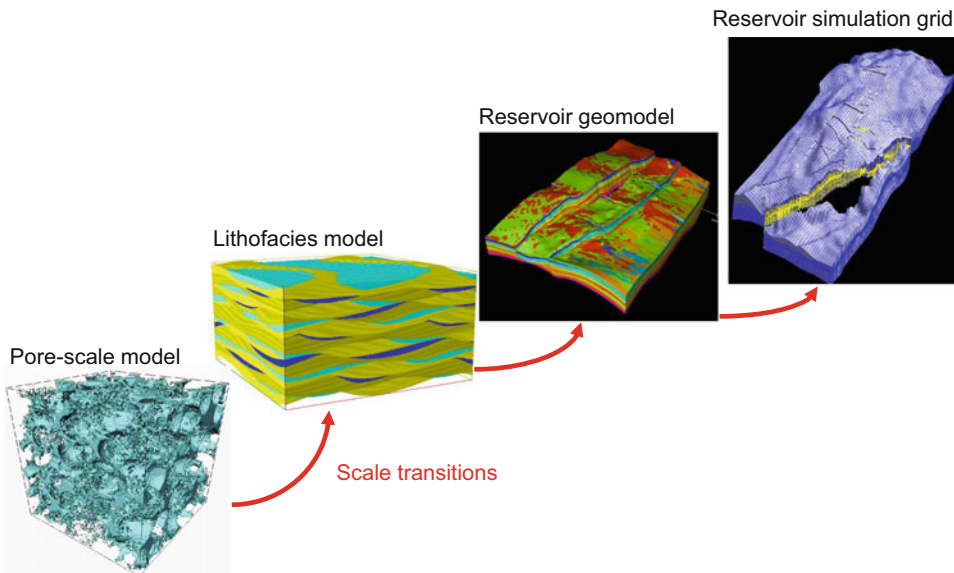


**Fig. 4.18** Examples of geologically-based reservoir simulation models at four scales: (a) model of pore space used as the basis for multi-phase pore network models (50 $\mu$ m cube); (b) model of lamina-sets within a tidal bedding facies (dimensions 0.05 m  $\times$  0.3 m  $\times$  0.3 m); (c) facies architecture model from a sector of the Heidrun field

showing patterns of tidal channel and bars (dimensions 80 m  $\times$  1 km  $\times$  3 km); (d) reservoir simulation grid for part of the Heidrun field illustrating grid cells displaced by faults in true structural position (dimensions 200 m  $\times$  3 km  $\times$  5 km). (Equinor image archives, © Equinor ASA, reproduced with permission)

and the principles which govern macroscopic flow properties. In this discussion, we assume four scales – pore, lithofacies, geomodel and reservoir. This gives us three scale transitions:

1. *Pore to lithofacies*, where a set of pore-scale models is applied to models of lithofacies architecture to infer representative or typical flow behaviour for that architectural element. The lithofacies is a basic concept in the description of sedimentary rocks and presumes an entity that can be recognised routinely. The lamina is the smallest sedimentary unit, at which fairly constant grain deposition processes can be associated with a macroscopic porous medium. The lithofacies comprises some recognisable association of laminae and lamina sets. In certain cases, where variation between laminae is small, pore-scale models could be applied directly to the lamina-set or bed-set scales.
2. *Lithofacies to geomodel*, where a larger-scale geological concept such as a sequence stratigraphic model, a structural model or a diagenetic model, postulates the spatial arrangement of lithofacies elements. Here, the geomodel is taken to mean a geologically-based model of the reservoir, typically resolved at the sequence or zone scale.
3. *Geomodel to reservoir simulator*. This stage may often only be required because of computational limitations, but may also be important to ensure good transformation of a geological model into 3D grid optimised for flow simulation, e.g. within the constraints of finite-difference multiphase flow simulation. This third step is routinely taken by practitioners, whereas steps 1 and 2 tend to be neglected.

Features related to structural deformation (faults, joints and folds) occur at a wide range of scales (Walsh et al. 1991; Yielding et al. 1992) and do not naturally fall into a step-wise upscaling scheme. Structural features are typically incorporated at the geomodel scale. However, effects of smaller scale fractures may also be incorporated as effective properties (as transmissibility multipliers) using upscaling

approaches. The incorporation of two-phase fault transmissibility into reservoir simulators is considered thoroughly by Manzocchi et al. (2002). Conductive fractures may also affect sandstone reservoirs, and are often the dominant factor in carbonate reservoirs. Approaches for multi-scale modelling of fractured reservoirs have also been developed (e.g. Bourbiaux et al. 2002) and will be developed further in Chap. 6.

The focus over the last few decades has been to include increasingly more detail into the geomodel, with only one upscaling step being explicitly performed. Full-field geomodels are typically in the size range of 1–10 million cells with horizontal cell sizes of 25–100 m and vertical cell sizes of order 1–10 m. There are also examples where a large number of grid cells are applied to sector or near-wellbore models reducing cell sizes to the dm-scale. Upscaling of the near-well region requires methods to specifically address radial flow geometry (e.g. Durlofsky et al. 2000).

More recent focus on explicit small-scale lithofacies modelling includes the use of million cell models with mm to cm size cells (e.g. Ringrose et al. 2003; Nordahl et al. 2005). Numerical pore-scale modelling employs a similar number of network nodes at the pore scale (e.g. Øren and Bakke 2003). Model resolution is always limited by the available computing power, and although continued efficiencies and memory gains are expected in the future, the use of available numerical discretisation at several scales within a hierarchy is preferred to efforts to apply the highest possible resolution at one of the scales (typically the geomodel). There is also an argument that advances in seismic imaging coupled with computing power will enable direct geological modelling at the seismic resolution scale. However, even when this is possible, seismic-based lithology prediction (using seismic inversion) will require smaller-scale modelling of the petrophysical properties within the seismically resolved element (see Chap. 2).

Upscaling methods impose further limitations on the value and utility of models within a multi-scale framework. In conventional upscaling – from a geological model to a reservoir simulation

grid – there are various approaches used. These cover a range which can be classed in terms of the degree of simplification/complexity:

1. *Averaging of well data directly into the flow simulation grid.* This approach essentially ignores explicit upscaling and neglects all aspects of smaller scale structure and flows. The approach is fast and simple and may be useful for quick assessment of expected reservoir flows and mass balance. It may also be adequate for very homogeneous and highly permeable rock sequences.
2. *Single-phase upscaling only in  $\Delta z$ .* This commonly-applied approach assumes a simulation grid designed with the same  $\Delta x$  and  $\Delta y$  as the reservoir model grid. The approach is often used where complex structural architecture provides very tight constraints to the design of the flow modelling grid. Upscaling involves averaging methods but ensures a degree of representation of thin layers or baffles/barriers. Also, where seismic data gives a good basis for the geological model in the horizontal dimensions, vertical upscaling of fine-scale layering to the reservoir simulator scale is typically required.
3. *Single-phase upscaling in  $\Delta x$   $\Delta y$  and  $\Delta z$ .* With this approach, multi-scale effective flow properties (permeability and porosity) are explicitly estimated and using widely available upscaling tools (diagonal tensor or full-tensor permeability upscaling methods). Multiphase flow effects are however neglected.
4. *Multi-phase upscaling in  $\Delta x$   $\Delta y$  and  $\Delta z$ .* This approach represents an attempt to calculate effective multiphase flow properties for larger scale models. The approach has been used rather too seldom due to demands of time and resources. However, the development of steady-state solutions to multiphase flow upscaling problems (Smith 1991; Ekran and Aasen 2000; Pickup and Stephen 2000) has led to wider use in field studies (e.g. Pickup et al. 2000; Kløv et al. 2003).

These four levels of upscaling complexity help define the number and dimensions of models required. The number of scales modelled is

typically related to the complexity and precision of the answer sought. Improved oil recovery (IOR) strategies and reservoir drainage optimisation studies are often the reason for starting a multi-scale approach. A minimum requirement for any reservoir model is that the assumptions used for smaller scale processes (pore scale, lithofacies scale) are explicitly stated. CO<sub>2</sub> storage modelling also generally requires a relatively high resolution grid, with VE upscaling often the main focus (Chap. 7).

There is a tendency to downplay the rather profound upscaling assumptions which are usually made. For example, a typical set of assumptions commonly used might be:

We assume that two special core analysis measurements represent all pore-scale physical flow processes and that all effects of geological architecture are adequately summarised by the arithmetic average of the well data.

Assumptions like these are rarely stated, although often implicitly assumed. Preferably, some form of explicit modelling at each scale should be performed using 3D multiphase upscaling methods. At a minimum, it is recommended to explicitly define pore-scale and geological-scale models, and to determine a rationale for associating the pore-scale with the geological scale, as in the example shown in Fig. 4.18.

### 4.3.3 Which Scales to Focus On? (The REV)

Geological systems present us with variability at nearly every scale (Fig. 4.19). To some extent they are fractal (Turcotte 1992), showing similar variability at all scales. However, geological systems are more accurately described as *multi-fractal* – showing some scale-independent similarities – but dominated by process-controlled scale-dependent features (Ringrose 1994). However you describe them, geological systems are complex, and we need an approach for simplifying that complexity and focussing on the important features and length scales.

The Representative Elementary Volume (REV) concept (Bear 1972) provides the essential

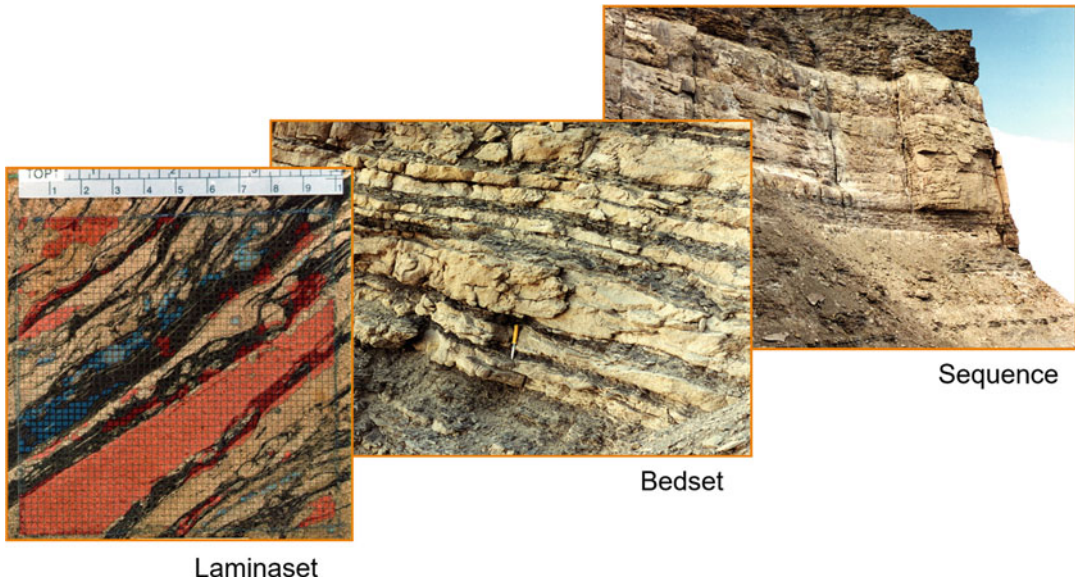
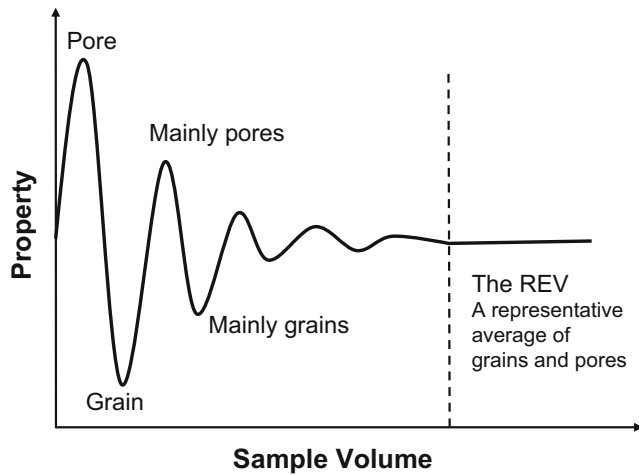


**Fig. 4.19** Multi-scale variability in a heterolithic (tidal delta) sandstone system: laminaset scale, core photograph with measured permeability (*red* indicates >1 Darcy); bedset scale, interbedded sandy and muddy bedsets (hammer for scale); sequence-stratigraphic scale, sand-dominated para-sequence between mudstone units. (Photos A. Martinius/Equinor © Equinor ASA, reproduced with permission)

**Fig. 4.20** The representative elementary volume (REV) concept (After Bear 1972)



framework for understanding measurement scales and geological variability. This concept is fundamental to the analysis of flow in permeable media – without a representative pore space we cannot measure a representative flow property nor treat the medium as a continuum in terms of the physics of flow. The original concept (Fig. 4.20) refers to the scale at which pore-scale fluctuations

in flow properties approach a constant value both as a function of changing scale and position in the porous medium, such that a statistically valid macroscopic flow property can be defined, as illustrated in Fig. 4.21.

The pore-scale REV is thus an essential assumption for all reservoir flow properties. However, rock media have several such scales where

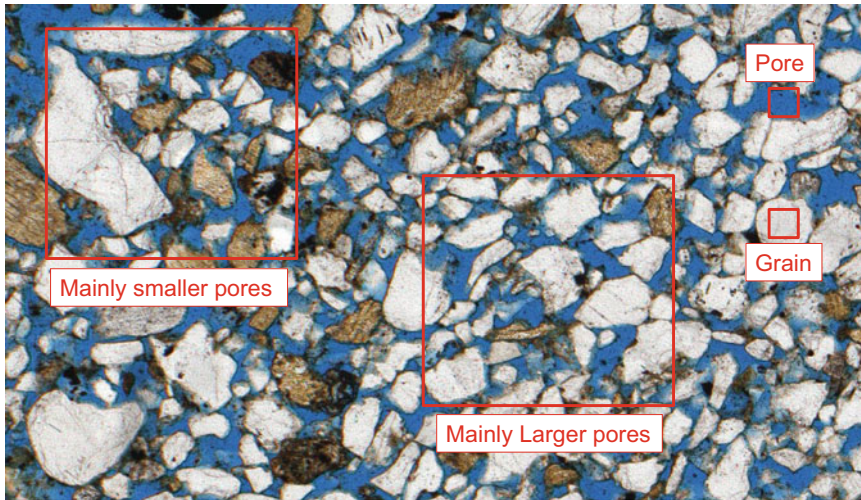
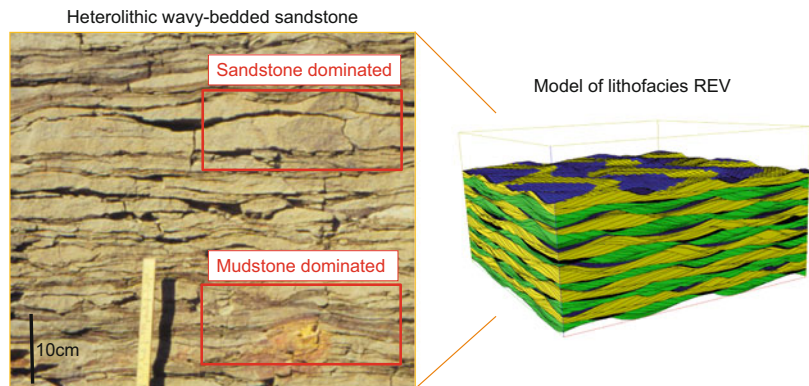


**Fig. 4.21** The pore-scale REV illustrated for an example thin section (the whole image is assumed to be the pore-scale REV). (Photo K. Nordahl/Equinor © Equinor ASA, reproduced with permission)

**Fig. 4.22** The lithofacies REV illustrated for an example heterolithic sandstone. (Photo K. Nordahl/Equinor © Equinor ASA, reproduced with permission)



smaller-scale variations approach a more constant value. It is therefore necessary to develop a multi-scale approach to the REV concept. It is not at first clear how many averaging length scales exist in a rock medium, or indeed if a REV can be established at the scale necessary for reservoir flow simulation. Despite the challenges, some degree of representativity of estimated flow properties is necessary for flow modelling within geological media, and a multi-scale REV framework is required.

Several workers (e.g. Jackson et al. 2003; Nordahl et al. 2005) have shown that an REV can be established at the lithofacies scale, e.g. at around a length-scale of 0.3 m for tidal heterolithic bedding (Fig. 4.22). In fact, the concept of representivity is inherent in the definition of a lithofacies, a recognisable and mappable

subdivision of a stratigraphic unit. The same logic follows at larger geological scales, such as the parasequence, the facies association or the sequence stratigraphic unit. Recognisable and continuous geological units are identified and defined by the sedimentologist, and the reservoir modeller then seeks to use these units to define the reservoir modelling elements (cf. Sect. 2.4).

As a general observation, core plug data is often not sampled at the REV scale and therefore tends to show a wide scatter in measured values, whereas wireline log data is often closer to a natural REV in the reservoir system. The true REV – if it can be established – is determined by the geology and not the measurement device. However, wire-line log data usually needs laboratory core data for calibration, which presents us

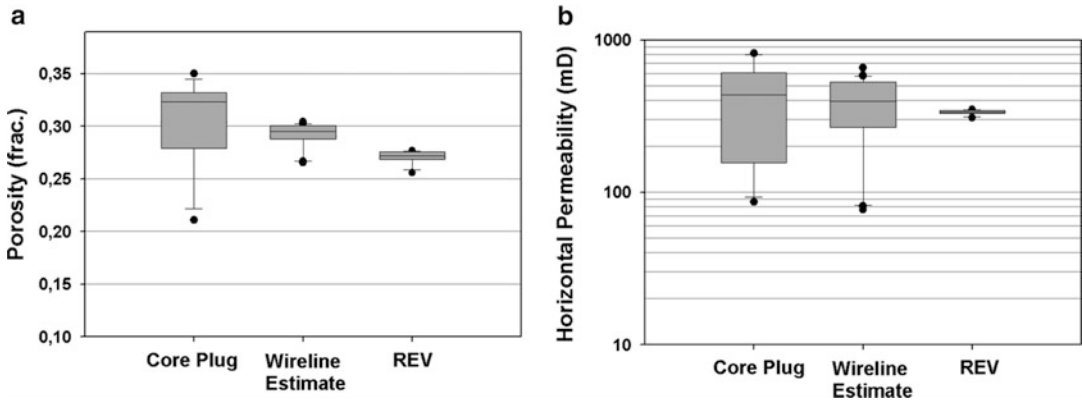


**Fig. 4.23** Assessment of the lithofacies REV, from Nordahl et al. (2005). Comparison of porosity (a) and horizontal permeability (b) estimated or measured from different sources and sample volumes. The lower and upper limits of the box indicate the 25th and the 75th percentile while the whiskers represent the 10th and the

90th percentile. The *solid line* is the median and the *black dots* are the outliers. The values at the REV are measured on the bedding model at a representative scale (with the distribution based on ten realisations). (Redrawn from Nordahl et al. 2005, *Petrol Geoscience*, v. 11 © Geological Society of London [2005])

with a dilemma: how should we integrate different scales of measurement?

Nordahl et al. (2005) performed a detailed assessment of the REV for porosity and permeability in a heterolithic sandstone reservoir unit (Fig. 4.23). This example illustrates how apparently conflicting datasets from core plug and wireline measurements can in fact be reconciled within the REV concept. The average and spread of the two datasets differ – the core plugs at a smaller scale record high degree of variability whereas the wireline data provides a more averaged result at a larger scale. Both sets of data can be integrated into a petrophysical model at the lithofacies REV. Nordahl and Ringrose (2008) extended this concept to propose a multi-scale REV framework (Fig. 4.24), whereby the natural averaging length scales of the geological system can be compared with the various measurement length scales.

Whatever the true nature of rock variability, it is a common mistake to assume that the averaging inherent in any measurement method (e.g. electrical logs or seismic wave inversion) relates directly to the averaging scales in the rock medium. For example, samples from core are often at an inappropriate scale for determining representativity (Corbett and Jensen 1992; Nordahl et al. 2005). At larger scales, inversion of reservoir properties from seismic can be

difficult or erroneous due to thin-bed tuning effects. Instead of assuming that any particular measurement gives us an appropriate average, it is much better to relate the measurement to the inherent averaging length scales in the rock system.

So how do we handle the REV concept in practice? The key issue is to find the length scale (determined by the rock architecture) where the measurement or model gives a representative average of the smaller-scale natural variations (captured artistically by the sculpture shown in Fig. 4.25). At the pore-scale this volume is typically around a few  $\text{mm}^3$ . For heterogeneous rock systems the REV is of the order of  $\text{m}^3$ . The challenge is to find the representative volumes for the reservoir system of interest in the subsurface.

#### 4.3.4 Handling Variance as a Function of Scale

Typical practice in reservoir studies is to assume that an average measured property for any rock unit is valid and that small-scale variability can be ignored. Put more simply, we often assume that the average log-property response for a well through a reservoir interval is the ‘right average.’ A statistician will know that an arbitrary sample is

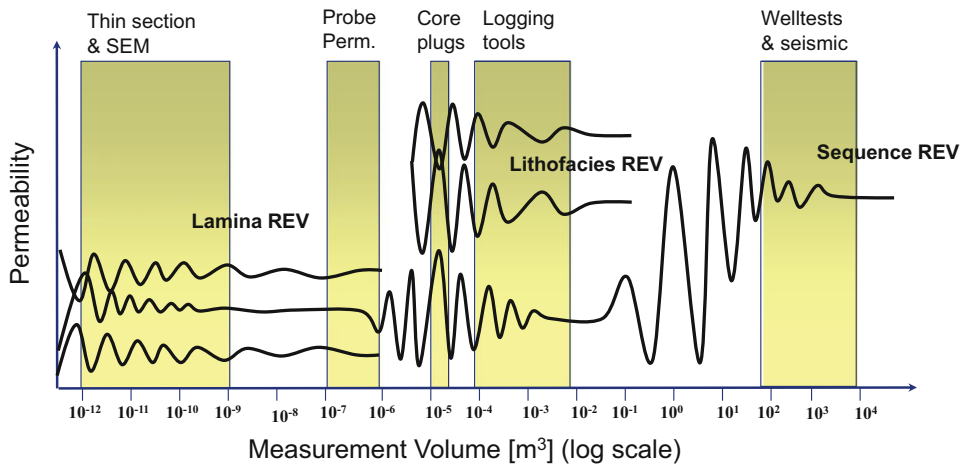


**Fig. 4.24** Sketch illustrating multiple scales of REV within a geological framework and the relationship to scales of measurement. (Adapted from Nordahl and Ringrose 2008)

**Fig. 4.25** Rock sculpture by Andrew Goldsworthy (NW Highlands of Scotland) elegantly capturing the concept of the REV



rarely an accurate representation of the truth. Valid statistical treatment of sample data is an extensive subject treated thoroughly in textbooks on statistics in the Earth Sciences – e.g. Size (1987), Davis (2003), Isaaks and Srivastava (1989) and Jensen et al. (2000).

The challenges involved in correctly inferring permeability from well data are illustrated here using an example well dataset (Fig. 4.26 and Table 4.2). This 30 m cored-well interval is from a tidal deltaic reservoir unit with heterolithic

lithofacies and moderate to highly variable petrophysical properties (the same well dataset is discussed in detail by Nordahl et al. 2005).

Table 4.2 compares the permeability statistics for different types of data from this well:

- High resolution probe permeameter data;
- Core plug data;
- A continuous wireline-log based estimator of permeability for the whole interval;
- A blocked permeability log as might be typically used in reservoir modelling.



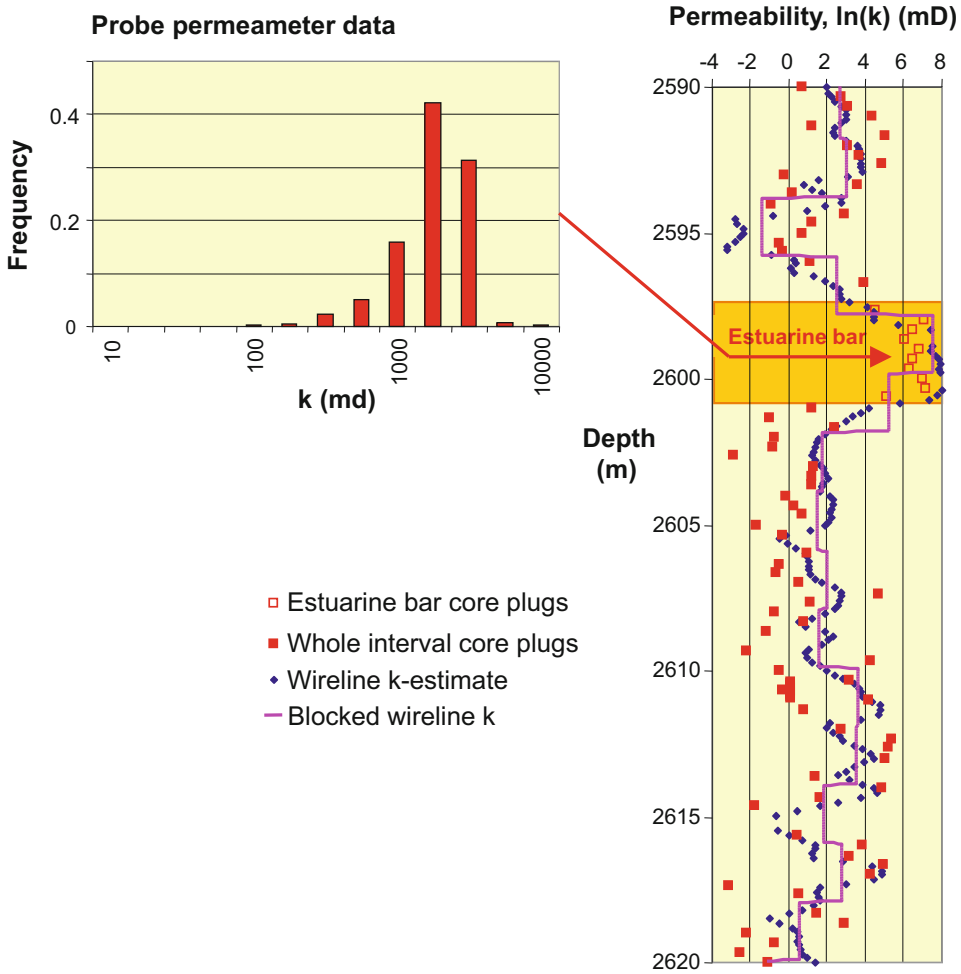


**Fig. 4.26** Example dataset from a tidal deltaic flow unit illustrating treatment of permeability data used in reservoir modelling. (Redrawn from Ringrose et al. 2008, The Geological Society, London, Special Publications 309 © Geological Society of London [2008])

**Table 4.2** Variance analysis of example permeability dataset

|                                      | Estuarine bar lithofacies    |                                       |                              | Whole interval (flow unit) |                         |                       |
|--------------------------------------|------------------------------|---------------------------------------|------------------------------|----------------------------|-------------------------|-----------------------|
|                                      | (a) Probe-k data             | (b) Probe data upscaled to plug scale | (c) Core plug data           | (d) Core plug data         | (e) Wireline-k estimate | (f) Blocked well data |
| Scale of data                        | 10 × 10 cm; 2 mm spaced data | 2 × 2 cm squares of 2 mm-spaced data  | c.15–30 cm spaced core plugs | c.15–30 cm spaced plugs    | 15 cm digital log       | 2 m blocking          |
| N =                                  | 2584                         | 25                                    | 11                           | 85                         | 204                     | 16                    |
| Mean ln(k)                           | 7.14                         | 7.14                                  | 6.39                         | 1.73                       | 2.32                    | 2.17                  |
| $\sigma^2$ ln(k)                     | 0.38                         | 0.30                                  | 0.99                         | 8.44                       | 5.94                    | 4.80                  |
| Variance adjustment factor, <i>f</i> | –                            | 0.79                                  | –                            | –                          | –                       | 0.81                  |

Statistics for  $\ln(k)$  are shown as the population distributions are approximately log normal. It is well known that the sample variance should reduce as sample scale is increased. Therefore, the reduction in variance between datasets (c) and (d) – core data to reservoir model – is expected. It is, however, a common mistake in multi-scale reservoir modelling for an inappropriate variance to be applied in a larger scale model, e.g. if core plug variance was used directly to represent the upscaled geomodel variance.

Comparison of datasets (a) and (b) reveals another form of variance that is commonly ignored. The probe permeameter grid (2 mm spaced data over a 10 cm  $\times$  10 cm core area) shows a variance of 0.38 [ $\ln(k)$ ]. The core plug dataset for the corresponding lithofacies interval (estuarine bar), has  $\sigma^2 \ln(k) = 0.99$ , which represents variance at the lithofacies scale. However, blocking of the probe permeameter data at the core plug scale shows a variance reduction factor of 0.79 up to the core plug scale (column 2 in Table 4.2). Thus, in this dataset (where high resolution measurements are available) we know that a significant degree of variance is missing from the datasets conventionally used in reservoir modelling.

Improved treatment of variance in reservoir modelling is clearly needed and presents us with a significant challenge. The statistical basis for treating population variance as a function of sample support volume is well established with the concept of *Dispersion Variance* (Isaaks and Srivastava 1989):

$$\begin{array}{rcc} \sigma^2(a, c) & = & \sigma^2(a, b) + \sigma^2(b, c) \\ \text{Total} & & \text{Variance} \quad \text{Variance} \\ \text{variance} & & \text{within blocks} \quad \text{between blocks} \end{array} \quad (4.14)$$

where:

a, b and c represent different sample supports  
(in this case,  $a = \text{point values}$ ,  $b = \text{block values}$   
and  $c = \text{total model domain}$ )

The variance adjustment factor,  $f$ , is defined as the ratio of block variance to point variance and can be used to estimate the correct variance to be applied to a blocked dataset. For the example dataset (Table 4.2 and Fig. 4.26) the variance adjustment factor is around 0.8 for both scale adjustment steps.

With additive properties, such as porosity, treatment of variance in multi-scale datasets is relatively straightforward. However, it is much more of a challenge with permeability data as flow boundary conditions are an essential aspect of estimating an upscaled permeability value (see Chap. 3). Multi-scale geological modelling is an attempt to represent smaller scale structure and variability as an upscaled block permeability value. In this process, the principles guiding appropriate flow upscaling are essential. However, improved treatment of variance is also critical. There is, for example, little point rigorously upscaling a core plug sample dataset if it is known that the dataset is a poor representation of the true population variance.

The best approach to this rather complex problem, is to review the available data within a multi-scale REV framework (Fig. 4.24). If the dataset is sampled at a scale close to the corresponding REV, then it can be considered as fairly reliable and representative data. If however, the dataset is clearly not sampled at the REV (and is in fact recording a highly variable property) then care is needed to handle and upscale the data in order to derive an appropriate average. Assuming that we have datasets which can be related to the REV's in the rock system, we can then use the same multi-scale framework to guide the modelling length scales. Reservoir model grid cell dimensions should ideally be determined by the REV length scales. Explicit spatial variations in the model (at scales larger than the grid cell) are then focussed on representing property variations that cannot be captured by averages. To put this concept in its simplest form, mapping REV's against the three pore-field scale steps introduced in Sect. 4.3.2, consider the following:

1. *From pore scale to lithofacies scale:* Pore-scale models (or measurements) are made at the pore-scale REV and then spatial variation at the lithofacies scale is modelled to estimate rock properties at the lithofacies-scale REV.
2. *From lithofacies scale to geomodel scale.* Lithofacies-scale models (or measurements) are made at the lithofacies-scale REV and then spatial variation at the geological architecture scale is modelled to estimate reservoir properties at the scale of the geological-unit REV (equivalent to reservoir model elements).
3. *From geomodel to full-field reservoir simulator.* Representative reservoir elements are modelled at the full-field reservoir simulator scale to estimate dynamic flow behaviour based on reservoir properties that have been correctly upscaled and are (arguably) representative.

There is no doubt that multi-scale modelling within a multi-scale REV framework is a challenging process, but it is nevertheless preferred to ‘throwing in’ some weakly-correlated random

noise into an arbitrary reservoir grid and hoping for a reasonable outcome. The essence of good reservoir model design is that it is based on some sound geological concepts, an appreciation of flow physics, and a multi-scale approach to determining statistically representative properties.

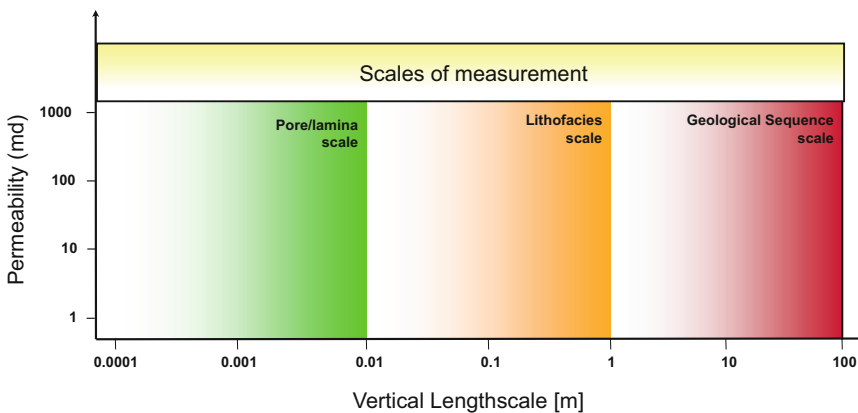
Every reservoir system is somewhat unique, so the best way to apply this approach method is try it out on real cases. Some of these are illustrated in the following sections, but consider trying Exercise 4.2 for your own case study.

**Exercise 4.2**

Find the REV’s for your reservoir?

Use your own knowledge a particular geological reservoir system or outcrop to sketch on the most likely scales of high variability and low variability (the REV) – similar to Fig. 4.21 – using the sketch below. Note that the horizontal axis is given as a vertical length scale (dz, across bedding) to make volume estimation easier.

\*\*\*



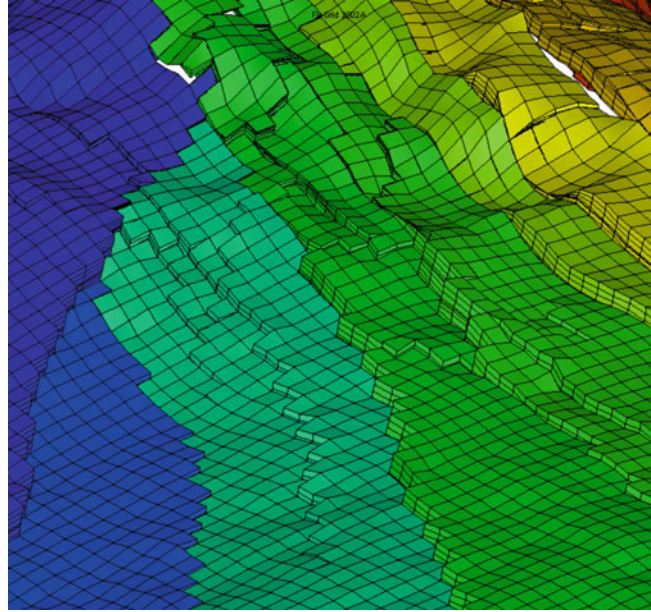
**4.3.5 Construction of Geomodel and Simulator Grids**

The choice of grid and grid-cell dimensions is clearly important. Upscaled permeability, the balance of fluid forces, and reservoir property variance are all intimately connected with the model length scale. The construction of 3D reservoir

models from seismic and well data remains a relatively time consuming task requiring considerable manual work both in construction of the structural framework and, not least, in construction of the grid for property modelling (Fig. 4.27).

Problems especially arise due to complex fault block geometries including reverse faults and Y-faults (Y-shaped intersections in the vertical

**Fig. 4.27** Example reservoir model grid (Heidrun Field fault segments, colour coded by reservoir segment). (Equinor image archives, © Equinor ASA, reproduced with permission)



plane). Difficulties relate partly to the mapping of horizons into the fault planes for construction of consistent fault throws across faults. Currently, most commercial gridding software is not capable of automatically producing adequate 3D grids for realistic fault architectures, and significant manual work is necessary. Upscaling procedures for regular Cartesian grids are well established, but the same operation in realistically complex grids is much more challenging.

The construction of 3D grids suitable for reservoir simulation is also non-trivial and requires significant manual editing. There are several reasons for this:

- The grid resolution in the reservoir and simulation models are different, leading to missing cells or miss-fitting cells in the simulation model. The consequences are overestimation of pore volumes, possibly wrong communication across faults, and difficult numerical calculations due to a number of small or ‘artificial’ grid cells.
- The handling of Y-shaped faults using corner point grid geometries is difficult. Similarly, whereas the use of vertically stair-stepped faults improves the grid quality and flexibility, it does not fully represent the fault geometry – special attention must be paid to the estimation of fault seal and fault transmissibility. There is generally insufficient information in the grid itself for these calculations, and the calculation of fault transmissibility must be calculated based on information from the conceptual geological model.
- The handling of inclined reverse faults using stair-step geometry in a corner point grid requires a higher total number of layers than required for an un-faulted model.
- Regions with fault spacing smaller than the simulation grid spacing give problems for appropriate calculation of fault throw and zone-to-zone communication. Gridding demands that smaller-scale faults are merged and a cumulated fault throw is used in the simulation model. This is not generally possible with currently available gridding tools, and an effective fault transmissibility, including non-neighbour connections, must be calculated based on information from the geomodel, i.e. using the actual geometry containing all the merged faults.
- Flow simulation accuracy depends on the grid quality, and the commonly used numerical discretisation schemes in commercial simulators have acceptable accuracy only for

‘near’ orthogonal grids. Orthogonal grids do not comply easily with complex fault structures, and most often compromises are made between honouring geology and keeping ‘near-orthogonal’ grids.

Figure 4.28 illustrates how some of these problems have been addressed in oilfield studies (Ringrose et al. 2008). After detailed manual grid construction including stair-step faults to handle Y-faults, smaller faults are added directly into the flow simulation grid. However, some gridding problems cannot be fully resolved using the constraints of corner point simulation grids and optimal, consistent and automated grid generation based on realistic geomodels is a challenge. The use of unstructured grids reduces some of the gridding problems, but robust, reliable and cost efficient numerical flow solution methods for these unstructured grids are not generally available. For improved and consistent solutions for construction of structured grids and associated transmissibilities have been proposed see Manzocchi et al. (2002) and Tchelepi et al. (2005).

### 4.3.6 Which Heterogeneities Matter?

There are a number of published studies in which the importance of different multi-scale geological factors on reservoir performance have been assessed. Table 4.3 summarizes the findings of a selection of such studies in which a formalised experimental design with statistical analysis of significance has been employed. The table shows only the main factors identified in these studies (for full details refer to sources). What is clear from this work is that several scales of heterogeneity are important for each reservoir type. While one can conclude that stratigraphic sequence position is the most important factor in a shallow marine depositional setting or that vertical permeability is the most important factors in tidal deltaic setting, each case study shows that both larger and smaller-scale factors are generally significant. This is a clear argument in favour of explicit multi-scale reservoir modelling.

Furthermore, in the studies where the effects of structural heterogeneity were assessed, both structural and sedimentary features were found to be significant. That is to say, structural features

**Fig. 4.28** Illustration of the transfer of a structural geological model to a reservoir simulation grid. (Redrawn from Ringrose et al. 2008, The Geological Society, London, Special Publications 309 © Geological Society of London [2008])

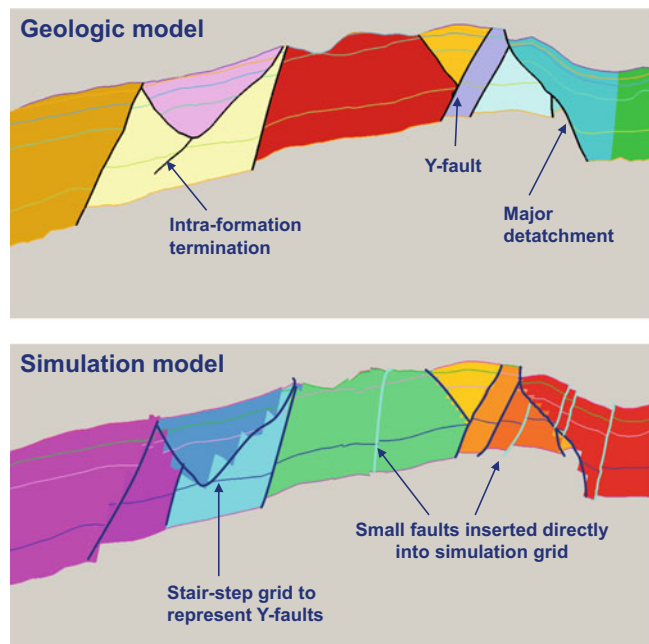


**Table 4.3** Summary of selected studies comparing multi-scale factors on petroleum reservoir performance

|                           | Shallow marine <sup>a</sup> | Faulted shallow marine <sup>b</sup> | Fluvial <sup>c</sup> | Tidal deltaic <sup>d</sup> | Fault modelling <sup>e</sup> |
|---------------------------|-----------------------------|-------------------------------------|----------------------|----------------------------|------------------------------|
| Sequence model            | V                           | V                                   |                      |                            | V                            |
| Sand fraction             | S                           | S                                   | V                    | S                          | n/a                          |
| Sandbody geometry         |                             |                                     | S                    | S                          | n/a                          |
| Vertical permeability     | S                           | S                                   |                      | V                          | n/a                          |
| Small-scale heterogeneity |                             |                                     | S                    | S                          | n/a                          |
| Fault pattern             | n/a                         | S                                   | n/a                  | n/a                        | S                            |
| Fault seal                | n/a                         | S                                   | n/a                  | n/a                        | S                            |

V Most significant factor, S Significant factor, n/a not assessed

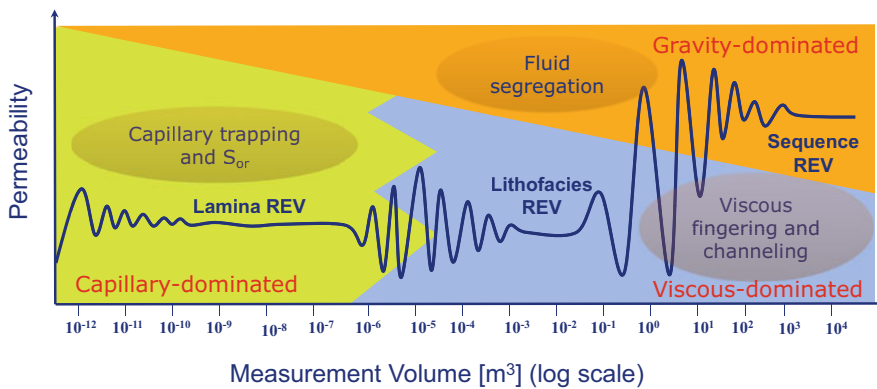
<sup>a</sup>Kjønsvik et al. (1994)

<sup>b</sup>England and Townsend (1998)

<sup>c</sup>Jones et al. (1993)

<sup>d</sup>Brandsæter et al. (2001a)

<sup>e</sup>Lescoffit and Townsend (2005)

**Fig. 4.29** Sketch illustrating the dominant fluid forces influencing different heterogeneity length-scales

and uncertainties cannot be neglected and are fully coupled with stratigraphic factors.

Another important aspect of how to approach this question is to consider how the fluid forces will interact with the heterogeneity in terms of the REV (Fig. 4.29). Pore and lamina-scale variations have the strongest effect on capillary-dominated fluid processes, whereas the sequence stratigraphic (or facies association) scale have the largest effect on flow processes in the viscous-dominated regime. Gravity operates at all scales, but gravity-fluid effects are most important at the larger scales, where significant fluid segregation occurs, that is, when both capillary forces and applied pressure gradients fail to compete effectively against the gravity stabilisation of the fluids involved.

Several projects have demonstrated the economic value of multi-scale modelling in the context of oilfield developments. An ambitious study of the structurally complex Gullfaks field (Jacobsen et al. 2000) demonstrated that 25 million-cell reservoir model grid (incorporating structural and stratigraphic architecture) could be upscaled for flow simulation and resulted in a significantly improved history match. Both stratigraphic barriers and faults were key factors in achieving improved pressure matches to historic well data. This model was also used for the assessment of IOR using CO<sub>2</sub> flooding.

Multi-scale upscaling has also been used to assess complex reservoir displacement processes, including gas injection in thin-bedded reservoirs (Fig. 4.30) (Pickup et al. 2000; Brandsæter et al.

**Fig. 4.30** Gas injection patterns in a thin-bedded tidal reservoir modelled using a multi-scale method and incorporating the effects of faults in the reservoir simulation model. (From a study by Brandsæter et al. 2001b)

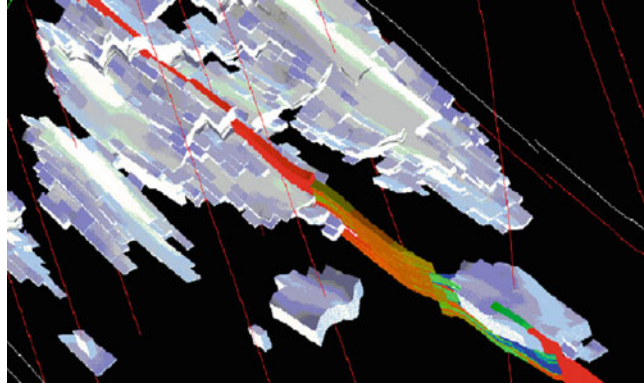
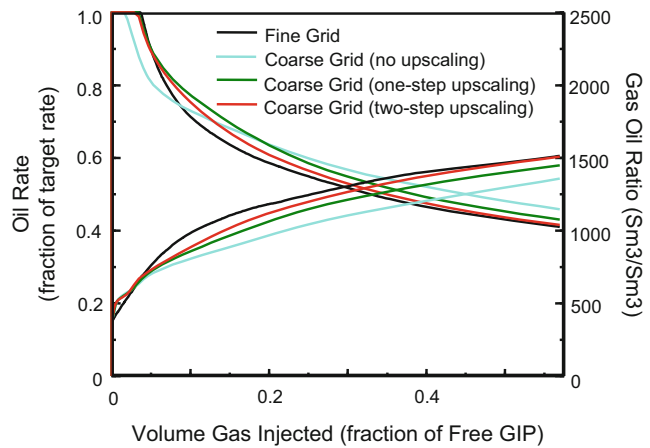


**Fig. 4.31** Effect of multi-scale upscaling on estimates of oil rate and GOR for the gas injection case study shown in Fig. 4.30. (Redrawn from Pickup et al. 2000, ©2000, Society of Petroleum Engineers Inc., reproduced with permission of SPE. Further reproduction prohibited without permission)



2001b, 2005), water-alternating-gas (WAG) injection on the Veslefrikk Field (Kløv et al. 2003), depressurization on the Statfjord field (Theting et al. 2005) and CO<sub>2</sub> storage field performance (Zhou et al. 2020).

These studies typically show of the order of 10–20% difference in hydrocarbon recovery factors when advanced multi-scale effects are implemented, compared with conventional single-scale reservoir simulation studies. For example, Fig. 4.31 shows the effect of one-step and two-step upscaling for the gas injection case study (illustrated in Fig. 4.30). The coarse-grid case without upscaling gives a forecasting error of over 10% when compared to the fine-grid reference case, while the coarse-grid case with two-step upscaling gives a result very close to the fine-grid reference case.

## 4.4 The Way Forward

### 4.4.1 Potential and Pitfalls

Multi-scale reservoir modelling has moved from a conceptual phase, with method development on idealised problems, into a practical phase with more routine implementation on real reservoir cases. The modelling methods have achieved sufficient speed and reliability for routine implementation (generally using steady-state methods on near-orthogonal, corner-point grid systems). However, a number of challenges remain which require further developments of methods and modelling tools. In particular:

- Multi-scale modelling within a realistic structural geological grid is still a major challenge.

- Handling of variance from multiple-scale datasets is frequently incorrect or neglected.
- The tool-set for upscaling is still incomplete and far from integrated; for example multi-phase flow, gridding and fault seal are generally treated in separate software packages and require a degree of manual data-file conversion.

Software tool developments will undoubtedly steadily resolve these challenges, but what ultimately is the goal? We suggest the overall target of reservoir modelling is multi-scale (pore-to-field) modelling and data integration. The level of detail involved depends very much on the task at hand – we return to the foundational issue of the model purpose (Chap. 1). Some problems are essentially pore-scale, e.g. will a different fluid displacement mechanism such as CO<sub>2</sub> injection make a difference to ultimate oil recovery or will capillary trapping be effective in a gas storage scheme? Other problems are essentially large-scale, e.g. does this gas field have sufficient volumes to justify a billion dollar investment? Nevertheless, executing either of these projects in detail will require a multi-scale analysis.

#### 4.4.2 Pore-to-Field Workflow

The following summarises a typical geologically-based workflow within a multi-scale design framework. We define four dominant length scales:

- Pore scale:  $\mu\text{m}$ -cm scale;
- Lithofacies scale: cm-m scale;
- Geomodel (rock and property architecture) scale: 10 m–10 km scale;
- Reservoir simulator scale (typically some coarsening up of the full-field reservoir geomodel): 100 m–10 km scale.

These scales are based both on the nature of rock heterogeneity and the principles for establishing macroscopic flow properties. These four scales give the three scale transitions introduced in Sect. 4.3.2: pore to lithofacies;

lithofacies to geomodel and geomodel to reservoir simulator.

At each scale we define flow properties for each cell (or pore) in the model and then use a numerical upscaling method to determine the upscaled flow property. The upscaled flow property is then used as input in the next scale up. A realistic illustration of this workflow for the pore to lithofacies scale is shown in Fig. 4.32. Here we assume we can define two different pore-scale rock types, e.g. coarse well-sorted sand and fine-grained sand.

Flow functions for each rock type are defined either from Special Core Analysis (SCAL) or from pore network modelling, preferably both. Secondly, we assume we have a selection of different rock models: e.g. trough cross-bedded sandstone lithofacies (as in Fig. 4.32). These models should correspond to the selection of modelling elements described in Sect. 2.4. For each lithofacies element, pore-scale properties are assigned to each lamina (or bed). Upscaling is performed to calculate the lithofacies-scale flow properties – the absolute and relative permeabilities for each flow direction. These flow properties are then assigned to each cell in the reservoir model, with further upscaling to the simulator, if necessary.

For most cases, to make this explicit pore-to-field upscaling computationally feasible, we use steady-state approximations to multi-phase flow, e.g. capillary limit and viscous limit methods. These steady-state approximations have been reviewed and discussed by, for example, Ekran and Aasen (2000) and Pickup and Stephen (2000). Published examples of the pore to lithofacies to full-field multi-scale workflow include Pickup et al. (2000), Theting et al. (2005) and Rustad et al. (2008).

#### 4.4.3 Essentials of Multi-scale Reservoir Modelling

We conclude this chapter with a check-list of essential questions that need to be asked for any reservoir flow-modelling problem:



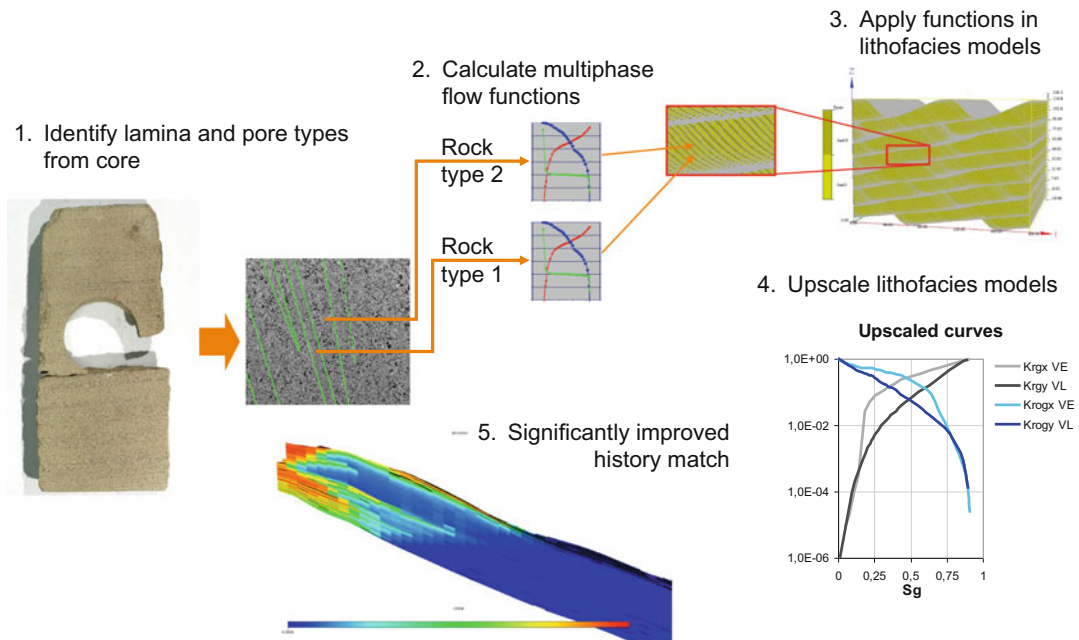


**Fig. 4.32** Pore to lithofacies modelling workflow. (Photos K. Nordahl & A. Rustad/Equinor © Equinor ASA, reproduced with permission)

1. Have you identified the main reservoir elements that impact on flow?

*Hint:* Use the HFU concept of petrophysically distinct units and check against Flora's rule (Sect. 2.4.4).

2. Are your rock properties estimated at the REV?

*Hint:* Try to relate your model length scales (grid sizes) to the natural rock architecture length scales using the multi-scale REV sketch.

3. What length scale has the largest influence on the flow process?

*Hint:* Some flow processes ignore small-scale variations while other flow processes may be strongly controlled by them. Use Flora's rule (Figs. 2.16 and 2.17) or scaling group theory (Sect 4.2.3).

4. Are your flow forecasts (based on single-phase or multi-phase flow equations) using *representative* rock properties and *appropriate* fluid properties.

*Hint:* What really controls your flow process –  $k_{\text{effective}}$ ,  $k_{\text{fracture}}$ ,  $k_{\text{relative}}$ ,  $k_v$  or  $P_c$ ?

Are you reasonably happy with your assumptions? Press 'run' on the simulator and review the outcomes. Finally, when reviewing model outcomes (forecasts) remember the challenge of human bias and the goal of making informed decisions (covered next, in Chap. 5). Reservoir models are part of a learning process – if the model just confirms your presumptions you haven't learned very much; but if it identifies some new insights, processes or phenomena you were not aware of then the model was 'useful'. We will return to this theme in Chap. 8.

## References

- Abbaszadeh M, Fujii H, Fujimoto F (1996) Permeability prediction by hydraulic flow units – theory and applications. SPE Form Eval 11(4):263–271
- Bakke S, Øren P-E (1997) 3-D pore-scale modelling of sandstones and flow simulations in pore networks. SPE J 2:136–149
- Barker JW, Thibeau S (1997) A critical review of the use of pseudo relative permeabilities for upscaling. SPE Reserv Eng 12(5):138–143

- Bear J (1972) *Dynamics of fluids in porous media*. Elsevier, New York
- Behbahani H, Blunt MJ (2005) Analysis of imbibition in mixed-wet rocks using pore-scale modeling. *SPE J* 10(4):466–474
- Blunt MJ (1997) Effects of heterogeneity and wetting on relative permeability using pore level modeling. *SPE J* 2(1):70–87
- Bourbiaux B, Basquet R, Cacas M-C, Daniel J-M, Sarda S (2002) An integrated workflow to account for multi-scale fractures in reservoir simulation models: implementation and benefits. SPE paper 78489 presented at Abu Dhabi international petroleum exhibition and conference, Abu Dhabi, United Arab Emirates, 13–16 October
- Brandsæter I, Wist HT, Næss A, Li O, Arntzen OJ, Ringrose P, Martinius AW, Lerdahl TR (2001a) Ranking of stochastic realizations of complex tidal reservoirs using streamline simulation criteria. *Pet Geosci* 7:53–63
- Brandsæter I, Ringrose PS, Townsend CT, Omdal S (2001b) Integrated modelling of geological heterogeneity and fluid displacement: Smørbukk gas-condensate field, Offshore Mid-Norway. SPE paper 66391 presented at the SPE reservoir simulation symposium, Houston, TX, 11–14 Feb 2001
- Brandsæter I, McIlroy D, Lia O, Ringrose PS (2005) Reservoir modelling of the Lajas outcrop (Argentina) to constrain tidal reservoirs of the Haltenbanken (Norway). *Pet Geosci* 11:37–46
- Bryant S, Blunt MJ (1992) Prediction of relative permeability in simple porous media. *Phys Rev A* 46:2004–2011
- Bryant S, King PR, Mellor DW (1993) Network model evaluation of permeability and spatial correlation in a real random sphere packing. *Transp Porous Media* 11:53–70
- Campbell CV (1967) Lamina, laminaset, bed, bedset. *Sedimentology* 8:7–26
- Chierici GL (1994) *Principles of petroleum reservoir engineering*, vol 1. Springer, Berlin, p 2
- Coats KH, Dempsey JR, Henderson JH (1971) The use of vertical equilibrium in two-dimensional simulation of three-dimensional reservoir performance. *Soc Petrol Eng J* 11(01):63–71
- Corbett PWM, Jensen JL (1992) Estimating the mean permeability: how many measurements do you need? *First Break* 10:89–94
- Corbett PWM, Ringrose PS, Jensen JL, Sorbie KS (1992) Laminated clastic reservoirs: the interplay of capillary pressure and sedimentary architecture. SPE paper 24699, presented at the SPE annual technical conference, Washington, DC
- Dake LP (2001) *The practice of reservoir engineering*, Rev edn. Elsevier, Amsterdam
- Davis JC (2003) *Statistics and data analysis in geology*, 3rd edn. Wiley, New York, 638 pages
- Doyen PM (2007) *Seismic reservoir characterisation*. EAGE Publications, Houten
- Durlafsky LJ, Milliken WJ, Bernath A (2000) Scaleup in the near-well region. *SPE J* 5(1):110–117
- Ekran S, Aasen JO (2000) Steady-state upscaling. *Transp Porous Media* 41(3):245–262
- England WA, Townsend C (1998) The effects of faulting on production from a shallow marine reservoir – a study of the relative importance of fault parameters. *Soc Petrol Eng*. <https://doi.org/10.2118/49023-MS>
- Gozalpour F, Ren SR, Tohidi B (2005) CO<sub>2</sub> EOR and storage in oil reservoir. *Oil Gas Sci Technol* 60(3):537–546
- Haldorsen HH (1986) Simulator parameter assignment and the problem of scale in reservoir engineering. In: Lake LW, Caroll HB (eds) *Reservoir characterization*. Academic, Orlando, pp 293–340
- Haldorsen HH, Lake LW (1984) A new approach to shale management in field-scale models. *Soc Petrol Eng J* 24:447–457
- Huang Y, Ringrose PS, Sorbie KS (1995) Capillary trapping mechanisms in water-wet laminated rock. *SPE Reserv Eng* 10:287–292
- Huang Y, Ringrose PS, Sorbie KS, Larter SR (1996) The effects of heterogeneity and wettability on oil recovery from laminated sedimentary. *SPE J* 1(4):451–461
- Isaaks EH, Srivastava RM (1989) *Introduction to applied geostatistics*. Oxford University Press, New York
- Jackson MD, Mugeridge AH, Yoshida S, Johnson HD (2003) Upscaling permeability measurements within complex heterolithic tidal sandstones. *Math Geol* 35(5):499–519
- Jacobsen T, Agustsson H, Alvestad J, Digranes P, Kaas I, Opdal S-T (2000) Modelling and identification of remaining reserves in the Gullfaks field. Paper SPE 65412 presented at the SPE European petroleum conference, Paris, France, 24–25 October
- Jensen JL, Lake LW, Corbett PWM, Goggin DJ (2000) *Statistics for petroleum engineers and geoscientists*, 2nd edn. Elsevier, Amsterdam
- Jones A, Doyle J, Jacobsen T, Kjønsvik D (1993) Which sub-seismic heterogeneities influence waterflood performance? A case study of a low net-to-gross fluvial reservoir. In: De Haan HJ (ed) *New developments in improved oil recovery*, vol 84, Geological society special publication. Geological Society, London, pp 5–18
- King MJ, Mansfield M (1999) Flow simulation of geologic models. *SPE Reserv Eval Eng* 2(4):351–367
- Kjønsvik D, Doyle J, Jacobsen T, Jones A (1994) The effect of sedimentary heterogeneities on production from a shallow marine reservoir – what really matters? SPE paper 28445 presented at the European petroleum conference, London, 25–27 Oct 1994
- Kløv T, Øren P-E, Stensen JÅ, Lerdahl TR, Berge LI, Bakke S, Boassen T, Virnovsky G (2003) SPE paper 84549 presented at the SPE annual technical conference and exhibition, Denver, CO, USA, 5–8 October

- Kyte JR, Berry DW (1975) New pseudo functions to control numerical dispersion. *SPE J* 15:276–296
- Lescoffit G, Townsend C (2005) Quantifying the impact of fault modeling parameters on production forecasting for elastic reservoirs. In: *Evaluating fault and cap rock seals*, vol 2, AAPG special volume Hedberg series. AAPG, Tulsa, pp 137–149
- Li D, Lake LW (1995) Scaling fluid flow through heterogeneous permeable media. *SPE Adv Technol Ser* 3 (1):188–197
- Li D, Cullick AS, Lake LW (1996) Scaleup of reservoir-model relative permeability with a global method. *SPE Reserv Eng* 11(3):149–157
- Mallet JL (2008) Numerical earth models. European Association of Geoscientists and Engineers, Houten, p 147
- Manzocchi T, Heath AE, Walsh JJ, Childs C (2002) The representation of two-phase fault-rock properties in flow simulation models. *Pet Geosci* 8:119–132
- McDougall SR, Sorbie KS (1995) The impact of wettability on waterflooding: pore-scale simulation. *SPE Reserv Eng* 10(3):208–213
- Miall AD (1985) Architectural-element analysis: a new method of facies analysis applied to fluvial deposits. *Earth-Sci Rev* 22:261–308
- Neasham JW (1977) The morphology of dispersed clay in sandstone reservoirs and its effect on sandstone shaliness, pore space and fluid flow properties. SPE paper 6858 presented at the SPE annual technical conference and exhibition, Denver, CO, 9–12 Oct 1977
- Nilsen HM, Herrera PA, Ashraf M, Ligaarden I, Iding M, Hermanrud C, Lie KA, Nordbotten JM, Dahle HK, Keilegavlen E (2011) Field-case simulation of CO<sub>2</sub>-plume migration using vertical-equilibrium models. *Energy Procedia* 4:3801–3808
- Nordahl K, Ringrose PS (2008) Identifying the representative elementary volume for permeability in heterolithic deposits using numerical rock models. *Math Geosci* 40(7):753–771
- Nordahl K, Ringrose PS, Wen R (2005) Petrophysical characterisation of a heterolithic tidal reservoir interval using a process-based modelling tool. *Pet Geosci* 11:17–28
- Nordbotten JM, Celia MA (2011) Geological storage of CO<sub>2</sub>: modeling approaches for large-scale simulation. Wiley, Hoboken
- Øren P-E, Bakke S (2003) Process-based reconstruction of sandstones and prediction of transport properties. *Transp Porous Media* 12(48):1–32
- Pickup GE, Stephen KS (2000) An assessment of steady-state scale-up for small-scale geological models. *Pet Geosci* 6:203–210
- Pickup GE, Ringrose PS, Sharif A (2000) Steady-state upscaling: from lamina-scale to full-field model. *SPE J* 5:208–217
- Pickup GE, Stephen KD, Zhang M, Ma J, Clark JD (2005) Multi-stage upscaling: selection of suitable methods. *Transp Porous Media* 58:119–216
- Rapoport LA (1955) Scaling laws for use in design and operation of water-oil flow models. *Am Inst Min Metallur Petrol Eng Trans* 204:143–150
- Renard P, de Marsily G (1997) Calculating equivalent permeability: a review. *Adv Water Resour* 20:253–278
- Ringrose PS (1994) Structural and lithological controls on coastline profiles in Fife, Eastern Britain. *Terra Nova* 6:251–254
- Ringrose PS, Corbett PWM (1994) Controls on two-phase fluid flow in heterogeneous sandstones. In: Parnell J (ed) *Geofluids: origin, migration and evolution of fluids in sedimentary basins*, vol 78, Geological Society special publication. Geological Society, London, pp 141–150
- Ringrose PS, Sorbie KS, Corbett PWM, Jensen JL (1993) Immiscible flow behaviour in laminated and cross-bedded sandstones. *J Pet Sci Eng* 9:103–124
- Ringrose PS, Jensen JL, Sorbie KS (1996) Use of geology in the interpretation of core-scale relative permeability data. *SPE Form Eval* 11(03):171–176
- Ringrose PS, Skjetne E, Elfeinbein C (2003) Permeability estimation functions based on forward modeling of sedimentary heterogeneity. SPE 84275, Presented at the SPE annual conference, Denver, USA, 5–8 Oct 2003
- Ringrose PS, Martinius AW, Alvestad J (2008) Multiscale geological reservoir modelling in practice. In: Robinson A et al (eds) *The future of geological modelling in hydrocarbon development*, vol 309, Geological Society special publications. Geological Society, London, pp 123–134
- Rubin DM (1987) Cross-bedding, bedforms and palaeocurrents, vol 1, Concepts in sedimentology and palaeontology. Society of Economic Paleontologists and Mineralogists Special Publication, Tulsa
- Rustad AB, Theting TG, Held RJ (2008) Pore-scale estimation, upscaling and uncertainty modelling for multiphase properties. SPE paper 113005, presented at the 2008 SPE/DOE improved oil recovery symposium, Tulsa, OK, UK, 19–23 Apr 2008
- Size WB (ed) (1987) Use and abuse of statistical methods in the earth sciences, IAMG studies in mathematical geology, no. 1. Oxford University Press, Oxford
- Smith EH (1991) The influence of small-scale heterogeneity on average relative permeability. In: Lake LW et al (eds) *Reservoir characterisation II*. Academic, San Diego
- Sorbie KS, Feghi F, Pickup GE, Ringrose PS, Jensen JL (1994) Flow regimes in miscible displacements in heterogeneous correlated random fields. *SPE Adv Technol Ser* 2(02):78–87
- Stone HL (1991) Rigorous black oil pseudo functions. SPE paper 21207, presented at the SPE symposium on reservoir simulation, Anaheim, CA, 17–20 Feb 1991
- Tchelepi HA, Jenny P, Lee C, Wolfsteiner C (2005) An adaptive multiscale finite volume simulator for

- heterogeneous reservoirs. SPE paper 93395 presented at the SPE reservoir simulation symposium, The Woodlands, Texas, 31 January–2 February
- Theting TG, Rustad AB, Lerdahl TR, Stensen JÅ, Boassen T, Øren P-E, Bakke S, Ringrose P (2005) Pore-to-field multi-phase upscaling for a depressurization process. Presented at the 13th European symposium on improved oil recovery, Budapest, Hungary, 25–27 Apr 2005
- Todd MR, Longstaff WJ (1972) The development, testing, and application of a numerical simulator for predicting miscible flood performance. *J Petrol Technol* 1972:874–882
- Towler BF (2002) Fundamental principles of reservoir engineering, vol 8, SPE textbook series. Henry L. Doherty Memorial Fund of AIME, Society of Petroleum Engineers, Richardson
- Turcotte DL (1992) *Fractals and chaos in geology and geophysics*. Cambridge University Press, Cambridge
- Walsh J, Watterson J, Yielding G (1991) The importance of small-scale faulting in regional extension. *Nature* 351:391–393
- Weber KJ (1986) How heterogeneity affects oil recovery. In: Lake LW, Carroll HB (eds) *Reservoir characterisation*. Academic, Orlando, pp 487–544
- Weber KJ, van Geuns LC (1990) Framework for constructing clastic reservoir simulation models. *J Pet Technol* 42:1248–1297
- Wen R, Martinius AW, Næss A, Ringrose PS (1998) Three-dimensional simulation of small-scale heterogeneity in tidal deposits – a process-based stochastic method. In: Buccianti A et al (eds) *Proceedings of the 4th annual conference of the international association of mathematical geology*, Naples, pp 129–134
- Yielding G, Walsh J, Watterson J (1992) The prediction of small-scale faulting in reservoirs. *First Break* 10 (12):449–460
- Yortsos YC (1995) A theoretical analysis of vertical flow equilibrium. *Transp Porous Media* 18(2):107–129
- Zhou D, Fayers FJ, Orr FM Jr (1997) Scaling of multi-phase flow in simple heterogeneous porous media. *SPE Reserv Eng* 12(03):173–178
- Zhou Q, Yang X, Zhang R, Hosseini SA, Ajo-Franklin JB, Freifeld BM, Daley TM, Hovorka SD (2020) Dynamic processes of CO<sub>2</sub> storage in the field: 1. Multiscale and multipath channeling of CO<sub>2</sub> flow in the hierarchical fluvial reservoir at Cranfield, Mississippi. *Water Resour Res* 56(2):e2019EF001360

## Abstract

The preceding chapters have highlighted a number of ways in which a reservoir model can go right or wrong. In terms of the potential impact on a commercial decision, however, nothing compares with the mishandling of uncertainty. An incorrect saturation model, for example, can easily give a volumetric error of 10% or 20%. A flawed geological concept could have a higher impact still. Mishandling of uncertainty, however, can eas-

ily result in the whole modelling and simulation effort becoming worthless.

The cause of this may be the misuse of software or misleading data, but the prime reason is more personal: our behaviour and our design choices. Our aim is to stimulate a model design strategy that can overcome data limitations and personal bias and give us a useful way of quantifying model forecast uncertainty.



*Foresee the trees*

## Keywords

Uncertainty · Root cause · Scenarios · Multi-determinism · Experimental design · Ensembles · Forecasting · Bias · Heuristics ·

Availability · Overconfidence · Anchoring · Priming

## 5.1 The Issue

### 5.1.1 Modelling for Comfort

In Chap. 1 we identified the tendency for modelling studies to become a panacea for decision making – modelling for comfort rather than analytical rigour (Bentley 2015). It is certainly often the case that reservoir modelling is used to hide uncertainty rather than illustrate it. We have a natural tendency to gravitate towards a best guess – the anchoring heuristic of Kahneman and Tversky (1974) – and the management processes in many companies, striving for a best technical case, inadvertently encourages the guesswork.

In a situation of dramatic under-sampling the guess is often wrong and influenced unconsciously by behavioural biases of the individuals or teams involved (Kahneman 2011). Best-guess models therefore tend to be misleading and their role is reduced to one of providing comfort to support a business decision, one which has perhaps already been made. In this case we are indeed simply ‘modelling for comfort’, a low value activity, rather than taking the opportunity to use modelling to identify a significant business risk (modelling for *discomfort*).

### 5.1.2 Modelling for Discomfort – Quantifying Uncertainty and Exposing Risk

Useful modelling can be thought of as ‘reasonable forecasting.’ A convenient metaphor for this is our ability to predict the image on a picture from a small number of sample points.

We illustrate this graphically in Fig. 5.1 using sampled sections from a landscape photograph. A routine modelling workflow would lead us to analyse and characterise each sample point – the

process of reservoir characterisation. Data-led modelling with no underlying concept and no application of trends could produce the stochastic result shown in Fig. 5.2. This representation assumes data stationarity, is statistically consistent with the underlying data set and would pass a simple QC test comparing the frequency of occurrences of elements in the data and in the model; yet the result is clearly meaningless and adds no value.

Application of logical deterministic trends to the modelling process, as described in Chap. 2, would make a better representation, one which would at least fit an underlying landscape concept, e.g. the sky is more likely to be at the top, the grass at the bottom (Fig. 5.3). Furthermore, there is an anisotropy ratio we can use so that we can predict better spatial correlation laterally (the sky is more likely to extend laterally over the image, rather than vertically).

If the texture from this pixel-based approach, analogous to SIS (Sect. 2.7.2), is deemed unrepresentative of landscapes, an object-based alternative may be preferred (Fig. 5.4). Grass is accordingly arranged in clusters, broadly elliptical, as are sky colours (clouds) and the rocky areas are arranged into ‘hills’, anchored around the data points they were observed in. A rough representation is beginning to take shape.

The model representations in Figs. 5.2, 5.3 and 5.4 each adhere to the same element proportions, and in this sense all ‘match’ the data, although with strongly contrasting textures. Assuming we then proceeded to add petrophysical properties to the landscape elements (Chap. 3) and re-scaled the image for flow simulation (Chap. 4), these images would produce strongly contrasting fluid-flow forecasts.

Using these different images as possible alternative realisations could be one way of exploring uncertainty, but we argue this would be a poor route to follow as it simply explores software

**Fig. 5.1** An undersampled picture – our task is to determine the image

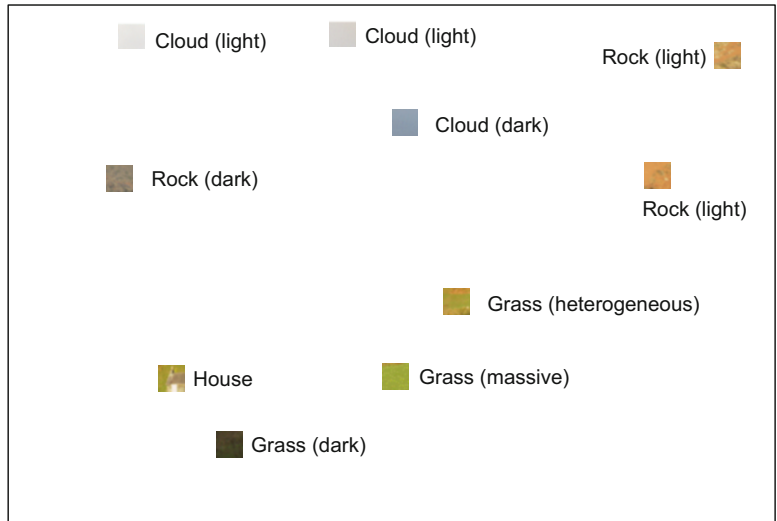


**Fig. 5.2** Stochastic model representation of the data in Fig. 5.1, assuming stationarity

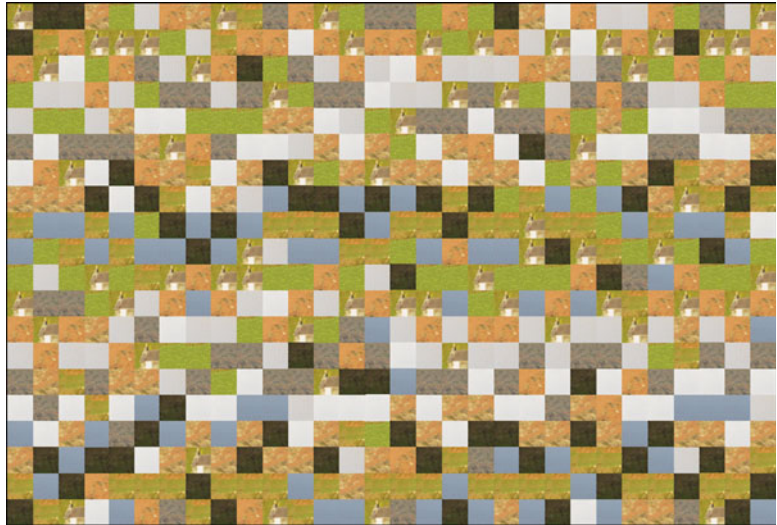


**Fig. 5.3** Overlay of deterministic trends on the stochastic model in Fig. 5.2, overcoming stationarity

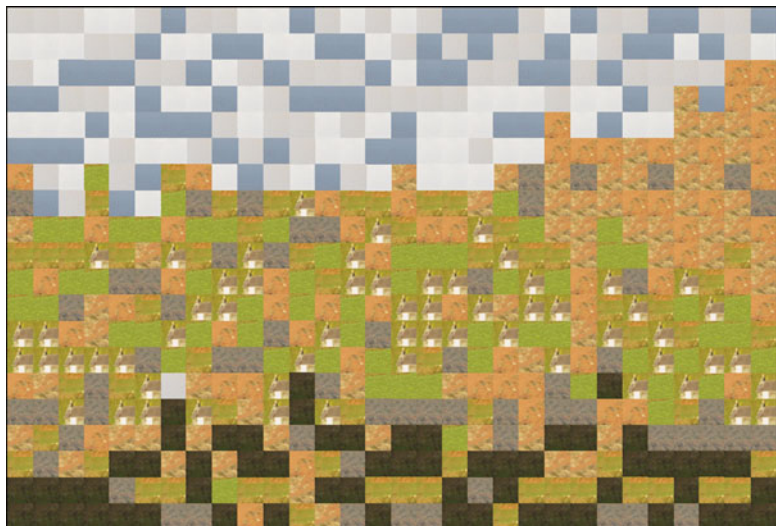


**Fig. 5.4** Object model alternative to Fig. 5.3, maintaining deterministic trends and embracing a loose alignment of lozenge shapes

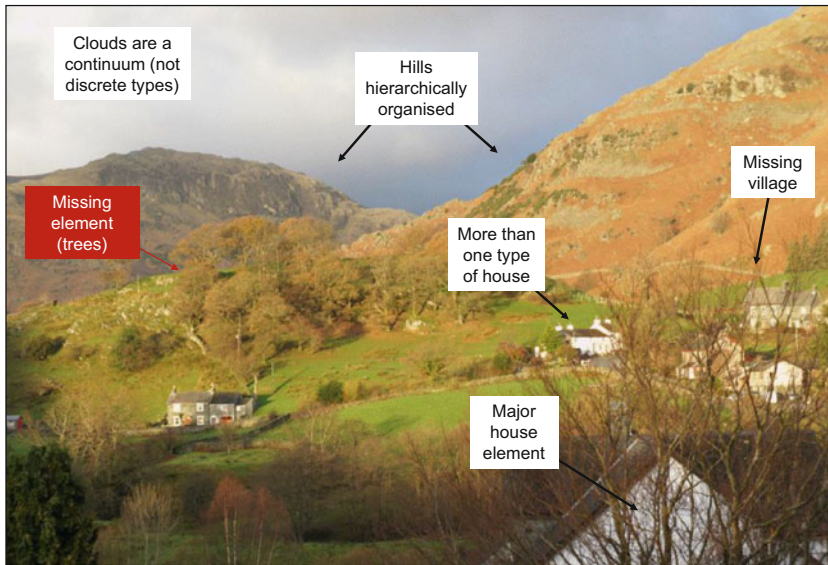


**Fig. 5.5** Reality: the data set was unable to detect key missing elements (notably the trees); these elements are therefore also absent from the simple probabilistic model, even with a useful deterministic trend imposed

options and does not tackle the validity of the initial sample. Reference to the actual image (Fig. 5.5) reveals a familiar theme:

$$data \neq model \neq truth$$

Even though most aspects of the image were sampled, and the applied deterministic trends were reasonable, there are significant errors in the representation – object modelling of the sky was inappropriate, hierarchical organisation was missed, and even some aspects of the

characterisation (grass vs. rocks) were oversimplified. There are also some modelling elements missing, most noticeably: *there were no trees*. Rearranging the data and detailed statistical analysis of the original samples does not reveal the missing elements. On reflection, we can see that the aim of reproducing the statistical content of the sample dataset brings with it a major flaw in all the models.

Could the missing elements in Fig. 5.5 have been foreseen, given that they were absent in the



data sample? We would argue yes, to a large extent. From the data set it is possible to establish a concept of hilly countryside in a temperate climate – the ‘expert judgement’ of Kahneman and Klein (2009). Having established this, there are certain aspects which are consistent with the concept, not actually seen by the sample data but can be anticipated. Based on a temperate countryside concept we can ask:

- Could there be more than one type of house? *Yes.*
- Could there be a small village? *Yes.*
- Is there likely to be a structure to the clouds? *Yes.*
- Could the hills be logically arranged, ones with greater contrast in the foreground? *Yes*
- Could there be trees?

On the issue of trees, these are highly likely to be present given the underlying concept of the image and they are also likely to be under-sampled. We can *expect* them.

The parallels with reservoir modelling are hopefully clear: we need to use concepts to honour the data but work beyond it to include missing but logical elements. Outcrop and sub-surface analogues are often used to identify plausible elements in reservoir modelling. If these elements are important to the field development (open natural fractures, discontinuous but high permeability layers, cemented areas, sealing sub-seismic faults, thin shales) then the presence or absence of these features becomes the important uncertainty.

We can always ask ourselves: “*could there be trees?*”

---

## 5.2 Differing Methodologies

The practice of model-based uncertainty quantification followed on logically from the emergence of the integrated reservoir modelling tools for field development planning in the 1990s, the subject matter of this book (see also Cosentino 2001; Towler 2002). Appreciating the numerous uncertainties involved in constructing such

models, the desire for multiple modelling naturally arose. Although not universal, the application of multiple modelling techniques is now common, with alternative models described variously as ‘runs’, ‘cases’, ‘realisations’, ‘scenarios’ or ‘ensembles’. These terms can broadly be defined as:

*Run* – one complete model build, of any type.

*Case* – a set of parameter values, usually with defined ranges.

*Realisation* – a model outcome based on statistical sampling of parameters in a case.

*Scenario* – a deterministic real-world outcome based on a reservoir concept and a development plan.

*Ensemble* – strictly: ‘a group of items viewed as a whole rather than individually’, in this case a collection of model run results, typically statistical realisations but can also be applied to a suite of deterministic scenarios.

The different terminologies are more than semantic, the essential difference being whether the work is anchored on a best guess or a set of alternative cases and whether those cases are generated deterministically (conceptually) or probabilistically (statistically) (Fig. 5.6).

The contrasting approaches to model-based uncertainty-handling broadly fall into these three end-members, or combinations of these, described below.

### 5.2.1 Best Guess, or ‘Rationalist’ Approaches

In this instance a preferred model is chosen as a base case (Fig. 5.7). The model is either run as a technical best guess, or with a range of uncertainty added to that guess. This may be either a percentage factor of the input parameters, e.g.  $\pm 10\%$  of the base case porosity,  $\pm 10\%$  of the base case net sand content etc., or of the model output itself, e.g.  $\pm 20\%$  of the base case volumes in-place (Fig. 5.7a). Alternatively, the range can be specified as separate low and high cases flanking the base case (Fig. 5.7b). This approach can be viewed as ‘traditional’ determinism.

**Fig. 5.6** Alternative approaches to uncertainty handling

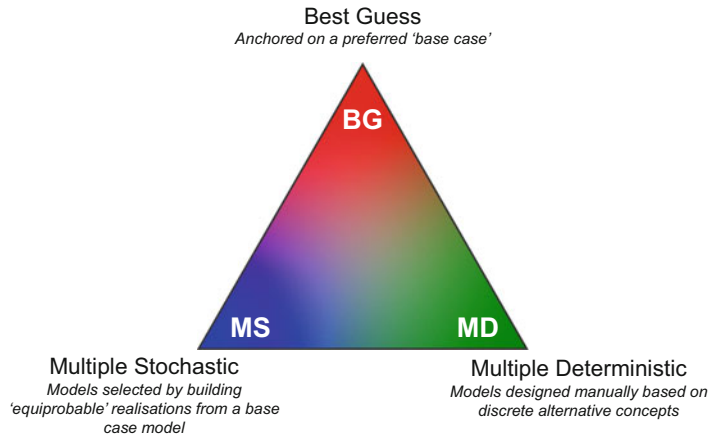
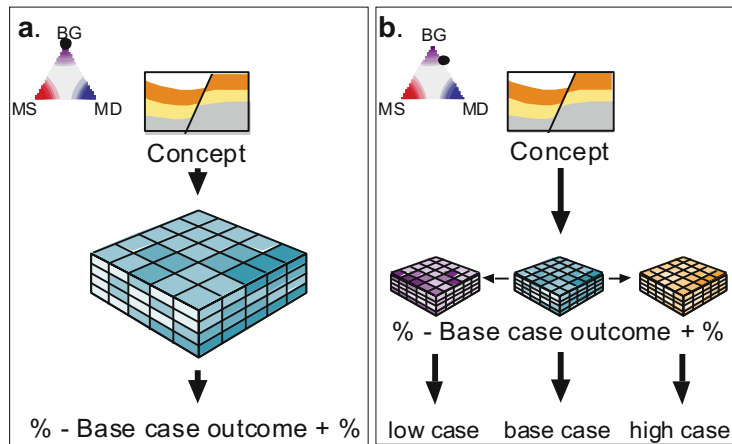


**Fig. 5.7** Base case–dominated, rationalist approaches. (Redrawn from Bentley and Smith 2008, The Geological Society, London, Special Publications 309 ©Geological Society of London [2008])



**5.2.2 Multiple Stochastic Approaches**

In this instance a large number of models are probabilistically generated by geostatistical simulation (Fig. 5.8). The deterministic guidance lies in the choice of the boundary conditions for the simulations, such as assumed correlation lengths for rock modelling and parameter ranges for property modelling, and setting degrees of dependence between input parameters.

The stochastic aspect is the parameter sampling which is based on random selection but guided by a starting seed value, which allows a probabilistic run to be replicated. The random sampling process is comparable with that used to generate heterogeneity in a standard geostatistical model build, but here applied to generating multiple, equally probable model

realisations. The technique allows a large ensemble of realisations to be generated in one run, which can be combined into a probability distribution.

Yarus and Chambers (1994) give several examples of this approach, and the options and choices are reviewed by Caers (2011).

**5.2.3 Multiple Deterministic Approaches**

These avoid a preferred base-case model and are not statistically generated (Fig. 5.9) – they are discrete deterministic scenarios, defined by van der Heijden (1996) in the context of corporate strategic planning as:

**Fig. 5.8** Multiple stochastic approaches. (Redrawn from Bentley and Smith 2008, The Geological Society, London, Special Publications 309 ©Geological Society of London [2008])

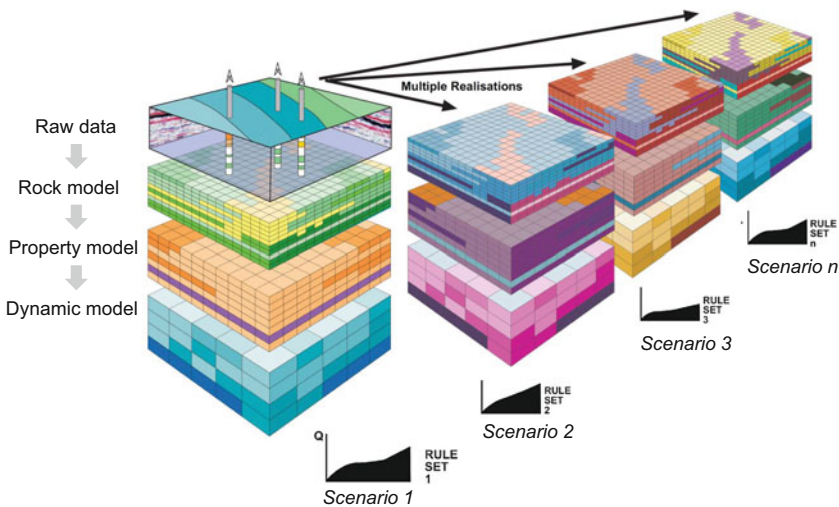
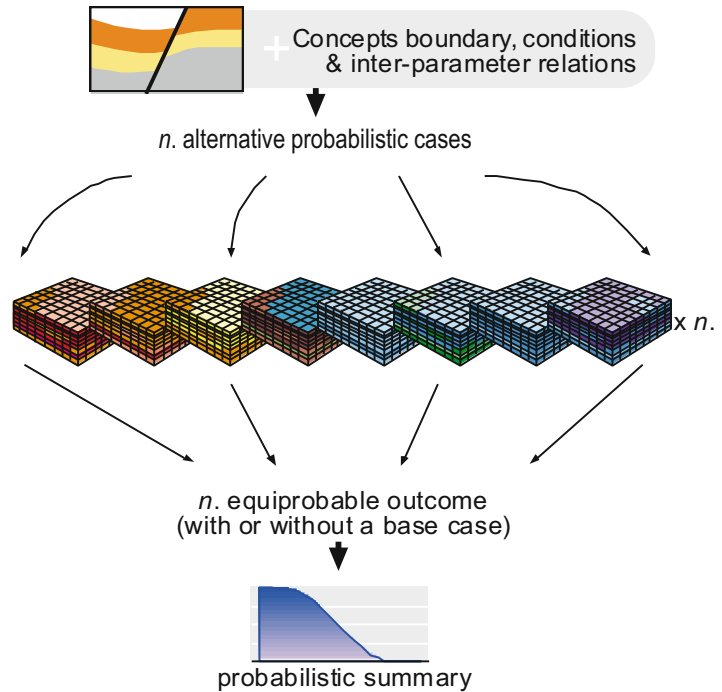


**Fig. 5.9** Multiple-deterministic, ‘scenario-based’ approach

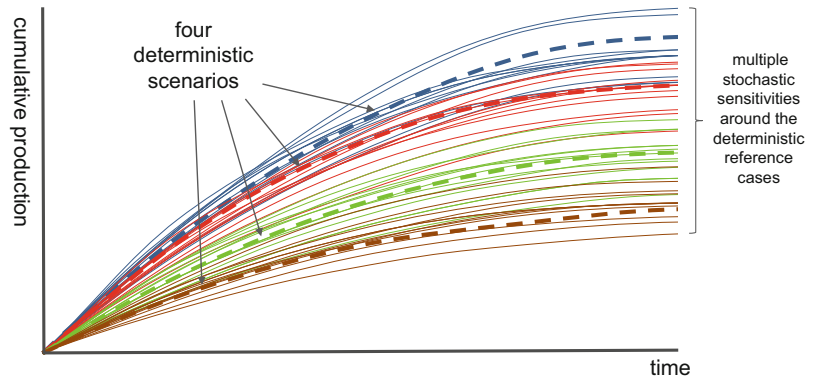
a set of reasonably plausible, but structurally different futures

a complete static-dynamic model outcome based on an underlying reservoir concept with an associated development plan tailored to optimise its development.

In the context of reservoir modelling, we adopt the definition of ‘scenario’ from Bentley and Smith (2008) as:

A reservoir and simulation model ‘scenario’ is therefore one of several plausible futures.

**Fig. 5.10** Multiple-deterministic and multiple-stochastic approaches combined; based on four initial deterministic realisations (bold lines: blue, red, green and brown) a broad ensemble is created by generating multiple stochastic realisations around each of the four deterministic realisations



In this approach a smaller number of models are built compared to the multiple stochastic approach, each one reflecting a complete real-world outcome following an explicitly-defined reservoir concept – a scenario. Geostatistical simulation may be applied in the building of the 3D model but the *selection* of the model realisations is made manually rather than by statistical sampling from input parameters (van de Leemput et al. 1996; Bentley and Woodhead 1998)

Geostatistical simulation is a key tool required to build an individual scenario but the *design* of each scenario is deterministic. This distinguishes scenario modelling from multiple stochastic modelling which may be based on statistical sampling from a single initial design.

The techniques merge if multiple stochastic cases are built from a suite of multiple deterministic concepts to generate an ‘ensemble’ (Fig. 5.10).

There is therefore a toolbox of options for model-based quantification of uncertainty, varying in emphasis from those which are deterministically vs. probabilistically guided and varying in complexity from simple tools (a guess or a toss of a coin) to complex model ensembles (Fig. 5.11). Furthermore, tools may be combined.

It would be dogmatic to suggest that one technique is right for all cases: different model purposes predicate different choices. We would argue though, as throughout this book, for three guiding principles:

1. Any approach should be founded on firm subsurface concepts (*if you can sketch it you can model it*);

2. The modelling should not be restricted to statistically insufficient data sets ( $data \neq model \neq truth$ ), and
3. Workflows should be adopted in a way which minimises predictable biases.

The third of these principles is introduced below, and we believe it is central to the avoidance of significant errors in model-based uncertainty quantification.

## 5.3 Bias

### 5.3.1 The Limits of Rationalism

The rationalist approach, described above as the ‘best-guess’ method, is effectively simple forecasting – and puts faith in the ability of an individual or team to make a reasonably precise judgement in the absence of sufficient data. If presented as the best judgement of a group of professional experts this appears reasonable. The weak point is that the best guess is only reliable when the system being described is well ordered and well understood, to the point of being highly predictable (Mintzberg 1990). It must be assumed that enough data is available from past activities to predict a future outcome with confidence, and the system being modelled is broadly stable. This is generally not the case in subsurface analysis, in spite of which there is a strong tendency for individuals, teams or managers to desire a best guess, and to subsequently place too much confidence in that guess (Baddeley et al. 2004). This is

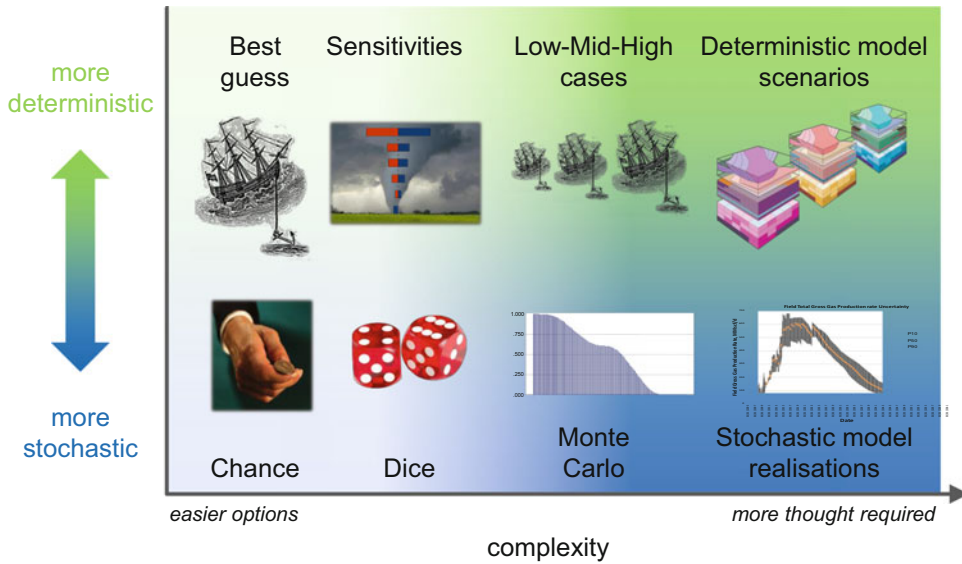


**Fig. 5.11** Quantification of uncertainty – choices

especially the case if that outcome gives comfort to a preferred decision (Bentley 2015).

It is often stated that for mature fields, a simple, rationalist approach may suffice because uncertainty has reduced through the field life cycle. This is also a fallacy. Although, the *magnitude* of the initial development uncertainties such as ultimate recovery tends to decrease with time, we generally find that as the field life cycle progresses new, more subtle, uncertainties arise and these now drive the decision making. For example, in the landscape image in Fig. 5.5, 100 samples would significantly improve the ability to describe the image, but this is still insufficient to specify the location of an unsampled house, which is key if the purpose is to locate the last house. Furthermore, some uncertainties systematically *increase* over the life cycle, simply because of our intervention in reservoir, such as injecting water. The injection pattern is simple at the start of field life but can become very complex in mature fields and locating a floodfront is key to choosing late life infill targets; the impact of uncertainties in terms of their ability to erode value may be as great near the end of the field life as at the beginning (Fig. 5.12).

We would argue that field life-cycle uncertainty is *U-shaped*: impacts on commercial decisions can be as great at the end of field life (infill drilling, EOR campaigns, decisions on

cessation of production or asset sale) as they are at start of field life when development planning is taking place (Fig. 5.13).

Despite this, rationalist, base-case modelling remains common across the industry, particularly in mature fields. In a review of 90 modelling studies conducted by the authors and colleagues across many companies, field modelling was based on a single, best-guess model in 36% of the cases (Smith et al. 2005). This was the case, despite a bias in the sampling from the authors' own studies, which tended to be scenario-based. Excluding the cases where the model design was made by the authors, the proportion of base case-only models rose to 60%.

### 5.3.2 The Limits of Geostatistics

Geostatistical simulation allows definition of ranges for variables, followed by rigorous sampling and combination of parameters to yield a range of results, which can be interpreted probabilistically. If the input data can be specified accurately, and if the combination process maintains a realistic relationship between all variables, the outcome can be good.

In practice, however, input data is imperfectly defined and the 'reasonableness' of the automated combination of variables is hard to verify.

**Fig. 5.12** Uncertainty vs. the field life cycle: ranges for some parameters generally decrease over time, such as ultimate recovery, whereas others increase, such as the distribution of injected water in a waterflood

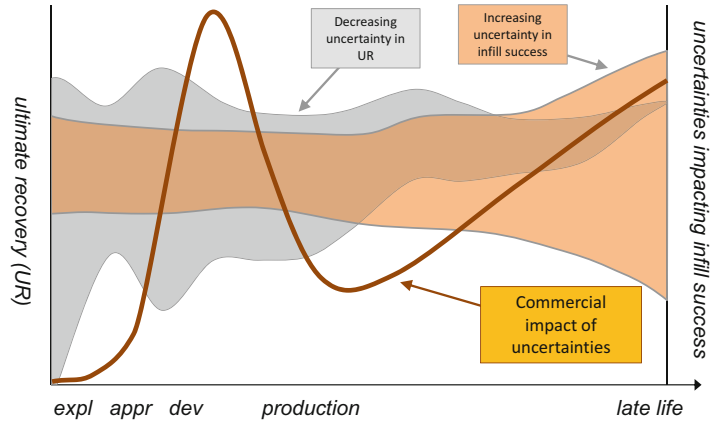
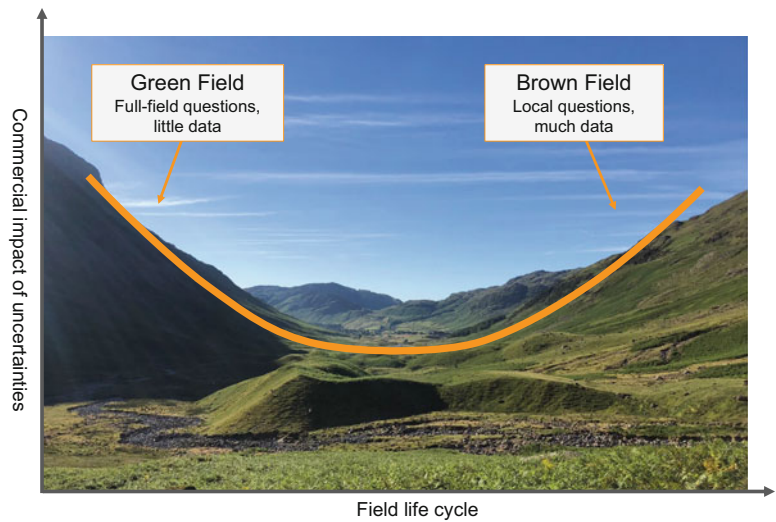


**Fig. 5.13** Uncertainty vs. the field life cycle: ‘U-shaped’



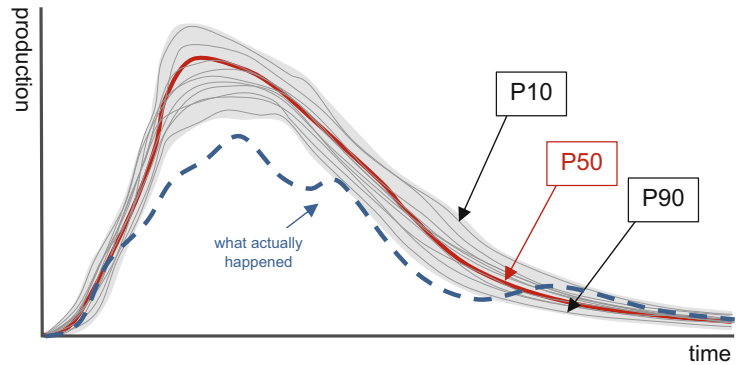
Statistical rigour is sometimes applied to data sets which are not statistically significant and an apparently exhaustive analysis may have been conducted on insufficient data. This is not a weakness of the geostatistical tool, it is a shortcoming of incomplete data followed by unwise application. Recall the geostatistical guidance from Pyrcz and Deutsch (2014):

Geostatistical methods aim to reproduce (the) input statistics; geostatistical models have no predictive power with respect to these statistics.

The geostatistical tools can only work with the conceptual starting point(s) provided. A common

pitfall is to make an exhaustive ensemble of realisations based around a single concept. No matter how many realisations are run, they are all rooted in the same base concept and although P90, P50 and P10 forecasts can be extracted from the ensemble, these are only P90-50-10 in the context of the parameters provided, and usually assume equiprobability of all realisations (which cannot be proven). If the underlying best guess concept is significantly in error the extracted forecasts are meaningless (Fig. 5.14). An approach like the one shown in Fig. 5.12 would have yielded a better outcome.

**Fig. 5.14** A probabilistic ensemble for field lifecycle production forecasts based around a single erroneous concept; the shaded area represents a cloud of forecast realisations: wrong several hundred times instead of just once



The validity of a statistical outcome may also be weakened by centre-weighting of the input data to variable-by-variable best-guesses, which creates an inevitability that the ‘most likely’ probabilistic outcome will be close to the initial best guess (Wynn and Stephens 2013). The geostatistical simulation itself is thus ‘anchored’.

We therefore argue that the application of geostatistical simulation does not in itself compensate for a natural tendency towards a rationalist best guess – it often tends to simply reflect it. Simulations which anticipate alternative concepts would require a form of artificial intelligence which is currently unavailable to reservoir and simulation modellers, although new machine learning approaches may evolve to address this need. The crucial step is therefore to select a workflow which removes the opportunity for anchoring on a best guess and avoids other sources of bias in the workflow itself.

### 5.3.3 Cognitive Limits – Heuristics

Human bias is a principal source of error in forecasting, arguably the largest. Most modellers have anecdotes about failed projects and missed opportunities, painful at the time, amusing in the re-telling but ultimately not useful in terms of improving performance. Progress has been made in the social sciences, however, in the elucidation of common patterns of behaviour (biases), mostly stemming from the work of Tversky and

Kahneman (1974), built on by many others and summarised in Kahneman (2011). They define ‘heuristics’ as:

a simple procedure that helps find adequate, though often imperfect, answers to difficult questions.

Once identified, named and recognised in a study, the opportunity arises to correct for biases, or define workflows which avoid the bias altogether. Four common heuristics, widely identified and understood in general science, have a particular bearing on reservoir and simulation modelling. These are described below.

*Anchoring and adjustment:* anchoring has been mentioned earlier in this section as the process of selecting a best guess in the face of uncertainty. Even when trying to establish a range of outcomes, once an initial preference is anchored upon we find it hard to embrace significantly different alternatives; if we adjust away from the initial guess to establish a range, such as in low-mid-high case modelling, the tendency is to remain too close to the original anchor point: ‘anchoring and adjustment’.

This is illustrated in Fig. 5.15, which shows the results from volumetric estimates made using a case study by individuals on a series of training courses (see also Chellingsworth et al. 2011). The parameter being estimated is field volume (STOIIP, MMstb) and each of the 191 blue lines represent the P90-P10 volume range estimated by one individual – an estimate made at the 80% confidence level. Individuals were asked to make their best estimate first, and were provided

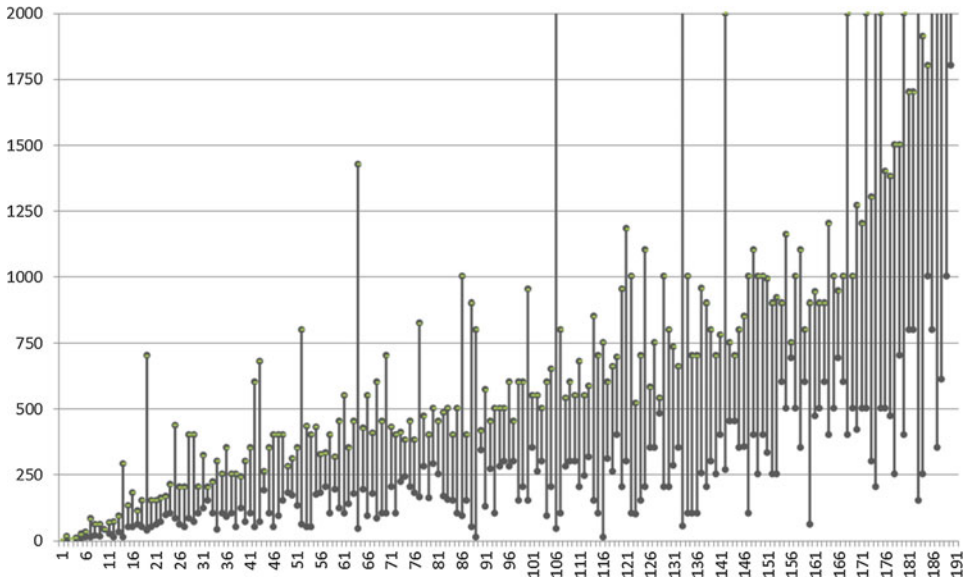


**Fig. 5.15** Individual low case (P90) and high case (P10) estimates of an oil field STOIIP (MMstb)

with map and log data to achieve this. They were then asked to estimate P90 and P10. If the estimates were accurate, the blue lines would largely overlap. They clearly do not.

The extreme cases clearly represent calculation errors, but even excluding these, the estimates (with one or two notable exceptions) are generally too narrow. The ‘truth case’ model for the field had a volume of 474 Mstb. In order for 80% of the group to bracket the truth case with their estimates, the P10s have to be doubled and the P90s halved. There is a factor 2 error in the high/low case adjustments.

*Availability* is a heuristic which explains in part why our anchor points often go down in the wrong place. Availability is defined as the error of mistaking the *ease* with which something comes to mind with its *likelihood*. For statistically-led modelling, the principal ‘available’ influence is the data itself. Reflection to the adage that data  $\neq$  model  $\neq$  truth is a prompt to consider whether the data set is truly a fair statistical sample – it usually isn’t. For concept-led modelling, the available knowledge is often a recent field study which is still fresh in the mind. It helps to reflect in a peer review setting whether our current model is simply reflecting the

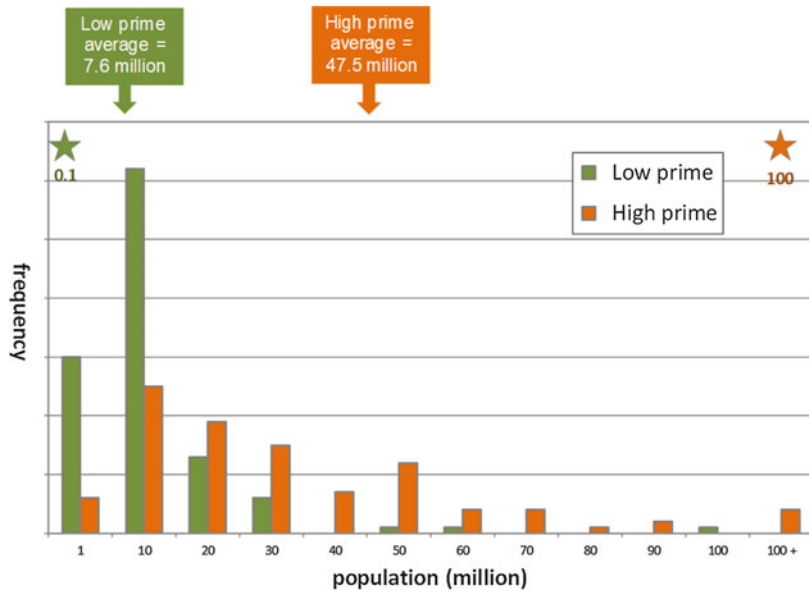
recent experiences of the new modellers. This draws on the expertise of domain experts, which itself comes with an associated and familiar heuristic: overconfidence.

*Overconfidence* is a heuristic related to the inability to adjust sufficiently away from an anchor point. In subsurface engineering generally, which is characterised by niche skills, expert advice will be given and it is a requirement of the modelling team to decide whether this is advice based on expertise (useful) or bias (not useful) (Kahneman 2011). A well-publicised exhaustive study of 28,000 estimates made by experts in the field of professional forecasting showed no correlation between their forecasts and the subsequent real-world outcomes (Tetlock 2007). However, Tetlock and Gardner (2015) identify ‘super-forecasters’ who are able to consistently overcome heuristics such as availability and overconfidence and analysed their approach. The outcome is a challenge to us all as success appears to lie with individuals who are consistently *open-minded, careful, curious and self-critical*.

*Affect* is another heuristic which causes anchors to be placed wrongly, and which also encourages overconfidence. Slovic et al. (2007) identified the tendency for probability to be



**Fig. 5.16** The priming effect: 1150 individuals asked to estimate a country's population but first primed with an unreasonably low or high suggestion: although unreasonable, the prime anchors a subsequent estimation resulting in a sixfold difference between the high- and low-prime groups



biased according to whether a particular outcome is 'liked'. The case in his study involved views concerning the risks associated with nuclear power, and showed that individuals who were predisposed in favour would consider benefits to be high and risks to be low, and visa versa. *Affect* has a place in model-based field studies, in which optimistic or pessimistic model outcomes are favoured not because they are conceptually more or less reasonable or statistically more or less likely, but because they are personally 'liked', or they support a preferred management view or perhaps support a decision which has already been made. *Affect* is therefore a causative factor of 'modelling for comfort' (Bentley 2015) and best resolved by stringent peer review from unbiased experts.

*Priming* is a behaviour which illustrates our general susceptibility to bias, and which is commonplace in groups when individuals are exposed to the opinion of others. Fig. 5.16 shows the results of a simple priming exercise run during our courses, involving the estimation of a country's population. Groups are given one or two prior estimates to consider, one very high (100 million) and one very low (100,000) and then asked to make a better best guess. Based on a dataset of 1150 individuals, those with the high

prime are averaging a best guess of 47.5 million, and those with the low prime 7.6 million, a factor of approximately 6 different. We are easily primed.

Overcoming these common heuristics makes a case for good quality peer review. 'Good quality' in this case is the joint identification of these named behaviours, and is preferable to reviews which simply offer additional subjective opinion. The process can also be helped by using a workflow which does not expose the modelling process to strong biases, notably anchoring. The suggested approach is scenario-based, which can be used as the basis for a multi-deterministic or multi-stochastic workflows. Both are grounded in a simple uncertainty list, described below.

## 5.4 Towards an Unbiased Methodology

We therefore have an array of methods at our disposal for quantifying uncertainty but limits in terms of the capabilities of statistical methodology (given our generally insufficient data sets) and our cognitive ability to avoid bias in the choice of scenarios to explore.

A recommended approach, before any significant modelling starts, is to work the list of key uncertainties interactively, express these in some simple format such as a probability or scenario tree, then choose an efficient methodology to build a suite of models. These first steps require some careful thought, as discussed below.

### 5.4.1 The Uncertainty List

The key to success for any form of multi-model building approaches (deterministic scenarios *or* statistical ensembles) lies in deriving an appropriate list of key uncertainties, a matter of experience and unbiased judgement. However, there is a strong tendency to conceptualise key uncertainties for at least the static reservoir models in terms of the parameters of the in-place fluid estimation, *i.e.* when asked to define the key uncertainties in the field, modellers will often quote parameters such as ‘porosity’ or ‘net sand’ as key factors. If the model-build progresses with these as the key uncertainties to test, this will most likely be represented as a range for a continuous variable, anchored around a best guess.

A better approach is to question why ‘porosity’ or ‘net sand count’ are considered significant uncertainties. It will either emerge that the uncertainty is not that significant or, if it is, then it relates to some underlying root cause, such as heterogeneous diagenesis, or some local facies control which has not been extracted from the data analysis.

For example, in Fig. 5.17 a probability density function (PDF) for an uncertain net-to-gross parameter is shown. A superficial approach to model uncertainty would involve taking the PDF, inputting it to a geostatistical algorithm and allowing sampling of the spread (commonly assumed to be Gaussian) to account for the uncertainty. As the figure illustrates, this would be misleading, because the range is underpinned by alternative geological concepts. The real need is to understand the depositional environment, and build contrasting, but realistic, architectural models – the basis for two scenarios. The uncertainty in the net-to-gross

parameter within each scenario is a higher level consequence of the underlying uncertainty in depositional environments, and will probably not be Gaussian.

In defining key uncertainties, the need is therefore to chase the source of the uncertainty to the underlying causative factor – ‘root cause analysis’ – and model the conceptual range of uncertainty of that factor with discrete cases, rather than simply input a data distribution for a higher level parameter such as net-to-gross.

### 5.4.2 Scenario Trees

A convenient way to express the final selection of root cause uncertainties is to arrange them in a simple ‘scenario tree’. These are comparable to the decision trees described by Bratvold and Begg (2010) but simpler in that there are no decision nodes, just a hierarchical description of uncertainties, optionally with associated probabilities added. The rationalising process is important as it prompts a conversation about the significance of issues raised in the context of the modelling purpose (Chap. 1) and is the opportunity to reduce the number of scenarios and better see the ‘wood from the trees’.

An example is given below from a study in which eight uncertainties are initially identified – the ‘long list’ covering both static and dynamic model parameters established to be important for the field development (Fig. 5.18). For each case, alternative high/low cases are defined, avoiding the heuristic of anchoring on a preferred best guess. Even without the unnecessary mid-case, if the eight uncertainties are viewed as independent, such that any high/low case can be combined, there are  $2^8 = 256$  alternative cases which can be defined – a large number. In order to avoid unnecessary modelling, the short list can be rationalised into a long list by considering the following:

- Are these all *root cause* uncertainties?
- Are some issues *insensitive* in the context of the model purpose?

**Fig. 5.17** Root-cause analysis: defining the underlying causative uncertainty. (Redrawn from Bentley and Smith 2008, The Geological Society, London, Special Publications 309 © Geological Society of London [2008])

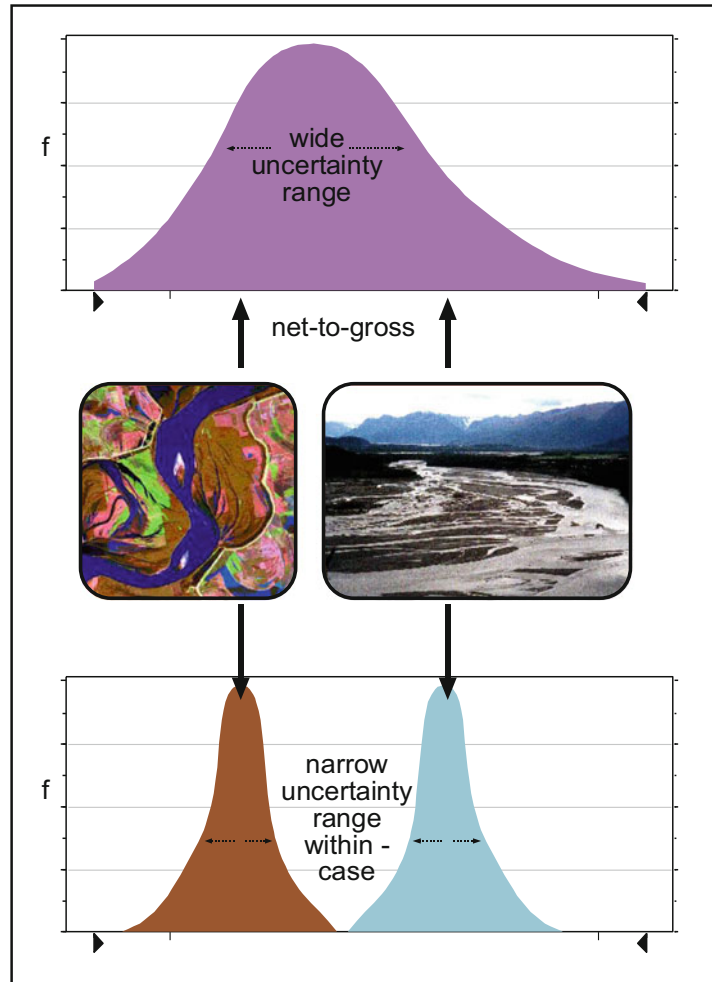


**Fig. 5.18** Initial long-list of uncertainties identified in a study of a channelised system under water injection: yellow boxes are static model uncertainties, blue boxes dynamic model uncertainties

|   |  |
|---|--|
| Flanks <i>shallow</i><br><i>deep</i>            | NTG <i>high</i><br><i>low</i>                                      |
| Contacts <i>common</i><br><i>stacked</i>        | Sand dist. <i>amalgamated sheets</i><br><i>non-amalg. channels</i> |
| Faults <i>sealing</i><br><i>open</i>            | Rel Perms <i>favourable</i><br><i>unfavourable</i>                 |
| Fluids <i>single API</i><br><i>variable API</i> | Injectivity <i>good</i><br><i>poor</i>                             |

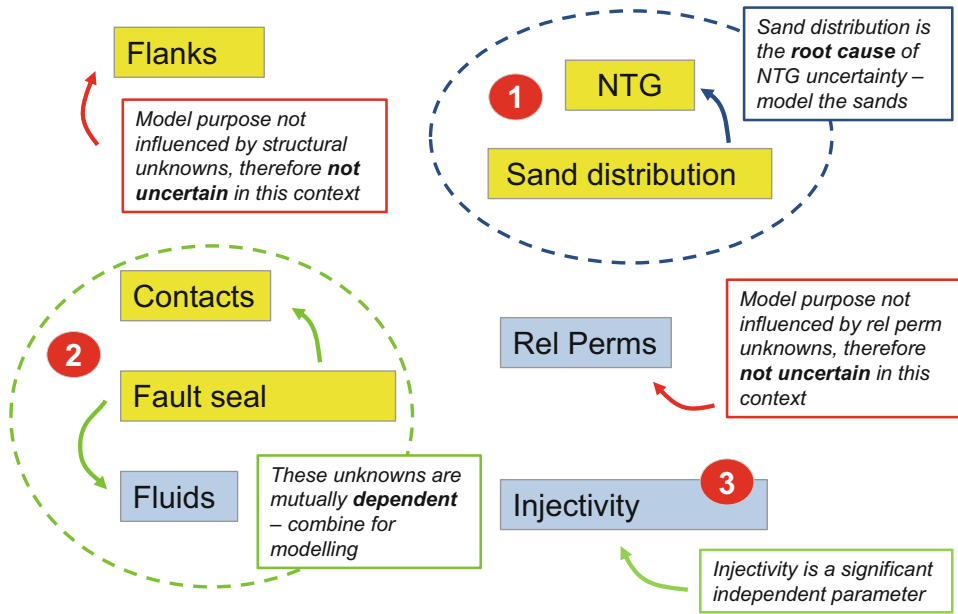


**Fig. 5.19** The long-list from Fig. 5.18 reduced to a short-list of three key uncertainties

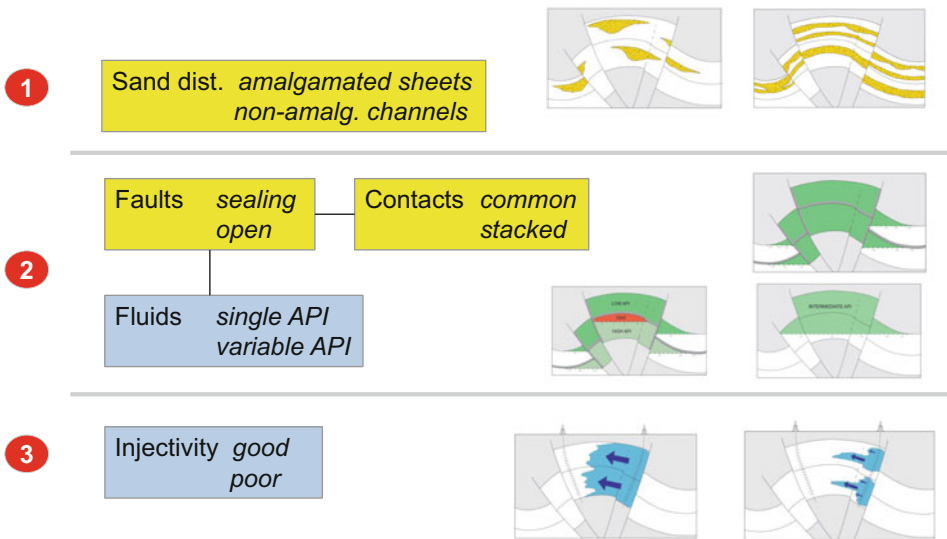


**Fig. 5.20** The three short-listed key uncertainties from Fig. 5.18, sketched

- Are some issues *dependent*, in which case they should be handled together in the context of a shared root cause?

Figure 5.19 offers an analysis of the long-list of the eight uncertainties in Fig. 5.18 and reduces it to a short-list of three once root cause,

dependency and sensitivity vs. model purpose are taken into account.

The three short-listed uncertainties from Fig. 5.19 are rearranged and sketched as a reality check: *if you can sketch it, you can model it* (Fig. 5.20) and presented as a scenario tree in Fig. 5.21.

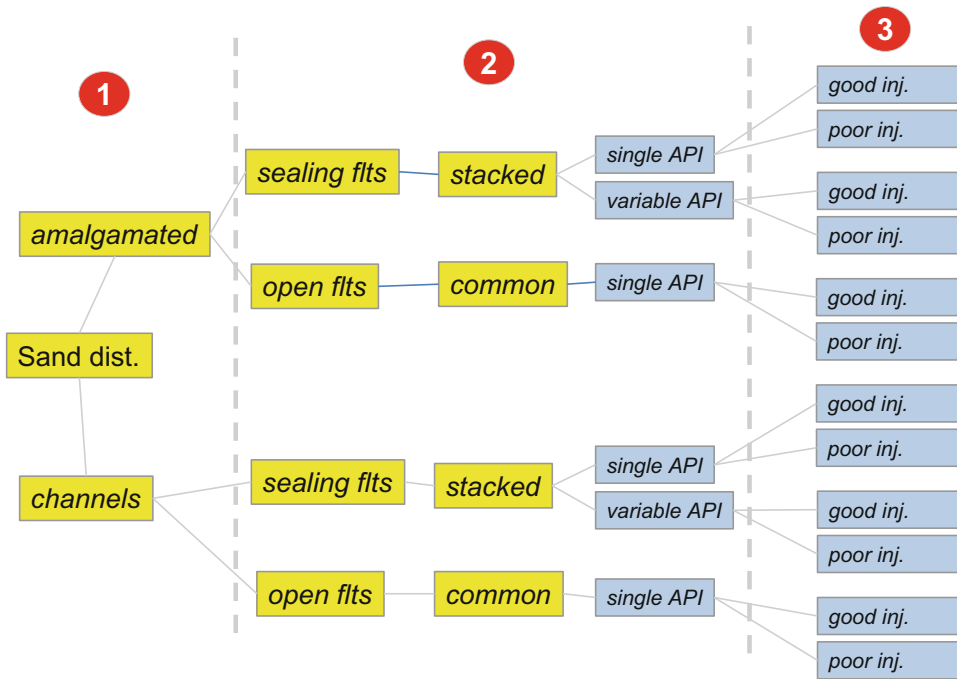


**Fig. 5.21** A scenario tree, laying out the original unknowns in terms of the three key uncertainties in Fig. 5.20

The scenario tree presents 12 independent cases. The process presented has generated a range of outcomes without anchoring on a best guess up-front, and the rationalisation itself has provided opportunities to sense check the significance of unknowns in a cross-discipline environment, where the other common heuristics can be considered.

The 12 cases can either be run and viewed as a multi-deterministic 12-model ensemble then used directly as the basis for scenario modelling, or they can be used as the basis for a building a larger, statistical ensemble.

Before embarking on either of these approaches, it is worthwhile simply running the most and least favourable cases and checking the outcome against the decision being made – the original purpose of the modelling. If the same decision would be made in any outcome, then the decision has been arrived at!

The remaining purpose of modelling is then simply to run out a forecast range to accompany the decision, if required, and at this point (the end of the work) a reference case for planning can be

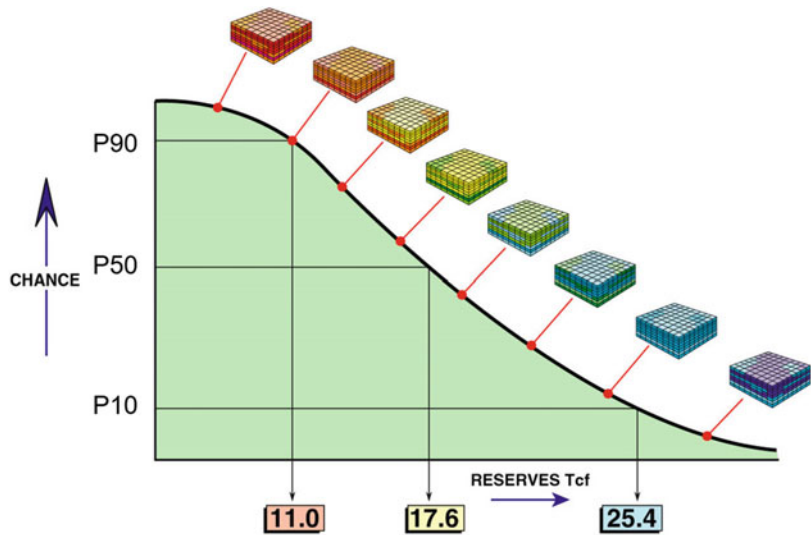
selected, if needed. This brings us to the final, non-trivial issue of how to post-process the results of our chosen methodology and extract forecasts which can be used to give quantitative estimates of resources as a guide to decision-making.

## 5.5 Post-processing the Ensemble

After a few multi-modelling iterations, whether multi-deterministic or multi-stochastic, it is common to accumulate a very large number of model realisations. The full ensemble is rarely a deliverable in itself, and results must be distilled into forecast ranges, often specifically a reference case (with or without a range) or in the form of P90-P50-P10 estimates for accounting subsurface fluids, whether these be extracted hydrocarbons or stored fluids or both. This raises the question of how to post-process the ensemble, and what meaning to put on the values.

A number of post-processing options are described below and surrounding issues are discussed.

**Fig. 5.22** Resource ranges based on multi-deterministic scenarios



### 5.5.1 Scenarios

Of the multi-modelling approaches described in the sections above, the most transparent and easy to communicate is the small ensemble of deterministic scenarios. Each is clearly linked to an underlying concept, dependencies are clearly maintained through the modelling process and the validity of each of the cases can be discussed and discarded if wished. The range is clearly defined by the spread of scenarios, and any end-member cases which are considered too extreme can be removed (whilst cognicant of the pitfalls of the overconfidence and affect heuristics from Sect. 5.3.3). Preferred cases can be selected for planning, as appropriate.

The difficulty comes when presenting statistical measures such as P90-P50-P10. Fig. 5.22 shows a suite of 8 scenarios, considered equiprobable and arranged in order of outcome on a reverse cumulative plot which is labelled following a convention of P90 as the low case and P10 as the high.

As the number of cases is small the choice of a near-median case as ‘P50’ carries some logic but the attribution of ‘P10’ and ‘P90’ labels is clearly arbitrary. For a small number of scenarios the lowest and highest cases are often simply taken as the P10 and P90: an instance of applying statistical labels in a non-statistical situation.

The ‘scenario approach’ as presented here (and as outlined in Bentley and Smith 2008) is essentially a non-statistical procedure designed to establish a range of outcomes, not anchored on a base case. The allocation of P90-P50-P10 terminology is subjective and should be declared as such in reporting. It should be noted, however, that low-mid-high case modelling carries even less statistical rigour and simple base case modelling carries none. In this respect ‘scenarios’ is a more robust method of generating a range and selecting reference cases for onward planning and reporting.

### 5.5.2 Exhaustive Deterministic Ensembles

One way of overcoming the lack of statistical rigour in a small ensemble of scenarios is simply to run many more. Examples of this are illustrated in Figs. 5.23, 5.24 and 5.25. Fig. 5.23 shows the outline structure to a probability tree built from the long-list of uncertainties rather than a rationalised short-list (Chellingsworth and Kane 2013).

The tree in Fig. 5.23 yielded 324 independent model realisations, run by combining deterministically-constructed cases in a software workflow manager, without any probabilistic

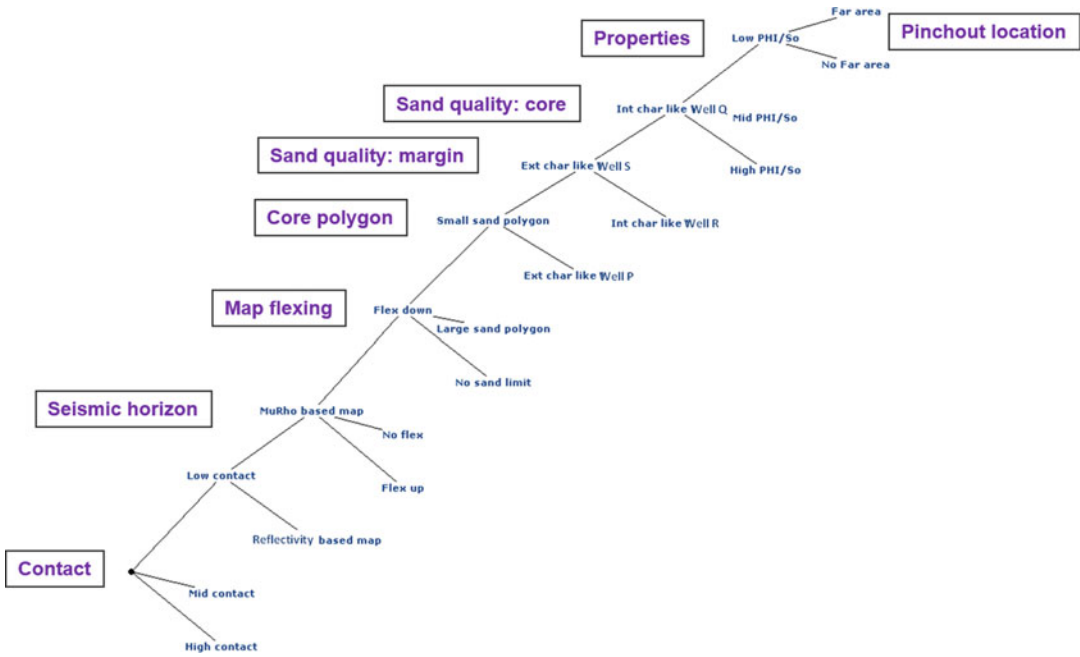


**Fig. 5.23** A large probability tree based on an uncertainty long-list

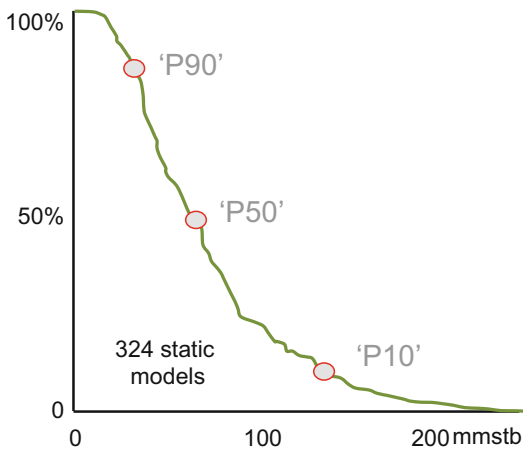


**Fig. 5.24** Reverse cumulative for an exhaustive multi-deterministic model ensemble (Chellingsworth and Kane 2013)

sampling of input parameters. The resulting realisations are shown in Fig. 5.24 on a reverse cumulative plot.

In this case, equiprobability has not been assumed, but weights have been applied to each case based on an uncertainty-by-uncertainty peer-

assisted discussion. P90, P50 and P10 percentiles are then extracted from the weighted ensemble of realisations.

This approach requires more manual model management than that in Sect. 5.5.1 but offers a more statistically valid ensemble of models, whilst maintaining the benefits of concept-driven, un-anchored, scenario-based models.

### 5.5.3 Variance Mapping

Simpler tools can offer a powerful way of illustrating results to support specific decisions. An example of this is illustrated in Figs. 5.25 and 5.26: a map of variance.

This is taken from a small multi-deterministic ensemble of 7 short-listed cases. The model purpose is to quantify a range of volumetric uncertainty during an appraisal programme and illustrate quantitatively where best to target appraisal wells in order to narrow the volume range for development planning. Each model case is run and a model of the hydrocarbon

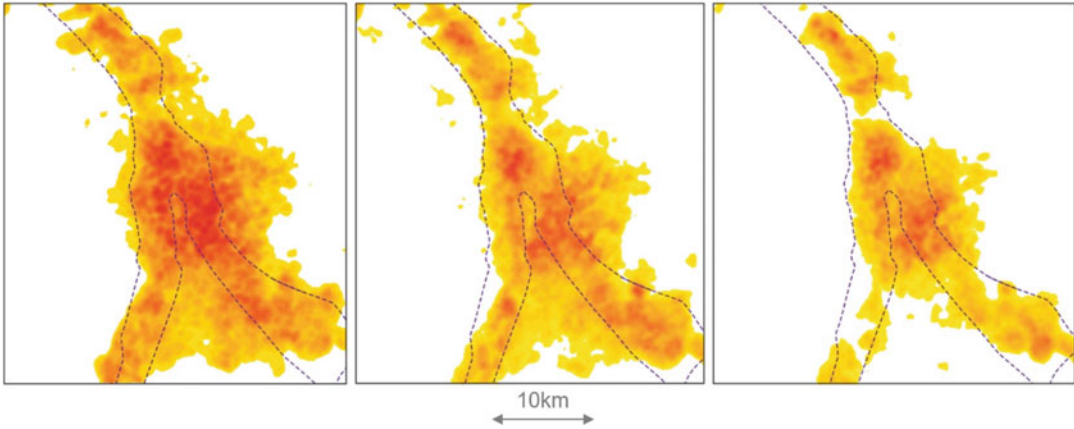


**Fig. 5.25** Example realisations for hydrocarbon distribution from a multi-deterministic ensemble based on underlying uncertainties in sand distribution and reservoir

quality; the mapped property is equivalent hydrocarbon pore column, with longer columns represented by hotter colours

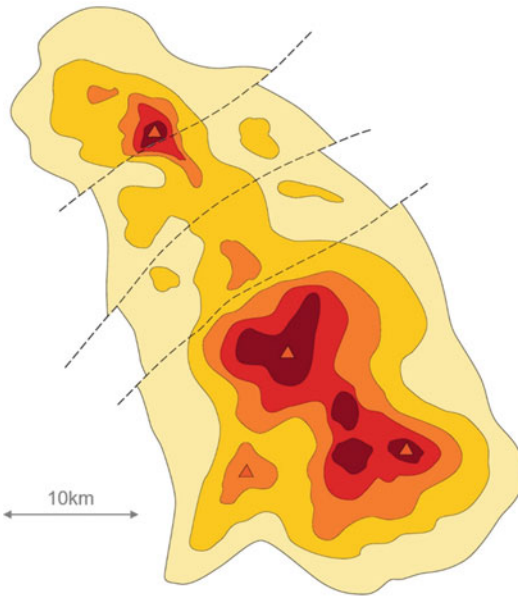


**Fig. 5.26** A variance map, showing the spread of volumetric results from the multi-deterministic ensemble; hot colours indicate areas where uncertainty is highest and hence where appraisal wells (shown as triangles) are best targeted to reduce volumetric uncertainty

distribution is made, and converted into a hydrocarbon pore column model, three of which are shown in Fig. 5.25. The pore column property has been derived from models capturing

alternative concepts for sand distribution (the prime uncertainty) with associated reservoir quality properties, and naturally reduces to zero at the (known) hydrocarbon-water contacts.

A logical expression applied to the pore column property in a model calculator finds the minimum and maximum column at each vertical location, which can then be presented as a 2D map showing where the spread in volumes is occurring – a simple measure of variance (Fig. 5.26).

Assuming the (unbiased) expert knowledge of the field has gone into the selection of key uncertainties and their low/high alternatives have been reasonably defined without *overconfidence* and limited *adjustment*, then the alternative deterministic concepts for sand distribution and consequent property variation which drive the results are a good reflection of the volumetric uncertainty in the field. The workflow compared the alternative models with no recourse to a base case or best guess, reducing the susceptibility to *anchoring*. The simple map in Fig. 5.26 therefore captures in one image the sum total of the useful knowledge pertinent to the question in hand, and puts the asset team in a good place for practical decision-making. Four appraisal wells were located and drilled based on this map.



### 5.5.4 Sampling Probabilistic Ensembles

A very large model ensemble can be more quickly and efficiently generated by probabilistic sampling of input parameters, as described in Sect. 5.2. The approach offers a statistically rich ensemble from which reference model(s) can be extracted for onward modelling, usually by organising all the realisations in rank order and selecting the 10th, 50th and 90th percentiles, as illustrated in Fig. 5.14. The difficulty is that models close to those percentiles can vary dramatically in nature and different models which have roughly the same outcomes for one analysis, such as ultimate recovery, may have very different outcomes when passed forward for a subsequent part of the analysis such as surface engineering.

Moreover, as discussed in Sect. 5.3.2, the apparent rigour of extracting statistical percentiles is undermined by the unprovable assumption of model equi-probability, even assuming all the statistically sampled cases are valid and that uncertainty space has been fully sampled (including all the trees).

Better approaches of extracting measures from ensembles are described in the following sections.

### 5.5.5 Experimental Design and Sensitivity Analysis

Methods for linking deterministic concepts with probabilistic outputs are a desirable solution to link the non-statistical world of scenarios with the statistical rigour of the multi-stochastic workflows. One method of attempting this is using Experimental Design ('ED') – a well-established technique in the physical and engineering sciences (e.g. Box and Hunter 1957) more recently applied in reservoir modelling and simulation studies, e.g. Egeland et al. 1992; Yeten et al. 2005; Li and Friedman 2005.

The broad approach is to define key uncertainties and run a small number of cases to determine a functional relationship between the

uncertainties ('factors') and the model outcome ('the 'response') and use multiple runs of the proxy function to generate the statistical spread. The type of design depends on the purpose of the study and on the degree of interaction between the variables. A simple approach is the Plackett-Burmann formulation, which assumes no interactions between the variables and that a relatively small number of experiments are sufficient to approximate the behaviour of the system. More elaborate designs such as D-optimal or Box-Behnken (e.g. Alessio et al. 2005; Cheong and Gupta 2005; Peng and Gupta 2005), attempt to analyse different orders of interaction between the uncertainties and require a significantly greater number of experiments. The value of elaboration in the design needs to be assessed – *more is not always better* – and depends on the model purpose, with some practitioners using ED simply as a screening tool to determine the significance of specific uncertainties – a sensitivity analysis.

A useful aspect of a simple ED is that the workflow involves careful consideration of each uncertainty independently, so can work from an uncertainty short-list, and starts by working with end-members so is intrinsically not anchored from the start. There need be no base case up-front.

The combination of Plackett-Burmann ED with the scenario-based approach is illustrated by the case below from a mature field re-development plan involving multiple-deterministic scenario-based reservoir modelling and simulation (Bentley and Smith 2008). The purpose of the modelling was to build a series of history-matched models that could be used as screening tools for a field development.

As with all scenario-based approaches, the workflow started with a listing of the uncertainties, which in this case were deemed to be:

- top reservoir structure;
- architectural connectivity;
- thin-bed effectiveness;
- sand quality;
- reservoir orientation and
- fluid contacts.

| Realisation | Structure | Quality | Contacts | Architecture | Thin beds | Orientation | Response |
|-------------|-----------|---------|----------|--------------|-----------|-------------|----------|
| 1           | -1        | 1       | 1        | 1            | -1        | 1           | 1178     |
| 2           | -1        | -1      | 1        | 1            | 1         | -1          | 380      |
| 3           | -1        | -1      | -1       | -1           | -1        | -1          | 109      |
| 4           | 1         | -1      | 1        | 1            | -1        | 1           | 1105     |
| 5           | -1        | -1      | -1       | 1            | 1         | 1           | 402      |
| 6           | 1         | -1      | 1        | -1           | -1        | -1          | 1078     |
| 7           | 1         | 1       | -1       | 1            | 1         | -1          | 1176     |
| 8           | 1         | -1      | -1       | -1           | 1         | 1           | 1090     |
| 9           | -1        | 1       | -1       | -1           | -1        | 1           | 870      |
| 0           | -1        | 1       | 1        | -1           | 1         | -1          | 932      |
| 11          | 1         | 1       | -1       | 1            | -1        | -1          | 1201     |
| 12          | 1         | 1       | 1        | -1           | 1         | 1           | 1245     |
| 13          | 0         | 0       | 0        | 0            | 0         | 0           | 956      |
| 14          | 1         | 1       | 1        | 1            | 1         | 1           | 1656     |

**Fig. 5.27** Plackett-Burmann matrix showing high/low combinations of model uncertainties and the resulting response (resource volumes in Bscf)

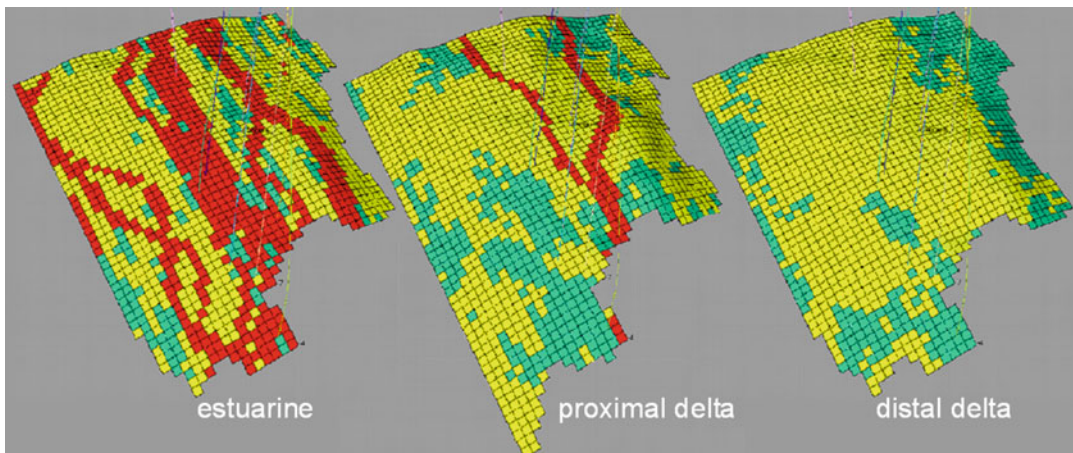


**Fig. 5.28** Alternative reservoir architectures (Images courtesy of Simon Smith). (Redrawn from Bentley and Smith 2008, The Geological Society, London, Special Publications 309 © Geological Society of London [2008])

These six uncertainties were combined using a 12-run Plackett-Burmann ED which specified alternative combinations of the uncertainties, assuming independence (Fig. 5.27). High cases for each uncertain factor are represented by +1, the low case by -1. In this case two additional runs were added, one using all the mid points from a previous best guess (represented by zeros) and one using all the low values as a sensitivity.

The 14 models were built (Fig. 5.28 shows samples of the three discrete cases for alternative

reservoir architectures) and the resource volume, or 'response', determined for each run. A linear least-squares function was derived from the results, capturing the relationship between the response and the individual uncertainties, the so-called 'proxy function' in which the relative impact of the individual uncertainties on the resource volumes is captured by a coefficient specific to the influence of each uncertainty.

The likelihood of each uncertainty occurring in between the defined end-member cases (between the '1' and the '-1') is reflected in

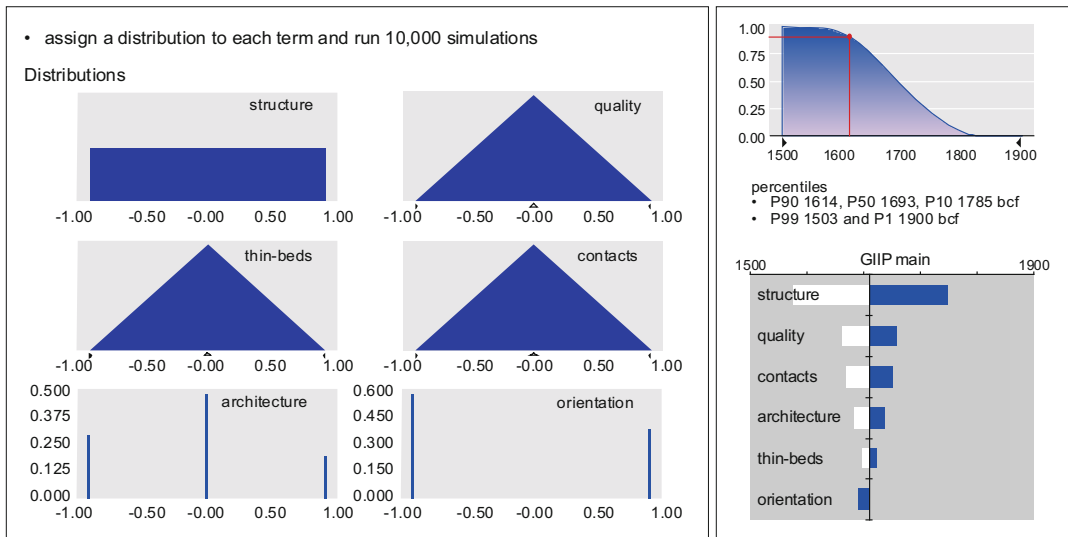


**Fig. 5.29** Parameter ranges and distribution shapes for each uncertainty and the resulting reverse cumulative ‘S curve’ and summary of sensitivities on a tornado plot

parameter distribution functions (Fig. 5.29) and parameters with a central tendency such as sand quality are distinguished from parameters with discrete alternative possibilities, such as the architectures illustrated in Fig. 5.28. The distributions are then sampled by standard Monte-Carlo analysis to generate a probabilistic distribution.

The attractions of the workflow are that it makes a link between discrete multiple-deterministic models and probabilistic reporting, it focuses on the end-members and therefore minimises the anchoring heuristic and it neatly captures sensitivities in tornado diagrams or simple spider plots which can be used to steer further data gathering.

The technique has its limitations however (see discussion in Caers 2011). A central point is that it has to be clearly reasonable to express the relationship between uncertainties and outcomes in a simple proxy function in the first place. A line can be fitted through any data set, even if the fit is a poor one. This is valid in situations in which the impact of factors vary smoothly in relationship to the response value, but is often not the case in geology where the underlying relationships are more complex: non-linearities, discrete step-

changes and hierarchy. The approach may nevertheless be useful as a screening tool and supports the thought process of pushing ranges wider than the overconfidence heuristic would otherwise encourage.

### 5.5.6 Clustering

Rather than reducing the ensemble to a proxy function another option, which also helps understand the ensemble response itself, is to spot patterns in the results: clustering.

Caers (2011) describes a process of unsupervised clustering, in which three clusters are identified in uncertainty space from a larger model ensemble (Fig. 5.30). The number of desired forward models is selected, in this case three, and entered into parameter space which is itself divided into three. The nodal points of each zone are then moved into the centre of the resulting clusters and parameter space is redefined accordingly. The large number of runs is thereby clustered and one realisation for each cluster is carried forward for further working.

A similar principle, but approached manually (deterministically) is simply to pick the clusters

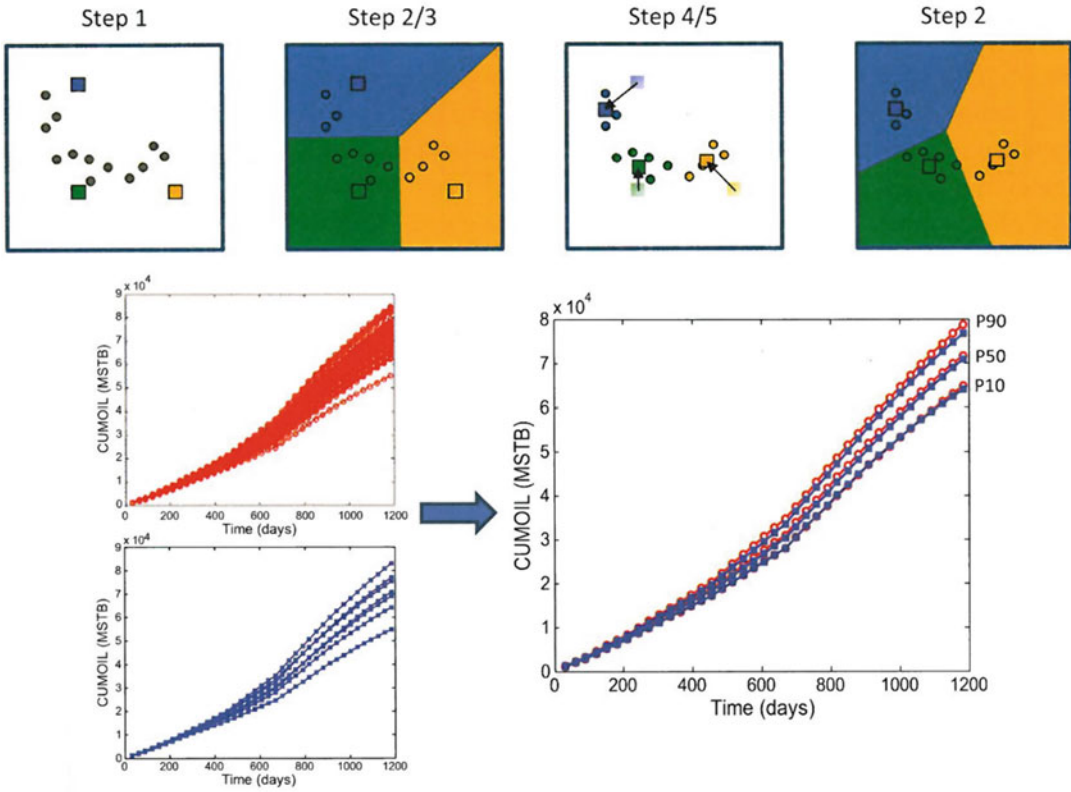
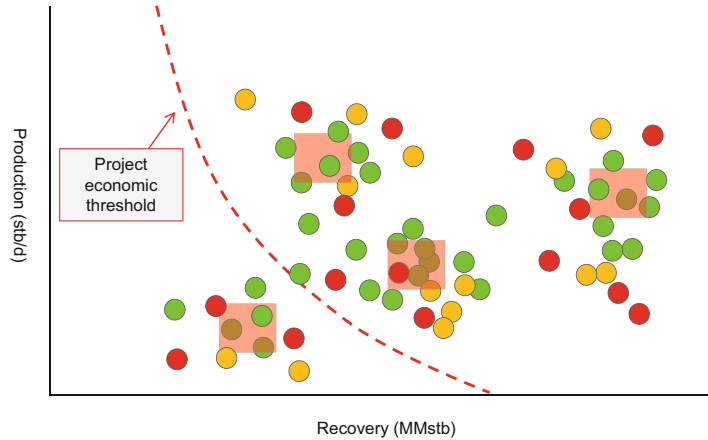


**Fig. 5.30** Unsupervised clustering, identification of three representative cases from a larger model ensemble. (Reproduced from Caers 2011)

**Fig. 5.31** Supervised clustering: manual selection of representative models from a multi-deterministic ensemble, plotted against the outcomes of interest (production and ultimate recovery) and an indication of the economic threshold of the project being studied



judged to be significantly contrasting. This is illustrated in Fig. 5.31 for a field study in which an infill strategy decision is being made (Oxlade and Bentley 2015). To support this, a number of

conceptually driven static/dynamic model pairs were run, with the significant outputs being ultimate recovery and field production rate. The model outcomes are therefore plotted against

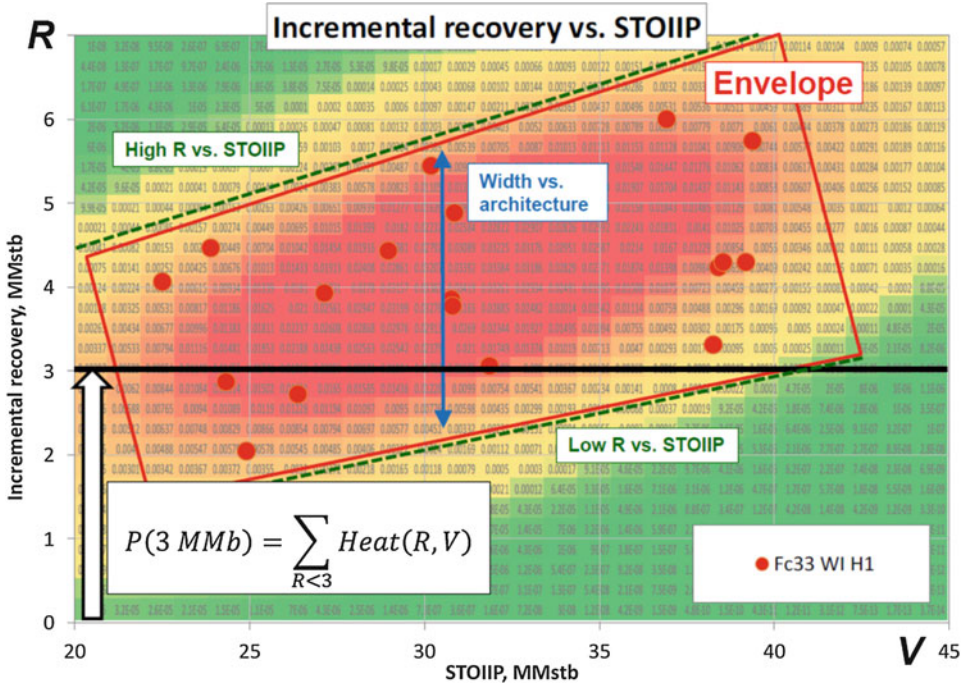


**Fig. 5.32** A heat map for identifying patterns in a spread of model ensemble results. Results are expressed in terms of volume and recovery and the parameters driving the envelope of outcomes are identified. Image courtesy of Ed Stephens

these outcomes and the spread on the plot in Fig. 5.31 is effectively a visual representation of uncertainty associated with the decision.

Project risk is illustrated by the red dashed line showing where the economic break-even points occur relative to those outcomes. Individual runs are colour-coded according to the ease with which the history match was achieved. The plot may already be enough to make the decision at hand but if further analysis is required, or representative forecasts generated, these can be chosen by picking usefully contrasting cases based on an understanding of the causative aspects which generate those results. In the case shown in Fig. 5.31 four are indicated: a failure case, a high success case and two cases which meet the economic hurdle but in different ways (one with better recovery and one with better rates).

If the clusters are not immediately obvious from a scatterplot, a ‘heat map’ may be useful, simply showing where in parameter space the greatest density of model outcomes are occurring. A heat map from a model ensemble for a mature

field study is shown in Fig. 5.32 based on Stephens (2015). In this case the outputs of interest are STOIP and incremental recovery, and a commercial threshold sits at a recovery of 3MMstb. The uncertainty can be quantified by defining an envelope around the cluster of results, the envelope having an associated spread of STOIP and recovery values. The probability (risk) of the project failing can be quantified from the ‘heat’ values themselves.

### 5.5.7 Updating Reservoir Uncertainty with New Information

What happens when new information arrives that changes your subjective view of the reservoir model? Changing the input data will obviously change the model, whatever approach you are using to handle uncertainty. Ideally we need a form of ‘supervised clustering’ that is influenced by the arrival of new data. The Bayesian statistical framework does exactly that, and offers a way

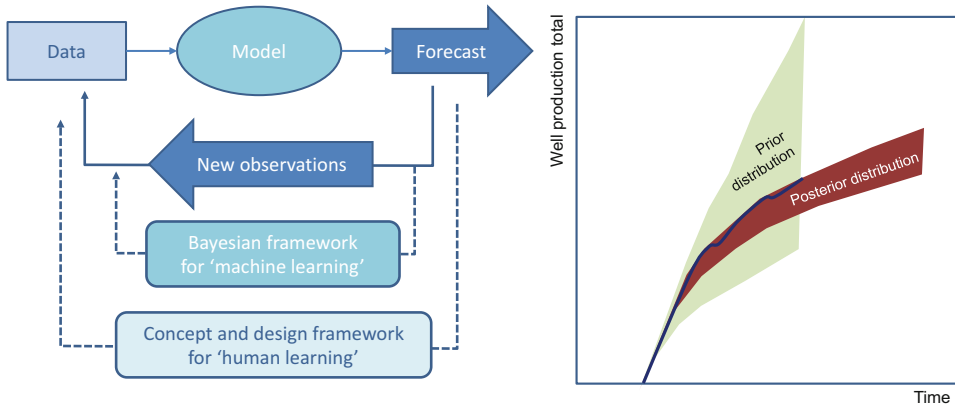


**Fig. 5.33** Reservoir forecasting with Bayesian updates (left), where a large initial range in forecasts (the prior) is updated using observed data (heavy line) leading to an

improved forecast with reduced uncertainty (the posterior). Right-hand sketch based on results from Seiler et al. (2011)

of forecasting where the ‘prior’ distribution is, adjusted using new data to define a modified ‘posterior’ distribution, e.g. Subbey et al. 2004; Wen and Chen, 2005. In adapting the general Bayesian formulation to reservoir forecasting, the Bayesian update can be posed as a *series* of updates where measured data are processed sequentially in time in a recursive sequence (Seiler et al. 2011). The statistical method for doing this is to use the Ensemble Kalman Filter (EnKF), an approach for updating complex datasets which is used in many branches of earth science (Evensen 2009.) The EnKF is a Monte Carlo approach which allows implementation of the Bayesian update by adjusting the covariance matrix. The concept is illustrated by the simple sketch in Fig. 5.33.

This approach has been widely used, and can be adapted to incorporate new production data (Wen and Chen 2005; Slotte and Smorgrav 2008), new geological information (Seiler et al. 2011) and observations from time-lapse seismic monitoring (Skjervheim et al. 2005). The approach is also readily adapted to automated ‘machine learning’ approaches for reservoir forecasting, where reservoir forecasting is run in a loop with regular updates as new data becomes available (Hanea et al. 2015).

While these modelling tools for handling uncertainty during forecasting potentially offer

the practitioner more speed and agility at handling a very complex data set, the human mindset and its inherent bias must not be forgotten in the process (Fig. 5.33). The underlying geological concepts and the reservoir model design should provide the overall ‘loop’ in the work process, and smart model update tools should be used to guide the reservoir modeller in what is ultimately a ‘human learning’ process.

### 5.5.8 Distinguishing and Illustrating Risk vs. Uncertainty

Risk and uncertainty are related terms and are often a source of confusion in subsurface discussions and decision-making. Reservoir modelling and simulation offer an opportunity to clarify (rather than confuse further) these terms, but some clear definitions are required. For most organisations:

- *uncertainty* is simply the inability to describe something accurately; the thing in question clearly exists, it just cannot be specified precisely;
- *risk* is highly contextual and requires careful definition; there must be a risk of something either happening or not happening – an impact, with an associated chance.

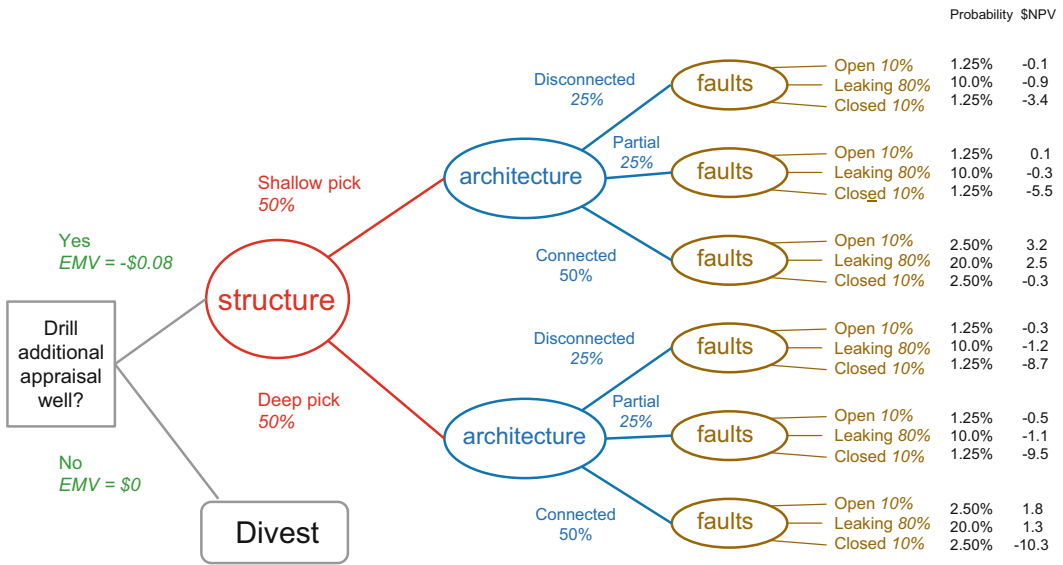


**Fig. 5.34** A decision tree quantifying risks and uncertainties associated with an appraisal drilling vs. divestment decision. Each of the outcomes is a static-dynamic model pair, overlain on which are the likelihoods. Combined with an estimate of the net present

value associated with each realisation and weighted with the associated probabilities, an expected momentary value (EMV) can be calculated (in this case negative, leading to the decision to divest the asset)

The plots in Figs. 5.31 and 5.32 distinguish subsurface uncertainties quantified by modelling from the project risks derived from those uncertainties. Once identified from modelling, a simple way of connecting the outcomes to the point of decision-making is by extending the scenario trees described in Sect. 5.4.2 to full decision trees (Bratvold and Begg 2010). Figure 5.34 shows a decision tree in which the value of drilling an infill well is assessed. Each branch of the tree is a model realisation. The probabilities attached to each branch, if not simply equal, can be informed by subjective judgement of the chances attached to the uncertain components of each realisation (in this case structure, reservoir architecture and fault transmissibility). With reference to some decision risk threshold, such as those illustrated in Fig. 5.31 and 5.32, the risk associated with the decision can be quantified.

The intent is to use modelling to expose risks as well as quantify uncertainty, to facilitate

communication and sometimes create discomfort before a key decision is made.

## 5.6 Summary

The hidden nature of the subsurface and the limitation of our sampling techniques means that all attempts to describe reservoirs carry significant uncertainty. These uncertainties have an impact on decisions made in relation to the subsurface, from quantifying subsurface resources to designing reservoir development plans or evaluating a storage scheme. Reservoir modelling and simulation aid in the description and quantification of these uncertainties and can be used to help mitigate risks which may significantly impact the success of a project.

However, there is no standard technique for quantifying uncertainty using reservoir and simulation models. Techniques vary from simple choice of low, mid and high cases to the building

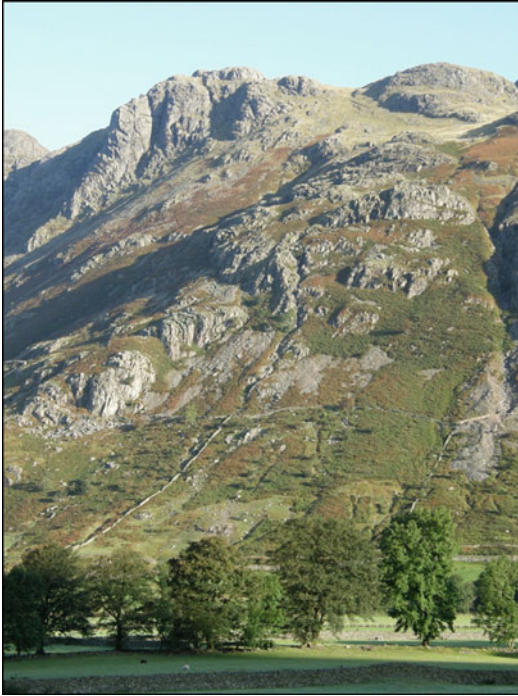


**Fig. 5.35** We can anticipate trees

of large model ensembles involving potentially thousands of runs. All techniques are preferable to building a single case, which is essentially just a guess.

Whichever technique is chosen, it is important to recall that each carries some subjective interpretational step, whether it is the obvious manual selection of a model to be the ‘P90’ or ‘P10’ case, or the more subtle input parameter range selection in a stochastic ensemble. In each case, it is important to understand which technique is being applied, how the models are being post-processed and where the subjective steps lie, such that they can be opened up to unbiased expert review.

Success in any of these techniques requires the identification of key uncertainties up-front. If the issues which could cause a business decision to fail are identified, then the modelling workflow will capture this and the decision risk can be mitigated or the decision changed. If a significant uncertainty is missed, no amount of modelling of any kind can compensate.

The key to success is therefore the formulation of the uncertainty list, including the identification

of issues not explicit in the current data set, but which can be anticipated with thought. There may be trees and the best chance of seeing them is to develop the mind-set of successful forecasters (Tetlock and Gardner 2015): analyse the problem and be *open-minded, careful, curious and self-critical* (Fig. 5.35).

## References

- Alessio L, Bourdon L, Coca S (2005) Experimental design as a framework for multiple realisation history matching: F6 further development studies. In: SPE 93164 presented at SPE Asia Pacific Oil and Gas conference and exhibition, Jakarta, 5–7 April 2005
- Baddeley MC, Curtis A, Wood R (2004) An introduction to prior information derived from probabilistic judgements: elicitation of knowledge, cognitive bias and herding. In: Curtis A, Wood R (eds) Geological prior information. Informing science and engineering, The Geological Society special publications, vol 239. The Geological Society, London, pp 15–27
- Bentley MR (2015) Modelling for comfort. *Pet Geosci* 22:3–10
- Bentley M, Smith S (2008) Scenario-based reservoir modelling: the need for more determinism and less anchoring. In: Robinson A et al (eds) The future of geological modelling in hydrocarbon development, The Geological Society special publications, 309. The Geological Society, London, pp 145–159
- Bentley MR, Woodhead TJ (1998) Uncertainty handling through scenario-based reservoir modelling. In: SPE paper 39717 presented at the SPE Asia Pacific conference on integrated modelling for asset management, Kuala Lumpur, 23–24 March 1998
- Box GEP, Hunter JS (1957) Multifactor experimental designs for exploring response surfaces. *Ann Math Stat* 28:195–241
- Bratvold RB, Begg S (2010) Making good decisions. Society of Petroleum Engineers, 207pp
- Caers J (2011) Modeling uncertainty in the earth sciences. Wiley (published online)
- Chellingsworth L, Kane P (2013) Expectation analysis in the assessment of volume ranges in appraisal and development – a case study (abstract). In: Presented at the Geological Society conference on Capturing Uncertainty in Geomodels – Best Practices and Pitfalls, Aberdeen, 11–12 December 2013. The Geological Society, London
- Chellingsworth L, Bentley M, Kane P, Milne K, Rowbotham P (2011) Human limitations on hydrocarbon resource estimates – why we make mistakes in data rooms. *First Break* 29(4):49–57
- Cheong YP, Gupta R (2005) Experimental design and analysis methods for assessing volumetric uncertainties. *SPE J* 10(3):324–335



- Cosentino L (2001) *Integrated reservoir studies*. Editions Technip, Paris, 310 p
- Egeland T, Hatlebakk E, Holden L, Larsen EA (1992) Designing better decisions. In: SPE paper 24275 presented at SPE European petroleum computer conference, Stavanger, 25–27 May 1992
- Evensen G (2009) *Data assimilation: the ensemble Kalman filter*. Springer
- Hanea R, Evensen G, Hustoft L, Ek T, Chitu A, Wilschut F (2015) Reservoir management under geological uncertainty using fast model update. In: SPE Reservoir Simulation symposium. Society of Petroleum Engineers
- Kahneman D (2011) *Thinking fast and slow*. Farrar, Straus and Giroux, New York, 499 p
- Kahneman D, Klein G (2009) Conditions for intuitive expertise: a failure to disagree. *Am Psychol* 64:515–526
- Li B, Friedman F (2005) Novel multiple resolutions design of experiment/response surface methodology for uncertainty analysis of reservoir simulation forecasts. In: SPE paper 92853, SPE Reservoir Simulation symposium, The Woodlands, 31 January–2 February 2005
- Mintzberg H (1990) The design school, reconsidering the basic premises of strategic management. *Strateg Manag J* 6:171–195
- Oxlade R, Bentley M (2015) It ain't what you do, it's the way that you do it: decision-led modelling workflows for mature fields. In: Presented at the Geological Society conference on Recognising the Limits of Geomodelling, Aberdeen, 4–5 March 2015. The Geological Society, London
- Peng CY, Gupta R (2005) Experimental design and analysis methods in multiple deterministic modelling for quantifying hydrocarbon in place probability distribution curve. In: SPE paper 87002 presented at SPE Asia Pacific conference on integrated modelling for asset management, Kuala Lumpur, 29–30 March 2004
- Pyrzcz MJ, Deutsch CV (2014) *Geostatistical Reservoir Modeling*, 2nd Edition, Oxford University Press, New York, p. 448
- Seiler A, Evensen G, Skjervheim JA, Hove J, Vabø JG (2011) Using the ensemble Kalman filter for history matching and uncertainty quantification of complex reservoir models. Large-scale inverse problems and quantification of uncertainty. Wiley Ser. Comput. Stat, pp 247–271
- Skjervheim JA, Evensen G, Aanonsen SI, Ruud BO, Johansen TA (2005) Incorporating 4D seismic data in reservoir simulation models using ensemble Kalman filter. In: SPE annual technical conference and exhibition, Society of Petroleum Engineers, 1 January 2005
- Slotte PA, Smorgrav E (2008) Response surface methodology approach for history matching and uncertainty assessment of reservoir simulation models. In: Europec/EAGE conference and exhibition, Society of Petroleum Engineers, 1 January 2008
- Slovic P, Finucane ML, Peters E, MacGregor DG (2007) The affect heuristic. *Eur J Oper Res* 177:1333–1352
- Smith S, Bentley MR, Southwood DA, Wynn TJ, Spence A (2005) Why reservoir models so often disappoint – some lessons learned. Petroleum Studies Group meeting, Geological Society, London. Abstract
- Stephens E (2015) 'Envelope of Outcomes' method for forecast probability distribution. In: Presented at the Geological Society conference on recognising the limits of geomodelling, Aberdeen, 4–5 March 2015. The Geological Society, London
- Subbey S, Christie M, Sambridge M (2004) Prediction under uncertainty in reservoir modeling. *J Pet Sci Eng* 44(1–2):143–153
- Tetlock PE (2007) *Expert political judgment: how good is it? How can we know?* 2nd edn. Princeton University Press, Princeton, 368pp
- Tetlock PE, Gardner D (2015) *Superforecasting: the art and science of prediction*. Crown, New York
- Towler BF (2002) *Fundamental principles of reservoir engineering*, SPE textbook series, vol 8. Henry L. Doherty Memorial Fund of AIME, Society of Petroleum Engineers, Richardson
- Tversky A, Kahneman D (1974) Judgement under uncertainty: heuristics and biases. *Science* 185:1124–1131
- van de Leemput LEC, Bertram D, Bentley MR, Gelling R (1996) Full-field reservoir modeling of Central Oman gas/condensate fields. *SPE Reserv Eng* 11(4):252–259
- van der Heijden K (1996) *Scenarios: the art of strategic conversation*. Wiley, New York, 305pp
- Wen XH, Chen WH (2005). Real-time reservoir model updating using ensemble Kalman filter. In: SPE Reservoir Simulation symposium, Society of Petroleum Engineers
- Wynn T, Stephens E (2013) Data constraints on reservoir concepts and model design (abstract). In: Presented at the Geological Society conference on Capturing uncertainty in geomodels – best practices and pitfalls, Aberdeen, 11–12 December 2013
- Yarus JM, Chambers RL (1994) *Stochastic modeling and geostatistics principals, methods, and case studies*. AAPG Comput Appl Geol 3:379
- Yeten B, Castellini A, Guyaguler B, Chen WH (2005) A comparison study on experimental design and response surface methodologies. In: SPE 93347, SPE Reservoir Simulation symposium, The Woodlands, 31 January–2 February 2005

## Abstract

Every reservoir is in some way unique. There are nevertheless generic issues pertinent to certain reservoir types and, in terms of model design, there are issues which inevitably require attention.

We don't aim to cover all possible reservoir types but we do hope to indicate trains of thought which we have found fruitful in modelling studies. Along the way, we can elicit distinctions between models for clastic

and carbonate reservoirs and some courses of action to take if the reservoir turns out to be fractured (which all reservoirs are).

If all reservoirs were just tanks of sand, this task would be trivial. In practice, geology and fluid dynamics combine in complex and intriguing but ultimately understandable ways. Adapting a line from Leo Tolstoy's *Anna Karenina*:

Homogeneous reservoirs are all alike; every heterogeneous reservoir is heterogeneous in its own way.



*Fault damage zone within aeolian sandstones, Moray Coast, Scotland*

We have chosen to group siliciclastic reservoirs by common depositional settings, namely: aeolian, fluvial, tidal-deltaic, shallow-marine and deep-marine. We then go on to consider carbonate and fractured reservoirs as ‘types’.

In practice, many carbonate reservoir systems contain siliciclastic units, and both sandstone and carbonate reservoirs may be significantly influenced by the presence of faults and joints. The main issue is to identify the key characteristics of the reservoir under consideration as a starting point for the reservoir model design which will be unique to that reservoir.

### Keywords

Clastic reservoirs · Carbonate reservoirs · Fractured reservoirs · Fluvial · Aeolian · Deep marine · Shallow marine · Percolation theory · Connectivity · Heterogeneity · Relative confinement · Pore fabric · Faults · Joints · Effective properties

## 6.1 Aeolian Reservoirs

Aeolian systems typically produce high net-to-gross (or at least high sand fraction) reservoir systems with blocky responses on open hole logs. Consequently, there is a tendency to treat them as ‘sand tanks’, a tendency encouraged by well-behaved porosity-permeability relationships resulting from the excellent sorting capability of the wind.

The risk is therefore that aeolian systems can be over-simplified, particularly because important heterogeneities are often found at a scale below log resolution. The highly laminated nature of aeolian strata and the strong permeability contrasts between some of these strata are belied by relatively benign log responses.

Aeolian systems are, however, very well organised with distinct generic bedform types, and thus lend themselves well to modelling, and multi-scale modelling in particular. The highly laminated heterogeneity is typically well

organised and therefore within reach of geologically-based reservoir modelling tools.

### 6.1.1 Elements

The component model elements of aeolian systems are well understood. Fryberger (1990a) describes aeolian systems in terms of four main facies: dune, interdune, sandsheet and sabkha, within which four principal types of bedding recur:

1. grainflow strata, resulting from avalanches down the steep side of dunes;
2. grainfall strata, dropped from airborne transport;
3. wind ripple laminations, a product of saltation, and
4. adhesion strata, resulting from drifting sands adhering to damp surfaces.

The aeolian bedding types usually have dune morphologies and have predictable reservoir property contrasts (Weber 1987, Fig. 6.1). As a rule of thumb, dune systems offer the best quality reservoirs, and it is the well-sorted, mostly coarse-grained grainflow beds on the slip faces of the dunes which typically carry the highest permeabilities within the dunes (Heward 1991).

Figure 6.2 shows some typical  $k/\phi$  relationships for these elements; with grain flow sands on the slip face typically offering an order of magnitude uplift in permeability for any given porosity class.

### 6.1.2 Effective Properties

The effective properties of some elements of aeolian systems are captured well by standard log and core measurements. However, for other elements, especially the different lamina types, this is predictably not the case, and a consideration of the multi-scale REV<sub>s</sub> for aeolian systems distinguishes the elements which require more attention (see Chap. 4 for a description of Representative Elementary Volumes, the ‘REV’). The

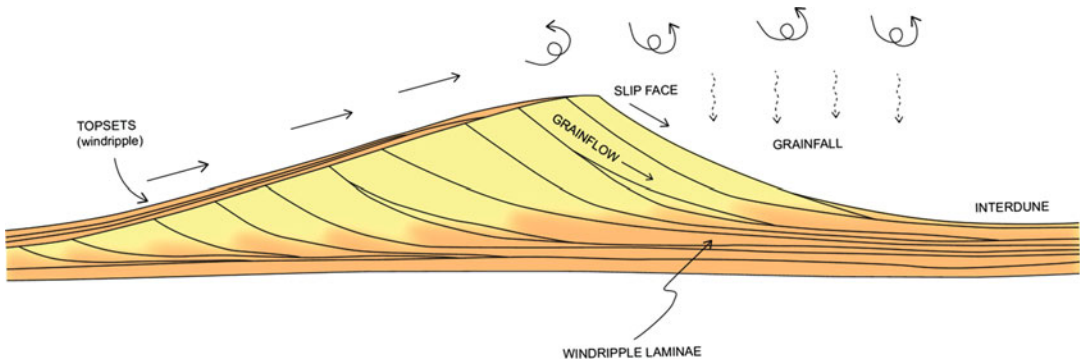


**Fig. 6.1** Typical elements of aeolian systems

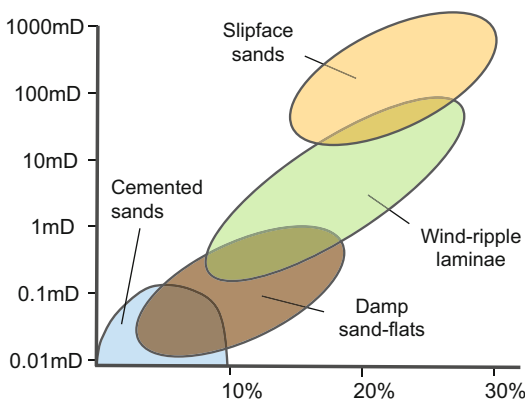


**Fig. 6.2** Typical petrophysical contrasts within aeolian systems

excellent exposure of the dune system shown in Fig. 6.3 reveals many heterogeneities, which can be summarised in terms of permeability length scales and a hierarchical arrangement of REV's, as shown in Fig. 6.4.

The REV summary in Fig. 6.4 is derived from observations such as those in Fig. 6.5, which shows the contrast between thicker grainflow beds and the fine laminations of the wind-ripple strata. The values used to build the REV plot are based on mini-permeameter data, calibrated against core data from an analogue oil-field over comparable lithologies.

The more blocky, homogeneous grainflow beds achieve an REV at a relatively fine scale, and this would be measured reasonably well by core plugs. Log data would offer a good measure of average porosity on the metre-scale, which

could be calibrated against core plug data, and the orderly  $k/\phi$  relationship from core plug data (e.g. Fig. 6.2) would lead to a reasonable estimate of the effective permeability of the interval.

The wind ripple bed sets are more heterogeneous and a larger sample volume is required to derive an effective average property. At the lamina scale, permeability is highly variable. Crucially, this occurs on a scale slightly smaller than the core-plug, core plugs neither representing the permeability of the coarse-grained laminae, nor giving a representative average of good and poor laminae. Log data will measure a reasonable average porosity over both good and bad laminae, but not necessarily the same average as would be measured from core plugs. Put another way, the scales of the measurements do not coincide with the scale of the REV.

Small-scale modelling could be used to provide a better range of estimates of the effective permeability as a function of scale for wind ripple intervals.

Model-based handling of aeolian laminae is comparable to the handling of thin bed heterolithics (described in the tidal deltaic and deep-water sections), the main difference being the more predictable form of the well-organised aeolian bed sets. The effective properties of fine scale heterogeneity have, for example, been explored using small-scale models by Pickup and Hern (2002), who show how the effective permeability of an interval varies depending on the presence or absence of



**Fig. 6.3** Dune core exposed at Clashach Cove, Moray Firth, Scotland

**Fig. 6.4** Permeability length scales for the Clashach outcrop (Fig. 6.3)

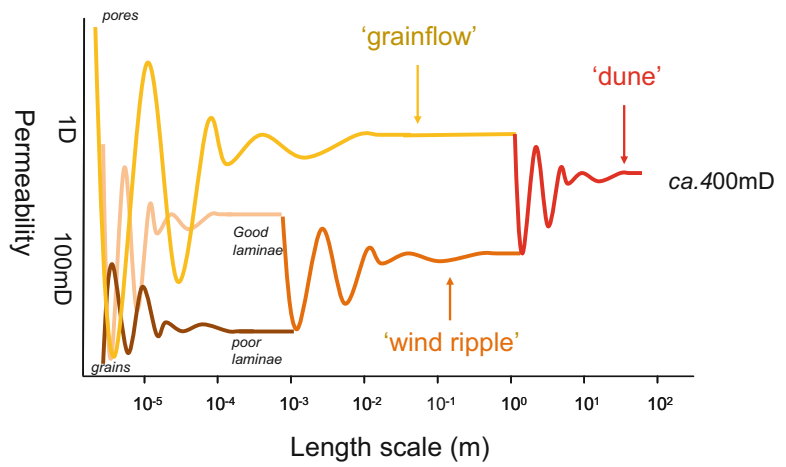


**Fig. 6.5** Components of the dune system; *top photo*: grainflow bedsets; *middle photo*: wind-ripple bedsets with dedicated petrophysicist for scale; *bottom photo*: permeability contrasts between wind-ripple laminae emphasised by weathering. The *red boxes* approximate REV's for each element

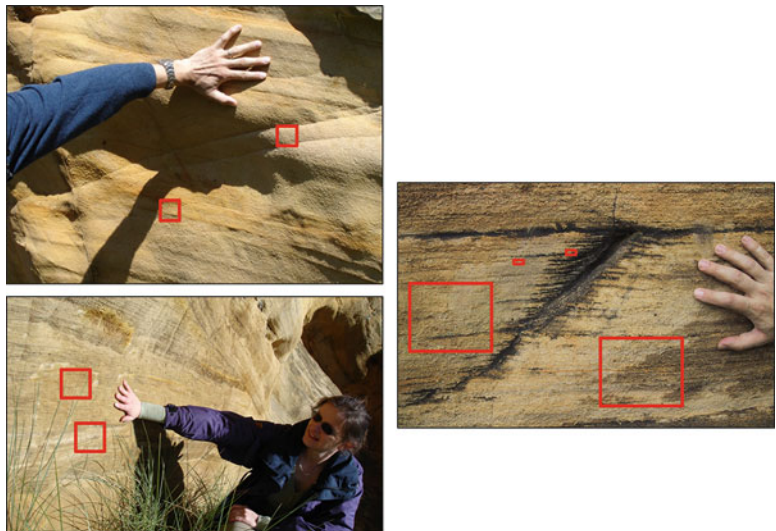
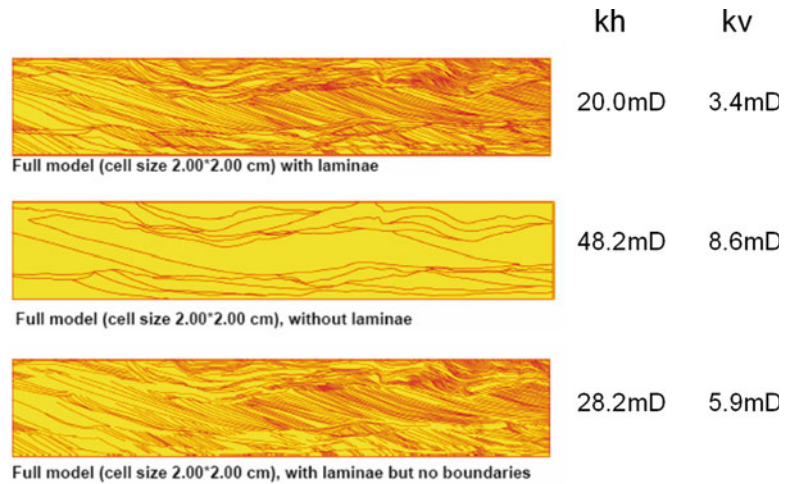


**Fig. 6.6** Effective permeability in aeolian laminae. Assuming: no-flow boundaries, 3 cm wind ripple laminae (0.6 mD) and 60 mD grainflow bedsets; bounding surface 6 cm thick. (Pickup and Hern 2002). (Redrawn from Pickup and Hern 2002, reproduced with kind permission from Springer Science+Business Media B.V)



laminae and the baffling effect of bounding surfaces (Fig. 6.6).

The effective permeability of small-scale aeolian architecture can therefore usually be quantified, and the main question for reservoir modelling is how the REV is architecturally organised on a larger scale. This is less predictable and two principal issues recur when modelling aeolian architecture:

1. How do the aeolian elements stack on a well-spacing scale, and
2. Does the resulting pattern impart a large-scale effective anisotropy on a producing reservoir?

### 6.1.3 Stacking

Strongly contrasting dune architectures are reported for linear, barchan and star dunes, with stacking patterns governed by the hierarchical arrangement of bounding surfaces (e.g. Fig. 6.7).

The hierarchical packaging of dune systems by bounding surfaces has been well described (Hunter 1977; Kocurek 1981; Fryberger 1990b) and the potential impact of their arrangement on reservoir sweep efficiency investigated, e.g. by Ciftci et al. (2004). In the Ciftci et al. study, aeolian bounding surfaces were seen to act as barriers to flow, based on observations from the Tensleep Sandstone in Wyoming, whereas in the Scottish outcrop example shown in Fig. 6.5 the

bounding surfaces are clearly open to flow. Either scenario is possible.

Assuming the permeability of the bounding surfaces can be determined, the central questions for forecasting flow (sweep efficiency) are:

- which reservoir element is the connecting medium, and
- what is the scale of the element distribution relative to the well spacing for a given production mechanism, such as water injection?

If high permeability slip-face sands are embedded in poorer quality sands on a scale significantly below that of the well spacing, the permeability of the overall system is dominated by the poorer quality unit (Fig. 6.8). In this case it can be argued that explicit modelling of the 'detail' is not necessary because irregularities in the sweep pattern disperse over the inter-well volume and the permeability of the reservoir system will start to approximate a predictable average.

However, if the slip-face sands connect, or congregate preferentially in specific units, the heterogeneity needs to be explicitly captured.

### 6.1.4 Aeolian System Anisotropy

For aeolian systems the key is therefore to identify the dune types and internal stacking patterns.

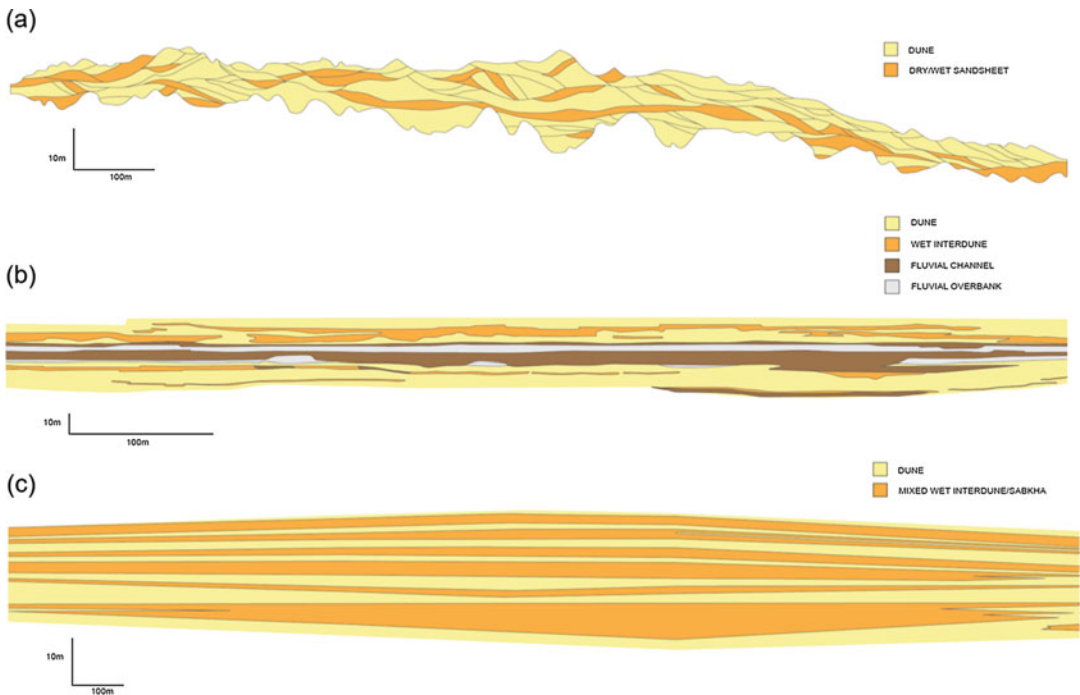


**Fig. 6.7** Contrasting dune architectures: (a) dry aeolian systems; (b) fluvial-aeolian system; (c) sabkha aeolian systems. (Image courtesy C.Y. Hern 2000)

A strong overprint on aeolian architecture is commonly the effect of changing base levels (the ‘stokes surfaces’ of Stokes 1968) or climatic fluctuations, as exemplified by the work of Meadows on Triassic reservoirs of the Irish Sea (Meadows and Beach 1993). As these trends are operating on a regional (basin) scale, high degrees of correlation within-field can occur. Productivity is driven by inter-well connectivity along correlatable dry-dune belts, such as that shown in Fig. 6.7 (lower image).

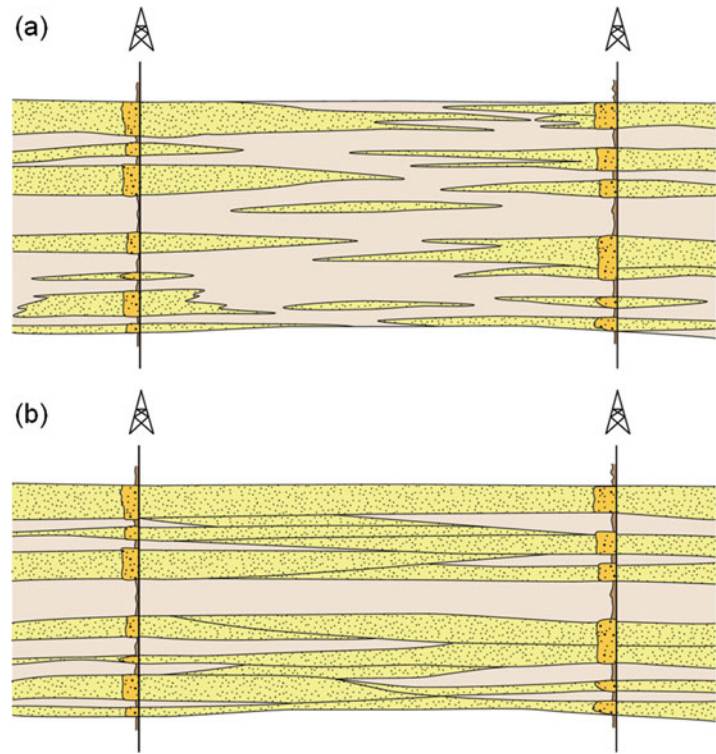
On a regional scale, even without base level changes, effective permeability anisotropy occurs if the dune systems are themselves strongly anisotropic (Krystinik 1990), with effective permeabilities parallel and perpendicular to dune ridges varying by up to an order of magnitude. Well spacing and preferred sweep directions are influenced by such anisotropy, which places value on the interpretation of dune type, and this can be imparted on reservoir models using variograms (for pixel-based workflows) or the superimposition of trends (discussed in Chap. 2).

### 6.1.5 Laminae-Scale Effects

A final important issue for aeolian systems, characterised by the widespread presence of fine-scale laminated lithologies, is whether these laminated elements in the reservoir system promote capillary trapping effects. That is, are the multiphase flow effects of strongly contrasting laminations important and adequately represented in the reservoir model?

This has been studied by Huang et al. (1995) who showed the impact of capillary forces on both the initial hydrocarbon distribution and the water-flood oil recovery. The low-permeability laminae cause a trapping effect due to locally high water saturations during water-oil displacement (see Chap. 4). The impact of small-scale heterogeneity on multiphase flow also depends on wettability (Huang et al. 1996), and wettability can vary within-reservoir – in this case more oil-wet in the poorer-permeability laminae and more water-wet in the higher permeability laminae. Capillary trapping will generally be a more important issue to consider in more water-wet systems.

**Fig. 6.8** Finding the connecting medium: comparing the length scale of the heterogeneity with the length scale of the development question (in this case, the well spacing). In (a) the connecting medium is the poor quality element, whereas in (b) the good quality elements are connecting



If determined to be important, the rock unit associated with capillary trapping (e.g. in grainfall or wind ripple strata) needs to be defined and included as a discrete modelling element. The impact of that element can then either be modelled explicitly as a 3D object or captured as part of an REV in small-scale models used to determine effective properties for a larger scale model.

## 6.2 Fluvial Reservoirs

### 6.2.1 Fluvial Systems

Fluvial reservoirs were one of the first reservoir types to receive the attention of object-based (Boolean) geological modelling efforts (Haldorsen and MacDonald 1987; King 1990; Holden et al. 1998; Larue and Hovadik 2006). Locating sand-rich channel objects within a more or less muddy background is the key issue, and this lends itself to some form of probabilistic modelling. Establishing the degree of

connectivity between channels is a key factor which determines hydrocarbon recovery so the proportion of channel sands is important as well as the internal character of the channels, which varies enormously.

Fluvial reservoirs fall into two broad groups architecturally: braided and meandering. Braided channels are formed in wide braid-plain systems (Fig. 6.9) with high sediment flux, whereas meandering channels form in more mature channel systems with overall lower sediment discharge. Braided systems tend to have a higher density of channels, which have lower sinuosity, whereas meandering systems tend to have a lower density of channels, with higher individual channel sinuosity.

Individual channels are typically grouped to form multi-channel complexes, and when we look at any individual channel we find it usually contains hierarchically-organised components, e.g. channel fill, barforms (Fig. 6.9), point bars, lateral accretion surfaces and over-bank deposits.



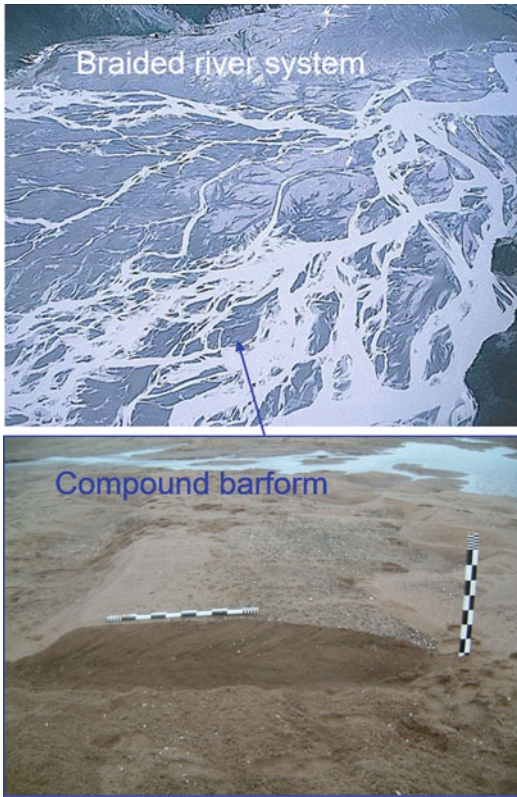


**Fig. 6.9** A modern braided fluvial system, with inset showing a compound barform. (Photo A. Martinus/Equinor © Equinor ASA, reproduced with permission)

Fluvial sandbody architecture is covered in detail elsewhere, notably by Miall (1985, 1988), and many resources have been devoted to understanding fluvial sandbody architecture at outcrop (e.g. Dreyer et al. 1993) as illustrated in Fig. 6.10.

### 6.2.2 Geometry

The key questions to ask when modelling fluvial reservoirs are typically geometric:

1. What is the fluvial system: braided or meandering, or something in between?
2. What is the channel density? Channel proportion well over 50%, or much less?
3. What is the channel sinuosity?
4. What are the typical channel dimensions?

5. Should we be focussing on individual channels or multi-channel complexes?
6. What is the internal channel architecture? Is it essentially sand-rich, and therefore effectively homogeneous, or is it composed of many variable elements including muddy, silty and sandy sub-elements?

Figure 6.11 shows examples of high-resolution models of meandering channel systems, illustrating typical model elements. In one example (Fig. 6.11, left) the focus is on channel stacking patterns and internal channel fill. The overbank crevasse-splay sands (green) have been represented as simple ellipsoids, whereas the sinuous channels have been modelled in more detail with layers of sand (yellow) and silt (purple) in the channel fill, and lateral accretion surfaces (red), all within a muddy background (blue). Alternatively (Fig. 6.11, right), less effort may be given to the internal channel architecture and more attention paid to capturing the channel types, intersections and connectivity.

Whatever the approach, the key issue is not to attempt to model all lithofacies but to define the appropriate *modelling elements*. Typical modelling elements for a fluvial system are:

- One or two channel elements, e.g. coarse-grained channel lag deposits and the main (typically finer) active channel fill.
- Discrete barforms within the channel complexes.
- Overbank deposits giving thin lateral communication paths within the non-reservoir background.
- Mudstone-dominated background facies (the floodplain).

### 6.2.3 Connectivity and Percolation Theory

Understanding sandstone connectivity in fluvial reservoirs is nearly always the dominant issue, and is best understood in terms of *percolation theory*, which describes the statistics of connectivity. In the context of sandstone connectivity,

**Fig. 6.10** The Escanilla Formation (Pyrenees, Spain) – a fluvial channel analogue illustrating large-scale stacked channel architecture. (Photo, Equinor image archive, © Equinor ASA, reproduced with permission)

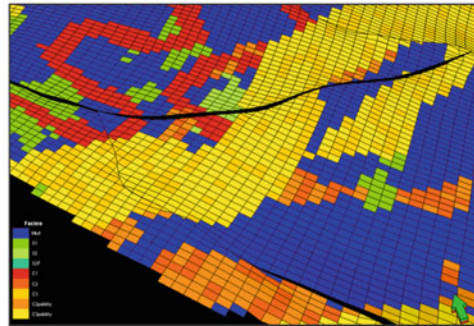
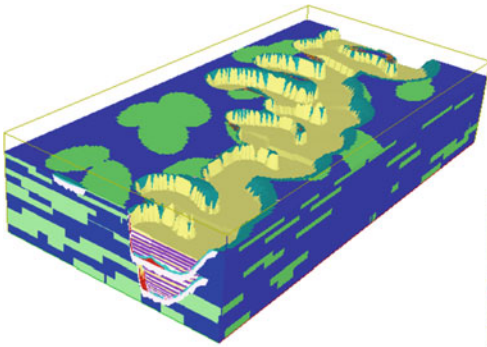


**Fig. 6.11** Example models of fluvial systems. *Left:* stacked meandering channel systems with heterogeneous fill (model area approximately 1 km × 2 km); *right:* model of mutually erosive channels (*yellow, red*) and crevasse

splays (*green*) – channels approximately 200–1000 m wide (*left image*, R. Wen/Geomodelling Corp., reproduced with permission)

the essential problem is whether we can say a sandstone observed in one well will connect with a sandstone observed in another well (Fig. 6.12).

Percolation theory, widely used in many branches of applied physics, describes connectivity in a statistical network using probability theory. To summarise the concept, it has been found

that by adding conducting elements randomly in a non-conductive network or lattice, connectivity occurs (statistically) when a predictable number of nodes or sites are filled. This point is the percolation threshold,  $p_c$ . The value for  $p_c$  depends on the dimensions and geometry of the system being considered. The theory is applied to a wide range of physical phenomena (de Gennes

**Fig. 6.12** Simple illustration of the sand connectivity problem

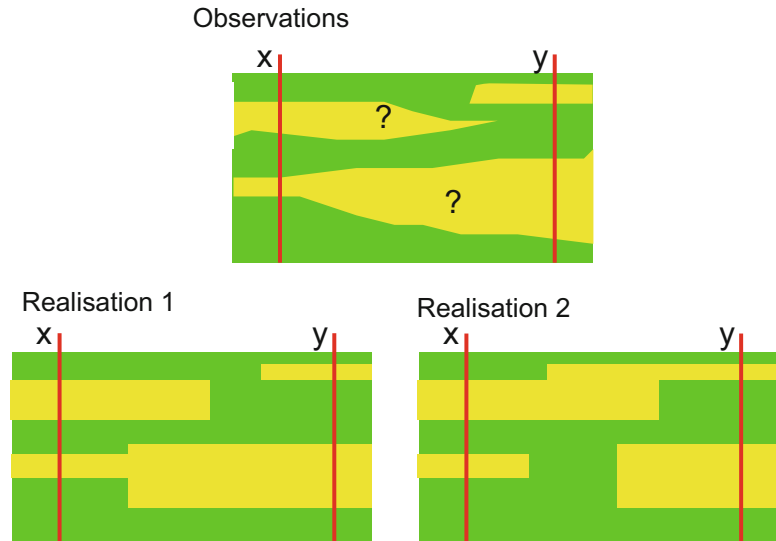


**Table 6.1** Some example percolation thresholds

| System  | Percolation threshold | References                  |
|---|-----------------------|-----------------------------|
| Square lattice (bond percolation)                           | 0.5000                | Stauffer and Aharony (1994) |
| Simple cubic lattice (site percolation)                     | 0.3116                | Stauffer and Aharony (1994) |
| Simple cubic lattice (bond percolation)                     | 0.2488                | Stauffer and Aharony (1994) |
| Overlapping sandstone objects (rectangles in 2D)            | ~0.667                | King (1990)                 |
| Overlapping sandstone objects (boxes in 3D)                 | ~0.25                 | King (1990)                 |
| Multiple stochastic models of intersecting sinuous channels | ~0.2 to ~0.6          | Larue and Hovadik (2006)    |

1976) and has been widely applied in subsurface flow studies (e.g. Stauffer and Aharony 1994). King (1990) showed how the theory can be applied to overlapping sand bodies in reservoir characterisation studies and Table 6.1 shows some example percolation thresholds.

When the theory is applied to permeability (Deutsch 1989; King 1990; Renard and de Marsily 1997) we find that the effective permeability,  $k_{\text{eff}}$ , in such a system follows a power law defined by  $p_c$ :

$$\begin{aligned} \text{For } p < p_c \quad k_{\text{eff}} &= 0 \\ \text{For } p > p_c \quad k_{\text{eff}} &= A(p - p_c)^e \end{aligned}$$

where:

$A$  and  $e$  are characteristic constants.

The simple case of 2D overlapping sand bodies is illustrated in Fig. 6.13 (based on results from King 1990). For more realistic systems, the problem is how the constants are to be estimated. However, all object-based geological reservoir models will tend to exhibit characteristics related to percolation phenomena, and it is useful to establish the expected connectivity behaviour of the system at hand. A simple reference point is that a reservoir with a sand volume fraction of around 0.25 would be expected to be close to the percolation threshold (in 3D) and therefore have connectivity strongly dependent on the sand volume fraction and geometrical assumptions.

Larue and Hovadik (2006) completed a very comprehensive analysis of connectivity in models

**Fig. 6.13** Illustration of the sand connectivity and effective permeability using percolation theory for a 2D system

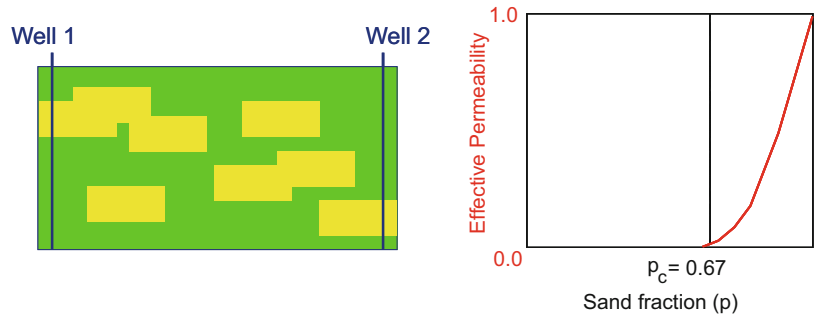
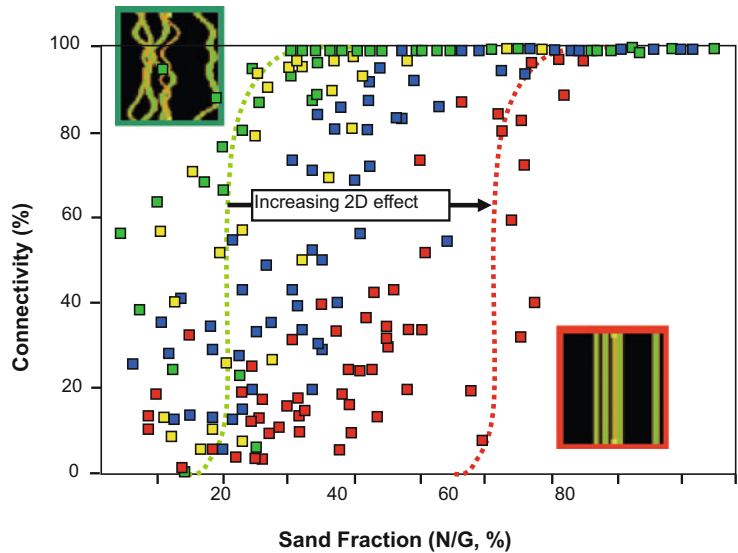


**Fig. 6.14** Connectivity as a function of channel sandstone fraction ( $N/G$ ), for a wide range of stochastic 3D channel models (Redrawn from Larue and Hovadik 2006). Sinuous channels (*green*) show characteristic 3D percolation behaviour, while straighter channels (*red*) show more 2D percolation behaviour. *Yellow* and *blue* points have intermediate sinuosity. (Redrawn from Larue and Hovadik 2006, Petroleum Geoscience, v. 12 © Geological Society of London [2006])



of channelized fluvial reservoirs (Fig. 6.14). They showed that actual connectivity (measured in terms of percolation exponents) varies enormously, depending on the details of the channel system, especially the sinuosity. In general, for 3D models, the rapid fall in connectivity occurs around the 20% sand fraction, a little lower than the theoretical value of 25% due to sinuosity and overlap of sandstone objects. However, as the sinuosity and dispersion in channel orientation reduces, 3D channel systems begin to behave like 2D systems, with the rapid change in connectivity occurring around the 60% sand fraction – close to the theoretical value of 66.7%.

This wide range in reservoir connectivity for fluvial channel models highlights the need for

careful model design based on good characterisation of the fluvial depositional system at hand. There is no point in making an attractive-looking fluvial reservoir model if it ‘misses the target’ with regard to the likely sandstone connectivity.

## 6.2.4 Hierarchy

Figure 6.15 illustrates the multi-scale nature of fluvial channels – the ‘channel’ is composed of several sandstone bodies, and each sandstone has variable lithofacies types (typically trough cross-bedded and ripple-laminated sandstones). Although challenging, these multiple scales

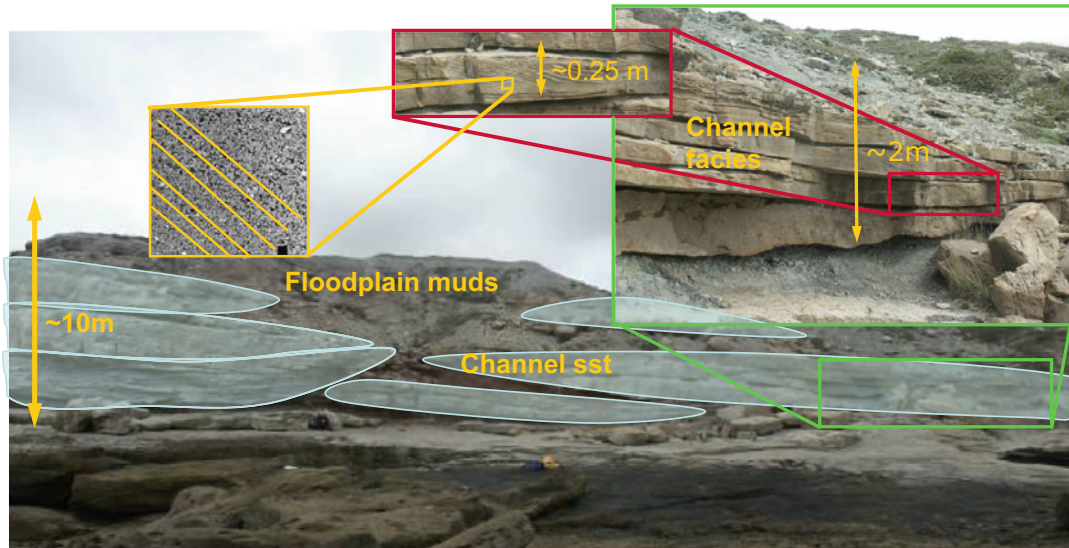


**Fig. 6.15** Hierarchy of sedimentary structures in fluvial channel system (Lourinha Formation, Portugal). (Photo K. Nordahl/Equinor © Equinor ASA, reproduced with permission)

lend themselves well to a multi-scale modelling approach. The detail within each channel cannot practically be modelled field-wide, but the effective permeability of a generic channel – the ‘channel REV’ – can be quantified through small-scale modelling (Chap. 4) and fed into a larger model, field-scale if necessary. Keogh et al. (2007) give a good review of the use of probabilistic geological modelling methods for building geologically-realistic multi-scale models of fluvial reservoirs.

## 6.3 Tidal Deltaic Sandstone Reservoirs

### 6.3.1 Tidal Characteristics

Tidal deltaic reservoir systems have earned a special focus in reservoir studies, because although they represent only one class of deltaic systems they present special challenges. Delta systems can be fluvial-, wave- or tidal-dominated. In terms of reservoir modelling, fluvial-dominated or wave-dominated delta systems could generally be handled using similar modelling approaches to those used for fluvial

and shallow marine settings. However, the influence of tidal processes tends to result in highly heterolithic reservoirs and these are now appreciated as being a widespread and important class of reservoir, e.g. offshore Norway, Alaska, Canada, Venezuela and Russia.

They form in estuarine settings (Dalrymple et al. 1992) where tidal influences prevail (Dalrymple and Rhodes 1995). They have highly complex architectures and stacking patterns, with bars, channels and inter-tidal muddy deposits intermixed and difficult to correlate laterally. The oscillatory nature of tide-dominated currents results in mixed sandstone/mudstone lithofacies, conveniently referred to as ‘heterolithics’. Heterolithics are defined as sedimentary packages with a strongly bimodal grain-size distribution, typified by moderate to high frequency alternation of sandstone layers with siltstone/clay layers in which layer thicknesses are commonly at the centimetre to decimetre scale (Martinius et al. 2001, 2005).

These represent particularly challenging reservoir systems because they display:

- generally marginal reservoir quality;
- highly variable net-to-gross ratios;
- highly anisotropic reservoir properties;

- fine-scale heterogeneities which are not easily handled with conventional reservoir modelling tools.

Recovery factors in heterolithics are typically low, in the range 15–40%.

### 6.3.2 Handling Heterolithics

Typically, the first inspection of heterolithic sandstones facies (e.g. Fig. 6.16) leads to the response “so where is the reservoir?” Often, the sandstone is so intermixed with the mudstone and siltstone that identification of good and bad reservoir elements becomes difficult, as does the integration of thin-bedded well logs with seismic data (Fig. 6.17).

In object-based reservoir modelling, it is conventional to model the reservoir (the foreground facies) against a background of non-reservoir, but in heterolithic, tide-dominated reservoir systems, there is often a gradation between reservoir and non-reservoir. In these systems, it is therefore essential to represent both background and foreground facies explicitly, e.g. Brandsæter et al. (2001a, b, 2005).



**Fig. 6.16** Example tidal heterolithic facies from core – in this case an inter-tidal wavy-bedded unit showing flow ripples and some bioturbation. (Photo A. Martinus/Equinor © Equinor ASA, reproduced with permission)

It was in this context that many of the concepts for total property modelling (*cf.* Fig. 3.33) and multi-scale modelling (*cf.* Fig. 4.1) were developed, and when working these fields it was quickly evident that multi-scale modelling was not optional for tidal-delta systems – it was essential.

Some form of effective flow property has to be estimated for the heterolithics, because neither core data, well logs or seismic give direct indicators of the presence of sandstone or high quality reservoir zones. There are many possible approaches to multi-scale modelling in such systems, but as a guide, Fig. 6.18 illustrates the workflow for upscaling heterolithic tidal deltaic reservoir systems, developed by Nordahl et al. (2005) and Ringrose et al. (2005). Core data is interpreted, ideally with the aid of near-wellbore models, to allow rescaling of core and wireline logs to the lithofacies REV. Rock property models at the lithofacies REV are then used to estimate flow functions. These could be permeability as a function of mud/sand ratio, e.g.  $k_v = f(V_m)$ , as shown in Fig. 6.18, or any other useful function such as acoustic properties as a function of porosity or water saturation as a function of  $k_h$ . Upscaled flow functions are then applied to the reservoir scale directly, or as part of further upscaling steps at the geological architecture scale.

The extra effort involved in multi-scale modelling of tidal deltaic systems clearly pays off in terms of the value gained by achieving realistic oil recovery factors from these relatively low quality reservoirs (Elfenbein et al. 2005).

## 6.4 Shallow Marine Sandstone Reservoirs

### 6.4.1 Tanks of Sand?

Shallow marine sandstones are among the most prolific class of reservoirs in terms of volumes of oil produced and are characterised by especially good recovery factors – up to 70% or even 80% (Tyler and Finlay 1991). They account for a

**Fig. 6.17** Tidal deltaic sand log shown alongside the corresponding seismic section, where only the thickest sands are evident on seismic

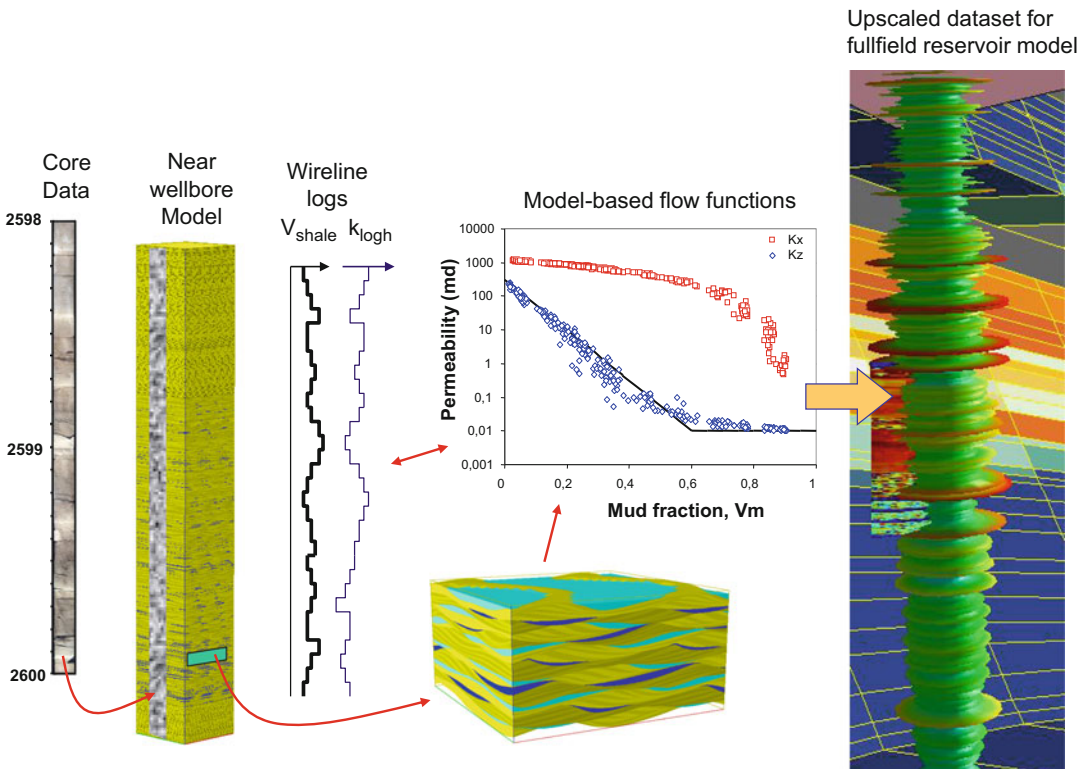
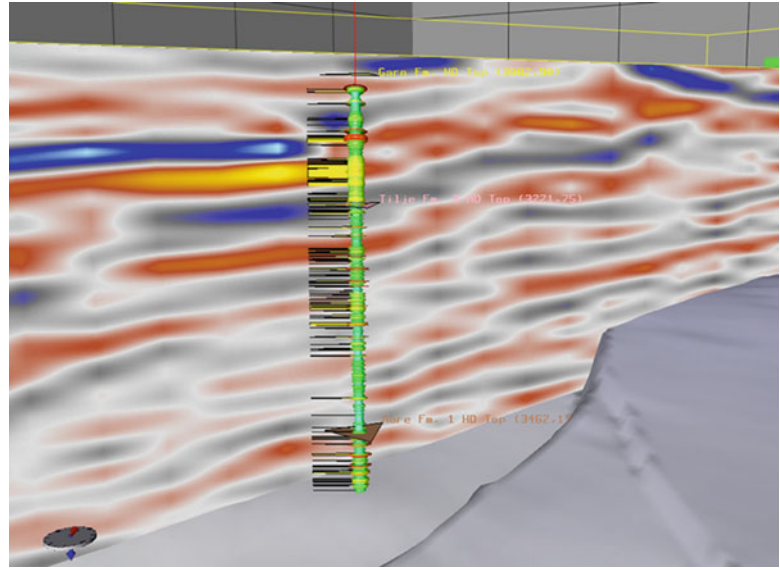


**Fig. 6.18** Workflow for upscaling heterolithic tidal deltaic reservoir systems

large portion of the Jurassic North Sea reservoirs and the majority of onshore US oilfields. They might well be regarded as an ‘easy’ reservoir in terms of oilfield development and are indeed one of the few reservoir types to occasionally behave

like ‘tanks of sand’ – the reservoir engineering ideal. However, shallow marine (paralic) reservoir systems are in fact very varied and can contain important heterogeneities at the sub-log scale.

Under the shallow marine group we include fluvial- and wave-dominated deltaic systems which characteristically build out into true shallow marine shoreface and offshore transition zones. The principal depositional settings involved are:

- delta plain and delta front;
- upper shoreface, usually storm and wave dominated;
- middle and lower shoreface, mainly below the fair-weather storm wave base;
- offshore and offshore transition zone, mud-dominated or heterolithic.

For a fuller discussion of the sedimentology and stratigraphy of these systems refer to the literature, including Van Wagoner et al. (1990), Van Wagoner (1995), Reading (1996), and Howell et al. (2008).

Alongside a wide range of depositional processes, including wave- and storm-action, fluvial delta dynamics and re-adjustments to base level changes, shallow marine systems are characterised by active benthic fauna, ‘worms and critters’, which churn up and digest significant quantities of the sandstone deposits. The trace fossils from these creatures (the ichnofacies) provide an important stratigraphic correlation tool, and give vital clues about the depositional setting (e.g. Bromley 1996; McIlroy 2004). They can also modify the rock properties.

### 6.4.2 Stacking and Laminations

Many reservoir characterisation and modelling studies of these systems have been published, (Weber 1986; Weber and van Geuns 1990; Corbett et al. 1992; Kjønsvik et al. 1994; Jacobsen et al. 2000; Howell et al. 2008). The last of these was part of a very comprehensive analysis of the geological factors which most affect oil production in faulted shallow marine

reservoir systems (Manzocchi et al. 2008a, b). They concluded the most important factors were:

1. The large-scale sedimentary stacking architecture, determined by the aggradation angle and progradation direction, and
2. The small-scale effects of laminations on two-phase flow, determined by the shape of the capillary pressure function.

That is, both the large-scale architecture and the small-scale laminations are important in these systems (as also concluded by Kjønsvik et al. 1994).

In wave-dominated, shallow-marine settings, fine scale laminations are common in the form of swaley or hummocky cross-stratified lithofacies (Fig. 6.19). These represent bedforms produced as the result of either wave-related oscillatory currents at the seabed or unidirectional currents (Allen and Underhill 1989) and are visible in core as bedsets with low-angle intersections (typically  $<5^\circ$ ). The laminations are sub-log scale and may be poorly sampled at the core-plug scale too, but make a significant contribution to flow heterogeneity. Such heterogeneity lends itself well to effective property modelling using small-scale models, such as that shown in Fig. 6.19.

### 6.4.3 Large-Scale Impact of Small-Scale Heterogeneities

To illustrate the dynamic interplay of geological factors with flow processes in shallow marine reservoirs, we use the case study presented by Ciammetti et al. (1995). They used a detailed outcrop model of a shallow marine parasequence (1370 m long and 45 m high) to study the effects of geological architecture on a simulated water-flood (Fig. 6.20).

Of the many cases run, the three cases shown in Fig. 6.21 illustrate the main effects. Water override generally occurs due to the coarsening-up (permeability increasing upwards) nature of the prograding shallow-marine parasequence.



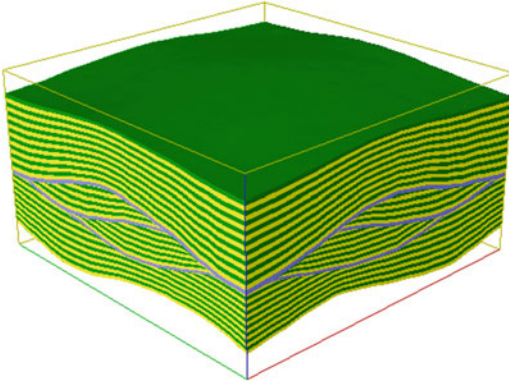


**Fig. 6.19** Example model of hummocky cross stratification (HCS) from a shallow marine shoreface system (model is  $2.5 \times 2.5 \times 0.5$  m)

This is generally positive, as it is in opposition to gravity which drives the water downwards, thus giving a balance between gravity slumping and viscous override of the water front.

Geologically-based upscaling captures this effect better than simple averaging and the application of rock curves. However, failure to include the effects of thin shales in the model, easy to overlook in log analysis, gives a reduced water override, and leads to an over-optimistic estimate of oil recovery.

All these models included the effects of capillary-dominated two-phase flow at the lamina scale (via upscaling). Omission of small-scale lamina architecture leads to differences in oil recovery of at least 5% (less recovery if small-scale effects are neglected), as shown by the oil production curves (Fig. 6.21). It is quite intriguing that for this shallow-marine case study, both the small-scale lamination and the coarsening-up permeability profile give a positive effect on recovery. In part, this explains why shallow marine reservoirs have such good overall recovery factors. Thin shales, however, have a negative impact.

The small-scale (microscopic) effects of capillary forces in causing strong directional anisotropy on two-phase immiscible flow processes (Fig. 6.22) are surprising to many, although the effect has been clearly documented using modelling (Corbett et al. 1992; Ringrose et al. 1993), laboratory analysis (Huang et al. 1995)

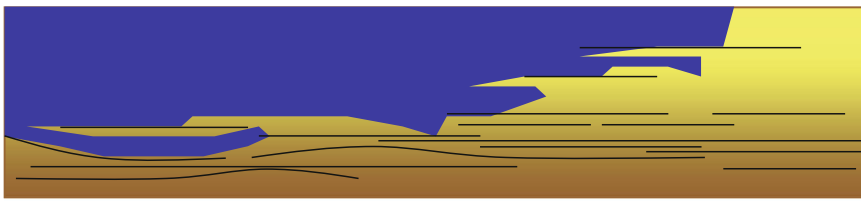
and full-field history matching (Rustad et al. 2008).

Reluctance to acknowledge the importance of small-scale heterogeneities may also be due to the fact that the effect operates at a scale much smaller than most models can resolve, and so must be incorporated implicitly using upscaled relative permeability functions. Here, the fluid system itself plays a determining role. The geological factors discussed above are for water displacing oil, an immiscible flow process. Gas displacing oil (generally a miscible flow process) tends to be most influenced by the large-scale permeability architecture. Strong gas over-ride should be expected, driven by both gravity and viscous forces working in concert, leading to a gas thief zone at the top of any progradational shallow marine unit, in contrast to the waterflood shown in Fig. 6.20.

The same parasequence model was used by Carruthers (1998) to simulate oil migration into a detailed model of a rock formation. Oil was introduced at the base and allowed to invade the rock model, using a capillary-dominated invasion-percolation technique (Carruthers and Ringrose 1998). The result (Fig. 6.23) illustrates how a capillary-dominated drainage flow process picks out critical flow pathways, filling individual sand layers as local accumulations. If oil migration is allowed to continue out of the model then little more than a few percent of the rock volume is contacted by oil. However, imposition of a structural closure on the model would result in the unit back-filling to create an oil reservoir.

In summary, shallow marine reservoir systems generally provide us with a ‘dream ticket’ for oil recovery. This is due partly to geology – shallow marine systems are generally laterally-continuous, sand-rich and well-sorted – but also due to the positive interaction between flow processes and geology. Two-phase flow effects at the lamina-scale and the coarsening up profile both have a positive effect on lateral water injection strategies; the geology assists the reservoir engineer. The small scale factors are nevertheless important and need to be included in any modelling exercise.

**Waterflood with thin shales**



**Waterflood without thin shales**



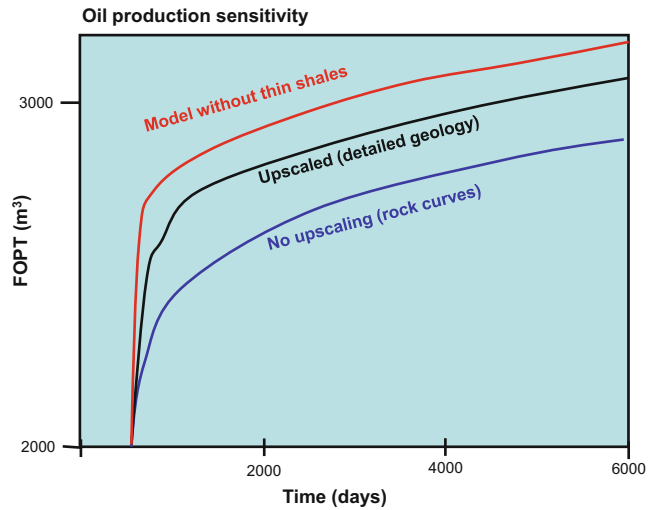
Coarsening up sequence

Model is 1370m by 45m with 10X1m grid cells

**Fig. 6.20** Detailed flow modelling of a shallow marine parasequence – Grassy member, Blackhawk Formation, Book Cliffs, Utah. Images show waterflood flow front (blue) prior to breakthrough at a producing well on the

right. (Redrawn from Ciammetti et al. 1995, ©1994, Society of Petroleum Engineers Inc., reproduced with permission of SPE. Further reproduction prohibited without permission)

**Fig. 6.21** Oil production profiles for three cases from the shallow marine outcrop simulations FOPT field oil production total. (Redrawn from Ciammetti et al. 1995, © 1994, Society of Petroleum Engineers Inc., reproduced with permission of SPE. Further reproduction prohibited without permission)



Other flow processes, such as gas injection, would not benefit in the same way from the geology so care is needed to ensure a rock model design that fits the flow process at hand. For a gas injection scheme, the most important geological feature is likely to be the location and continuity of the parasequence tops.

## 6.5 Deep Marine Sandstone Reservoirs

Deep marine systems are dominated by processes associated with density flows: gravity-driven currents moving sediments in suspension or by traction and depositing them along continental

**Fig. 6.22** Anisotropic relative oil permeability for an example shallow marine facies (wavy-bedded facies, Rannoch Formation, Ringrose and Corbett 1994). (Redrawn from Ringrose and Corbett 1994, The Geological Society, London, Special Publications, No. 78 © Geological Society of London [1994])

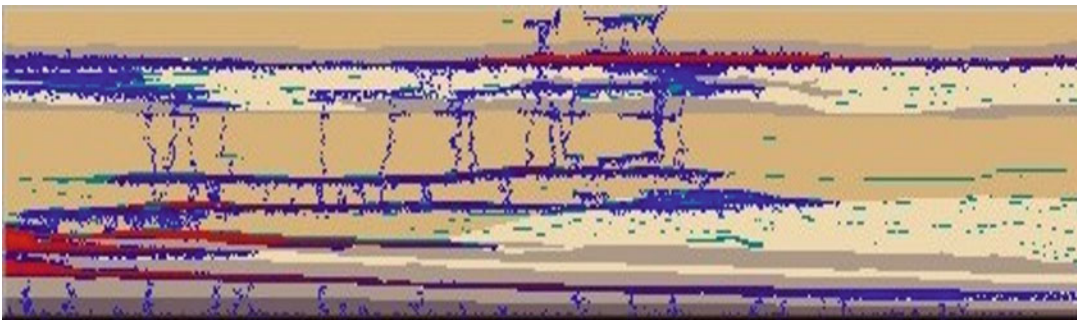
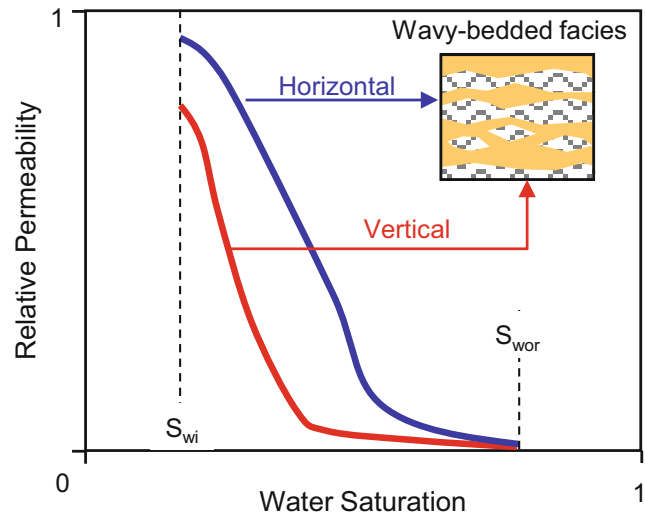


**Fig. 6.23** Simulation of oil migration into shallow marine rock unit (Carruthers 1998) (Redrawn from Carruthers 1998, drawing courtesy of D. Carruthers)

margins. Deep-water systems include but are not synonymous with ‘turbidites’ (Kneller 1995).

Emphasis in deep marine reservoirs has been placed firmly on depositional geometries and reservoir frameworks which are commonly determined from seismic, in some cases of spectacular quality. In reservoir modelling, the strength has been the ability to integrate seismic attributes into conditioned reservoir models; the weakness has been in the underestimation of small-scale heterogeneities and in not seeing what lies below seismic resolution.

The tendency to miss significant reservoir features has been encouraged by the observation that seismic data and reservoir simulation work at similar resolutions. It is therefore tempting to avoid sub-seismic architecture and work directly from ‘seismic-to-simulation’. This can work, but requires the seismic to be fortuitously resolved at the REV scale pertinent to the model purpose. This can be the case for gas reservoirs but, recalling Flora’s guiding rule (Chap. 2), this is unlikely to be the general case for oil reservoirs.

Sub-seismic architectural understanding is usually required, and there are a considerable range of possibilities. The question to ask is: “What’s inside the seismic loop?”, and for model-related issues a consideration of *confinement* is a good place to start.

### 6.5.1 Relative Confinement

Confinement describes the extent to which a submarine gravity flow ‘feels’ physically constrained by surrounding topography. Is the flow being funnelled through a narrow canyon (‘confined’) or is it depleting on to the floor of a large open basin (‘unconfined’)? Confinement is important as a concept because it is the primary underlying factor guiding the permeability architecture we are attempting to capture in reservoir modelling and simulation (Stanbrook et al. 2020).

In confined systems, new density flows tend to erode into deposits of earlier flows and hence sands from different flows tend to amalgamate (Fig. 6.24). The erosional elements of the new flow are typically sand-rich and the fill within the erosional scour will also tend to be sand-rich, whether deposited by the initial confined flow or subsequent flows through the same conduit. The amalgamation of sand-rich units results in permeability architectures with favourable  $k_v/k_h$  ratios unless individual sandy depositional elements are draped by muds.

In unconfined systems, flows are more depletive, less erosive and prone to the generation of a

more layer-cake architecture (Fig. 6.24). Sand amalgamation is limited and the finer-grained, lower-permeability units separating the sands tend to remain continuous. The resulting  $k_v/k_h$  ratio is low.

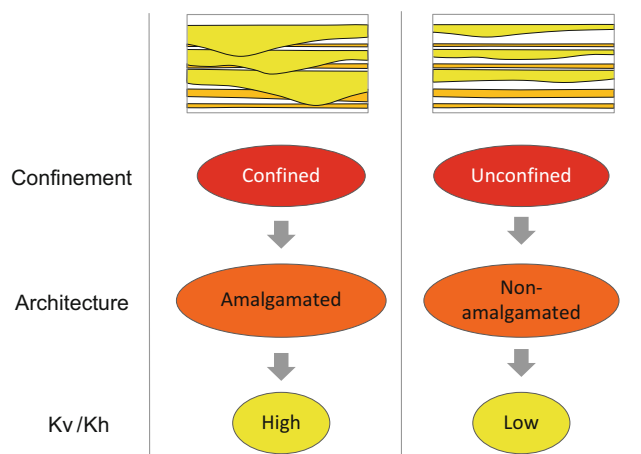
The degree of confinement and the resulting amalgamation ratio therefore link directly to permeability architecture (Stephen et al. 2001) and an understanding of the reservoir in terms of confinement is an essential aspect of the conceptual sketch which we have argued underpins any good modelling exercise (Chap. 2).

Figure 6.25 illustrates the degree of confinement in terms of two controlling factors: the size of the gravity flow depositing the sediment and the size of the container it flows in to. Similar geometries may result from large flows entering a large basin as those from small flows entering a smaller basin (e.g. Stanbrook and Clark 2004). Confinement is thus a *relative* issue, and a series of flows making up one gross reservoir interval may be a combination of confined and unconfined components. Variations in confinement, via changes in amalgamation ratio, lead to variations in permeability architecture,  $k_v/k_h$  ratio and recovery efficiency.

### 6.5.2 Seismic Limits

Once a reservoir prospect has been identified from seismic attributes and proven by drilling, the reservoir often becomes clearly ‘visible on

**Fig. 6.24** Summary of the effect of confinement on deep-water reservoir architecture



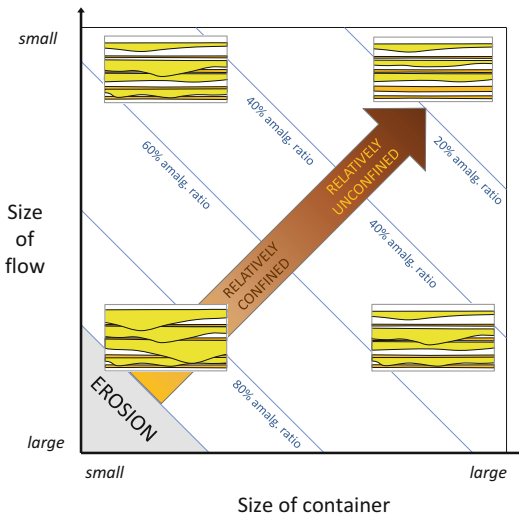


**Fig. 6.25** The relationship between permeability architecture (anisotropy expressed in terms of an amalgamation ratio) and key underlying controls on confinement. (Based on discussions in the field with D. Stanbrook and E. Stephens)

seismic' leading to three common tendencies in reservoir modelling:

1. To limit the field description to the observed seismic attributes.
2. To treat the reservoir as largely connected within-attribute.
3. If high N/G sands are encountered initially, to assume the field is relatively tank-like within the seismically-constrained envelope.

These simplifying tendencies may occasionally work (the rare 'sand tank' reservoir) but sub-seismic heterogeneities usually emerge during the producing life of a field.

A distinctive feature of deep water systems is the predominance of stratigraphic traps. Unlike structurally closed fields, where there is a geometric limit to how much volume can be contained in a defined closure, the addition of previously undetected connected HCIIP beyond the seismically-observed reservoir can be considerable. This is particularly the case in unconfined systems and the challenge is therefore to see beyond the seismic, particularly if the reservoir has a stratigraphic trap with no direct means of defining the field extent.

For reservoir modelling, the possibility of unseen HCIIP requires a concept, and ideas on confinement (and hence likely connectivity) can be tested against information from material balance. There is therefore greater emphasis than usual on starting the modelling exercise with guidance from dynamic data, as this can inform the first conceptual sketches of the reservoir.

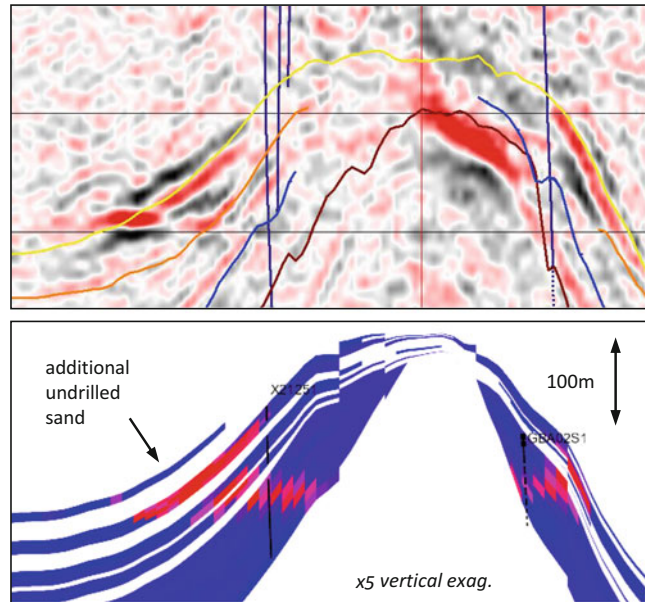
The example shown in Fig. 6.26 is from a gas field in the UK Central North Sea modelled after 5 years of production (Bentley and Hartung 2001). The structure is a small field in which gravity flows were observed to onlap a palaeotopographic high above a salt dome. Models limited to observations of sand intervals in the wells could be history matched but simple matches could only be achieved if additional volumes were present in beds not initially identified from seismic. In the analysis of uncertainty, it was therefore valid to consider scenarios including additional, unobserved reservoir sands, an interpretation which would be consistent with additional confined flows depositing around the palaeo high. 4D seismic data from this field subsequently supported this hypothesis.

### 6.5.3 Thin Beds

Incorrect representation of thin beds is prevalent in deep water stratigraphic traps where significant undrilled sub-seismic HCIIP may be present. Even when penetrated by wells, the thin beds may be unresolved on logs and reservoir pay intervals will typically be underestimated.

The impact of the log sampling problem in a reservoir modelling workflow is illustrated in Fig. 6.27. Modellers will usually check blocked property (porosity) logs against raw log data as a QC step, but this is only worthwhile if the raw data points are valid in the first place. If not, the subsequent cross-plotting of incorrect blocked log data with permeability data is invalid. An important error occurs if the core plug data is not sampling an REV, which tends to be the case in finely laminated intervals ('heterolithics'). The resulting permeability values inserted into model cells are somewhat

**Fig. 6.26** *Top*: amplitude change after 5 years of production in gravity flows overlapping a salt dome; *bottom*: forward-modelled acoustic impedance change in the sand-rich layers, including an additional upper layer not seen in the wells (Bentley and Hartung 2001). (Redrawn from Bentley and Hartung 2001, ©EAGE reproduced with kind permission of EAGE Publications B.V., The Netherlands)



meaningless numbers, which are then upscaled for simulation. The resulting simulation forecasts are unlikely to be useful.

A less error-prone workflow is illustrated in Fig. 6.28, in which the important step is to decouple the handling of porosity and permeability. The porosity log may not reflect the porosity of the thin net reservoir beds correctly, but it may be a reasonable average of porosity in the net/non-net package. The logging tool is effectively measuring an upscaled porosity, which can be applied to a cell with  $N/G = 1$  at least as a first approximation of the pore volume. The validity of this can be checked with reference to core data.

Permeability cannot be directly derived by transforming the log-average of core values, however, and this is where the modelling of porosity and permeability is decoupled. Effective permeability can instead be calculated using small-scale modelling based on data which samples the REV's of the small scale reservoir elements, as described in Chap. 4, and illustrated in this chapter for tidal heterolithics and fine aeolian laminae. The input data may be core plug permeabilities, mini-permeameter data or estimates from thin sections – whichever scale samples the appropriate REV. The final outcome should be checked against well test data.

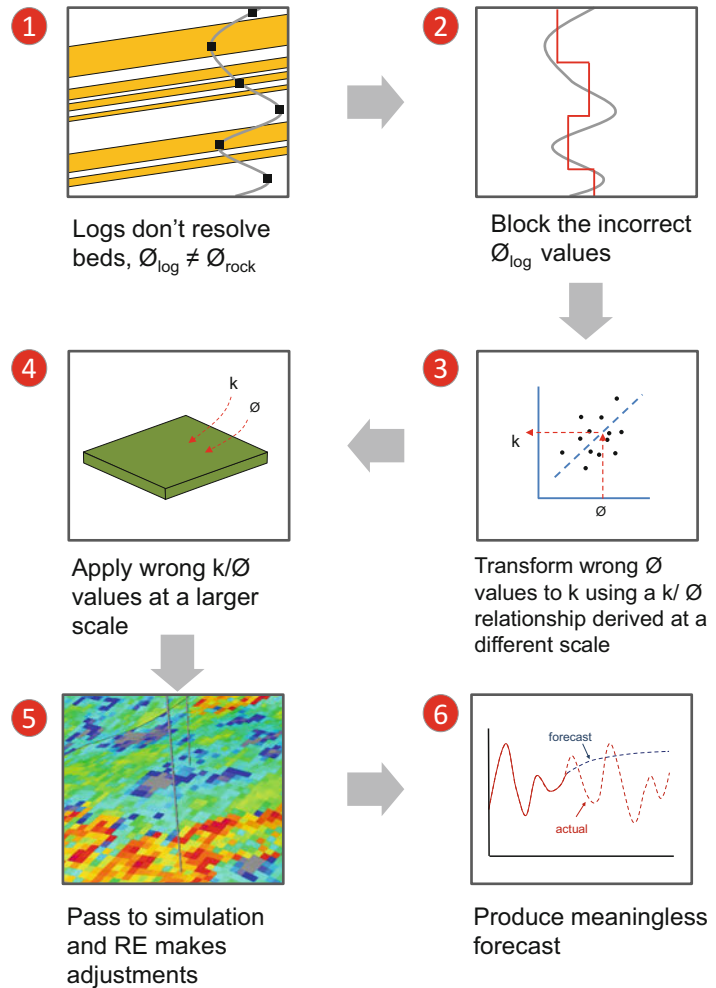
#### 6.5.4 Small-Scale Heterogeneity in High Net-to-Gross 'Tanks'

For confined systems in which the reservoir is detectable from seismic attributes, it is tempting to work directly from seismic and treat the field as a 'tank of sand', albeit an irregularly-shaped one. What tends to be overlooked is the contribution of low-net thin beds within the generally high N/G system; the inverse condition of the 'thin bed' scenarios described above.

An example of this is shown below from the well-studied high N/G ratio reservoir analogues of the Annot region in SE France (Pickering and Hilton 1998). Massive sand intervals are partitioned by thin but extensive heterolithic intervals with low permeability (Fig. 6.29a). These thin heterogeneous intervals (Fig. 6.29b) would be poorly resolved on logs. The issue is whether or not such heterolithic intervals would have significant vertical permeability and how laterally extensive the intervals would be, i.e. do they constitute barriers or baffles?

Without very good log resolution a similar logic is needed to that applied to thin beds – effective permeability needs to be estimated from small-scale modelling. This is a simpler exercise, however, as the focus is vertical

**Fig. 6.27** Modelling of thin beds: when it goes wrong



permeability; the horizontal permeability in the gross sand interval will always be dominated by the high N/G sands above and below the heterolithics.

The heterolithic facies can be extensive, even in high N/G systems, and in this example can be traced along the cliff line for 4 km (Fig. 6.30). The impact of this architecture is illustrated in 2D sections through a 3D model (Fig. 6.31), in which the heterolithic intervals seen in Fig. 6.29a,b are included as discrete elements with contrasting effective vertical permeabilities.

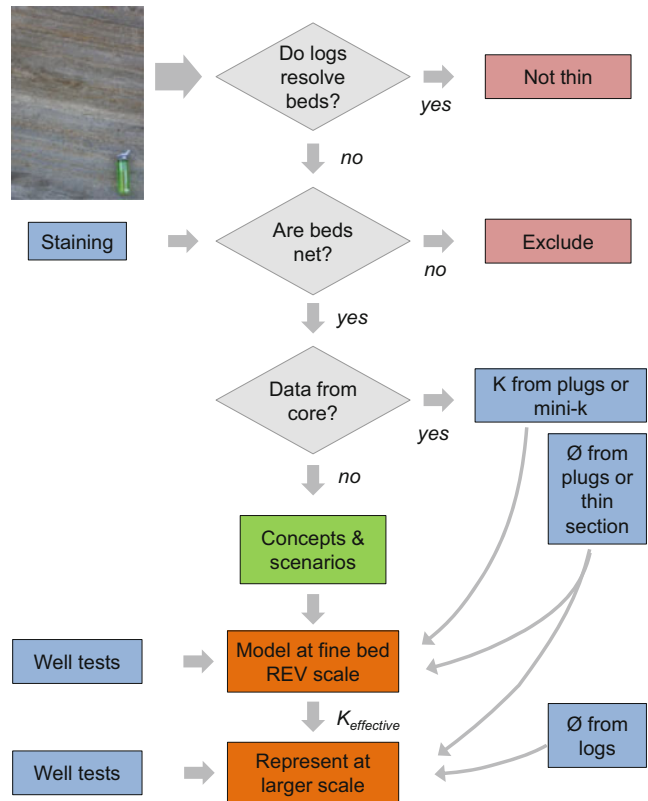
The effective vertical permeability in the heterolithic units determines the sweep pattern. In this case the heterogeneity improves recovery; water breakthrough times increase from 3 months

to 3 years and recovery increases from 21% to 37% (after 16 years of production) as the baffling effect of the low-permeability interval holds back water coning. The addition of higher permeability channels within the sheet-like sands (the ‘Jardin de Roi’ section in Fig. 6.31) has the reverse effect by provoking earlier water breakthrough. Both the heterolithic facies and the channel facies are likely to be sub-seismic, and these effects will be missed by ‘seismic-only’ workflows.

### 6.5.5 Summary

Despite huge advances in deep marine reservoir developments, the experiences of the last

**Fig. 6.28** Reservoir modelling in thin beds: a better approach, partly decoupling the modelling of porosity and permeability modelling



decade confirm that no matter how good the seismic data is, there is typically essential sub-seismic heterogeneity in deep marine systems, especially in fields to be developed under waterflood. Once under production, 4D seismic is an invaluable tool to help explain field behaviour, but by this time the biggest investment decisions have been made. Even with 4D data, key heterogeneities may remain sub-seismic.

Reservoir modelling in deep marine systems therefore requires an understanding of the fine-scale architectural concepts, steered by an overarching understanding of relative confinement.

## 6.6 Carbonate Reservoirs

To the frustration of some sedimentologists, carbonate reservoir modelling suffers from two common labels:

1. Carbonate systems are as varied as siliciclastic systems, but whilst much attention is paid to different types of clastic reservoir, carbonates are often lumped as one (as in this chapter), and
2. Carbonates are seen as ‘just difficult.’

The bias towards clastic systems in reservoir modelling is certainly strong (consider the common occurrence of fluvial channel examples in geostatistical work, despite fluvial systems being a minority case globally), but the principles of model design described in chapters 1–5 apply equally well to all reservoir types. Are carbonates more difficult to model? Not necessarily, but they do tend to be different, as reviewed by Burchette (2012).

For carbonate reservoir modelling, five areas are highlighted for consideration:

1. Depositional architecture
2. Pore fabric



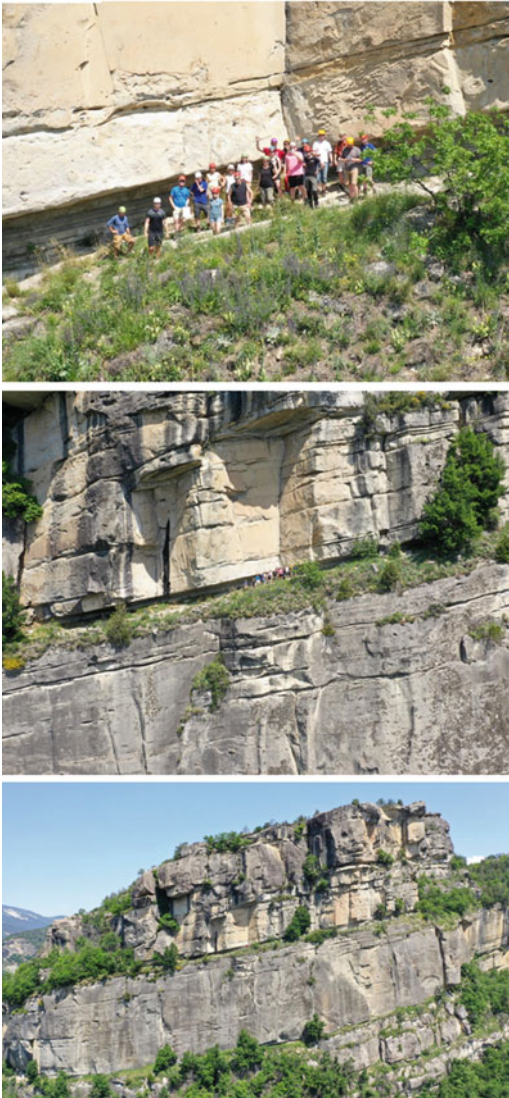


**Fig. 6.29a** Thin bed heterolithics in the otherwise very high N/G of the Gres d'Annot, outcrops above Annot town. (Drone images courtesy of John Howell)

3. Diagenesis
4. Fractures
5. Hierarchies of scale (the carbonate REV)

### 6.6.1 Depositional Architecture

Where reservoir heterogeneity is controlled by original depositional patterns and processes, carbonate modelling is open to the same options for



**Fig. 6.29b** The ‘lost heterogeneity’ – heterolithics are low (but not zero) permeability elements in the system which act as baffles; the key heterogeneity is sub-log scale and effective permeability is commonly erroneous in reservoir models. Gres d'Annot, outcrops at the Scafferels, above Annot town

rock modelling as those which apply for siliciclastic reservoir models. An important difference is the more limited reservoir modelling database for carbonates, and the tendency therefore to rely more on modern environmental analogues (Burchette 2012). However, the link to modern analogues is weaker than for clastic systems simply because of the organic aspect of carbonate sedimentology – modern day organisms do not necessarily build carbonate reservoirs in the same way as their ancestors, and current climatic changes do not always match those of the past. There is therefore a greater need to derive geometric data from stratigraphically and environmentally appropriate settings than is the case for many clastic reservoirs.

In the example shown in Fig. 6.32, outcrop analogues for the Shuaiba reservoir are drawn from examples in Provence (Leonide et al.

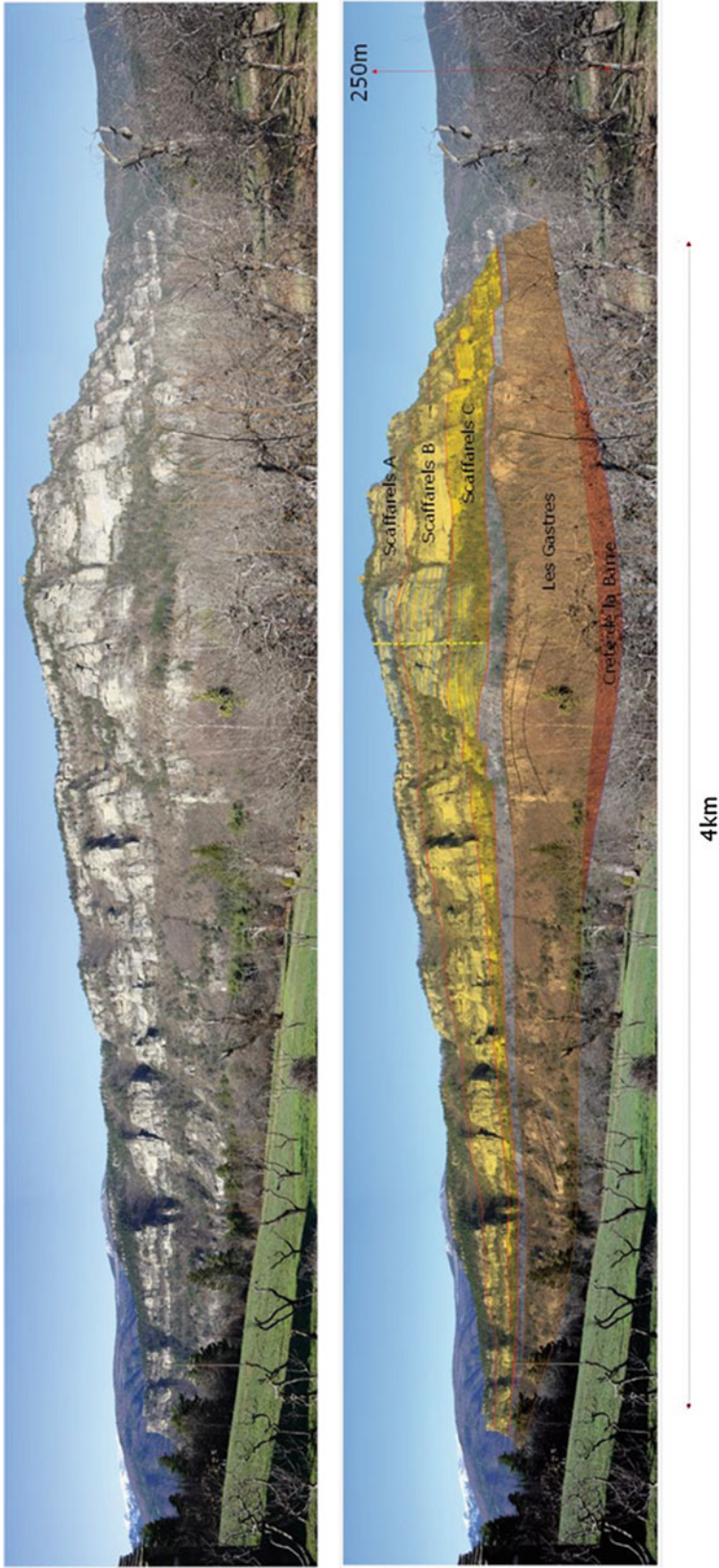


**Fig. 6.30** Architecture of the Gres d'Annot of the Coulomp Valley; the heterolithics in Fig. 6.29a,b are at the base of the unit labelled 'Scaffarels A'

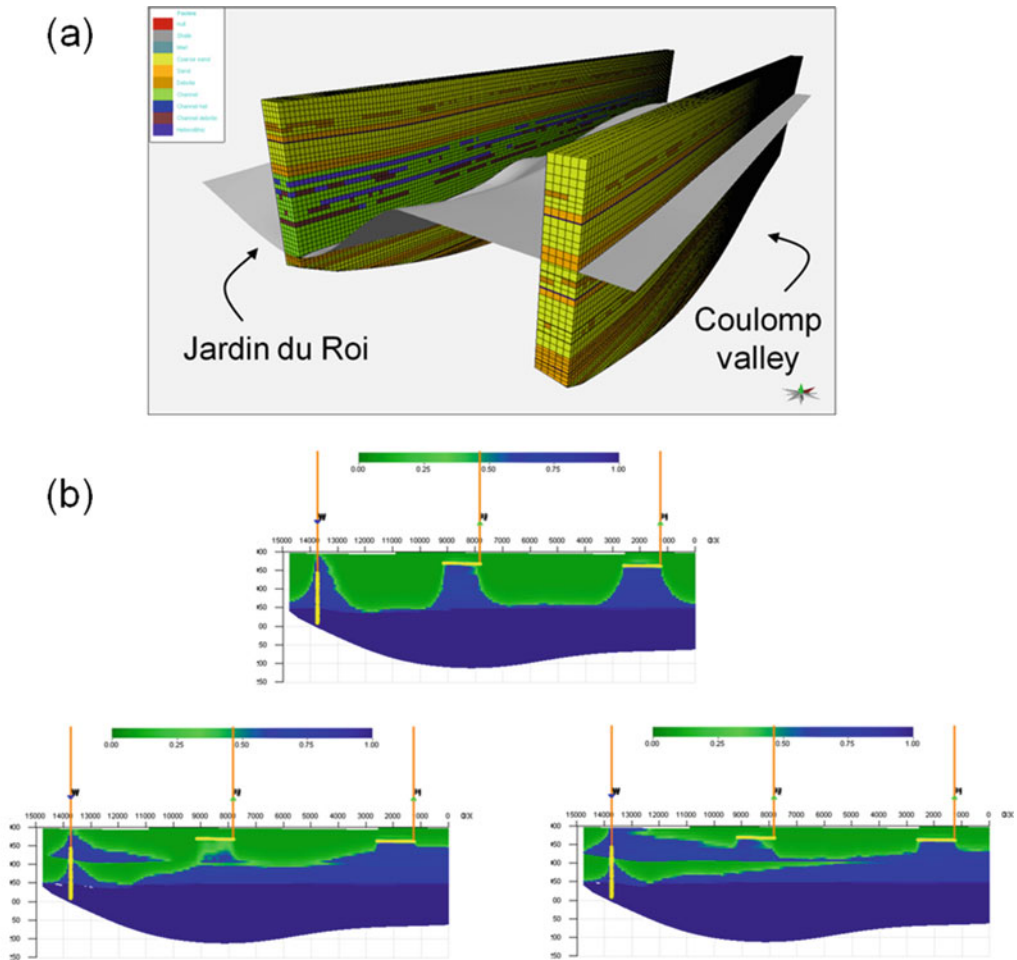


**Fig. 6.31** Modelling the Gres d'Annot. (a) Static well model sections with heterolithics in orange. (b) Impact of heterolithics in a high N/G reservoir (Coulomp Valley section) on sweep efficiency during a water flood of a viscous oil; green = oil, blue = water, injection from

left. Production is from horizontal wells in the upper reservoir. Upper image: no heterolithics; lower left: heterolithics with effective  $k_v = 1$  mD; lower right: heterolithics with effective  $k_v = 0.1$  mD. (Unpublished images from E. Stephens & M. Bentley)

2012) and detailed mapping of limestone facies provides insight into the distribution of reservoir types in age-equivalent Middle Eastern reservoirs. Even here, though, the palaeoenvironments between reservoir and analogue locations differ – the two areas lay on opposite sides of the ancient Tethys Ocean and are characterised by different faunal assemblages.

Other carbonate environments display impressive lateral continuity and might appear to make little call on the rock modelling toolbox. This is reported from field studies by Palermo et al.

(2012) working on the Muschelkalk, where laterally consistent reservoir properties have been measured in platform carbonates and traced over several 100's of metres, contrasting markedly with very abrupt vertical variations. Similar patterns are common in platform carbonates of the Middle East (Fig. 6.33).

This extreme anisotropy is also familiar in carbonate-evaporite sequences where heterogeneities are controlled laterally by gentle basin-wide chemical gradients but vertically by fluctuations in basin inputs and outputs, such as

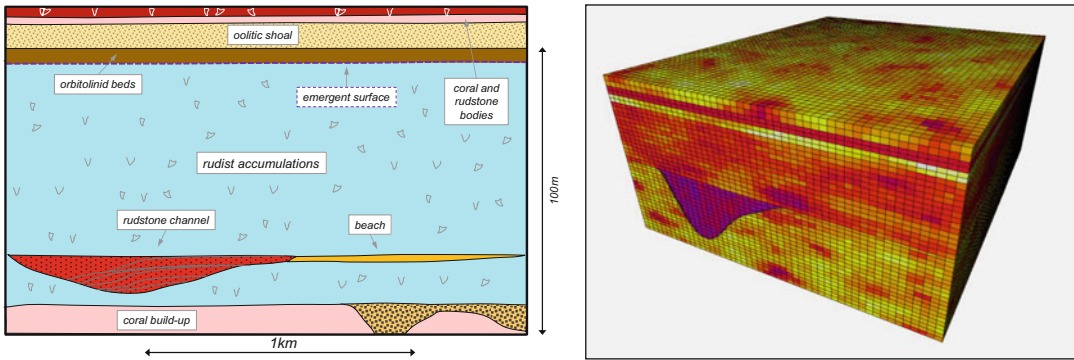


**Fig. 6.32** Facies interpretation of a platform margin from outcrops near Rustrel, France (Leonide et al. 2012) (left) and a cellular representation of the same (right). (Left

image redrawn from Leonide et al. 2012, © SEPM Society for Sedimentary Geology [2012], reproduced with permission)

**Fig. 6.33** Highly layered platform carbonates from the Natih-E at Jabal Madmar, Oman



periodic connection and disconnection with open seawater and periodic basin desiccation (Fig. 6.34).

Similar high frequency, laterally-correlatable cyclicity is also common in chalk fields, and the regularity can be picked out from vertical variograms of porosity and permeability measured on core (Almeida and Frykman 1994) (Fig. 6.35).

Depositional environments can therefore dictate the need for simple, very thinly layered models, or heterogeneous object-based models, although the latter potentially lack good analogue data. In this respect, carbonate modelling workflows may be comparable to workflows for clastic reservoirs.

### 6.6.2 Pore Fabric

Where carbonates and clastics differ most markedly is in their pore fabric. Clastic systems can generally be broken down into elements with reasonable porosity-permeability relationships, reflecting a consistency of pore type for a given model element. This is often not the case in carbonates, where there may be little or no relationship between porosity and permeability.

The underlying reason is pore size distribution, which can vary over very short distances in carbonates owing to the irregularity of pore shapes. Not all carbonates behave this way: as pore shapes become more uniform, such as in some chalks or well sorted grainstones, regular

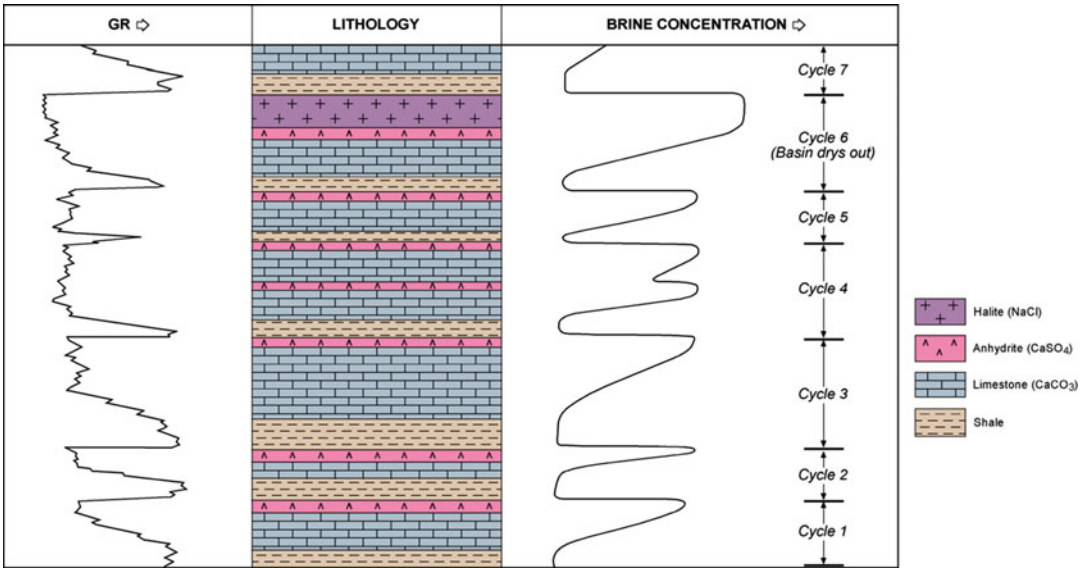


**Fig. 6.34** Vertical distribution of elements in a carbonate-evaporite interval; individual 5 m thick cycles are correlatable for 10's of km laterally

$k/\phi$  relationships emerge. However, classifying core plug data using the Dunham (1962) descriptive scheme, useful for objective description of the lithology in terms of texture, often fails to break a reservoir system down into elements with clear  $k/\phi$  relationships.

A pragmatic method of carbonate characterisation at the pore scale is presented in Lucia (1983) and the summaries given by Lucia (2007) remain a very good starting point for characterising carbonate reservoirs as a basis for reservoir modelling. Lucia classifies pore systems into two broad groups:

1. Inter-particle, in which porosity exists between grains or crystals, and
2. Vuggy (everything else).

Vuggy systems divide again into separate-vug and touching-vug fabrics. Any carbonate classification system can be mapped onto this simple scheme, and indeed Lucia (2007) subdivides the scheme to accommodate common carbonate descriptive terms (moldic pores, fenestral pores, breccias, etc.). The advantage of Lucia's scheme is that it captures heterogeneity in terms of *pore fabric* which lends itself to petrophysical characterisation, and it is therefore more

predictive for a property such as permeability than the Dunham scheme.

With reservoir modelling in mind, a generalisation of Lucia's scheme is shown in Fig. 6.36. This is set against the Dunham classification but with joint systems separated out, rather than being treated as a special case of touching-vug fabrics, as in the Lucia classification scheme. The latter distinction is made here because of the dramatically different permeability of connected fractures and the different scale on which connected joint systems work (see next section). Lucia's work is primarily focussed on carbonate sedimentology and petrophysics, with fractures given a reduced role; the modified scheme proposed in Fig. 6.36 allows for the fracture classifications of Nelson (2001) to be overlain.

The typical porosity-permeability characteristics of the Lucia rock fabrics are shown in Fig. 6.37, with a fracture group added alongside.

These classification schemes attempt to isolate the underlying controls on rock properties, particularly permeability. It should however be emphasized that if the origin of reservoir permeability for any given case is not known and cannot be characterised conceptually, there is

**Fig. 6.35** A variogram for vertical porosity measured in chalk core (Almeida and Frykman 1994). The pattern is a ‘hole’ variogram, showing alternating high and low variance between porosity values, suggesting regular 12 m layering. (Redrawn from Almeida and Frykman 1994, AAPG© 1994, reprinted by permission of the AAPG whose permission is required for further use)

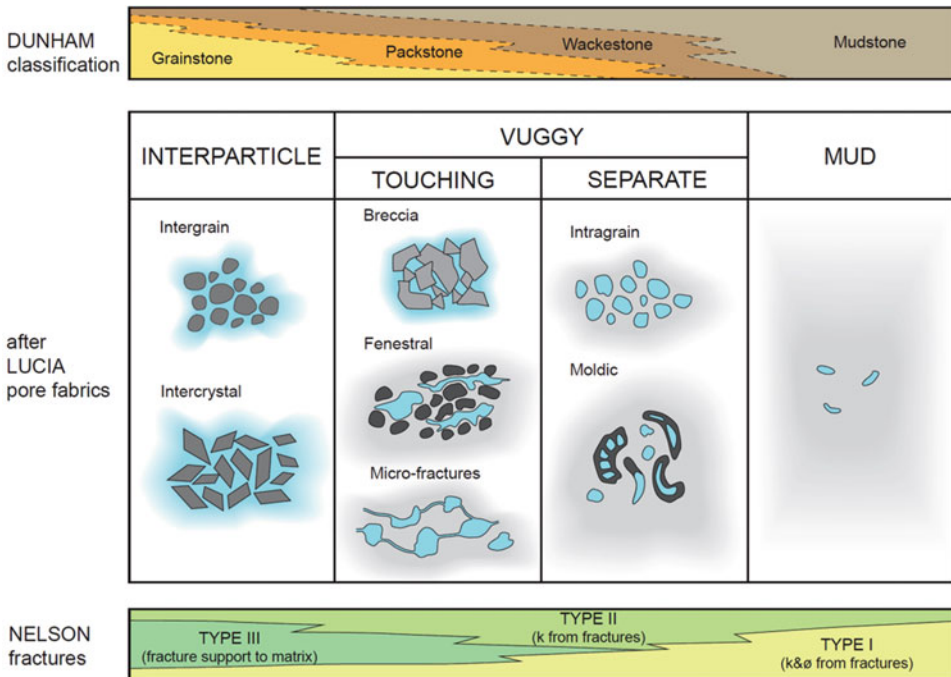
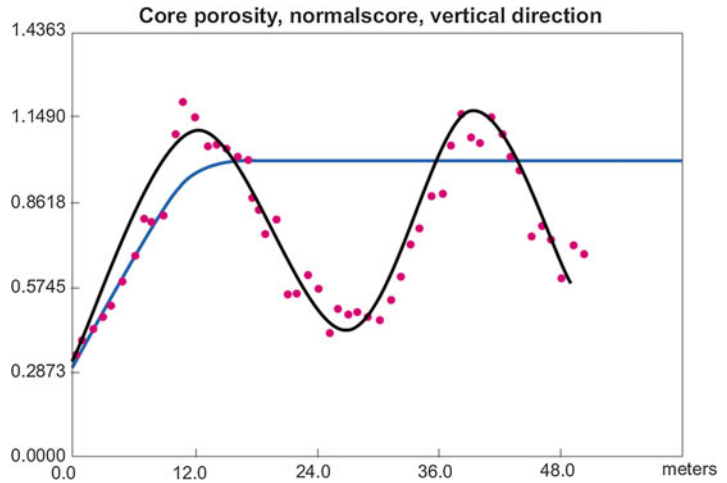


**Fig. 6.36** Carbonate pore fabrics; modified after Lucia (2007) for selecting reservoir modelling elements but including fracture sets, mudstone, the Dunham classification and the typical overlap with Nelson’s fracture classification

little point in embarking on a model, certainly if the end-result is simulation. Simple log-based porosity modelling and the application of a log-linear transform from porosity to permeability is likely to produce a weak model.

### 6.6.3 Diagenesis

A second important difference between clastic and carbonate reservoir characterisation is the complexity of the diagenetic history as this will provide much of the back-story to the concept for

small-scale permeability architecture, necessary for understanding and predicting flow. For reservoir modelling, the diagenesis storyline needs to be converted into a model parameter which can be overlain, or may completely replace, the

depositional architecture. In clastics, it is unusual for the original depositional fabric to be completely obscured during diagenesis but in carbonates this is much more common, to the point that traditional rock modelling as described in Chap. 2 may no longer be necessary, and the process of modelling can begin with effective property modelling (Chap. 3).

In this case, the desired reservoir model may ‘simply’ be a description of the diagenetic history, parameterised into a set of overlying trends or functions. The example in Fig. 6.38 illustrates this for a thick carbonate-evaporite interval in which diagenesis dominates the depositional fabric and matrix permeability is controlled by dolomitisation. The conceptual model is for the expulsion of dolomitising fluids due to compaction in the basin centre, leading to best reservoir properties along the basin margins. The permeability distribution can therefore be modelled regionally by applying trends sensitive to depth and structural location. The porosity model is generated from upscaled (core-calibrated) porosity logs, but there is no porosity-permeability relationship *per se*.

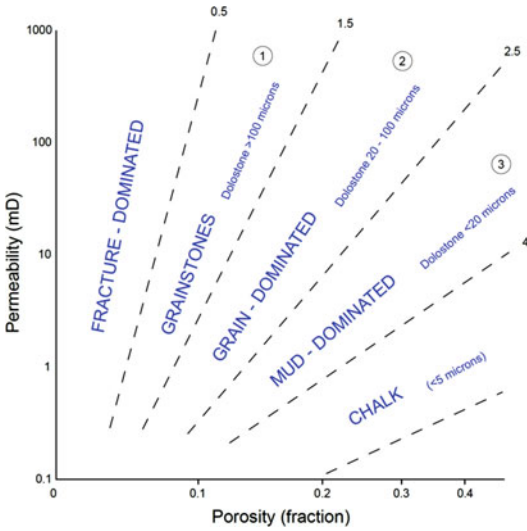


**Fig. 6.37** Pore fabric  $k/\phi$  transforms. (Modified after Lucia 2007)

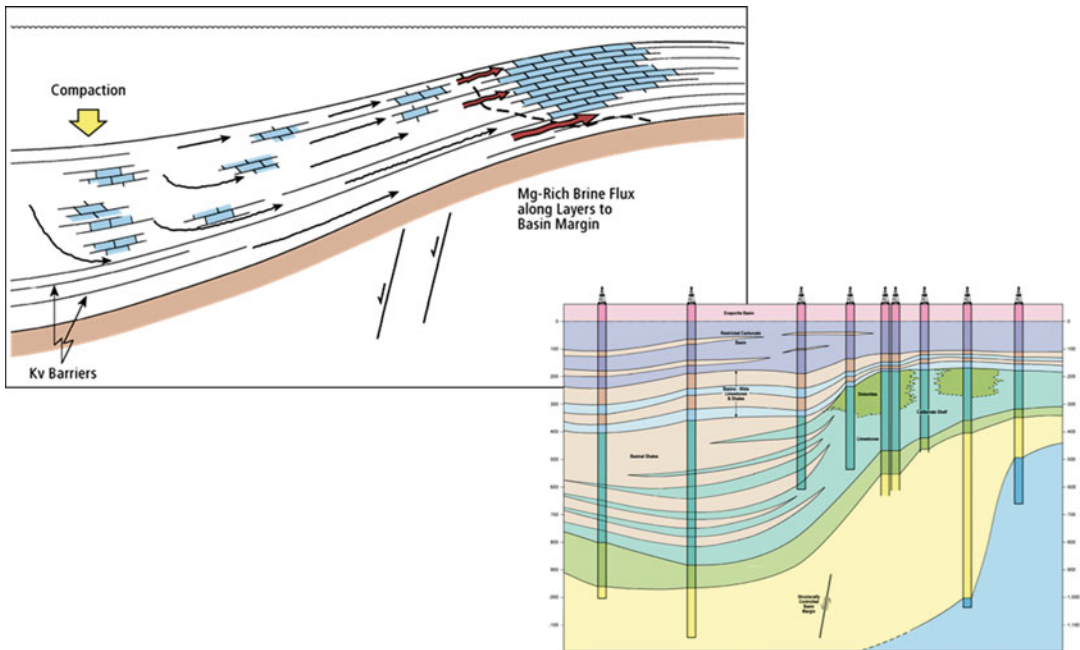


**Fig. 6.38** Localisation of high permeability dolomite along structurally-controlled basin margins

### 6.6.4 Fractures and Karst

A third important difference between carbonates and clastics lies in the mechanical properties of limestones and dolomites. These predispose carbonates to natural fracturing, notably jointing, to a much greater extent than their more argillaceous, clastic counterparts. Near-surface dissolution processes in carbonate rocks result in karst topography in which flow is dominated by the fractures (Fig. 6.39).

Fractured reservoirs are discussed separately below, and it suffices to say here that in the absence of information to the contrary it is wise

to assume some degree of natural fracturing occurs in *any* carbonate reservoir.

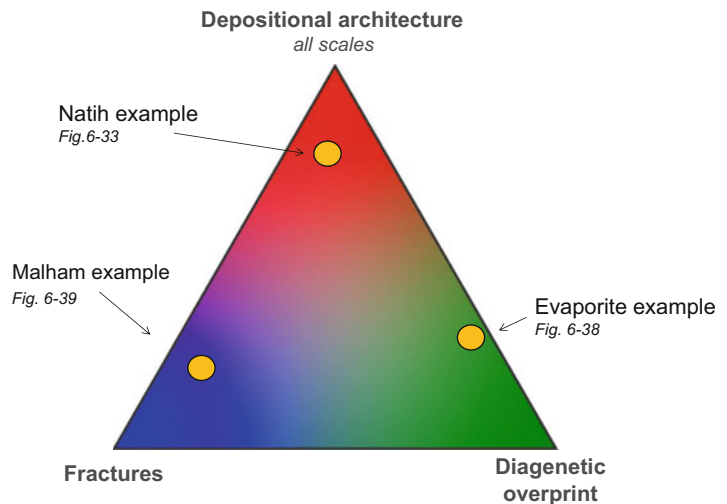
### 6.6.5 Hierarchies of Scale – The Carbonate REV

A starting point for the characterisation of a carbonate reservoir for reservoir modelling is therefore to view the depositional architecture, the diagenesis and fracture patterns all as potential inputs, and determine the relative importance of each on permeability, at the scale of interest (Fig. 6.40).

**Fig. 6.39** Karstified natural fracture system in limestone, Malham Tarn, UK



**Fig. 6.40** Ternary diagram of influences on carbonate reservoir modelling with examples from this section





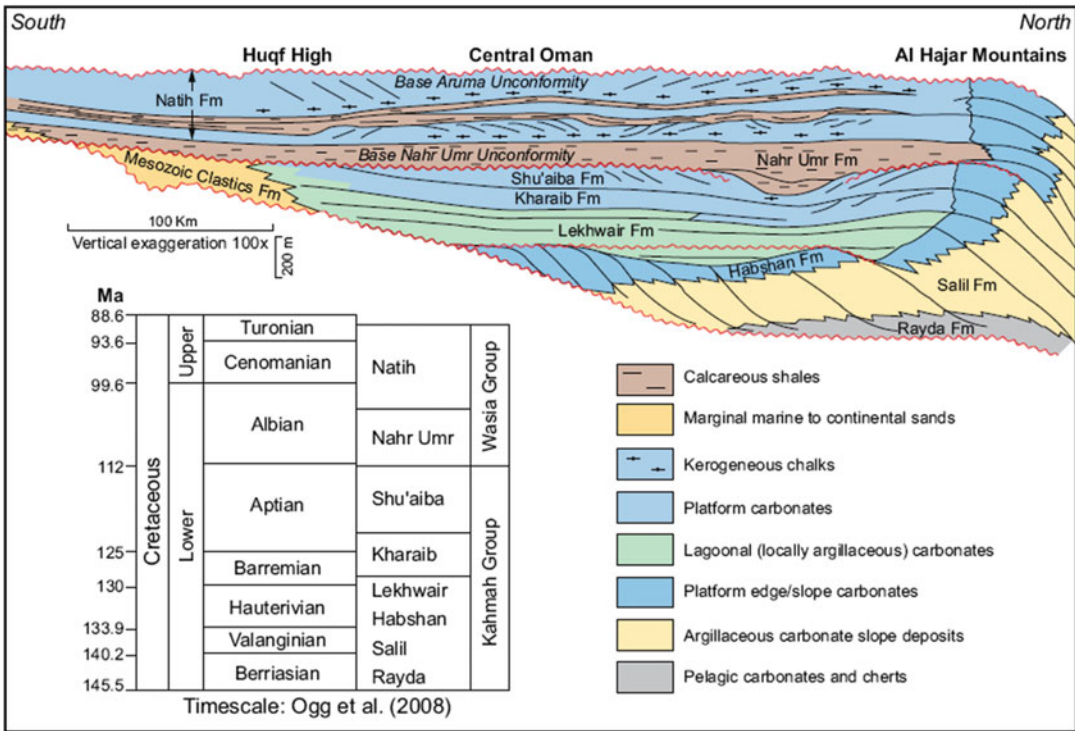


**Fig. 6.41** Sequence-based framework for the Kahmah and Wasia Group reservoirs in North Oman. (After Droste and Van Steenwinkel 2004)

Having determined dominant influences on reservoir quality, these then need to be placed in a large-scale framework, which for carbonate environments is usually a sequence-based hierarchy, such as the example from Oman (Droste and Van Steenwinkel 2004; Fig. 6.41).

A key topic for attention in carbonate reservoir modelling is how to take interpretations of small-scale pore fabric (Fig. 6.36) and map these onto a large-scale chronostratigraphic framework such as that in Fig. 6.41. In a clastic reservoir the route would be via depositional architecture (facies & facies associations), but this only applies to carbonates at one tip of the ternary of influences (Fig. 6.40). Even then the task remains of finding the REV for the intermediate scales between pore and region. Carbonate modelling requires the integration of all three nodes of the ternary in Fig. 6.40, encapsulating the model purpose (Chap. 1) and the scale at which the model purpose applies – the ‘scale of the question’.

These issues have been further explored in recent studies (e.g. Kazemi et al. 2012) which

relate to the hierarchies of REV (described in Chap. 4). An example of how this can be done is shown in Fig. 6.42, working up from the pore scale. The problem at hand is the value of infill drilling in a platform-margin reservoir; the scale of the question is therefore the well spacing, in this case 500–1000 m. The reservoir is characterised by local sponge build-ups in a bioclastic background, as observed at outcrop analogue (centre of Fig. 6.42). In this case, permeability does relate to the original depositional architecture, which places this case at the top apex of the ternary plot (Fig. 6.40). The difficulty is that the pore fabric in the sponges is not sampled in a representative way by core plugs, so the core-based data source for permeability estimation is insufficient.

As in the case of thin beds in siliciclastic reservoirs, a solution lies in the decoupling of porosity and permeability modelling, but this time at the pore fabric scale (Fig. 6.42). The sponge-dominated model element is a

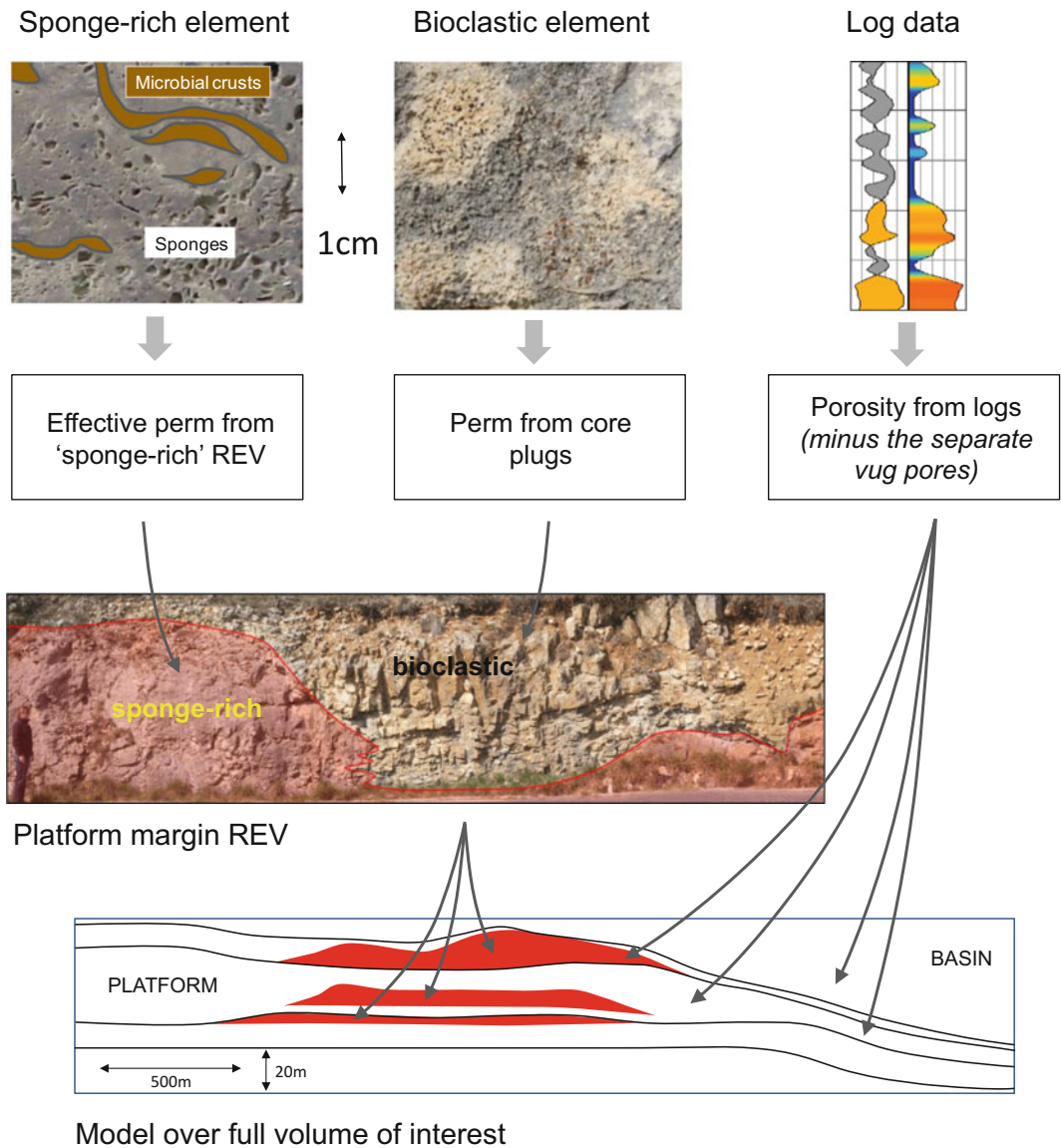


**Fig. 6.42** Workflow for modelling pore-scale detail in a larger scale carbonate model for a platform margin. *Top*: pore scale elements, the REV for one of which is captured at the core plug scale, the other requiring effective property modelling to quantify; *middle*: outcrop analogue guiding the concept for architectural arrangement of elements

within a layer, the second REV scale; *lower*: sequence-based framework showing the location of the sponge-dominated REVs, scale informed from the work of Leonide et al. (2012). Porosity is modelled directly from logs

combination of separate-vug and touching-vug pore fabric in a very low permeability mudstone background mixed with algal crusts which have no effective porosity. Small-scale modelling can deliver estimates of the effective permeability of the sponge-rich element which can be combined

with the bioclastic element at the next scale up (layer scale). The inter-particle permeability for the bioclastic facies is, however, sampled reasonably well at the core plug scale, so this part of the layer-scale model can be populated directly from core data.

The effective permeability of the layer-scale model can be determined by a small model on the scale of metres (the outcrop-analogue scale and the ‘platform margin’ REV), and this can be fed into the sequence-based framework of the larger scale model, scaled appropriately to answer the infill well spacing question. Note that a full-field model is not required to address the question at hand.

Meanwhile, porosity can simply be derived from logs upscaled into the largest scale model, unless there is a reason to believe the averaging of the tool is significantly non-additive (see Chap. 3). A common cause for this in carbonates is non-contributing vuggy pore space (porosity that does not contribute to flow), and this needs to be compensated for in the petrophysical model (see Lucia 2007, for a suitable approach).

The handling of porosity and permeability is therefore largely decoupled in this workflow. This is necessary here, not because there is no clear  $k/\phi$  relationship, but because the relationship is not captured at the scales at which the porosity and permeability data are gathered. Arguably, average porosity could also be derived from the multi-scale models. The disadvantage of this approach is that the average porosity variation captured by the field-wide log dataset would be missed, and this would degrade the other main model purpose, which is to estimate pore volume across the volume of interest.

Small-scale complexity does not therefore rule out reservoir modelling, it simply means an alternative workflow is required, in which the modelling of porosity and permeability may be decoupled. Porosity may justifiably be modelled from log values. Permeability may need to be forward-modelled from small-scale data, accompanied by an architectural concept for permeability distribution – the conceptual sketch.

### 6.6.6 Conclusion: Forward-Modelling or Inversion?

Are carbonate reservoirs more difficult to model than clastic reservoirs? We would suggest not necessarily, but the model designs *will* be

different (Agar and Hampson (2014) give a good summary of future directions in carbonate modelling). The same design elements apply to all reservoirs: concept – element selection – architectural arrangement – algorithm choice – model scaling – uncertainty-handling, but different choices will be made.

The total property modelling concept (Chap. 3) is especially applicable to carbonate reservoirs, as is the multi-scale effective property modelling approach (in place of simple poro-perm cross-plots) described in Chap. 4. The need to overlay an open natural fracture network on the matrix properties is also more common.

When carbonate reservoir modelling becomes especially involved (e.g. multi-scale, with matrix and fractures), the expectation of an accurate forward model of the reservoir should be reduced, and more emphasis placed on inversion from production data. This philosophy is explored further in the section on fractured reservoirs, below.

## 6.7 Fractured Reservoirs

All reservoirs are to some extent influenced by fractures. For some reservoirs the effects of fracturing are minor and can be neglected, whereas for other reservoirs the structural effects are so important that the sedimentary and diagenetic aspects turn out to play only a minor role. It is also often true that the effects of fractures are initially assumed to be of little importance, but once more production data accumulates the fractures start to reveal themselves and are often unexpectedly open to flow. As the interest in reservoirs changes from production to disposal and storage this is increasingly the case, and increasingly of interest in reservoir modelling.

When reservoir flow performance becomes influenced by fracture systems, it is necessary to adjust modelling workflows to include fracture properties as an element in the sense introduced in Chap. 2: “*three-dimensional rock bodies which are petrophysically and/or geometrically distinct from each other in the specific context of the reservoir fluid system*”.

The properties of such elements were discussed in Chap. 3 alongside the modelling of matrix properties. In this section, approaches for applying those fracture properties across a larger scale reservoir system are explored.

### 6.7.1 Fracture Concepts

Pivotal to a reasonable representation of a fractured reservoir is a clear understanding of the predominant fracture mechanism operative in a field, and hence an understanding of the resulting fracture type – the *underlying concept*. This is true for all reservoir modelling exercises but is particularly acute in the case of fractured reservoirs which tend to be conceptualised rather narrowly in one of two arche types:

1. Regular, dense, open fracture systems which dominate flow: the classical ‘naturally fractured reservoirs’ of Aguilera (1980).
2. Faulted reservoirs, in which the fractures are well-spaced 2D planes picked from seismic, and interpreted as sealing or non-sealing.

This is a limited representation. Reference to analogue outcrops illustrates that true fracture systems are often a blend of these two arche types, and in all cases the fractures themselves are three-dimensional elements, even though broadly planar. Yet reservoir modelling packages treat fractures as 2D features by default.

Section 3.8 considered the properties of fractures as three-dimensional elements and key to this was the distinction between fracture types, notably:

- *joint systems* (tensile fractures) which are often open and if so are typically more permeable than the host matrix and
- *fault systems* (shear fractures) which can be sealing or open but, if open, are typically less permeable than the host matrix.

The distinction between joint and fault systems blurs when both occur together, notably in fault damage zones, which can be an intricate mixture between open and closed fractures and

may include both small-scale faults and joints. Hence the need for a clear concept of the fracture system present in the reservoir and how the fractures relate to the larger scale reservoir framework, both structural and stratigraphic: *the sketch*.

Figure 6.43 shows two common large-scale structural settings, faults and folds, both in mechanically layered stratigraphy. The upper pictures show the analogue and the lower sketches draw out the relationship between the fractures and the larger-scale framework they sit in: the architecture.

The distribution of fracture types is related to the large-scale structural setting and is therefore somewhat predictable if the fracture mechanisms are understood; once this is ascertained, and the properties of the fractures as 3D elements within that concept are estimated, the appropriate workflow can be chosen: *if you can sketch it, you can model it*.

The optimal workflow is rarely the default offered in the common modelling software packages. This is therefore an issue of model design, and is considered below in terms of common naturally fractured reservoir types.

### 6.7.2 Low Density, Compartmentalised Fracture Systems (Fault-Dominated)

Low density fracture systems, with fracture zones widely spaced (decimetre to kilometre) are typically fault-dominated systems with joints restricted to the fault damage zones.

In terms of conceptualizing the large scale framework, this is a matter of interpreting the kinematic setting, guided by the regional tectonic model and observations from seismic. The principle settings are extensional (dominated by normal faults), compressional (dominated by reverse or thrust faults) and wrench (dominated by strike-slip faults). All intermediate cases between these three end-member cases are possible, hence the terms ‘oblique-slip’, ‘transtensional’ and ‘transpressional’ to cover hybrid cases on the ‘tectonic spectrum’ (McCoss 1986, Fig. 6.44). Faults also tend to reactivate, for example normal

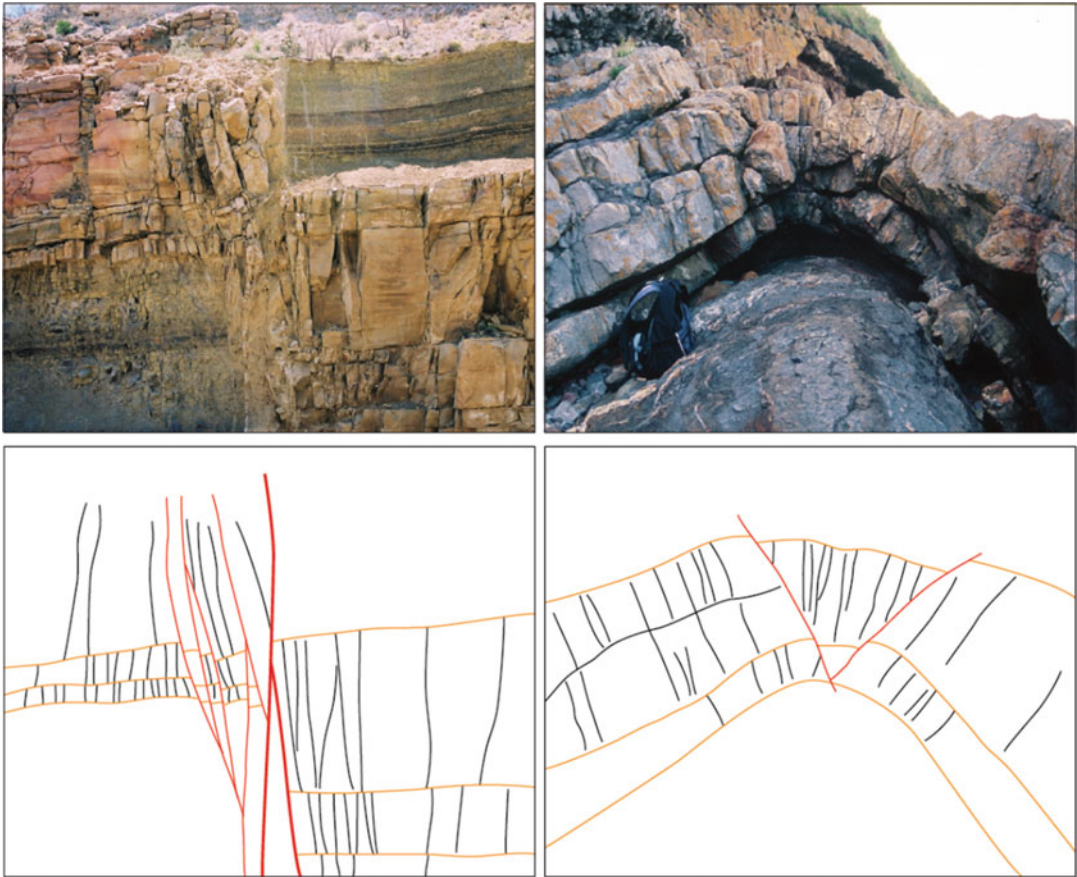


**Fig. 6.43** Architectural arrangement of fracture types in contrasting settings. Left: fault-related fracturing in deep marine sediments from Brushy Canyon, USA; right: fold-

related fracturing in limestones from Northumberland, UK. Faults are indicated in red, joints in grey

faults in extensional basins may subsequently experience reverse fault motion during later phases of basin compression – the process of ‘structural inversion’.

Note that rocks are always in net compression at shear failure, irrespective of whether the regional tectonic picture is described as ‘extensional’, ‘compressional’ or ‘strike-slip’, the latter terms simply describing the relative position of the principal stresses at failure. This follows the founding structural principle of Anderson (1905) which relates the stress system to the style of faulting, in which  $\sigma_1 > \sigma_2 > \sigma_3$  and the three axes are differently aligned to create normal, reverse and strike-slip displacements (Fig. 6.44). For a fuller understanding of the processes

involved in shear we refer you to texts such as Twiss and Moores (1992) and Mandl (2000).

Faults form as part of a network (Fig. 6.45), and a key characteristic of fault networks is their scale invariance – similar fault patterns can be observed on a range of scales. They are fractal, although the smaller-scale, sub-seismic faulting tends to be neglected in reservoir models.

On closer inspection, faults such as those in Fig. 6.45, although clearly planar features, reveal their three-dimensionality (Fig. 6.46).

In reservoir modelling and simulation we are concerned with the effects of faults on fluid flow and also their tendency to compartmentalise the reservoir volume. There are four main activities in the model build:

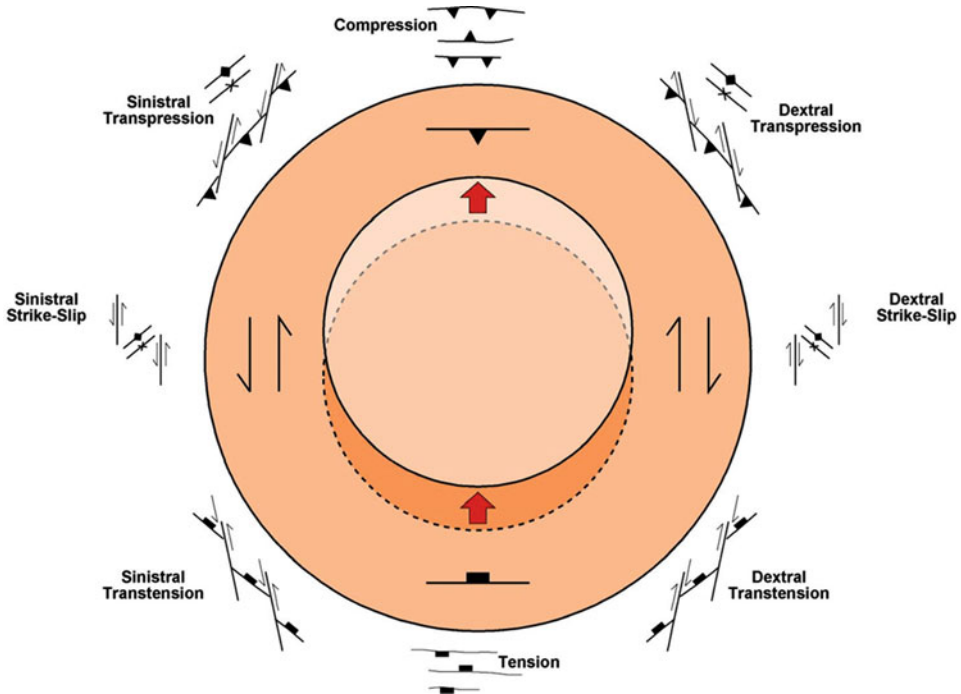


**Fig. 6.44** The ‘tectonic spectrum’ after McCoss (1986), summarising the intermediate cases between the Andersonian end-member fault categorisation relating faults to the principal stress directions (extension, strike-slip and compression)

**Fig. 6.45** Normal fault network in interbedded clastics; large-scale shear fractures attended by smaller-scale shear fractures, but forming an overall low density fracture system, Somerset, UK

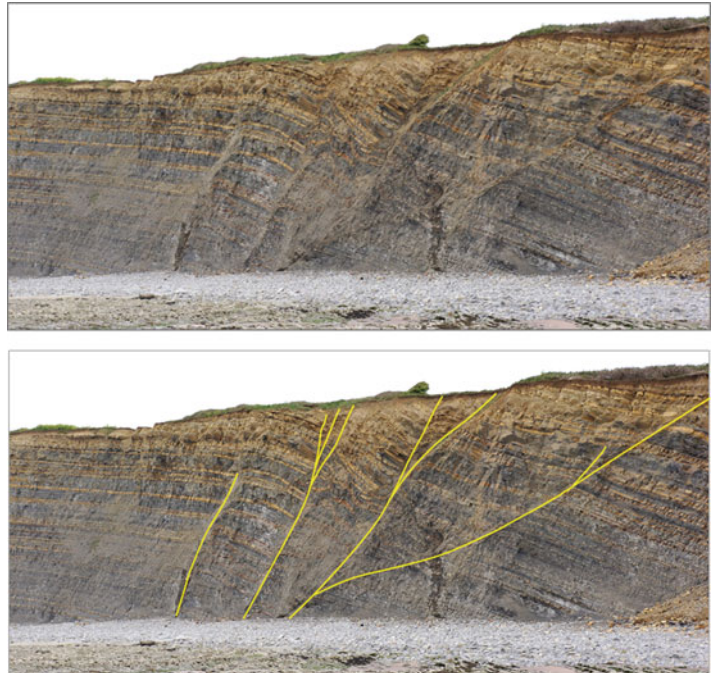
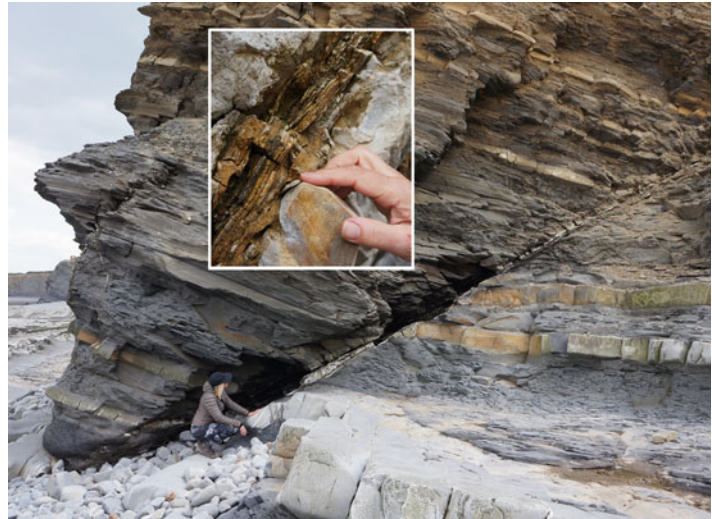


**Fig. 6.46** Normal fault in interbedded clastics; the inset shows the detail of the fault zone: planar, but three dimensional, Somerset, UK



1. Representing the irregular fault network reasonably in a relatively regular cellular framework.
2. Capturing layer juxtapositions around the fault zones accurately.
3. Considering the impact of the sub-seismic fault network.
4. Applying properties to the fault zone elements and considering three dimensional flow effects within the fractured volume.

**Representing the Network** For sealing faults the precise geometry of a given fault is not crucial; the priority is identifying compartments and allocating volumes between compartments reasonably in the context of the model purpose. Fig. 6.47 shows the conversion of a structural interpretation from seismic into a simpler representation of fault compartments. As long as the volumes within-compartment are maintained, and the addition of compartmentalising sub-seismic faults is plausible within the kinematic concept and also with production data and material balance, then the representation is reasonable.

**Layer Juxtapositions** If faults are not fully sealing then attention needs to be paid to the 3D mapping of layers and faults around fault

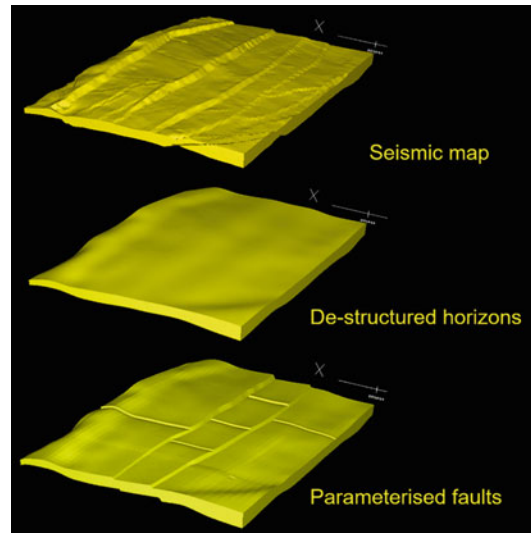


**Fig. 6.47** Example workflow for modelling faults from seismic data (central fault block is ~1 km wide). (Equinor image archive, © Equinor ASA, reproduced with permission)

zones. Layer juxtapositions across faults and lateral fault intersections are rarely resolved accurately from seismic as image quality tends to deteriorate close to faults. It is therefore typically necessary to edit the raw seismic interpretations to produce a network which is structurally plausible (Fig. 6.48).

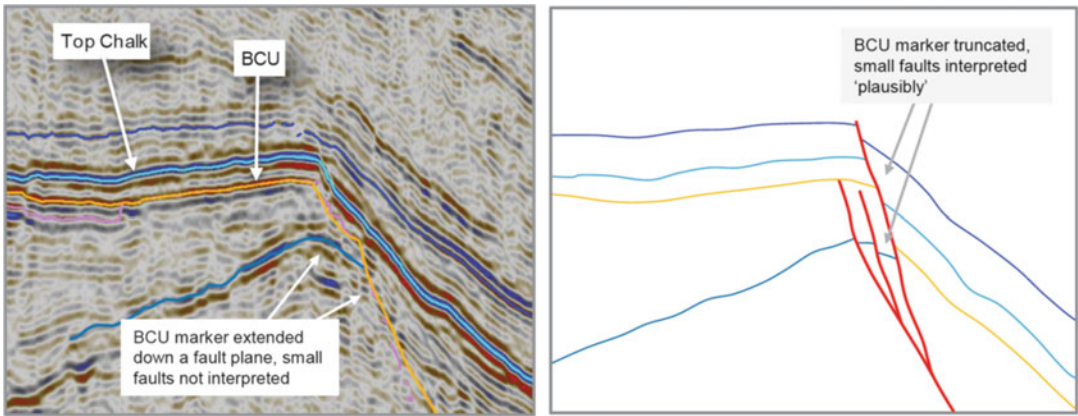
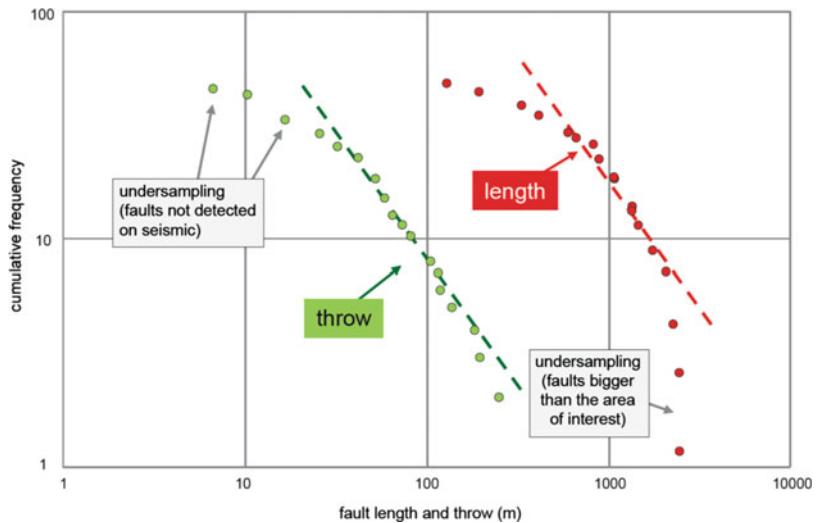


**Fig. 6.48** Editing the raw seismic fault and layer interpretation (left) to restore plausible geometries (right)

**Fig. 6.49** Faults are fractal – networks display scale invariance in terms of geometries; one large seismic fault is an indication of many smaller, sub-seismic faults



**The Sub-seismic Fault Network** Fault systems, unlike joint systems, are fractal in nature (Scholz and Aviles 1986; Walsh et al. 1991) so fault networks show size and property distributions which usually follow a power law (Fig. 6.49). Walsh and Watterson (1988) showed that for many real fault datasets the length of a fault, L, is correlated with the maximum displacement on the fault, D, such that:

$$D = L^2/P \tag{6.1}$$

where:

P is a rock property factor.

A 10 km-long fault would typically have a maximum displacement of around 100 m. Similar relationships between fault thickness and displacement have also been established by Hull (1988) and Evans (1990).

If the structural concept for the field is one of faults which are baffling to flow then a large-scale fault network, mapped from seismic, can be expected to be accompanied by smaller-scale faults causing some effective permeability reduction on a cell scale (see Lescoffit and Townsend 2005 for a description of the impact of fault seal on production forecasting). Any such adjustments



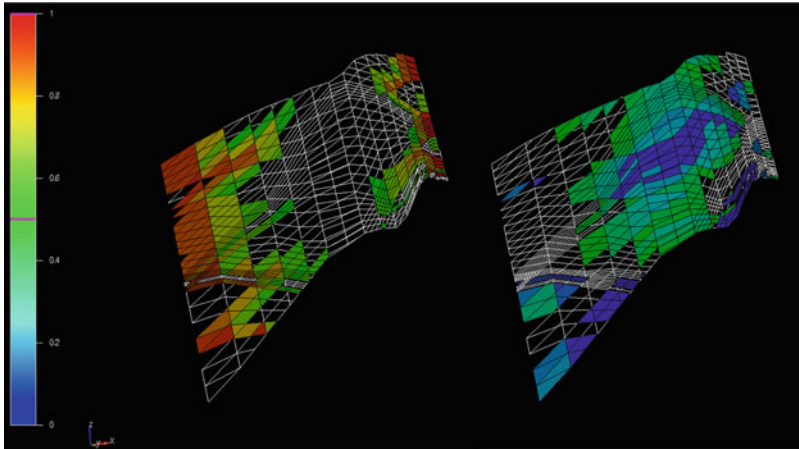


**Fig. 6.50** Example fault-plane mesh (circa 5 km long and 100 m high) showing hanging-wall to footwall grid connections with estimated fault transmissibility multipliers: *hot colours* representing higher

transmissibility at fault margins (*left*) and *cold colours* representing lower transmissibility closer to the centre of the fault (*right*). (Equinor image archive, © Equinor ASA, reproduced with permission)

to permeability should honour the overall structural concept, distinguishing regions affected by faults and those not and honouring structural anisotropy in  $k_x$  and  $k_y$ .

**Applying Properties to Fault Zone Elements** Properties of sealing fault zones were discussed in Sect. 3.8 and representation of those properties in reservoir simulation models came down to transmissibility multipliers on the simulation cell boundary (Fig. 6.50) with or without multi-phase effects or alteration of the cells adjacent to the fault plane as a proxy for the damage zone. The latter option allows detailed analysis of the effects of faults on flow, but is rarely used because it may be computationally demanding, and involves the overwriting of the matrix properties.

### 6.7.3 Low Density Fracture Systems, Open to Flow (Fault-Dominated)

The discussion above concerns situations in which low density fracture systems tend to reduce permeability *across* the fault zone. There is now an increasing awareness that even if a fault core is

sealing, the fractures in the fault damage zone may be open to flow *up or along* the fault zone.

The fault zone in Fig. 6.51 from the Urganian Limestone in Provence illustrates this. This is a normal fault with a well-defined slip plane and a highly sheared and sealed fault core. The core is surrounded by a highly heterogeneous damage zone, widest at this location in the footwall. The damage zone contains small faults and a large number of open joints with a typical spacing of ca.10 cm. Although the core appears to be sealing, the damage zone is open to flow, reflected in the karstification of the fault zone which is open to a depth (surveyed by divers and ROVs) of 300 m below the location of the photograph. The fault core is therefore sealing laterally, but is open to flow in the plane of the damage zone, both vertically and laterally.

Figure 6.52 shows a simple model of the Vaucluse system producing under waterflood from horizontal wells. The simulation illustrates the dominance of the fracture network, with high permeability matrix layers providing only secondary shortcuts for the flood front. This is an oil wet system with fracture permeability in the damage zone captured as an REV; with little imbibition expected in the matrix, this has been approximated using a single porosity/single

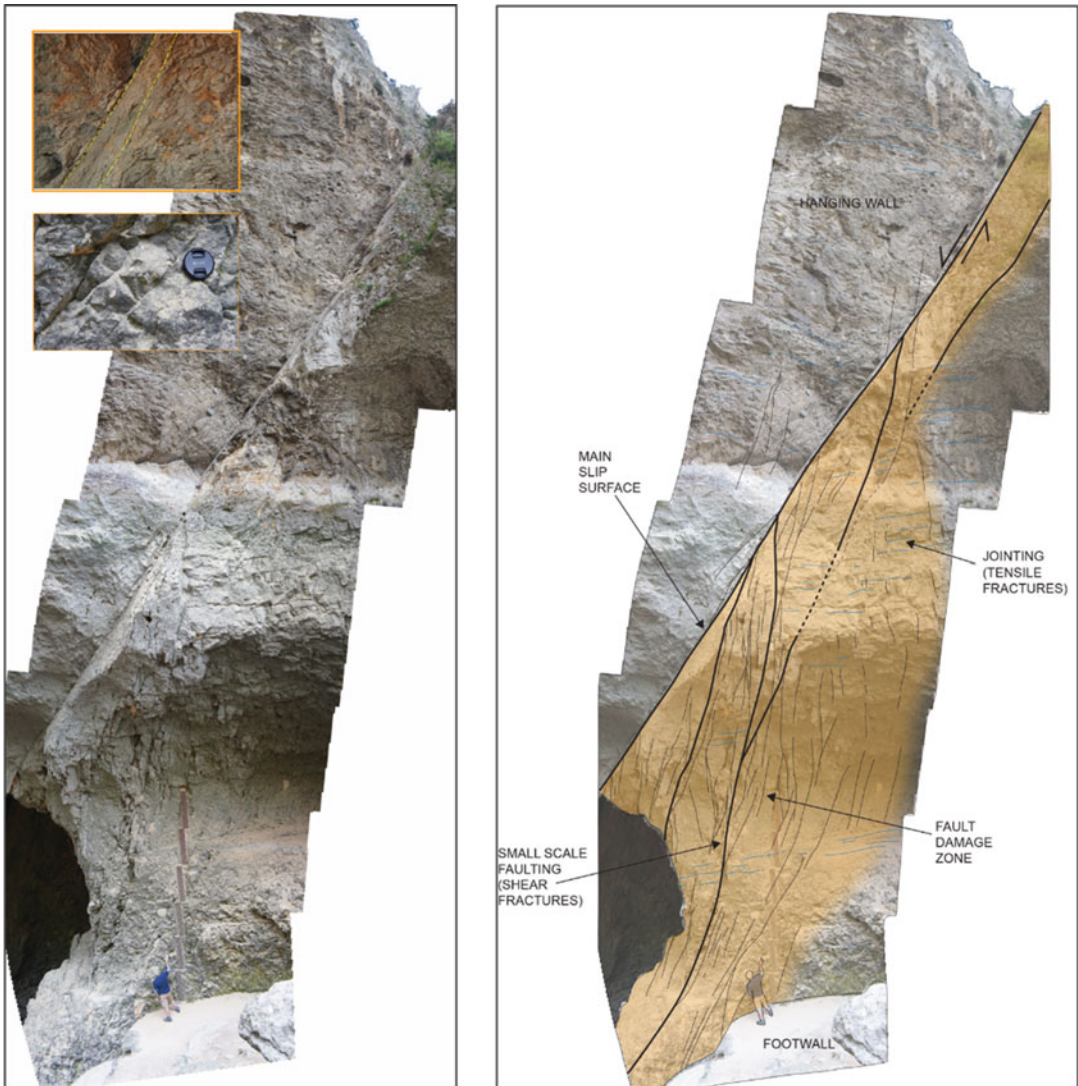


**Fig. 6.51** Open fractures in a fault damage zone in the Urgonian Limestone: upper left inset shows the highly deformed fault core, bounded by yellow dashes, lower

left inset shows closely-spaced open joints in the damage zone; note high degree of asymmetry in the damage zone, Fontaine-de-Vaucluse, France

permeability simulation. For different wettabilities, a more complex representation is required (see next section).

The same phenomenon is prone to occur in the subsurface in reservoirs which are faulted and mechanically brittle enough for tensile failure in the fault footwalls and hangingwalls. This can occur in carbonates or in clastics, typically

phyllosilicate-poor clastics, lacking ductile components to accommodate strain.

The Douglas Field in the East Irish Sea provides an example of this in a siliciclastic system, for which a simple modelling workflow was designed (Bentley and Elliott 2008, based on unpublished work in a similar field by Hadwin). The interpretation of open damage zones was

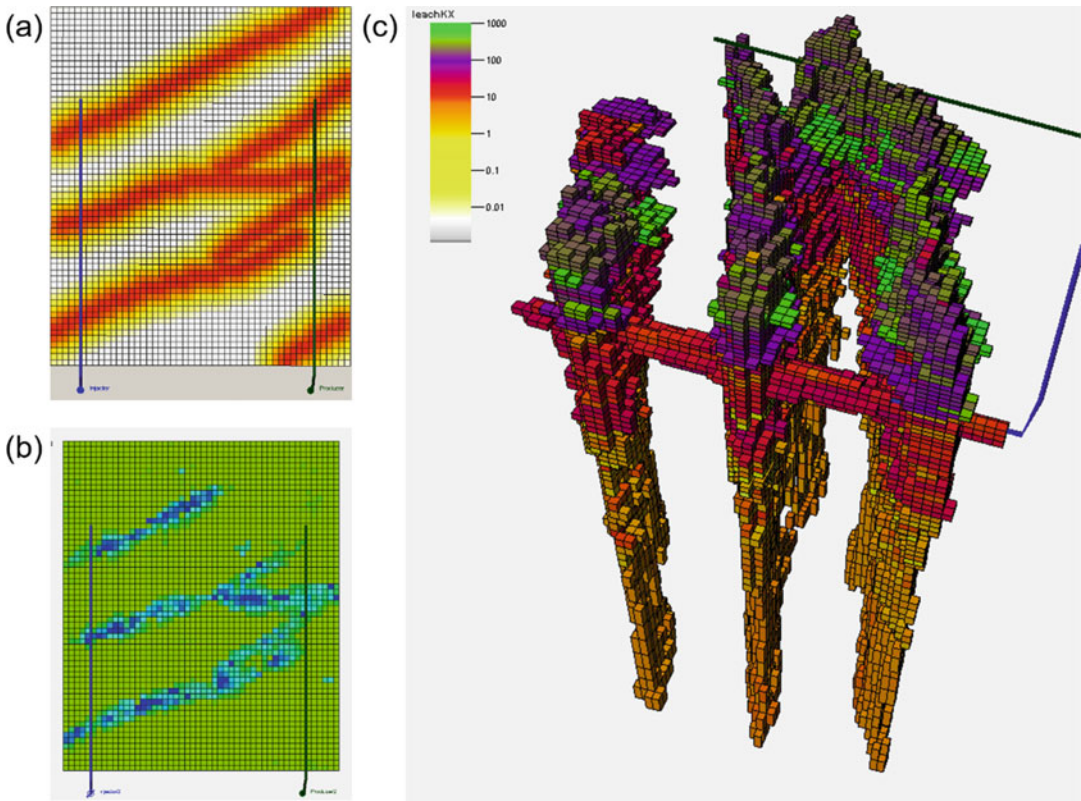


**Fig. 6.52** Waterflood simulation of the karstified natural fracture system in Fig. 6.51 from the Fontaine du Vacluse, Provence: (a) map view of the horizontal producer/injector pair, ornament indicates damage zone permeability (hot colours = higher perm); (b) saturation changes in the model under waterflood (blue = high  $S_w$ , green = high  $S_o$ ), injection well on the left; (c) overview

of the waterflood, expressed in terms of mobility ratio in the model, where  $M = M_w/M_o = (k_{rw}/\mu_w)/(k_{ro}/\mu_o)$ . The short-circuiting of the flood through the fracture system is clear, with only secondary ingress into the matrix (around the injector) and when the fracture system crosses high permeability layers in the matrix. Image courtesy of Ed Stephens

prompted by the anomalous water-cut behaviour of some wells and the inability to match history using conventional simulation modelling of the reservoir matrix. The anomalous behaviour took three forms:

1. Water breakthrough was not matched in wells drilled close to or through major faults.
2. Gas breakthrough was not matched in wells following gas disposal/injection in one well.
3. Flowing bottom-hole pressures were not matched in most wells.

Three activities were initiated: a visit to the core store, an inspection of outcrop analogues, and a re-design of the reservoir modelling

approach based on an updated concept for the reservoir architecture.

The revised concept which emerged from these studies was one of zones of damage around seismic-scale faults containing both permeability-reducing and permeability-enhancing elements. The sealing elements were small shear fractures, observed as deformation bands in quartz-rich layers or as small discrete faults in more mud-rich intervals, and the master fault slip surfaces themselves juxtaposing reservoir against non-reservoir. Evidence of fracturing in the core material is sparse, as the core was taken in vertical appraisal wells, but fracturing was nevertheless observed locally in core as deformation bands and



**Fig. 6.53** Open fractures associated with deformation bands in Ormskirk Sandstone core from the Douglas Field. Left: open fault with slickensides and oil residue;

right: fault zone at an analogue outcrop showing a 1 m damage zone in the fault footwall, Wirral, UK

rare faulted intervals. One fault plane in particular was well preserved in core, was not cemented and, crucially, was observed to be hydrocarbon stained (Fig. 6.53, left). At the outcrop, open joints were clearly visible in fault footwalls (Fig. 6.53, right).

The structural concept which emerged from the review is summarised in Fig. 6.54. Although major faults were tending to seal to lateral cross-flow, either through juxtaposition, the formation of a sealing fault gouge or the generation of deformation bands, the damage zones around the faults included open fractures, either joints or small faults. The joints will tend to be stratigraphically sensitive and bed-limited to the quartz-rich intervals, but the slip surfaces will be through-going. The major faults were therefore exhibiting a tendency to seal normal to the plane of faulting but to be open to flow vertically or laterally along the open damage zones.

In order to model the effects of this concept, involving both conductive fractures and sealing faults, an approach to modelling the fault damage zones was implemented, using artificial wells ('pipes') to create flow conduits along suspected fracture zones.

The pipes were assigned with open flow completions in each simulation grid block along the fracture corridor to allow cross-flow within the formation. Altering the radii of the pipes provided a method of history matching the rapid onset of water production. The resulting flood front pattern is shown in Fig. 6.55, with water migrating up the pipes as a proxy for open fractures in the damage zones, connecting with high permeability layers in the upper dune sands in response to pressure depletion at the wells.

The approach readily allowed a successful history match, replicating the observed water breakthrough patterns, the gas-oil ratio changes and the recorded flowing bottom-hole pressures.

This example illustrates the importance of the conceptual structural geological model as a foundation for modelling. In this case, failure of the initial conceptual model to include the effects of low-density fracture systems was the source of the difficulty in matching the dynamic production data. The change in the geological interpretation was prompted by an accumulation of production data which was inconsistent with the existing interpretations of the field. Once sense-checked against core data, outcrop data and structural

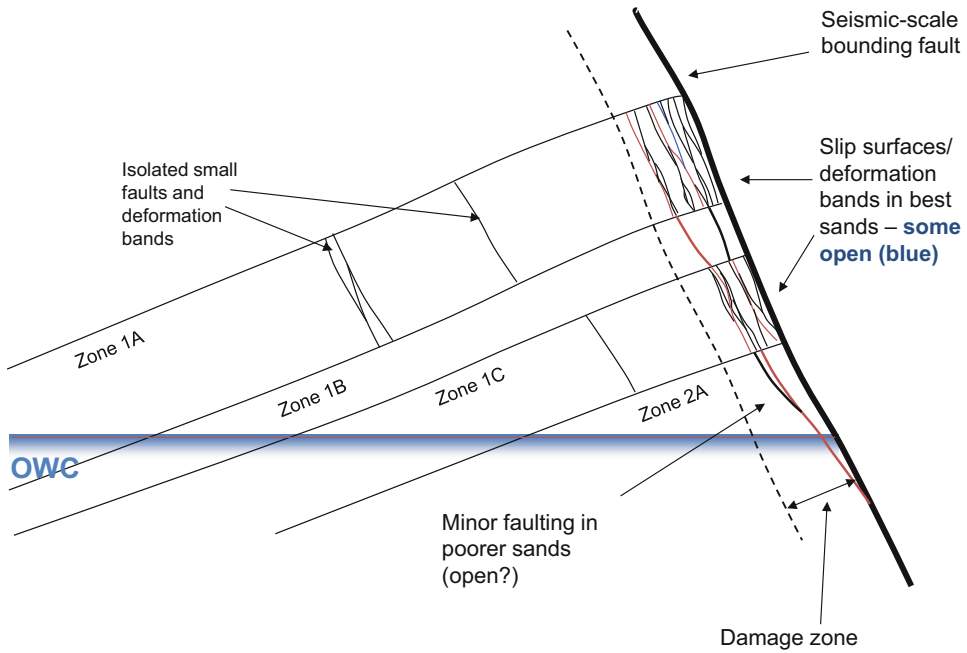


**Fig. 6.54** Structural concept for the major fault terraces in the Douglas field. (Redrawn from Bentley and Elliott 2008, ©2008, Society of Petroleum Engineers Inc.,

reproduced with permission of SPE. Further reproduction prohibited without permission)

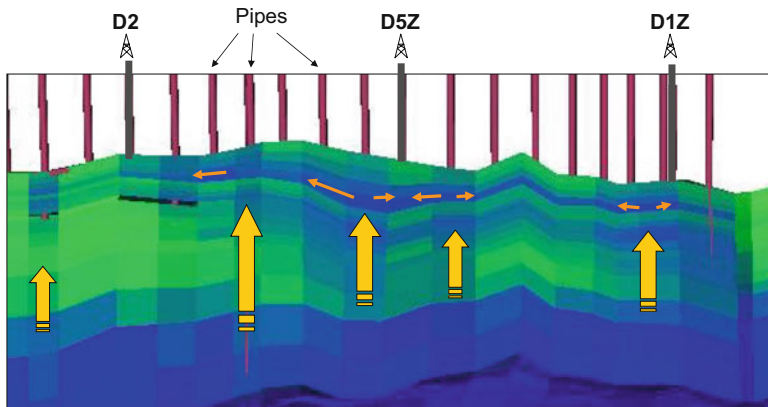


**Fig. 6.55** Use of 'pipes' (dummy wells) to represent open fault damage zones in the Douglas Field. The view is towards the footwall of a seismic-scale fault; blue = water; green = oil, pipes (red) are positioned in simulation grid cells adjacent to the fault. Water is drawn up the damage

zone and along the highest permeability matrix towards the producers (black) in response to depletion. (Redrawn from Bentley and Elliott 2008, ©2008, Society of Petroleum Engineers Inc., reproduced with permission of SPE. Further reproduction prohibited without permission)

geological principles, a new model emerged which was not only geologically plausible but also led to significantly improved interpretation of rather complex subsurface flow behaviour.

This case also highlights the importance of understanding faults as heterogeneous 3D zones, rather than simply 2D planes of offset.

### 6.7.4 High Density Fractured Reservoirs – Open to Flow (Joint-Dominated)

High density fracture networks, in which several fractures may occur per metre over extensive areas, are typically joint sets (Fig. 6.56).

It is these networks which petroleum engineers are typically referring to when the term ‘naturally fractured reservoir’ is used. Analytical reservoir engineering solutions for describing flow in naturally fractured reservoirs typically reference stylised geometries of joint systems (Aguilera 1980), describing the matrix blocks between the fractures as ‘sheets’, ‘match-sticks’ or ‘sugar cubes’ (Fig. 6.57).

The properties of joint sets are influenced strongly by the mechanical properties of layers within the host rock – more brittle beds form joints more readily – so joints are often bed-limited. Mechanical stratigraphy is therefore important in

understanding joint patterns. Unlike fractal fault networks the statistics of joint sets (in terms of frequency vs. size) are typically log-normal.

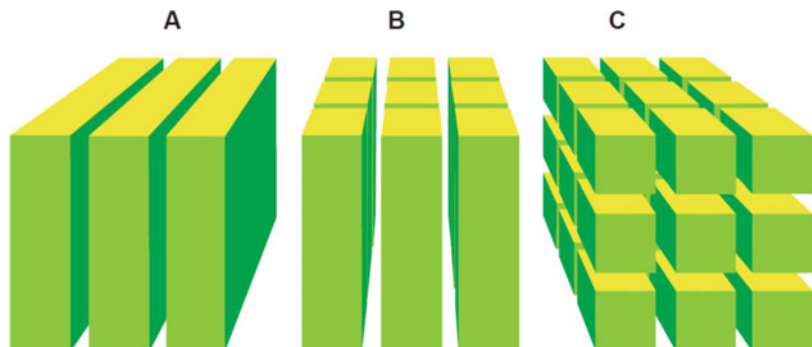
There are numerous ways of modelling high-density fracture systems. From the reservoir simulation viewpoint, the focus is on whether the fracture and matrix should both be permeable and porous, i.e. should neighbouring grid cells connect through the matrix, the fractures, or both. Hence, the distinction between dual-permeability/dual-porosity models, dual-permeability/single-porosity, or single-permeability/single-porosity models. Another workflow choice is whether the fractures are to be modelled as explicit or implicit model properties. The two alternatives are described below.

**Explicit – Discrete Fracture Network (DFN) Models** DFNs involve building digital representations of the actual fracture planes (Fig. 6.58).

**Fig. 6.56** Plan view of an open joint system, with two main joint sets, one abutting the other, Somerset, UK



**Fig. 6.57** Stylised joint systems, (a) sheets; (b) match-sticks; (c) sugar cubes



DFN packages were designed for high density networks and were built for classic joint-dominated naturally fractured reservoirs. Having built them, specialist simulators are then required to model flow through the discrete fracture planes (Fig. 6.59).

From a software perspective, fracture modelling algorithms are less mature than standard modelling tools. They also tend to be

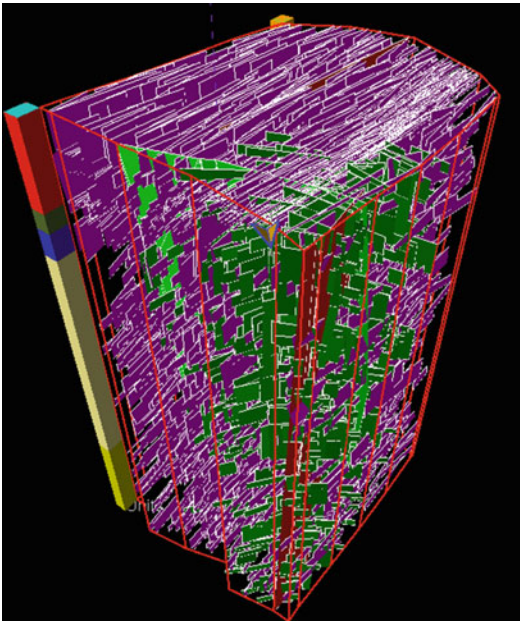
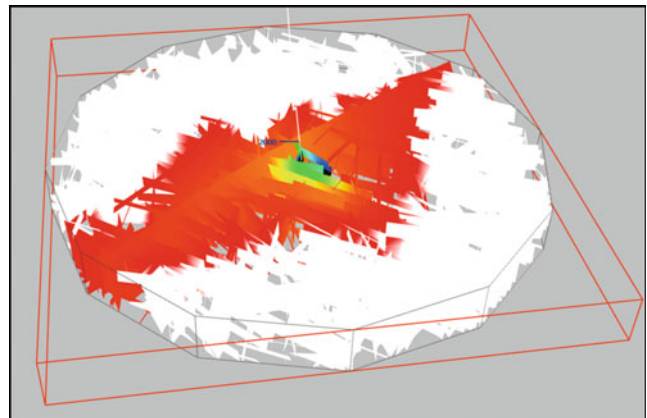


**Fig. 6.58** Discrete Fracture Network (DFN) models: a static fracture model for a near-wellbore volume. (Image courtesy of Tim Wynn)

**Fig. 6.59** Dynamic modelling of a flowing fracture network during a well test. (Image courtesy of Tim Wynn)



incomplete representations, in that there is only so much detail the current algorithms can capture explicitly e.g. are fractures assumed to have constant properties and are joints simply located stochastically rather than in logical abutting patterns such as that in Fig. 6.56? Technical guidance for correctly upscaling multiphase fracture properties is also limited.

Whilst appearing to offer an ultimate solution to the fracture modelling need, the DFN solution is therefore not always manageable or practical, and high levels of approximation must often be accepted to implement this approach. Attempts at full-field DFN models – literally modelling every crack in the reservoir – are generally unrealistic and at a certain level of approximation it can be queried whether the discrete model description is adding much value beyond visualisation.

The more successful implementations of DFN models are those built at the well-model scale, and used to match well test data, e.g. Figs. 6.58 and 6.59. The outputs from this type of explicit fracture modelling in terms of effective permeabilities become the inputs to more implicit modelling methods at the full-field scale, as discussed below.

**Implicit Fracture Property Models** Implicit methods abandon the aspiration to represent every fracture as an explicit plane in the model, and instead treat the dense fracture systems as a

volumetric property of a standard cellular model – effectively a fracture REV.

Simulators can accomplish this when working in ‘dual permeability’ mode. Two modelling grids are set up: one to handle the matrix properties and one to handle the fractures. The two grids exist in the same geographic space and a functional relationship termed the ‘shape factor’, sigma, is used to control how the two cellular frameworks should ‘talk to each other’ and exchange fluids. A common assumption is that capillary flow processes dominate the fluid exchange between the matrix block and the fracture network, while viscous flow processes dominate in the fracture network. Note also that flow in fractures is governed by Poiseuille’s Law (Sect. 3.8).

Given that dual-permeability simulation models need implicit fracture properties, modelling workflows can be devised to provide these inputs from standard geocellular modelling software packages. One such example is shown in Fig. 6.60, following a workflow described in Fig. 6.61, involving the production of reservoir property models for fracture permeability, fracture density, fracture porosity and fracture geometry (affecting the shape factor).

The advantage of implicit fracture modelling methods is that they can be applied in conventional modelling packages, and therefore easily combined with standard workflows for modelling the matrix (the right hand side of Fig. 6.61).

The same logic can be applied to the dynamic model, in which the effective flow properties for a

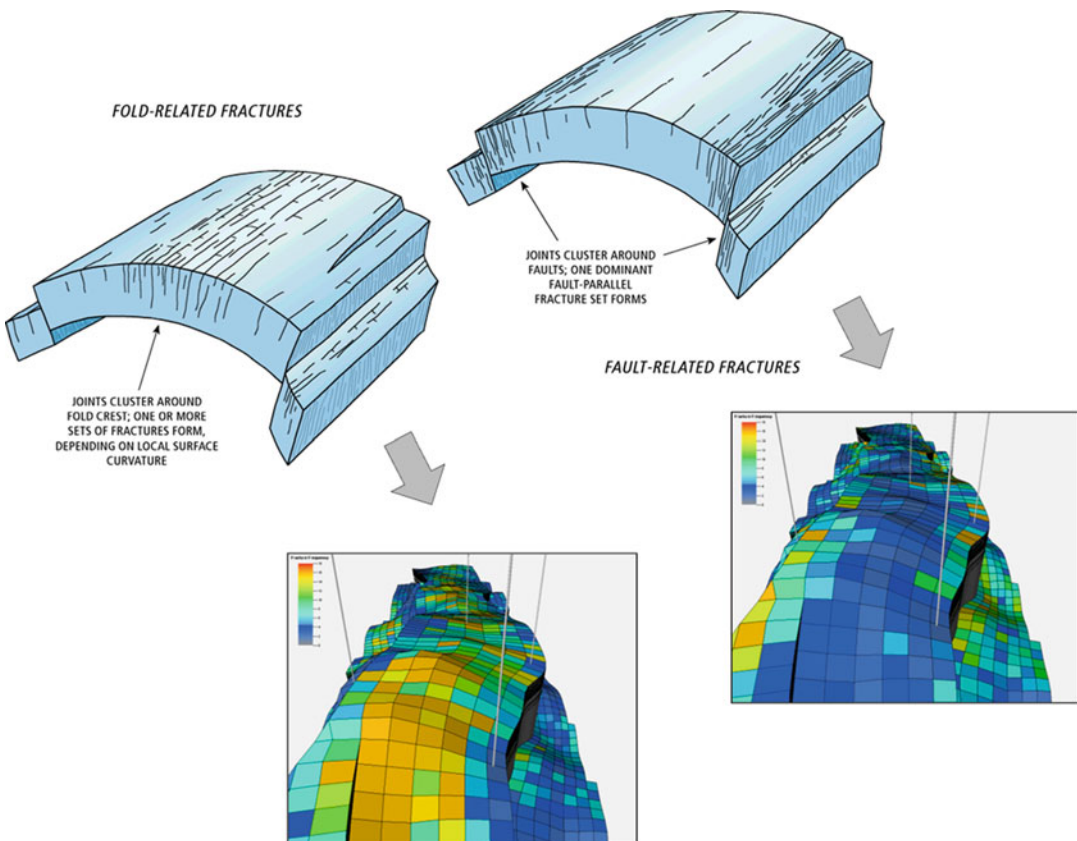


**Fig. 6.60** Alternative concepts for fracture distribution (fold- or fault-related), and property models for fracture density which honour those concepts implicitly (*hot colours* = higher fracture density)



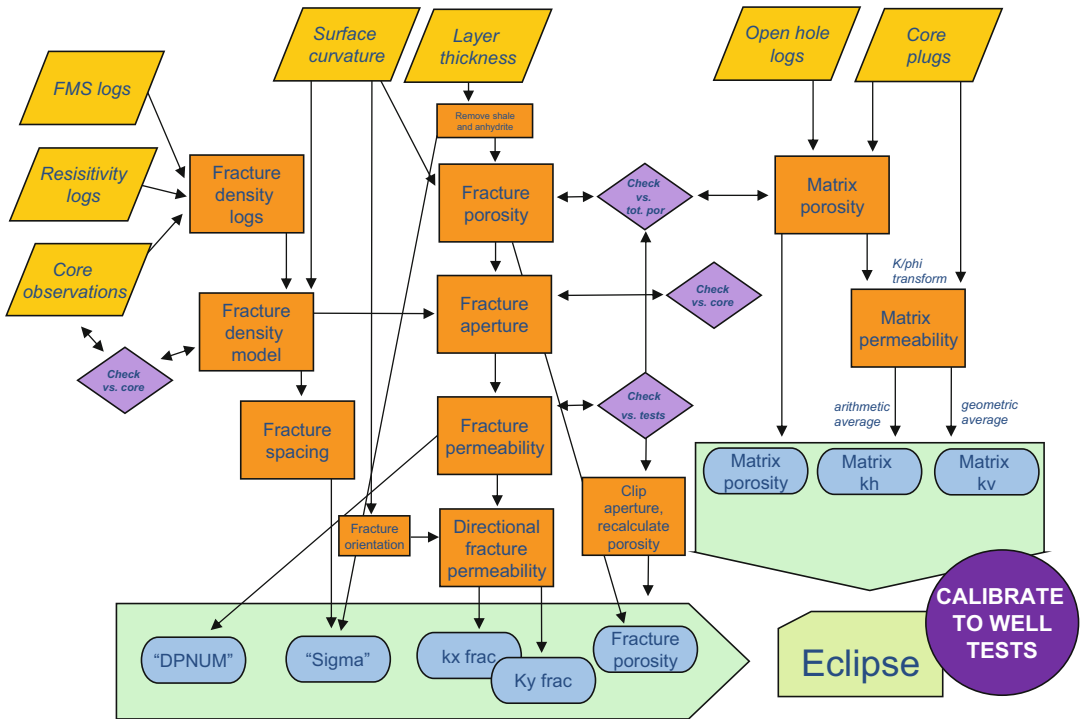


**Fig. 6.61** Workflow for implicit static description of fractures, feeding into standard dual-permeability simulations

fracture REV can be established using small-scale models, and applied directly in a standard single porosity, single permeability simulator. Numerous assumptions must be made along the way, and it is important to check whether the underlying fracture concept has been compromised in the process. This is particularly the case for ensuring an appropriate level of network connectivity on the cell-to-cell scale: if the concept is for field-wide fracture continuity in a particular direction, is that appropriately represented in the dynamic model?

The choice of whether a dual-porosity, dual-permeability simulator is required rather than a simpler standard simulator relates to the matrix properties and in particular the wettability of the rock. If the matrix is tight, and flow only occurs in the fractures (the ‘Type I’ fractured reservoirs of Nelson 2001), standard reservoir and simulation modelling tools can be used. One such case is illustrated in Figs. 6.62 and 6.63 from a fractured granite reservoir. The grid cell shape is closer to cubic than usual ( $dx = dy = dz$ ) such that the

narrow fault core can be represented as a cellular model element, as can the surrounding damage zone.

The cellular values for effective, block-scale permeability were derived from a well test using a small-scale DFN model around the tested well bore and distributed stochastically using SGS through the deterministically-constructed reservoir architecture (Fig. 6.63). The static models were then passed through to a standard black oil reservoir simulator.

If the matrix blocks are permeable and matrix-fracture fluid interaction is important, more complex dual porosity-permeability modelling may be required. This introduces the importance of wettability, as matrix blocks which are water-wet (such as chalk) will imbibe water from a flooded fracture system through capillary imbibition, the displaced matrix oil draining back into the fracture system. A perfectly oil-wet reservoir, by comparison, will not imbibe water into the matrix.

Figures 6.64 and 6.65 illustrate this with example small-scale models related to the

**Fig. 6.62** Static model for a fractured granite, with heterogeneity captured in terms of structural model elements

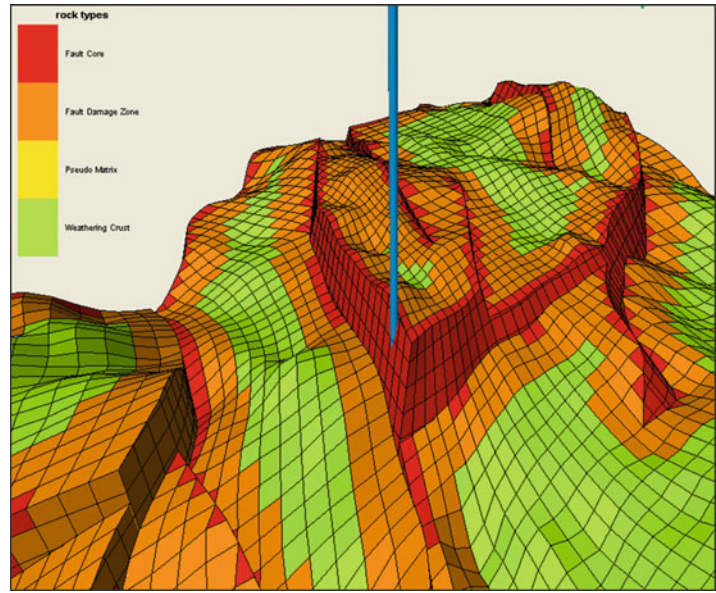
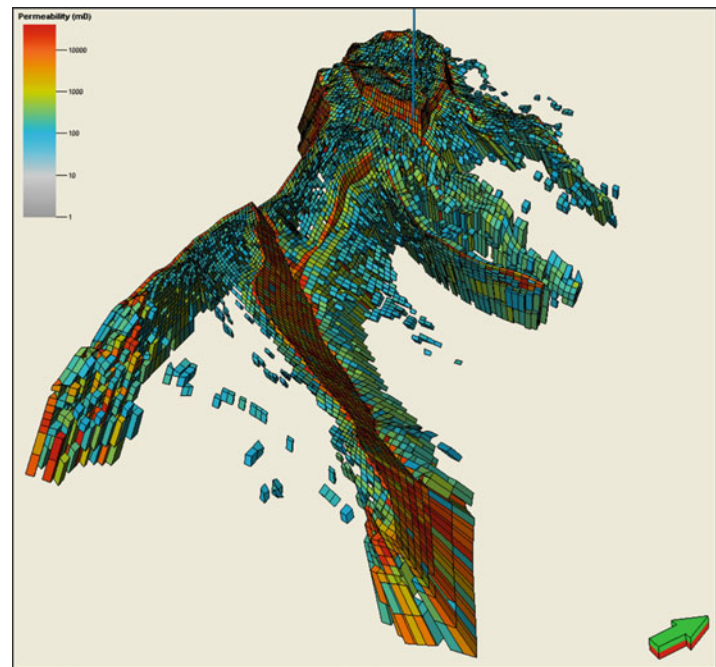


**Fig. 6.63** Effective, block-scale permeability across the full-field model illustrated in Fig. 6.62; with non-reservoir granite cells filtered out



fractured Urgonian Limestone outcrops of the Callanques of Cassis in France.

Three styles of dense jointing are described in Fig. 6.64 relating to the mechanical properties of the layering. The upper images show the outcrops, the central images the

interpretation and the lower images the model representations.

In Fig. 6.65, the models from Fig. 6.64 are simulated in a dual porosity, dual permeability simulator to illustrate the contrasting reservoir behaviours of water-wet and oil-wet matrix

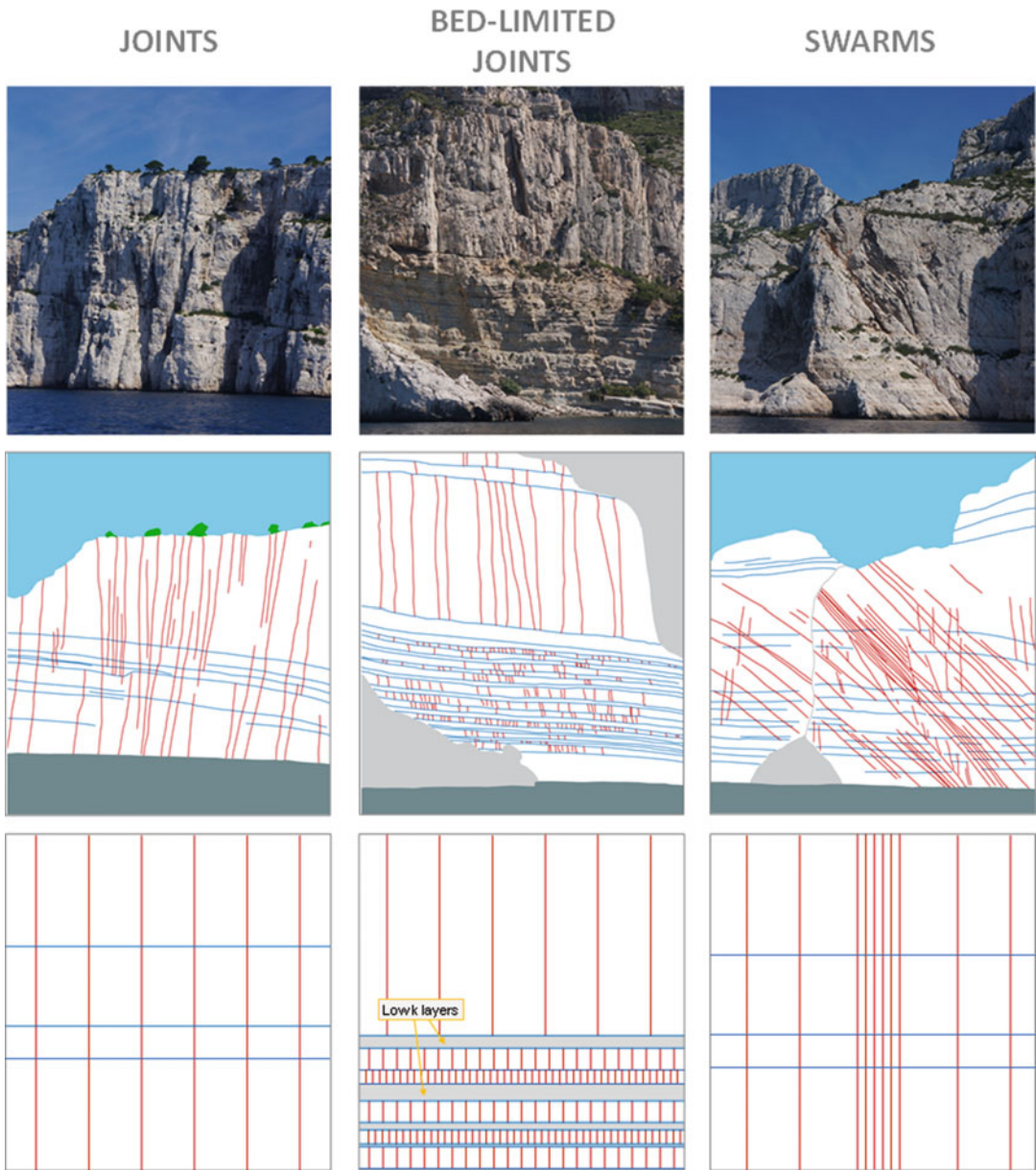


**Fig. 6.64** High density fracture (joint) systems with interpretations and model representation below; Cassis, France

blocks, and the different behaviour of the contrasting fracture patterns under gas-oil gravity drainage.

Suffice to say, central to all of this analysis is a clear understanding of the fracture mechanisms at work in these reservoirs over geological time to produce the architectures and distribution of elements seen today.

### 6.7.5 Forward-Modelling or Inversion in Fractured Reservoirs?

In discussing carbonate reservoirs (Sect. 6.6), the point was made that once a significant number of assumptions have been made in a complex modelling workflow it can be questioned whether attempts to forward-model reality from limited

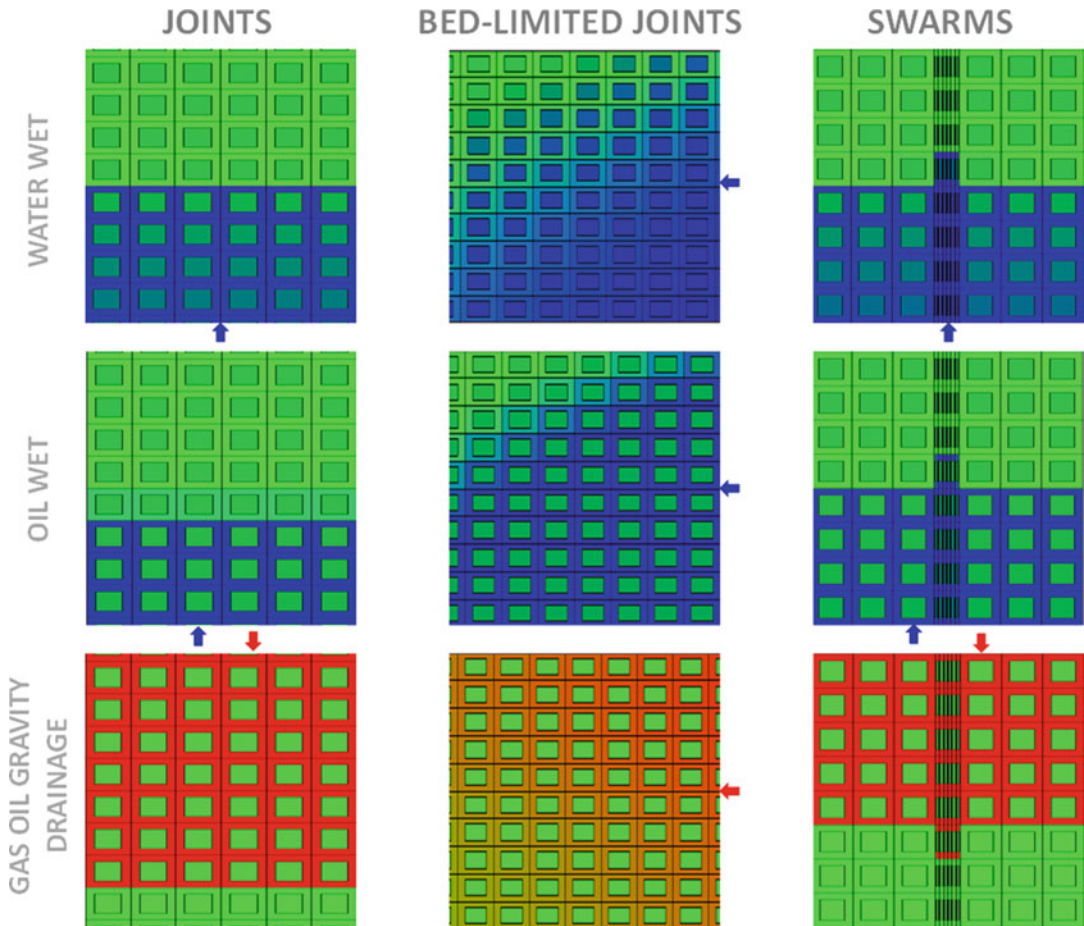


**Fig. 6.65** Simulation of the models in Fig. 6.63 using a dual-porosity, dual-permeability simulator; colours are fluid saturation (green = oil, blue = water, red = gas).

Image courtesy of TRACS (comparative realisations by Richard Oxlade)

data are still valid. This is particularly the case for fractured reservoirs, where necessary static field data is limited and the sensitivity to missing data is high. For example, fracture permeability is particularly sensitive to fracture aperture, yet *in situ* aperture data is extremely difficult to determine. Average aperture can be back-calculated if fracture density and gross fracture porosity are known, but fracture porosity is also difficult to measure and even estimates of fracture density are usually built on very limited data sets. Many assumptions must be made, in addition to those routinely made for modelling the matrix properties. By definition, fractured reservoir

models involve a greater degree of approximation than models for un-fractured reservoirs.

Because of this, there is a greater reliance on using production data, and in this sense fracture models are typically ‘inverted’ from production data rather than forward-modelled from logs and core only. Indeed, one of the most useful roles of DFN software is to reconcile well test data with potential fracture network properties – the missing fracture data is effectively inverted from the well test data.

This is captured in the workflow shown in Fig. 6.61 in which the forward modelling steps culminate in the need to ‘calibrate to well tests’,

after which several of the fracture parameters may need to be significantly adjusted. It is not uncommon for orders of magnitude permeability adjustments to be made in order to reconcile models with production data; in matrix-only reservoirs the permeability adjustments are more normally no more than a factor 2 or 3, or none at all.

This leads to some general implications for the use of fracture models:

1. In inversion-style workflows the production data is often treated as representative for the whole field; if based on a single well test, this is unlikely to be the case.
2. The inversion process is itself non-unique.
3. Because of the above, base-case fracture models are of even less value than base-case matrix models – multi-model uncertainty-handling based on alternative fracture concepts and scenarios is essential.

## 6.8 Fit-for-Purpose Recapitulation

The preceding sections have discussed different reservoir types in terms of their geology, identifying the key issues for reservoir modelling with an underlying assumption that we are generally talking about oil fields. However, as pointed out in Chap. 2 (Fig. 2.14) and then developed further in Chap. 4 (Fig. 4.29) the type of fluid is as important as the type of rock system. The effects of fluid physics have to be considered alongside the effects of rock architecture, and this applies whether flow out of the rock (production) or flow into the rock (injection and storage) are being modelled.

To reiterate the underlying principle, for any given reservoir architecture (clastic, carbonate or structurally complex fields) the impact of the reservoir heterogeneities on flow depends on the fluid system. Using the handy rule of thumb (Flora's rule, Chap. 2):

- A gas reservoir is only sensitive to 3 orders or more of magnitude of permeability variation.

- An oil reservoir is typically sensitive to 2 orders of magnitude of permeability variation.
- Heavy oil reservoirs or lighter crudes under secondary recovery (waterflood) are sensitive to 1 order of magnitude of permeability variation.

This is only a rule of thumb, but reminds us to consider the fluid system before launching into a detailed reservoir modelling study. Gas reservoirs under depletion will require much less modelling and characterisation effort than oil reservoirs under waterflood, and heavy oil reservoirs may require very intense efforts to identify the critical effects of rock architecture on the fluid displacement mechanism.

One important caveat to this principle is that it assumes you know what the permeability variation of your reservoir is *a priori*. We know from our discussion of the treatment of generally incomplete subsurface datasets (Chap. 3) that a few core plugs from an appraisal well may give a false impression of the permeability variation in the reservoir. Several gas reservoir developments started with the assumption that internal permeability variations in the reservoir were insignificant, and that a 'reservoir tank' model was therefore adequate, only to find later that certain previously unidentified high-k thief zones or barriers did in fact have a major impact on the gas depletion rates.

Every heterogeneous reservoir is heterogeneous in its own way. Although this is true, generic issues can be extracted for different reservoir types, as the preceding pages have aimed to illustrate. These common features should allow the reservoir modeller to achieve a fit-for-purpose approach to the case at hand. In all cases three things are essential:

1. Developing good conceptual reservoir models.
2. Understanding how the fluid system interacts with the reservoir heterogeneity.
3. Maintaining alternative concepts in order to handle uncertainties.

## References

- Agar SM, Hampson GJ (2014) Fundamental controls on flow in carbonates: an introduction. *Pet Geosci* 20 (1):3–5. <https://doi.org/10.1144/petgeo2013-090>
- Aguilera R (1980) Naturally fractured reservoirs. Penwell Corp, 521pp
- Allen PA, Underhill JR (1989) Swaley cross stratification produced by unidirectional flows, Beneliff Grit (Jurassic), Dorset, U.K. *J Geol Soc Lond* 146:241–252
- Almeida AS, Frykman P (1994) Geostatistical modeling of chalk reservoir properties in the Dan field, Danish North Sea. In: Computer application, vol 3. The American Association of Petroleum Geologists, Tulsa, pp 273–286
- Anderson EM (1905) The dynamics of faulting. *Trans Edinb Geol Soc* 8(3):387–402
- Bentley M, Elliott A (2008) Modelling flow along fault damage zones in a sandstone reservoir; an unconventional modelling technique using conventional modelling tools in the Douglas Field, Irish Sea, UK. In: SPE paper 113958 presented at Europec/EAGE conference and exhibition, Rome, Italy, 9–12 June 2008
- Bentley M, Hartung M (2001) A 4D surprise at Gannet B; a way forward through seismically-constrained scenario-based reservoir modelling. In: Extended abstract, EAGE annual conference, Amsterdam
- Brandsæter I, Wist HT, Næss A et al (2001a) Ranking of stochastic realizations of complex tidal reservoirs using streamline simulation criteria. *Petrol Geosci Spec Issue* 7:S53–S63
- Brandsæter I, Ringrose PS, Townsend CT, Omdal S (2001b) Integrated modeling of geological heterogeneity and fluid displacement: Smørbukk gas-condensate field, Offshore Mid-Norway. In: SPE paper 66391. Society of Petroleum Engineers, Richardson, pp 11–14. <https://doi.org/10.2118/66391-MS>
- Brandsæter I, McIlroy D, Lia O, Ringrose PS (2005) Reservoir modelling of the Lajas outcrop (Argentina) to constrain tidal reservoirs of the Haltenbanken (Norway). *Pet Geosci* 11:37–46
- Bromley RG (1996) Trace fossils: biology, taphonomy and applications. Chapman & Hall, London
- Burchette TP (2012) Carbonate rocks and petroleum reservoirs: a geological perspective from the industry. *Geol Soc Lond Spec Publ* 370(1):17–37
- Carruthers DJF (1998) Transport modelling of secondary oil migration using gradient-driven invasion percolation techniques. PhD thesis, Heriot-Watt University, UK
- Carruthers DJF, Ringrose PS (1998) Secondary oil migration: oil-rock contact volumes, flow behaviour and rates. In: Parnell J (ed) Dating and duration of fluid flow and fluid rock interaction, Geological Society special publication, 144. The Geological Society, London, pp 205–220
- Ciammetti G, Ringrose PS, Good TR, Lewis JML, Sorbie KS (1995) Waterflood recovery and fluid flow upscaling in a shallow marine and fluvial sandstone sequence. In: SPE 30783, presented at the SPE annual technical conference and exhibition, Dallas, USA, 22–25 October 1995
- Ciftci BN, Aviantara AA, Hurley NF, Kerr DR (2004) Outcrop-based three-dimensional modeling of the Tensleep Sandstone at Alkali Creek, Bighorn Basin, Wyoming. In: Integration of outcrop and modern analogs in reservoir modeling. American Association of Petroleum Geologists, Tulsa, pp 235–259. [archives.datapages.com](http://archives.datapages.com)
- Corbett PWM, Ringrose PS, Jensen JL, Sorbie KS (1992) Laminated clastic reservoirs: the interplay of capillary pressure and sedimentary architecture. In: SPE paper 24699, presented at the SPE annual technical conference, Washington, DC
- Dalrymple RW, Rhodes RN (1995) Estuarine dunes and bars. In: Perillo GME (ed) Geomorphology and sedimentology of estuaries, Developments in sedimentology, 53. Elsevier, Amsterdam, pp 359–422
- Dalrymple RW, Zaitlin BA, Boyd R (1992) Estuarine facies models: conceptual basis and stratigraphic implications. *J Sediment Petrol* 62:1130–1146, *Geoscience* 11:37–46
- de Gennes PG (1976) La Percolation: un concept unificateur. *La recherche* 7:919
- Deutsch C (1989) Calculating effective absolute permeability in sandstone/shale sequences. *SPE Form Eval* 4:343–348
- Dreyer T, Fält L-M, Høy T, Knarud R, Steel R, Cuevas J-L (1993) Sedimentary architecture of field analogues for reservoir information (SAFARI): a case study of the fluvial Escanilla formation, Spanish Pyrenees. In: Flint S, Bryant ID (eds) Quantitative description and modeling of clastic hydrocarbon reservoirs and outcrop analogues, Special publication of the International Association of Sedimentologists, vol 15. Blackwell Publishing Ltd
- Droste H, Van Steenwinkel M (2004) Stratal geometries and patterns of platform carbonates: the Cretaceous of Oman. In: Eberli GP, Maserferro JL, Rick Sarg JF (eds) Seismic imaging of carbonate reservoirs and systems, AAPG memoir 81. American Association of Petroleum Geologists, Tulsa, pp 185–206
- Dunham RJ (1962) Classification of carbonate rocks according to depositional texture. In: Classification of carbonate rocks: a symposium, vol 1. American Association of Petroleum Geologists, Tulsa, p 108
- Elfenbein C, Ringrose P, Christie M (2005) Small-scale reservoir modeling tool optimizes recovery offshore Norway. *World Oil* 226(10):45–50
- Evans JP (1990) Thickness-displacement relationships for fault zones. *J Struct Geol* 12(8):1061–1065
- Fryberger SG (1990a) Eolian stratification. In: Fryberger SG, Krystinik LF, Schenk CJ (eds) Modern and ancient eolian deposits: petroleum exploration and production. SEPM Rocky Mountain Section, Denver, pp 4–1–4–12
- Fryberger SG (1990b) Bounding surfaces in eolian deposits. In: Fryberger SG, Krystinik LF, Schenk CJ

- (eds) Modern and ancient eolian deposits: petroleum exploration and production. SEPM Rocky Mountain Section, Denver, pp 7-1–7-15
- Haldorsen HH, MacDonald A (1987) Stochastic modeling of underground reservoir facies (SMURF). In: SPE paper 16751, presented at the 62nd annual technical conference and exhibition of the society of petroleum engineers, Dallas, TX, 27–30 September 1987
- Hern CY (2000) Quantification of Aeolian architecture and the potential impact on reservoir performance. PhD, unpublished thesis, Institute of Petroleum Engineering, Heriot-Watt University
- Heward AP (1991) Inside Auk: the anatomy of an eolian oil reservoir. In: Miall AD, Tyler N (eds) The three-dimensional facies architecture of terrigenous clastic sediments and its implications for hydrocarbon discovery and recovery. SPEM, Tulsa, pp 44–56
- Holden L, Hauge R, Skare Ø, Skorstad A (1998) Modeling of fluvial reservoirs with object models. *Math Geol* 30(5)
- Howell JA, Skorstad A, MacDonald A, Fordham A, Flint S, Fjellvoll B, Manzocchi T (2008) Sedimentological parameterization of shallow-marine reservoirs. *Pet Geosci* 14(1):17–34
- Huang Y, Ringrose PS, Sorbie KS (1995) Capillary trapping mechanisms in water-wet laminated rock. *SPE Reserv Eng* 10:287–292
- Huang Y, Ringrose PS, Sorbie KS, Larter SR (1996) The effects of heterogeneity and wettability on oil recovery from laminated sedimentary structures. *SPE J* 1(4):451–461
- Hull J (1988) Thickness-displacement relationships for deformation zones. *J Struct Geol* 10(4):431–435
- Hunter RE (1977) Basic types of stratification in small eolian dunes. *Sedimentology* 24:361–387
- Jacobsen T, Agustsson H, Alvestad J, Digranes P, Kaas I, Opdal S-T (2000) Modelling and identification of remaining reserves in the Gullfaks field. In: Paper SPE 65412 presented at the SPE European petroleum conference, Paris, France, 24–25 October
- Kazemi A, Shaikhina D, Pickup G, Corbett P (2012) Comparison of upscaling methods in a heterogeneous carbonate model. In: SPE 154499 presented at SPE Europec/EAGE annual conference, Copenhagen, Denmark, 4–7 June 2012
- Keogh KJ, Martinus AW, Osland R (2007) The development of fluvial stochastic modelling in the Norwegian oil industry: a historical review, subsurface implementation and future directions. *Sediment Geol* 202(1):249–268
- King PR (1990) The connectivity and conductivity of overlapping sand bodies. In: Buller AT et al (eds) North Sea oil and gas reservoirs II. Graham and Trotman, London, pp 353–358
- Kjønsvik D, Doyle J, Jacobsen T, Jones A (1994) The effect of sedimentary heterogeneities on production from a shallow marine reservoir – what really matters? In: SPE paper 28445 presented at the European petroleum conference, London, 25–27 October 1994
- Kneller BC (1995) Beyond the turbidite paradigm: physical models for deposition of turbidites and their implications for reservoir prediction. In: Hartley AJ, Prosser DJ (eds) Characterisation of deep marine clastic systems, Special publication 94. Geological Society, London, pp 31–49
- Kocurek GA (1981) Significance of interdune deposits and bounding surfaces in eolian dune sands. *Sedimentology* 28:753–780
- Krystinik LF (1990) Early diagenesis in continental eolian deposits. In: Fryberger SG, Krystinik LF, Schenk CJ (eds) Modern and ancient eolian deposits: petroleum exploration and production. SEPM Rocky Mountain Section, Denver, pp 79–89
- Larue DK, Hovadik J (2006) Connectivity of channelized reservoirs: a modelling approach. *Pet Geosci* 12(4):291–308
- Leonide P, Borgomano J, Masse JP, Doublet S (2012) Relation between stratigraphic architecture and multi-scale heterogeneities in carbonate platforms: the barremian-lower aptian of the monts de vacluse, S.E. France. *Sediment Geol* 265:87–109
- Lescoffit G, Townsend C (2005) Quantifying the impact of fault modeling parameters on production forecasting for clastic reservoirs. In: Evaluating fault and cap rock seals, AAPG special volume Hedberg series, no. 2. American Association of Petroleum Geologists, Tulsa, pp 137–149
- Lucia FJ (1983) Petrophysical parameters estimated from visual descriptions of carbonate rocks: a field classification of carbonate pore space. *J Pet Technol* 35(03):629–637
- Lucia FJ (2007) Carbonate reservoir characterization: an integrated approach. Springer, Berlin
- Mandl G (2000) Faulting in brittle rocks: an introduction to the mechanics of tectonic faults. Springer, New York
- Manzocchi T, Carter JN, Skorstad A et al (2008a) Sensitivity of the impact of geological uncertainty on production from faulted and unfaulted shallow-marine oil reservoirs: objectives and methods. *Pet Geosci* 14:3–15
- Manzocchi T, Heath AE, Palanathakumar B, Childs C, Walsh JJ (2008b) Faults in conventional flow simulation models: a consideration of representational assumptions and geological uncertainties. *Pet Geosci* 14(1):91–110
- Martinus AW, Kaas I, Næss A, Helgesen G, Kjærefjord JM, Leith DA (2001) Sedimentology of the heterolithic and tide-dominated Tilje formation (Early Jurassic, Halten Terrace, offshore mid-Norway). In: Martinsen OJ, Dreyer T (eds) Sedimentary environments offshore Norway – paleozoic to recent, Norwegian Petroleum Society, special publications, 10. Elsevier, Amsterdam, pp 103–144
- Martinus AW, Ringrose PS, Brostrøm C, Elfenbein C, Næss A, Ringås JE (2005) Reservoir challenges of heterolithic tidal hydrocarbon fields (Halten Terrace, Mid Norway). *Pet Geosci* 11:3–16

- McCoss A (1986) Simple constructions for deformation in transpression/transension zones. *J Struct Geol* 8 (7):15–718
- McIlroy D (2004) Some ichnological concepts, methodologies, applications and frontiers. *Geol Soc Lond Spec Publ* 228:3–27
- Meadows NS, Beach A (1993) Controls on reservoir quality in the Triassic Sherwood sandstone of the Irish Sea. In: *Petroleum geology conference series, vol 4*. Geological Society, London, pp 823–833
- Miall AD (1985) Architectural-element analysis: a new method of facies analysis applied to fluvial deposits. *Earth Sci Rev* 22:261–308
- Miall AD (1988) Reservoir heterogeneities in fluvial sandstones: lessons learned from outcrop studies. *Am Assoc Pet Geol Bull* 72:882–897
- Nelson RA (2001) *Geologic analysis of naturally fractured reservoirs*, 2nd edn. Butterworth-Heinemann, Houston
- Nordahl K, Ringrose PS, Wen R (2005) Petrophysical characterisation of a heterolithic tidal reservoir interval using a process-based modelling tool. *Pet Geosci* 11:17–28
- Palermo D, Aigner T, Seyfang B, Nardon S (2012) Reservoir properties and petrophysical modelling of carbonate sand bodies: outcrop analogue study in an epicontinental basin (Triassic, Germany). *Geol Soc Lond Spec Publ* 370(1):111–138
- Pickering KT, Hilton VC (1998) *Turbidite systems of SE France*. Vallis Press, London
- Pickup GE, Herm CY (2002) The development of appropriate upscaling procedures. *Transp Porous Media* 46:119–138
- Reading HG (ed) (1996) *Sedimentary environments: processes, facies and stratigraphy*, 3rd edn. Blackwell Science, London
- Renard P, de Marsily G (1997) Calculating equivalent permeability: a review. *Adv Water Resour* 20:253–278
- Ringrose PS, Corbett PWM (1994) Controls on two-phase fluid flow in heterogeneous sandstones. In: Parnell J (ed) *Geofluids: origin, migration and evolution of fluids in sedimentary basins*, Geological Society special publication No. 78. Geological Society, London, pp 141–150
- Ringrose PS, Sorbie KS, Corbett PWM, Jensen JL (1993) Immiscible flow behaviour in laminated and cross-bedded sandstones. *J Pet Sci Eng* 9:103–124
- Ringrose PS, Nordahl K, Wen R (2005) Vertical permeability estimation in heterolithic tidal deltaic sandstones. *Pet Geosci* 11:29–36
- Rustad AB, Theting TG, Held RJ (2008) Pore-scale estimation, upscaling and uncertainty modelling for multiphase properties. In: *SPE paper 113005*, presented at the 2008 SPE/DOE improved oil recovery symposium, Tulsa, OK, UK, 19–23 April 2008
- Scholz CH, Aviles CA (1986) The fractal geometry of faults and faulting. In: Das S et al (eds) *Earthquake source mechanics*, vol 37. American Geophysical Union, Washington, DC, pp 1–341
- Stanbrook DA, Clark JD (2004) The Marnes Brunes Inférieures in the Grand Coyer remnant: characteristics, structure and relationship to the Grès d'Annot. In: Joseph P, Lomas SA (eds) *Deep-water sedimentation in the Alpine Basin of SE France: new perspectives on the Grès d'Annot and related systems*, Special publications, 221. Geological Society, London, pp 285–300
- Stanbrook DA, Bentley MR, Stephens E (2020) How to interpret Turbidites: the role of relative confinement in understanding reservoir architectures. In: *Extended abstract, presented at the AAPG ACE*
- Stauffer D, Ahorony A (1994) *Introduction to percolation theory*, rev 2 edn. Routledge/Taylor & Francis Group, London
- Stephen KD, Clark JD, Gardiner AR (2001) Outcrop based stochastic modelling of turbidite amalgamation and its effects on hydrocarbon recovery. *Pet Geosci* 7:163–172
- Stokes WL (1968) Multiple parallel-truncation bedding planes – a feature of wind-deposited sandstone formations. *J Sediment Petrol* 38:510–515
- Twiss RJ, Moores EM (1992) *Structural geology*. Freeman and Co, New York, 532 pp
- Tyler N, Finlay RJ (1991) Architectural controls on the recovery of hydrocarbons from sandstone reservoirs. In: Miall AD, Tyler N (eds) *The three dimensional facies architectures of terrigenous clastic sediments and its implications for hydrocarbon discovery and recovery*, SEPM concepts in sedimentology and palaeontology, vol 3. SEPM, Tulsa, pp 1–5
- Van Wagoner JC (1995) Sequence stratigraphy and marine to nonmarine facies architecture of foreland basin strata. In: Van Wagoner JC, Bertram GT (eds) *Sequence stratigraphy of foreland basin deposits*, AAPG memoir, 64. American Association of Petroleum Geologists, Tulsa, pp 137–224
- Van Wagoner JC, Mitchum RM, Campion KM, Rahmanian VD (1990) Siliciclastic sequence stratigraphy in well logs, cores, and outcrops, AAPG methods in exploration series, No. 7. American Association of Petroleum Geologists, Tulsa
- Walsh JJ, Watterson J (1988) Analysis of the relationship between displacements and dimensions of faults. *J Struct Geol* 10(3):239–247
- Walsh J, Watterson J, Yielding G (1991) The importance of small-scale faulting in regional extension. *Nature* 351:391–393
- Weber KJ (1986) How heterogeneity affects oil recovery. In: Lake LW, Carroll HB (eds) *Reservoir characterisation*. Academic, Orlando, pp 487–544
- Weber KJ (1987) Computation of initial well productivities in aeolian sandstone on the basis of a geological model, Leman gas field, U.K. In: Tillman RE, Weber KJ (eds) *Reservoir sedimentology*, SEPM special publication, 46. Society of Economic Paleontologists and Mineralogist, Tulsa, pp 333–354
- Weber KJ, van Geuns LC (1990) Framework for constructing clastic reservoir simulation models. *J Pet Technol* 42:1248–1297



## Abstract

Same rocks – different fluids

What happens if the objective of your model changes dramatically – can the same rock model be applied to multiple dynamic objectives? We have developed the argument that the importance of different scales and types of heterogeneity depends on the flow processes – geomodels for gas depletion are quite different from geomodels purposed for water or gas injection. What about completely different objectives, such as permanent storage of CO<sub>2</sub> or seasonal storage of air or hydrogen?

Here we develop the question of how to align the reservoir model design to different objectives, focussing especially on the energy transition for which storage and management of subsurface fluid resources will be as important as fluid extraction. We will focus on the case of CO<sub>2</sub> storage, but also draw insights relevant to the seasonal storage of gas, air and hydrogen.



Imagining fluids in the subsurface using two glasses – one with olive oil and water and one with sparkling wine and CO<sub>2</sub>. Images courtesy of Britta Paasch

## Keywords

CO<sub>2</sub> storage · Trapping mechanisms · Phase behaviour · Storage complex · Sleipner · 4D seismic · Capillary forces · Rock mechanics · Fluid migration · Fluid pressure · Heterogeneity · Gas storage · Hydrogen storage

## 7.1 Displacements of Different Fluids

Historically, geological reservoir modelling has been focused on the extraction of oil and gas, with water or gas injection being the dominant fluid recovery mechanisms. Many gas and oil fields are also produced by simple pressure depletion. Whatever the mechanism chosen, two-phase flow of water and hydrocarbon is the main process, with either the hydrocarbon or the water being the wetting phase. For CO<sub>2</sub> storage, the main fluid process is CO<sub>2</sub> displacing saline water – a CO<sub>2</sub>-brine system where CO<sub>2</sub> is the non-wetting phase. In the deep subsurface, CO<sub>2</sub> exists as a liquid or dense (super-critical) phase, which is a fluid we do not naturally have an intuitive understanding of from everyday life.

To get a better appreciation of the subsurface flow processes, consider two glasses with mixing fluids – one with oil and water and one with CO<sub>2</sub> and water (or champagne), illustrated in the frontispiece. It might surprise you that CO<sub>2</sub> in the subsurface is more like the oil-water analogue than the CO<sub>2</sub>-bubbles analogue. This is because CO<sub>2</sub> at depth is very different from CO<sub>2</sub> at surface conditions. The interfacial tension for olive-oil/water at room temperature is around 32 mN/m (Sahasrabudhe et al. 2017) which is quite similar to dense-phase CO<sub>2</sub>/brine in the subsurface (Naylor et al. 2011), and the density of liquid CO<sub>2</sub> is more like oil than gas. For further discussion of this comparison see Ringrose (2020). To appreciate CO<sub>2</sub> storage processes in the subsurface we therefore need to think about a non-wetting phase with an interfacial tension and density similar to an oil-water system, but a liquid with a viscosity much lower than oil.

---

## 7.2 Geological Storage of CO<sub>2</sub>

Geological storage of CO<sub>2</sub> is an emerging topic, likely to gain significant traction in the coming decade as the nations of the world strive to meet their emissions reduction targets. CO<sub>2</sub> storage is an established technology, although currently

limited to a handful of projects (Ringrose 2020). The basic concept is to store CO<sub>2</sub> captured from sites of anthropogenic CO<sub>2</sub> emissions underground in rock formations, thus isolating CO<sub>2</sub> from the atmosphere. The two main domains of storage are:

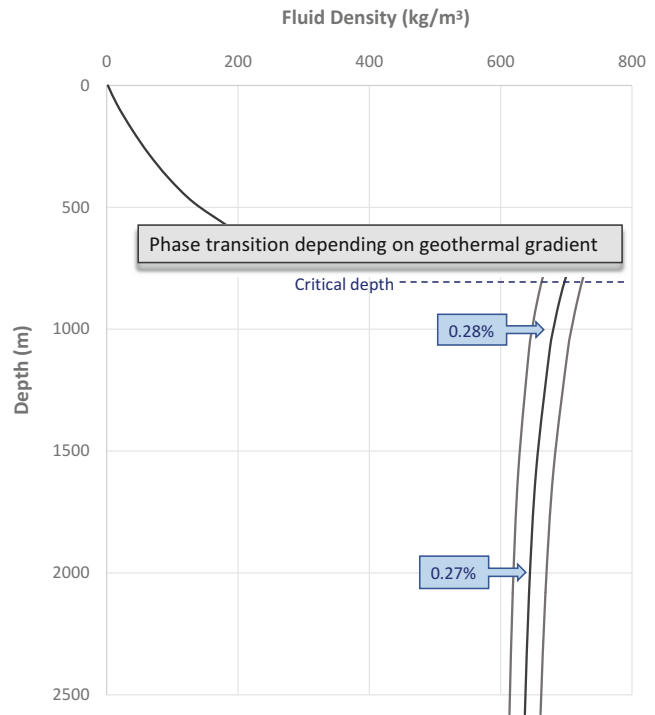
1. Storage in saline aquifer formations.
2. Storage in depleted oil and gas reservoirs.

Less important classes of porous rock formations which could be used include coal beds, shale units, volcanic rocks and underground caverns. Here, we focus on the case of saline aquifer formations where the rock-fluid interactions are best understood. However, many of the processes involved apply equally well to other storage domains and to storage as part of CO<sub>2</sub> EOR projects. CO<sub>2</sub> storage in basalt formations has also been recently demonstrated as part of a geothermal CCS project in Iceland (Aradóttir et al. 2011; Gislason and Oelkers 2014).

The behaviour of CO<sub>2</sub> has some similarities to a gas in the subsurface, but also many differences. The underlying concept is that we store the CO<sub>2</sub> relatively deep (greater than ~800 m) to ensure that CO<sub>2</sub> is in a dense form – either a liquid or as a super-critical phase (Fig. 7.1). At these depths CO<sub>2</sub> is in a liquid or dense phase having a density around 700 kg/m<sup>3</sup> (slightly less dense than water), but having a viscosity that is more similar to hydrocarbon gases (CO<sub>2</sub> viscosity is around 0.06 cP at 1500 m depth). So, when handling a fluid with liquid-like density and gas-like viscosity in the geological reservoir, the hydrocarbon field experience does not directly apply. Fortunately, we now have experience of modelling and monitoring from several CO<sub>2</sub> storage projects, so the theory and the practice is in place. The question of how CO<sub>2</sub> behaves in heterogeneous rock formations, however, is very much a topic to explore.

The depth of storage is also important for storage security, as one or more effective storage sealing units are essential for the concept. As we approach depths of around 1 km or more we enter the domain of compacted and cemented rocks which should provide the required

**Fig. 7.1** CO<sub>2</sub> density versus depth diagram for typical subsurface conditions in the North Sea. The dark line is the density function at the Sleipner location assuming a geothermal gradient of 35 °C/km ( $\pm 2$  °C/km, grey lines). The CO<sub>2</sub> phase transition occurs somewhere between 550 m and 750 m depth, depending on local temperature, leading the generally assumed ‘critical depth’ of 800 m; blue boxes show relative volume occupied by CO<sub>2</sub> in the subsurface compared to surface volumes



low-permeability sealing units, e.g. shales, faults, and salt units. At these depths we know from experience that natural gas has been trapped beneath geological seals for millions of years, and so the potential for long-term trapping of CO<sub>2</sub> at these depths is also clearly possible.

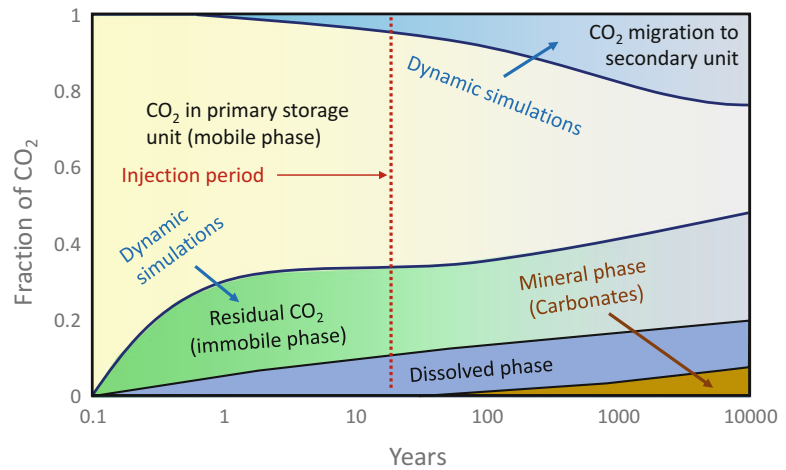
The processes involved in trapping and containing CO<sub>2</sub> in the subsurface can be summarized into geological, physical and chemical factors:

- *Geological trapping mechanisms*, controlled by regional geological structure, basin history, the geometry of structural and stratigraphic traps and the rock architecture of the storage complex.
- *Physical trapping mechanisms* related to fluid flow processes, principally capillary interfaces between fluids and retention of CO<sub>2</sub> as a residual phase.
- *Geochemical trapping mechanisms*, comprising CO<sub>2</sub> dissolution in the brine phase, CO<sub>2</sub> precipitation as mineral phases and CO<sub>2</sub> sorption/absorption, e.g. on clay minerals.

These mechanisms were conceptually combined in the IPCC special report (Benson et al. 2005) into a trapping versus time diagram establishing the concept that the various trapping mechanisms should work together to increase storage security as a function of time. Figure 7.2 shows a version of the trapping mechanisms diagram based on experience gained so far in understanding how these mechanisms are expected to function over time within the storage complex, discussed further in Ringrose (2020). Our interest here is on understanding what we need to know for designing appropriate geological models. The main objectives for modelling CO<sub>2</sub> storage sites are to demonstrate secure long-term storage, or more specifically to estimate the rate and magnitude of the trapping mechanisms as a function of time:

- How quickly does the mobile-phase plume grow and eventually stabilise?
- How quickly will migration into secondary storage units occur (if at all)?
- What is the fraction of CO<sub>2</sub> which will end up in the residual, dissolved and mineral phases?

**Fig. 7.2** Framework for forecasting the fate of CO<sub>2</sub> in the storage complex



Dynamic flow simulations will generally be used to make these assessments, but the length of time involved means that the focus of the modelling efforts in the injection period may be very different from the long-term (post-injection) period. For example, it may be acceptable to neglect geochemical reactions in the operational period and just focus on forecasting the mobile and residual phase within the primary storage unit.

Another fundamental difference between modelling for CO<sub>2</sub> storage and hydrocarbon reservoir modelling is the volume and coverage of the model. CO<sub>2</sub> storage workflows, along with the legislative frameworks for storage permits, have developed the concept of the *storage complex* which comprises a large subsurface domain including the storage units, the sealing formations and faults and a wider study area, e.g. area of review, site boundary, monitoring or survey areas.

In terms of the regulations governing CO<sub>2</sub> storage, the storage complex is defined under the EU CCS Directive (EC 2009) as follows:

Sufficient data shall be accumulated to construct a volumetric and three-dimensional static (3-D)-earth model for the storage site and storage complex, including the caprock, and the surrounding area, including the hydraulically connected areas.

The EU Directive goes on to define ‘leakage’ as ‘any release of CO<sub>2</sub> from the storage complex’, while ‘significant irregularity’ means ‘any

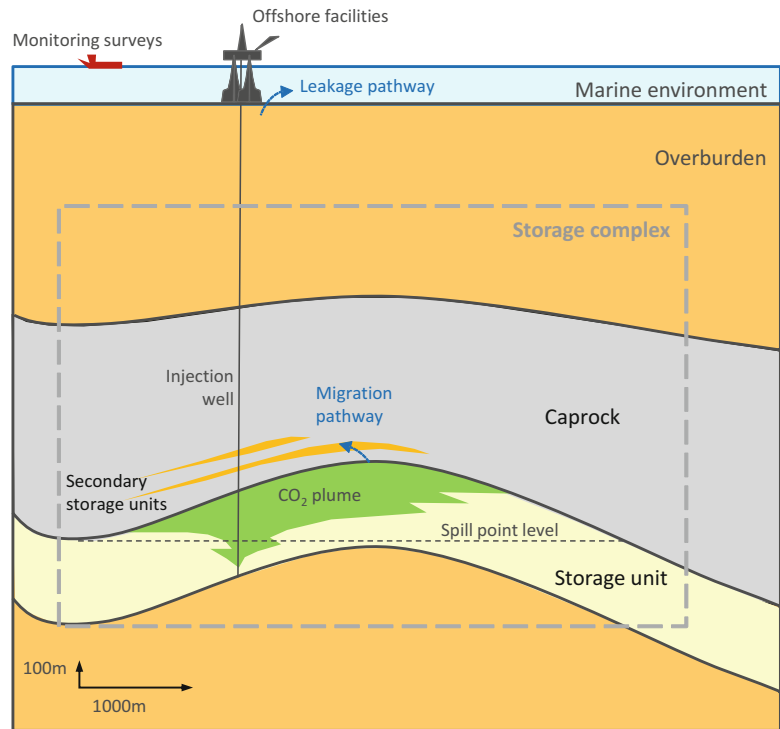
irregularity in the injection or storage operations or in the condition of the storage complex itself, which implies the risk of a leakage or risk to the environment or human health.’ Note that different regions/continents have different regulatory frameworks in place, but the EU Directive gives a good basis for understanding the concepts involved. In the United States, sequestration is permitted by the Environmental Protection Agency, under a provision for Class VI wells addressing the legal process for sequestration of carbon dioxide deep underground.

This framework has several implications for geological modelling for CO<sub>2</sub> storage objectives – mainly that a much larger gross rock volume needs to be considered. Figure 7.3 illustrates the main concepts and terms involved in defining the CO<sub>2</sub> storage complex. Each project will need to define specifically what is covered by the storage complex, but what is clear is that it must involve multiple rock units from the deeper storage units and upwards to include the sealing and overburden units.

### 7.3 CO<sub>2</sub> Storage Modelling Objectives

Modelling for CO<sub>2</sub> storage involves assessing the expected efficacy of the various trapping mechanisms – structural trapping, residual trapping, dissolution of CO<sub>2</sub> in the brine phase

**Fig. 7.3** Sketch illustrating the definition and coverage of the CO<sub>2</sub> storage complex (offshore setting)



and precipitation of CO<sub>2</sub> as minerals (Fig. 7.2). A sketch illustrating how these processes might develop within a migrating CO<sub>2</sub> plume is shown in Fig. 7.4. As mentioned above, projects will generally focus on plume migration, structural trapping and residual trapping which are most important for the injection phase, and only include solubility and mineral trapping when considering longer term storage timeframes.

Essential to modelling CO<sub>2</sub> storage sites is the inclusion of a reasonably accurate equation of state (EOS) for CO<sub>2</sub> and some explicit treatment of CO<sub>2</sub> dissolution in the brine phase. In other respects, CO<sub>2</sub>-brine systems are fairly similar to other two-phase flow problems. There are several options for the choice of the CO<sub>2</sub> equation of state:

- Peng-Robinson and Soave-Redlich-Kwong are two commonly-used cubic equations of state, because they are relatively simple to implement and are widely used in modelling packages (see Li and Yan 2009, for a

discussion of different cubic EOS equations used for handling CCS processes).

- Span and Wagner (1996) proposed a more accurate but also more demanding EOS for CO<sub>2</sub> which is often used in assessing detailed system behaviour and complex mixtures (Span et al. 2013).

Whatever choice is made for the EOS used, an appreciation of the phase behaviour of CO<sub>2</sub> is essential. Within the storage unit CO<sub>2</sub> is in the liquid or dense (supercritical) phase – a phase we are not very familiar with at surface conditions. Furthermore, as we take the gas/vapour-phase CO<sub>2</sub> from surface conditions (at the capture plant), via compression and liquefaction, and inject it at the wellhead, we take the CO<sub>2</sub> through a series of phase transitions. This is illustrated in Fig. 7.5, using the examples of CO<sub>2</sub> storage at Sleipner and Snøhvit. At Sleipner with an injection depth of 1 km, the CO<sub>2</sub> at the well head and bottom-hole conditions is very close to the triple point, where the phase is very sensitive to small

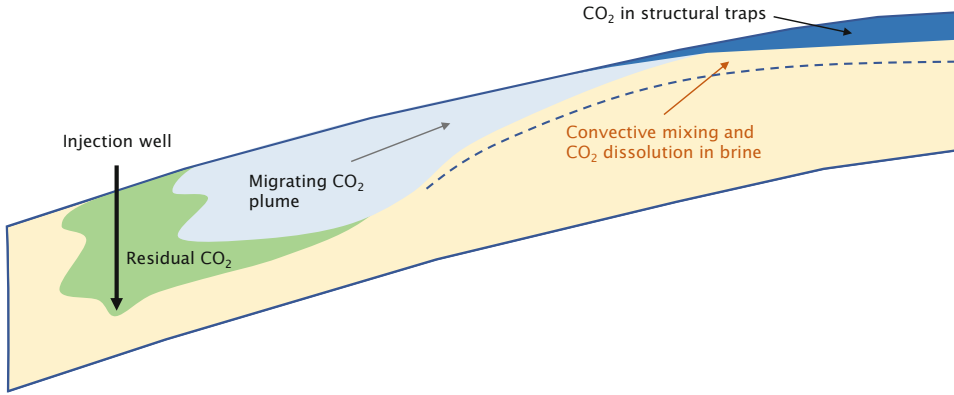


**Fig. 7.4** Sketch illustrating CO<sub>2</sub> storage flow processes

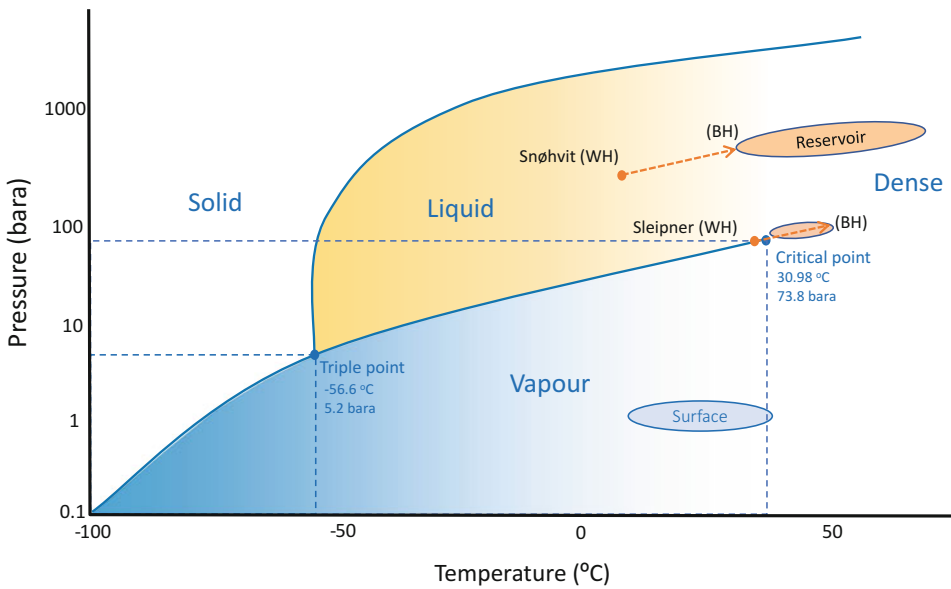


**Fig. 7.5** CO<sub>2</sub> phase diagram with approximate wellhead (WH) and bottom-hole (BH) conditions for the Sleipner and Snøhvit projects

changes in pressure and temperature. At Snøhvit with an injection depth of around 2.4 km, the CO<sub>2</sub> is well within the liquid phase at the wellhead moving into the dense phase in the reservoir.

In addition to having a very different fluid to consider, CO<sub>2</sub> storage projects have some other important differences when compared to the conventional practices for modelling hydrocarbon field developments:

- CO<sub>2</sub> injection projects usually start with very few wells (perhaps none initially) and generally need to forecast expected behaviour out

from the injection well and with very few well-control constraints. This contrasts with oilfield modelling which is often focused on history matching observations from multiple wells, and in this sense CO<sub>2</sub> projects are an exercise in forward modelling with much less data to calibrate against.

- Injection of a low viscosity fluid (CO<sub>2</sub>) into a higher viscosity fluid (brine) gives an unstable mobility ratio and inherently leads to viscous-fingering behaviour, to a much greater extent than we are familiar with in oil reservoirs as the viscosity contrast is more marked.

This setting makes forecasting CO<sub>2</sub> storage behaviour somewhat more challenging than oil field simulation as the fluids are particularly sensitive to reservoir heterogeneities. We generally have less subsurface information available and yet we need to forecast an unstable displacement of a fluid with quite variable fluid properties. Flow simulation for CO<sub>2</sub> storage projects is inherently a forecasting activity, where the objectives are to understand the ‘expected behaviour’ and the likely ‘range of outcomes’. In their review of three large-scale storage projects, Eiken et al. (2011) pointed out that the actual CO<sub>2</sub> plume development at the Sleipner, In Salah and Snøhvit projects was strongly controlled by unobserved reservoir heterogeneities that were discovered from monitoring data (especially seismic data) during the injection phase. Project experience so far (Ringrose 2020) clearly points to the need to be iterative about the project design, using site monitoring data to update the reservoir model, in addition to monitoring fluid saturation and pressure.

To summarize, the modelling objectives for CO<sub>2</sub> storage projects differ significantly from hydrocarbon reservoir production projects. For CO<sub>2</sub> storage the following overall objectives are paramount:

1. Understand the behaviour of the whole storage complex (not just the injection unit).
2. Quantify the different trapping mechanisms as a function of time.
3. Aim to demonstrate long-term storage integrity.

In the following two sections we will consider the fluid dynamic aspects and reservoir heterogeneity aspects of this problem.

---

## 7.4 Understanding the CO<sub>2</sub> Storage Process

Studies of the CO<sub>2</sub> storage process show that filling of a porous rock formation with CO<sub>2</sub> is somewhat like the process of hydrocarbon charging of rock formations over geological time, in contrast to the process of oil and gas production.

Oil and gas migration studies have demonstrated the importance of capillary sealing phenomena in controlling the size of oil and gas accumulations, e.g. Berg 1975. In terms of dynamic modelling, the most appropriate process for replicating migration of a buoyant non-wetting phase is Invasion Percolation (IP), which represents a capillary/gravity dominated flow system using percolating clusters in a medium controlled by capillary threshold pressures. The IP concept, introduced by Wilkinson and Willemsen (1983), has been widely applied to multiphase flow problems at the pore scale (e.g. Blunt 2001) and for modelling basin-scale oil migration (e.g. Carruthers and Ringrose 1998). The method also lends itself to modelling CO<sub>2</sub> storage processes (Cavanagh and Ringrose 2011; Cavanagh et al. 2015; Meckel 2013; Trevisan et al. 2015, 2017a). When using the IP method to represent a migrating immiscible buoyant fluid invading a water-wet porous medium, the condition is used whereby migration of the non-wetting phase cluster occurs if:

$$\Delta\rho g dz > P_t \quad (7.1)$$

where:

$\Delta\rho$  is the fluid density difference for the cluster with vertical dimension  $dz$

$P_t$  is the threshold capillary pressure for largest available pore which can be invaded by the cluster (if this condition is not satisfied, the cluster is immobile)

$g$  is acceleration due to gravity

More generally, and especially during the injection phase of a CO<sub>2</sub> storage project, multiphase Darcy-flow approaches are used to simulate the process of CO<sub>2</sub> filling the porous media. Figure 7.6 shows example CO<sub>2</sub>-brine relative permeability curves where both the drainage and imbibition flooding cycles were measured, resulting in a measured residual CO<sub>2</sub> saturation of 22% ( $S_w = 0.78$ ). However, the CO<sub>2</sub>-brine relative permeability function depends very much on the flow rates and rock heterogeneity. Figure 7.7 shows a set of measurements for CO<sub>2</sub>-brine drainage relative permeability curves from a

**Fig. 7.6** Example CO<sub>2</sub>-brine relative permeability curves from data published by Bennion and Bachu (2006). (Cardium Sandstone sample with IFT = 56.2 mN/m)

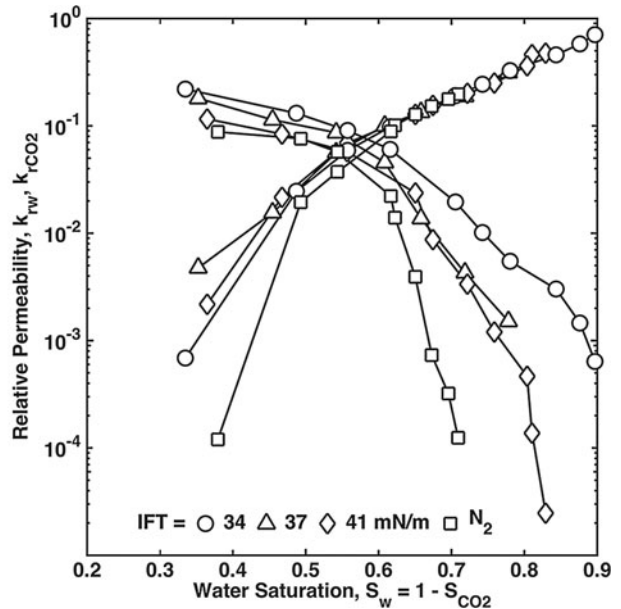
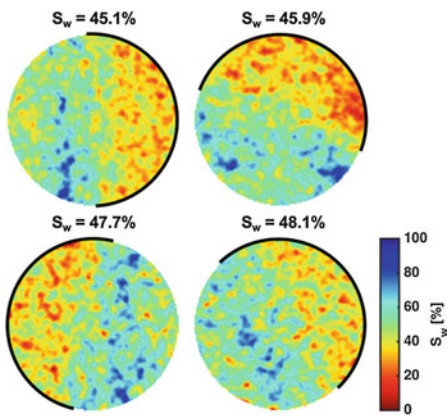
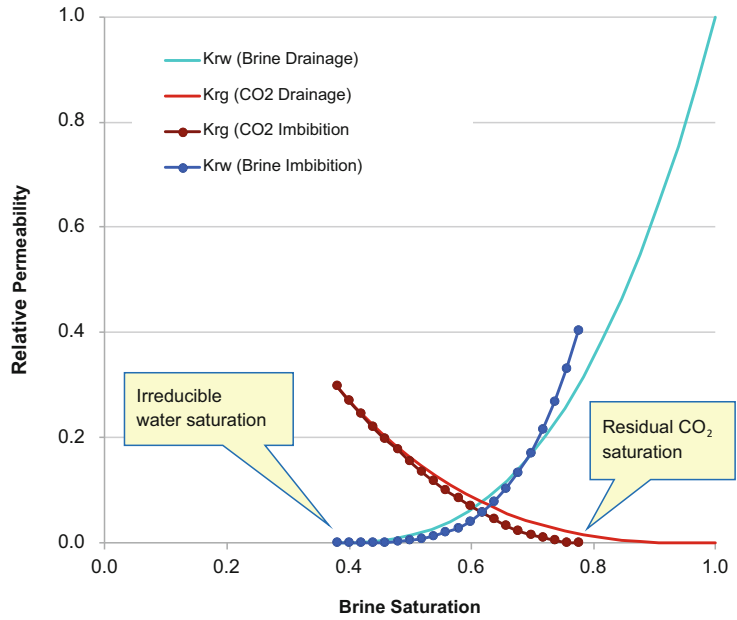


**Fig. 7.7** Saturation maps (left) and relative permeability functions (right) for core-flood experiments in a Bentheimer sandstone core with a two-layer heterogeneity (from Reynolds and Krevor 2015). Experiments 2, 4, 6 and 8 (clockwise from top left) were conducted at conditions close to the capillary limit, with varying interfacial

tensions of IFT = 37 mN/m (Exp. 2), IFT = 41 mN/m (Exp. 4), IFT = 34 mN/m (Exp. 6) and with Nitrogen (Exp. 8). Black lines indicate the high-permeability half of the core. (Image © 2015 American Geophysical Union, reproduced with permission)



set of experiments by Reynolds and Krevor (2015) who show that near capillary-limit conditions, the CO<sub>2</sub>-brine system flow functions are very sensitive to heterogeneity in capillary pressure, whereas under viscous-dominated conditions the rock structure plays a more limited role. Note the strong contrast in saturation between the two halves of the core (Fig. 7.7, left), with a higher non-wetting phase saturation in the high-porosity half, and a clearly heterogeneous displacement process.

Reynolds et al. (2017) further developed the understanding of CO<sub>2</sub>-brine flow systems, using a series of flow experiments with fluids imaged using a fast synchrotron X-ray CT experimental system. They observed a process of dynamic (episodic) fluid connectivity occurring during the imposed steady-state multiphase flow boundary conditions in the sandstone sample (Fig. 7.8). Note that here nitrogen was used as the non-wetting phase as an analogue to supercritical CO<sub>2</sub>. Thus, the flow process at the pore-scale is driven by episodic connections between non-wetting phase ganglia. This work indicates that the large-scale CO<sub>2</sub> storage process (CO<sub>2</sub> drainage into a brine-saturated medium) is

governed by episodic fluid connectivity behaviour at the pore-scale.

Transferring this understanding of pore-scale processes up to the metre-scale, we can gain important insights from another set of experiments performed in large sand packs by Trevisan et al. (2017b). These experiments were carefully set up using surrogate fluids (that mimic the density and viscosity contrasts of CO<sub>2</sub> and brine at reservoir conditions) and sand packs with contrasting permeability structure. A homogeneous sand case was contrasted with a bedded heterogeneous system, using different grain sizes to create a heterogeneous permeability architecture with a log-normal permeability distribution. The model was set with a gentle slope, with a 3° dip angle, to create a component of lateral migration.

For the homogeneous sand pack an inverted cone geometry was observed (Fig. 7.9a) with some asymmetry caused by the slope, and with up-dip migration immediately beneath the cap-rock surface. This behaviour corresponds very well to predictions from flow theory, as explained by Nordbotten and Celia (2006). For the heterogeneous case, a careful procedure using different sieve sizes was used to deposit beds with contrasting grain sizes in a two-dimensional rectangular array to mimic natural sedimentary heterogeneity. In this case the ‘inverted cone geometry’ was broken up by pore-scale capillary-pressure contrasts to create multiple accumulations of CO<sub>2</sub> (proxy fluid) connected by feeder pathways (Fig. 7.9b). This observed flow behaviour is best explained by the migration of non-wetting phase ganglia in a percolating flow system where local accumulations only migrate further once the local capillary threshold pressure has been exceeded. The result is a more distributed filling of the porous medium with saturations that are locally higher than would occur in the homogeneous case. Small-scale rock heterogeneity thus enhances the effectiveness of CO<sub>2</sub> storage, due to capillary trapping at the bed scale. A similar process was found to hinder oil recovery in hydrocarbon reservoirs (Ringrose et al. 1993; Huang et al. 1995). Studies of the efficiency of CO<sub>2</sub> storage in geological

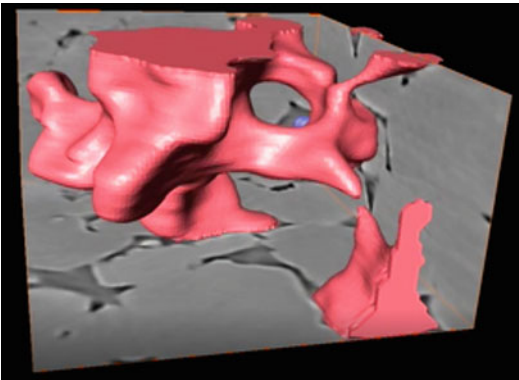
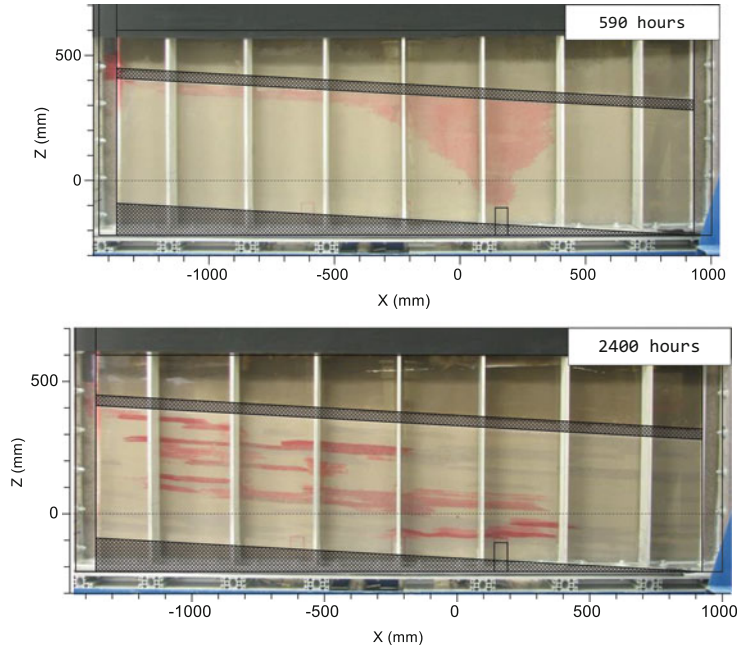


**Fig. 7.8** Snap-shot from a time-lapse movie showing episodic connectivity of N<sub>2</sub> ganglia for steady-state multiphase flow in a sandstone sample. (From an experiment described in Reynolds et al. 2017). Image shows a 720 × 720 × 360 μm sub-volume. Nitrogen (N<sub>2</sub>) is used here as an analogue for CO<sub>2</sub> to illustrate the nature of non-wetting phase ganglia in a porous medium. The two large ganglia (pink) display episodic snap-off behaviour at the point where they nearly touch in this image. (Image courtesy of Sam Krevor)

**Fig. 7.9** Example flow migration experiments from Trevisan et al. (2017b) using a proxy fluid pair to mimic migration of supercritical CO<sub>2</sub> in the deep subsurface: (a) homogeneous base case experiment after 590 h (pink region shows saturations in the range of 0.05 to 0.35); (b) heterogeneous experiment after 2400 h (pink region shows saturations in the range of 0–05 up to 0.8). (Images © 2016, American Geophysical Union, reproduced with permission)



formations, will therefore need to take some account of these effects, as has been done using detailed outcrop models (Veloso et al. 2016) or for real injection sites (Hovorka et al. 2004).

At the field scale, the overall dynamics of CO<sub>2</sub> injection can be predicted from flow theory. For a viscous-dominated assumption, the flow process is essentially governed by the mobility ratio of the two fluids. For example, Nordbotten and Celia (2006) showed that the radius of the expanding plume  $r_{\max}$  can be estimated by:

$$r_{\max} = \sqrt{\frac{\lambda_c}{\lambda_b} \frac{Q_{\text{well}} t}{\pi B \varphi}} \quad (7.2)$$

where:

$\lambda_c$  and  $\lambda_b$  are the fluid mobilities for CO<sub>2</sub> and brine

$Q_{\text{well}}$  is the volume injected over time  $t$  into a horizontal saline aquifer unit with thickness  $B$

Note that for each phase, the fluid mobility is the ratio of relative permeability to viscosity,  $\lambda_i = k_i/\mu_i$ . Fluid mobility is also usefully summarized by the mobility ratio  $\lambda_r = \lambda_c / \lambda_b$ .

This approximation could apply for high injection rates close to the injection well. For example, a typical first-order estimate  $r_{\max}$  for injection of one million tonnes (Mt) of CO<sub>2</sub> into a 50 m-thick aquifer is 550 m, or 11 times the aquifer thickness. This assumes a porosity of 0.3 and a mobility ratio,  $\lambda_r$ , of 4. However, as the viscous force decreases away from the well gravity effects will play a bigger role and the fluid density difference will drive a process of gravity segregation, with the CO<sub>2</sub> tending to collect at the top of the aquifer layer or in micro accumulations within the aquifer layer. These fluid dynamic effects, and the interaction of the gravity-viscous-capillary force balance becomes quite complex, but the principles are essential to understand. Ringrose (2020) provides a fuller discussion, with extensive treatments on the flow dynamics given by Nordbotten and Celia (2012) and Niemi et al. (2017).

These observations can be used to point to some important principles for building reservoir models for CO<sub>2</sub> storage:

- The fluid physics must be well understood – a buoyant non-wetting fluid filling a porous brine-saturated medium.

- The CO<sub>2</sub> migration process is likely to be controlled by small-scale rock heterogeneity.
- Barriers and baffles to flow will play an important role because they act as capillary interfaces.

At the next scale up – the full-field scale – we can also learn about typical CO<sub>2</sub> plume growth geometry from large-scale CO<sub>2</sub> injection projects. The Sleipner CCS project is particularly valuable due to its long history (in operation since 1996) and excellent quality of time-lapse seismic imaging of the CO<sub>2</sub> plume (Chadwick et al. 2010; Furre et al. 2015, 2017). Figure 7.10 shows an example seismic cross section where time-lapse data (seismic reflection amplitude difference) gives a good indication of the presence of CO<sub>2</sub>. Note that seismic imaging of CO<sub>2</sub> in layer 9 is excellent, but that in deeper layers signal degradation occurs due to inelastic attenuation and transmission loss caused by the overlying CO<sub>2</sub> layers, and especially a velocity pull-down effect. What is clear is that CO<sub>2</sub> has filled multiple layers in a stacked sequence.

Using the seismic images at the field scale, we can also estimate the overall storage efficiency at Sleipner. For example, the overall storage efficiency is estimated to be ~5.2% as of 2013

(Ringrose 2020) using the seismic monitoring dataset (Furre et al. 2017) to measure the plume extent as a fraction of the storage volume. This only gives a macroscopic view of the overall occupancy of the available pore space with CO<sub>2</sub>. In detail, the plume distribution is highly complex, being influenced by the *in situ* temperature/density gradients (Cavanagh et al. 2015; Williams et al. 2018) and the properties of the shale baffles, which are breached in several places (Furre et al. 2019).

The effect of the shale baffles in controlling the vertical and lateral migration of CO<sub>2</sub> within the Sleipner Utsira formation has been extensively studied, e.g. from Zweigel et al. 2004 to Williams et al. 2018. An example Invasion Percolation simulation of the multi-layer CO<sub>2</sub> plume at Sleipner is shown in Fig. 7.11, from a study by Santi (2019). This study, building on previous work by Cavanagh et al. (2015), shows that the Invasion Percolation approach can successfully replicate the observed plume behaviour: a stacked series of CO<sub>2</sub> accumulations ponded beneath shale layers and then migrating upwards, either by exceeding the capillary threshold pressure of the shales or by finding breaches in the shales. However, the migration behaviour is very sensitive to the shale properties, which are poorly

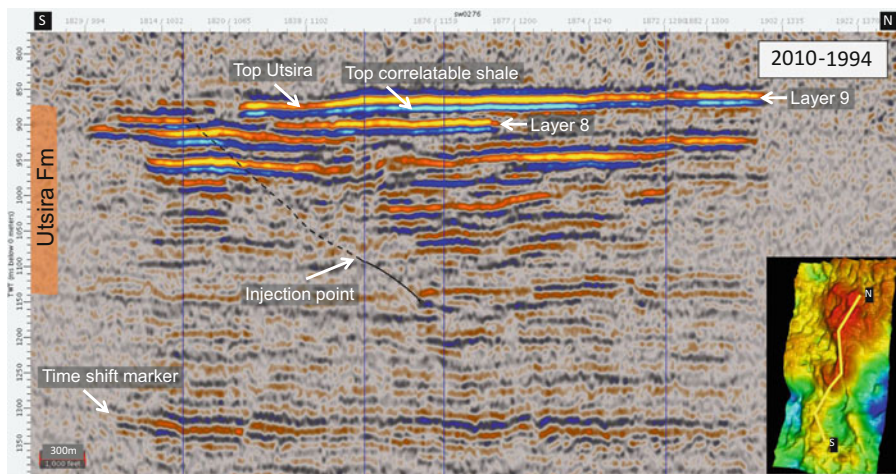


**Fig. 7.10** Seismic section (N-S) at Sleipner showing time-lapse amplitude-difference data when comparing 2010 and 1994 surveys, modified from Furre et al.

(2015). (Image courtesy of Equinor and partners of the Sleipner Production Licenses)

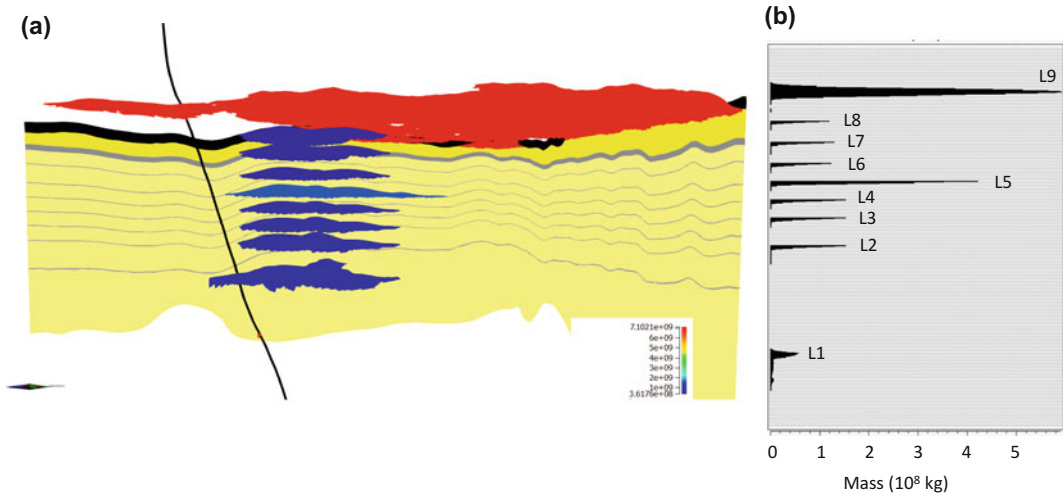


**Fig. 7.11** Example Invasion Percolation simulation of the CO<sub>2</sub> plume at Sleipner after injection of 12.08 Mt. (in 2010): (a) total CO<sub>2</sub> mass distribution in 3D model (field of view  $\sim 6 \times 0.2$  km); (b) CO<sub>2</sub> mass

accumulated per layer; the model shows a sensitivity case and is not precisely history matched. (From Santi 2019, reproduced with permission)

determined due to lack of core data (see Singh et al. 2010 for estimates of properties). In the example shown in Fig. 7.11, no breaches in the shales are modelled, but rather the threshold pressures of continuous shales are adjusted to get an approximate match to the observed mass distributions per layer. Other studies of the plume dynamics at Sleipner have successfully applied multi-phase Darcy-flow simulation approaches, in which the need to capture gravity segregation effects using vertically-integrated saturation functions is clearly evident (Gasda et al. 2013; Nilsen et al. 2017; Cowton et al. 2018).

At the full-field scale, the choices made about *in situ* fluid properties and the approach to handling thermal effects becomes important. Often, a practitioner will assume a fixed CO<sub>2</sub> density and a constant temperature, which may be acceptable for a single rock unit. However, models of a multi-layer system or a larger model domain are likely to require explicit modelling of thermal effects, dynamic changes in CO<sub>2</sub> density and relative permeability hysteresis. These thermal effects have been assessed for the well-

calibrated case at Sleipner (Williams and Chadwick 2017; Williams et al. 2018) and future studies should see increasing use of coupled modelling approaches.

To summarise the insights gained on understanding the CO<sub>2</sub> storage process, we generally expect to see an inverted-cone geometry as the buoyant plume spreads within the storage unit and then migrates up-dip. This behaviour is clearly evident from monitoring data at the Snøhvit CO<sub>2</sub> injection project (Fig. 7.12), where reservoir simulation calibrated to time-lapse seismic imaging data reveals the likely nature of up-dip migration of the CO<sub>2</sub> plume (Grude et al. 2013; Osdal et al. 2014). Time-lapse seismic data cannot reveal the thin leading edge of the migrating plume (Fig. 7.12a), so a degree of forecasting calibrated to monitoring data will always be required. The plume geometry is very much affected by the density difference between CO<sub>2</sub> and brine (the gravity force) but also by the details of the rock heterogeneity, especially barriers and baffles to flow, as summarised in Fig. 7.13.

**Fig. 7.12** CO<sub>2</sub> injection into the Stø Fm at Snøhvit: (a) baseline survey seismic section around injection point; (b) seismic difference data comparing 2012 repeat survey and baseline survey; (c) corresponding reservoir simulation of the CO<sub>2</sub> plume after 0.8Mt CO<sub>2</sub> injected into this unit. (Modified from Osdal et al. (2014); images courtesy of Equinor and the Snøhvit Licence partners, reproduced with permission)

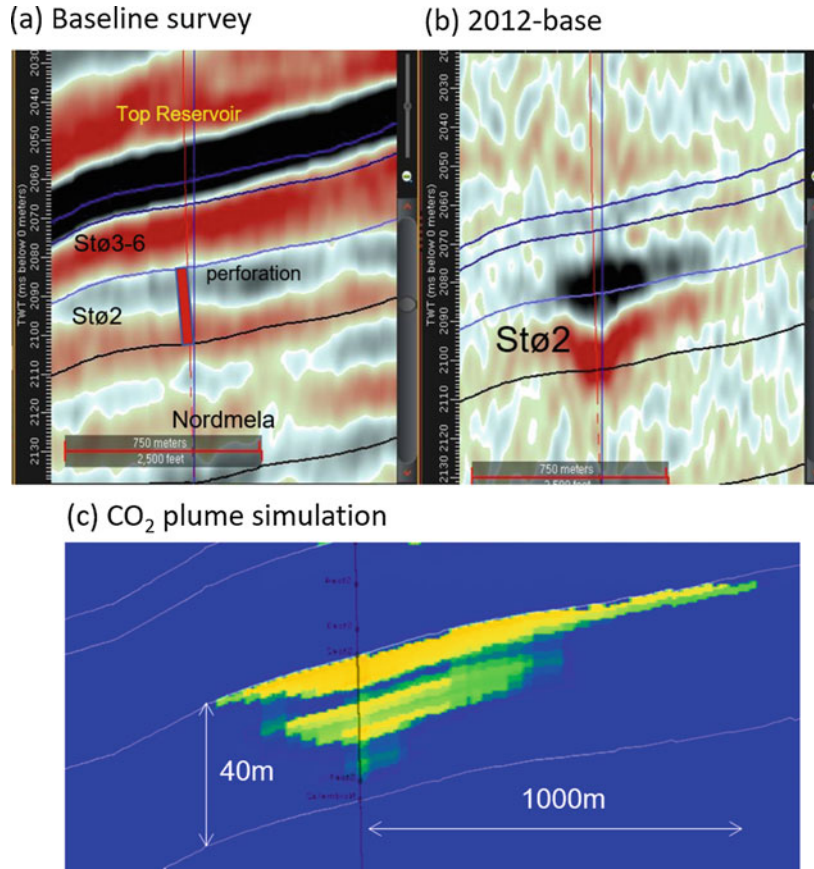
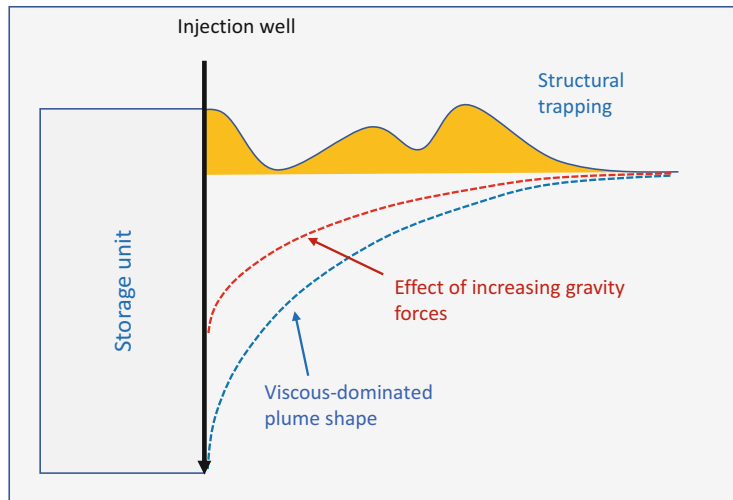


**Fig. 7.13** Simple sketch of factors affecting a CO<sub>2</sub> plume



## 7.5 The Influence of Geological Heterogeneity

The seismic imaging datasets at the Sleipner and Snøhvit CO<sub>2</sub> injection projects give clear indications of the importance of sedimentary heterogeneity in controlling CO<sub>2</sub> migration within the storage unit. A general finding of these projects is that the time-lapse seismic responses, which are strongly influenced by saturation changes (CO<sub>2</sub> displacing brine), also reveal geological features that were not imaged on the pre-injection seismic reflection data. This is illustrated in Fig. 7.14 which shows examples from layer 9 at the Sleipner storage site (Fig. 7.14a) and from the time-lapse amplitude map for the Tubåen reflector at the Snøhvit CO<sub>2</sub> injection project (Fig. 7.14b). In both cases, sandstone channel or bar forms can be seen to constrain the spatial growth of the plume.

For the case of CO<sub>2</sub> plume growth in layer 9 at Sleipner, Williams and Chadwick (2017) identify linear features from isochore maps, which probably correspond to channels or bar forms. Differential subsidence appears to have created a slight topographical high along these channels, with the CO<sub>2</sub> migrating northwards along these two features and beneath the overlying sealing layer. A brief reminder from sedimentology is useful here – recall that ‘channels’ tend to be filled with bar forms, which is why preserved channels are often stacked barforms.

The reason why CO<sub>2</sub> flows along channel/bar features could be an effect of a permeability contrast but is more likely to be due to shale baffles (bounding surfaces to the sand bodies) constraining the CO<sub>2</sub> within the feature. This interpretation is supported by well-test analysis of pressure data at Snøhvit which reveals the presence of a partial flow barrier at around 100 m from the injection well (Hansen et al.

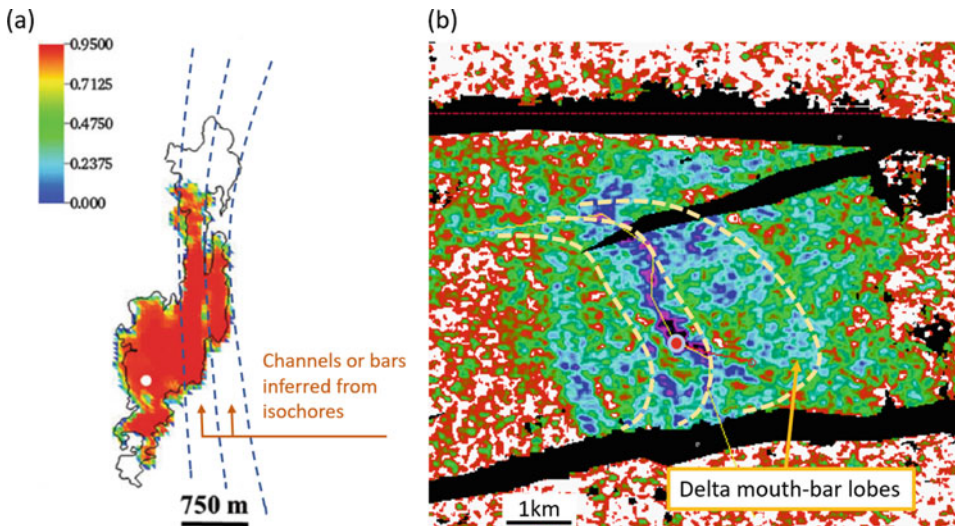
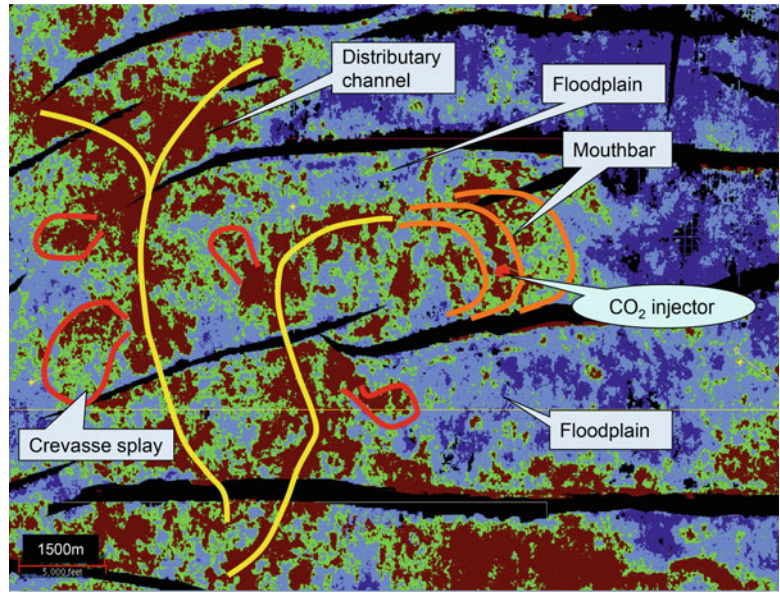


**Fig. 7.14** Influence of reservoir architecture on plume migration: (a) model of CO<sub>2</sub> distribution in Layer 9 at Sleipner at the time of the 2010 seismic monitor survey with annotations to show suspected channel or bar forms inferred from seismic isochore maps (colours indicate CO<sub>2</sub> saturation, outline of the 4D seismic anomaly shown by black line, modified from Williams and Chadwick 2017); (b) time-lapse RMS amplitude map for the Tubåen Fm. reflector at the Snøhvit CO<sub>2</sub> injection project with

annotations to show suspected delta mouth-bar lobes. (Modified from Hansen et al. 2013 and Grude et al. 2013). The highest CO<sub>2</sub> saturations correspond to the highest amplitudes (purple) which form a sinuous feature, interpreted as a channel or bar; the lower amplitudes (green) reveal the presence of smaller amounts of CO<sub>2</sub>. The red dot shows the injection well location. (Image ‘a’ is © 2017 by the Authors, published by Elsevier Ltd. and reproduced with permission)

**Fig. 7.15** Acoustic impedance map of the Tubåen Fm reflector at the Snøhvit CO<sub>2</sub> injection site, annotated with depositional features related to the interpreted depositional environments; brown and green colours show higher acoustic impedance indicating higher sand fraction, black features are faults. (Modified from Hansen et al. 2013, image courtesy of Equinor)



2013). To put this discussion of the Snøhvit case in context, Fig. 7.15 shows an interpretation of the depositional environment of the early Jurassic Tubåen Fm storage unit, in the region around the injector. Several depositional features of the fluvio-deltaic system are evident on the acoustic impedance map: distributary channels, crevasse splays and mouth bars. These lithofacies can also be identified from a sedimentological interpretation of core data. This then provides a convincing explanation for the origin the sinuous high CO<sub>2</sub>-saturations feature evident from the time-lapse seismic data (Fig. 7.14b). The CO<sub>2</sub> most likely has filled a mouth-bar sandstone unit intersected by the injection well, with some CO<sub>2</sub> finding a pathway outwards from this unit into the Tubåen-1 unit as a whole.

Clearly then, geological architecture has an important role in controlling the migration paths and fluid distribution of the expanding CO<sub>2</sub> plume. The details are, however, hard to predict. It will be a challenge for future reservoir models of aquifer/reservoir units intended for CO<sub>2</sub> storage to decide on how much detail is needed to make a realistic estimate of the plume behaviour, which will control the ultimate storage capacity. However, assessment of contrasting geological scenarios and plume forecasting within reasonable bounds of uncertainty is quite realistic, and advisable.

To gain an appreciation for the nature of the thin shales and barform features which clearly control CO<sub>2</sub> migration at the Sleipner and Snøhvit CO<sub>2</sub> storage sites, it is useful to look at well-exposed outcrop analogues. No outcrop analogue is a perfect match, but the well-exposed barrier-island bar system exposed near Pano, in the Spanish Pyrenees, provides some excellent examples of the architectural features involved. This Eocene sandstone body is interpreted as part of a transgressive barrier-island bar system prograding over shallow-marine shoreface facies and associated tide-dominated lagoonal facies (Donselaar 1996). In the examples shown in Fig. 7.16, we see the low-angle clinofolds of the main barrier-island bar overlying a package of shallow marine and lagoonal sediments, showing hummocky cross stratification and thin shale layers, typically less than 10 cm thick. These bounding surfaces and thin shales are broadly analogous to the features observed to constrain the CO<sub>2</sub> plume at Sleipner in the shallow-marine Utsira Formation. These thin shales within a very sand-rich stratigraphic unit will be inherently hard to detect in the subsurface but are important to appreciate as they could have a significant effect on CO<sub>2</sub> migration paths. At Sleipner, numerous thin shales were detected from well-log data prior to injection (Zweigel et al. 2004), but it was unknown which or how

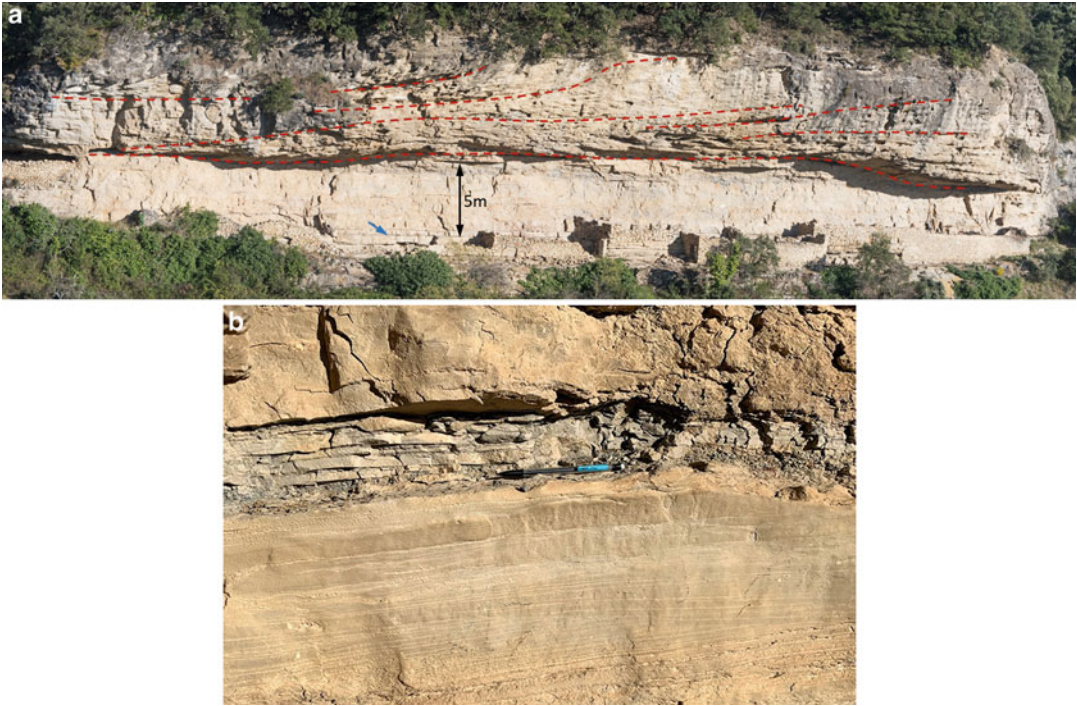


**Fig. 7.16** Outcrop images of the barrier island bar system of the Eocene Pano formation exposed near the village of Pano, northern Spain (Donselaar 1996), showing: (a) bounding surfaces of bar forms which overlie a shallow-marine shoreface system; (b) laterally-extensive thin

shales, 7-10 cm thick, within shoreface sandstones dominated by hummocky cross stratification (blue arrow indicates location of image b). (Upper image courtesy of Allard Martinus, Equinor)

many of these would impede vertical migration of  $\text{CO}_2$ . Time-lapse seismic data subsequently revealed 8 intra-formational shales as having a significant control on the actual plume distribution (cf. Figures 7.10 and 7.11, above).

In developing an appreciation of  $\text{CO}_2$  migration behaviour in stratified sedimentary systems, Krishnamurthy et al. (2019) performed a series of laboratory experiments, using a non-wetting phase fluid as a surrogate for supercritical  $\text{CO}_2$  injected at the base of a cross-stratified bead pack. Figure 7.17 shows images of fluid distribution for one of their experiments, under low-rate capillary-dominated flow conditions. The permeability and capillary-entry-pressure contrasts in the cross-stratified sand pack result in multiple accumulations of the  $\text{CO}_2$ -proxy fluid in the cross-stratified units with vertical migration pathways feeding successive traps as the injection

continues (Fig. 7.17a). After injection was stopped, only a minor degree of fluid redistribution was observed (Fig. 7.17b). The intermittency map (Fig. 7.17c) reveals the dynamic nature of the flow process with only limited parts of the migrating clusters being active at any one time, revealing the episodic disconnection and reconnection of the non-wetting phase.

These observations regarding the nature of  $\text{CO}_2$  storage flow processes at multiple scales are reviewed here as a guide to the reservoir model design that will be required for  $\text{CO}_2$  storage projects. We have focussed on the effects of stratigraphic barriers, but structural barriers (faults large and small) may also be important, either as flow baffles or as flow conduits. Detailed predictions are probably futile, due to the inherently random nature of migrating buoyant clusters of dense-phase  $\text{CO}_2$  in geological strata.



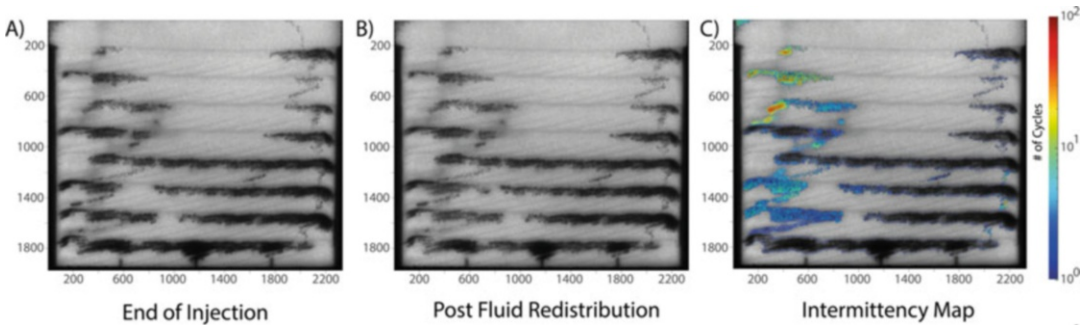


**Fig. 7.17** Digital images showing the migration of a non-wetting phase fluid (laboratory surrogate for supercritical CO<sub>2</sub>) in a cross-stratified bead pack ( $0.6 \times 0.6 \times 0.02$  m) from an experiment by Krishnamurthy et al. (2019): (a)

situation at the end of injection; (b) after fluid redistribution; (c) flow intermittency cycles during post breakthrough. (Images © 2019, American Geophysical Union, reproduced with permission)

Some degree of plume forecasting is, however, quite realistic. The fluid physics is well understood and the macroscopic nature of CO<sub>2</sub> plumes – the inverted cone geometry – has been observed in accordance with theory. Reservoir characterisation for CO<sub>2</sub> storage will therefore need to focus on the nature of bounding surfaces, baffles and faults within the sandstone units, as much as on the target sandstone units themselves. Regular monitoring of CO<sub>2</sub> storage plumes will also be essential in order to detect migration patterns and regularly update the reservoir models in a ‘modelling-monitoring loop’ workflow. Within the regulatory frameworks for CO<sub>2</sub> storage this activity is part of the requirement for *conformance monitoring*, with fit-for purpose workflows successfully demonstrated for several projects (Eiken et al. 2011; Furre et al. 2017; Dance et al. 2019).

## 7.6 Handling Pressure and Rock Deformation

With all injection projects, the response of the formation to elevated pressure (sustained or cyclic) becomes an important, often dominant, theme. The guiding principle is that injection pressure (or operating pressure cycles) must be kept below the fracture pressure of the sealing formation,  $P_{\text{frac}}$  (Fig. 7.18). In some cases, it

may be acceptable to exceed the fracture pressure of the injection unit (the reservoir) as long as the containing formation (the seal) is not compromised.

We can differentiate three major classes of underground storage of gases or liquids:

1. Storage in natural porous rock formations;
2. Storage in engineered salt caverns;
3. Storage in underground tanks (steel or concrete).

We will neglect the third category as this is an engineering problem, but the first two categories concern understanding geological systems and therefore a degree of reservoir modelling (Fig. 7.19).

Salt caverns, created by solution mining in domed or bedded salt formations, have become highly desirable as a solution for seasonal storage of natural gas, hydrocarbons, air or hydrogen. Typical cavern dimensions are 40–60 m in diameter and 300–1000 m in vertical height, with a pillar-wall thickness between caverns of 2 to 3 times the cavern diameter (Istvan et al. 1997). There are thousands of salt caverns in operation globally. The engineering and operation of salt cavern storage systems is covered elsewhere, e.g. Bérest et al. (2001, 2007), and there is now growing interest in the use of salt caverns for storage of hydrogen or compressed air as a complement to renewable energy systems, e.g. Ozarslan 2012; Raju and Khaitan 2012.

**Fig. 7.18** Conceptual graph illustrating the operational pressure ‘window’ in a subsurface injection project: operating fluid pressure needs to be kept below the fracture pressure of the sealing formation,  $P_{frac}$ . In some cases, fault or fracture zones create potential local points of weakness, where  $P_{fault-slip}$  may be less than the formation fracture pressure

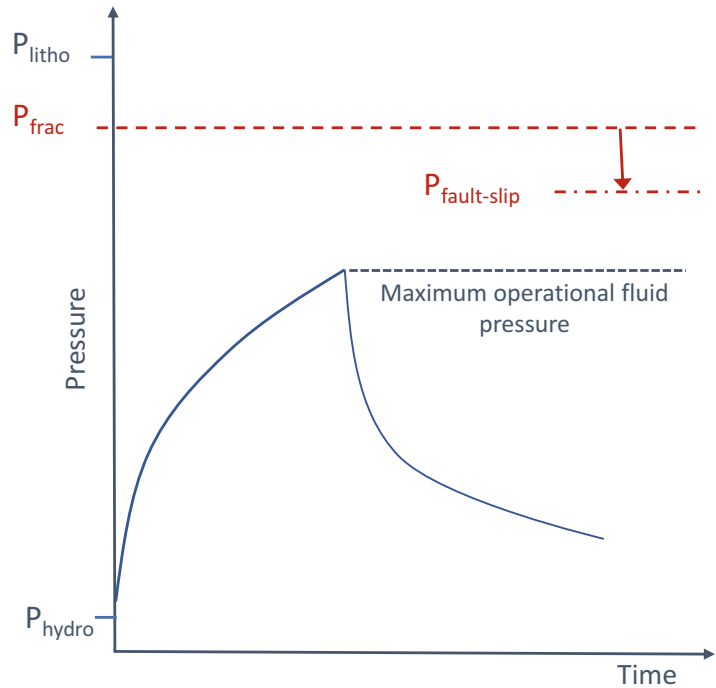
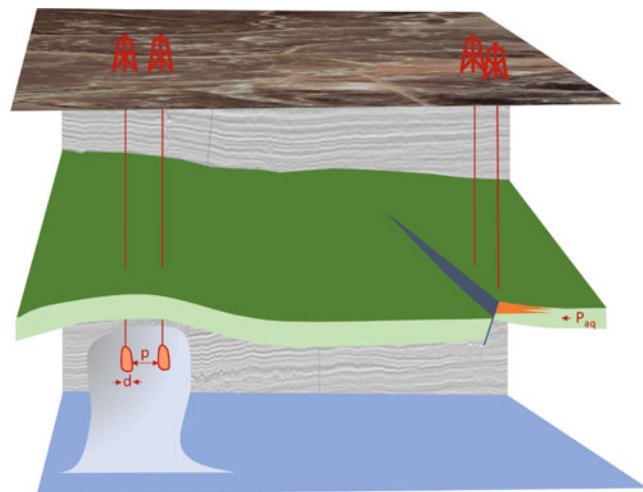


**Fig. 7.19** Sketch contrasting the two main domains for subsurface gas storage: salt caverns (left) and porous rock formations beneath structural closures (right). Key parameters controlling the geomechanics of salt caverns are the diameter,  $d$ , and the pillar wall thickness,  $p$ , while regional aquifer pressure support,  $P_{aq}$ , is a key factor controlling storage in porous rock formations



In a recent study, Otto (2017) explains the many aspects involved in characterisation and modelling of the subsurface as part of planning a new salt cavern gas storage facility at Jemgum in the Lower Saxony Basin of Germany. Much as for other uses of the subsurface, 3D depth-migrated seismic data were used to plan the gas storage project and to identify key uncertainties related to the mapping of the salt interface,

associated faults and the overlying fluvial system strata (Fig. 7.20). Planned caverns were expected to have an average diameter of 83 m and a minimum salt pillar width of 200 m. Otto (2017) went on to explain the site-characterization tasks specific to salt cavern planning, including:

- Seismic-attribute analysis and seismic interpretation;

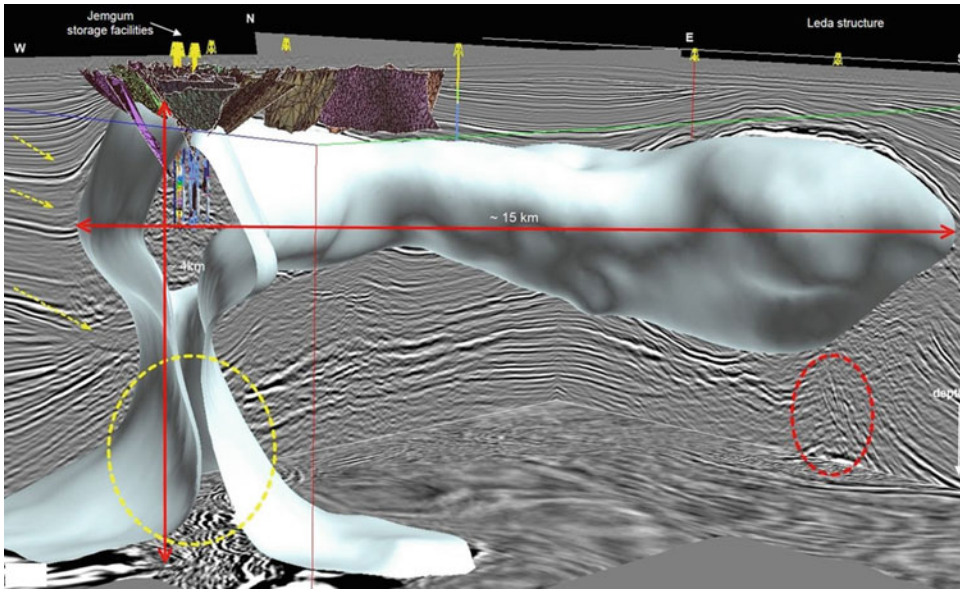


**Fig. 7.20** Interpretation of geological features around a salt diapir system for planning gas storage at the Jemgum site in the Lower Saxony Basin, NW Germany, from Otto (2017). The yellow ellipse indicates the stem of Jemgum diapir and the red ellipse indicates the salt weld beneath

the Leda salt diapir, with the two becoming joined into one salt canopy. Meshes show faults planes within the overburden of the salt structure. (Image © Geological Society of London 2017, reproduced with permission)

- Fault detection and construction of a structural framework;
- Determination of 3D distances between the cavern walls and salt interfaces;
- Mapping of shallow subsurface anomalies within the post-salt overburden;
- Identification of intra-salt seismic anomalies (anhydrite stringers or salt spines);
- Risk analysis, focused on potential migration pathways detected during the structural subsurface analysis.

The important geological aspects of what might at first appear to be a purely engineering problem, are to detect and map heterogeneities and discontinuities that might impact the drilling and solution mining process and to assess risks related to potential migration pathways which could lead to gas leakage during operations.

Salt caverns are now sought after for use as storage facilities as a complement to fluctuating renewable power systems. A well-studied example is the Huntorf power plant in northern

Germany, where two salt caverns having a total volume of around  $3 \times 10^5 \text{ m}^3$  are used for compressed air energy storage (CAES), delivering up to 321 MW of power for 3 h (Crotogino et al. 2001). Hydrogen storage in salt caverns is also envisaged as a key component of renewable energy systems. Currently, there are four sites in operation that store hydrogen in salt caverns (Lord et al. 2014). The storage of hydrogen brings additional operational challenges for underground storage, because hydrogen is a small and light molecule that reacts quickly with many natural elements and can lead to embrittlement of steel infrastructure. Note that the hydrogen ( $\text{H}_2$ ) molecule has a kinetic diameter 24% smaller than the methane molecule ( $\text{CH}_4$ ) and a density about 9 times lower than methane at standard conditions ( $\text{H}_2$  density at STP is 0.089 g/L).

Saline aquifers and depleted oil and gas reservoirs are also being evaluated as potential future options for large-scale storage of hydrogen (Pfeiffer et al. 2017; Pfeiffer and Bauer 2019) or for CAES (Wang and Bauer 2017). What these

early scoping studies show is that high-permeability sandstone aquifers can, in principle, be suitable for cyclic storage of compressed air or hydrogen, but that a suitable dome/fault block architecture is needed together with a responsive regional aquifer, allowing rapid recharge of pressure during depletion. Geochemical reactivity and potential losses to the formation are important concerns for hydrogen storage. The number of wells, the optimal placement of wells, the internal reservoir architecture, and the regional aquifer behaviour are all key factors to assess. However, natural gas storage in depleted gas reservoirs is already widely implemented and provides a framework for other gas storage options (see, for example, Mokhtab et al. 2018).

Whatever system is chosen for gas storage, an appreciation of the rock mechanical response to fluid pressure increase is needed, including episodic or cyclic fluid pressure fluctuations. An important feature for salt caverns is that the halmostatic pressure (the pressure gradient of salt as a viscous fluid) is a critical reference (Bérest et al. 2001), as it is significantly higher than the hydrostatic pressure. For all systems, defining a maximum admissible pressure, governed by mechanical failure limits of the rock containment system or the well-cement

bonds, is the overriding operational control issue. We focus here on the case of injection into a porous stratigraphic reservoir unit, with many of the concepts being also relevant to salt caverns (Fig. 7.19).

A brief summary of the extensive topic of rock mechanics is important as a basis to this discussion. Figure 7.21 shows a summary of rock mechanical failure concepts, using the Mohr diagram and based on a full treatment of the topic given by Jaeger et al. (2009). Depending on the stress state of the rock, described by the principal stresses  $\sigma_1$ ,  $\sigma_2$  and  $\sigma_3$ , rock failure is most likely to occur on a shear fracture at an angle of roughly  $30^\circ$  from the maximum stress vector, as summarized by the Mohr diagram. A minimum shear stress is generally needed to initiate failure, termed the rock cohesion,  $C$ , and the failure line is determined by rock strength and the angle of internal friction,  $\phi$ . Increasing the pore pressure will reduce effective stress, eventually leading to failure. Generally, high stress anisotropy in brittle rocks at depth leads to shear failure, but lower stress anisotropy can result in tensile failure. Real rock systems are of course more complex than suggested by this simple model, and modes and points of failure are difficult to predict in detail. Furthermore, most rocks exhibit a more complex

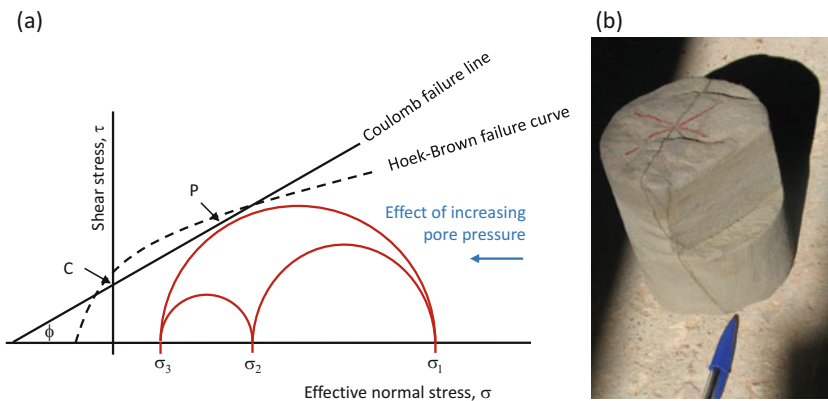


**Fig. 7.21** (a) Summary of rock failure concepts using the Mohr diagram to describe stress states leading to shear failure of a rock. The Coulomb failure line indicates the point of shear failure,  $P$ , for a rock with principal stresses  $\sigma_1$ ,  $\sigma_2$  and  $\sigma_3$ ;  $\phi$  is the angle of internal friction and  $C$  is the cohesion (the finite shear stress needed to initiate failure).

Increasing pore pressure reduces effective stress. Real rocks typically follow a more complex failure line such as a Hoek-Brown curve derived from fitting rock failure experiments. (b) An example fractured sandstone core sample displaying natural cemented fractures

failure line such as the Hoek-Brown curve shown in Fig. 7.21a, a function derived from fitting a curve to many rock failure experiments Jaeger et al. (2009).

A further important challenge is that underground rock systems do not only comprise intact rock – they also contain a set of discontinuities, fractures and faults inherited from the geological history of changing tectonic episodes over time. This means that certain faults and fractures within the storage unit may fail before the expected failure point of intact rock. This is illustrated in Fig. 7.18 where the pressure causing fault slip,  $P_{\text{fault-slip}}$ , may be less than the formation fracture pressure,  $P_{\text{frac}}$ . Storage projects therefore need to assess both the mechanical limits of the key formations involved and the mechanical limits of faults and fractures exposed to pressure changes. This frames an important part of the design goals for reservoir models of CO<sub>2</sub> storage sites – understand the rock mechanical response to injection.

Ideally, injection projects wish to keep the pressure below the level where mechanical failure of the rock can occur (Fig. 7.18). In this situation, an elastic response to pressure changes will still occur, but the deformation will most likely be

small and reversible. Take the case of elevated injection pressure into a reservoir unit such as sketched in Fig. 7.22. What degree of rock strain should we expect? Fjær et al. (2008) proposed a useful reference model to estimate the vertical strain,  $\Delta h$ , caused by an increase in formation pressure,  $\Delta P$ . Assuming a thin laterally extensive reservoir, they showed that  $\Delta h$  can be estimated analytically by:

$$\frac{\Delta h}{h} = \alpha \frac{(1 + \nu)(1 - 2\nu)}{(1 - \nu)E} \Delta P \quad (7.3)$$

Where,  $\alpha$  is Biot’s coefficient,  $\nu$  is Poisson’s ratio, and  $E$  is Young’s modulus. If we take an illustrative example and using some typical values for rock mechanical properties ( $\alpha = 1$ ;  $\nu = 0.2$ ,  $E = 6\text{GPa}$ ), then the vertical strain,  $\Delta h$ , in a 20-m thick reservoir unit would be:

- 9 mm for a pressure increase of 3 MPa (30 bar)
- 15 mm for a pressure increase 6 MPa (60 bar)

This is a linear elastic effect and could be considered as a typical expected rock mechanical response to elevated injection pressures.

A well-studied example of rock mechanical response to CO<sub>2</sub> injection is the In Salah CCS project in Algeria (Rutqvist et al. 2010; Ringrose

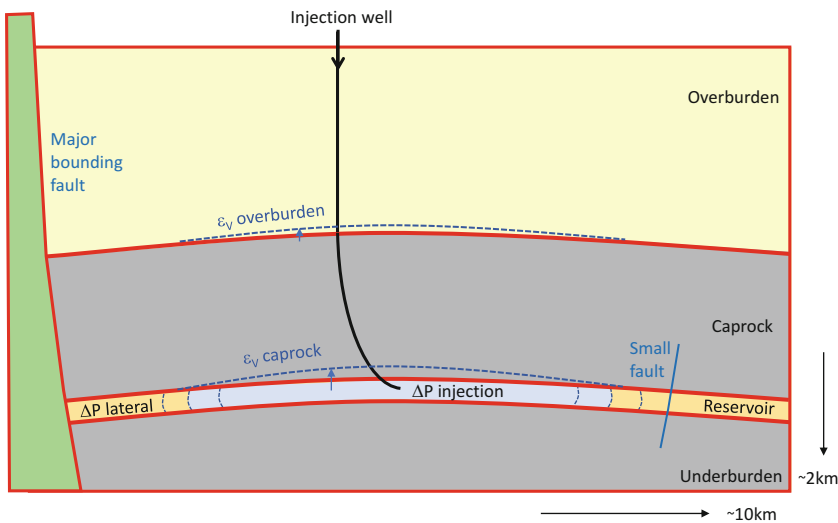


**Fig. 7.22** Illustration of rock strain response to elevated injection pressure in a porous stratigraphic reservoir unit,  $\Delta P$  = change in fluid pressure;  $\epsilon_v$  = vertical component of rock strain

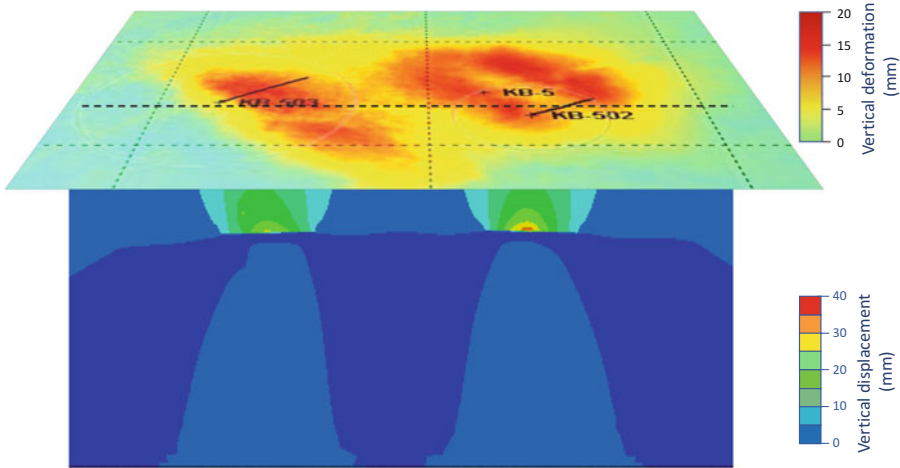


**Fig. 7.23** Observed and modelled vertical displacements resulting from pore pressure increase associated with CO<sub>2</sub> injection at the In Salah project. (Modified from Gemmer et al. 2012). Surface map shows vertical surface displacement pattern determined from InSAR observations at

August 2009 and section shows output from a linear-elastic geomechanical model. The section is 15 km across and 6 km deep; the injection interval is at 2 km depth

et al. 2013). At this onshore injection site, high quality satellite-based radar interferometry measurements (InSAR) of surface deformation could be clearly linked to the subsurface pressure field associated with CO<sub>2</sub> storage (Vasco et al. 2010). This enabled a detailed and informative determination of how a rock mass responds to injection pressure. Figure 7.23 shows an example result from the study by Gemmer et al. (2012), where observed surface displacement (InSAR data) could be used to validate modelled deformation using a linear-elastic geomechanical model. Note how the maximum vertical displacement at the reservoir interval (up to 40 mm) decays towards the surface where a maximum of 20 mm of surface uplift was observed. The precise nature of the rock mechanical response depends very much on the detailed mechanical properties of the reservoir and overburden sequence and the discontinuities within the rock mass (White et al. 2014), and careful characterisation of the overburden units – the ‘mechanical stratigraphy’ – is key to successful forecasting of the rock mechanical response.

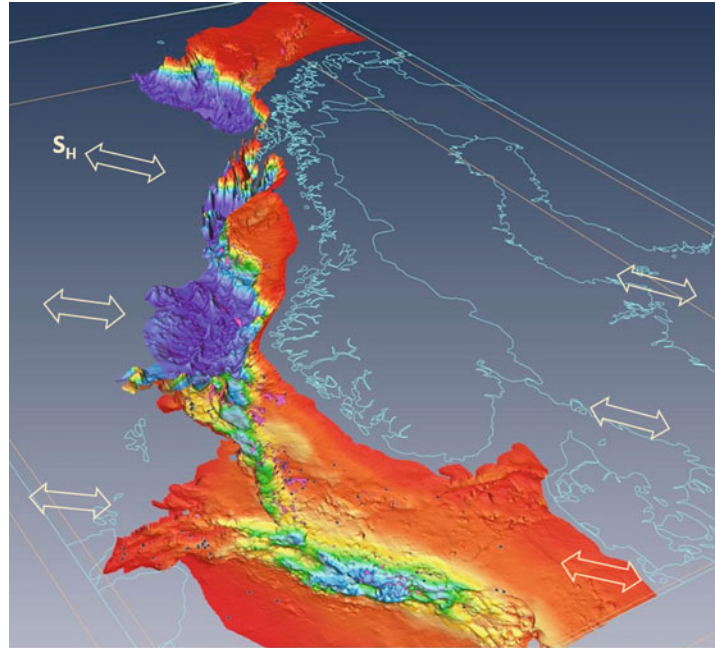
An essential part of the workflow for geomechanical assessment of CO<sub>2</sub> storage

projects is to characterise the structural architecture and the present-day state of stress, generally assessing the tectonic history as part of that process. Determining the stress field orientation and magnitudes of stress vectors is often a major uncertainty. The regional view of the North Sea and adjacent offshore basins shown in Fig. 7.24 indicates the first order trends in the stress field dictated by plate-tectonic boundary forces (Heidbach et al. 2007a). However, within each basin second- and third-order variations in stress patterns are observed leading to significant variations in the stress field (Heidbach et al. 2007b).

In a geomechanical analysis of the Snøhvit CO<sub>2</sub> storage project, Chiamonte et al. (2015) developed a probabilistic analysis of fault reactivation risk using available stress and rock mechanical data. Their approach and workflow offer a good basis for geomechanical analysis in future projects, and can be summarised in the following steps:

1. Determine the *in situ* stress state by quantifying the magnitude and orientation of the three principal stresses: the vertical stress

**Fig. 7.24** Topographic view of the Base Cretaceous Unconformity surface (10xVE) of the North Sea and adjacent basins, with main oil and gas fields in magenta and first-order trends in the orientation of the maximum horizontal compressional stress ( $S_H$ ). (Image courtesy of Nils Erik Janbu, reproduced with permission from Equinor ASA; regional stress trends are inferred from Heidbach et al. 2007a)



( $S_v$ ) and the minimum and maximum horizontal stress vectors ( $S_{Hmin}$ ,  $S_{Hmax}$ ).

2. Assess uncertainty ranges in these estimates by analysis of wellbore fractures in image logs and reported stress measurements from wells in the region.  $S_v$  is generally accurately constrained by integrating density logs,  $S_{Hmin}$  magnitudes can be estimated from available well tests (ideally extended leak-off tests) whereas  $S_{Hmax}$  is typically very poorly constrained.
3. Assess a likely range in the stress field, especially for  $S_{Hmax}$ , using poro-elastic theory to estimate upper and lower bound values, including alternative stress orientations.
4. Then estimate the fault-slip tendency for the mapped faults in the vicinity of the injection wells using the contrasting stress-state scenarios to generate a series of probabilistic outcomes (or a simple sensitivity analysis may also suffice).

This approach to integrated uncertainty analysis of potential fault slip associated with  $CO_2$  injection is important for the risk assessment itself, but also valuable for quantifying the underlying uncertainties, which can be then be

managed by a focussed monitoring programme, with pressure monitoring and passive seismic monitoring as appropriate. In fact, full foresight of the fracturing potential for a  $CO_2$  storage project is unrealistic, the main goal is to ensure an acceptably low probability of injection-induced events. During operations the initial design can be then adjusted using real-time analysis of pressure time-series datasets, as demonstrated by Bohloli et al. (2017).

## 7.7 Model Design Futures for the Energy Transition

In this chapter we have reviewed insights and key focus topics for modelling  $CO_2$  storage and other storage options such as cyclic storage of hydrogen or compressed air. It is hard to anticipate how fast this field will grow in the drive for a low- $CO_2$  emissions society. Probably quite rapidly. Although the underlying reservoir modelling principles are similar across all applications (have a geological concept, understand static-dynamic interactions and maintain alternative scenarios), some aspects of storage are more

unique. Introducing a low-viscosity, non-wetting fluid into a brine-saturated porous medium is fundamentally different from oil and gas extraction. Flow barriers and baffles are probably a more important aspect of the reservoir characterisation, and understanding the rock mechanical response to injection is often critical.

In anticipation of the projected growth in CO<sub>2</sub> storage activities globally, Ringrose and Meckel (2019) outlined a framework for CO<sub>2</sub> storage project development within the framework of basin-scale stratigraphy and subsurface pressure constraints. The necessary storage resources are clearly available – the challenges are more about financial incentives and business drivers. Assuming modern society wishes to fulfil the objective of the 2015 Paris climate accord, thereby changing our energy systems to limit global warming to less than 2 °C, then CO<sub>2</sub> storage must become a very significant activity over the coming decades. The analysis by Ringrose and Meckel (2019) indicates that about 12,000 CO<sub>2</sub> injection wells will be needed globally by 2050 to achieve the Paris agreement goals.

Although the low-carbon energy transition is clearly underway, the pace of change is unclear. In all scenarios, reservoir modelling and wise use of subsurface reservoirs will be important. Ideally the skills learned from the petroleum age will be quickly adapted to the ‘low-carbon’ world, where CO<sub>2</sub> storage and hydrogen storage could become as commonplace as hydrocarbon field developments currently are.

## References

- Aradóttir ES, Sigurdardóttir H, Sigfússon B, Gunnlaugsson E (2011) CarbFix: a CCS pilot project imitating and accelerating natural CO<sub>2</sub> sequestration. *Greenhouse Gases Sci Technol* 1(2):105–118
- Bennion B, Bachu, S (2006) Dependence on temperature, pressure, and salinity of the IFT and relative permeability displacement characteristics of CO<sub>2</sub> injected in deep saline aquifers. Paper SPE 102138, presented at the 2006 SPE Annual Technical Conference and Exhibition, San Antonio, TX, USA, September 24–27
- Benson S, Cook P, Anderson J, Bachu S, Nimir HB, Basu B, Heidug W (2005) Underground geological storage. In: IPCC special report on carbon dioxide capture and storage. Cambridge University Press, New York, pp 195–276
- Bérest P, Brouard B, Durup JG (2001) Tightness tests in salt-cavern wells. *Oil Gas Sci Technol* 56(5):451–469
- Bérest P, Brouard B, Karimi-Jafari M, Van Sambeek L (2007) Transient behavior of salt caverns—interpretation of mechanical integrity tests. *Int J Rock Mech Min Sci* 44(5):767–786
- Berg RR (1975) Capillary pressures in stratigraphic traps. *AAPG Bull* 59(6):939–956
- Blunt MJ (2001) Flow in porous media—pore-network models and multiphase flow. *Curr Opin Colloid Interface Sci* 6(3):197–207
- Bohlooli B, Ringrose P, Grande L, Nazarian B (2017) Determination of the fracture pressure from CO<sub>2</sub> injection time-series datasets. *Int J Greenhouse Gas Control* 61:85–93
- Carruthers D, Ringrose P (1998) Secondary oil migration: oil-rock contact volumes. *Geol Soc Lond, Spec Publ* 144(1):205–220
- Cavanagh AJ, Ringrose PS (2011) Simulation of CO<sub>2</sub> distribution at the In Salah storage site using high-resolution field-scale models. *Energy Procedia* 4:3730–3737
- Cavanagh AJ, Haszeldine RS, Nazarian B (2015) The Sleipner CO<sub>2</sub> storage site: using a basin model to understand reservoir simulations of plume dynamics. *First Break* 33(6):61–68
- Chadwick AG, Williams N, Delepine V, Clochard K, Labat S, Sturton M, Buddensiek M, Dillen M, Nickel A, Lima R, Arts F, Neele P, Rossi G (2010) Quantitative analysis of time-lapse seismic monitoring data at the Sleipner CO<sub>2</sub> storage operation. *Lead Edge* 29:170–177. <https://doi.org/10.1190/1.3304820>.
- Chiaromonte L, White JA, Trainor-Guitton W (2015) Probabilistic geomechanical analysis of compartmentalization at the Snøhvit CO<sub>2</sub> sequestration project. *J Geophys Res Solid Earth* 120(2):1195–1209
- Cowton LR, Neufeld JA, White NJ, Bickle MJ, Williams GA, White JC, Chadwick RA (2018) Benchmarking of vertically-integrated CO<sub>2</sub> flow simulations at the Sleipner Field, North Sea. *Earth Planet Sci Lett* 491:121–133
- Crotogino F, Mohmeyer KU, Scharf R (2001) Huntorf CAES: more than 20 years of successful operation. In: Proceedings of the Solution Mining Research Institute (SMRI) Spring Meeting, Orlando, FL, USA, 15–18 April 2001. Solution Mining Research Institute (SMRI), Clarks Summit, pp 351–357
- Dance T, LaForce T, Glubokovskikh S, Ennis-King J, Pevzner R (2019) Illuminating the geology: post-injection reservoir characterisation of the CO<sub>2</sub>CRC Otway site. *Int J Greenhouse Gas Control* 86:146–157
- Donselaar ME (1996) Barrier island coasts and relative sea level rise: preservation potential, facies architecture and sequence analysis. Ph.D thesis, University of Delft, NUGI 816
- EC (2009) DIRECTIVE 2009/31/EC OF THE EUROPEAN PARLIAMENT AND OF THE COUNCIL OF



- 23 April 2009 on the geological storage of carbon dioxide and amending Council Directive 85/337/EEC, European Parliament and Council Directives 2000/60/EC, 2001/80/EC, 2004/35/EC, 2006/12/EC, 2008/1/EC and Regulation (EC) No 1013/2006
- Eiken O, Ringrose P, Hermanrud C, Nazarian B, Torp TA, Høier L (2011) Lessons learned from 14 years of CCS operations: Sleipner, In Salah and Snøhvit. *Energy Procedia* 4:5541–5548
- Fjær E, Holt RM, Raaen AM, Risnes R, Horsrud P (2008) *Petroleum related rock mechanics*, 2nd edn. Elsevier, 514 p
- Furre AK, Kiær A, Eiken O (2015) CO<sub>2</sub>-induced seismic time shifts at Sleipner. *Interpretation* 3.3(2015):SS23–SS35
- Furre AK, Eiken O, Alnes H, Vevatne JN, Kiær AF (2017) 20 years of monitoring CO<sub>2</sub>-injection at Sleipner. *Energy Procedia* 114:3916–3926
- Furre A, Ringrose P, Santi AC (2019) Observing the invisible—CO<sub>2</sub> feeder chimneys on seismic time-lapse data. 81st EAGE conference and exhibition 2019. European Association of Geoscientists & Engineers.
- Gasda SE, Nilsen HM, Dahle HK (2013) Impact of structural heterogeneity on upscaled models for large-scale CO<sub>2</sub> migration and trapping in saline aquifers. *Adv Water Resour* 62:520–532
- Gemmer L, Hansen O, Iding M, Leary S, Ringrose P (2012) Geomechanical response to CO<sub>2</sub> injection at Krecbba, In salah, Algeria. *First Break* 30(2)
- Gislason SR, Oelkers EH (2014) Carbon storage in basalt. *Science* 344(6182):373–374
- Grude S, Landrø M, Osdal B (2013) Time-lapse pressure–saturation discrimination for CO<sub>2</sub> storage at the Snøhvit field. *Int J Greenhouse Gas Control* 19:369–378
- Hansen O, Gilding D, Nazarian B, Osdal B, Ringrose P, Kristoffersen JB et al (2013) Snøhvit: the history of injecting and storing 1 Mt CO<sub>2</sub> in the fluvial Tubåen Fm. *Energy Procedia* 37:3565–3573
- Heidbach O, Fuchs K, Müller B, Reinecker J, Sperner B, Tingay M, Wenzel F (2007a) The World Stress Map – Release 2005, 1:46,000,000. Commission of the Geological Map of the World, Paris
- Heidbach O, Reinecker J, Tingay M, Müller B, Sperner B, Fuchs K, Wenzel F (2007b) Plate boundary forces are not enough: second- and third-order stress patterns highlighted in the World Stress Map database. *Tectonics* 26: TC6014. <https://doi.org/10.1029/2007TC002133>.
- Hovorka SD, Doughty C, Benson SM, Pruess K, Knox PR (2004) The impact of geological heterogeneity on CO<sub>2</sub> storage in brine formations: a case study from the Texas Gulf Coast. *Geol Soc London Spec Publ* 233 (1):147–163
- Huang Y, Ringrose PS, Sorbie KS (1995) Capillary trapping mechanisms in water-wet laminated rocks. *SPE Reserv Eng* 10(4). <https://doi.org/10.2118/28942-PA>
- Istvan JA, Evans LJ, Weber JH, Devine C (1997) Rock mechanics for gas storage in bedded salt caverns. *Int J Rock Mech Min Sci* 34(3–4):142–1e1
- Jaeger JC, Cook NG, Zimmerman R (2009) *Fundamentals of rock mechanics*. Wiley, New York
- Krishnamurthy PG, Meckel TA, DiCarlo D (2019) Mimicking geologic depositional fabrics for multiphase flow experiments. *Water Resour Res* 55 (11):9623–9638
- Li H, Yan J (2009) Impacts of equations of state (EOS) and impurities on the volume calculation of CO<sub>2</sub> mixtures in the applications of CO<sub>2</sub> capture and storage (CCS) processes. *Appl Energy* 86(12):2760–2770
- Lord AS, Kobos PH, Borns DJ (2014) Geologic storage of hydrogen: scaling up to meet city transportation demands. *Int J Hydrogen Energy* 39(28):15570–15582
- Meckel TA (2013) Digital rendering of sedimentary-relief peels: implications for clastic facies characterization and fluid flow. *J Sediment Res* 83(6):495–501
- Mokhatab S, Poe WA & Mak JY (2018) *Handbook of natural gas transmission and processing: principles and practices*. Cambridge, MA Gulf Professional Publishing.
- Naylor M, Wilkinson M, Haszeldine RS (2011) Calculation of CO<sub>2</sub> column heights in depleted gas fields from known pre-production gas column heights. *Mar Pet Geol* 28(5):1083–1093
- Niemi A, Bear J, Bensabat J (2017) *Geological storage of CO<sub>2</sub> in deep saline formations*. Springer, Dordrecht
- Nilsen HM, Krogstad S, Andersen O, Allen R, Lie KA (2017) Using sensitivities and vertical-equilibrium models for parameter estimation of CO<sub>2</sub> injection models with application to Sleipner data. *Energy Procedia* 114:3476–3495
- Nordbotten JM, Celia MA (2006) Similarity solutions for fluid injection into confined aquifers. *J Fluid Mech* 561:307–327
- Nordbotten JM, Celia MA (2012) *Geological storage of CO<sub>2</sub>: modeling approaches for large-scale simulation*. Wiley, Hoboken
- Osdal B, Zadeh HM, Johansen S, Gonzalez RR, Wærum GO (2014) Snøhvit CO<sub>2</sub> monitoring using well pressure measurement and 4D seismic. In: Fourth EAGE CO<sub>2</sub> geological storage workshop. European Association of Geoscientists & Engineers
- Otto B (2017) The importance of detailed geological characterization for future expanded use of gas storage in the sustainable energy context. *Pet Geosci* 23 (3):327–338
- Ozarslan A (2012) Large-scale hydrogen energy storage in salt caverns. *Int J Hydrog Energy* 37(19):14265–14277
- Pfeiffer WT, Bauer S (2019) Comparing simulations of hydrogen storage in a sandstone formation using heterogeneous and homogenous flow property models. *Pet Geosci* 25(3):325–336
- Pfeiffer WT, Beyer C, Bauer S (2017) Hydrogen storage in a heterogeneous sandstone formation: dimensioning and induced hydraulic effects. *Pet Geosci* 23 (3):315–326

- Raju M, Khaitan SK (2012) Modeling and simulation of compressed air storage in caverns: a case study of the Huntuorf plant. *Appl Energy* 89(1):474–481
- Reynolds CA, Krevor S (2015) Characterizing flow behavior for gas injection: relative permeability of CO<sub>2</sub>-brine and N<sub>2</sub>-water in heterogeneous rocks. *Water Resour Res* 51(12):9464–9489
- Reynolds CA, Menke H, Andrew M, Blunt MJ, Krevor S (2017) Dynamic fluid connectivity during steady-state multiphase flow in a sandstone. *Proc Natl Acad Sci* 114(31):8187–8192
- Ringrose P (2020) How to store CO<sub>2</sub> underground: insights from early-mover CCS projects. Springer Briefs in Earth Sciences. ISBN 978-3-030-33113-9
- Ringrose PS, Meckel TA (2019) Maturing global CO<sub>2</sub> storage resources on offshore continental margins to achieve 2DS emissions reductions. *Sci Rep* 9(1):1–10. <https://doi.org/10.1038/s41598-019-54363-z>
- Ringrose PS, Sorbie KS, Corbett PWM, Jensen JL (1993) Immiscible flow behaviour in laminated and cross-bedded sandstones. *J Pet Sci Eng* 9(2):103–124
- Ringrose PS, Mathieson AS, Wright IW, Selama F, Hansen O, Bissell R et al (2013) The In Salah CO<sub>2</sub> storage project: lessons learned and knowledge transfer. *Energy Procedia* 37:6226–6236
- Rutqvist J, Vasco DW, Myer L (2010) Coupled reservoir-geomechanical analysis of CO<sub>2</sub> injection and ground deformations at In Salah, Algeria. *Int J Greenhouse Gas Control* 4(2):225–230
- Sahasrabudhe SN, Rodriguez-Martinez TH, O'Meara M, Farkas BE (2017) Density, viscosity, and surface tension of five vegetable oils at elevated temperatures: measurement and modeling. *Int J Food Prop* 20(sup2):1965–1981
- Santi AC (2019) Factors impacting multi-layer plume distribution in CO<sub>2</sub> storage reservoirs. Masters dissertation, University of Lisbon, Portugal. <https://repositorio.ul.pt/handle/10451/37821>
- Singh VP, Cavanagh A, Hansen H, Nazarian B, Iding M, Ringrose PS (2010) Reservoir modeling of CO<sub>2</sub> plume behavior calibrated against monitoring data from Sleipner, Norway. In: SPE annual technical conference and exhibition. Society of Petroleum Engineers.
- Span R & Wagner W (1996) A new equation of state for carbon dioxide covering the fluid region from the triple point temperature to 1100 K at pressures up to 800 MPa. *J Phys Chem Ref Data*, 1996; 25: 1509–1596.
- Span R, Gernert J, Jäger A (2013) Accurate thermodynamic-property models for CO<sub>2</sub>-rich mixtures. *Energy Procedia* 37:2914–2922
- Trevisan L, Pini R, Cihan A, Birkholzer JT, Zhou Q, Illangasekare TH (2015) Experimental analysis of spatial correlation effects on capillary trapping of supercritical CO<sub>2</sub> at the intermediate laboratory scale in heterogeneous porous media. *Water Resour Res* 51(11):8791–8805
- Trevisan L, Krishnamurthy PG, Meckel TA (2017a) Impact of 3D capillary heterogeneity and bedform architecture at the sub-meter scale on CO<sub>2</sub> saturation for buoyant flow in clastic aquifers. *Int J Greenhouse Gas Control* 56:237–249. <https://doi.org/10.1016/j.ijggc.2016.12.001>.
- Trevisan L, Pini R, Cihan A, Birkholzer JT, Zhou Q, González-Nicolás A, Illangasekare TH (2017b) Imaging and quantification of spreading and trapping of carbon dioxide in saline aquifers using meter-scale laboratory experiments. *Water Resour Res* 53(1):485–502. <https://doi.org/10.1002/2016WR019749>
- Vasco DW, Rucci A, Ferretti A, Novali F, Bissell RC, Ringrose PS, Wright IW (2010) Satellite-based measurements of surface deformation reveal fluid flow associated with the geological storage of carbon dioxide. *Geophys Res Lett* 37(3)
- Veloso FM, Frykman P, Nielsen CM, Soria AR, Meléndez MN (2016) Outcrop scale reservoir characterisation and flow modelling of CO<sub>2</sub> injection in the tsunami and the barrier island—tidal inlet reservoirs of the Camarillas Fm. (Galve sub-basin, Teruel, NE Spain). *Int J Greenhouse Gas Control* 55:60–72
- Wang B, Bauer S (2017) Compressed air energy storage in porous formations: a feasibility and deliverability study. *Pet Geosci* 23(3):306–314
- White JA, Chiaramonte L, Ezzedine S, Foxall W, Hao Y, Ramirez A, McNab W (2014) Geomechanical behavior of the reservoir and caprock system at the In Salah CO<sub>2</sub> storage project. *Proc Natl Acad Sci* 111(24):8747–8752
- Wilkinson D, Willemsen JF (1983) Invasion percolation: a new form of percolation theory. *J Phys A Math Gen* 16(14):3365
- Williams GA, Chadwick RA (2017) An improved history-match for layer spreading within the Sleipner plume including thermal propagation effects. *Energy Procedia* 114:2856–2870
- Williams GA, Chadwick RA, Vosper H (2018) Some thoughts on Darcy-type flow simulation for modelling underground CO<sub>2</sub> storage, based on the Sleipner CO<sub>2</sub> storage operation. *Int J Greenhouse Gas Control* 68:164–175
- Zweigel P, Arts R, Lothe AE, Lindeberg EB (2004) Reservoir geology of the Utsira Formation at the first industrial-scale underground CO<sub>2</sub> storage site (Sleipner area, North Sea). *Geol Soc London Spec Publ* 233(1):165–180

## Abstract

It ain't what you do, it's the way that you do it

There is a tendency in the reservoir modelling community to build detailed, full-field models and the bigger the computer, the bigger the model. Although individual models now run very quickly, the turn-around times for reservoir studies have not necessarily changed over recent decades, despite the

huge increases in computing power and the increased sophistication of modelling and simulation software. Often these models are not fit-for-purpose, and the decision at hand could have been made via more efficient routes. We tend, in this sense, to work at a level of maximum inefficiency.

The reason is workflow. In this section we therefore look at alternative workflows which take us away from the 'default' of a single detailed full-field model.



The Forth Bridge in Edinburgh, Scotland; a visual metaphor for iterative workflows

---

**Keywords**

Resource models · Decision models · Truth models · Front-end loading · Agile · Iteration · Integration · History matching · Bayesian Evidential Learning

---

## 8.1 The Detailed, Full-Field Model Default

Modelling and simulation software packages are toolboxes, and guidance in their usage generally comes in the form of a recommended workflow. We illustrated a standard workflow in Fig. 1.10 and the steps involved in a typical model build are usefully summarised by Cannon (2018). The linear workflow helps practitioners learn the modelling process and usually results in a full-field model, with a grid cell count designed to capture the main features in the reservoir (reef build-ups, channels, correlatable shales etc.) but not so many features that the simulation run times are inconveniently long. Capturing the effects of more detail can be tackled through upscaling (Chap. 4), although with increased computing power many practitioners favour static and dynamic modelling at a single scale in order to ‘avoid the upscaling issue’. This tendency to put everything into a single manageable (?) model is what we refer to as the ‘detailed full-field default’.

The default often lets us down when it comes to supporting decisions. This is particularly the case in mature fields, where the models tend to become large and unwieldy, the integration of production data is time-consuming and the incremental nature of accumulating data means models tend to become ‘patched’ by local updates. Patches to the static model are usually made around new wells and often much larger patches are added to the dynamic model to keep the model production history consistent with the actual field history – the process of ‘history-matching’. Models are also commonly passed hand-to-hand between practitioners to the point that ownership

is lost. The update and maintenance of the ‘field model’ becomes a job in itself, often separate from the process of managing the field. The modelling process thus loses its value.

As the previous chapters have progressively argued, there are many alternative model types and several alternative workflows (Fig. 8.1).

In this chapter we explore alternative routes to decision making which offer a more efficient option to the detailed, full-field default.

---

## 8.2 Resource and Decision Models

The simple solution to avoid the ‘default’ is to let go of the assumption that one model must serve all purposes.

Different purposes were reviewed in Chap. 1. For greenfield development planning, a full-field approach is generally desirable, possibly supplemented by small-scale models to capture significant heterogeneity which has been lost at the full-field scale. For mature fields, full-field modelling is more arduous as the data volume is larger, particularly dynamic data, and yet the questions being asked later in field life are not necessarily full-field questions. Using every piece of data each time any decision has to be made may appear ‘integrated’, but is the least efficient course of action. On the other hand, there is a need to at least maintain the full-field data set – some data items, notably seismic, are almost universally acquired on a full-field basis.

The tension between data and purpose can be relieved by decoupling the two. It is therefore useful to distinguish between the ‘resource model’ and the ‘decision model’ (Bentley and Ringrose 2017) (Fig. 8.2).

The *resource model* is effectively a 3D database containing all field data pertinent to the management of the field. This includes the spatially located data such as wells and seismic, but also the associated dynamic data from the field (time-series data); everything required to build any type of model. By definition, this is full-

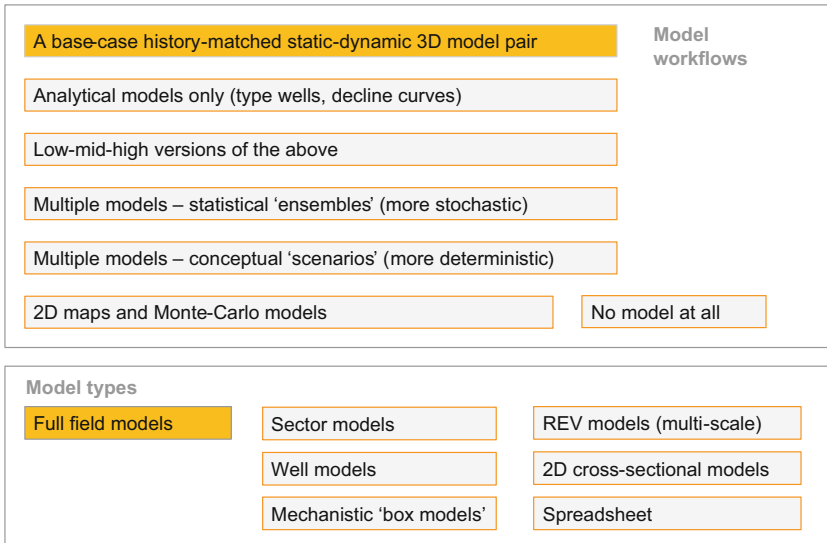


**Fig. 8.1** Modelling and simulation options: alternative workflows and alternative model types

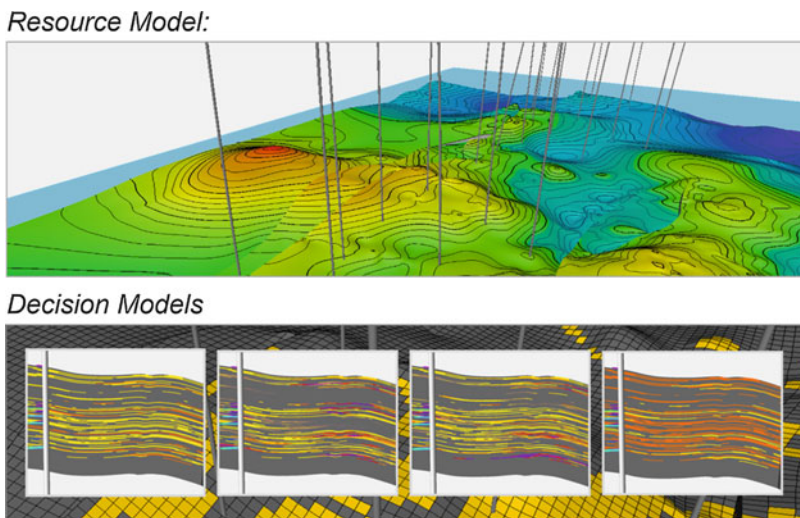


**Fig. 8.2** Resource models vs. decision models

field, and would generally be contained in a modelling package so it can be visualised. Resource volumes, full-field by definition, would naturally come from the resource model. The 3D database can also accumulate the stream of injection and production data as it becomes available, along with new static data elements as they are acquired (a new well, or a new vintage of seismic). However, this does not necessarily need to be turned into a full-field, history-matched simulation model.

The *decision model* is something which is built in answer to a specific development question, and it is this type of model which should be fit-for-purpose. As stressed in Chap. 1, different purposes call upon different model designs and in mature fields in particular these are commonly not full-field. The decision models should live for the life of the question at hand and, once answered, can be archived until a new question emerges, which may demand a different type of decision model.

The decision model therefore lasts for the season, whereas the resource model is ‘evergreen’ – at least until the field life cycle itself concludes.

An example of this distinction is given by Oxlade and Bentley (2015) for a mature oil field in France. The field is a low net-to-gross (10–30%) fluvial reservoir filled with a light oil undergoing waterflood and the development question was whether a five spot infill drilling campaign would be commercial. Modelling and simulation work commenced and it quickly became apparent that the static-dynamic iteration of a full-field model at the resolution needed to capture production behavior was time-consuming – too time-consuming to support the decision on infill drilling in the time available for planning. The default workflow was therefore abandoned in favour of a multi-scale approach with static-dynamic iteration in small sectors (Fig. 8.3). A full-field static resource model was built to calculate in-place volumes and provide a representation of the permeability architecture to which an injection scheme would be sensitive (Fig. 8.3c). A coarse full-field material balance sand/shale model was also built to understand connectivity on a field scale and match field pressures in the area of interest (Fig. 8.2b). The model used for decision-making was a hybrid, in which the sector where the intended 5-spot injection pattern was to be tested was extracted from the resource model and embedded in the material balance model to honour sector boundary conditions.

Uncertainties pertinent to the infill question were explored using alternative models for the sector only. These were scenario-based, constructed as described in Sect. 5.2.3. Each model was manually re-matched for each static realisation in the sector – a relatively straightforward process involving a few wells local to the sector with relatively low water cuts. Well-by-well detailed matches across the whole field were not necessary. Development scenarios - infill wells with different well spacings and water flood patterns - were tested against each combination of uncertainties.

The models provided the confidence for the infill programme pilot. This was successfully

implemented the following year and has subsequently been extended across the field. There was no single ‘full-field model’ and a traditional, detailed, history-matched full-field model was not required to get to the decision point.

The workflow described above was highly fit-for-purpose and much more efficient in terms of both manpower and computing power than detailed full-field modelling. The contrast between this and a more traditional, linear process is shown in Fig. 8.4. A key feature of the approach was fast iteration, and this is explored further in the next section.

---

### 8.3 Iterative Workflows – The Forth Bridge

Building on the idea of parallel working and accelerated project timelines illustrated by the example above and adopting concepts of front-end loading, Oxlade and Bentley (2015) proposed a generic workflow which is particularly applicable for mature fields in which the default workflow often disappoints.

The conceptual model uses the Forth Bridge in Edinburgh as a visual metaphor in which the cantilevers represent short periods of team-based working and the nodes between the cantilevers represent meeting points when the disciplines come together to compare findings and plan for the next work segment (Fig. 8.5). The passage across the bridge itself is linear, as is study time.

The generic content of each node and cantilever is predictable:

- *Node* – problem definition (the kick-off)
- *Cantilever* – data review
- *Node* – definition of uncertainties – the long list
- *Cantilever* – analysis of significant uncertainties – root cause analysis
- *Node* – review uncertainties – the short list
- *Cantilever* – initial static/dynamic models to test commercial sensitivity
- *Node* – decision on modelling – worth it or not? If worthwhile, choose a fit-for-purpose model design

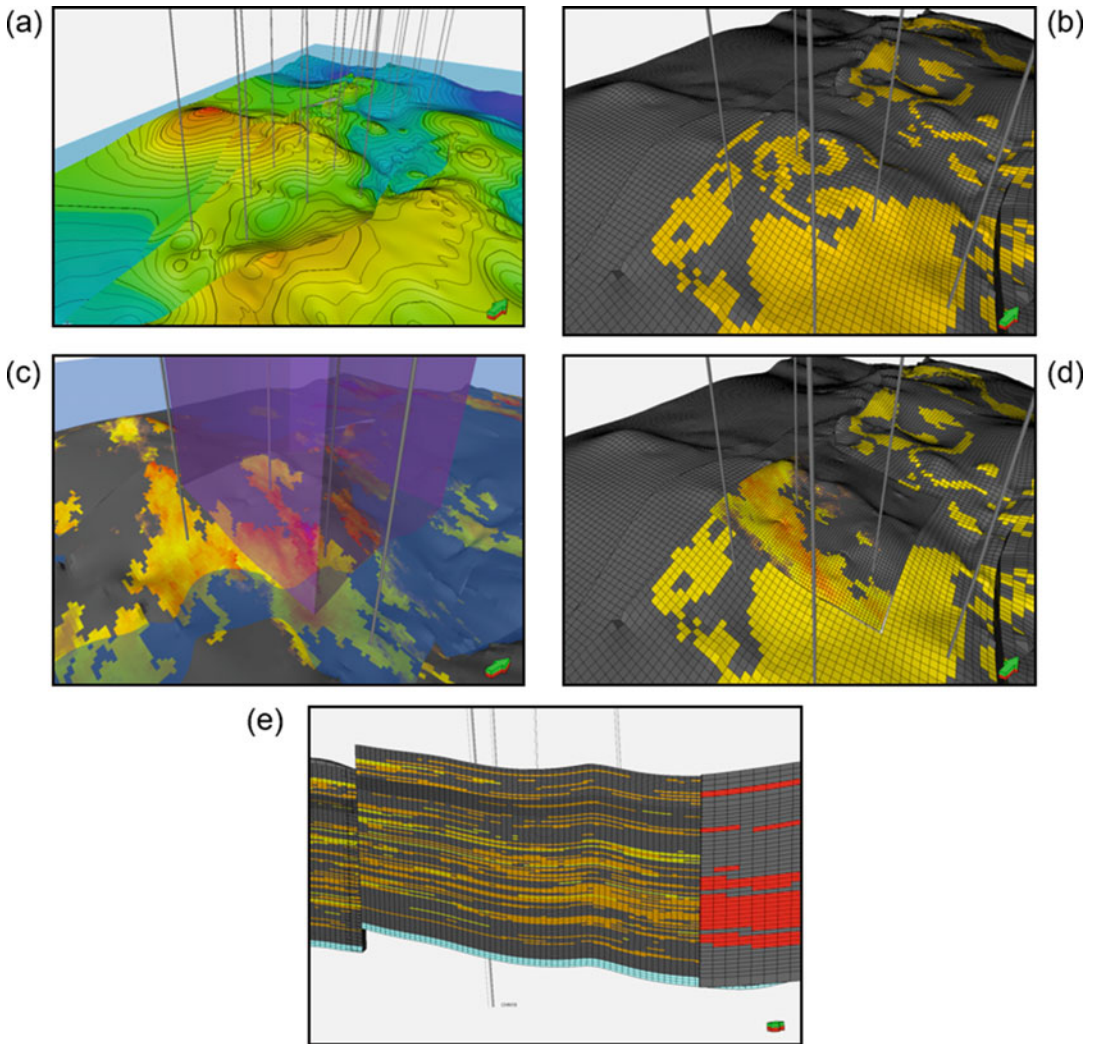


**Fig. 8.3** Resource and decision models, an application: (a) top structure map for the mature field; (b) full-field simple material balance model to work out gross water-flood and pressure gradients; (c) resource model with appropriate static reservoir heterogeneity, used for in-place volumes; (d) the decision model, in this case a

sector model on the scale of the proposed infill 5-spot pattern; embedded in the material balance model; (e) checking the join between different model resolutions in (d), ornament is model elements, grey – non-reservoir. (Oxlade and Bentley 2015)

- *Cantilever* – the larger modelling exercise
- *Last node* – the decision

Work in the early cantilevers is short – measured in days or weeks. The early modelling choices are not known at the outset – the problem has to be defined, deconstructed and worked - and hence the study plan (the ‘framing’) is *not*

constructed at the kick-off, as too little is known at this point. Framing is better done at later nodes once some understanding has been achieved. The outcome may be that detailed full-field models are not required to support the decision at hand; potentially, ‘big modelling’ is not required at all.

The approach is useful in mature fields with large volumes of data where the pursuit of the

**Fig. 8.4** Working sequentially (the default) vs. working in parallel, showing the potential time dividend available from abandoning the default workflow

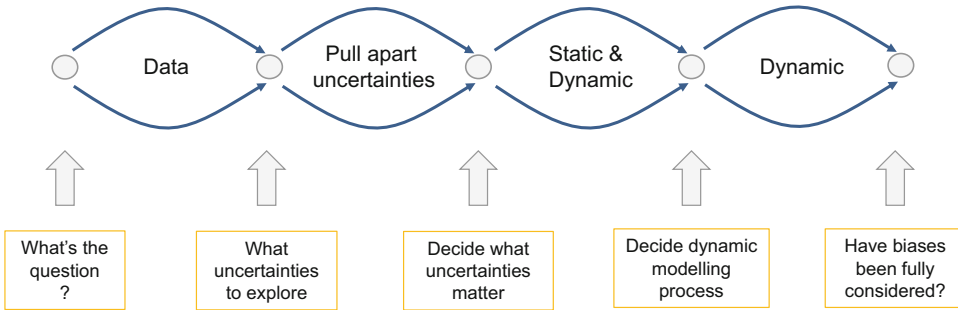
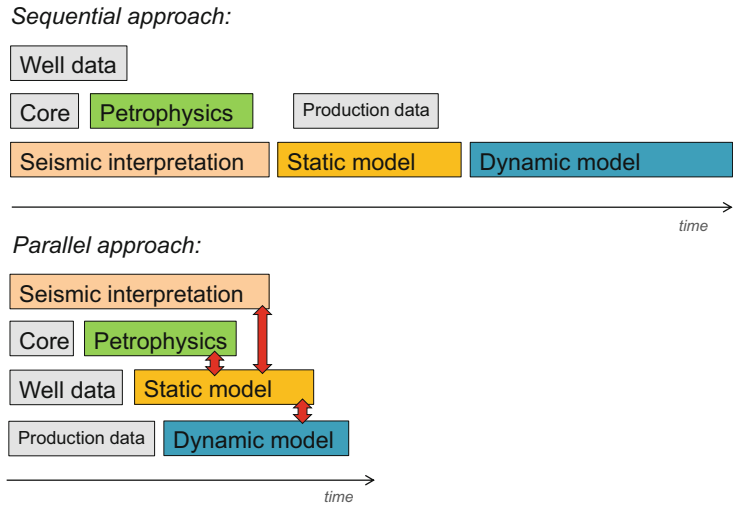


**Fig. 8.5** Integrated, iterative project working

history match can distract us from thinking about the uncertainties associated with the decisions that we need to make: infill well locations, value of workovers, water injection patterns, options for EOR etc. Worse still, the process of history matching can lead us to believe we understand our reservoirs more deeply than we really do, and blind us to the uncertainties and associated decision risks (the ‘affect’ heuristic of Slovic et al. 2007).

This generic ‘node and cantilever’ workflow represents an integrated approach to modelling

workflows and decision making and has the following characteristics:

- (a) All disciplines are involved throughout the project.
- (b) Key points of integration bring teams together, akin to gates in a typical project management process.
- (c) Risk and uncertainty are considered near the start of the project and refined through time, rather than being considered at the end.



- (d) The cantilevers represent fast learning loops for teams to develop understanding.
- (e) Points of integration need to be planned and require project management.
- (f) The nodes are effectively ‘gates’, not just progress meetings; teams shouldn’t launch on to the next cantilever without agreeing the next steps.
- (g) The number of cantilevers is not prescribed and can be changed along the path; the real Forth Bridge has three cantilevers, the project bridge may have many.

This workflow has much in common with ‘agile’ work processes, which have their foundation in software development in the 1990s, and is consistent in style with the ‘Scrum’ management techniques described by Sutherland and Schwaber (Sutherland 2014). Although there are subtle differences in definition and use, the general ideas are comparable: the aim is to break down a big complex problem into shorter, simpler work components which can be managed iteratively to generate results more quickly and efficiently.

In the world of reservoir model design, this means a more nimble design in which understanding and learning in the early phases of a modelling project are used to adjust the model design to efficiently arrive at a decision point. Models therefore become focussed on the few uncertainties that would change a decision, rather than defaulting to large, complex model(s) that try to represent every uncertainty, large or small, to be used for every purpose.

This raises two workflow-related questions that need to be confronted:

- What is our approach to model updates and full-field history matching?
- What if our chosen modelling workflow gives an unclear forecast?

---

## 8.4 Handling Dynamic Data

At the start of the field life, models are matched to well test data from the exploration and appraisal campaign, a relatively simple process that helps optimise an initial field development plan.

As field life progresses, dynamic data accumulates and models inevitably require adjustments in order to match the field history. These adjustments can become significant for oilfields developed by waterflooding, particularly if the fields are fractured, where production ‘surprises’ (unexpected water breakthrough in wells) are common. The surprises occur because of inevitable imperfections in the subsurface description, recall: model  $\neq$  truth (Sect. 3.3.1). ‘Geological surprises’ also tend to dominate the evolution of CO<sub>2</sub> storage projects, which typically have very limited well data, such that 4D seismic or pressure monitoring data bring new insights as the projects progress (Ringrose 2020). The question is what to do about this. There are two generic approaches, which we summarise below.

### 8.4.1 History-Matching

The common response to new data is to either update the static model and rematch the simulation model to the updated history, or to simply adjust the simulation model in the geographic vicinity of the new data to achieve a match – the process of adding ‘patches’. The simulation models are then used in a forecasting mode to predict the future.

The matching process can be very time-consuming. Although this can be alleviated using automated history-matching algorithms or machine learning (e.g. Buckle et al. 2019), there are some issues to consider:

1. The adjustments are typically required because of some error (or unknown) in the underlying static description: without identifying and correcting the error, adjusting the parameters in the simulator is effectively following the principle that *‘two wrongs make a right’*. This erodes the quality of the resulting forecast.
2. Matching to production data is an inverse problem, and is non-unique; there are many parameters which can be adjusted in a simulator to approximate a match. A single history match is therefore not a good basis for forecasting.

3. Treating the history match as a tool for the QC of a forecast is based on the assumption that the behaviour of the field is completely encapsulated in the production history as experienced by the wells (or as seen on 4D seismic) – potentially ignoring the underlying reasons for the unpredicted behaviour. This situation becomes more likely later in field life, at which point it often becomes apparent that earlier models were highly inaccurate descriptions of the subsurface, which begs the questions: “Were they worth building? Did the early models mislead the decision-making?”

Kahneman (2011) summarises this nicely:

The illusion that we understand the past fosters overconfidence in our ability to predict the future

The solution to this challenge, especially early in life of a field development project, is to make history matches based on multiple realisations (multi-deterministic scenarios, or a statistical ensemble, as described in Sect. 5.2) and to generate a range of forecasts to overcome the lack of uniqueness in a single match. Useful guidelines for more open-minded and intelligent history matching are:

- In all but the most exceptional of circumstances, avoid local ‘patching’ around wells, making only global adjustments to parameters;
- Global adjustments must be related to an uncertainty in some underlying reservoir concept, and should be achieved by iterating the static model accordingly;
- If some concept-based models significantly mis-match the new data, review and adjust the underlying concept, and ultimately be prepared to abandon it, if necessary;
- Consider ‘trees’ – the likely unknowns (Sect. 5.1.2); unexpected dynamic data may be alerting us to a hitherto unseen aspect of the reservoir character such as the presence of open fractures, in which case the underlying reservoir concepts should be reviewed.

For mature fields the guidelines above still apply, but the volume of data tends to increase

the complexity of the matching process significantly, and a decision to completely rebuild based on a new concept will be time-consuming. This can be helped by automatic model updates and algorithm-based assisted history matching (Buckle et al. 2019; Seiler et al. 2011) but although automation makes useful time savings, some of that time will be lost in the necessary QC of the automation process. Human intervention is inevitably still required to make adjustments to the reservoir concept (as noted in Sect. 5.5.7), and for spotting ‘trees’.

#### 8.4.2 History-Comparing

An alternative approach is to learn by *comparing* with history rather than attempt to *match* it all, as there is typically important information associated with the initial mismatch.

This was achieved manually in the case of the infill well decision described in Sect. 5.5.6 (Fig. 5.32) in which a set of multi-deterministic scenarios were run and matched closely in wells located in the vicinity of the infill decision, but only approximately matched in wells further away. A simple traffic light system (green for good matches, amber for partial matches and red for poor matches) was applied to each static-dynamic model pair and used to judge their worth subjectivity. The matching exercise was therefore limited and more emphasis was placed on *comparing* realisations with history.

A statistically more rigorous version of history-comparing is described by Scheidt et al. (2014, 2018), who return to Bayesian principles to make the comparison: Bayesian Evidential Learning (BEL). The BEL approach is based on the idea that by making a suite of reservoir models and comparing these with information such as production data, a statistical model can be built which describes the relationship between the data and the model forecasts. The statistical model itself can then be used to make the forecasts (Fig. 8.6).

This is a fundamentally different approach to traditional history matching, placing the emphasis on understanding patterns in the data rather than

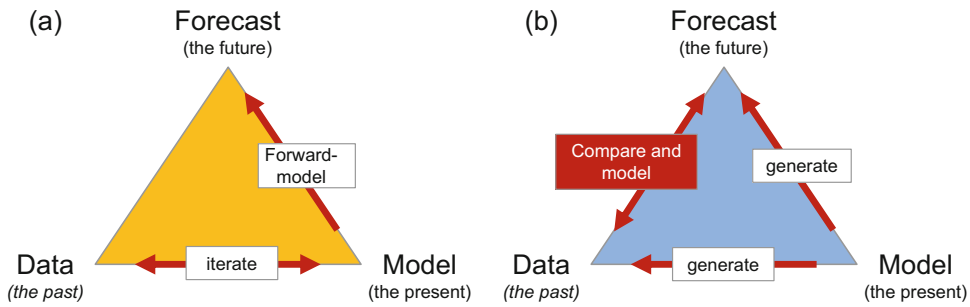


**Fig. 8.6** (a) Standard modelling workflow, forward-modelling a forecast from the data and the model; (b) the Bayesian Evidential Learning (BEL) alternative, start with

model hypotheses, generate data samples and forecasts and model their relationship. (Modified after Scheidt et al. 2018)

simply matching it by non-unique adjustment of model parameters.

## 8.5 'Truth Models'

Another alternative to the default workflow of the detailed full-field model is to focus effort on simply understanding the performance of the reservoir *at the scale of interest* pertinent to the decision at hand.

This is a return to the theme of smaller-scale modelling aiming to capture the impact of small-scale reservoir heterogeneities on larger-scale flow processes, including the use of pseudo-functions and physics-based averaging approaches (e.g. Coats et al. 1971; Weber and van Geuns 1990; Lake et al. 1990; Stephen et al. 2001; Manzocchi et al. 2002; Jackson et al. 2003). These workers put much thought into techniques for capturing small-scale heterogeneities implicitly as permeability multipliers or pseudo-relative permeability curves (e.g. Hearn 1971; Pickup et al. 2000), and the discipline of effective property modelling which emerged to calculate properties, notably permeability, appropriate for use in coarser representations of the sub-surface (e.g. Muggeridge 1991).

With increasing computing power, these efforts to capture multi-scale effects in reservoir models have been downplayed and there is often a view that the issue of heterogeneity can be taken care of by reducing grid cell size by a factor. In

Chap. 4 we argued that this is in many cases an illusion, especially for reservoirs which are characterised by small-scale heterogeneity under secondary or tertiary recovery processes. Essential heterogeneity is still being lost.

We support a quest to unearth this 'lost heterogeneity', and advocate the use of increased computing power to assess the impact of small-scale heterogeneities in much the same way as the early effective property models, but with much higher resolution and with no compromise to a 'full physics' representation in a simulator. For example, Ringrose et al. (2005) used multiple million-cell models to estimate the effects of cm-scale sedimentary bedding on large-scale reservoir models.

Bentley and Stephens (2018) define 'truth models' as:

static-dynamic models which have cellular resolution at the scale of the underlying data, but which are sized at the scale of the development question at hand.

The 'scale of the data' is typically the size of a core plug, on which most rock analysis is done in laboratories (notably permeability), but for some properties it may be the well-log resolution scale. The 'scale of the question' references the inevitability that all subsurface development questions have an associated scale of interest (see also Sect. 2.4.4):

- In cases of production by displacement, e.g. waterflooding or EOR, the interest is usually focused on the well spacing.

- In the analysis of well stimulation the interest is usually near wellbore.
- For production by depletion, the interest is at the scale of the depleting container, which may be an isolated fault block, or could be full-field.
- For CO<sub>2</sub> injection projects the questions of concern typically cover the whole storage complex – reservoir and sealing systems.

So, models generally need to be sized at the scale of the question, in order to address that question. Models for gas fields are therefore usually full-field, or at least full-compartment, to capture the depleting volume, whereas models for infill planning can generally be analysed at the inter-well or inter-pattern scale.

This definition of ‘truth modelling’ is computationally demanding, as models are being built with no upscaling from the underlying source data – potentially, they only upscale from the pore scale to the core-plug or well-log scale. Running full-fluid physics, accounting for the effects of capillary pressure, also slows run times, as does the inclusion of all rock types – the ‘total property modelling’ of Ringrose (2008)

(discussed in Chap. 3). With full heterogeneity and full physics included, the models explicitly reveal the subtle interplay of heterogeneity and fluid-force interaction which are often missed in the default full-field model, and help us understand why our model forecasts are inaccurate, and generally over-optimistic.

An example is given below, built to understand a waterflood in a highly heterogeneous single bed under waterflood. The example is outcrop-based, using a well-exposed bed in a Devonian dryland river system exposed at Swan Lake Bay in Pembrokeshire, Wales (Fig. 8.7). The bed architecture is internally highly heterogeneous and the rock properties (core data) from analogue producing fields are allocated to the element description, as shown in Fig. 8.7. All candidate elements are included, in order to illustrate their relative importance, and permeabilities range from several hundred millidarcies in the best sandstones to microdarcies in the silts.

Static/dynamic models were constructed at the same scale, with a grid cell size of 5 cm by 1 cm selected to represent the scale of data (core plugs) and sized to address development questions for a line-drive waterflood. For this purpose a 2D

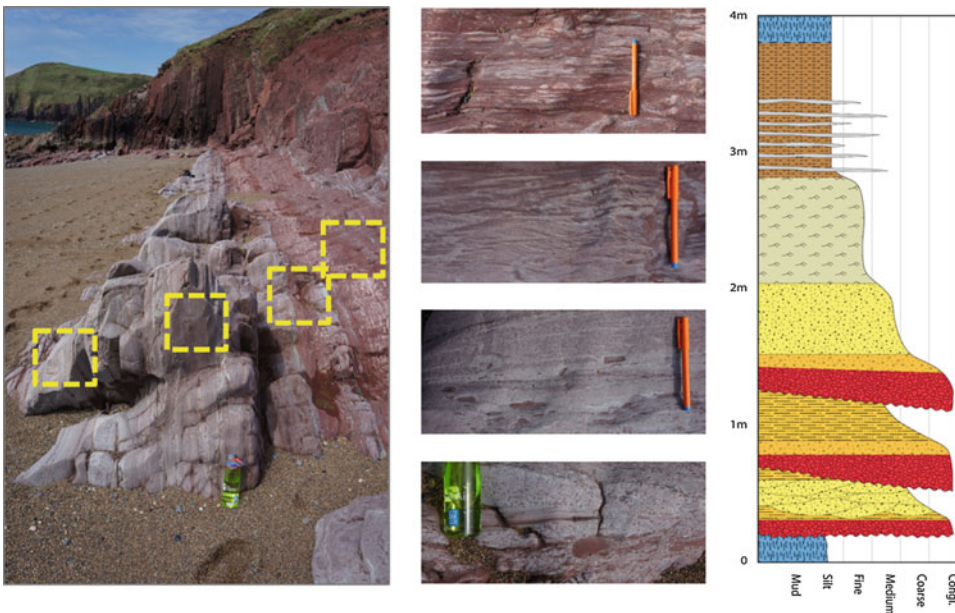


**Fig. 8.7** A single heterogeneous bed from fluvial red beds at Swan Lake Bay, Pembrokeshire, Wales

model of a producer-injector pair at typical offshore well spacing (400 m) was sufficient. The bed itself is 4 m high, resulting in a 2D model with 3.2 million grid cells (Fig. 8.8).

Dynamic models of the static representation in Fig. 8.8 are shown in Fig. 8.9. For these cases, the impact of the three forces at work in a reservoir (viscous, gravity, capillary) are explored and the images show the progress of a water floodfront through the single bed at a resolution not achievable in a full-field model.

Having set the model up, an opportunity is created for understanding the production process (in this case displacement) at a resolution not

achievable in a full-field model. One example is given in Fig. 8.10 – an analysis of remaining oil after waterflooding.

The model illustrates the location of remaining oil behind the floodfront in the lower portion of the bed and the performance of the truth model can be compared with a standard scale model grid cell (shown by the white box in Fig. 8.10). In this case the average  $S_{or}$  in the coarse model is reasonably accurate, but the truth model allows the identification of the specific elements which are poorly swept, and also their location. The truth model also resolves phase segregation in the lower units, and therefore has lower flowing

**Fig. 8.8** Swan Lake Bay 'truth model'; the concept sketch of the outcrop (top) used to build a static model using multi-point statistics. (Image courtesy of Tom Buckle and Rhona Hutton)

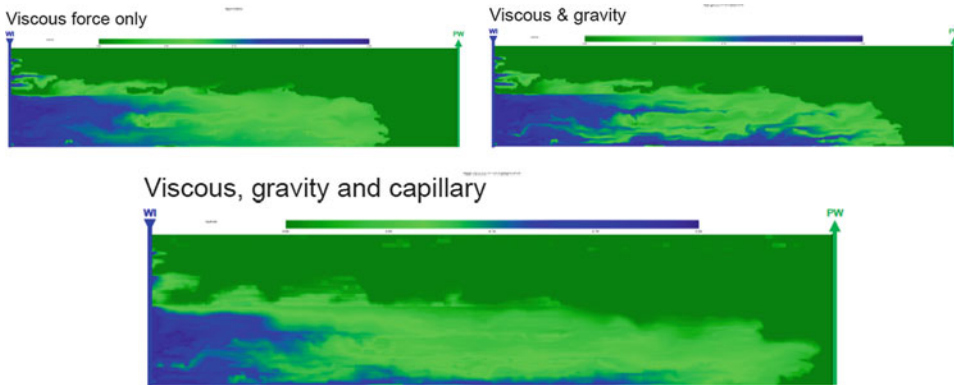
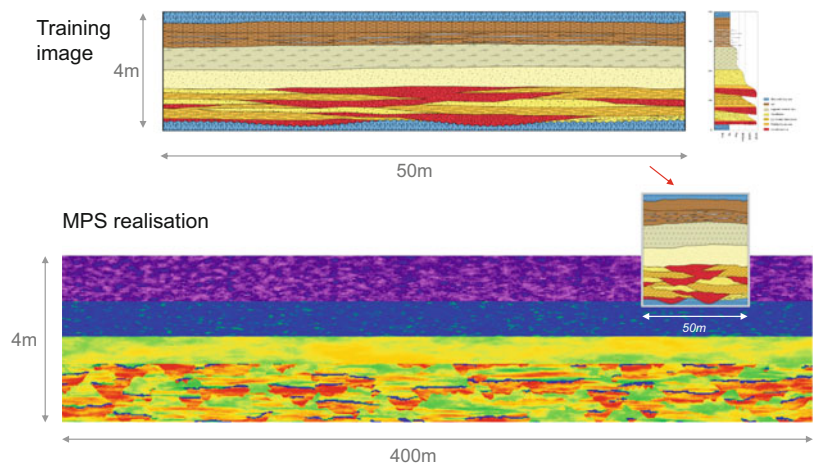


**Fig. 8.9** Swan Lake 'truth models' under waterflood, used to understand the impact of different forces; models are ornamented to show water relative permeability,

reflecting the passage of injected water through the bed. (Image courtesy of Ed Stephens)

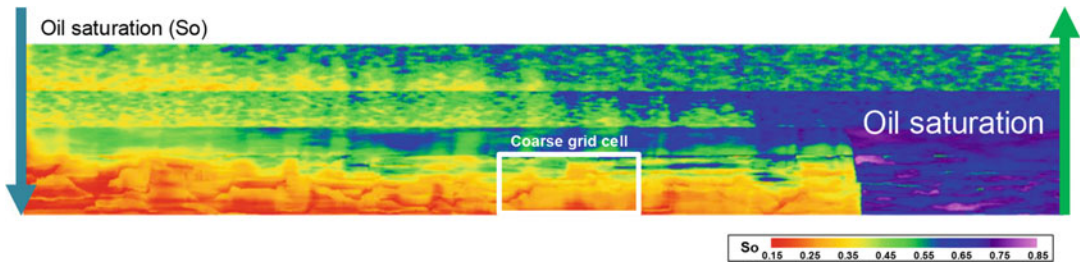


**Fig. 8.10** Swan Lake truth model ornamented for residual oil saturation; the model illustrates the location of the remaining oil behind the floodfront and in the poorer

quality sub-layers where viscous sweep is ineffective but capillary forces have an impact. (Image courtesy of Ed Stephens)

water cut in the cell as well as higher average water and oil reperms (Ed Stephens, pers. comm.). Moreover, the truth model illustrates resource potential in the upper portion of the bed, which would typically be excluded from a larger-scale model, either at the petrophysical analysis stage, or by removal of low pore volume cells in the simulator. With the poor quality elements included and full physics honoured, the effects of capillary imbibition into the upper parts of the bed from the injected water flooding the lower bed, and the incremental oil draining into the lower bed, can be quantified.

Truth models, as defined here, help explain why some coarser model representations over- or under-predict. The point is to *learn* about the true processes and interactions that might be occurring as a basis to designing the ‘decision model.’ The case shown here, compared to the coarse model equivalent, typically produced forecast differences of 10–20% in terms of water flood breakthrough times and generated different production profile shapes as simple piston-like displacement was replaced by a more complex production tail. Moreover, truth modelling simply deepens the understanding of how reservoirs are behaving – ‘modelling for understanding’ – a theme explored in the final chapter.

## References

- Bentley M, Ringrose P (2017) Future directions in reservoir modelling: new tools and ‘fit-for-purpose’ workflows. Geological Society, London, Petroleum Geology Conference series 8:537–546
- Bentley M, Stephens E (2018) Complex construction vs. Simple deconstruction: Alternative workflows and the role of ‘Ultimate Truth’ Models. Conference Proceedings, 80th EAGE Conference and Exhibition, p. 1–5
- Buckle T, Hutton R, Demyanov V, Arnold D, Antropov A, Kharyba E, Pilipenko M, Stulov L (2019) Improving local history match using machine learning generated regions from production response and geological parameter correlations. Fourth EAGE Conference on Petroleum Geostatistics, Florence
- Cannon S (2018) Reservoir modelling – a practical guide. Wiley, Chichester, p 312
- Coats KH, Dempsey JR, Henderson JH (1971) The use of vertical equilibrium in two-dimensional simulation of three-dimensional reservoir performance. Soc Petrol Eng J 11(01):63–71
- Hearn CL (1971) Simulation of stratified waterflooding by Pseudo relative permeability curves. J Pet Technol 23 (7)
- Jackson MD, Muggerridge AH, Yoshida S, Johnson HD (2003) Upscaling permeability measurements within complex heterolithic tidal sandstones. Math Geol 35 (5):499–519
- Kahneman D (2011) Thinking, fast and slow. Macmillan, New York
- Lake LW, Kasap E, Shook M (1990) Pseudofunctions — the key to practical use of reservoir description. In: Buller AT, Berg E, Hjelmeland O, Kleppe J, Torsæter O, Aasen JO (eds) North Sea oil and gas reservoirs—II. Springer, Dordrecht
- Manzocchi T, Heath AE, Walsh JJ, Childs C (2002) The representation of two-phase fault-rock properties in flow simulation models. Pet Geosci 8(2):119–132
- Muggerridge A (1991) Generation of effective relative permeabilities from detailed simulation of flow in heterogeneous permeable media. In: Lake LW, Carroll HB, Wesson TC (eds) Reservoir characterisation II. Academic Press Inc, San Diego, pp 197–223
- Oxlade R, Bentley MR (2015) It ain’t what you do it’s the way that you do it – decision-led modelling workflows

- for mature fields. Geol Soc conf: Reservoir Modelling Technical limits, Aberdeen, Scotland, UK
- Pickup GE, Ringrose PS, Sharif A (2000) Steady-state upscaling: from lamina-scale to full-field model. *SPE J* 5(2):208–217. SPE-62811-PA. <https://doi.org/10.2118/62811-PA>
- Ringrose PS (2008) Total-property modeling: Dispelling the Net-to-Gross Myth (see associated supplementary discussion and response). *SPE Reserv Eval Eng* 11(5): 866–873
- Ringrose P (2020) How to store CO<sub>2</sub> underground: insights from early-mover CCS projects. Springer, Cham
- Ringrose P, Nordahl K, Wen R (2005) Vertical permeability estimation in heterolithic tidal deltaic sandstones. *Pet Geosci* 11(1):29–36
- Scheidt C, Renard P, Caers J (2014) Prediction-focused subsurface modelling: Investigating the need for accuracy in flow-based inverse modelling. *Math. Geosci* 1–19
- Scheidt C, Li L, Caers J (Eds.) (2018) Quantifying uncertainty in subsurface systems (Vol. 236). John Wiley & Sons
- Seiler A, Evensen G, Skjervheim JA, Hove J, Vabø JG (2011) Using the ensemble Kalman filter for history matching and uncertainty quantification of complex reservoir models. *Large-Scale Inverse Problems and Quantification of Uncertainty*. Wiley Ser. Comput. Stat, pp. 247–271
- Slovic P, Finucane ML, Peters E, MacGregor DG (2007) The affect heuristic. *Eur J Oper Res* 177:1333–1352
- Stephen KD, Clark JD, Gardiner AR (2001) Outcrop-based stochastic modelling of turbidite amalgamation and its effects on hydrocarbon recovery. *Pet Geosci* 7:163–172
- Sutherland J (2014) *Scrum: the art of doing twice the work in half the time*, vol 248. Crown Publishing, London
- Weber KJ, van Geuns LC (1990) Framework for constructing clastic reservoir simulation models. *J Pet Technol* 34:1248–1297

## Epilogue – Modelling for the Energy Transition

# 9

### Abstract

We will never cease to be interested in how fluids flow in the subsurface.

The same reservoir and simulation technologies which have been developed and honed in the pursuit of oil and gas resources will continue to be required in the future, for a declining production of hydrocarbons, continuing interest in geothermal energy, increasing disposal of CO<sub>2</sub> and storage of energy itself. This is in addition to the long-standing needs to manage water, understand earthquakes and predict hydrothermal systems and even volcanic

plumbing. All of these require a technical understanding of fluid flow in the subsurface and draw on the skills discussed in this text, and more. Hence we have emphasised in this second edition the use of modelling technologies for carbon storage, an issue of immediate urgency to meet the challenge of managing climate change. Perilous as it is to predict the future, and at the risk of dating this book as soon as it is written, it is worth closing with comments on possible ways ahead. In this last chapter we summarise our current position, draw together some of the developments which may become standard tools in the future and close with a thought on the purpose of modelling itself: understanding.



Multiscale geological bodies and associated erosion, Lower Antelope Canyon, Arizona. (Photo by Jonas Bruneau, © EAGE reproduced with permission of the European Association of Geoscientists & Engineers)



## Keywords

Data · Analogues · Workflows · Surface-based modelling · Process-based modelling · Rapid reservoir modelling · Modelling for understanding · Energy transition

## 9.1 Synopsis – The Story So Far

This book set out to offer practical advice and guidelines on the design and construction of subsurface reservoir models. The overall objective has been to promote the skills and procedures for the design of fit-for-purpose models that allow the reservoir modeller to make useful estimates of resources and forecasts of fluid behaviour, both within reasonable bounds of uncertainty.

We organised the discussion under eight thematic headings:

1. Model Purpose
2. The Rock Model
3. The Property Model
4. Upscaling Flow Properties
5. Handling Uncertainty
6. Generic reservoir types
7. Models for storage
8. Workflows

In order to achieve good model design within each of these themes, we need to access a selection of data manipulation and mathematical modelling tools, including those for seismic analysis, petrophysical analysis, geological modelling, statistical estimation, fluid flow simulation and analysis of outcomes. This is a rather long list of tools and functions, typically handled by several different computer software packages often linked by spreadsheets. The quest for a fully integrated subsurface data package will no doubt continue, and we welcome those efforts, but is likely to be compromised by the development of new niche tools, and we live with this. The primacy of the geological concept in deciding what information to capture in a reservoir model does, however, give us a framework for addressing the subsurface data integration challenge. The first

step in reservoir modelling is always to *think* rather than *click*.

We have tried to hold two important themes in balance:

1. *The rock*: the conceptual geological model. The first concept, “it’s a river-dominated delta system”, could be wrong but that is better than having no concept formulated at all. Better still, we should have several reservoir concepts that can be tested and refined during the modelling process, e.g. “we think it’s a fluviually dominated system, but there are indications of tidal influence so we need to test tidal versus fluvial deltaic models.”
2. *The fluid*: the physics of the system. Fluid flows have their own natural averaging processes. Not all geological detail matters, and the geological heterogeneities that do matter depend on the fluid flow system. Low viscosity fluids are more indifferent to rock heterogeneity than high viscosity fluids and all multiphase fluid systems are controlled by the balance of capillary, viscous and gravity forces on the fluid displacement processes.

Because rock-fluid interactions are multi-scale – from the microscopic pore-scale ( $\mu\text{m}$ ) to the macroscopic rock architecture scale (km) – we need a framework for handling data as a function of scale. The concept of the Representative Elementary Volume (REV) has been identified as absolutely fundamental to understanding and using reservoir property data. If your measurements are not representative and your flow properties are estimated at the wrong length scale the modelling effort is undermined and the outcomes generally poor. The multi-scale REV concept gives us a framework for determining which measurements and averages are useful and which model scales and grid sizes allow us to make reasonable forecasts given that data. This is not a trivial task, but it does give us a basis for deciding how confident we are in our analysis of flow properties.

Subsurface data analysis leads us quickly into the domain of ‘lies and statistics.’ Geostatistical tools are immensely useful, but also very prone to misuse. A central challenge in reservoir

modelling is that the data we have is usually imperfect and statistically insufficient. When making estimates based on incomplete data we cannot rely on statistics alone – we must employ intuition and hypothesis. To put this simply in the context of reservoir data, if we wish to know the porosity and permeability of a given reservoir unit that answer is seldom found in a simple average. The average can be wrong for several reasons:

- Some data points could be missing – incomplete sampling.
- The model elements could be wrongly identified – the porosity data from two distinct rock types do not necessarily give us the average of reservoir element 1 or 2.
- We may be using the wrong averaging method – effective permeability is especially sensitive to the choice of averaging (the usefulness of the arithmetic, harmonic and geometric averages are controlled by the rock architecture).
- We may be estimating the average at an inappropriate scale – estimates close to the scale of the REV are always more robust.
- The average may be the wrong choice – many reservoir issues are about the inherent variability, not the average.

Because of these issues, we need to know which average to use and when. Averaging is essentially a form of upscaling; we want to know which large-scale value represents the effects of small-scale variations evident within the reservoir. It is useful to recall the definition of the upscaled block permeability,  $k_b$  (Sect. 3.2):

$k_b$  is the permeability of a homogeneous block, which under the same pressure boundary conditions will give the same average flows as the heterogeneous region the block is representing.

If the upscaled permeability is closely approximated by the arithmetic average of the measured (core plug) permeability values, then that average is useful. If not, then other techniques need to be applied, such a numerical estimation methods or a power average.

Assuming, then, that we have the first four elements of reservoir design in place – a defined

model purpose, a rock model based on explicit geological concepts, a property model estimated at an REV, and then upscaled appropriately – we have the issue of uncertainty, as no amount of careful reservoir model design will deliver the ‘right’ answer. The model purpose might be redefined, the geological concept could be false, the property model may be controlled by an undetected flow unit, and upscaling may yield multiple outcomes.

In order to handle reservoir uncertainty we have advocated the use of scenario-based thinking, whether this is expressed in multi-deterministic concepts or a statistical ensemble. It may at first appear dissatisfying to argue that there may be several possible outcomes after a concerted period of reservoir data analysis, modelling and simulation. The asset manager of financial investor usually wants only one answer, and becomes highly irritated by the ‘two-handed’ geologist (“*on the one hand the answer may be this, but on the other hand. . .*”). Some education about reservoir forecasting is needed at all levels. It is never useful to say that the sky tomorrow will be a shade of grey on average. It is however, accurate to say that the skies tomorrow may be blue, white or grey – depending on the weather patterns and the time of day – and it is useful to present more explicit scenarios with probabilities, such as that there is a 60% of blue sky tomorrow and a 10% chance of cloud (assuming this is based on a sound analysis of weather patterns).

In the same way, scenarios describing alternative plausible reservoir realities do provide useful forecasts. For example, who wouldn’t invest in a reservoir development or energy storage plan where nine out of ten fully integrated and upscaled model scenarios gave a positive outcome, but where one negative scenario helped identify potential downsides that would need to be mitigated in the proposed plan?

The road to happiness is therefore *good reservoir model design*, conceptually-based and appropriately scaled. The outcome, or forecast, should encompass multiple scenarios, using geostatistical tools guided by deterministic concepts. Reservoir and simulation models integrate knowledge, allow us to forecast futures,

quantify value and hence help make significant commercial and environmental decisions.

This is where we are now. Based on current needs and trends, what are the foreseeable developments that may lie just around the corner? We capture these under four themes:

- Use of analogues and data
- Restoring lost heterogeneity
- New algorithms
- Modelling for understanding

---

## 9.2 Use of Analogues and Data

Reservoir systems are complex, so the ambition of reservoir modellers to understand the effects of ancient subsurface rock strata on fluid flow processes several km beneath the surface is a bold venture. We may recall the underlying principles of geology to guide us in that process. One of the founders of geology, Sir Archibald Geikie (1905), established the principle:

The present is the key to the past

This concept is now so embedded in geology that we can easily forget it. We use our understanding of modern depositional processes to interpret ancient systems. Modern aeolian processes in the Sahara desert (Fig. 9.1) can tell us a lot about how to correctly describe a North Sea reservoir built from Permian aeolian sands. The many efforts to understand outcrop analogues for subsurface reservoir systems (Fielding and Crane 1987; Miall 1988; Brandsæter et al. 2005; Howell et al. 2008; Cabello et al. 2011; Keogh et al. 2014; Puig et al. 2019) are devoted to this goal and will continue to bring important new insights into the reservoir description of specific types of reservoir.

A wide range of imaging techniques are now being used in outcrop studies (Pringle et al. 2006; Rittersbacher et al. 2014; Nyberg et al. 2015; Cawood et al. 2017) in order to obtain more quantitative and multi-scale information from outcrop analogues of reservoir systems. These include digital aerial photogrammetry, digital terrain models, ground penetrating radar, satellite

imaging, differential GPS location data, ground-based laser scanning (LIDAR), all hugely expanded in use since the arrival of drones. While these new high-resolution outcrop datasets provide valuable information at faster rates of acquisition, they still require sound geological interpretation to make sense of the data and to apply them to reservoir studies.

Despite the growing body of knowledge, reservoirs will always present us with surprises and for this reason, and because of the inherent challenge of the estimation of inter-well reservoir properties, reservoir forecasting will always carry large uncertainties. In the process of making forecasts about the subsurface we therefore employ a variation of Geikie's dictum, because we use our knowledge of the geological record to make these forecasts, such that:

The past is the key to the future

This principle has grown in use in the last decades, and formally elaborated as a branch of geological research by Doe (1983). Geological forecasting has received most attention in the study of climate change (Sellwood and Valdes 2006), but also in the fields of earthquake hazard forecasting and in subsurface fluid flow modelling.

In reservoir modelling studies we use *the past is the key to the future* principle in several ways:

1. We use our knowledge of the rock system to make credible 3D models of petrophysical properties giving us some confidence in our flow predictions. This principle is axiomatic to the proposed basis for reservoir model design – that there must be some level of belief in the reservoir concepts embodied in the model for there to be any value in the forecasts made using that model.
2. We use our experience from other similar reservoirs to gain confidence about new reservoirs. This includes the 'petroleum play' concept and the use of subsurface reservoir analogues; we have much more confidence in reservoir forecasting in a mature petroleum basin than we do in a frontier province. This is now extending to the field of CO<sub>2</sub> disposal,

**Fig. 9.1** Modern dune systems in the Sahara, central Algeria. (Photo B. Paasch, reproduced with permission)



where we build on experiences of early schemes such as those at Sleipner and Snøhvit (Chap. 7) to plan CCS schemes globally (Ringrose 2020).

3. We use our growing body of knowledge on rock-fluid interactions to make better forecasts of fluid flow. One important example of this is the role of wetting behaviour in multiphase flow. There was a time (1950–1980s) when most petroleum engineers assumed water-wet behaviour for oil mobility functions, i.e. the oil had negligible chemical interaction with the rock. The growing appreciation that most rock systems are mixed wet (that is, they contain both water-wet and oil-wet pores controlled by the surface chemistry of silicate, carbonate and clay minerals) led to improved two- and three-phase relative permeability functions and to the use of different chemicals and altered water salinity to improve oil mobility. The tools available for understanding rock-fluid interactions are constantly improving. New technology is being applied at the macroscopic scale, such as the use of advanced inversion of seismic data and electromagnetic data (Constable and Srnka 2007) and at the nanoscopic to microscopic scale, such as the use of scanning electron microscopes (SEM) to study pore-surface mineralogy (Fig. 9.2).

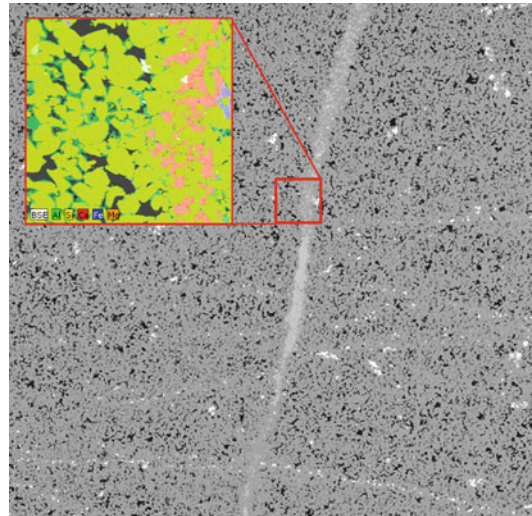


**Fig. 9.2** SEM petrography and spectroscopic analysis used to identify pore mineralogy and their controls on porosity and permeability. A fracture filled with carbonate cements (*pink*) and a sandstone pore space with grain coatings of chlorite (*green*) can be identified using the Energy-Dispersive X-ray Spectroscopy (EDS) image, shown on the *inset* which is 500 $\mu$ m across. (Photo T. Boassen/Equinor © Equinor ASA, reproduced with permission)

4. We match dynamic model forecasts to historical production data. The amount of effort we invest in this process and the value we gain can be questioned, as discussed in Sect. 8.4 and reflected upon in Sect. 9.5 below.

### 9.3 Restoring Lost Heterogeneity

We suggest the near future will see renewed interest in the importance of modelling fine scale detail in the more heterogeneous components of reservoirs. Much effort was expended in researching this field in the early years of modelling and simulation, and was essential to make the relatively simple models of that period predict reasonably. With increasing computing power and software sophistication this has become less common with practitioners, even though the literature contains significant knowledge of the issues and researchers continue to improve understanding of fluid flow in the more challenging reservoir types. The reason behind this seems to be a perception among practitioners that current model size and complexity should be enough to capture all the necessary detail in a single big model. As pointed out in Chap. 8 this is often not the case, and multi-scale questions may become increasingly important because:

- Most oil and gas fields are mature and remaining production is coming from the poorer quality, more heterolithic zones;
- More mature fields are being produced by EOR techniques, which are more sensitive to reservoir heterogeneities than primary production techniques;
- Many of the new fields coming on stream are in more heterogeneous, tight or unconventional reservoirs;
- CO<sub>2</sub> storage is gaining importance, and storage capacity is strongly influenced by reservoir heterogeneity and capillary interactions, in fact it may rely on them.

This is manifestly the case in highly heterolithic reservoirs, but even in simpler reservoirs a 10% heterolithic content is likely to have more than a 10% impact on a production forecast. We need to recover this ‘lost heterogeneity’.

The extent of this can be assessed by examining analogue outcrops with an appropriate focus – here we may return to the well-studied outcrop near Annot Town referenced in Sect. 6.5.4.

A current, high-resolution simulation model would represent the Annot outcrop (Fig. 9.3a) with a cell architecture similar to that in Fig. 9.3b. This would be a ‘big model’ on a field scale, and although cell resolution in the thick sand units is perhaps too high for most purposes, the resolution is insufficient to capture necessary detail in the heterolithic interval. This can be tackled by varying the cell size (Fig. 9.3c) but even if the significant cell size variation is managed in a simulator this still fails to capture the detail in the heterolithic interval which would significantly baffle fluid flow in the whole system. A better solution is to adopt the multi-scale techniques described in Chap. 4 and the workflows of Chap. 8 and pursue a design such as that in Fig. 9.3d.

The knowledge and techniques required to capture lost heterogeneity are available, but require more widespread adoption by practitioners; many current and future model purposes will require them.

---

### 9.4 New Workflows

In addition to the better use of analogues and fuller application of techniques for capturing heterogeneity, new modelling techniques are emerging which may find general application and support both these initiatives.

A general theme is a move away from grid-centric modelling (Bentley & Ringrose 2017) (Fig. 9.4). Conventional reservoir simulators use a finite-difference gridding scheme where only small deviations from an orthogonal grid can be accepted. The modelling approach is governed by the demands of the flow simulator such as computational limits on the number of grid cells, and convergence of the numerical flow solutions. This generally results in distortion and oversimplification of the reservoir architecture that the flow model is attempting to represent. Handling of structural features such as fracture systems is particularly challenging (Sect. 6.7). Moreover, the construction and update of a fixed corner-point grid is typically time-consuming and

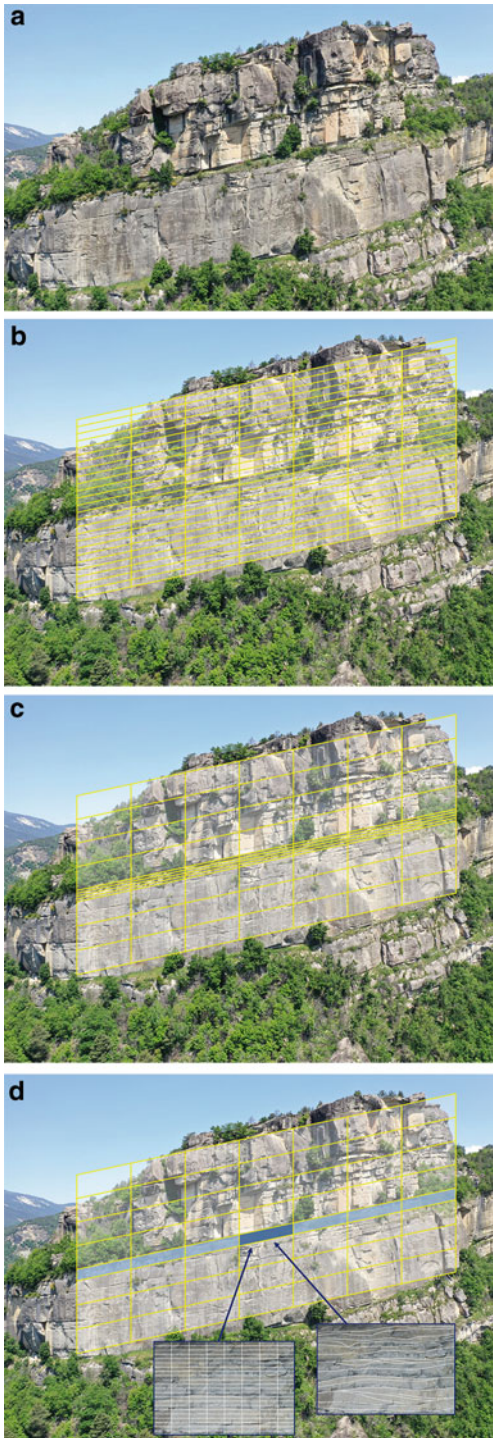


**Fig. 9.3** Capturing scales of heterogeneity at the analogue outcrop near Annot Town shown in Figs. 6.29–31: (a) the exposed outcrop at the Scafferels, approximately 100 m high; (b) a simulation grid overlay with typical grid

tends to be the ‘efficiency bottleneck’ in most modelling projects (Fig. 9.4a).

Current research seeks more efficient alternatives and one vision incorporates surface-based modelling, with gridding only called upon for the forecasting moment (Fig. 9.4b). This opens a path for new tools which offer the opportunity for more nimble model workflows, described below.

### 9.4.1 Surface-Based Models

Commonly, methods for geological reservoir modelling are either object-based, beloved of sedimentologists, pixel-based, such as indicator simulation, focused on geostatistical estimation (exploiting two-point spatial statistics) and more recently texture-based approaches using multi-point geostatistics, the latter requiring the use of training images (Sect. 2.7 and see Mariethoz and Caers 2014 for further discussion). All these techniques require the allocation of rock properties to a pre-defined 3D grid which remains fixed for the duration of the modelling project (Fig. 9.4a).

A different approach is to consider depositional process in an attempt to re-create geological history and build a rock architecture using the sequential build-up of 2D surfaces and 2D structural frameworks. Some tools are available now such as SBED for small-scale clastic depositional architectures (Wen et al. 1998; Nordahl et al. 2005, Fig. 9.5) and 3DMove for creating or recreating structural architectures (Zanchi et al. 2009).

The chief merit of these process-based methods is geological realism, but the level of detail required makes significant demands on

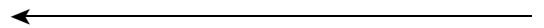


**Fig. 9.3** (continued) cell sizes – the grid is unnecessarily fine for the thick layers and too coarse for the heterolithic interval; (c) an improved cell size distribution, although still insufficient to capture the cm-scale detail in the heterolithic; (d) a multi-scale model alternative with on-scale small-scale effective property models for the heterolithic interval, either grid- or surface-based (drone images courtesy of John Howell, University of Aberdeen)

**Fig. 9.4** Alternative workflows: (a) grid-centric; (b) workflows based around a disposable grid

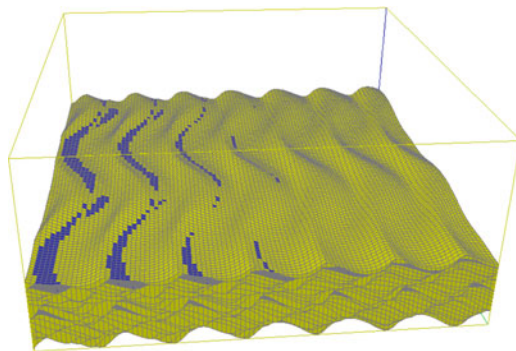
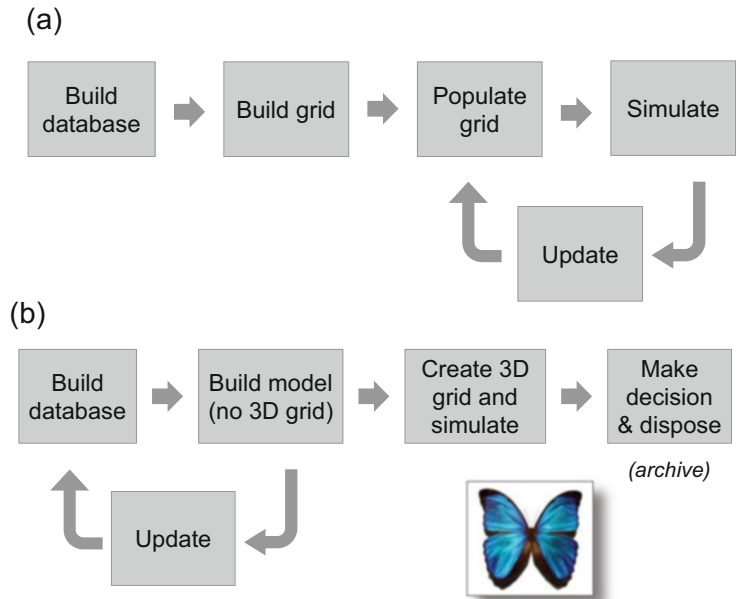


**Fig. 9.5** Surface-based representation of reservoir architecture using SBED: tidal bedding model (left) converted to a permeability cube (right). (Modified from Ringrose et al. 2005 © Geological Society of London [2005])

flexible, hierarchical, gridding algorithms. An integrated numerical description of the subsurface is captured by the GeoChron model (Mallet 2014) and represents an important step towards building these algorithms.

A step towards making this process nimble is captured by the Rapid Reservoir Modelling initiative, with sketch-based techniques drawn from advances in 3D digital graphics (Jackson et al. 2015; Zhang et al. 2020). If you can sketch it, you can indeed model it. An example of this application is shown in Fig. 9.6, in which a stacked

channel architecture is sketched directly into a drawing package and automatically rendered into 3D using a hierarchy of 2D surfaces. The flow performance of the sketch is then quantified by applying an orthogonal grid on the surface-based architecture.

### 9.4.2 Disposable Grids

The example in Fig. 9.6 is an illustration of the schematic in Fig. 9.4b in which the 3D grid appears only for the purpose of a final calculation and may then be effectively disposed of (or ‘archived’); the ‘evergreen’ or living part of the workflow is the surface-based representation which underlies it.

The concept of the ‘disposable grid’ can be taken one step further by the application of a flexible mesh (Fig. 9.7). This is a complete move away from the relatively regular grids required by finite-difference simulators to finite-volume flow simulation methods which allow more grid flexibility. These have been developed and applied to multi-scale reservoir systems including complex structural architectures, e.g. Jenny et al. 2006; Geiger et al. 2004; Coumou

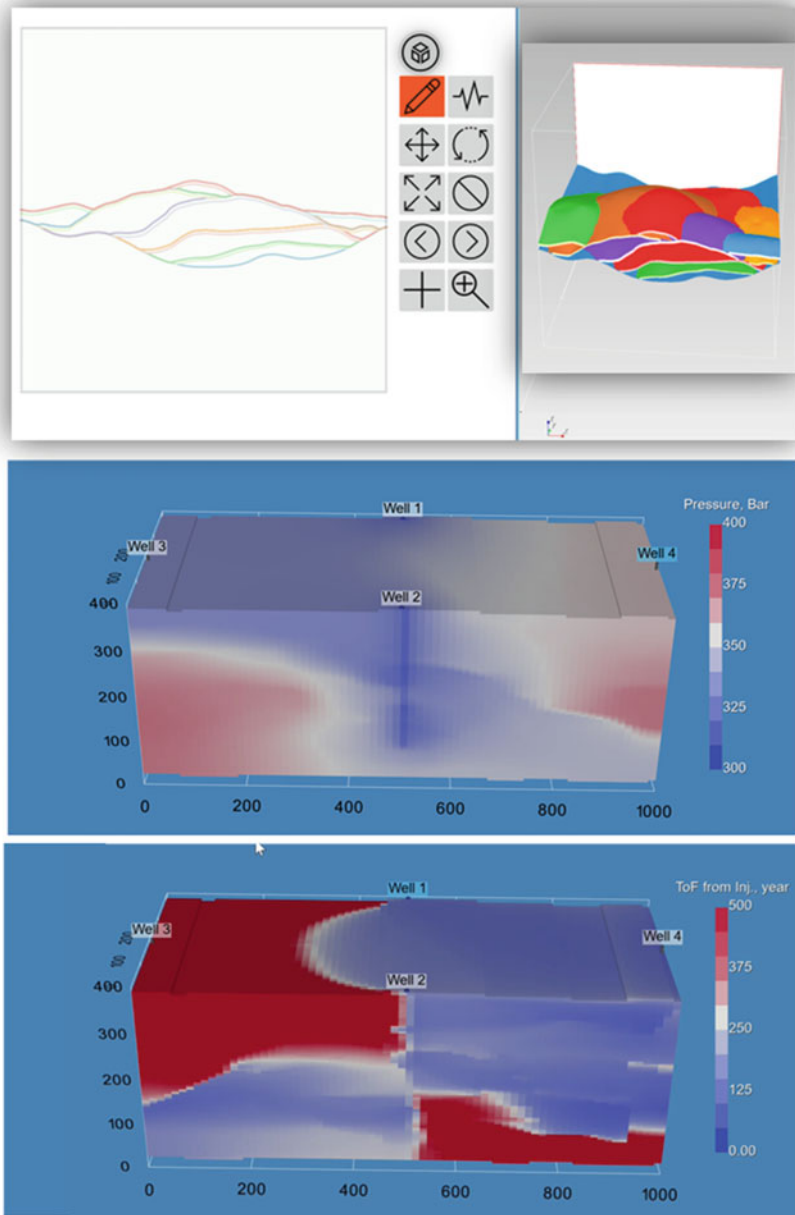


**Fig. 9.6** Surface-based representation of reservoir architecture using a sketch-based interface, and calculation of flow properties for a given well pattern and production mechanism: ‘Rapid Reservoir Modelling’. (Image

courtesy the Rapid Reservoir Modelling consortium, [www.rapidreservoir.org](http://www.rapidreservoir.org), Heriot-Watt University, Imperial College London, University of Calgary)

et al. 2008; Jacquemyn et al. 2019). The methodology allows detailed geological features such as fracture zones to be explicitly included in the flow simulation (Matthäi et al. 2007). This can be taken one step further by making the mesh

adaptive (Jackson et al. 2013, 2014), in which case the grid moves with every time-step to focus computational effort in the parts of the volume where greatest changes are occurring, such as around a floodfront (Fig. 9.7b). By these



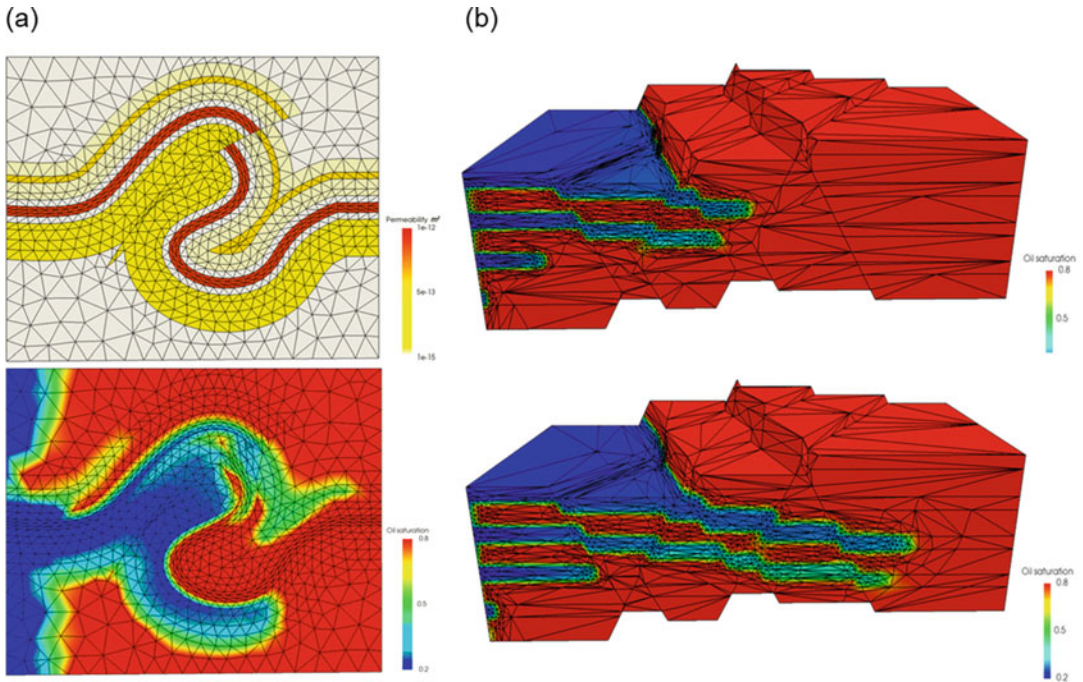


**Fig. 9.7** Meshes: (a) unstructured grids which allow highly irregular geometries to be modelled and simulated; (b) an adaptive mesh, in which the mesh moves with each time-step to focus computational effort in portions of the volume where change is occurring, such as a flood front –

a truly ‘disposable’ grid. The approaches require an underlying subsurface description of the reservoir, which may be 2D surface- or 3D grid-based. (Images courtesy of the Novel Reservoir Modelling and Simulation (NORMS) group, Imperial College London)

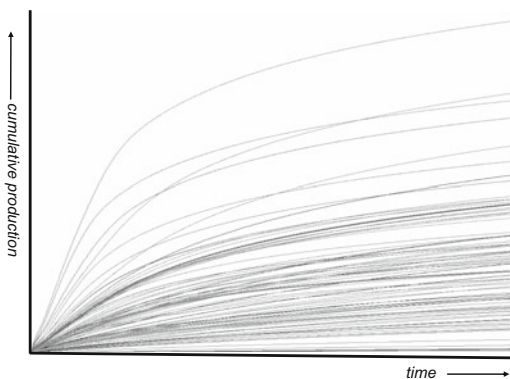


**Fig. 9.8** Multiple production forecasts for a static/dynamic model ensemble supporting a mature field infill decision; when the work illustrates that the outcome is simply not known

means the step away from 3D grid-centric modelling is finally made.

The meshes can be combined with the surface-based techniques described above, as the mesh

requires some underlying description of the subsurface. In this approach the ‘fixed’ aspect is the underlying surface-based representation and the conceptual understanding of the reservoir, both of which evolve steadily through a field life cycle – the ‘resource model’ of Chap. 8. The grid itself becomes a variable, to be built and discarded quickly once a decision has passed – the ‘decision models’.

## 9.5 Stepping Beyond the Solution – ‘Modelling for Understanding’

Sometimes modelling does not yield a simple solution, and this final section reflects on the thought that the best value activity may simply be to model for *improved understanding* of a subsurface process.

Figure 9.8 shows production forecasts based on a mature field case in which a decision on infill

drilling was being made using sector models. The work was of a high technical quality, with uncertainties carefully explored and quantified using an ensemble-based technique.

Uncertainties were significant, and the work illustrated that plausible outcomes ranged from a very positive cumulative production to effectively zero production and commercial failure, with all possibilities in-between. Other than capturing a slight bias to the downside, the technical work is essentially illustrating that the uncertainty is high and future outcomes are unclear. As this was apparent from a cursory inspection of the initial uncertainties, it begged the question “*what was the point of all that modelling work?*”

This is an extreme case, but raises the question of why we model at all, if the honest outcome of our efforts is only to illustrate that we don’t know the answer. This is an uncomfortable conclusion that we are generally loath to acknowledge out of technical-professional pride; it is a conclusion we fear will not go down well with superiors and is one of the causative factors behind the paradigm of ‘modelling for comfort’ introduced back in Chap. 1. It may, however, be a true reflection of our situation. So what should we do?

An improvement on modelling for comfort is to abandon the notion that are we trying to finesse a solution every time we study the subsurface. Sometimes the uncertainties are too great and modelling only serves to illustrate this rather

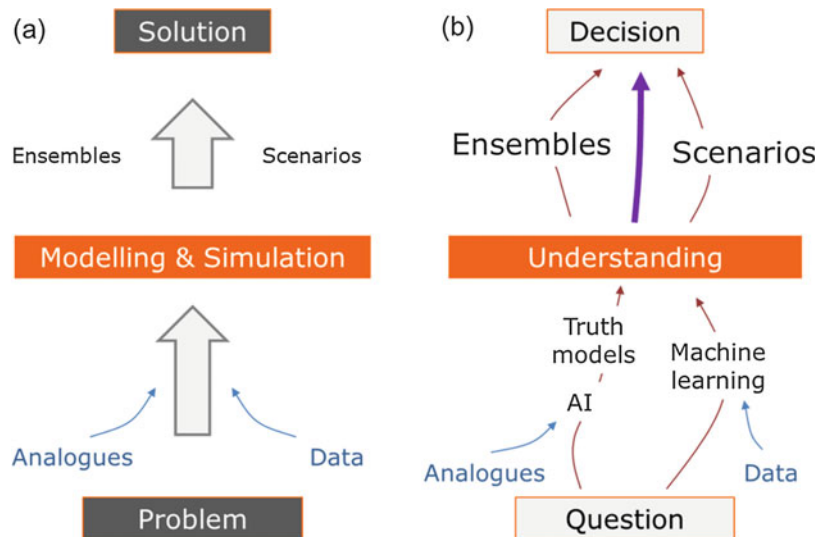
than to resolve those uncertainties. In this case we can benefit by simply stepping away from the idea that there is a subsurface problem, and that we have engaged in a modelling and simulation study to find ‘the solution’ (Fig. 9.9a).

The alternative is to replace the formulation of a ‘problem’ with that of a ‘question’, and the notion of a ‘solution’ with a ‘decision’ (Fig. 9.9b). We don’t actually need to conceptualise subsurface issues as problems and, as Fig. 9.8 illustrates, we cannot always come up with clear solutions. We will, however, always have questions and in a commercial world we will always have to make decisions and this applies equally to the storage projects of the energy transition as it has done to historical resource extraction projects.

Framed in this way, we can re-evaluate many of our modelling and simulation efforts and overcome some of the frustrations of modelling for comfort and the inefficiencies of the detailed full-field model default. Workflows such as the resource/decision models of Sect. 8.2 and the truth models of Sect. 8.4 fit into this framework neatly:

- The ‘resource model’ is simply a data base and is not a decision-making tool in itself.
- Truth models are there to generate understanding, as are the recent advances in machine learning which offer tremendous insights into

**Fig. 9.9** Alternative workflows: (a) the pursuit of an optimal solution; (b) the pursuit of understanding to support a decision



our data and particularly into the management of production data – but they do not make decisions for us.

- Artificial intelligence (AI) is a candidate for decision-making but needs a place within a framework of statistically insufficient, highly subjective, concept-based modelling; a potential role for AI lies in the construction of truth models based on a wealth of knowledge from outcrop analogue data (Fig. 8.12b).

All of the above requires thinking and modelling with the purpose of generating improved understanding, based on which (on the next cantilever of the decision-making process; Sect. 8.3) we can go forward and quantify uncertainties associated with the decision at hand. As discussed in Chap. 5, this can be explored using statistical ensembles, with or without machine learning, or deterministic scenarios or some combination of both.

If the outcome of this work is likely to give an answer similar to Fig. 9.8 then we may realise that our modelling work so far has been enough, we have all the understanding we need or can generate, and are in the position to stop modelling and make the next decision (which might be to collect new data). If, however, the modelling is leading us towards an improved or more precise understanding then we are perhaps evolving towards a solution.

Either way, the future of reservoir modelling must be more about improved understanding and less about finding the ‘right answer.’ This evidence-based learning approach to modelling the subsurface is likely to be the dominant paradigm for the near future – especially since careful use of resources is increasingly vital to our society, whether this be for the continued use of remaining hydrocarbon resources or for the growing efforts in CO<sub>2</sub> management, emissions reductions and subsurface energy storage.

---

## References

Bentley MR, Ringrose P (2017) Future directions in reservoir modelling: new tools and ‘fit-for-purpose’

- workflows. *Geol Soc Lond Pet Geol Conf Ser* 8:537–546
- Brandsæter I, McIlroy D, Lia O, Ringrose PS (2005) Reservoir modelling of the Lajas outcrop (Argentina) to constrain tidal reservoirs of the Haltenbanken (Norway). *Pet Geosci* 11:37–46
- Cabello P, Falivene O, López-Blanco M, Howell JA, Arbués P, Ramos E (2011) An outcrop-based comparison of facies modelling strategies in fan-delta reservoir analogues from the Eocene Sant Llorenç del Munt fan-delta (NE Spain). *Pet Geosci* 17:65–90
- Cawood AJ, Bond CE, Howell JA, Butler RWH, Totake Y (2017) LiDAR, UAV or compass-clinometer? Accuracy, coverage and the effects on structural models. *J Struct Geol* 98:67–82
- Constable S, Srnka LJ (2007) An introduction to marine controlled-source electromagnetic methods for hydrocarbon exploration. *Geophysics* 72(2): WA3–WA12.
- Coumou D, Matthäi S, Geiger S, Driesner T (2008) A parallel FE–FV scheme to solve fluid flow in complex geologic media. *Comput Geosci* 34:1697–1707
- Doe BR (1983) The past is the key to the future. *Geochem Cosmochem Acta* 47:1341–1354
- Fielding CR, Crane RC (1987) An application of statistical modelling to the prediction of hydrocarbon recovery factors in fluvial reservoir sequences. *SEPM Spec Publ* 39
- Geiger S, Roberts S, Matthäi SK, Zoppou C, Burri A (2004) Combining finite element and finite volume methods for efficient multiphase flow simulations in highly heterogeneous and structurally complex geologic media. *Geofluids* 4:284–299
- Geikie A (1905) *The founders of geology*. Macmillan, p 299. Reprinted by Dover Publications, New York, 1962
- Howell JA, Skorstad A, MacDonald A, Fordham A, Flin S, Fjellvoll B, Manzocchi T (2008) Sedimentological parameterization of shallow-marine reservoirs. *Pet Geosci* 14:17–34
- Jackson MD, Gome JLMA, Mostaghimi P, Percival JR, Tollit BS, Pavlidis D, Blunt MJ (2013) Reservoir modeling for flow simulation using surfaces, adaptive unstructured meshes, and control-volume-finite-element methods. *SPE reservoir simulation symposium*. Society of Petroleum Engineers
- Jackson MD, Hampson GJ, Saunders JH, El-Sheikh A, Graham GH, Massart BYG (2014) Surface-based reservoir modelling for flow simulation. *Geol Soc Lond Spec Pub* 387:271–292
- Jackson MD, Hampson GJ, Rood D, Geiger S, Zhang Z, Sousa MC, Amorim R, Brazil EV, Samavati FF, Guimaraes LN (2015) Rapid reservoir Modeling: prototyping of reservoir models, well trajectories and development options using an intuitive, Sketch-based interface. *Society of Petroleum Engineers*
- Jacquemyn C, Jackson MD, Hampson GJ (2019) Surface-based geological reservoir modelling using grid-free NURBS curves and surfaces. *Math Geosci* 51:1–28
- Jenny P, Lee SH, Tchelepi HA (2006) Adaptive fully implicit multi-scale finite-volume method for multi-

- phase flow and transport in heterogeneous porous media. *J Comp Phys* 217:627–641
- Keogh KJ, Leary S, Martinius AW, Scott AS, Riordan S, Viste I, ... & Howell J (2014) Data capture for multiscale modelling of the Lourinha Formation, Lusitanian Basin, Portugal: an outcrop analogue for the Statfjord Group, Norwegian North Sea. *Geol Soc Lond Spec Pub* 387(1): 27–56.
- Mallet J-L (2014) Elements of mathematical sedimentary geology: the geochron model. EAGE Publications, p 374
- Mariethoz G, Caers J (2014) Multiple-point geostatistics: stochastic modeling with training images. Wiley, Hoboken
- Matthäi SK, Geiger S, Roberts SG, Paluszny A, Belayneh M, Burri A, Heinrich CA (2007) Numerical simulation of multi-phase fluid flow in structurally complex reservoirs. *Geol Soc Lond Spec Pub* 292:405–429
- Miall AD (1988) Reservoir heterogeneities in fluvial sandstones: lessons learned from outcrop studies. *Am Assoc Petrol Geol Bull* 72:882–897
- Nordahl K, Ringrose PS, Wen R (2005) Petrophysical characterization of a heterolithic tidal reservoir interval using a process-based modelling tool. *Pet Geosci* 11:17–28
- Nyberg B, Buckley SJ, Howell JA, Nanson RA (2015) Geometric attribute and shape characterization of modern depositional elements: a quantitative GIS method for empirical analysis. *Comput Geosci* 82:191–204
- Pringle JK, Howell JA, Hodgetts D, Westerman AR, Hodgson DM (2006) Virtual outcrop models of petroleum reservoir analogues: a review of the current state-of-the-art. *First Break* 24:33–42
- Puig JM, Cabello P, Howell JA, Arbués P (2019) Three-dimensional characterisation of sedimentary heterogeneity and its impact on subsurface flow behaviour through the braided-to-meandering fluvial deposits of the Castissent Formation (late Ypresian, Tremp-Graus Basin, Spain). *Mar Pet Geol* 103:661–680
- Ringrose P (2020) How to Store CO<sub>2</sub> Underground: insights from early-mover CCS Projects. Springer.
- Ringrose P, Nordahl K, Wen R (2005) Vertical permeability estimation in heterolithic tidal deltaic sandstones. *Pet Geosci* 11(1): 29–36
- Rittersbacher A, Howell JA, Buckley SJ (2014) Analysis of fluvial architecture in the Blackhawk formation, Wasatch Plateau, Utah using large 3D photorealistic models. *J Sed Res* 84:72–87
- Sellwood BW, Valdes PJ (2006) Mesozoic climates: general circulation models and the rock record. *Sed Geol* 190:269–287
- Wen R, Martinius, AW, Næss A, Ringrose P (1998) Three-dimensional simulation of small-scale heterogeneity in tidal deposits – a process-based stochastic simulation method. In: IAMG 1998 Proceedings. International Association for Mathematical Geology
- Zanchi A, De Donatis M, Gibbs A, Mallet J-L (2009) Imaging geology in 3D. *Comput Geosci* 35:1–3
- Zhang Z, Geiger S, Rood M, Jacquemyn C, Jackson M, Hampson G, De Carvalho FM, Silva CCMM, Silva JDM, Sousa MC (2020) Fast flow computation methods on unstructured tetrahedral meshes for rapid reservoir modelling. *Comput Geosci* 24:641–661

# Nomenclature

| Symbol                   | Definition   |
|--------------------------|--|
| A                        | Area   |
| $AI_{p,s}$               | Acoustic impedance (p and s wave)  |
| $C_a$                    | Capillary number   |
| $C_v$                    | Coefficient of variation   |
| $E(p)$                   | Expected value for the variable, p   |
| $f$                      | Variance adjustment factor or frequency  |
| $f(x), g(x)$             | Functions of the variable x  |
| $F_D$                    | Fracture density   |
| g                        | Acceleration due gravity at the Earth's surface. ( $\sim 9.81 \text{ ms}^{-2}$ ) |
| H, h                     | Height or spatial separation (lag)   |
| HCIIP                    | Hydrocarbon volume initially in place  |
| $J(S_w)$                 | Water saturation function  |
| K                        | Constant of hydraulic conductivity or coefficient of permeability                |
| k                        | Permeability, or strictly the intrinsic permeability                             |
| $\mathbf{k}$             | Permeability tensor  |
| $k_b$                    | Block permeability   |
| $k_{\text{eff}}$         | Effective permeability   |
| $k_h, k_v$               | Horizontal and vertical permeability   |
| $k_{ro}, k_{rg}, k_{rw}$ | Relative permeability to oil, gas and water                                      |
| $k_x, k_y, k_z$          | Directional permeabilities in a Cartesian grid coordinate system                 |
| L                        | Length   |
| $\ln(x)$                 | Natural logarithm of x   |
| $N_o$                    | Sample number sufficiency statistic  |
| N/G                      | Net to gross ratio   |
| p, $p_c$                 | Statistical variable, critical value of p  |
| $P_c$                    | Capillary pressure   |
| PDF                      | Probability density function   |
| $\nabla P$               | Pressure gradient  |
| Q, q                     | Volume flux of fluid   |
| QC                       | Quality control  |

| Symbol                         | Definition  |
|--------------------------------|---|
| REV                            | Representative elementary volume                                  |
| STOIP                          | Stock tank oil initially in place                                 |
| $S_{ro}$                       | Remaining oil saturation  |
| $S_{wi}$                       | Initial water saturation  |
| $S_{wc}$                       | Connate water saturation  |
| $S_w, S_o, S_g$                | Water, oil and gas saturation                                     |
| u                              | Intrinsic flow velocity   |
| $V_m, V_s$                     | Volume fraction of mud and sand                                   |
| $V_{\text{shale}}$             | Volume fraction of shale  |
| $v_p$                          | Seismic compressional wave velocity                               |
| $v_s$                          | Seismic shear wave velocity                                       |
| X                              | General variable parameter  |
| $\delta X, \delta Y, \delta Z$ | Grid cell increment in X, Y, and Z                                |
| $\Delta X, \Delta Y, \Delta Z$ | System dimension in X, Y, and Z                                   |
| Z(x)                           | Spatial variable  |
| $\gamma(h)$                    | Semi-variance at distance h (the Variogram function)              |
| $\theta$                       | Angle (radians or degrees)  |
| $\kappa$                       | Number of standard deviations                                     |
| $\lambda$                      | Correlation length or power exponent                              |
| $\mu$                          | Mean value (statistics) or viscosity (physics)                    |
| $\pi$                          | Mathematical constant (ratio of circle circumference to diameter) |
| $\rho$                         | Correlation coefficient   |
| $\rho_g$                       | Grain density   |
| $\rho_b$                       | Bulk formation density  |
| $\sigma$                       | Standard deviation (statistics) or interfacial tension (physics)  |
| $\sigma_{1,2,3}$               | Principle components of the stress field                          |
| $\phi$                         | Porosity  |
| $\omega$                       | Weighting factor  |

(continued)

---

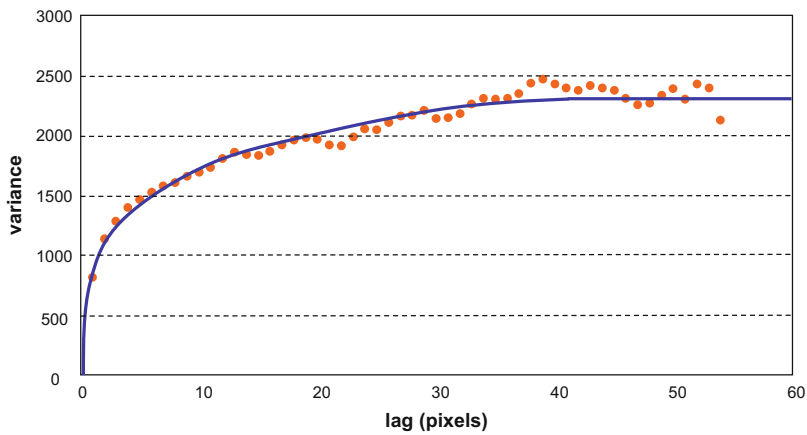
# Solutions

---

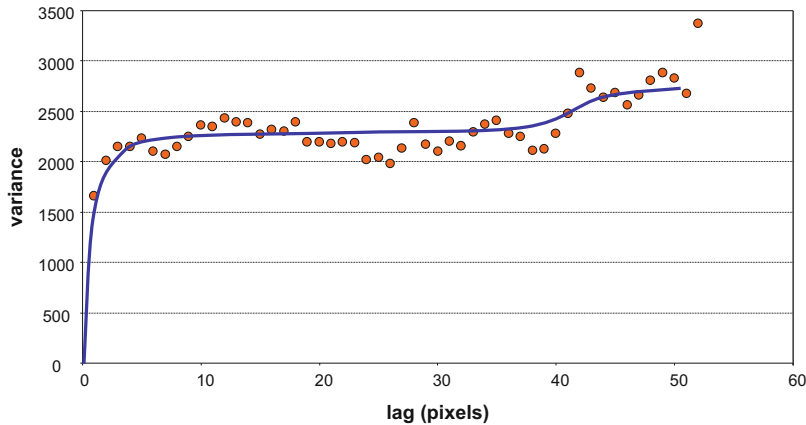
## Exercise 2.1. Estimation of Variograms for an Outcrop Image

Variograms for the pixelated grey-scale version of the outcrop image are shown below. If your sketch was close to these your intuition was pretty good.

- (a) Horizontal variogram with range of c. 40 pixels



(b) Vertical variogram with range of c. 5 pixels



### Exercise 3.1. Which Modelling Methods to Use?

There is no automatic right answer – the table is ordered in approximate correspondence between simpler approaches and complexity of purpose. 3D approaches are nearly always essential for well placement and design of IOR/EOR strategies, while 2D maps or simple averages may be quite adequate for initial fluids-in-place or reserves estimates.

### Exercise 3.2. Additive Properties

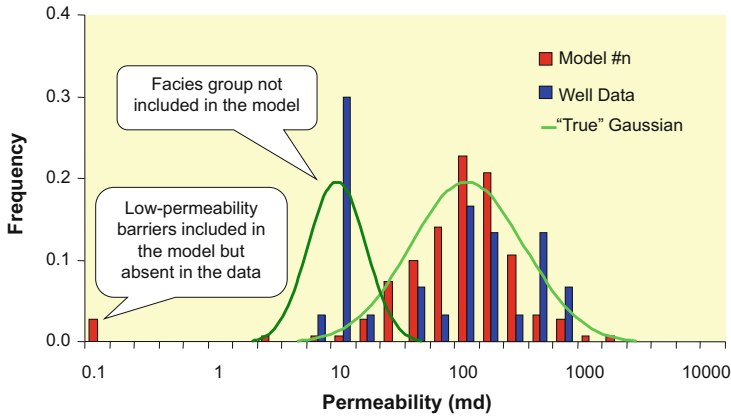
The key factor is that if the property involves a vector (e.g. related to field fluxes or gradients) then it is generally non-additive, while scalar properties are additive. The following properties are essentially additive: net-to-gross ratio, fluid saturation, porosity and bulk density. Permeability, formation resistivity, seismic velocity, and acoustic impedance are non-additive. However, fluid saturation could be considered non additive by virtue of its dependence on permeability.

### Exercise 3.3. Dimensions of Permeability

The SI unit for intrinsic permeability,  $k$ , is  $\text{m}^2$  and the dimensionless form of Darcy's law is  $[\text{L}\text{T}^{-1}] = ([\text{L}^2]/[\text{ML}^{-1}\text{T}^{-1}]) \cdot [\text{ML}^{-2}\text{T}^{-2}]$ . Note: One Darcy =  $0.987 \times 10^{-12} \text{ m}^2$ .

### Exercise 3.4. Comparing Model Distributions to Data

The warning indicator here is that although the arithmetic averages are similar, the geometric average of the well data is half the value for the model while the harmonic average of the model is much lower than the value for the well data. Two things are happening here illustrated in the graph below: (a) there is a facies group, or population, in the well data that has not been captured in the model and (b) the model has included some barriers that are not present in the data (due to insufficient sampling of thin shales). The model may in fact be quite a good one – if it is assumed that it captures the key features of the geology. Gaussian distributions are shown representing the hypothetical 'true' rock property distributions.



**Exercise 3.5. Bayes and the Cookie Jar**

The probability that Fred picked the cookie from the first cookie jar is 0.6 because:

$$P(A|B) = \frac{P(B|A) \times P(A)}{P(B)} = \frac{0.75 \times 0.5}{0.625} = 0.6 \text{ where}$$

- P(A) is the probability of picking jar 1;
- P(B) is the probability of getting a plain cookie;
- P(B|A) is the probability of getting a plain cookie assuming Fred picked from jar 1.

**Exercise 4.1. Permeability Upscaling for a Simple Layered Model**

- (a) The upscaled horizontal and vertical single-phase permeabilities are estimated using arithmetic and harmonic averages to give  $k_h = 550 \text{ md}$  and  $k_v = 181.8 \text{ md}$ .
- (b) Analytical values for the upscaled directional relative permeabilities for two values of  $P_c$  (assuming capillary equilibrium) are given below, where  $k_{rox}$  is the oil relative

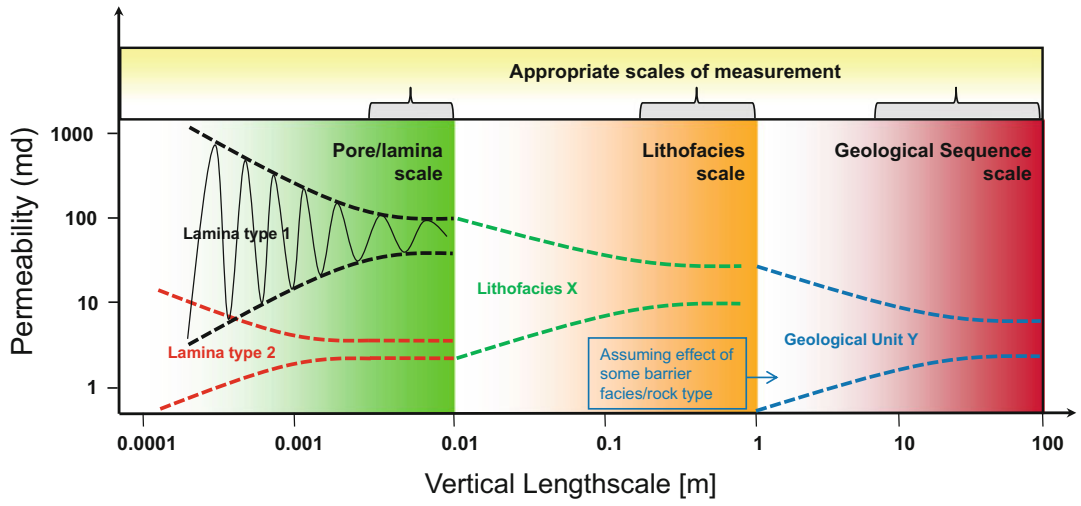
permeability in the horizontal direction, etc. (The method is illustrated in Fig. 4.9 and the complete upscaled curves are shown in Fig. 4.11.)

| $P_c$ | $S_w$ | $k_{rox}$ | $k_{roz}$ | $k_{rwx}$ | $k_{rwz}$ |
|-------|-------|-----------|-----------|-----------|-----------|
| 0.5   | 0.137 | 0.892     | 0.873     | 1.022E-05 | 3.058E-05 |
| 3     | 0.132 | 0.899     | 0.898     | 4.74E-08  | 1.419E-07 |

**Exercise 4.2. Find the REV's for Your Reservoir**

There is no correct answer – every reservoir is unique, although many lithofacies show characteristic behaviours. An example multi-scale REV sketch might look something like the example below. In practice we want to identify scales where the variance is relatively low and where an REV may be defined. Measurements will be most representative where an REV can be established. Reservoir models are best designed if their length scales (cell sizes and model domains) match the REV's. This may not always be possible.



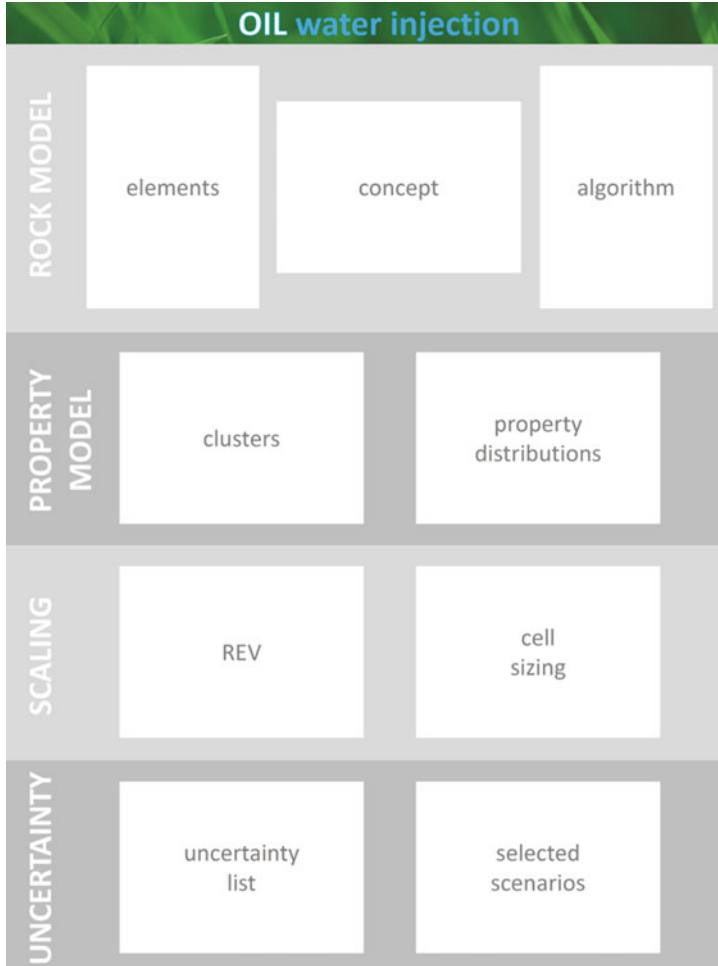


---

## Appendix A: A Template for Model Design

As a support for model design, we have developed a design template for use during reservoir modelling training events (below). The principle is that once the design components are agreed by an asset team (and ideally peer reviewed), we are in a good position to log on and build our models. The choices would always be fluid-dependent and purpose-

specific. The placeholders on the A0 poster are for A4 formatted hand-outs (shown on the following page) and examples of templates filled out for primary development planning for a clastic reservoir with contrasting fluid fills are illustrated on the final page.



**Model Elements**  
For your given field type, what elements will serve as the building blocks for a reservoir model?

**Conceptual Architecture**

**Algorithms and methodology**  
What algorithm(s) will you select for modelling, and what key parameters would you set (e.g. van genuchten)?

**Property Clusters**

**Property Distributions**  
Porosity  
NTG  
Total property modelling  
NTG modelling  
NTG defined by element choice  
NTG as a variable within element  
Enter the property distribution shape and end-points per model element  
Ring your choice(s) (may be different for different elements)

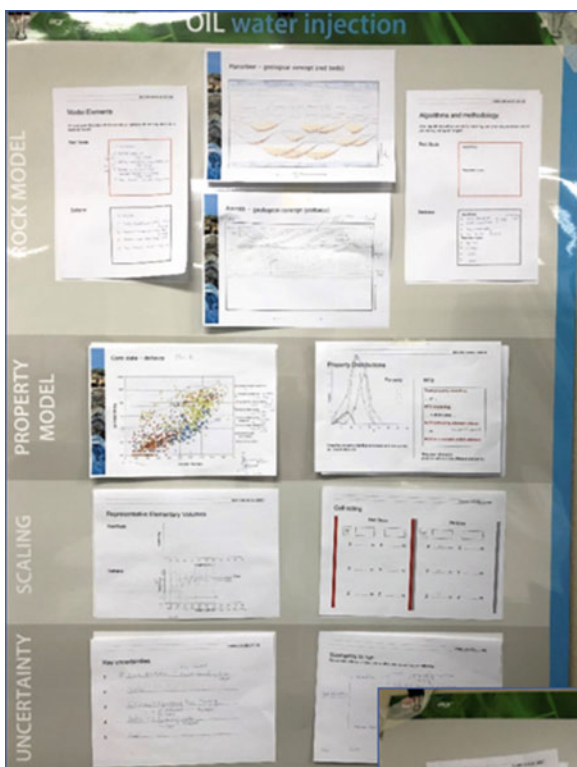
**Representative Elementary Volumes**  
Permeability  
Length scale (m)

**Cell sizing**  
Static  
Dynamic  
X \_\_\_\_\_ m X \_\_\_\_\_ m  
Y \_\_\_\_\_ m Y \_\_\_\_\_ m  
Z \_\_\_\_\_ m Z \_\_\_\_\_ m

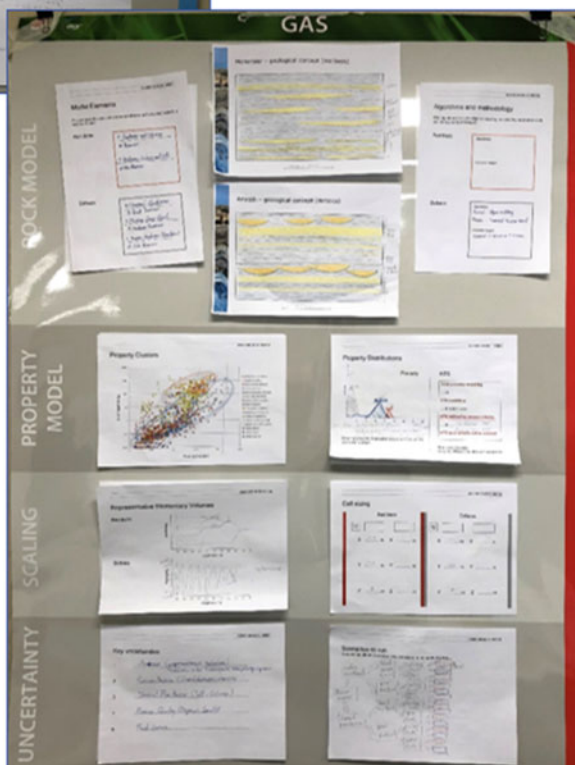
**Key uncertainties**  
1 \_\_\_\_\_  
2 \_\_\_\_\_  
3 \_\_\_\_\_  
4 \_\_\_\_\_  
5 \_\_\_\_\_

**Scenarios to run**  
Represent the alternative cases you would choose to run on a probability tree.

*(alternative conceptual sketches courtesy of Dave Cox, BP)*



Completed templates at the end of a course for alternative fluid fills: a light oil with water injection (left) and the same reservoir for a gas fill scenario (below).



# Index

## A

Acoustic impedance, 6, 7, 69, 215, 265, 305, 308  
Adaptive mesh, 300  
Additive properties, 4, 69, 154, 308  
    additivity, 69  
Aeolian, 39, 81, 139, 141, 196–201, 215, 294  
Aeolian reservoirs, 196–201  
Aeolian sandstone, 139, 195  
Aeolian systems, 196, 197, 199–200  
Affect, 66, 101, 102, 142, 144, 147, 176, 177, 182, 282  
Agile, 283  
Albert Einstein, 131  
Amalgamation ratio, 213, 214  
Amplitude extraction, 58  
Analogues, 1, 13, 14, 24, 33, 39, 41, 42, 46, 47, 59, 69, 81,  
    93, 121, 169, 197, 203, 215, 218, 220, 221,  
    226–229, 236, 237, 252, 259, 265, 286,  
    294–297, 302  
Anchored, 166, 169, 175, 178, 182, 185  
Anchoring, 166, 175, 177, 178, 181, 184, 187  
Anchoring and adjustment, 175  
Anchor point, 175, 176  
Andrew Goldsworthy, 152  
Anisotropy, 37–39, 42, 49, 50, 77, 106, 108–110, 121,  
    126, 166, 199–200, 206, 212, 214, 220, 234,  
    270  
Anisotropy ratio, 38, 39, 49, 108, 166  
Anna Karenina, 195  
Annot region, 215  
Annot Town, 218, 296, 297  
Anthropogenic CO<sub>2</sub>, 252  
Archibald Geikie, 294  
Arithmetic average, 67, 73, 74, 83, 105, 148, 293, 308  
Arithmetic mean, 73, 89, 108  
Artificial intelligence (AI), 302  
Assisted history matching, 284  
AVA, 95, 96  
Availability, 176  
AVA inversion, 96  
Average, 26, 28, 34, 35, 39–41, 48–51, 57, 67, 69, 71–75,  
    79, 83, 85, 90, 91, 100, 105, 108–112, 133,  
    135–137, 140, 148, 149, 151, 154, 197, 199,  
    215, 228, 245, 268, 287, 288, 292, 293, 308,  
    309

Averaging, 4, 28, 35, 40, 50, 65, 66, 72, 74, 100, 102, 108,  
    111, 127, 141, 144, 148, 150, 151, 177, 210,  
    228, 285, 292, 293  
AVO data, 95

## B

Balance of fluid forces, 142  
Balance of forces, 142, 143  
Barriers, 8, 18, 101, 102, 105–110, 120, 127, 148, 158,  
    199, 215, 246, 261, 262, 264–266, 274, 308  
Bayes  
    bayesian, 6, 92–93, 95–97, 189, 190, 284  
Bayesian Evidential Learning (BEL), 284  
Bayesian inference, 92  
Bayesian probabilistic, 6  
Bayesian statistics, 92–93, 96  
Behavioural biases, 166  
Best guess, 58, 166, 169–170, 172–175, 177, 184, 186  
Best-guess models, 166, 173  
Bias, vi, vii, 80, 86, 100, 101, 161, 166, 172–177, 190,  
    217, 301  
Biot's coefficient, 271  
Blocking, 100, 101, 105, 153, 154  
Block permeability ( $k_b$ ), 70, 71, 75, 77, 102, 104, 154, 293  
Book Cliffs, U., 211  
Boundary conditions, 32, 67, 71, 72, 75, 76, 102, 135,  
    138, 154, 170, 280  
Box-Behnken, 185  
Box-Cox transform, 83  
Braided, 39, 51, 201, 202  
Braided systems, 201  
Brushy Canyon, 118, 230

## C

Callanques of Cassis, 243  
Capillary imbibition, 242, 288  
Capillary number ( $C_a$ ), 144  
Capillary pressure  
    capillary-dominated, 142, 144, 158, 210  
    capillary equilibrium (CE), 110, 138–141, 309  
    capillary trapping, 141, 160, 200, 201, 259  
Capillary sealing, 257  
Capillary threshold pressure, 122, 124, 257, 259, 261  
Carbonate-evaporite sequences, 220

- Carbonate modelling, 218, 226
  - Carbonate pore fabrics, 223
  - Carbonate reservoirs, 22, 82, 147, 217–228, 244
  - Carbonate REV, 218, 225–228
  - Carbonates
    - environments, 82, 218, 220, 226
    - pore fabrics, 217, 221–224, 226, 227
    - pore type, 221
    - reservoir modelling, 217, 226, 228
  - Carbonate systems, 42, 217
  - CCS, 252, 254, 255, 271, 295
  - CCS project, 252, 261
  - Central limit theorem, 85, 86
  - Chalk fields, 221
  - Channel architecture, 202, 203, 298
  - Channel REV, 206
  - Chebyshev's inequality, 80
  - Chronostratigraphic framework, 226
  - Clustering, 187–189
  - CO<sub>2</sub>-brine flow systems, 259
  - CO<sub>2</sub>-brine relative permeability, 257, 258
  - CO<sub>2</sub> density *versus* depth, 253
  - CO<sub>2</sub> disposal, v, 24, 294
  - Coefficient of variation ( $C_v$ ), 80–82
  - CO<sub>2</sub> EOR projects, 252
  - CO<sub>2</sub> flooding, 7, 158
  - Cognitive limits, 175–177
  - CO<sub>2</sub> injection, 126, 160, 256, 261–265, 271, 272, 274, 286
  - Comfort, 1–2, 166, 173, 177, 301
  - CO<sub>2</sub> migration, 261, 264, 265
  - Conceptual geological model, 58, 292
  - Conceptual model
    - conceptual sketch, 13, 17, 52, 62, 214, 228
    - geological model, 4, 58, 237, 292
    - reservoir model, 13, 31, 223, 237, 246
  - Confined systems
    - confinement, 213, 214, 217
  - Connectivity, 53, 185, 200, 202–205, 214, 242, 259, 280
  - Contrast, 8, 24, 26, 29, 37, 43, 58, 67, 81, 103, 117, 118, 138, 169, 197, 210, 256, 257, 259, 280
  - CO<sub>2</sub> plume, 255, 257, 261–265
  - CO<sub>2</sub> plume growth, 261, 264
  - Core plug data, 150, 152, 153, 197, 222
  - Core plugs, 72, 106, 120, 134, 150–154, 197, 209, 215, 222, 226–227, 246, 285, 286, 293
  - Corey exponent, 136
  - Correlation
    - coefficient, 32–35, 58, 87
    - lengths, 47, 74, 90, 93–95, 170
  - Correlation coefficient, 32, 34, 35, 58, 305
  - Correlation lengths, 47, 74, 90, 93–95, 170, 305
  - CO<sub>2</sub> storage, 7, 8, 26, 27, 66, 69, 95, 126, 148, 159, 252–267, 271–274, 283, 296
  - CO<sub>2</sub> storage process, 252, 257–263
  - CO<sub>2</sub> storage projects, 252, 256, 257, 272, 283
  - CO<sub>2</sub> storage simulation, 138
  - Cross-correlation, 67, 87, 89
  - Cumulative distribution function (CDF), 83
  - Cut-offs, 78, 79, 86, 91, 97–105, 127
- D**
- Darcy
    - Darcy's law, 67, 70, 76, 77, 99, 135, 142, 308
  - Data-driven, 13, 31, 87, 88
  - Decision-making, vi, 173, 181, 184, 190, 191, 278, 280, 282, 301, 302
  - Decision model, 278–281, 300
  - Decision trees, 178, 191
  - Deep marine, 212–217, 230
  - Deep marine systems, 211, 217
  - Deep water, 197, 212–214
  - Determinism, vi, 4, 13, 28–34, 44, 54, 61, 62, 92, 169
  - Deterministic control, vi, 30, 32, 34, 54, 55
  - Deterministic trends, 18, 54–58, 166–168
  - DFN models, 78, 239, 240
  - Diagenesis
    - diagenetic, x, 13, 20, 22, 23, 46, 147, 223, 224, 228
  - Diagenetic elements, 22, 23
  - Diagonal tensor, 71, 148
  - Discrete fracture network (DFN), 78, 239–240, 245
  - Dispersion variance, 34, 154
  - Disposable grids, 298–300
  - Dolomites
    - dolomitisation, 22, 23, 224
  - D-optimal, 185
  - Douglas field, 16, 235, 237–238
  - Drainage and imbibition, 137
  - 3D seismic, 31, 58, 93, 97
  - Dual permeability, 78, 239, 241–243, 245
  - Dual permeability models, 78
  - Dual-permeability simulations, 241, 242, 245
  - Dual-permeability simulator, 245
  - Dual porosity models, 78, 239
  - Dune architecture, 199, 200
  - Dunham classification, 222, 223
  - Dynamic data, 69, 79, 92, 93, 95, 126, 214, 278, 283–285
- E**
- Earth model, 33, 58
  - Effective medium theory, 71, 107
  - Effective permeability ( $k_{\text{eff}}$ ), 71–74, 78, 83, 102, 106, 109, 124, 135, 197, 199, 200, 204, 205, 215, 218, 227, 233, 293
  - Effective porosity, 71, 86, 88
  - Effective Properties, 147, 196–199, 201, 209, 224, 227, 228, 285, 297
  - Effective property modelling, 209, 224, 227, 228, 285, 297
  - Effective vertical permeability, 216
  - Elastic properties, 96, 97
  - Endpoints, 135–137
  - Energy transition, v, 273–274, 291–302
  - Enhanced oil recovery (EOR), v, 7, 66, 67, 69, 99, 173, 252, 282, 285, 296, 308
  - Ensemble Kalman Filter (EnKF), 190
  - Ensembles, 169, 172, 174, 175, 178, 181–185, 187–190, 192, 284, 293, 300–302
  - EOR techniques, 296
  - Equation of state (EOS), 255
  - Eros, 65

- Evaporite, 220, 222, 224  
 Expected momentary value (EMV), 191  
 Experimental design (ED), 157, 185–187  
 Expert judgement, 169, 172  
 Expert review, 192
- F**
- Facies, 12, 13, 20, 44–46, 49, 50, 61, 69, 75, 84, 89, 94, 96–99, 108, 109, 119, 146, 150, 158, 178, 196, 202, 207, 212, 216, 220, 221, 226, 227, 265, 308  
 Facies trend simulation, 49, 50  
 Fault block geometries, 155  
 Fault compartments, 26, 232  
 Fault damage zones, 22, 23, 118, 195, 229, 234, 235, 237, 238  
 Fault framework, 15  
 Fault gouge, 119, 237  
 Faulting, 32, 117, 121, 230, 237  
 Fault juxtaposition diagrams, 119  
 Fault networks, 15–17, 117, 118, 230–233  
 Fault reactivation risk, 272  
 Fault rock, 119–124  
 Faults  
   damage zone, 22, 23, 118, 123, 229, 234, 235, 238  
   model, 8, 15  
   network, 15–17, 117, 118, 230–233, 239  
   rock properties, 121, 122  
   sticks, 16  
   terminology, 116  
 Fault sticks, 16  
 Fault system, 16, 119, 229, 233  
 Fault zone, 15, 119–124, 229, 232, 234, 237  
 Fault zone elements, 232  
 Field life cycle, 173, 174, 280, 300  
 Finite-volume flow simulation, 298  
 Fit-for-Purpose, ix, vi, 2, 8–9, 88, 93, 127, 246, 267, 280, 292  
 Fit-for-purpose models, vi, 2, 8–9, 292  
 Flexible mesh, 298  
 Flora's rule, 23–28, 33, 61, 161, 246  
 Flow barriers and baffles, 274  
 Flow boundary conditions, 72, 102, 154  
 Flow properties, vii, 75, 96, 97, 105, 121, 124, 126, 131–161, 241, 292, 299  
 Flow regime, 142  
 Flow simulation, 54, 76, 91, 133, 134, 138, 147, 150, 156–158, 166, 254, 257, 262, 298  
 Flow zone indicator, 69, 88  
 Fluid-force interaction, 286  
 Fluid forces, 111, 142–144, 155, 158, 286  
 Fluid mobility, 136, 260  
 Fluvial, 13, 14, 21, 39, 42, 43, 45, 49, 51–54, 58, 77, 81, 99, 144, 200–206, 209, 217, 268, 280, 286, 292  
 Fluvial reservoirs, 13, 14, 201–206  
 Fluvial systems, 39, 42, 49, 51–54, 144, 201–203, 217, 268  
 Fluvio-deltaic, 58, 265  
 Fluvio-deltaic system, 265  
 Fontaine du Vaucluse, Provence, 236  
 Force balance, 260  
 Forces, 60, 72, 79, 111, 132, 135, 136, 138–144, 155, 158, 200, 210, 260, 262, 263, 272, 286, 287, 292  
 Forth Bridge, 277, 280–283  
 Forth Bridge in Edinburgh, 277, 280  
 Forward-Modelling, 53, 124, 228, 244–245, 256  
 Fontainebleau sandstone, 87  
 Fourier transform, 95, 96  
 Fractal, 117, 148, 230, 233, 239  
 Fractional flow, 139  
 Fracture aperture, 68, 78, 124, 245  
 Fracture concepts, 229, 242, 246  
 Fracture networks, 78, 116, 125, 126, 228, 234, 239–241, 245  
 Fracture pattern, 224, 244  
 Fracture properties, 115–127, 228, 229, 240, 241  
 Fracture REV, 241, 242  
 Fractures  
   permeability, 68, 78, 126, 234, 240, 245  
   reservoirs, 115, 116, 127, 147, 224, 228–246  
   systems, 78, 115, 124, 125, 127, 225, 228, 229, 231, 234–238, 242  
 Fracture types, 229–230  
 Framing, 281  
 Franken field, 58–60  
 Free water level (FWL), 111, 113, 114  
 Frequency content, 32, 96  
 Front-end loading, 280  
 Funnelling, 45, 46, 48
- G**
- Gas injection, 7, 158, 159, 211, 252  
 Gaussian distribution, 80, 82, 308  
 Genetic element, 21–23  
 Genetic units, 20, 21  
 Geobodies, 32, 34  
 Geochemical trapping mechanisms, 253  
 GeoChron model, 298  
 Geo-engineer, 66  
 Geological hierarchy, 144  
 Geological trapping mechanisms, 253  
 Geomechanical model, 272  
 Geometric average, 74, 79, 108, 110  
 Geometric mean, 74, 75, 89, 108  
 Geomodel, 9, 109, 147, 154–157, 160  
 Geophysical imaging, 5  
 Geostatistical simulation, 36, 172, 173, 175  
 Geostatistical tools, 40, 174, 292  
 Geostatistics, 17, 28, 34–43, 47, 51, 173–175, 297  
 Geosteering, 4, 5  
 Glacial clastic systems, 42  
 The Golden Ass, 65  
 Gravity-capillary equilibrium (GCE), 138–140  
 Gravity/capillary ratio, 142  
 Gravity-fluid effects, 158  
 Greenfield, 278  
 Gres d'Annot (outcrop), 218–220  
 Grid-cell dimensions, 155



Grid resolution, 8, 95, 146, 156  
 Grids  
   gridding, 16, 105, 156, 157, 160, 296–298  
 Gullfaks field, 158

## H

Hard conditioning, 32, 34  
 Harmonic average, 74, 109, 140, 308, 309  
 Harmonic mean, 74, 75, 89  
 Hatnbanken, 93  
 Heat map, 189  
 Heriot-Watt University, 138, 299  
 Heterogeneity, 4, 12, 13, 17–20, 23–28, 33, 36, 37, 40, 42, 47, 57, 61, 81, 91, 127, 142–144, 146, 157–160, 170, 196, 197, 199–201, 207–210, 212, 214–219, 222, 243, 246, 257–259, 261, 262, 264–267, 269, 278, 281, 285, 286, 292, 294, 296  
 Heterolithic, 21, 72, 105, 108, 109, 144, 145, 149–152, 197, 206–209, 214–216, 218–220, 296, 297  
 Heterolithic facies from core, 207  
 Heterolithic reservoirs, 206, 296  
 Heuristics, 166, 175–178, 181, 182, 187, 282  
 Hierarchical packaging, 199  
 Hierarchy, 17–19, 32, 144, 146, 187, 205–206, 218, 225–228, 298  
 Hierarchy (geological), 17, 144, 146, 206  
 History-comparing, 284–285  
 History match, 158, 189, 282, 283  
 History-matching, 210, 237, 278, 283–284  
 Horizon interpretations, 15  
 Horizontal trends, 56–57  
 Hummocky cross stratification (HCS), 210, 265, 266  
 Hydraulic flow unit (HFU), 69, 88–89, 133, 161  
 Hydraulic units, 69  
 Hydrocarbon volume initially in place (HCIIP), 4, 214  
 Hydrodynamic gradients, 111, 112, 115, 122

## I

Imaging techniques, 294  
 Imbibition, 137, 140, 141, 234, 242, 257, 258, 288  
 Immiscible flow, 135, 210  
 Imperial College London, 299, 300  
 Implicit fracture modelling, 241  
 Improved oil recovery (IOR), 7, 66, 69, 148, 158, 308  
 Improved oil recovery/enhanced oil recovery (IOR/EOR), 7, 66, 308  
 Indicator kriging, 44, 47–49  
 In Salah, 8, 126, 271, 272, 274  
 Interfacial forces, 135  
 Interfacial tension, 110, 136, 141, 144, 252, 258  
 Invasion Percolation (IP), 210, 257, 261, 262  
 Inversion, 6, 58, 68, 69, 92, 96–98, 147, 151, 228, 230, 244, 246, 295  
 Iterative workflows, 277, 280–283

## J

Jabal Madmar, Oman (outcrop), 221  
 J-function, 111

Joints, 116, 118, 124, 147, 177, 222, 229–230, 233, 234, 237, 239–244  
 Joint systems, 222, 229, 233, 239, 244  
 Juxtapositions, 119, 232, 237

## K

$k_h$ , 17, 68, 72, 75, 79, 101, 102, 104–110, 207, 213, 242, 309  
 Karst, 225  
 Karstification, 234  
 Karstified natural fracture, 225, 236  
 Kinematic concept, 232  
 Knowledge capture, 66  
 Kozeny-Carmen, 69, 88  
 Kozeny-Carmen equation, 68, 88  
 Kraka field, 113–116  
 $k/\phi$  relationships, 88, 196, 197, 216, 222, 228  
 $k-\phi$  transform, 86–88, 224  
 Kriging, 44, 47–49, 69, 89–91, 96  
 $k_v/k_h$  ratio, 17, 68, 101, 105, 106, 108, 110, 213

## L

Lajas, 14, 93, 94  
 Laminae-Scale Effects, 200  
 Layer-cake, 20  
 Layer-cake architecture, 213  
 Length scales, 17, 18, 24, 26–28, 37, 49, 87, 90, 102, 127, 133, 134, 139, 142–144, 146, 148, 150, 151, 154, 155, 158, 161, 198, 201, 309  
 Leo Tolstoy, 195  
 Life-cycle, 173, 174, 280, 300  
 Lithofacies, 19–22, 72, 144–148, 150–155, 160, 161, 202, 205–207, 209, 265, 309  
 Lithofacies modelling, 134, 147, 161  
 Lithofacies REV, 151, 158, 207  
 Lithofacies-scale models, 155  
 Lithological, 17  
 Log-normal distribution, 74, 82, 83  
 Lost Heterogeneity, 218, 294, 296  
 Lourinha formation, Portugal, 206  
 Lower Antelope Canyon, Arizona, 291  
 Lucia classification, 222  
 Lucia rock fabrics, 222

## M

Machine learning, 190, 283, 301  
 Macroscopic, 17, 144, 147, 149, 160, 261, 267, 292  
 Marginal reservoir, 206  
 Marked point process, 44  
 Mark Rothko, 132, 133  
 Mature fields, 173, 185, 189, 278–281, 284, 296, 300  
 Meandering, 53, 94, 201–203  
 Meandering channel systems, 202, 203  
 Mechanical properties, 118, 225, 239, 243, 271  
 Mechanical stratigraphy, 118, 239, 272  
 Microscopic, 144, 210, 292, 295  
 Mini-permeameter data, 197  
 Mobility ratio, 24, 99, 236, 256, 260  
 Model concept, 13, 19, 22, 46, 61, 62

- Model design, x, ix, vi, vii, viii, 2, 7, 8, 12, 13, 15, 30–32, 34, 39, 65, 86, 93, 95, 99, 142, 155, 173, 190, 205, 217, 228, 229, 266, 273–274, 279, 280, 283, 292–294, 3011–314
- Model elements, 13, 18–28, 32, 42, 44, 46, 50, 59, 61, 69, 84, 86–88, 91, 93, 116, 146, 155, 196, 202, 221, 226, 242, 243, 281, 293
- Model ensemble, 172, 181, 183, 185, 187–189, 192, 300
- Modelling elements, 20, 160, 201, 202, 223, 250
- Modelling for comfort, 1, 2, 166, 177, 301
- Modelling for understanding, 288, 294, 300–302
- Model purpose, 1–9, 17, 24, 33, 91, 160, 178, 180, 212, 228, 232, 292, 293
- Mohr diagram, 116, 117, 270
- Monte Carlo, 29, 187, 190
- Monte-Carlo analysis, 187
- Multi-channel complexes, 201
- Multi-deterministic, 117, 181, 183, 184, 188, 284
- Multi-deterministic scenarios, 284
- Multi-phase, 101, 102, 122, 135–146, 148, 160, 161, 234, 262
- Multiphase flow, 121, 135, 138, 139, 143, 147, 148, 200, 257, 259
- Multiphase flow upscaling, 138, 148
- Multi-phase fluid flow, 142
- Multiple-deterministic models, 187
- Multiple deterministic scenarios, 126, 171
- Multiple models, 59, 169
- Multiple-stochastic, 170–172, 204
- Multiplicative, 4, 69
- Multi-point statistics (MPS), 44, 50–53, 287
- Multi-scale flow modelling, 132–134
- Multi-scale geological modelling, 154
- Multi-scale modelling, 132, 144, 147, 155, 158, 159, 196, 206, 207, 297
- Multi-scale reservoir modelling, 134, 144–159
- Multi-stochastic, 177, 181, 185
- N**
- Naturally fractured reservoir, 229, 240
- Navier-Stokes, 70
- Net-to-gross, 3, 56, 57, 69, 97, 99, 178, 179, 206, 215, 280, 308
- net sand, 99
- N/G ratio, 68, 69, 97–105, 206, 215, 306
- $N/G_{\text{sand}}$ , 68, 80, 99, 100
- Net-to-gross ratio, 69, 97, 99, 206, 306
- Normal distribution, 74, 80, 82–85
- Normal faults, 145, 231, 232
- Normal score transform, 83, 84
- Numerical methods, 75, 102, 132, 160, 293
- N-zero, 80, 82
- O**
- Object modelling
- object-based modelling, 32, 146
- Oil migration, 210, 212, 257
- Oman, 221, 226
- Open damage zones, 235, 237
- Open fracture properties, 124
- Ordinary kriging, 49
- Outcrop analogues, 1, 33, 42, 81, 227, 228, 236, 265, 294, 302
- Overconfidence, 176, 182, 187, 283
- Overconfidence heuristic, 187
- P**
- Pandora's box, 65
- Parasequences, 17, 22, 150, 209–211
- Paris climate accord, 274
- Patagonia, 14
- Peer review, 59, 176, 177, 311
- Pembrokeshire, Wales, 286
- Peng-Robinson, 255
- Percolation
- theory, 202–205
- threshold, 108, 109, 203, 204
- Permeability
- averages, 72–75
- tensors, 72, 75–77, 121, 126, 135, 148
- anisotropy, 106, 108, 121, 200
- upscaling, 71, 141, 148, 309
- Persephone, 65
- Petrophysical properties, 47, 69, 77, 91, 93, 109, 127, 138, 147, 152, 166
- Petter Dass Museum, 9
- Physical trapping mechanisms, 253
- Picasso, 132, 133
- Pipes, 237–238
- Pixel-based methods, 44, 48, 62
- Pixel-based modelling, 47–50, 146
- Plackett-Burmann, 185, 186
- Platform carbonates, 39, 220, 221
- Poiseuille's law, 77, 124, 241
- Poisson's ratio, 271
- Population statistics, 78, 83
- Pore networks, 86, 87, 137, 146, 160
- Pore-scale
- modelling, 145, 227
- models, 134, 147
- Pore size distribution, 110, 137, 221
- Pore-to-Field Workflow, 160
- Poro-perm cross-plots, 86
- Porosity, 3–5, 8, 12, 24, 35, 37, 43, 67–69, 71, 77, 78, 85–89, 91, 93, 95–97, 99, 101, 102, 111, 121, 132, 133, 145, 148, 151, 154, 169, 178, 196, 197, 207, 214, 215, 217, 221–222, 224, 226, 227, 234, 239–242, 245, 259, 260, 293, 295, 308
- The power average, 108, 293
- Power transform, 83
- Pressure gradient ( $\Delta P$ ), 24, 70, 71, 76, 78, 111, 113, 122, 135, 139, 142, 143, 158, 270, 281
- Priming, 177
- Principles of geology, 237, 273, 294
- Probabilistic
- probability, 29, 30, 54, 96
- ensembles, 175, 185

- Probability density function, 83, 305  
 Probability trees, 56, 178, 180–183, 191  
 Probability Volumes, 57  
 Probe permeability  
   probe permeameter, 73, 152, 154  
 Probe permeameter data, 152–154  
 Process-based, 44, 53–55, 62, 146, 297  
 Process-based methods, 44  
 Process-based model, 53–55  
 Process-Based Modelling, 53–54  
 Project risk, 189, 191  
 Property distributions, 12, 61, 89–97, 233, 308  
 Property modelling, 12, 40, 47, 53, 61, 78, 83, 86, 90,  
   92–97, 99, 101–105, 115, 127, 155, 207, 209,  
   223, 227, 228, 285  
 Proxy function, 185–187  
 Pseudo-relative permeability curves, 285  
 Purpose, vi, 1–2, 9, 12, 17, 27, 28, 33, 38, 65, 66, 69, 73,  
   82, 88, 89, 91, 93, 111, 127, 160, 172, 173, 178,  
   180, 181, 185, 212, 226, 228, 232, 246, 267,  
   277–280, 283, 286, 291–292, 296, 298, 302,  
   308, 311
- Q**  
 Quality control (QC), 15, 46, 53, 58, 61, 96, 166, 214, 284
- R**  
 Rapid reservoir modelling, 298, 299  
 Rationalist approaches, 169–170, 172, 173  
 Realisations, 47, 48, 50, 58, 89, 91, 94, 96, 151, 166, 169,  
   170, 172, 174, 175, 181–185, 187, 191, 245,  
   280, 284  
 Recovery efficiency, 213  
 Relative permeability, 68, 122, 123, 135–137, 139–141,  
   145, 210, 257, 258, 260, 262, 285, 287, 295,  
   309  
 Relative permeability curves, 136, 137, 139, 141, 257,  
   258, 285  
 Representative elementary volume (REV), 27, 133, 144,  
   148–152, 154, 155, 158, 161, 196, 197, 201,  
   206, 207, 212, 214, 215, 218, 225–228, 234,  
   241, 242, 292, 293, 309  
 Representativity, 150, 151  
 Reservoir analogue, 33, 69, 215  
 Reservoir flow simulation, 99, 101  
 Reservoir simulation, v, 2, 4, 6, 7, 100, 101, 105, 123, 146,  
   147, 157, 159, 212, 234, 262, 263  
 Reservoir simulators, 135, 138, 147, 148, 155, 160, 242,  
   296  
 Resource and decision model, 278–280  
 Resource model, 278–280, 300, 301  
 REV framework, 151, 154, 155  
 Risk, v, 3, 166–169, 177, 189–192, 196, 254, 269, 272,  
   273, 282  
 Rock-fluid interactions, 292, 295  
 Rock mechanics, 270–272  
 Rock model  
   rock modelling, 12, 32, 43–45, 47, 48, 50–52, 54,  
   57–62, 91, 93, 170, 218, 220  
 Rock types, 20, 86, 97, 111, 140–142, 160, 286, 293  
 Root cause, vii, 178–180, 280  
 Root-cause analysis, 179, 280
- S**  
 Salt caverns, 267–270  
 Sand trend map, 56  
 Saturation-height Functions, 111–112  
 Saturation model  
   saturation-height function, 111–112  
 SBED Studio, 9  
 Scale invariance, 230, 233  
 Scale transitions, 132, 133, 146, 147, 160  
 Scaling group theory, 161  
 Scaling laws, 135  
 Scanning electron microscopes (SEM), 139, 152, 295  
 Scenario approach  
   scenario-based modelling, 183, 185  
 Scenario-based, 171, 173, 177, 183, 185, 280, 293  
 Scenario-based thinking, 293  
 Scenario modelling, 172, 181  
 Scenarios, v, 3, 7, 17, 47, 126, 169–173, 177, 178,  
   181–183, 185, 199, 214, 215, 246, 265, 273,  
   274, 280, 284, 293, 302  
 Sealing fault zones, 234  
 Seismic, 2, 13, 67, 133, 169, 207, 257, 278, 292  
 Seismic data  
   4D seismic, v, 6, 7, 214, 264  
   seismic attributes, 4, 57, 58, 212–215, 268  
   seismic conditioning, 32–34, 58  
   seismic imaging, v, 5, 95, 147, 261, 262, 264  
   seismic interpretation, 2, 6, 15, 16, 232  
   seismic inversion, 6, 58, 68, 69, 92, 96–98, 147  
 Seismic resolution, 15, 147, 212  
 Sequential gaussian simulation (SGS), 47, 91, 92, 146, 242  
 Sequential indicator simulation (SIS), 44, 47–51, 57, 58,  
   60, 91, 92, 146, 166  
 Sequestration of carbon dioxide, 254  
 Shale gouge ratio (SGR), 119–121  
 Shallow marine, 157, 158, 206–212, 265  
 Shallow marine reservoirs, 209–210  
 Shallow marine (paralic) reservoir systems, 208  
 Shallow marine sandstones, 207–211  
 Shape factor, 78, 88, 125, 241  
 Shoreface, 17, 21, 22, 37, 42, 49, 50, 209, 210, 265, 266  
 Shoreface systems, 17, 42, 210, 266  
 Shuaiba, 218  
 Shuaiba reservoir, 218  
 Shuey approximation, 95  
 Shuiba, 11  
 Sigma, 125, 241  
 Siliciclastic, 119, 217, 218, 226, 235  
 Simple kriging, 48, 90  
 Simulation (reservoir simulation), v, 2, 4, 6, 7, 100, 101,  
   105, 122, 123, 146, 147, 157, 159, 212, 234,  
   262, 263  
 Simulator grids, 155–157  
 Single-phase flow, 135, 140, 161

## SIS

*See* Sequential indicator simulation (SIS)

Sleipner, 253, 255–257, 261, 262, 264, 265, 295  
 Sleipner Utsira formation, 261  
 Smørbuk field, 103  
 Snøhvit, 255–257, 262–265, 272, 295  
 Soave-Redlich-Kwong, 255  
 Soft conditioning, 32, 33, 57, 58  
 Spatial correlation, 36, 37, 49, 50, 89, 166  
 Spatial estimation, 89  
 Spatial heterogeneity, 36  
 Spatial variation, 35, 37, 40, 90, 154, 155  
 Special core analysis (SCAL), 139, 148, 160  
 Stair-stepped faults, 156  
 Standard error, 80, 81  
 Staffjord field, 159  
 Stationarity, 45, 48, 49, 55–60, 90, 166, 167  
 Statistical ensemble, 178, 181, 293, 302  
 Statistical methods, 80, 146, 177, 190  
 Steady-state, 71, 75, 76, 113, 138–142, 148, 159, 160, 259  
 Steady-state approximations, 160  
 Steady-state upscaling, 139, 140  
 Steady-state upscaling methods, 139, 140  
 Stochastic, vi, 5, 29, 93, 96, 98, 107, 166, 167, 170–172, 177, 192, 204, 205  
 Stochastic approaches, 170–172  
 Stochastic simulation, 93, 98  
 Storage, 7, 26, 66, 138, 191, 228, 252, 283, 291  
 Storage complex, 27, 253–255  
 Storage in engineered salt caverns, 267  
 Storage in natural porous rock formations, 267  
 Storage in underground tanks, 267  
 Storage of compressed air, 270  
 Storage of hydrogen, 267, 269  
 Stratigraphic, 2, 4, 15, 17–19, 22, 46, 61, 101, 102, 113, 144, 146, 149, 150, 157, 158, 209, 214, 229, 253, 265, 266, 270, 271  
 Stratigraphic barriers, 101, 102, 266  
 Stratigraphic correlation, 17, 18  
 Stratigraphic framework, 226  
 Stratigraphic inputs, 15, 17  
 Stratigraphy, 17–19, 22, 56, 93, 118, 209, 229, 239, 272, 274  
 Stress field, 126, 272, 273  
 Stress field orientation, 272  
 Stress-modelling, 126  
 Strike-slip faults, 230, 231  
 Structural barriers, 266  
 Structural concept, 16, 233, 237, 238  
 Structural elements, 22, 23  
 Structural framework, 13, 16, 17, 32, 155  
 Structural inputs, 13  
 Structural model, 2, 16, 18, 22, 147, 243  
 Sub-seismic faulting, 230  
 Sub-seismic fault network, 232  
 Subsurface energy storage, v, 302  
 Super-forecasters, 176  
 Surface-based models, 297–298  
 Swanson's mean, 86–88

Sweep efficiency, 199, 220

## T

Tectonic spectrum, 229, 231  
 Tensor permeability, 72, 75–77, 121, 126, 135, 148  
 Texture-based methods, 44  
 Texture-based modelling, 50, 51  
 Thief zone, 210, 246  
 Thin beds, 103–105, 112, 151, 185, 186, 197, 214–218, 226  
 Thrust faults, 229  
 Tidal, 7, 14, 73, 84, 94, 103, 108, 109, 145, 146, 149, 150, 152, 153, 157–159, 197, 206–208, 215, 292, 298  
 Tidal channel, 94, 146  
 Tidal delta, 94, 145, 149, 207  
 Tidal deltaic, 73, 84, 103, 108, 109, 145, 152, 153, 157, 158, 197, 206–208  
 Tidal deltaic reservoir, 73, 84, 109, 152  
 Tidal deltaic reservoir systems, 206, 208  
 Tidally-influenced delta, 39  
 Tidal reservoir, 7, 14, 159  
 Tilted oil-water contacts, 112–115  
 Time-lapse, 7, 190, 259, 261, 264–266  
 Time-lapse amplitude map, 264  
 Time-lapse seismic, 7, 190, 261, 264, 266  
 Timelines, 17, 18, 280  
 Total property modelling (TPM), 101–105, 207, 228, 286  
 TRACS, 245  
 Training image, 44, 51–55, 297  
 Transmissibilities, 101, 106, 107, 115, 120, 122, 123, 134, 147, 156, 157, 191, 232, 234  
 Transmissibility multiplier, 106, 107, 122, 123, 147, 234  
 Trees, 34, 168, 169, 178–183, 185, 191, 192, 284  
 Trend map, 45, 46, 57  
 Trends, 3, 18, 36, 37, 44–50, 54–58, 60–62, 86–89, 96, 122, 139, 166–168, 200, 224, 272, 273, 294  
 Trends (vertical, horizontal), 37, 48, 55–58, 139  
 Truncated Gaussian simulation (TGS), 91, 92  
 Truth models, 285–288, 301  
 TUDelft, 55  
 Turbidites, 212  
 Two-phase flow effects, 210

## U

Uncertainties, 3, 17, 80, 158, 166, 214, 265, 280, 292  
 handling, 29, 165–192, 228, 246, 292  
 uncertainty list, 177, 178, 192  
 University of Aberdeen, 297  
 University of Calgary, 299  
 Unstructured grids, 157, 300  
 Unsupervised clustering, 188  
 Upscaling  
 upscaled permeability, 70–72, 102, 140, 154, 155, 293  
 upscaled (block) permeability, 71, 75–77, 154, 293  
 Upscaling methods, 102, 127, 133, 138–142, 147, 148, 160  
 Urganian, 11, 118, 125, 234, 235, 243

**V**

Variance  
 adjustment factor, 153, 154  
 Variance mapping, 183–184  
 Variogram  
 semi-variogram, 35–43, 90, 91  
 Variogram function, 35, 36, 48, 90  
 Variogram model, 37, 38, 41, 42, 47, 49, 62  
 Vaucluse, 234, 235  
 Vertical equilibrium, 139  
 Vertical permeability, 68, 77, 101, 105–110, 158, 215, 216  
 Vertical trends, 37, 48, 55–58, 139  
 Vertical variograms, 37, 308  
 Viscosity, 24, 70, 76, 78, 135, 136, 142, 144, 252, 256,  
 259, 260, 274, 292  
 Viscous/capillary ratio, 142–144  
 Viscous-dominated, 142, 144, 259, 260  
 Viscous limit (VL), 138, 139, 160  
 Visualisation, 2–3, 5, 61, 240  
 Volcanic rocks, 252  
 Volumetrics,  $v$ , 2–4, 22, 70, 78, 116, 119, 127, 175, 183,  
 184, 241, 254  
 $V_p/V_s$ , 68, 97, 98  
 Vuggy systems, 222

**W**

Walther's Law, 55  
 Water alternating gas (WAG), 7, 69, 159  
 Waterflood, 7, 137, 141, 174, 200, 210, 211, 217, 234,  
 236, 281, 286, 287, 311  
 Water saturation, 27, 110, 111, 136, 200, 207  
 Water wet, 122, 124, 136, 141, 142, 200, 242, 257, 295  
 Well planning/plans, 2, 4–5, 66, 67, 91  
 Well test, 27, 71, 79, 109, 110, 126, 134, 215, 240, 242,  
 245, 246, 264, 273, 283  
 Wettability, 125, 141, 200, 235, 242  
 Wetting and non-wetting, 139  
 Workflow, 8, 12, 15, 16, 18, 19, 31, 34, 50, 53, 90, 93–97,  
 100, 102, 105, 119, 120, 124, 125, 127, 160,  
 161, 166, 172, 175, 177, 182, 184, 185, 187,  
 192, 200, 207, 208, 214–216, 221, 228–229,  
 232, 235, 239–241, 242, 245, 254, 267, 272,  
 277–288, 292, 296–297, 301

**Y**

Young's modulus, 271  
 Y-shaped faults, 156